Science
AAAS

Supplementary Materials for

Photocatalyzed oxidative cleavage of alkenes using CO_2 as an oxygen donor

Yuman Qin *et al*.

Corresponding authors: Matthias Beller, matthias.beller@catalysis.de; Shoubhik Das, shoubhik.das@uni-bayreuth.de

Science **392**, eaed6068 (2026)
DOI: 10.1126/science.aed6068

The PDF file includes:

Contents

1. General information

Commercial reagents were used without purification and reactions were run under CO_2 atmosphere with exclusion of moisture from reagents using standard techniques for manipulating air-sensitive compounds. $CDCl_3$ was purchased from Sigma Aldrich. $CHCl_3$, MeCN was purchased from Acros Organics-International. Dicyandiamide, 2-amino-5-(trifluoromethyl)benzonitrile and $Fe(NO_3)_3$•$9H_2O$ were purchased from Sigma Aldrich. Kessil lamps were purchased from Laser 2000 (UK) Ltd, with precise wavelengths (390 nm, 456 nm). ^1H NMR spectra (500 MHz) and ^{13}C NMR spectra (126 MHz) were recorded using Bruker Avance 500 spectrometer with $CDCl_3$ or DMSO-d_6 as solvent. NMR spectra were calibrated using the solvent residual signals ($CDCl_3$: δ ^1H = 7.26, δ ^{13}C = 77.00; DMSO-d_6: δ ^1H = 2.50, δ ^{13}C = 39.52). The following abbreviations were used to describe peak splitting patterns when appropriate: s = singlet, d = doublet, t = triplet, q = quartet, quint = quintet, dd = doublet of doublet, m = multiplet and br = broad singlet. Analytical thin layer chromatography (TLC) was performed using pre-coated TLC sheets ALUGRAM® SIL G/UV254 (Machery-Nagel) and spots were visualized using UV light (254 nm). Flash chromatography was performed on an automated chromatography system (Buchi) with on-line UV detection using commercial Silica Flash Cartridges and the indicated solvent and gradient system. High performance liquid chromatography (HPLC) of samples were prepared by dissolving 0.1−5.0 mg of the product in methanol or in acetonitrile and further diluting to a concentration of 10^{-5}−10^{-6} M with 50% methanol (or acetonitrile)/50% H_2O/0.1% formic acid.

2. Synthesis of Fe@f-gC_3N_4 photocatalyst

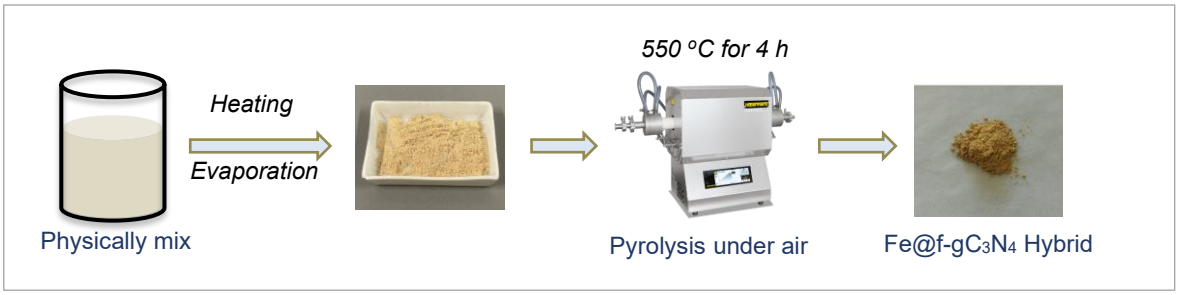

Fig. S1. The preparation procedure of atomically dispersed Fe photocatalyst

107 mmol of Dicyandiamide (DCDA, 9 g), 0.08 mmol of $Fe(NO_3)_3$•$9H_2O$ (0.032 g), and 0.8 mmol of 2-amino-5-(trifluoromethyl)benzonitrile (0.150 g) were stirred together in 45 mL of H_2O at 95 °C for 1 h in a closed system and then dried at 100 °C to remove water. Afterward, solids were ground to fine powders and heated to 550 °C at a rate of 2.2 °C/min and were kept at this temperature for 4 h under an aerobic atmosphere. After that, the oven was cooled down to room temperature, the resulting mixture was removed and ground in an agate mortar and used for the subsequent reactions. The as synthesized catalyst was named Fe@f-gC_3N_4.

3. Elemental analysis

Elemental (CHN) analyses was performed by using a UNICUBE® microelemental analyzer (Elementar). For precise sample preparation, a Mettler Toledo™ WXTS3DU microbalance and a Mettler Toledo™ MX5 microbalance were employed along with dedicated sample formers and pressing tools. During combustion, the system reached a maximum furnace temperature of 1,200 °C, with localized temperatures up to 1,800 °C achieved briefly when tin foil was used to promote sample ignition.

Table S1. Weight percentage of C, N, H in Fe@f-gC_3N_4

Sample	Weight (mg)	Method	Weight (%)		
			N	C	H
Fe@f-gC_3N_4	2.21	2 mg standard	57.61	33.13	1.85
Blank	1	Blank with O_2	0	0	0
Fe@f-gC_3N_4	2.17	2 mg standard	56.65	32.55	1.77
Blank	1	Blank with O_2	0	0	0
Fe@f-gC_3N_4	2.16	2 mg standard	57.63	33.09	1.83
Blank	1	Blank with O_2	0	0	0
	Average		57.30	32.92	1.82

4. Inductively coupled plasma optical emission spectrometry (ICP-OES)

The ICP-OES method was employed to determine the bulk elemental composition of Fe in fresh Fe@f-gC_3N_4 and spent Fe@f-gC_3N_4. The measurements were conducted with a 715-ES ICP emission spectrometer (Varian, Palo Alto, CA, USA). Before analyses, samples were dissolved in a mixture of HF and aqua regia at 200 °C and 60 bar through microwave-assisted digestion. The iron content in both the fresh and spent Fe@f-gC_3N_4 samples was determined to be 0.143 wt%.

5. Photoelectrochemical properties of Fe@f-gC_3N_4

5.1 UV-Visible-DRS spectroscopy

A UV-Visible spectrometer (UV-Vis, Shimadzu UV-2600i) coupled with a diffused reflectance spectra (DRS) integrating-sphere module (with $BaSO_4$ as the reference standard) was used for bandgap measurements.

Here, we use the Tauc plot method to calculate the bandgap width of catalysts. This method is based on the formula proposed by Tauc, Davis, and Mott, commonly known as the Tauc plot.

$$(\alpha h\nu)^{\frac{1}{n}} = A\left(h\nu - E_g\right) \quad (1)$$

where hv=hc/λ. Here, α is the absorption coefficient, h is Planck's constant, v is the photon frequency, c is the speed of light, and λ is the wavelength of light. E_g is the bandgap energy. The exponent n depends on the type of semiconductor: for direct bandgap semiconductors, n = 1/2; for indirect bandgap semiconductors, n = 2. A is a parameter dependent on the transmission probability.

Additionally, the band gap energy is usually determined from diffuse reflectance spectra. For UV-Vis diffuse reflectance spectroscopy (DRS) to measure the bandgap, reflectance (R) is typically measured. The Kubelka-Munk function $F(R_\infty)$ based on Kubelka-Munk theory is then used, which relates reflectance to absorbance and is given by:

$$F(R_\infty) = \frac{K}{S} = \frac{(1 - R_\infty)^2}{2R_\infty} \quad (2)$$

where $R_\infty = R_{sample}/R_{standard}$ is the reflectance of an infinitely thick specimen, while K and S are the absorption and scattering coefficients, respectively. Substitute $F(R_\infty)$ for α in equation 1 yields the form equation 3.

$$(F(R_\infty) \cdot h\nu)^{\frac{1}{n}} = A\left(h\nu - E_g\right) \quad (3)$$

Then plot $(F(R_\infty)\ h\nu)^{1/n}$ versus hv (**Fig. S2**) The linear portion of the plot is then extrapolated

to the horizontal axis, where the interception gives the bandgap energy (E_g). So, the band gap of Fe@f-gC_3N_4 is determined to be 2.63 eV.

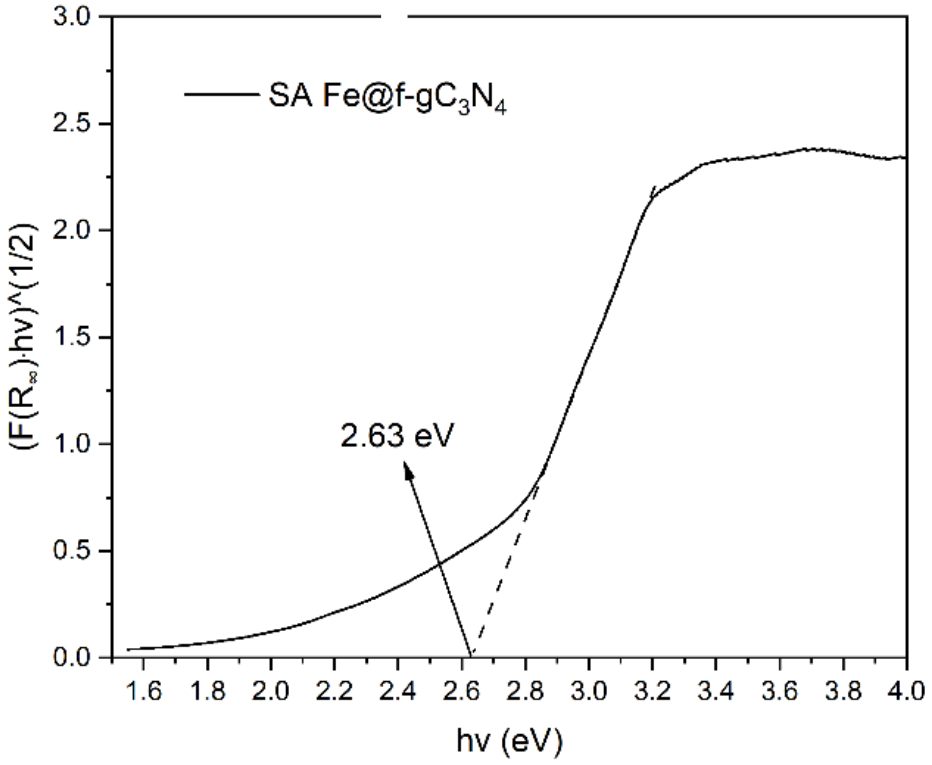

Fig. S2. Band gap of Fe@f-gC_3N_4 determined by Tauc plot

5.2 Mott-Schottky (MS) measurements

The Mott-Schottky experiments were performed in a three-electrode configuration cell, with obtained thin film electrode as the working electrode, Pt-foil electrode as the counter electrode, and silver chloride electrode (Ag (s)IAgCl (s)IKCl (aq) (3M)) as the reference electrode, respectively. Thin film electrodes were prepared by the drop-coating method, 12.5 mg of sample was added to the mixed solution of ethanol (50 μL) and Nafion solution (5 wt%, 10 μL) under sonication for 1h. Then 15 μL of the mixture was pipetted on the surface of a FTO glass to obtain 1 cm × 1 cm coating films, followed by drying at room temperature and further drying at 40 °C overnight in a vacuum oven. Additionally, the electrolyte solution was used as 0.5 M Na_2SO_4 (measured pH = 7.47) degassed by N_2. The measurements were conducted by using a Metrohm Autolab potentiostat-galvanostat PGSTAT204 workstation in the dark, at AC amplitude of 5 mV and frequency of 400Hz, 600Hz and 1000 Hz.

Then, to further clarify the electronic structure, electrochemical flat-band potential measurements were conducted. Typically, flat-band potential values are derived from the Mott-Schottky equation.

$$\frac{1}{C^2} = \frac{2}{\varepsilon\varepsilon_0 N_D}\left(E - E_{fb} - \frac{K_B T}{q}\right) \quad (4)$$

Here, C represents the space charge capacitance, N_D denotes the donor density, and ε, ε_0 are the dielectric constants of the film electrode and free space, respectively. E refers to the applied potential, E_{fb} is the flat-band potential, K_B is Boltzmann's constant, T is the temperature, and q is the electronic charge. The flat-band potential E_{fb} can be obtained by extrapolating the plot to

where $1/C^2 = 0$ (**Fig. S3**)

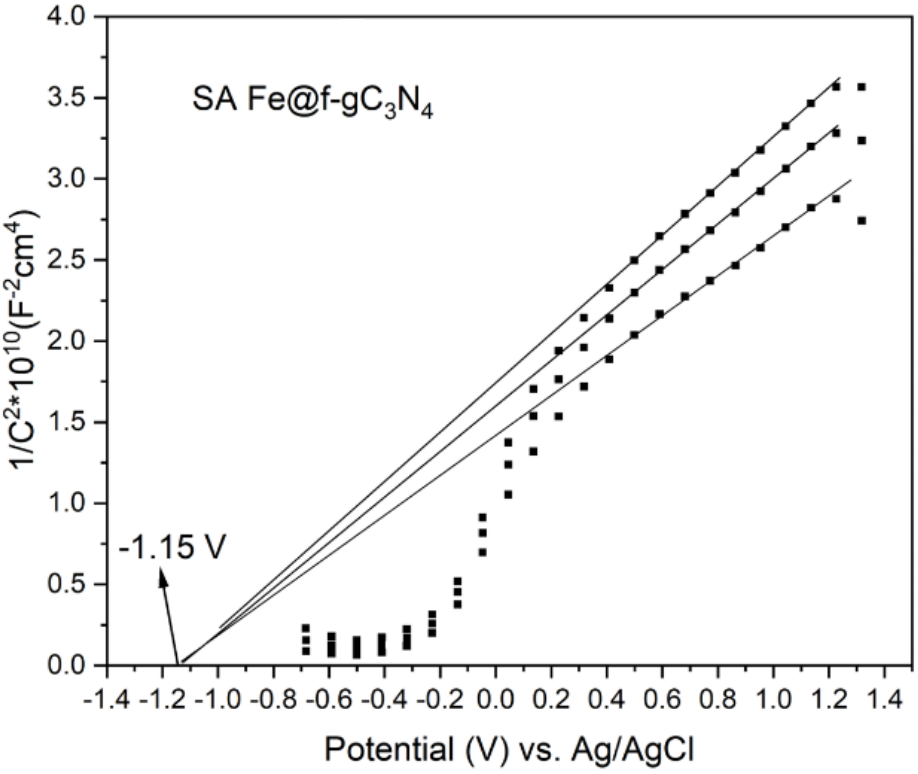

Fig. S3. Mott-Schottky plot of Fe@f-gC_3N_4

The positive slope of the Mott-Schottky curve suggested that the photocatalyst was *n*-type. Consequently, the flat band potential (E_{fb}) of Fe@f-gC_3N_4 was approximately -1.15 V (vs Ag (s)IAgCl (s)IKCl (aq) (3M)), as determined from the intersection between the Mott-Schottky plot and the baseline. In *n*-type semiconductor photocatalyst, the conduction band generally lies 0.1 to 0.2 eV above the flat-band potential, with this offset influenced by factors such as electron effective mass and carrier concentration. So, the conduction band of the Fe@f-gC_3N_4 can be calculated as -1.35 V (vs Ag (s)IAgCl (s)IKCl (aq) (3M)). Additionally, using the band gap energy E_g, the valence band (VB) can be determined by $E_{VB}=E_{CB}+E_g$. Therefore, the valence band (VB) of Fe@f-gC_3N_4 was at ca. +1.28 V (vs Ag/AgCl, 3M KCl). Convert to normal hydrogen electrode (NHE) reference electrode, E_{CB}=-1.15 V (vs NHE), E_{VB}=+1.48 V (vs NHE). Based on: $E_{SCE}=E_{NHE}-0.244V$, so E_{CB}=-1.39 V (vs SCE), E_{VB}=+1.24 V (vs SCE).

6. Experimental procedures

6.1 Setup for the C=C bond cleavage under CO_2 atmosphere

The reaction setup is depicted in **Fig. S4.** The reaction setup consists of a Kessil lamp (390 nm or 456 nm), cooling of the setup was performed by commercially available fans to keep the temperature around 30 °C. The light intensity was measured by Ophir StarLite power meter with 3A probe head. The light intensity of Kessil lamp (λ = 390 nm) was 0.17 W/cm^2 and Kessil lamp (λ = 456 nm) was 0.15 W/cm^2. The CO_2 was provided by a balloon (balloon diameter ~20 cm) filled with pure CO_2 gas (>99.9%) and the distance between lamp and reaction tube was 4~5 cm.

Fig. S4. Set up for the oxidative cleavage of alkenes

6.2 Investigations of the reaction conditions

A dry 15 mL Schlenk tube containing a stirring bar and a CO_2 balloon was equipped to its stopcock with 2 mm bore. The tube was charged with 5 mg of Fe@f-gC_3N_4 (0.064 mol% of Fe) and capped with a rubber plunger. Connected the tube and pump to do three vacuum-CO_2 cycles. After this, 0.2 mmol of *trans*-*β*-Methylstyrene (**1a**) and 2 mL solvent were added to the tube under CO_2 atmosphere, then the whole reaction tube was kept for 24 h under the irradiation of Kessil lamp (λ = 456 nm). After completing the reaction, 1,3,5-trimethoxybenzene as internal standard was added to the solution, the final reaction solution was filtered and concentrated under reduced pressure to produce the crude product. The product yield of **2a** was obtained by ^{1}H NMR analysis and the yield of acetic acid was quantified by gas chromatography with flame ionization detection (GC-Fid).

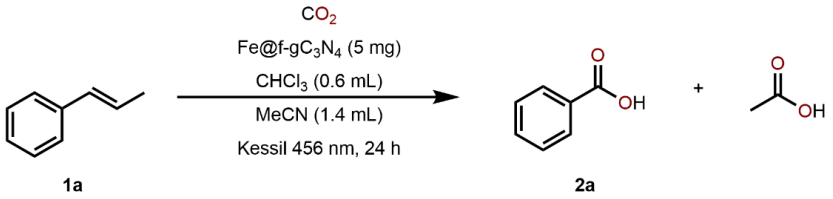

Table S2. Screening of reaction conditions, *: isolate yield

Reaction condition optimization					
Entry	**Solvent (0.1 M)**	**Light source**	**Additives (2.0 equiv.)**	**Catalyst (mg)**	**^{1}H NMR yield (%)**
1	DMA	456 nm	-	10	5
2	DMF	456 nm	-	10	5
3	DMSO	456 nm	-	10	5
4	MeCN	456 nm	-	10	15
5	MeCN	456 nm	CH_3OH	10	0
6	MeCN	456 nm	CH_3CH_2OH	10	0
7	MeCN	456 nm	CF_3CH_2OH	10	0
8	MeCN	456 nm	Et_3N	10	9
9	MeCN	456 nm	H_2O	10	13
10	1,4-Dioxane	456 nm	-	10	0
11	EtOH	456 nm	-	10	0
12	Toluene	456 nm	-	10	0
13	DCM	456 nm	-	10	30
14	$CHCl_3$	456 nm	-	10	59
15	DCE	456 nm	-	10	40
16	$CHCl_3$	456 nm	Et_3N	10	35
17	$CHCl_3$	456 nm	$(^iPr)_2NEt$	10	30
18	$CHCl_3$	456 nm	DABCO	10	0
19	$CHCl_3$	456 nm	CH_3COOH	10	43
20	$CHCl_3$	456 nm	CH_3OH	10	51
21	$CHCl_3$	456 nm	H_2O	10	54
22	$CHCl_3$	456 nm	K_2CO_3	10	17
23	$CHCl_3$	456 nm	K_2HPO_4	10	13
24	$CHCl_3$	456 nm	^{t}BuOK	10	13
25	$CHCl_3$: MeCN 1.0 : 1.0	456 nm	-	10	69
26	$CHCl_3$: MeCN 1.5 : 0.5	456 nm	-	10	57
27	$CHCl_3$: MeCN 0.8 : 1.2	456 nm	-	10	73
28	$CHCl_3$: MeCN 0.6 : 1.4	456 nm	-	10	78
29	$CHCl_3$: MeCN 0.4 : 1.6	456 nm	-	10	51
30	$CHCl_3$: MeCN 0.6 : 1.4	456 nm	-	5	82 (*76)
31	$CHCl_3$: MeCN 0.6 : 1.4	427 nm	-	5	30
32	$CHCl_3$: MeCN 0.6 : 1.4	Blue LED	-	5	13
Control experiments					

	Photocatalyst	Light	Atomsphere	^{1}H NMR yield (%)
33	gC_3N_4	456 nm	CO_2	26
34	f-gC_3N_4	456 nm	CO_2	17
35	Fe@gC_3N_4	456 nm	CO_2	38
36	-	456 nm	CO_2	0
37	Fe@f-gC_3N_4	456 nm	Ar	0
38	Fe@f-gC_3N_4	dark	CO_2	0

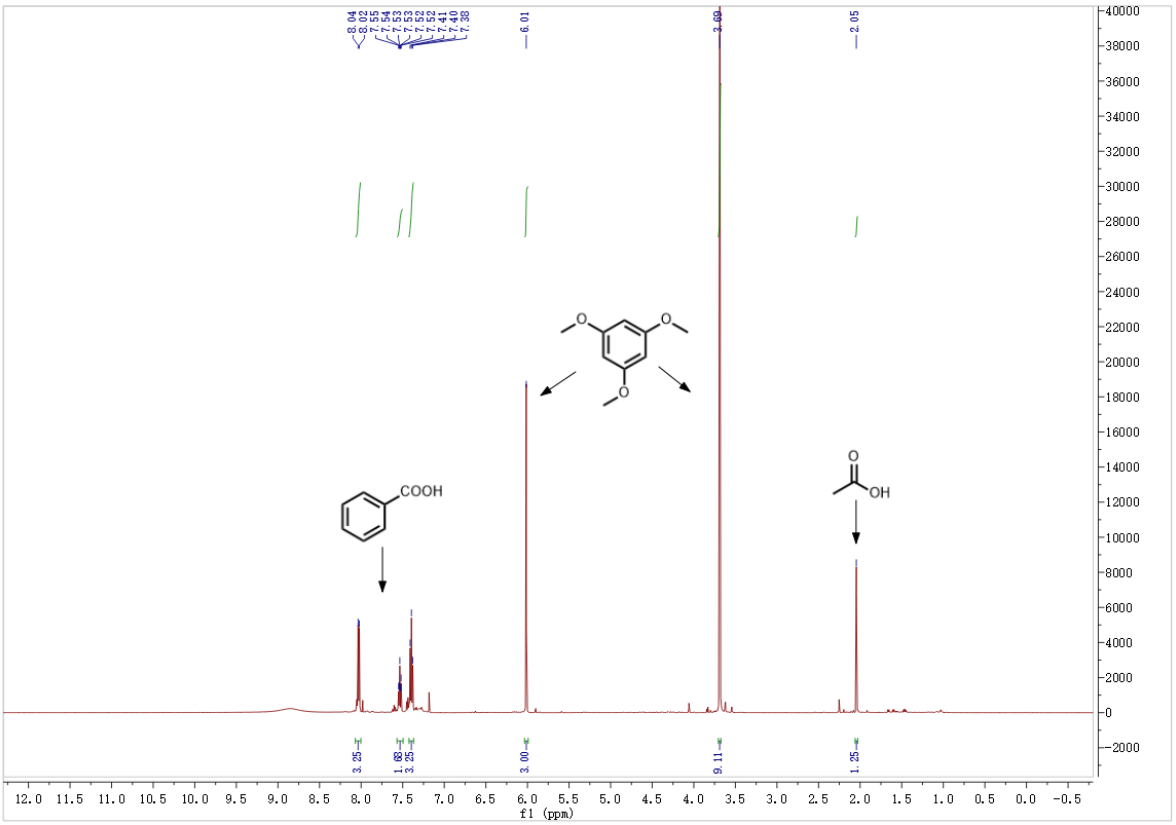

Fig. S5. Crude ^{1}HNMR spectra of standard reaction under optimal conditions (**Entry 30** in **Table S1**), with internal standard 17 mg

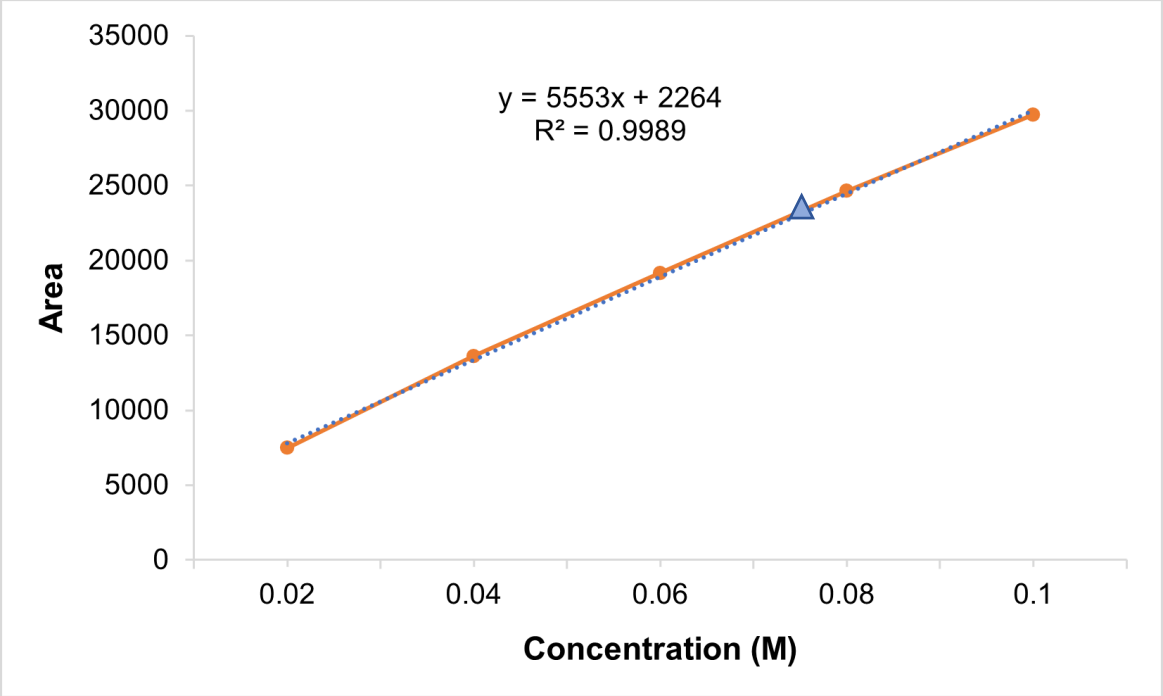

Fig. S6. Calibration curve of acetic acid in GC-FID

6.3 Correlation of activity to the band gap of various modified materials

We conducted control experiments using gC_3N_4, f-gC_3N_4, Fe@gC_3N_4, and Fe@f-gC_3N_4 under identical reaction conditions. The yields are summarized in **Table S2.** To investigate the correlation between catalytic activity and band structure of various modified materials, we measured the optical band gaps and band edge positions, as shown in **Fig. S7**. The results indicate that Fe@f-g-C_3N_4 and Fe@g-C_3N_4 possess higher valence band potentials (+1.24 V and +1.26 V vs. SCE, respectively), enabling efficient oxidation of $CHCl_3$ to initiate the reaction. However, Fe@f-g-C_3N_4 also exhibits a more negative conduction band potential (–1.39 V vs. SCE), which is more favorable for CO_2 reduction compared to the other materials. This dual advantage in both oxidative and reductive potentials makes Fe@f-g-C_3N_4 the most efficient photocatalyst among those tested, correlating well with its superior catalytic performance.

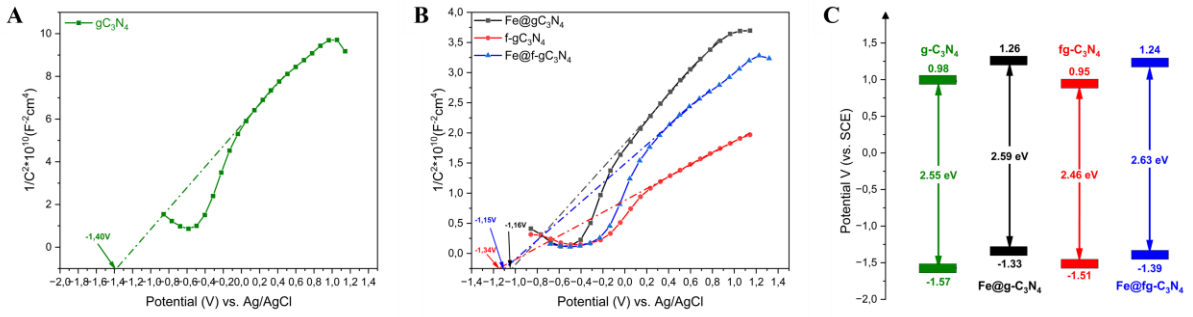

Fig. S7. (**A**) Mott–Schottky plots of bulk gC_3N_4; (**B**) Mott–Schottky plots of variants revealing their flat-band potential value collected at 1 kHz frequency; (**C**) Electronic band positions of the g-C_3N_4 and variants

6.4 Photocatalyst recycling experiments

To evaluate the stability of the Fe@f-gC_3N_4 catalyst, a recyclability test was performed using the model reaction in a 5 mmol scale. The recycled catalyst was employed for at least 10 consecutive runs under optimal conditions. For catalyst recovery, the solvent was removed under reduced pressure post-reaction. The residue was then treated with excess *n*-hexane, sonicated for 2 minutes, and centrifuged to collect the catalyst as a light-yellow precipitate. This washing procedure was sequentially repeated using MeOH and water, each followed by sonication and centrifugation. Finally, the recovered catalyst was dried at 120 °C before reused. The results indicated that the good stability of Fe@f-gC_3N_4. And the collected catalyst was later subjected to various characterization techniques to indicate its structural stability (Section **8**).

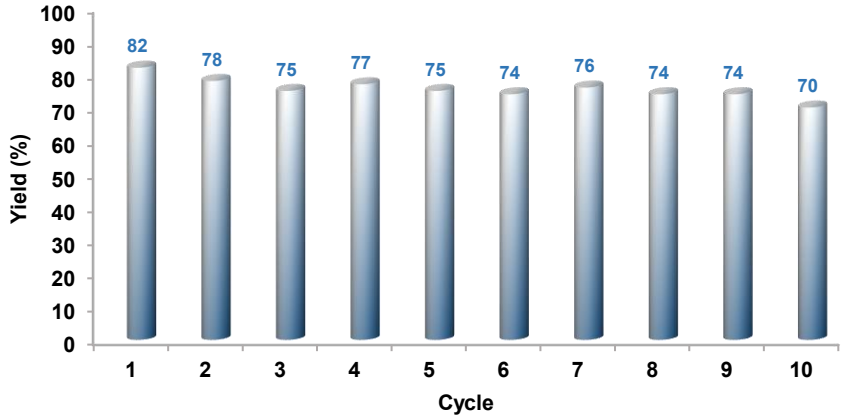

Fig. S8. Recycling experiments

6.5 Sheldon's hot filtration test

The Sheldon's hot filtration test was carried out to assure heterogeneous nature of the photocatalyst (Fe@f-gC_3N_4). The oxidation of *trans-β*-Methylstyrene (**1a**) was continued over the photocatalyst under optimized conditions for 3 h and then the reaction mixture was divided into two-halves. From one portion of the reaction mixture, the photocatalyst was removed by a 0.45 um filter and both parts of the reaction were further continued for another 21 h. On ^{1}H NMR analysis, it was revealed that no significant progress in reaction was achieved without the photocatalyst while the other portion led to 100% conversion of the starting material. The result is shown in **Fig. S9** and this further suggests the heterogeneity of this process.

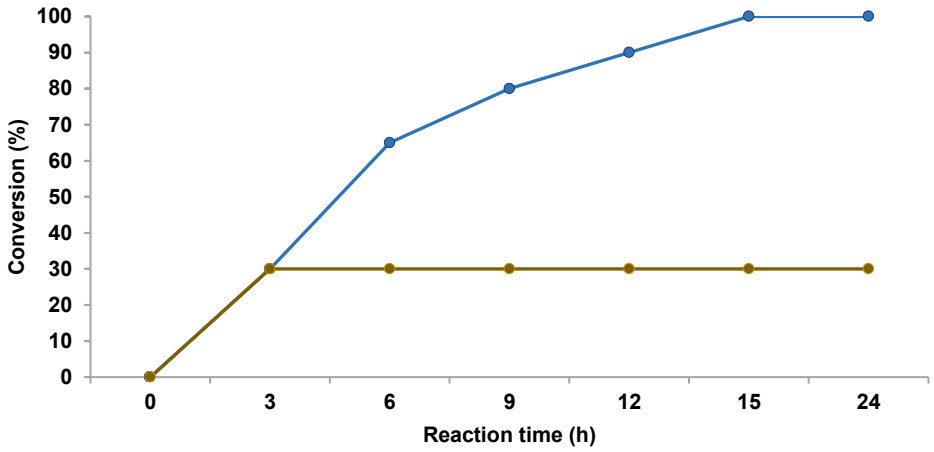

Fig. S9. Sheldon's hot filtration test

6.6 Scale-up experiments in continuous flow

A continuous flow cell setup was investigated using a UV-150 photochemical reactor (Vapourtec Ltd.). The system was configured for continuous flow operation with a Pyrex glass microreactor channel. And 10 mmol substrate, 250 mg (0.064 mol% Fe) of finely ground catalyst was packed into the reactor bed (catalyst bed length: 6 cm), along with 20 small glass beads (4 mm diameter) to ensure uniform catalyst distribution. To prevent catalyst leaching, a small piece of cotton and a silica pad were placed at both ends of the reactor bed. The flow rates of the reactant solution and CO_2 were set to 0.1 mL min^{-1} and 5 mL min^{-1}, respectively. Illumination was provided by a PR160L Kessil LED lamp (λ = 390 nm). The reaction was performed in a continuous circulation mode, in which the product mixture from one cycle was recycled and used as the reactant for the next cycle.

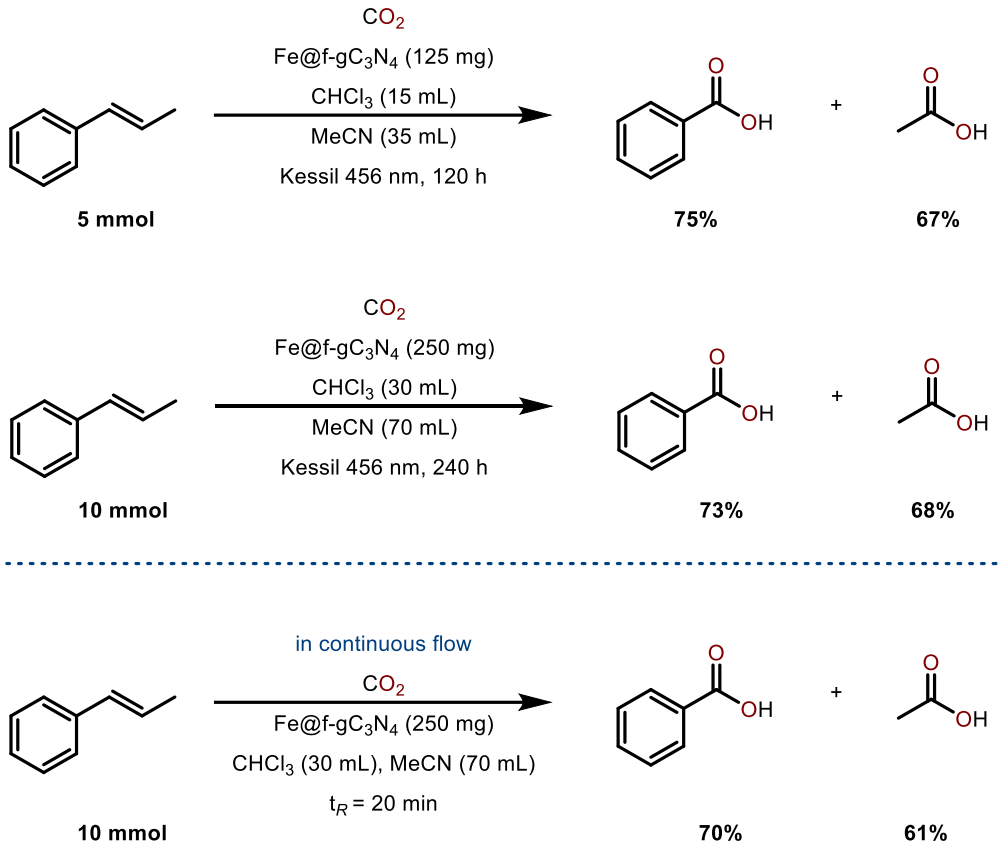

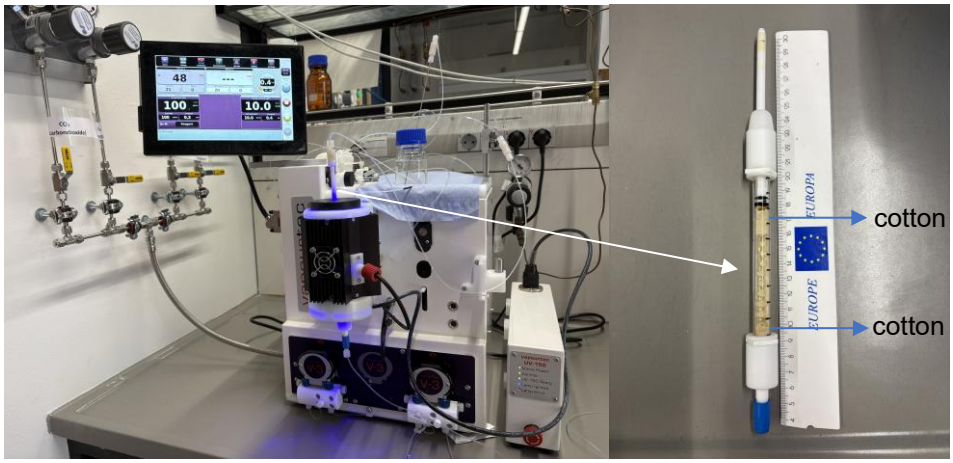

Fig. S10. Large-scale experiment in continuous flow

6.7 Long-term photostability test

The stability of the photocatalyst was further evaluated through a long-term reaction which was conducted continuously for >21 days without isolating the photocatalyst from the reaction system in flow. Gratifyingly, a steady accumulation of the product was observed throughout the reaction time, indicating sustained photocatalytic activity and excellent operational stability. To further validate the robustness of the catalyst, it was recovered after 21-days and subjected to a fresh reaction with substrate **1a**. The product, benzoic acid, was obtained in 80% yield.

6.8 Starting material preparation procedures

The starting material **1a-1p**, **1r-1t**, **1v**, **1w**, **1z**, **1aa**, **1ai-1am**, **1aw** were commercially available.

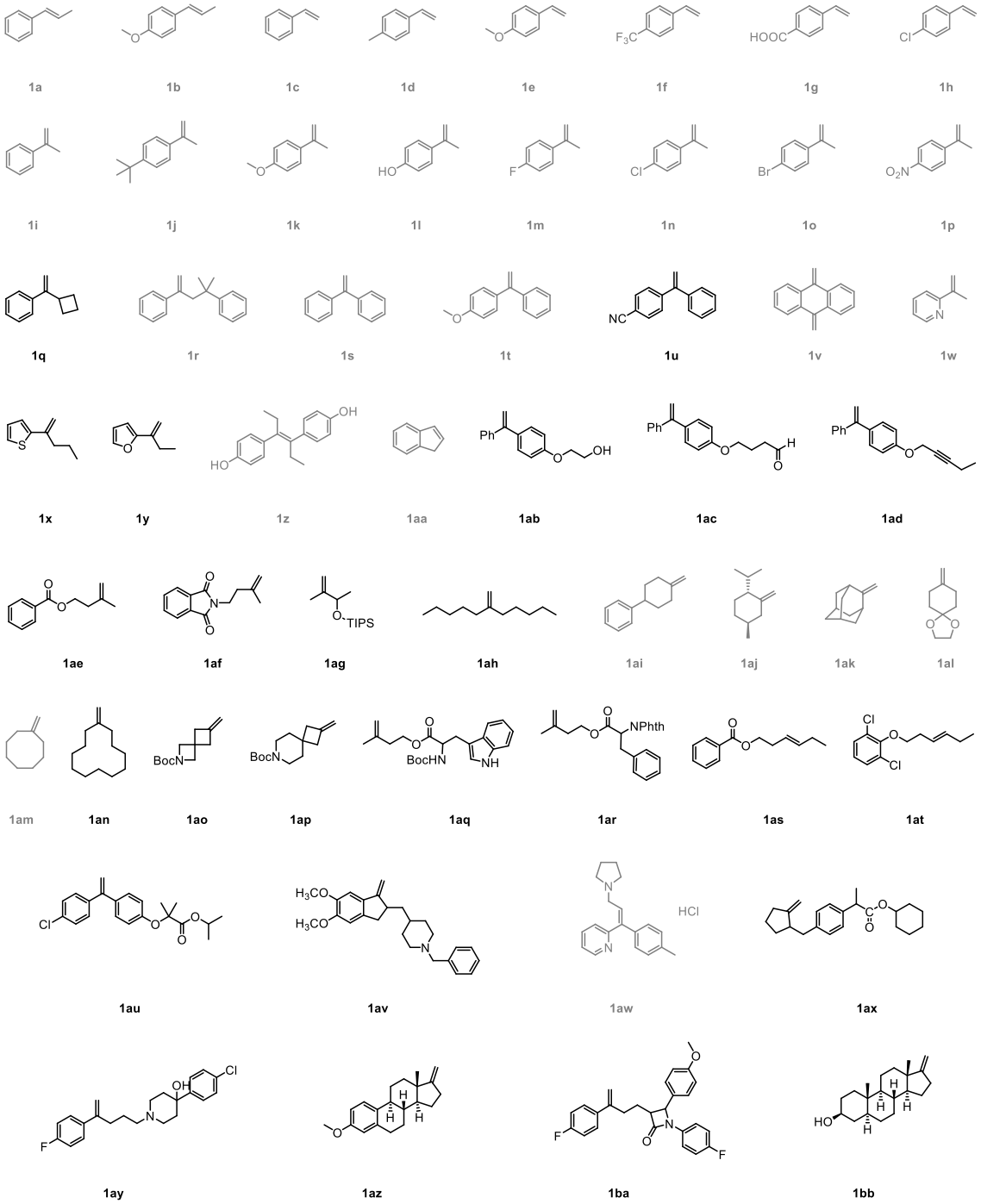

Fig. S11. Starting material scope

GP-1. 1u was prepared according to the following procedure (*59*)

$Pd(PPh_3)_4$ (0.03 equiv.) and arylboronic acids (1.2 equiv.) were added to an Schlenk tube. The tube was then evacuated and filled with argon. Acetic acid (0.15 equiv.), phenylacetylene (1.0 equiv.), and 1,4-dioxane (1 M) were added under argon flow. The mixture was stirred at 80 °C for 12 h and then cooled to room temperature. Et_2O and water were added to the tube, reaction mixture was extracted with Et_2O, then concentrated. The obtained crude sample was purified by flash chromatography.

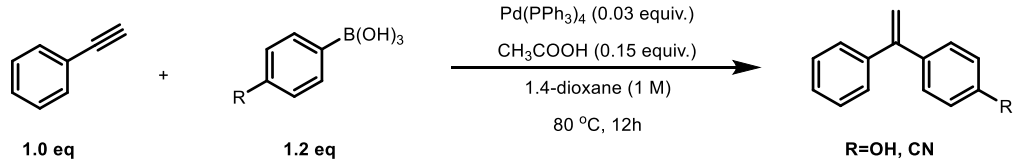

GP-2. **1q**, **1x**, **1y**, **1ah**, **1an, 1av, 1ax, 1az, 1bb** were prepared according to the following procedure (*60*)

A 50 mL Schlenk flask equipped with a stirring bar was charged with methyltriphenylphosphonium bromide (1.5 equiv.) in dry THF, NaH (1.5 equiv.) was added under argon at 0 ºC and stirred for 30 min. Then the corresponding ketone (1.0 equiv.) dissolved in THF was added drop wise and stirred overnight. The reaction was quenched by water in ice bath. Extracted the mixture with ethyl acetate. The organic phase dried over anhydrous Na_2SO_4 and concentrated in vacuo. The residue was purified by flash chromatography to afford pure alkene.

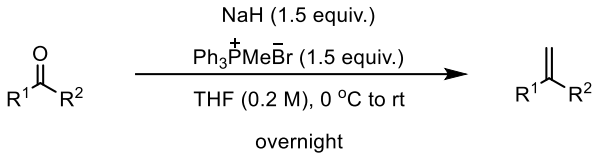

GP-3. **1ab-1ad, 1at** were prepared according to the following procedure

4-(1-phenylvinyl)phenol was prepared according to the GP 1.
When R was an ethanol group. To a solution of PPh_3 (1.1 eq), 4-(1-phenylvinyl)phenol (1.0 eq), and 2-(tert-butyldimethylsilyloxy)-ethanol (1.1 eq) in THF (0.5 M) was added DEAD (1.0 eq) in THF (5 mL) at 0 °C, and then the cooling bath was removed. The mixture was stirred at rt for 24h, and then H_2O was added. The mixture was extracted with Et_2O. The combined ether layers were washed with 3% H_2O_2, 1 N NaOH, and brine, and were dried over Na_2SO_4. The residue was dissolved in THF. H_2O and AcOH were added at 0 °C, the mixture was stirred for 6 h at room temperature, then it was slowly poured into a solution of Na_2CO_3 to make the pH about 8, and the mixture was extracted with EtOAc. The combined organic layers were dried over Na_2SO_4 and concentrated. The residue was purified by flash chromatography to give the pure compound **1ab**.

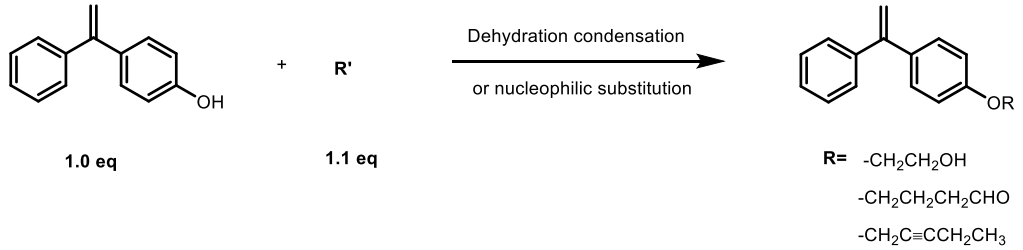

When R was a butyraldehyde group, 4-(4-(1-phenylvinyl)phenoxy)butan-1-ol was prepared according to the above method. Then 4-(4-(1-phenylvinyl)phenoxy)butan-1-ol (1.0 equiv.) was dissolved in CH_2Cl_2 (0.15 M). Dess-Martin periodinane (1.0 equiv.) was added and the reaction

was stirred for 16 h at room temperature. The reaction mixture was filtered and the solvent removed under reduced pressure. The residue was purified by flash chromatography to give the pure compound **1ac**.

When R was a pent-2-yne group. A mixture of 4-(1-phenylvinyl)phenol (1.0 eqiv.), K_2CO_3 (1.1 eqiv.) and the 1-bromopent-2-yne (1.1 equiv.) in acetone (0.1 M) was refluxed for 18–26 h (monitored by TLC). The mixture was hot filtered and evaporated to obtain a residue that was purified by flash chromatography to give the product **1ad**. Starting material **1at** was prepared using the same procedure from the corresponding 2,6-dichlorophenol and (*E*)-1-bromohex-3-ene.

GP-4. **1af** was prepared according to the following procedure (*61*)

A solution of azodicarboxylic acid diisopropyl ester (1.0 equiv.) in dry THF (0.5 M) was added dropwise to a solution of 3-methylbut-3-en-1-ol (1.0 equiv.), phthalimide (1.2 equiv.) and triphenylphosphine (1.1 equiv.) in dry THF (0.2 M) under Ar atmosphere at room temperature. The reaction mixture was stirred for 24 h, then concentrated under reduced pressure. The resulting residue was purified by flash chromatography to afford **1af**.

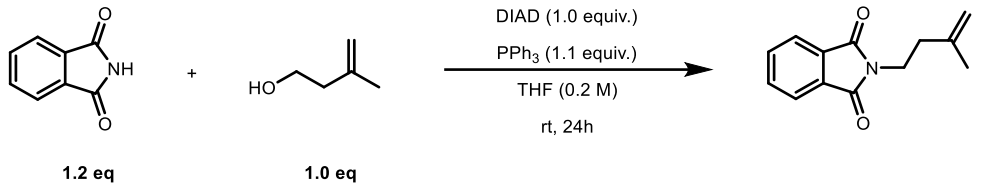

GP-5. **1ag** was prepared according to the following procedure (*62*)

To a solution of 3-methylbut-3-en-2-ol (1.0 equiv.) in DCM (0.1 M) were added imidazole (1.5 equiv.) and triisopropylsilyl chloride (1.2 equiv.). The reaction mixture was stirred at room temperature for 24 h. Water was then added, and the layers were separated. The aqueous phase was extracted with DCM, and the combined organic layers were washed with brine, dried over Na_2SO_4, filtered, and concentrated under reduced pressure. The resulting residue was purified by flash column chromatography to afford compound **1ag**.

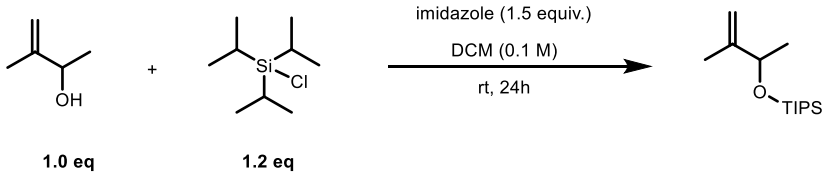

GP-6. **1ae, 1aq-1as** was prepared according to the following procedure (*63*)

To a solution of corresponding alchol (1.0 equiv.), dicyclohexylcarbodiimide (1.0 equiv.), 4-(dimethylamino)pyridine (0.1 equiv.) in DCM (0.5 M) were added carboxylic acid (1.2 equiv.). The reaction mixture was stirred at room temperature for overnight. The reaction mixture was then filtered and concentrated. The resulting residue was purified by flash column chromatography to afford compounds **1ae,** and **1aq-1as.**

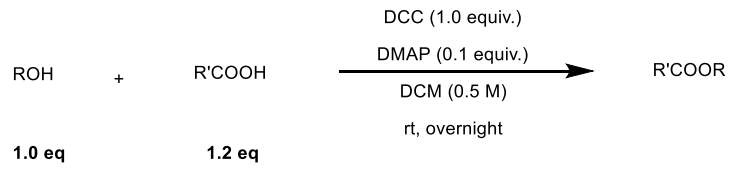

GP-7. **1au** was prepared according to the following procedure (*64*)

1-(4-chlorphenyl)-1-(4'-hydroxyphenyl)ethen was prepared according to the GP 1. Then KOH (1.0 equiv.) was added to a solution of 1-(4-chlorphenyl)-1-(4'-hydroxyphenyl)ethen (1.0 equiv.) in EtOH (0.5 M) at 0 °C. After 30 min, isopropyl 2-bromo-2-methylpropanoate (1.1 equiv.) was added and the mixture was refluxed for 16 h. After solvent evaporation the product was subjected to flash chromatograph to get the pure product.

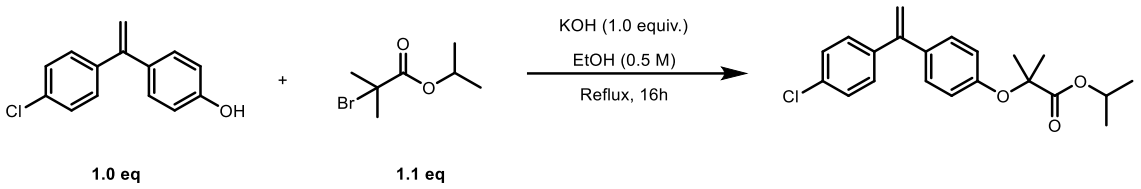

GP-8. **1ay** was prepared according to the following procedure (*65*)

1-(5-Chloropent-1-en-2-yl)-4-fluorobenzene was prepared according to GP-2. A mixture of 1-(5-chloropent-1-en-2-yl)-4-fluorobenzene (1.0 equiv.), piperidin-4-one (1.2 equiv.), KI (0.02 equiv.), and Na_2CO_3 (0.02 equiv.) in toluene (0.16 M) was heated at reflux for 72 h. After cooling to room temperature, the reaction mixture was filtered, washed with aqueous $NaHCO_3$, dried over anhydrous Na_2SO_4, filtered, and concentrated under reduced pressure. The crude product was purified by flash column chromatography to afford compound **3**. Compound **3** was then dissolved in THF (1.0 M) under an argon atmosphere and cooled in an ice bath. 4-Chlorophenylmagnesium bromide (1.2 equiv.) was added dropwise, and the reaction mixture was stirred overnight. The reaction was quenched with water and extracted with EtOAc. The combined organic layers were dried over Na_2SO_4, filtered, and concentrated under reduced pressure. Purification by flash column chromatography afforded compound **1ay**.

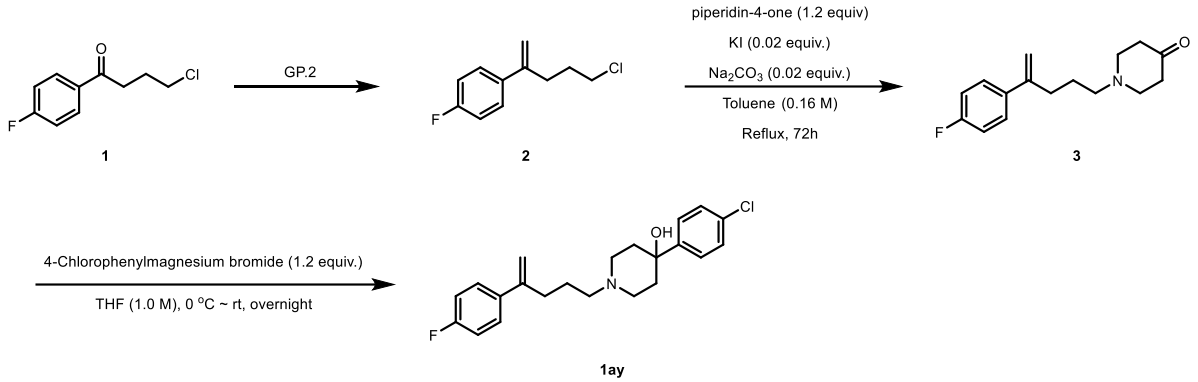

GP-9. **1ba** was prepared according to the following procedure (*66*)

Compound **1** (ezetimibe, 1.0 equiv.) was dissolved in dry DMF (1.0 M) under an argon atmosphere and cooled to 0 °C. K_2CO_3 (1.1 equiv.) was added portionwise, and the mixture was stirred at room temperature for 30 min. Methyl iodide (2.0 equiv.) was then added, and stirring was continued at room temperature for an additional 30 min. Water was added to quench the reaction, and the mixture was extracted with Et_2O. The organic phase was combined and dried over Na_2SO_4, filtered, and concentrated under reduced pressure to afford compound **2**. Then, methyltriphenylphosphonium chloride (1.0 mmol) and NaH (2.0 equiv.) were placed in a Schlenk tube, followed by addition of THF (0.7 M) and compound **2**. The reaction mixture was stirred at 40 °C under an air atmosphere (1 atm, balloon) and monitored by TLC. After completion, the reaction was quenched with water and extracted with EtOAc. The combined organic layers were concentrated under reduced pressure, and the residue was purified by flash column chromatography to afford compound **1ba**.

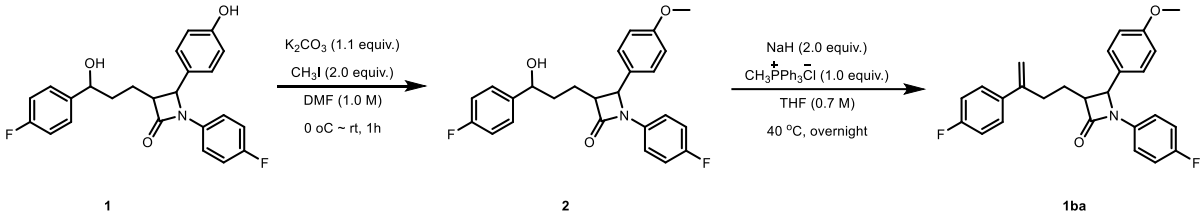

7. Mechanistic studies

7.1 Monitoring the reaction progress

To gain deeper insight into the reaction kinetics, time-course experiments were conducted. The yield evolution of both reaction intermediates and final products was monitored over time, as illustrated in **Fig. S12** and **Fig. S13**.

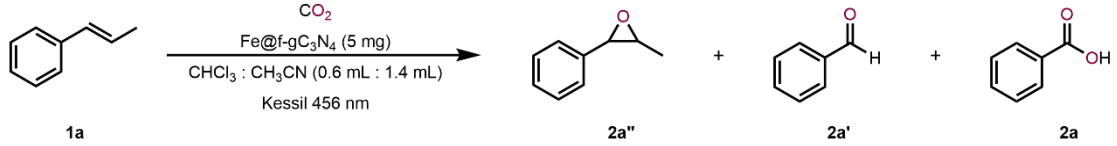

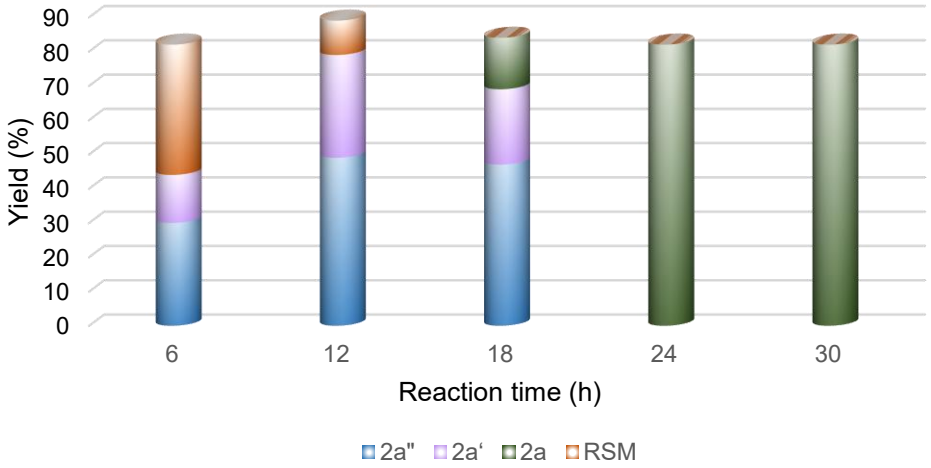

Fig. S12. Time course experiments. RSM: remaining of starting material

The epoxide **2a″** is obtained in 49% yield with in 12 h. When the reaction was conducted at a lower temperature (0 °C), the yield of epoxide **2a″** decreased to 15% (**Entry 2**). Actually, the epoxide formation requires a fine balance between reaction conditions and catalyst reactivity (**Entries 4–9**). In particular, we found that modulation of the metal center plays a decisive role. For example, when Au@f-g-C_3N_4 was employed as the catalyst, the epoxide yield increased to 68%. These results indicate that selective epoxidation is governed less by temperature and more by the nature of the metal–oxygen intermediate. It should be noted here that while Au-based system favor epoxide retention, the present study deliberately focuses on Fe to establish CO_2-to-oxygen transfer using an earth-abundant metal.

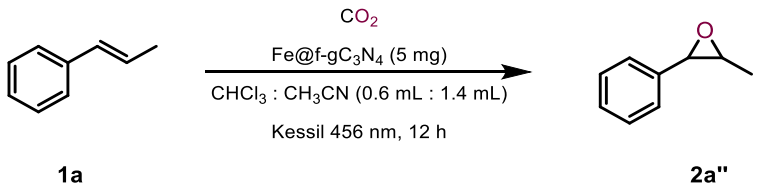

Table. S3 Reaction condition screening for the formation of epoxide

Entry	Variations from the standard condition	Yield of 2a″
1	nono	49%
2	Under 0 ℃	15%
3	Blue LED	7%
4	Co@f-gC_3N_4, 24h	44%
5	Mn@f-gC_3N_4, 24h	39%
6	Cu@f-gC_3N_4, 24h	36%
7	Zn@f-gC_3N_4, 24h	35%
8	Ir@f-gC_3N_4, 24h	41%
9	Au@f-gC_3N_4, 24h	68%

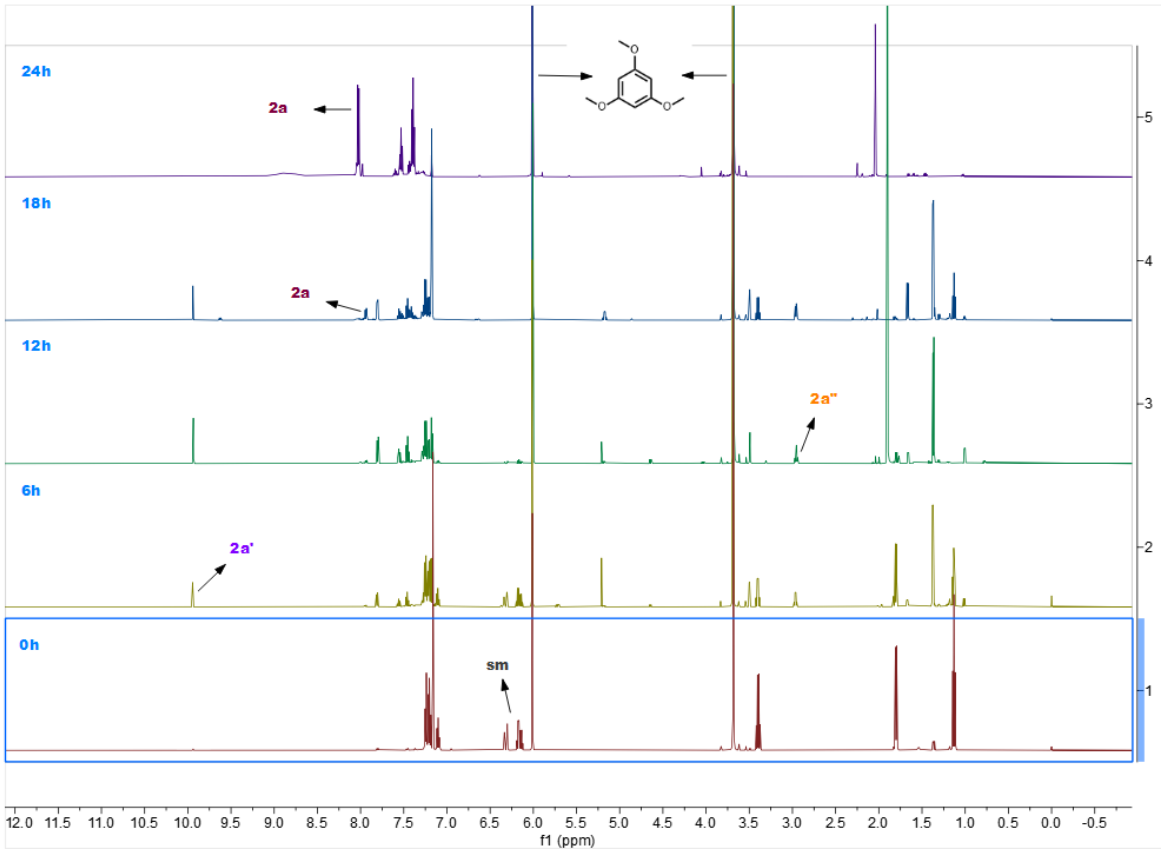

Fig. S13. Crude ^{1}H NMR spectra of time course experiments

7.2 $C^{18}O_2$-labeling experiment

To verify the origin of the oxygen in intermediates and benzoic acid, ^{18}O-labeled CO_2 experiments were conducted. When the reaction was performed with 97 % pure $C^{18}O_2$, all statistically possible ^{18}O labelled intermediates and product were observed by High Resolution Mass Spectrometry (HR-MS). The result was consistent with the proposed mechanism, in which the oxygen atom in epoxide, benzaldehyde and benzoic acid arises from the CO_2 molecule.

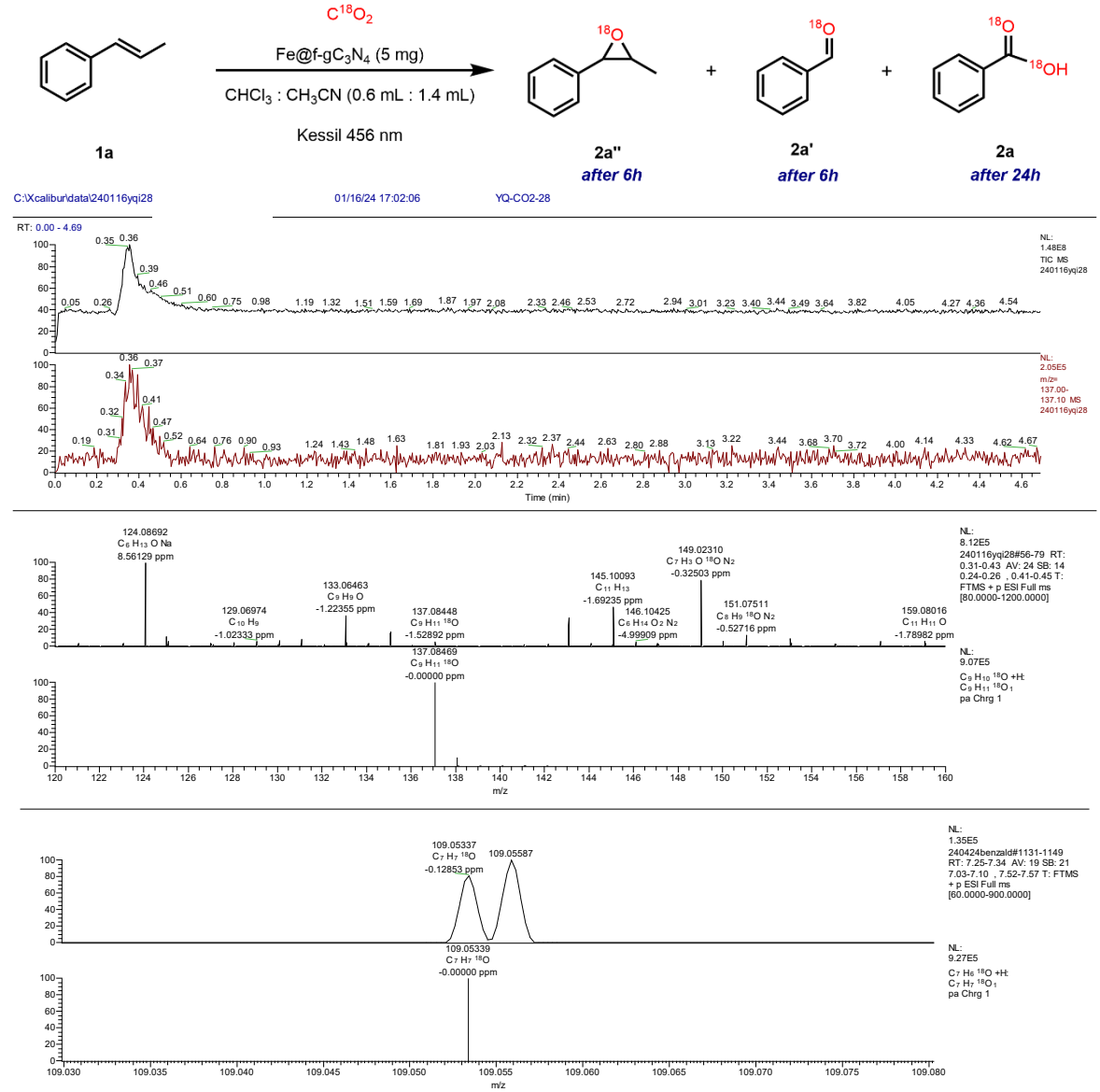

Fig. S14. HR-MS spectra of reaction solution after 6h

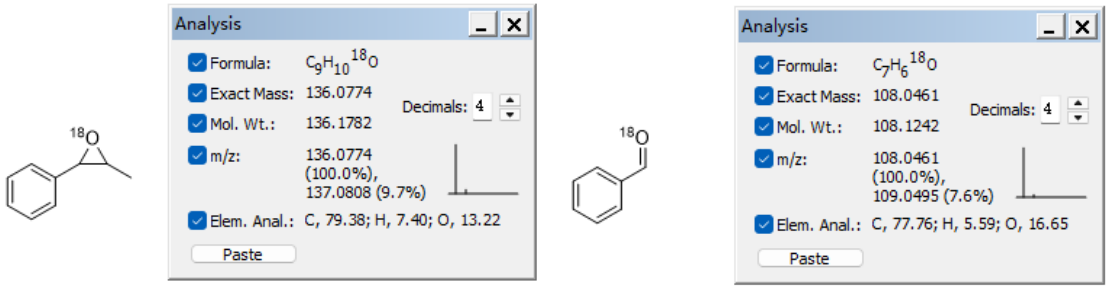

Fig. S15. MS of 2a″ and 2a'

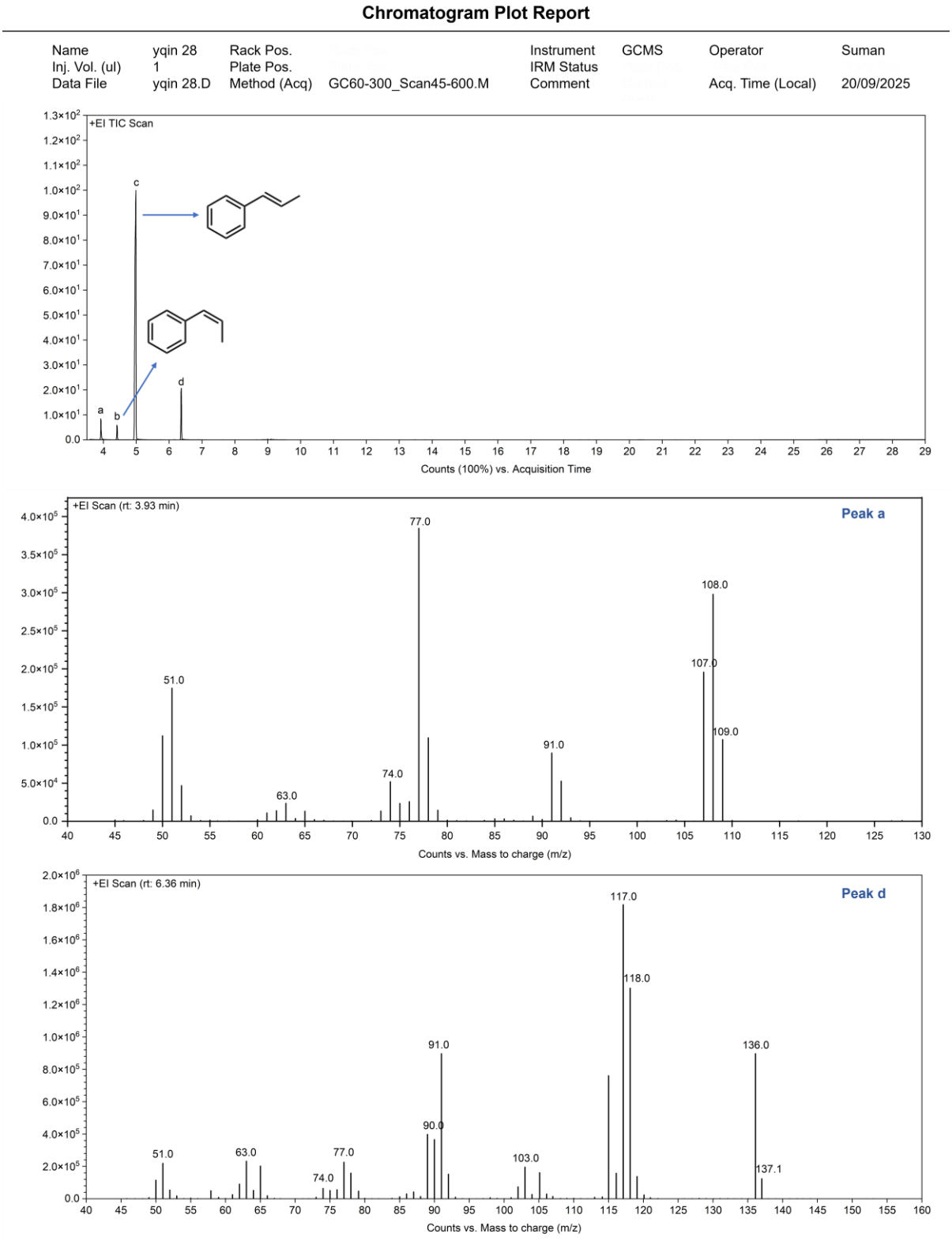

Fig. S16. GC-MS spectra of reaction solution after 6h

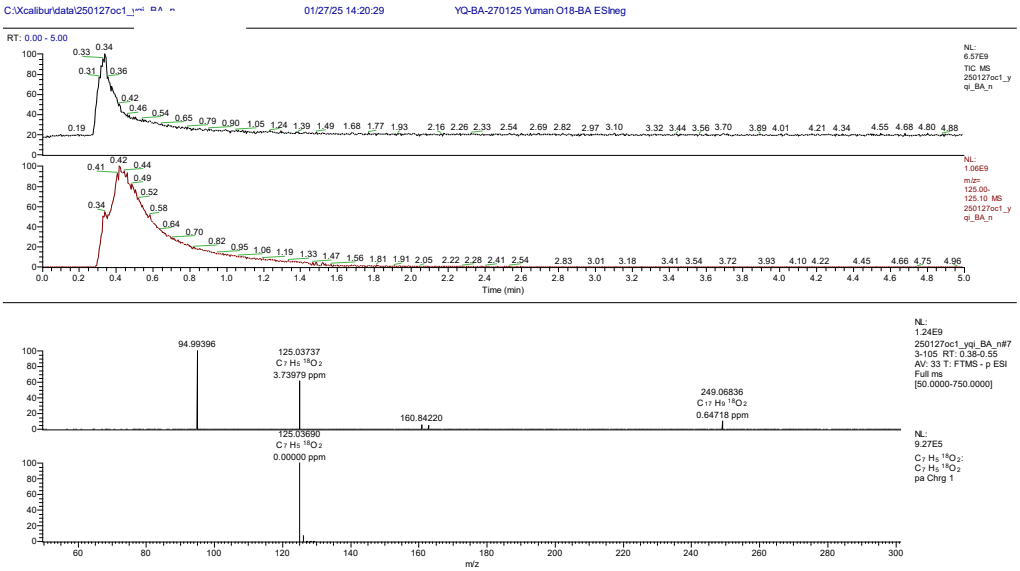

Fig. S17. HR-MS spectra of reaction solution after 24h

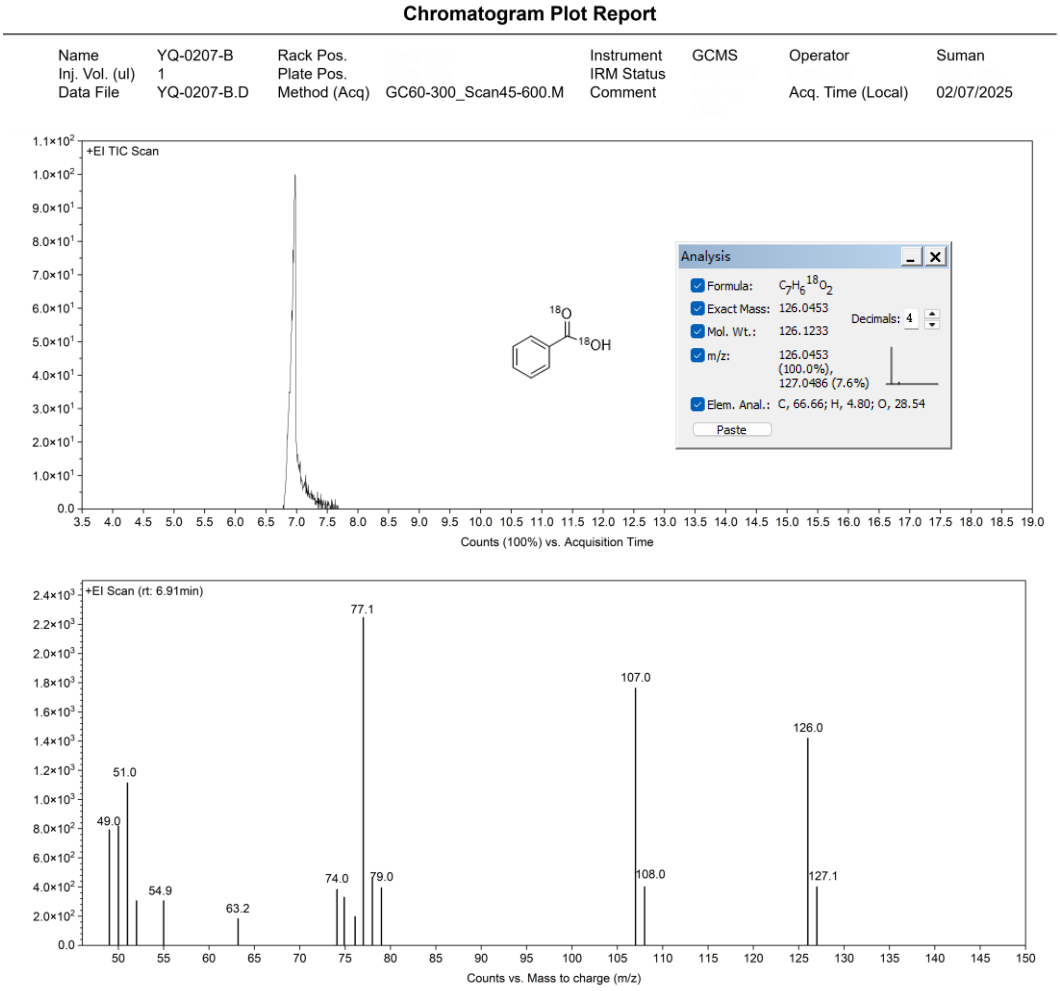

Fig. S18. GC-MS spectra of $C^{18}O_2$ labelling experiment

7.3 Investigation of gas products from CO_2

Upon completion of the model reaction, a 10 mL glass syringe was used to collect a gas sample, which was subsequently analyzed by head-space gas chromatography (GC), confirming the formation of CO and methane.

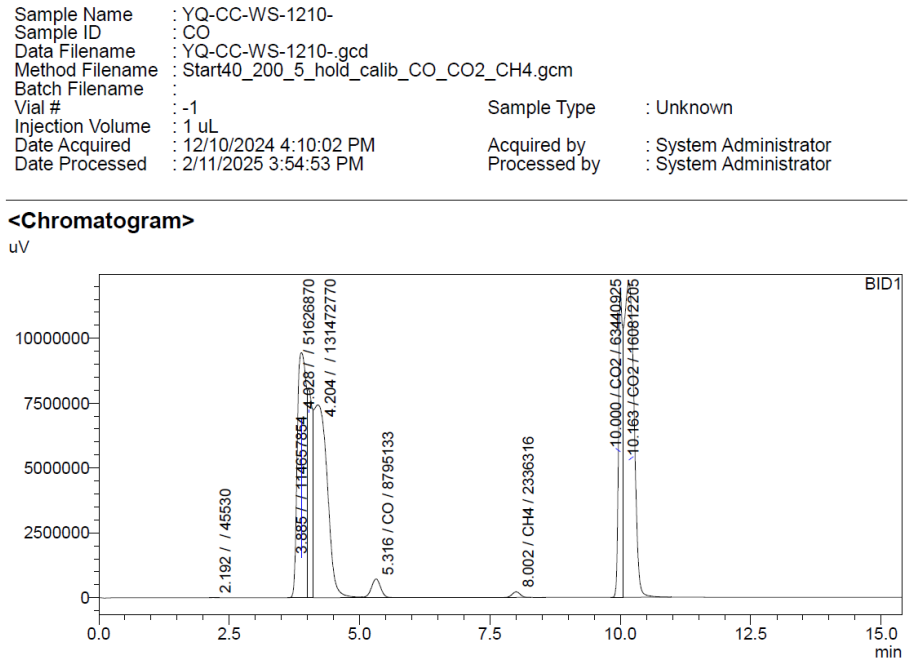

Fig. S19. Result of head-space GC after reaction

7.4 Quenching experiments

In a dry 15 mL Schlenk tube equipped with a 2 mm bore stopcock, a magnetic stirring bar was added along with a balloon filled with CO_2. The tube was charged with 5 mg of Fe@f-gC_3N_4 and the radical quencher (1.0 equiv.) before being sealed with a rubber septum. The setup underwent three vacuum-CO_2 cycles to ensure a CO_2 atmosphere. Subsequently, *trans-β*-methylstyrene (0.2 mmol), 0.6 mL $CHCl_3$ and 1.4 mL of MeCN were introduced under a CO_2 atmosphere. The reaction mixture was irradiated using a Kessil lamp (456 nm) for 24 h. Upon completion, 1,3,5-trimethoxybenzene was added as an internal standard. The reaction mixture was then filtered, and the solvent was removed under reduced pressure to yield the crude product. The yield of product **2a** was quantified by ^{1}H NMR analysis. The results are summarized in **Table S4**. When radical scavengers such as 2,2,6,6-tetramethyl-1-piperidinyloxyl (TEMPO) or 2,6-di-tert-butyl-4-methylphenol (BHT) were employed, the formation of 2a was significantly inhibited, indicating the involvement of radical intermediates. Moreover, no product was observed when $CuCl_2$ was used as a quencher, strongly suggesting a single-electron transfer (SET) pathway is involved in the reaction mechanism.

Table S4. Results of quenching experiments

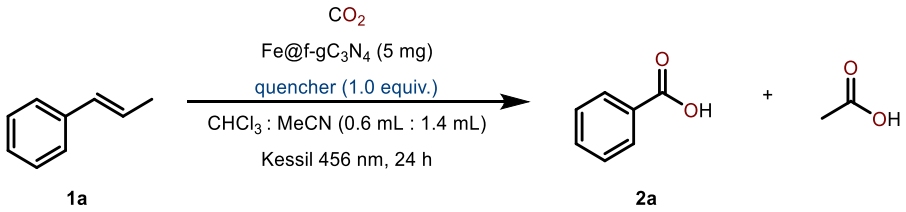

Entry	Quencher	Equiv.	Yield (%)	Conclusion
1	TEMPO	1.0	0	Radical
2	BHT	1.0	0	Radical
3	$CuCl_2$	1.0	0	SET

7.5 Radicals capture experiments

In a 15 mL Schlenk tube equipped with a 2 mm bore stopcock, a magnetic stirring bar was added along with a balloon filled with CO_2. The tube was charged with 5 mg of Fe@f-gC_3N_4 and the TEMPO (1.0 equiv.) before being sealed with a rubber septum. The setup underwent three vacuum-CO_2 cycles to ensure a CO_2 atmosphere. Subsequently, *trans*-*β*-methylstyrene (0.2 mmol), 0.6 mL $CHCl_3$ and 1.4 mL of MeCN were introduced under a CO_2 atmosphere. The reaction mixture was irradiated using a Kessil lamp (456 nm) for 24 h. Upon completion, the reaction mixture was filtered and quickly submitted to HR-MS measurement to identify the possible radical adducts. The results are summarized in **Fig. S20**. Under the optimized reaction conditions, no **2a** and acetic acid formed, radical adducts A and B were detected (**Fig. S21**).

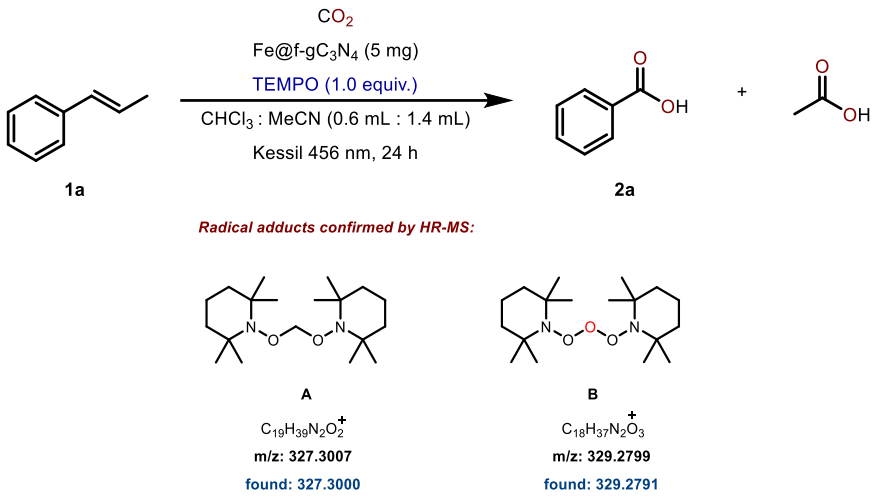

Fig. S20. Result of radical capture experiments

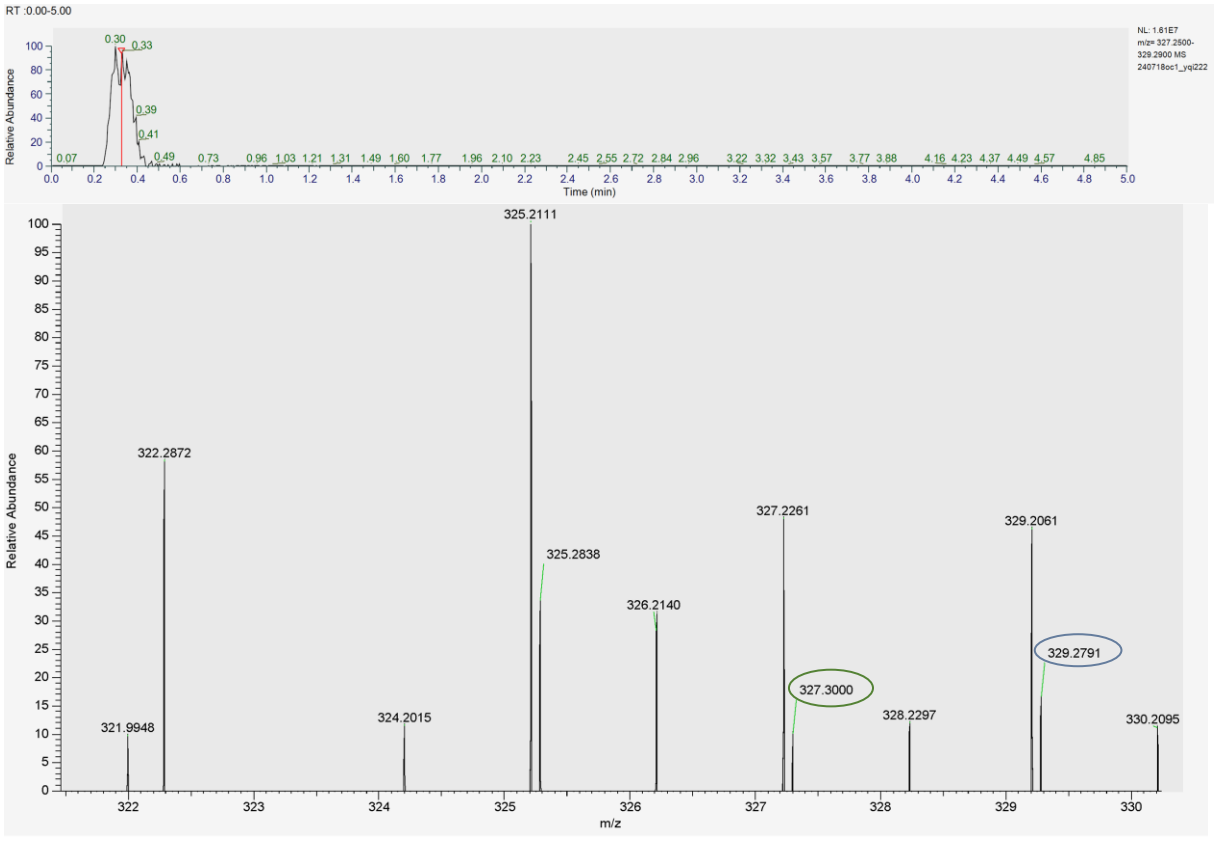

Fig. S21. HR-MS spectra of reaction with TEMPO

7.6 Investigation of the compounds originated from $CHCl_3$

To investigate the behavior of $CHCl_3$ in this reaction, a series of experiments were conducted under the conditions described in **Table S5**. The reaction solution was analyzed using Gas Chromatography-Mass Spectrometry (GC-MS), and the results confirmed the formation of Cl_3CCCl_3 from $CHCl_3$.

Table S5. Detection of compound from $CHCl_3$

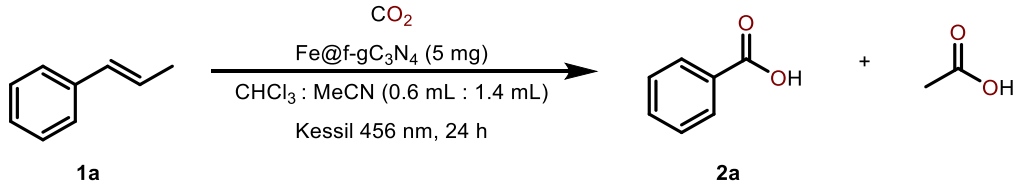

1a **2a**

Entry	Variations from standard conditions	Results
1	none	Cl_3CCCl_3
2	Without 1a	Cl_3CCCl_3
3	Using $CHCl_3$ (2 mL) as solvent	Cl_3CCCl_3

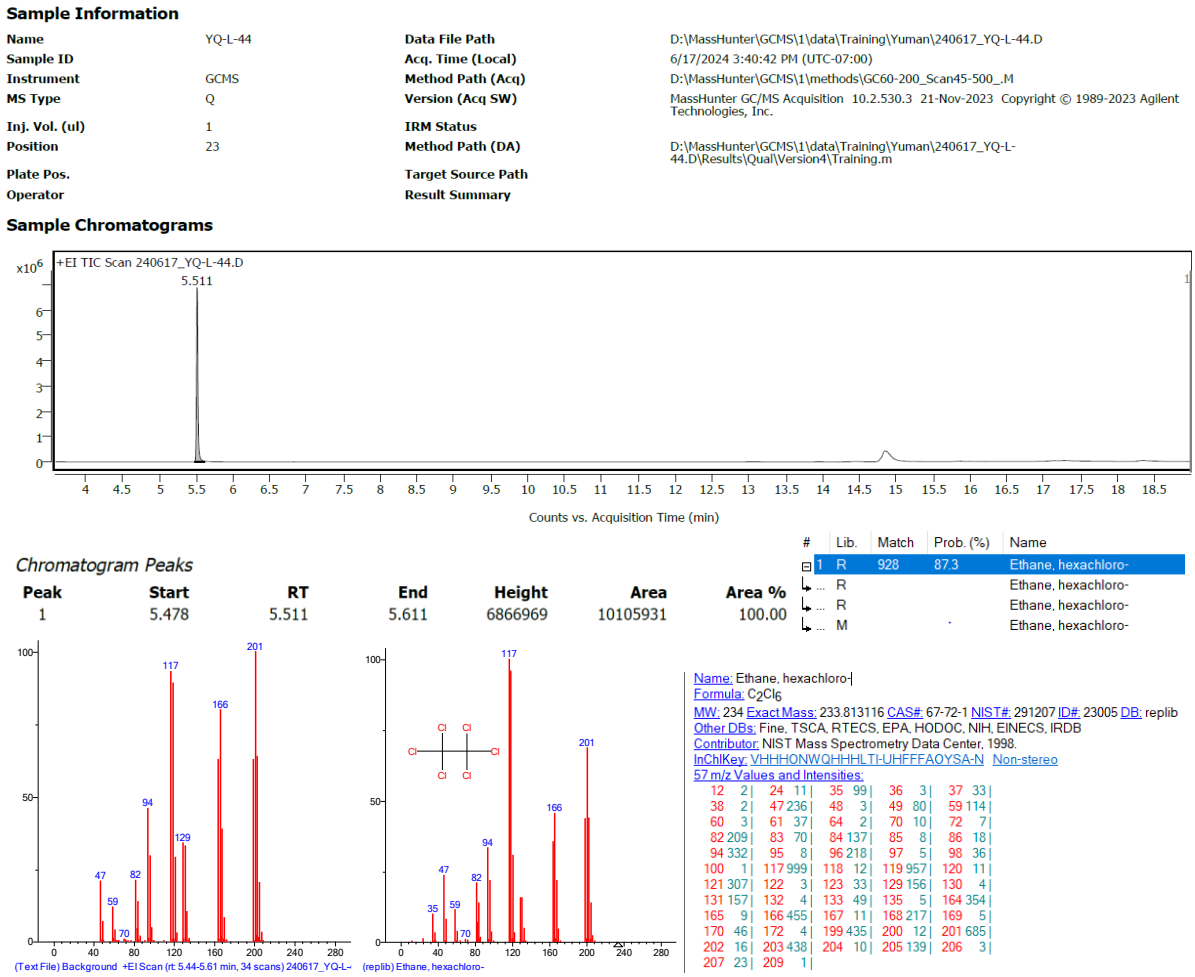

Fig. S22. GC-MS spectra of reaction solution under condition of entry 2

7.7 Isotope experiments

In a dry 15 mL Schlenk tube equipped with a 2 mm bore stopcock, a magnetic stirring bar was

added along with a balloon filled with CO_2. The tube was charged with 5 mg of Fe@f-gC_3N_4 before being sealed with a rubber septum. The setup underwent three vacuum-CO_2 cycles to ensure a CO_2 atmosphere. Subsequently, **1bc** (0.2 mmol), 0.6 mL $CHCl_3$ and 1.4 mL of MeCN were introduced under a CO_2 atmosphere. The reaction mixture was irradiated using a Kessil lamp (456 nm) for 24 h. Upon completion, 1,3,5-trimethoxybenzene as internal standard was added to the solution, the final reaction solution was filtered and concentrated under reduced pressure to produce the crude product. The D/H yield of **3a** and **4a** was obtained by ^{1}H NMR analysis (**Fig. S23**).

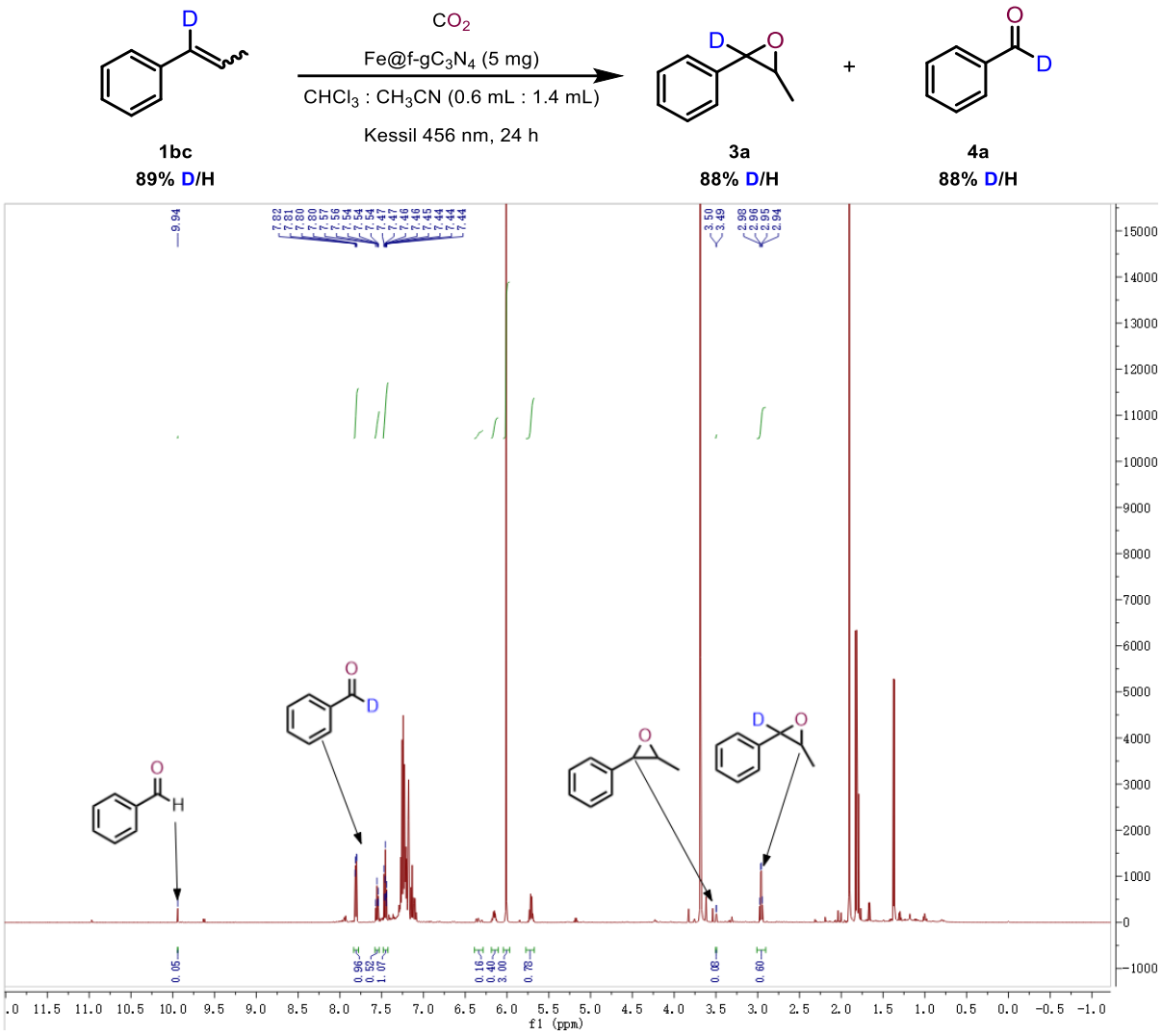

Fig. S23. Crude ^{1}H NMR spectra of isotope experiments

7.8 Demonstration of reaction stoichiometry

To provide an assessment of the carbon mass balance of this reaction, both the gaseous and liquid products formed during the reaction were carefully quantified. As a representative example, substrate **1z** was selected to rigorously track oxygen incorporation and the fate of carbon-containing species. The gaseous products, including CO and CH_4, were analyzed by headspace GC, and quantified using the method described in **Equation (3)**. The yields of C_2Cl_6 and residual $CHCl_3$ were determined by using GC-Fid analysis (**Fig. S24**). We first quantified the yield of **2z**, which was found to be 0.26 mmol. Based on this, we calculated that a minimum of 0.26 mmol of oxygen species (O) was required for complete the oxidation. We then made a theoretical estimation of the required reagent input and compared it with the experimentally

measured values. Notably, the actual quantities of each reagent exceeded the theoretical minimum, which is reasonable given the mild reaction conditions and the likely need for an excess of oxygen species to drive the transformation efficiently. The quantitative analyses confirmed a good overall carbon mass balance across the liquid and gas phases (**Table S6**).

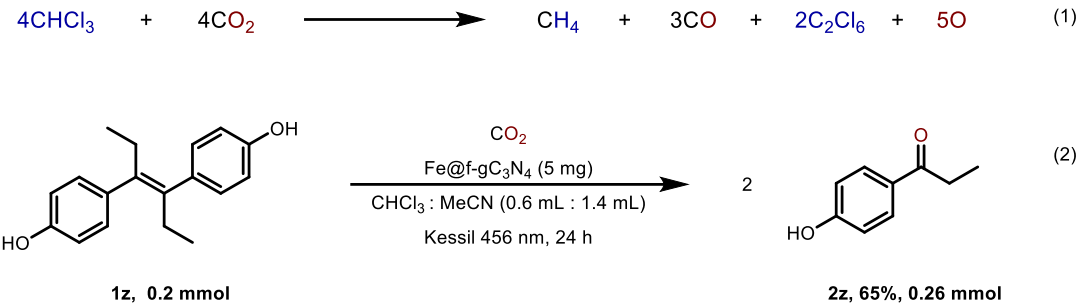

Table S6. Summary of the molar amount of reagent

Entry	Molar amount (mmol)						
	CO_2	$CHCl_3$	CH_4	CO	C_2Cl_6	[O]	2z
Theoretical values	0.20	0.20	0.05	0.15	0.10	0.26	0.26
Experimental values	0.24	0.24	0.06	0.18	0.12	0.30	0.26

The micro mole of gaseous product was calculated according to the following formula:

$$mmol = \frac{ppm \times P \times L}{1000 \times R \times T} \approx ppm \times 4.09 \times 10^{-5} \times L \quad (3)$$

Where: ppm = parts per million (v/v), P = pressure (atm), R = 0.08206 L·atm/mol·K; T = temperature (K), L= 0.21 L, At 1 atm and 25°C (298 K).

CH_4	6879 ppm	0.06 mmol
CO	18630 ppm	0.18 mmol

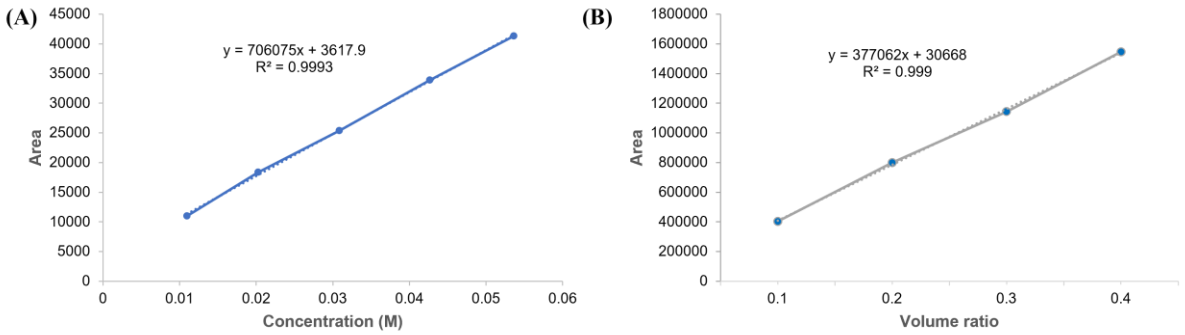

Fig. S24. Calibration curve of (**A**) C_2Cl_6 and (**B**) $CHCl_3$ in GC

7.9 EPR investigation

EPR spectra were recorded on an X-band Bruker EMX CW-micro EPR spectrometer equipped with an ER4119HS high-sensitivity resonator using a microwave frequency of ν≈9.7 GHz, a microwave power of 6.3 mW, a modulation frequency of 100 kHz and a modulation amplitude of 1 G, a scanning number of 1 and sweeping time of 30 s. The $h\nu = g\beta B_0$ equation was used

to calculate g values with ν and B_0 being the microwave frequency and resonance field, respectively. 2,2-Diphenyl-1-picrylhydrazyl (DPPH) was used as a standard (g = 2.0036 ± 0.0004) for calibration of the g value. The EPR spectra were simulated with MatlabR2023a using the EasySpin-5.2.36 module.

EPR spin trapping experiments with and without 5,5-dimethyl-1-pyrroline N-oxide (DMPO) were performed as following:

A 40 mL Schlenk tube equipped with a stirring bar, 3.0 mg of Fe@g-fC_3N_4 was sealed with a rubber septum after creating a CO_2 environment. This was achieved by applying a vacuum for 3 minutes and then purging with CO_2 for 30 s, repeated for a total of three cycles. Subsequently, 30 μL of starting material (**1a**), 1.4 mL MeCN, and 0.6 mL $CHCl_3$ (MeCN and $CHCl_3$: free O_2, H_2O) was added to the Schlenk tube under a CO_2 atmosphere. Then a CO_2 balloon was attached to the Schlenk tube using a needle. About 100 μL of this reaction mixture was taken out and mixed with 10 μL DMPO. Then about 50 μL of this mixture was transferred into a glass microcapillary tube (Hirschmann) and EPR spectra were recorded in dark and under irradiation (40 W Kessil lamp 456 nm) at room temperature. The remaining reaction solution in the Schlenk tube was then exposed to 456 nm irradiation using a Kessil lamp, positioned approximately 2 cm from the tube. The reaction proceeded with vigorous stirring at room temperature for several hours. After different reaction time, about 100 μL solution was taken out and mixed with 10 μL DMPO. Then about 50 μL of this mixture was transferred into a glass microcapillary tube (Hirschmann) and EPR spectra were recorded in dark and under irradiation (40 W Kessil lamp 456 nm) at room temperature. About 50 μL of reaction mixture without DMPO was also transferred into a glass microcapillary tube (Hirschmann) and EPR spectra were recorded under similar conditions.

In-situ EPR experiments were performed as following:

12 mg of fresh Fe@g-fC_3N_4 was added to a EPR tube which then was sealed with a rubber septum after creating a Ar environment. The EPR spectra of fresh Fe@g-fC_3N_4 in Ar was measured at 93K. Then, the EPR measurements were recorded at room temperature in the dark and during irradiation for 30min (40 W Kessil lamp 456 nm). After that, a CO_2 balloon was attached to the EPR tube using a needle, and the sample was irradiated for 30min (40 W Kessil lamp 456 nm) at room temperature, and the EPR spectra were recorded under these conditions before cooling to 93K for recording spectra at low temperature. Finally, the reaction mixture (0.2 mL) of *trans-β*-methylstyrene in a mixed solvent of $CHCl_3$ and MeCN was added into the EPR tube containing the catalyst under CO_2 atmosphere, which then was irradiation for 30min (40 W Kessil lamp 456 nm) at room temperature before cooling to 93K for recording spectra at this temperature. The spectrum of the used catalyst was compared with those of the fresh and pre-treated with CO_2 forms.

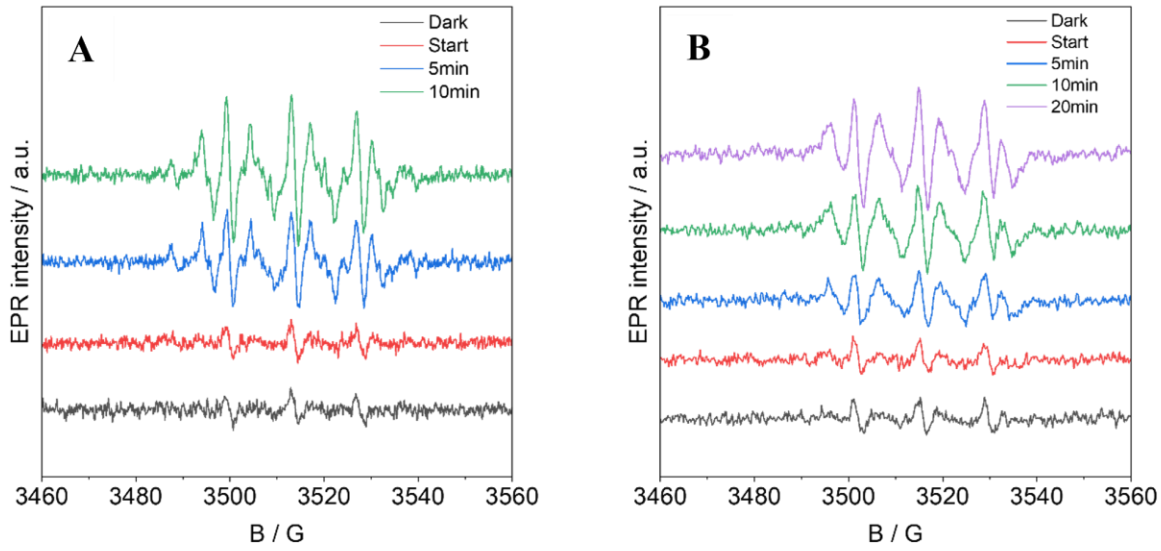

Fig. S25. EPR spectra of reaction mixtures in the presence of CO_2 and DMPO recorded at room temperature before and during irradiation (10min, 40 W Kessil lamp 456 nm) inside the resonant cavity of EPR spectrometer: reaction mixtures after (**A**) 20 min and (**B**) 3 h testing outside the resonant cavity of EPR spectrometer (40 W Kessil lamp 456 nm).

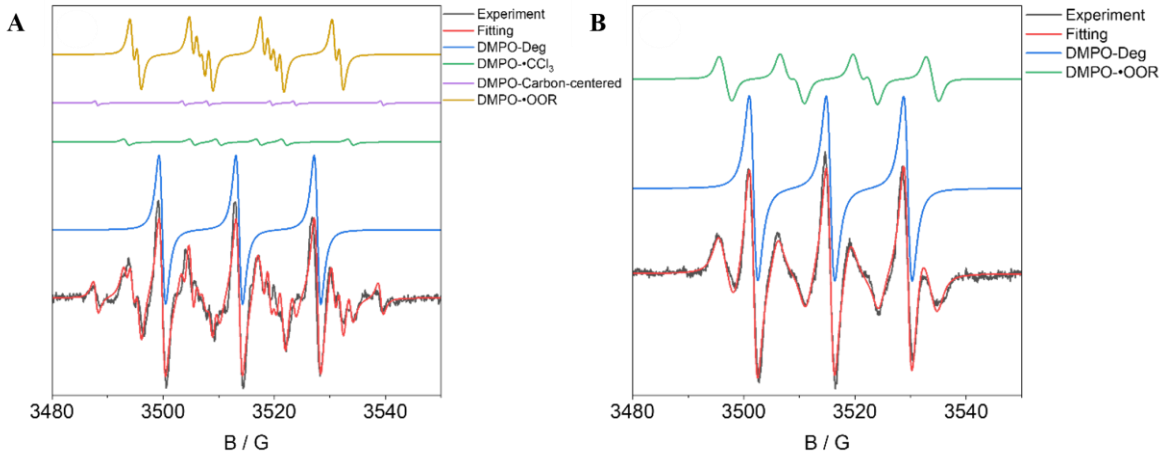

Fig. S26. EPR spectra DMPO-containing reaction mixtures recorded at room temperature after 10min irradiation inside the resonant cavity of EPR spectrometer together with fitting spectra and all simulated spectral components; reaction mixtures after: (**A**) 20 min and (**B**) 3 h testing outside the resonant cavity of EPR spectrometer (40 W Kessil lamp 456 nm).

The EPR spectra of reaction mixtures after testing for 20 min and 3 h shown no signal. Therefore, DMPO was used to trap any short-lived radicals generated during a photoreaction. After different times of irradiation outside of the resonant cavity of EPR spectrometer (40 W Kessil lamp 456 nm), DMPO was added to the reaction mixture and the EPR spectra were recorded before and during irradiation inside the resonant cavity. As seen in **Fig. S26A** and **S26B**, the EPR spectra of reaction mixture after 20 min and 3 h irradiation outside in the presence of DMPO shown weak triplet corresponding to the degradation of DMPO before irradiation during EPR measurements (black line). The intensity of this triplet increases upon irradiation. Moreover, a doublet of triplet signals with $A_N = 15.1$ G, $A_H^{\beta} = 21.0$ G is related to a carbon-centered radical DMPO adduct (DMPO-•CH_3), other doublet of triplet signals with

lower A_N = 12.0G and A_H^{β} = 16.59 G corresponding to DMPO-•CCl_3 radical adduct were formed within short time (5min), following by the formation of DMPO-•OOR radical adduct (A_N = 12.93 G, A_H^{β} = 10.45 G, A_H^{γ} = 1.3 G) after 10min irradiation (**Fig. S25A** and **Fig. S26A**) (*67-69*). After longer time irradiation outside (3 h), beside the triplet of DMPO degradation (DMPO-Deg) only the signals with A_N = 13.02 G, A_H^{β} = 10.48 G, A_H^{γ} = 1.3 G corresponding to DMPO-•OOR radical adduct (**Fig. 26B**) were formed upon irradiation inside the resonant cavity (**Fig. S25B** and **Fig. S26B**).

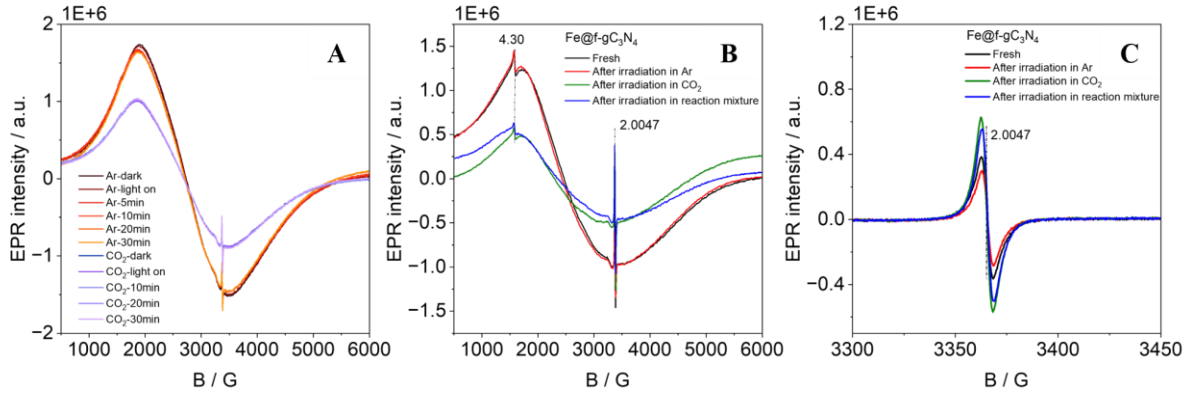

Fig. S27. (**A**) In-situ EPR spectra recorded at room temperature of Fe@f-gC_3N_4 catalyst in the dark and under irradiation in Ar atmosphere and CO_2 atmosphere; EPR spectra recorded at 93K of fresh Fe@f-gC_3N_4 catalyst, Fe@f-gC_3N_4 after irradiation in Ar for 30min, Fe@f-gC_3N_4 catalyst in CO_2 atmosphere after irradiation for 30min, Fe@f-gC_3N_4 in the reaction mixture after irradiation for 30min: (**B**) full range with a modulation amplitude of 5G; (**C**) narrow range with a modulation amplitude of 1G.

The EPR profiles at room temperature show only a broad signal from magnetically interacting iron and another signal at g = 2.0047 due to the localized *p*-conjugated structure of g-C_3N_4. The intensity of the broad signal decreased slightly during irradiation in Ar (**Fig. S27A**), indicating that the photoexcited electron reduce ferromagnetic Fe signal to an EPR-silent species. Notably, this ferromagnetic signal decreased more quickly and markedly in the presence of CO_2. This might be due to the oxidation of the ferromagnetic phase. Alternatively, it could be caused by spin disorder induced by CO_2-derived intermediates that have been adsorbed.

Their EPR profiles recorded at 93K in **Fig. S27B** show a signal at g = 4.3 from single sites, with similar intensity after irradiation in Ar. However, the intensity of this signal decreased after irradiation in CO_2 and in the reaction mixture, indicating the reduction of ferromagnetic Fe signal during these conditions. Moreover, the intensity of the signal at g = 2.0047 decreased slightly when irradiating in Ar, while it increased significantly under irradiating in CO_2 and the reaction mixture (**Fig. S27C**), indicating the localized p-conjugated structure of catalyst received new paramagnetic species under these conditions. These findings are in excellent agreement with our previous in-situ EPR experiments examining the formation of different radicals.

7.10 Step by step experiments

To confirm that epoxide and diol is an intermediate rather than a byproduct, stepwise experiments were conducted using epoxide (**2a″** and **1be**) as the starting material under optimal conditions. Similarly, a dry 15 mL Schlenk tube equipped with a 2 mm bore stopcock, a magnetic stirring bar and 5 mg of Fe@f-gC_3N_4 were added along with a balloon filled with

CO_2. The setup underwent three vacuum-CO_2 cycles to ensure a CO_2 atmosphere. Subsequently, epoxide (0.2 mmol), 0.6 mL $CHCl_3$ and 1.4 mL of MeCN were introduced under a CO_2 atmosphere. The reaction mixture was irradiated using a Kessil lamp (456 nm). Upon completion, the reaction mixture was filtered and quickly submitted to ^1H NMR. In both cases, the starting material successfully yielded the target products (**2a**).

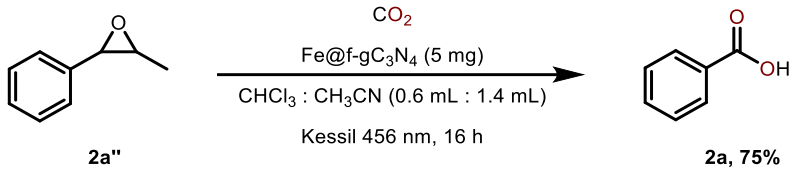

2a" **2a, 75%**

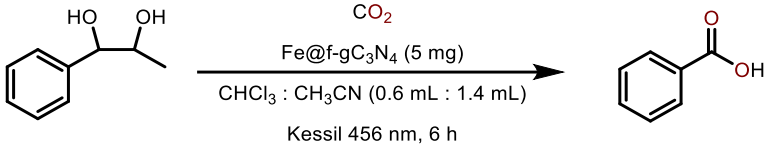

1be **2a, 85%**

7.11 Cyclization experiments

When we use substrate **1bd** as the starting material under the standard reaction conditions, we observed the formation of product **5a** in 71% yield. This result supported the hypothesis of the formation of 1,2-diol intermediate.

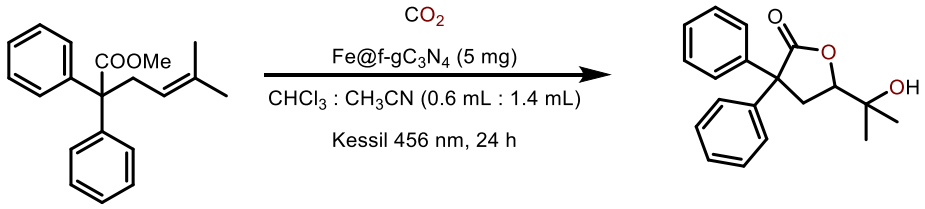

1bd **5a, 71%**

7.12 The light on/off experiments

Light on/off experiments were conducted using the model substrate (**1a**). After 6 hours of irradiation, the light was turned off for 3 hours, during which the yields of **1a**, **2a"**, **2a'**, and **2a** remained unchanged. Upon re-irradiation for another 3 hours, the yields of **2a"**, **2a'**, and **2a** increased with a corresponding decrease in **1a**. However, this progress plateaued again when the light was turned off for an additional 3 hours. This cycle was repeated three times, and the results, as shown in **Fig. S28**, clearly demonstrate that light plays a critical role in the reaction. The transformation ceased in the absence of light and resumed immediately upon re-illumination.

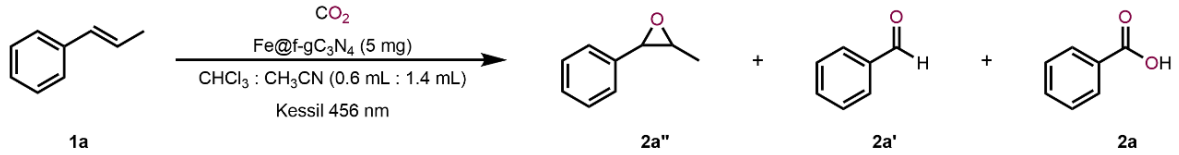

1a **2a"** **2a'** **2a**

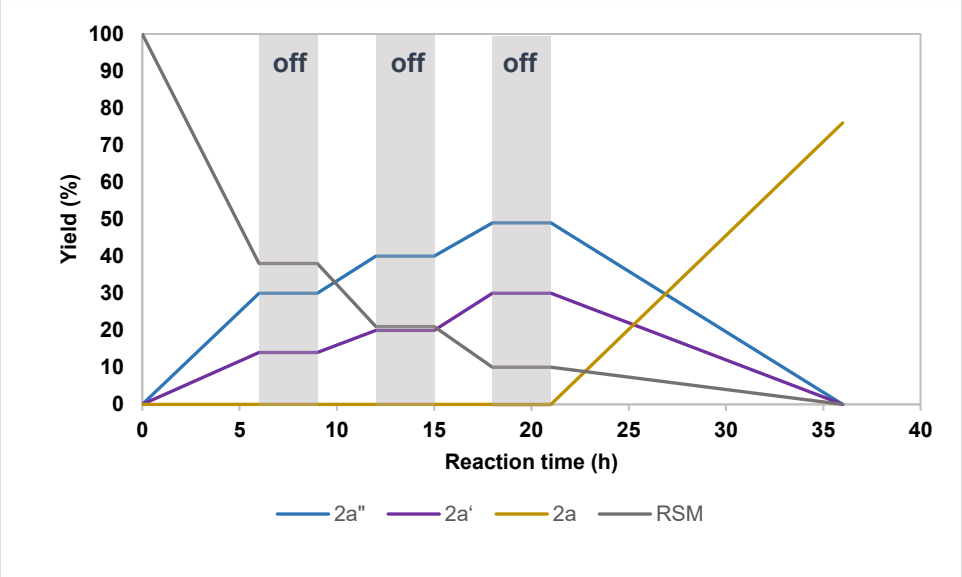

Fig. S28. Result of light on/off experiments

7.13 Apparent quantum yield (AQY) measurement

The Apparent quantum yield (AQY) of benzoic acid under standard conditions was calculated as follows.

The amount of formed product (mol):

M = 0.2 mmol x 78% = 0.156 mmol = 1.56 x 10^{-4} mol

The light intensity of Kessil lamp (λ = 456 nm) was 0.15 W/cm^2.

$$\eta = \frac{N_e}{N_p} \times 100\% = \frac{2 \times M \times N_A}{\frac{S \times P \times t}{h \times \frac{c}{\lambda}}} \times 100\% = \frac{2 \times M \times N_A \times h \times c}{S \times P \times t \times \lambda} \times 100\%$$

$$= \frac{2 \times 1.56 \times 10^{-4} \times 6{,}022 \times 10^{23} \times 6{,}63 \times 10^{-34} \times 3 \times 10^{8}}{1{,}3 \times 0{,}15 \times 24 \times 3600 \times 456 \times 10^{-9}} \times 100\%$$

$$= 0.49\%$$

M represents the amount of formed product (mol), N_A is the Avogadro constant (6.022 x 10^{23} mol^{-1}), h is the Planck constant (6.63 x 10^{-34} J·s), c is the light speed (3 x 10^8 $m \cdot s^{-1}$), S is the irradiation area (1.3 cm^2), P is the light intensity (0.15 $W \cdot cm^{-2}$), t is irradiation time (24 x 3600 s), λ is the wavelength of light (m).

7.14 Fluorescence quenching experiment

Steady-state photoluminescence spectra were recorded at 298 K by using a Jasco FP-8600 spectrofluorometer equipped with a 1 cm path length quartz cuvette. The excitation wavelength was set to 355 nm. For the measurements, 1 mg of Fe@f-g-C_3N_4 photocatalyst was dispersed in 3 mL of MeCN. Prior to data acquisition, the suspension was sonicated in an ultrasonic bath for 30 minutes to ensure uniform dispersion of the photocatalyst.

Fig. S29 shows the reduction of fluorescence intensity in solutions with different amounts and types of quencher. Upon increasing the fraction of $CHCl_3$, the fluorescence reduces, indicating an efficient interaction between $CHCl_3$ and the excited photocatalyst. In contrast, when *trans*-*β*-methylstyrene (**1a**) is added as quencher at the same concentration (0.9 M), less reduction in the fluorescence intensity is observed. The results demonstrate that $CHCl_3$ exhibits stronger quenching behavior, suggesting it serves as a primary hole scavenger in this reaction. These

findings support our proposed pathway that $CHCl_3$ undergoes oxidation by the valence band holes to generate trichloromethyl radicals (CCl_3•) and protons. The CCl_3• species subsequently undergo homocoupling to form C_2Cl_6, as supported by product analysis.

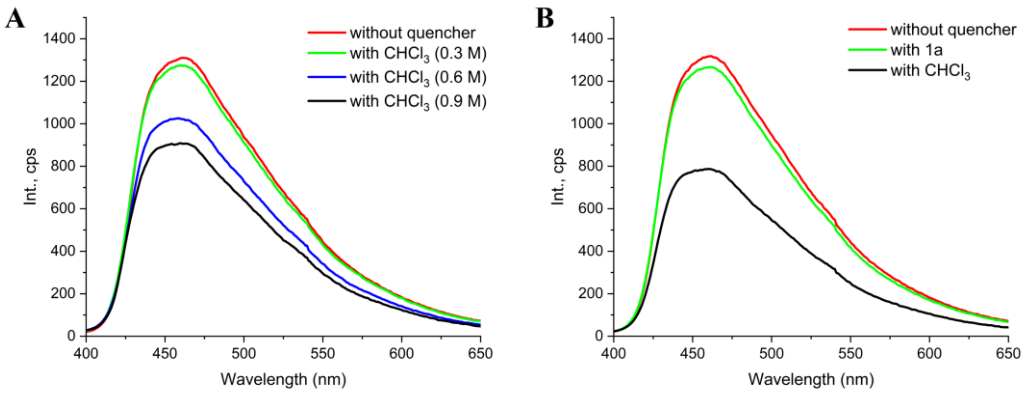

Fig. S29. Quenching of Fluorescence of Fe@f-g-C_3N_4 upon addition of $CHCl_3$. (**A**) Fluorescence spectra in neat MeCN and in MeCN:$CHCl_3$ mixtures at the moler concentrations indicated. (**B**) Comparison of fluorescence spectra in MeCN without quencher and with the quenchers **1a** and $CHCl_3$, added at the same mole fraction.

7.15 In-situ diffuse reflectance infrared fourier transform (DRIFT) spectroscopy

In-situ DRIFTS were collected on a Nicolet 6700 FTIR spectrometer by using a high-temperature Praying Mantis reaction cell (Harrick) with CaF_2 windows, equipped with a temperature control unit (Eurotherm). Each spectrum was obtained by averaging 64 scans recorded with a resolution of 4 cm^{-1}. In situ experiments were conducted by loading 25 mg of solid catalyst into the sample cup of the DRIFT reaction cell. The sample was pretreated by heating at a rate of 10 $K \cdot min^{-1}$ up to a temperature of 473 K for 2 h under a flow of He (13 $mL \cdot min^{-1}$) to clean the surface. Afterward, the cell was cooled under He flow. The dome of the DRIFT cell was removed, and a drop of *trans-β*-methylstyrene in a mixed solvent of $CHCl_3$ and MeCN was rapidly added to the catalyst with a pipette. Once the dome was replaced and under He flow, CO_2 was quickly admitted to the cell at a flow rate of 4 $mL \cdot min^{-1}$. The background spectrum was taken at this point. Then, the lamp was turned on, and spectra were collected over time under continuous radiation. The intensity of the signals is Given in log(1/R) scale. The reaction mixture (4 mL) of *trans-β*-methylstyrene in a mixed solvent of $CHCl_3$ and MeCN was prepared using the same ratio as in the catalytic test in a Schlenk tube and outgassed under the Schlenk system.

In general, the intensity of the bands was weak, with no carbon-containing surface intermediates were detected in the 1690–1360 cm^{-1} region due to strong background absorption in this spectral range, which hindered the extraction of mechanistic details. This limitation is consistent with previous reports on C_3N_4-based catalysts, where carbon-containing species were similarly undetectable within this region. The *trans-β*-methylstyrene oxidized to form epoxide species, as evidenced by a characteristic band at 1128 cm^{-1}. Upon irradiation, this band appeared as a negative feature in the time-resolved spectra (**Fig. S30**), suggesting further oxidation of the epoxide to the final carboxylic acid product. The latter was confirmed by the emergence of bands at 1730 cm^{-1} and 1330 cm^{-1}, in agreement with the catalytic test. Additionally, bands observed at 1290 and 1315 cm^{-1} are tentatively assigned to carboxylic acid species with different binding modes with the catalyst surface. These different interactions may explain the broadening of the 1730 cm^{-1} band.

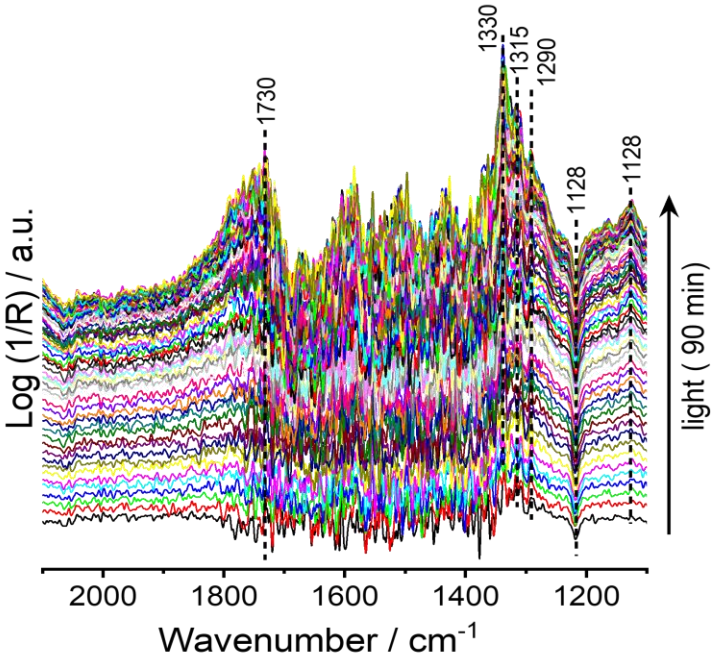

Fig. S30. Time-resolved in-situ DRIFTS spectra showing the oxidative cleavage of *trans-β*-methylstyrene over Fe@f-gC_3N_4 at RT under irradiation and CO_2 flow for 90 min

8. Characterization of Fe@f-gC_3N_4

8.1 STEM and EDX

Scanning transmission electron microscopy (STEM) measurements were carried out utilizing a probe aberration-corrected JEM-ARM200F (JEOL, Corrector: CEOS) operating at 200 kV. This microscope is equipped with a JED-2300 (JEOL) energy-dispersive X-ray spectrometer (EDX) having a silicon drift detector (dry SD60GV). For STEM imaging, both High-Angle Annular Dark Field (HAADF) and Annular Bright Field (ABF) detectors were employed. The solid samples were deposited onto a holey carbon-supported Cu grid (mesh 300) without any pre-treatment and subsequently transferred to the microscope for analysis.

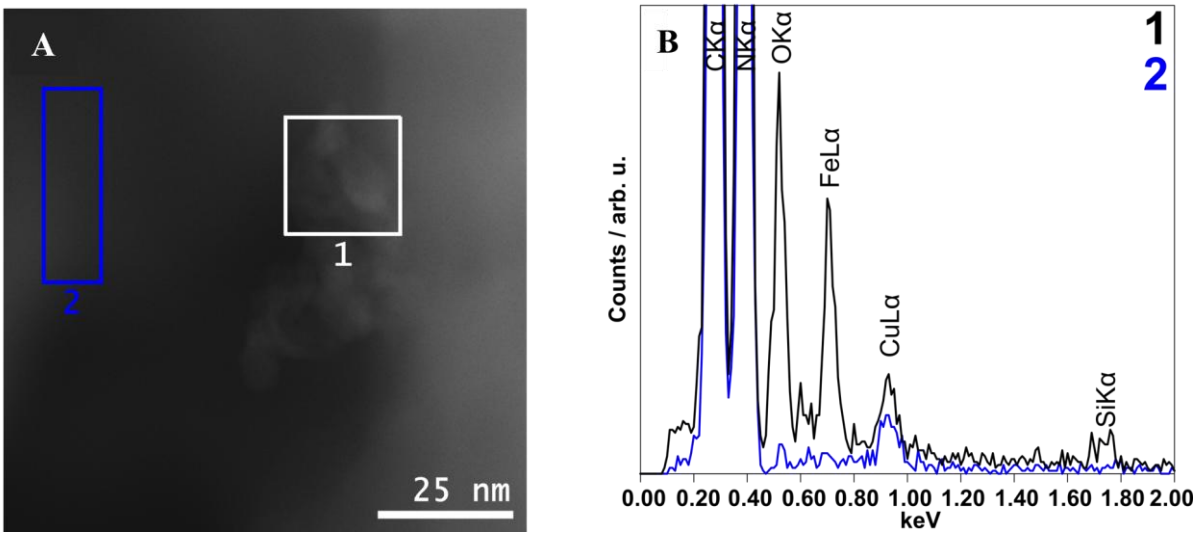

Fig. S31. STEM-HAADF image of Fe@f-gC_3N_4 (**A**), selected EDX spectra of Fe@f-gC_3N_4 (**B**) of the regions highlighted by rectangles in (**A**). Area 1 shows clearly a more intense O Kα signal when Fe is present, while area 2 shows just carbon and nitrogen and negligible amounts of oxygen

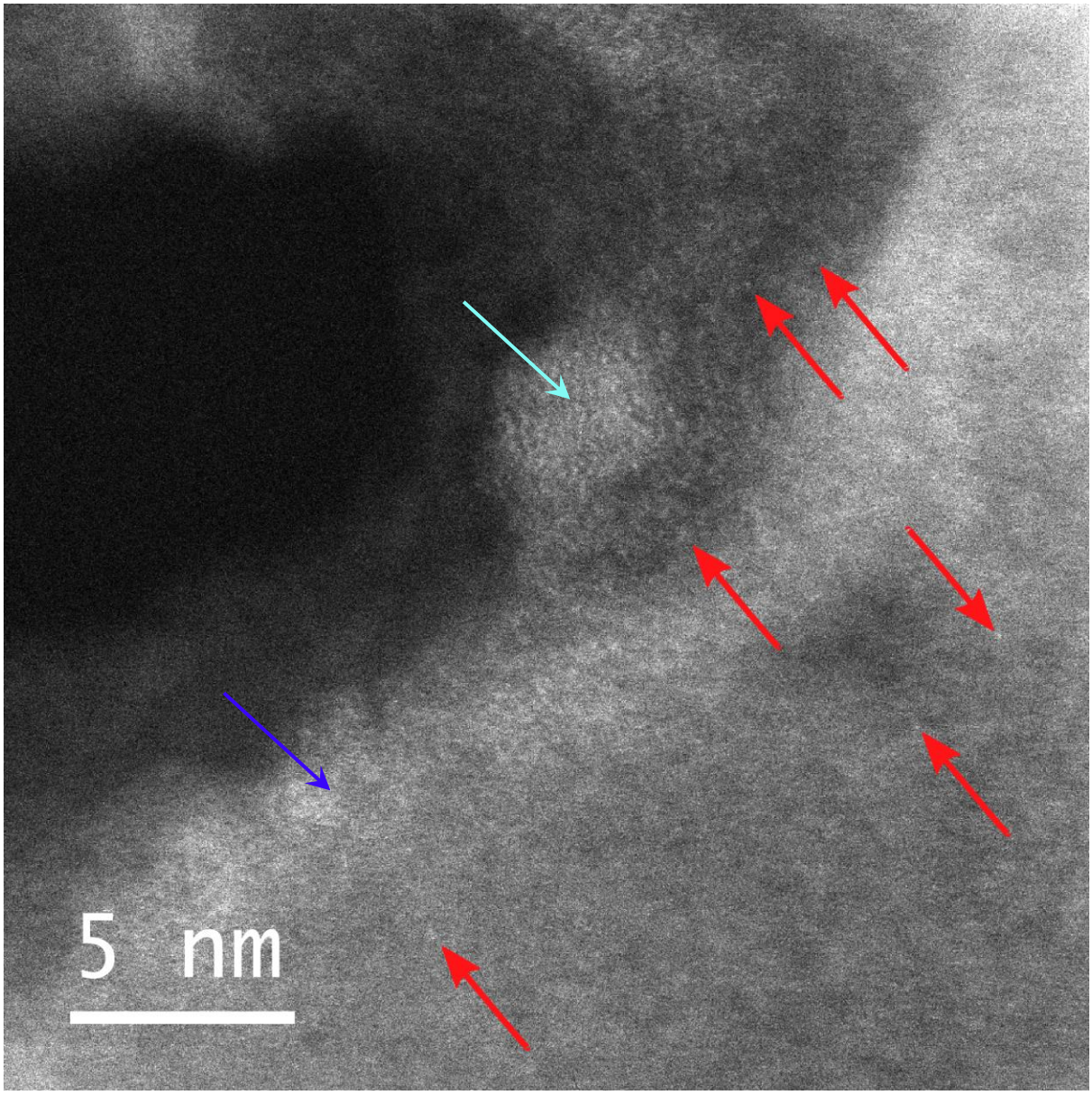

Fig. S32. Larger representation of the image depicted in **Fig. 3B** (in the manuscript) with the red arrows indicating single iron atoms, a blue arrow indicating surface enriched Fe species and cyan arrow indicating Fe containing nanoparticle

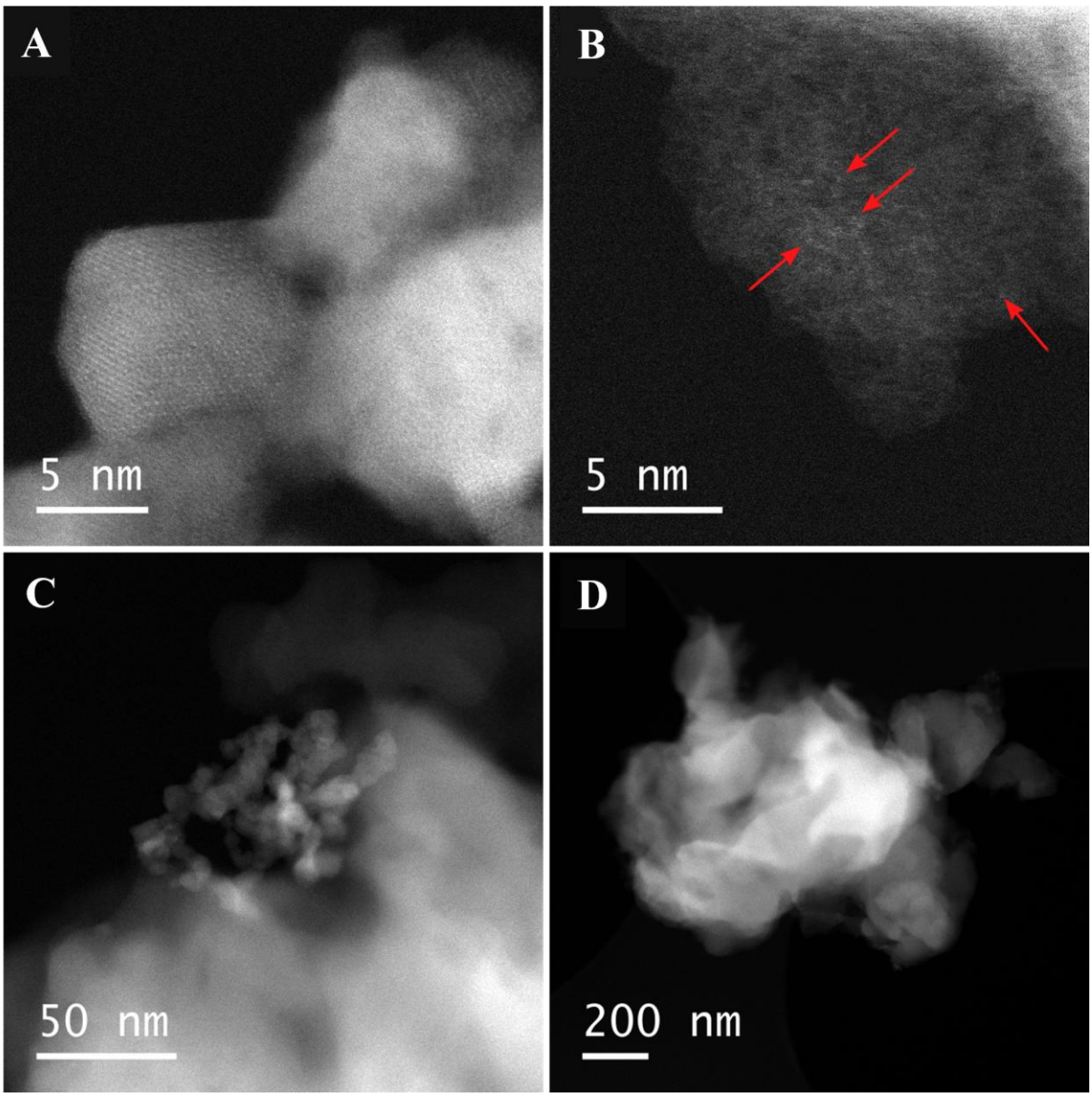

Fig. S33. Selected STEM-HAADF images of Fe@f-gC_3N_4 at different magnifications after 160 h of photocatalytic oxidation (456 nm) of *trans*-*β*-methylstyrene. The main structural features of the fresh material are also found here. Red arrows indicate single Fe atoms

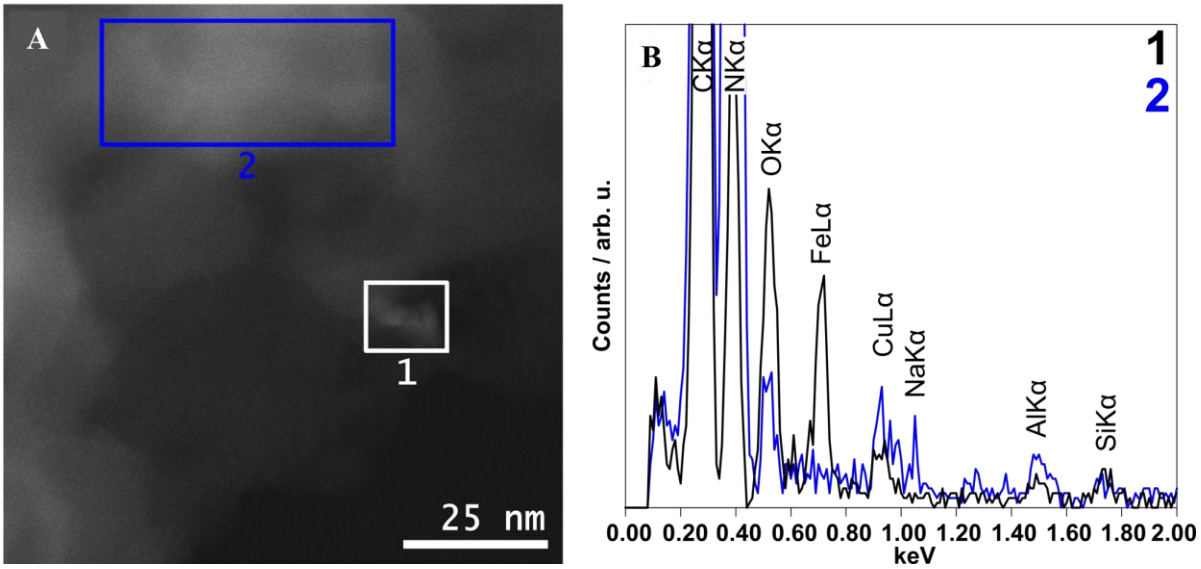

Fig. S34. Selected EDX spectra of Fe@f-gC_3N_4 after 160 h of (**A**) of the regions highlighted by rectangles in the STEM-HAADF image (**B**). Spectrum 1 shows clearly a more intense O Kα signal when Fe is present, while spectrum 2 shows just carbon and nitrogen and negligible amounts of oxygen

8.2 ^{57}Fe Mössbauer spectroscopy and magnetic measurements

^{57}Fe Mössbauer spectra were recorded at room temperature in transmission geometry in constant-acceleration mode with a sinusoidal waveform which determines the source motion using Mössbauer spectrometer from wissenschaftliche elektronik with a silicon drift detector from KETEK equipped with a 50 mCi^{57}Co(Rh) source. Magnetic measurements were collected using a SQUID MPMS-XL5 instrument from Quantum Design. The samples were prepared in gelatin capsules held in a plastic straw.

8.3 X-ray photoelectron spectroscopy (XPS)

X-ray photoelectron spectroscopy (XPS) measurements were carried out in a Prevac photoelectron spectrometer equipped with a hemispherical analyzer (VG SCIENTA R3000) using monochromatized aluminium Al Kα radiation (E = 1486.6 eV). Binding energy values were calibrated based on the position of the C 1s reference peak at 284.8 eV. The data were processed in the Casa XPS software.

The surface of the fresh sample contains small amounts of adventitious carbon contaminants (C 1s peak at 284.8 eV), as well as trace levels of oxidized N forms (a very weak N 1s peak at 404.4 eV). After the reaction, a substantial accumulation of C–C/C=C carbonaceous species is observed, as evidenced by a marked increase in the intensity of the C 1s peak at 284.8 eV. The symmetry of this peak and the absence of a shift toward higher binding energies exclude the presence of significant amounts of carbon–oxygen functionalities. Consequently, it can be inferred that this signal originates from strong adsorption of the alkene substrate or unoxidized reaction intermediates/products on the Fe@f-gC_3N_4 surface. The surface coverage by these species results in a noticeable decrease in the intensity of the C 1s, N 1s, and Fe 2p peaks attributed to the f-gC_3N_4 support and the Fe-containing active phase deposited on it.

The Fe 2p XPS spectrum exhibits relatively weak and broad peaks, primarily due to the low Fe content in the sample. In addition, this observation can be attributed to the specific photoemission characteristics of Fe when excited by X-ray radiation. In particular, the Fe 2p signal is affected by its relatively small photoionization cross-section and the intrinsic multiplet splitting and satellite structure, which distribute the intensity over a broad energy range.

Furthermore, inelastic background electrons contribute to a reduced apparent peak intensity. The Fe 2p XPS spectrum of the sample after the reaction does not show a significant change in the relative contributions of FeO_x and metallic Fe compared to the fresh photocatalyst. Despite the significant decrease in intensity (due to adsorption of the alkene substrate or unoxidized reaction intermediates/products on the Fe@f-gC_3N_4 surface, as show in **Fig. S35 A**), both components corresponding to FeOx and dispersed metallic Fe species are still visible in the Fe 2p region.

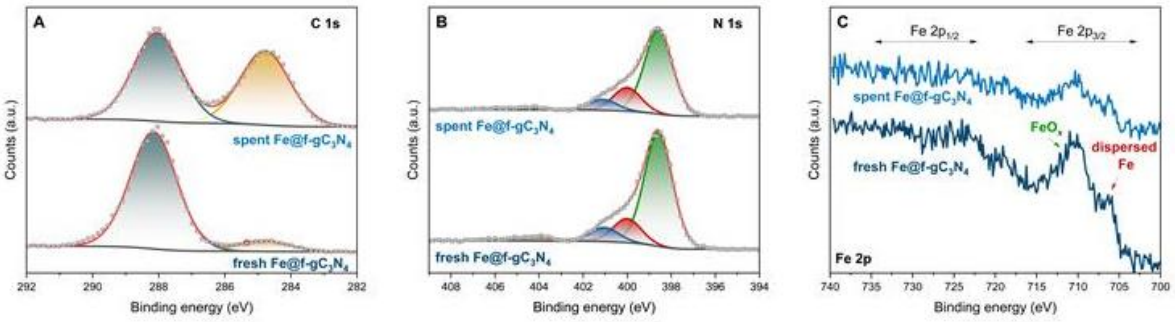

Fig. S35. High-resolution XPS spectra of C 1s (**A**), N 1s (**B**) and Fe 2p (**C**) for the fresh and spent sample

8.4 X-ray diffraction (XRD) measurements

X-ray diffraction (XRD) measurements of Fe@f-gC_3N_4 were conducted using a special glass capillary tube (No. 10, outer diameter 0.7 mm, Hilgenberg) and an Ag radiation source. Figure SXX presents the XRD patterns of both fresh and recycled Fe@f-gC_3N_4 catalysts.

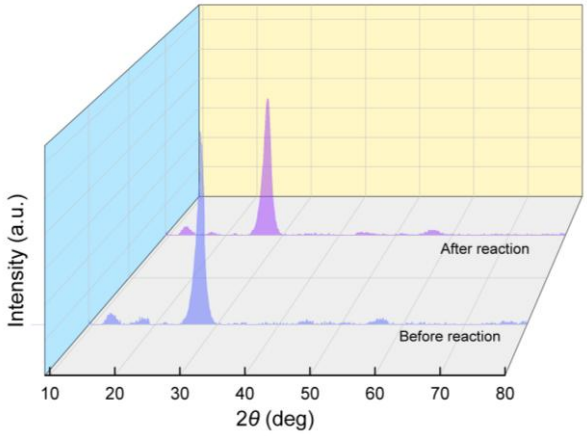

Fig. S36. XRD pattern of Fe@f-gC_3N_4 and recycled Fe@f-gC_3N_4

8.5 Fourier transform infrared (FT-IR) spectroscopy

A standard KBr pellet method was employed for transmission-mode FT-IR characterization of fresh and post reaction Fe@f-gC_3N_4 catalysts, using a Bruker Omni spectrometer.
We characterized the fresh and recycled (post-reaction) catalysts using FT-IR spectroscopy in transmission mode (**Fig. S37**). The sharp absorption peak around 808 cm^{-1}, which is assigned to the out-of-plane bending vibration of the triazine ring units in the g-C_3N_4 framework, remained in the same position before and after the reaction. Furthermore, the absorption bands in the 1200-1650 cm^{-1} range, which correspond to the stretching vibrations of the C-N and C=N bonds in the heterocyclic aromatic rings, showed negligible differences between the fresh and used samples. These results demonstrate that the catalyst remains structurally stable under the applied photocatalytic conditions.

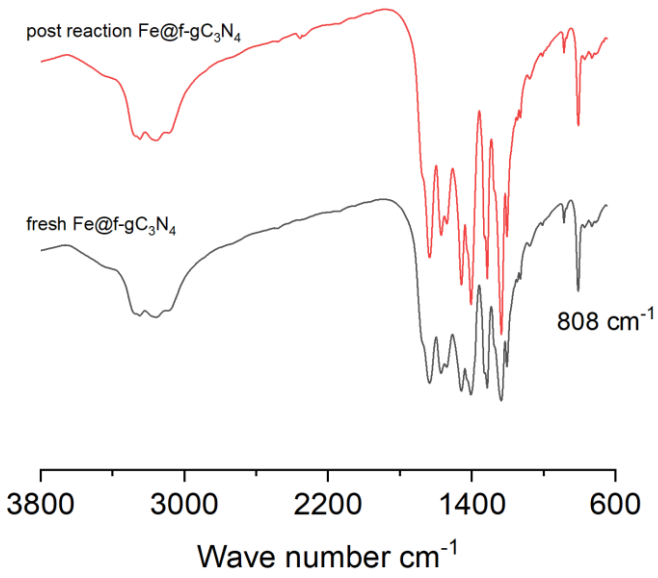

Fig. S37. IR spectra of fresh Fe@f-gC_3N_4 and recycled Fe@f-gC_3N_4

8.6 Brunauer–Emmett–Teller (BET) analysis

Porosity of Fe@f-gC_3N_4 was studied by N_2 adsorption-desorption measurements at -196 °C using a Micromeritics ASAP 2020 porosimeter. Prior to analysis, the sample was degassed under vacuum (10^{-3} Pa) at 250 °C for 6 h. Its specific surface area (S_{BET}) was determined using the Brunauer-Emmett-Teller method, while total pore volumes (V_{total}) were calculated from the amount of N_2 adsorbed at a relative pressure (p/p_0) of 0.99.

As shown in **Fig. S38**, the recorded low-temperature N_2 adsorption-desorption isotherm exhibits a shape characteristic of type II according to the IUPAC classification, indicating the non-porous nature of the Fe@f-gC_3N_4 material. The adsorption uptake becomes apparent only at the highest relative pressures, suggesting interparticle condensation, a phenomenon typical of finely dispersed materials. The determined S_{BET} value for Fe@f-gC_3N_4 is 7.0 m^2/g, while V_{total} = 0.08 cm^3/g.

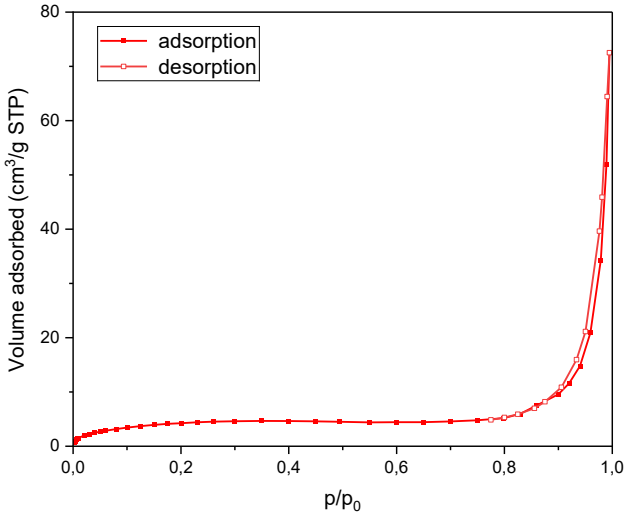

Fig. S38. Low-temperature N_2 adsorption-desorption isotherm of Fe@f-gC_3N_4

8.7 Solid-state nuclear magnetic resonance (ssNMR)

Solid-state magic-angle-spinning (MAS) ^1H and ^{19}F NMR spectra, as well as cross-polarization ^1H-^{15}N CPMAS NMR spectra were collected at a magnetic field of 14.1 T with a Bruker Avance-III spectrometer. The ^1H and ^{19}F MAS NMR spectra were acquired using a 1.3 mm

probehead and a 60 kHz MAS rate. These acquisitions involved a use of a rotor-synchronized, double-adiabatic spin-echo sequence with a 90° excitation pulse of 1.25 μs (2.50 for ^{19}F) followed by a pair of 50.0 μs tanh/tan short high-power adiabatic pulses (SHAPs) with 5 MHz frequency sweep. All pulses operated at the nutation frequency of 200 kHz (100 kHz for ^{19}F). 64 (16384 for ^{19}F) signal transients were acquired using a relaxation delay of 5.0 s. ^{1}H-^{15}N CPMAS NMR spectra were recorded using a 7 mm probe head with a 7 kHz MAS rate and 65 kHz spinal 64 proton decoupling. For ^{1}H-^{15}N CPMAS acquisition Hartmann-Hahn matched radiofrequency fields were applied for a contact interval of 5 ms and 32768 signal transients were collected using a relaxation delay of 2 s. The ^{1}H-^{13}C CPMAS acquisitions involved a contact interval of 1.5 ms, and 1024 scans collected with a relaxation delay of 2 s. Chemical shifts are reported with respect to TMS (^{1}H, ^{13}C), nitromethane (^{15}N), and trichlorofluoromethane (^{19}F). Calculations of ^{19}F NMR shifts were performed with the ORCA code (*70*, *71*). Geometry optimizations of the models and the subsequent (GIAO) NMR shifts calculations were performed at the revPBE-D4/pcseg-2 and DLPNO-MP2/aug-cc-pVTZ-J-un levels of theory, respectively. The $CFCl_3$ molecule treated at the same level of theory was used as a ^{19}F NMR shift reference.

Solid-state ^{19}F MAS NMR spectrum of the Fe@f-gC_3N_4 catalyst was used to estimate the fluorine content in the material (**Fig. S39**). Its ^{19}F NMR signal integral was related to that of the solid LiF recorded using the same NMR rotor and experimental conditions. The number of scans and pulse delay for LiF were set to 64 and 1000s, respectively, since LiF exhibits very slow relaxation. By assuming molar masses and densities of LiF and gC_3N_4 to be 25.939 and 92.060 g/mol, and 2.64 and 2.00 g/cm^3, respectively, and accounting for the difference in the number of signal transients collected for each sample, obtained fluorine content in the material could be represented as a molar ratio of gC_3N_4:$F_{0.0013}$. Based on this calculation, the fluorine content in Fe@f-gC_3N_4 catalyst is 0.027 wt%. However, we note that it is only an estimate, as the exact density of the Fe@f-gC_3N_4 catalyst is not known, and the ^{19}F NMR signal of the Fe@f-gC_3N_4 sample might not be fully relaxed, which could not be assessed due to very weak signal intensity. Because of the latter, it is highly probable that the real fluorine content in the material is higher than the above estimate.

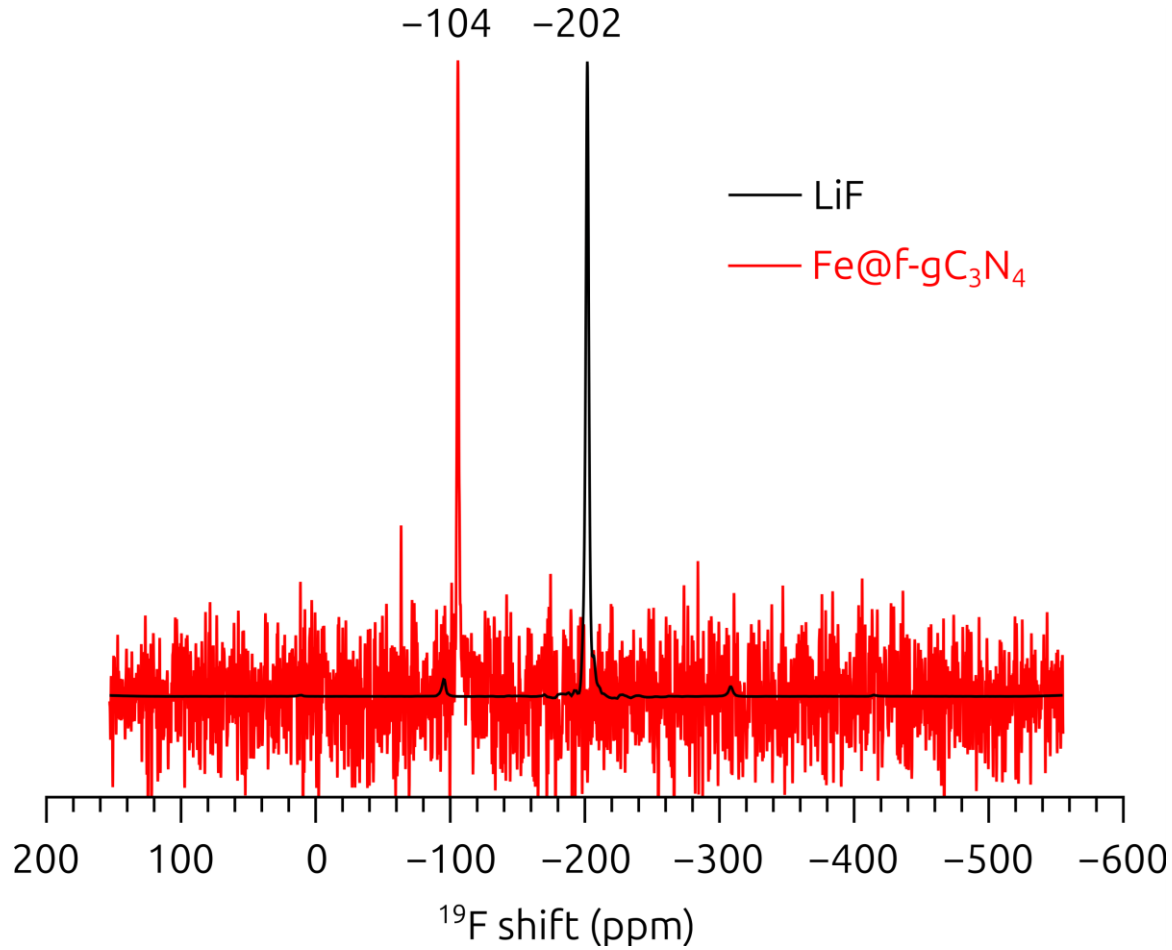

Fig. S39. ^{19}F MAS NMR spectra of solid LiF (black trace) and Fe@f-gC_3N_4 catalyst (red trace) recorded under the same experimental conditions. Spectrum of LiF corresponds to 64 signal transients, whereas spectrum of the catalyst was recorded with 16384 signal transients and its signal intensity plotted above is enhanced by a factor of 100 to match that of LiF.

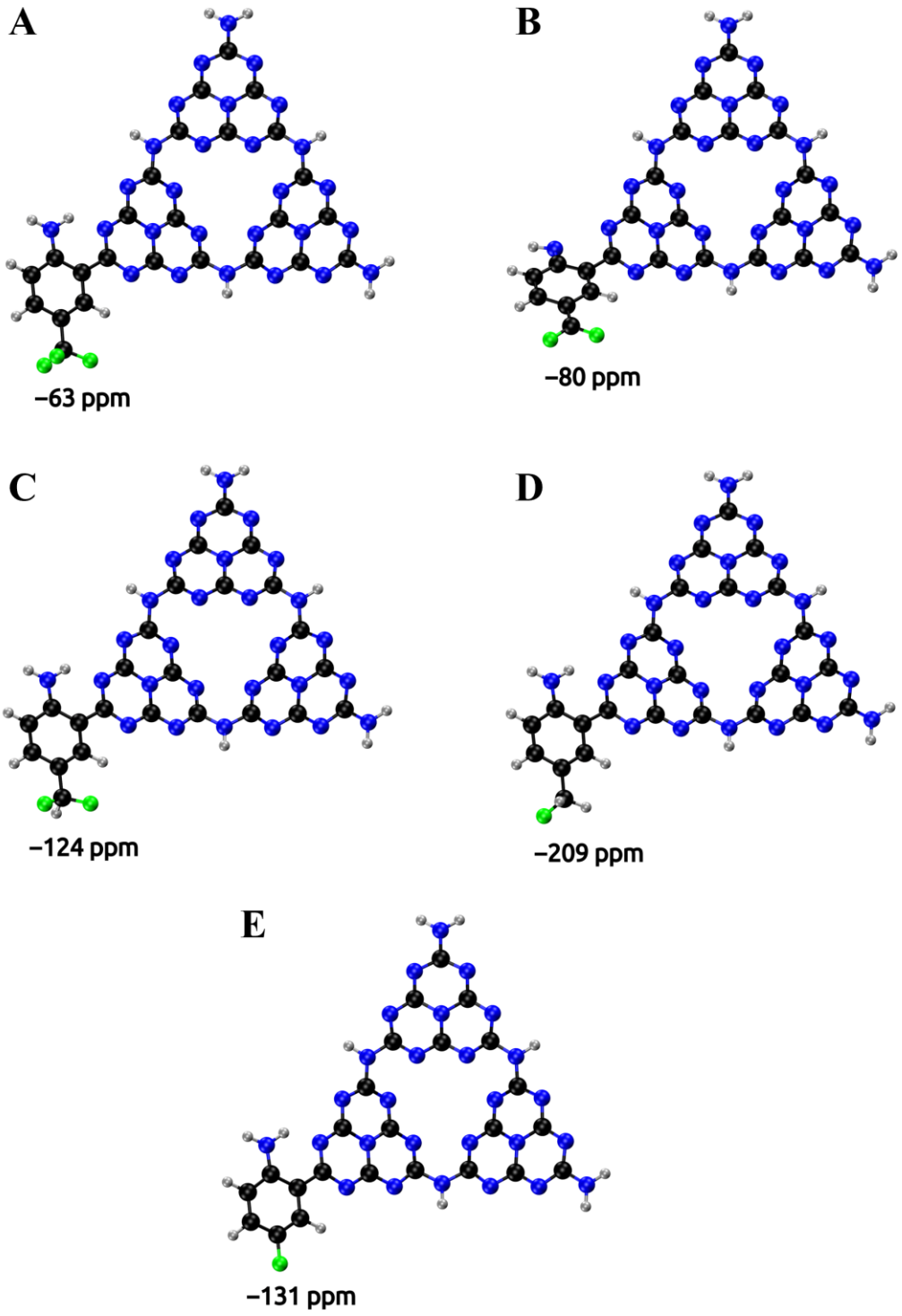

Fig. S40. ^{19}F NMR shifts calculated at the DLPNO-MP2/pcSseg-1 level of theory for the models of g-C_3N_4 modified with fluorinated aryl ligands. Models were geometry-optimized at the revPBE-D4/pcseg-1 level of theory. Model in panel (**A**) contains -CF_3 group, model (**B**) contains =CF_2 group, model (**C**) -CHF_2 group, model (**D**) -CH_2F group, and model (**E**) represents ArF moiety. Fluorine atoms are shown in green, nitrogen atoms in blue, carbon atoms in black, and protons in grey

Cartesian coordinates of the models (in Å)

Model a				**Model b**			
N	-4.663129	1.424074	-0.451114	N	-4.633085	1.466516	-0.327211
N	-3.478192	3.404807	-0.611682	N	-3.441530	3.445269	-0.444561
N	-1.119131	3.293739	-0.297961	N	-1.076767	3.311816	-0.188974
N	-2.421626	1.357261	0.141772	N	-2.379810	1.367293	0.213389
N	0.225347	5.240886	-0.525342	N	0.273406	5.258312	-0.386230
N	4.193835	-3.013102	1.080678	N	4.223822	-3.057366	0.917255
N	-1.424853	-4.564189	-0.997337	N	-1.445661	-4.518624	-1.086985
N	-0.873084	7.216377	-0.922739	N	-0.822290	7.250900	-0.697361
N	5.019912	-5.116268	1.483600	N	5.041735	-5.175070	1.254361
N	-2.205360	5.353357	-0.774374	N	-2.161577	5.391211	-0.575444
N	-0.114576	1.248780	0.371283	N	-0.069513	1.242904	0.397509
N	1.254951	3.184396	-0.133779	N	1.299678	3.185748	-0.080032
N	2.195832	1.102309	0.221533	N	2.236668	1.090109	0.200214
N	-3.719964	-0.560562	-1.162718	N	-3.722054	-0.502129	-1.126498
N	-4.855322	-2.559982	-0.586233	N	-4.867720	-2.508553	-0.600319
N	-5.967916	-0.485970	-0.257507	N	-5.944544	-0.437031	-0.157815
N	-7.143047	-2.490840	-0.001308	N	-7.157139	-2.432597	0.024516
N	-5.993237	-4.608786	-0.200560	N	-6.012401	-4.553712	-0.248570
N	-3.699500	-4.635219	-0.656642	N	-3.714223	-4.583129	-0.703090
N	-2.617785	-2.589570	-1.379184	N	-2.636246	-2.532554	-1.415696
N	3.253986	-0.917603	0.644611	N	3.291210	-0.945619	0.549621
N	2.044524	-2.887650	0.079093	N	2.055802	-2.892920	-0.037517
N	1.220900	-0.793841	-0.669226	N	1.234225	-0.776460	-0.721342
N	-0.007100	-2.707450	-1.106499	N	-0.016933	-2.670054	-1.179123
N	0.728545	-4.844667	-0.234796	N	0.718604	-4.832114	-0.369807
N	2.887739	-5.036170	0.638591	N	2.892798	-5.059896	0.456630
C	-8.346569	-4.570646	0.281443	C	-8.367551	-4.508605	0.208237
C	-3.446778	2.093534	-0.310555	C	-3.412308	2.123198	-0.190849
C	-2.295722	4.042941	-0.558871	C	-2.255149	4.074514	-0.399154
C	-1.219535	1.932915	0.080829	C	-1.177584	1.939955	0.148265
C	0.150709	3.928546	-0.310157	C	0.195712	3.940427	-0.209671
C	-0.953998	5.881185	-0.730703	C	-0.907051	5.910489	-0.544813
C	1.046657	1.881401	0.136251	C	1.089032	1.877004	0.158050
C	-4.782837	0.053057	-0.626056	C	-4.768790	0.100551	-0.540382
C	2.219564	-0.280169	0.064611	C	2.249595	-0.286855	0.006259
C	-3.705782	-1.890341	-1.066349	C	-3.718676	-1.832446	-1.071931
C	-6.018559	-1.825389	-0.286521	C	-6.025975	-1.773746	-0.247446
C	-7.102016	-3.854082	0.007748	C	-7.101986	-3.777747	-0.044084
C	-4.856388	-3.977873	-0.488732	C	-4.864239	-3.920206	-0.521075

C	-2.638598	-3.882053	-1.027497
C	3.204120	-2.261021	0.604282
C	1.070194	-2.114303	-0.591732
C	-0.167066	-3.994929	-0.784914
C	1.891191	-4.297062	0.154118
C	3.991926	-4.356997	1.044098
H	-1.722142	7.743989	-1.109254
H	0.040504	7.662988	-0.929176
H	5.860495	-4.661581	1.831044
H	4.915006	-6.127443	1.509498
H	-1.498845	-5.540837	-0.700463
H	3.076653	1.577658	0.422334
H	-5.517386	1.980844	-0.404993
C	-9.602373	-3.903665	0.530969
C	-8.307086	-5.987849	0.303018
C	-9.440185	-6.747376	0.555989
C	-9.396862	-8.249229	0.578849
C	-10.675170	-6.094030	0.799252
C	-10.750420	-4.714117	0.786735
N	-9.723668	-2.553341	0.527662
H	-10.620928	-2.124728	0.733602
H	-8.868351	-2.001425	0.359900
H	-11.708785	-4.216565	0.977030
H	-11.575146	-6.684897	1.000384
H	-7.342796	-6.465627	0.114365
F	-8.144503	-8.745170	0.370336
F	-10.215827	-8.794989	-0.380981
F	-9.838696	-8.749053	1.780709
Model c			
N	-4.672582	1.458513	-0.526252
N	-3.460589	3.422077	-0.691461
N	-1.107021	3.283860	-0.349563
N	-2.438855	1.367692	0.091298
N	0.264449	5.212102	-0.576086
N	4.116553	-3.074747	1.139642
N	-1.507841	-4.579871	-0.954823
N	-0.804545	7.198583	-0.998256
N	4.914733	-5.183221	1.570031
N	-2.161640	5.353268	-0.853673
N	-0.136208	1.232267	0.348577
N	1.263444	3.145692	-0.158197

C	-2.655694	-3.827506	-1.083849
C	3.230319	-2.286858	0.478565
C	1.074791	-2.096884	-0.671652
C	-0.180949	-3.963170	-0.884204
C	1.892464	-4.302239	0.008667
C	4.010253	-4.398178	0.854161
H	-1.672068	7.787700	-0.851448
H	0.093772	7.691929	-0.714930
H	5.890546	-4.734223	1.599525
H	4.927557	-6.185440	1.264409
H	-1.521972	-5.500161	-0.808110
H	3.122830	1.554874	0.401921
H	-5.484010	2.025116	-0.247997
C	-9.657324	-3.984905	-0.299982
C	-8.312175	-5.682459	0.908341
C	-9.517308	-6.393981	1.281918
C	-9.440568	-7.567983	1.974088
C	-10.806239	-5.819780	0.921321
C	-10.859785	-4.673879	0.193334
N	-9.654045	-3.031494	-1.187137
H	-10.631457	-2.810448	-1.449563
F	-8.307082	-8.157733	2.342246
H	-11.831334	-4.251413	-0.092687
H	-11.721925	-6.329836	1.238011
H	-7.335689	-6.072783	1.210355
F	-10.496884	-8.277899	2.366221
Model d			
N	-4.608488	1.470723	-0.467447
N	-3.422156	3.445833	-0.675271
N	-1.061884	3.337489	-0.370775
N	-2.365530	1.413884	0.119577
N	0.284778	5.276266	-0.650393
N	4.243024	-2.946295	1.132732
N	-1.379796	-4.532328	-0.907984
N	-0.812204	7.243989	-1.088660
N	5.065502	-5.041304	1.581783
N	-2.146961	5.387720	-0.889045
N	-0.057710	1.306836	0.341614
N	1.312668	3.227811	-0.214789
N	2.251545	1.152965	0.186749
N	-3.669667	-0.529168	-1.142032

N	2.173615	1.054860	0.224915	N	-4.807150	-2.516030	-0.528724
N	-3.752146	-0.550828	-1.199252	N	-5.913160	-0.433849	-0.227571
N	-4.912891	-2.524148	-0.584516	N	-7.092439	-2.431226	0.063481
N	-6.002544	-0.430602	-0.305495	N	-5.949036	-4.556026	-0.109802
N	-7.201111	-2.415138	-0.006584	N	-3.654658	-4.594621	-0.564214
N	-6.074480	-4.550088	-0.150254	N	-2.570880	-2.563238	-1.323217
N	-3.782662	-4.614766	-0.611733	N	3.307071	-0.859192	0.651107
N	-2.675548	-2.597576	-1.375359	N	2.092768	-2.838740	0.131024
N	3.204612	-0.972888	0.675736	N	1.271787	-0.760070	-0.661493
N	1.975440	-2.934162	0.122595	N	0.040815	-2.680766	-1.057366
N	1.182313	-0.838726	-0.653622	N	0.773522	-4.799916	-0.140040
N	-0.067218	-2.741513	-1.076636	N	2.932979	-4.976174	0.736044
N	0.638734	-4.878694	-0.180565	C	-8.303108	-4.502945	0.370384
N	2.789960	-5.086778	0.708364	C	-3.392043	2.140958	-0.345698
C	-8.424903	-4.472898	0.344744	C	-2.238677	4.082484	-0.642789
C	-3.449720	2.112850	-0.379018	C	-1.163301	1.985819	0.039974
C	-2.271017	4.045529	-0.629754	C	0.208776	3.969465	-0.403770
C	-1.229164	1.927594	0.039426	C	-0.894621	5.913638	-0.864751
C	0.170748	3.902333	-0.352308	C	1.103100	1.931927	0.087047
C	-0.904450	5.865629	-0.798915	C	-4.730460	0.095160	-0.612931
C	1.035414	1.847729	0.120632	C	2.272507	-0.232406	0.059293
C	-4.809556	0.085645	-0.678323	C	-3.657846	-1.857094	-1.021729
C	2.181800	-0.329315	0.081757	C	-5.968590	-1.774778	-0.235736
C	-3.755117	-1.878701	-1.077055	C	-7.059389	-3.796137	0.088987
C	-6.069180	-1.770313	-0.305146	C	-4.812700	-3.932515	-0.407980
C	-7.175749	-3.778549	0.042425	C	-2.594425	-3.849385	-0.949138
C	-4.931982	-3.939669	-0.455666	C	3.254123	-2.202874	0.640773
C	-2.713553	-3.882503	-0.998145	C	1.118951	-2.078475	-0.555779
C	3.138933	-2.315913	0.648937	C	-0.121987	-3.960765	-0.707836
C	1.014556	-2.156401	-0.562533	C	1.936926	-4.245931	0.236204
C	-0.244704	-4.023848	-0.743041	C	4.038317	-4.290142	1.125858
C	1.804979	-4.340870	0.210286	H	-1.661016	7.767875	-1.286374
C	3.898913	-4.416454	1.115040	H	0.102379	7.687802	-1.113851
H	-1.644855	7.735810	-1.196447	H	5.906803	-4.580159	1.918722
H	0.114477	7.633870	-0.995440	H	4.958964	-6.051411	1.630315
H	5.757706	-4.734776	1.919717	H	-1.454513	-5.502497	-0.591227
H	4.797266	-6.192672	1.606272	H	3.133716	1.631061	0.374451
H	-1.595800	-5.550343	-0.641928	H	-5.461947	2.029648	-0.436339
H	3.058572	1.521202	0.428554	C	-9.552701	-3.827511	0.628010
H	-5.519772	2.026952	-0.495207	C	-8.280281	-5.924230	0.384826
C	-9.676569	-3.785696	0.562604	C	-9.407075	-6.688295	0.657962

C	-8.395496	-5.888071	0.437484	C	-9.361142	-8.189375	0.669024
C	-9.531545	-6.633260	0.727211	C	-10.631616	-6.012559	0.909128
C	-9.469181	-8.138470	0.793028	C	-10.702223	-4.631460	0.894018
C	-10.759197	-5.956883	0.935951	N	-9.667975	-2.475034	0.623031
C	-10.827162	-4.576482	0.855209	H	-10.562347	-2.043129	0.833957
N	-9.789074	-2.434817	0.496502	H	-8.813921	-1.926531	0.442550
H	-10.683505	-1.992106	0.683445	H	-11.656925	-4.126898	1.086854
H	-8.929135	-1.895408	0.316557	H	-11.538338	-6.596409	1.107203
H	-11.781611	-4.064741	1.027943	H	-7.318309	-6.401714	0.173590
H	-11.660002	-6.530858	1.177667	F	-10.265611	-8.722101	-0.286069
H	-7.430414	-6.377367	0.282641	H	-8.348591	-8.557622	0.422894
F	-10.407863	-8.622071	1.698311	H	-9.667894	-8.599929	1.650905
F	-8.218921	-8.561152	1.213292				
H	-9.670969	-8.642829	-0.172699				

Model e

N	-4.609948	1.467740	-0.475429	H	3.130916	1.630340	0.378668
N	-3.424067	3.443654	-0.677857	H	-5.463603	2.026371	-0.444502
N	-1.064377	3.336005	-0.368692	C	-9.553217	-3.833260	0.617608
N	-2.367949	1.410762	0.115334	C	-8.257879	-5.929525	0.404150
N	0.281754	5.276175	-0.641161	C	-9.400656	-6.655334	0.668704
N	4.243723	-2.946886	1.131092	H	-7.302651	-6.427067	0.217955
N	-1.378190	-4.534444	-0.910295	C	-10.634556	-6.021833	0.913773
N	-0.815526	7.244389	-1.076474	C	-10.701058	-4.636444	0.887313
N	5.067901	-5.041887	1.577372	N	-9.673283	-2.478180	0.598845
N	-2.149550	5.386762	-0.884635	H	-10.567577	-2.046977	0.809594
N	-0.060464	1.304345	0.341222	H	-8.819433	-1.928876	0.423946
N	1.309920	3.227183	-0.208672	H	-11.657910	-4.135953	1.077044
N	2.249198	1.151964	0.189549	H	-11.523799	-6.626457	1.122131
N	-3.669831	-0.532229	-1.148414	F	-9.352165	-8.021043	0.698523
N	-4.806376	-2.518925	-0.532550				
N	-5.914651	-0.436967	-0.237305				
N	-7.092775	-2.434552	0.056614				
N	-5.947033	-4.558972	-0.110458				
N	-3.652830	-4.597051	-0.565863				
N	-2.570048	-2.565990	-1.327144				
N	3.305998	-0.859917	0.652115				
N	2.093503	-2.839813	0.129274				
N	1.271284	-0.760918	-0.661371				
N	0.041431	-2.682011	-1.058893				
N	0.775788	-4.801684	-0.144153				

N	2.935520	-4.977364	0.731344
C	-8.299783	-4.507348	0.370820
C	-3.393905	2.138211	-0.350466
C	-2.241011	4.080906	-0.641553
C	-1.165800	1.983419	0.039062
C	0.206024	3.968698	-0.397871
C	-0.897570	5.913379	-0.856255
C	1.100535	1.930457	0.089889
C	-4.731417	0.092180	-0.621031
C	2.271238	-0.233349	0.060470
C	-3.657360	-1.860028	-1.026443
C	-5.968950	-1.777846	-0.242705
C	-7.056611	-3.798744	0.086752
C	-4.810638	-3.935336	-0.409664
C	-2.592834	-3.851799	-0.951695
C	3.254246	-2.203685	0.640033
C	1.119232	-2.079563	-0.556840
C	-0.120460	-3.962527	-0.710572
C	1.938793	-4.247294	0.232679
C	4.040203	-4.290955	1.122275
H	-1.664344	7.768450	-1.273657
H	0.098758	7.689015	-1.097678
H	5.908694	-4.580544	1.915297
H	4.962028	-6.052132	1.624730
H	-1.452741	-5.504640	-0.593387

8.8 XANES and EXAFS

X-ray absorption spectra at the Fe K-edge (7112 eV) were collected in fluorescence mode at the ASTRA beamline of the SOLARIS National Synchrotron Radiation Centre. The experiment setup employed a Si (111) double-crystal monochromator, ensuring high energy resolution and minimizing harmonic contamination. To achieve accurate energy calibration, the absorption spectrum of a metallic Fe foil was measured at the Fe K-edge. Fe@f-gC_3N_4 and Fe@f-gC_3N_4_post samples were prepared by pressing a suitable amount of material into 1.3 cm diameter pellets under controlled pressure. Prior to spectral acquisition, the sample chamber was evacuated to a base pressure of 0 Pa to eliminate interference from ambient gases, after which it was backfilled with high-purity N_2 gas to provide an inert atmosphere and prevent sample oxidation or contamination during measurements. X-ray signal extraction and normalization were carried out using the ATHENA software, while the Fourier transform extended X-ray absorption fine-structure (FT-EXAFS) spectra were analyzed by Artemis, and both are part of the IFEFFIT suite of interactive programs (*72*).

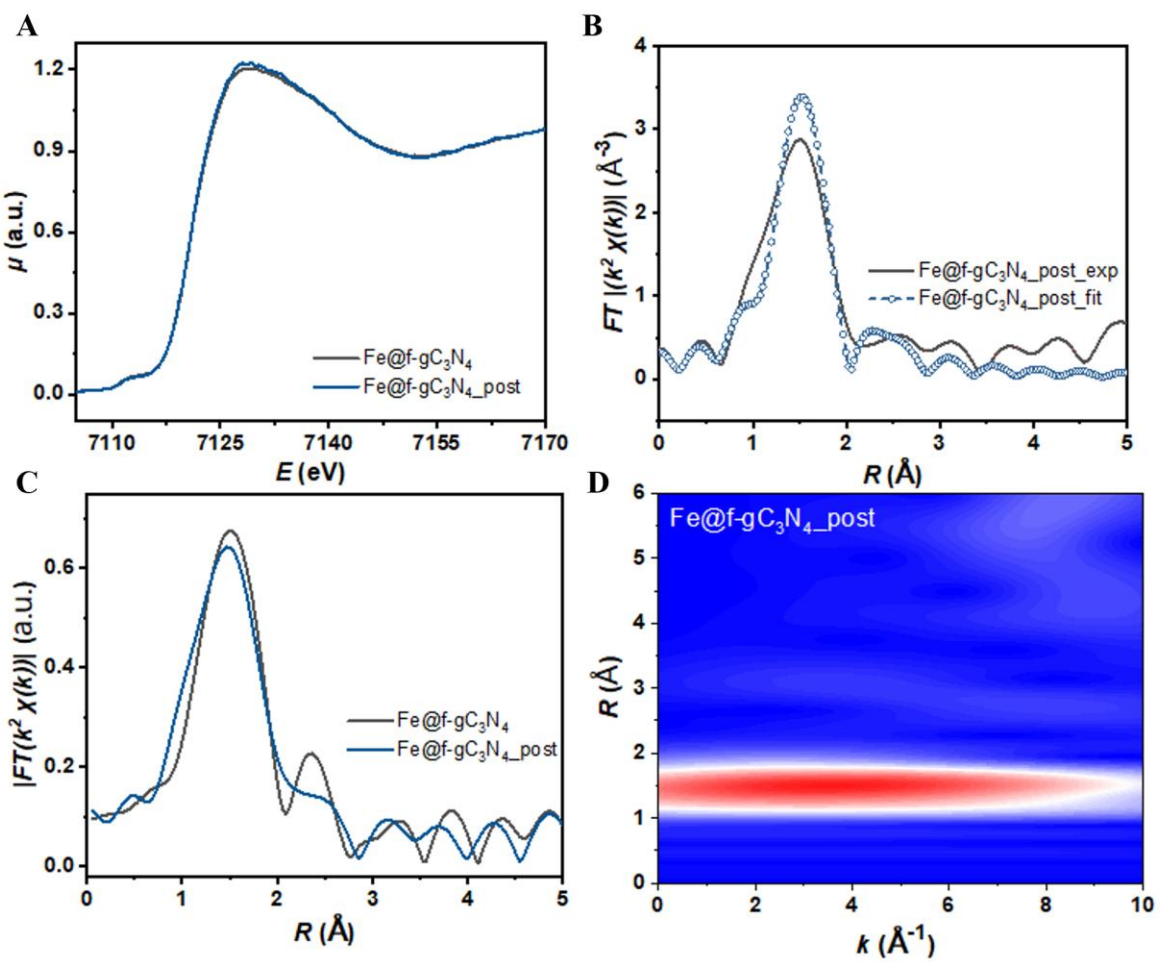

Fig. S41. (**A**) Normalized Fe K-edge XANES spectra, (**B**) corresponding fitting curves of FT-EXAFS spectra of Fe@f-gC_3N_4_post in R space. (**C**) k^3-weighted FT spectra of Ni in R spaces. (**D**) Wavelet transforms the k^3-weighted EXAFS spectrum of Fe@f-gC_3N_4_post

Table S7. Fitting parameters from the EXAFS analysis

Sample	Paths	Coordination number	Radical distance	Debye-factor	ΔE	R^2
Fe@ f-gC_3N_4	Fe-N/O	3.06 ± 0.19	2.020 ± 0.01	0.009	-1.52	0.015
	Fe-Fe	0.20	2.912 ± 0.03	0.009		
Fe@ f-C_3N_4_post	Fe-N/O	2.83 ± 0.31	1.994 ± 0.02	0.009	-1.08	0.02
	Fe-Fe	0.32	2.963 ± 0.10	0.009		

9. Density functional theory

We used the Gaussian 16 program (*73*) for optimizing the molecular adducts in acetonitrile solution (in agreement with the experiments) at the density functional theory (DFT) level with the B3LYP hybrid functional, the Grimme DFT-D3(BJ) empirical dispersion, the 6-31G(d,p) basis set for the C, N, O, F, and H atoms, and the def2-TZVPD basis set (*74*) for the metal center (Fe). Acetonitrile (ε = 35.69) was described as a continuum through the SMD approach (*75*). Saddle points were located using the Synchronous Transit-Guided Quasi-Newton (STQN) method (*76*).

We reproduced possible reaction pathways and activation energy barriers (saddle points) through the nudged elastic band (NEB) approach available in the Quantum Espresso package (*77*). Projector Augmented-Wave (PAW) pseudopotentials (*78*) and the generalized gradient

approximation (GGA) with the Perdew–Burke–Ernzerhof (PBE) functional (*79*) were used. Dispersion corrections were added according to the Grimme-D3 parametrization implemented in the QE package (80). Wave function and charge density cutoffs for the plane-wave basis sets of 50 and 500 Ry were employed, respectively. Single-particle wave functions were calculated spin-unrestricted by applying smearing of the one-particle levels of 0.002 Ry. The NEB calculations were performed considering as reactants and products the optimized geometries obtained with the Gaussian16 software and, depending on the complexity of the mechanism, 9 or 13 intermediate images. Time-dependent DFT (TDDFT) calculations on the optimized geometries at the ground states (70 excitations) were carried out to simulate the UV-vis spectra of the most stable complexes.

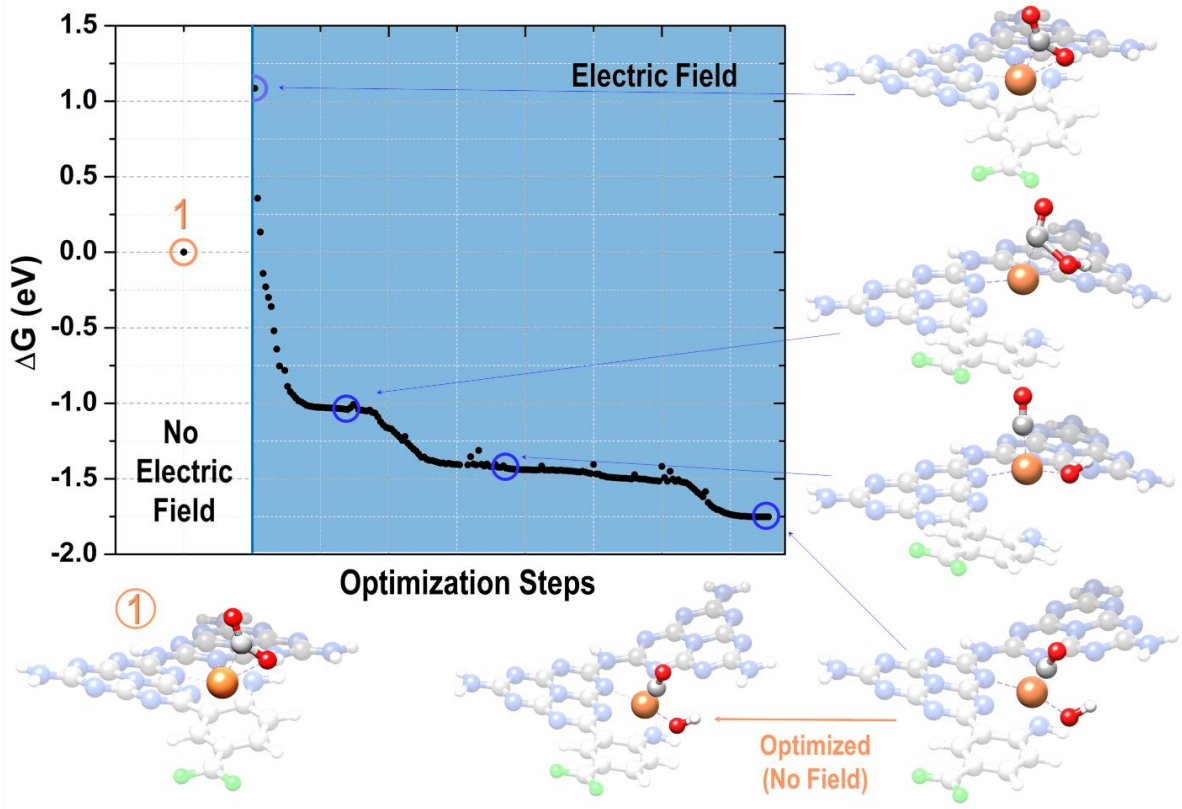

Fig. S42. Reaction pathway of the CO_2 reduction to CO and Fe-OH. In the optimized starting configuration (#1), the CO_2 molecule is adsorbed on the metal ion. The DFT minimum energy structures of the initial and final configurations are shown below the energy plot. The intermediate species sampled during the optimization in the presence of the electric field are displayed on the right of the plot. Color codes: C gray, N blue, F green, Fe orange, O red, H white

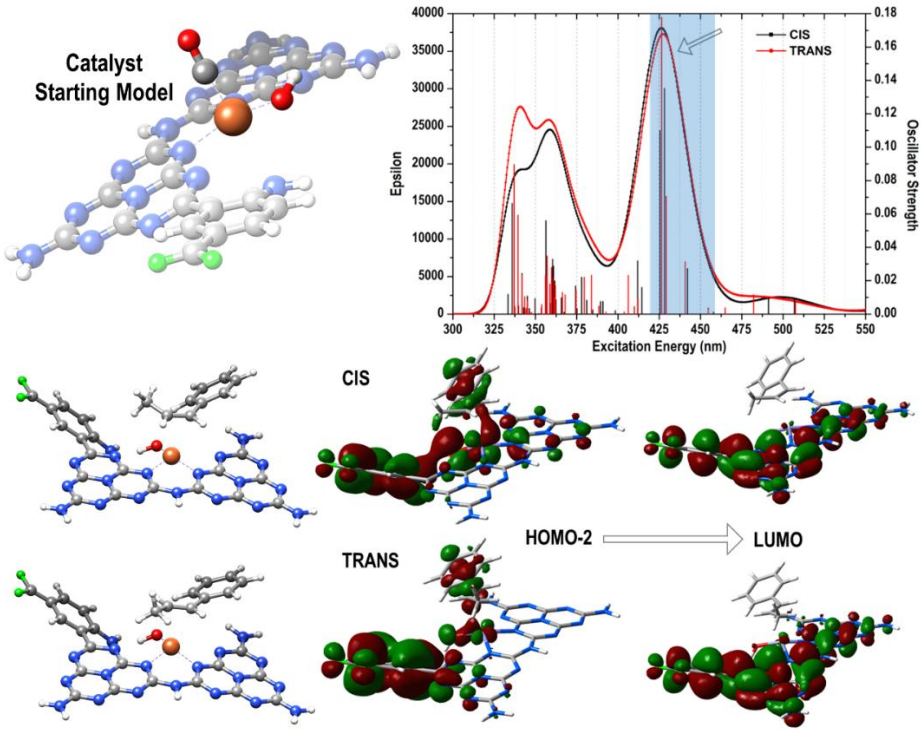

Fig. S43. Structure of the catalyst (top-left) with the Fe center presenting dissociated CO and OH adsorbed on it, as products of CO_2 activation. Simulated structures (bottom-left) and adsorption profiles (top-right) of CIS and TRANS methyl-styrene adsorbed on the Fe center; in the bottom-right panel, two single-particle transitions dominating the range of interest for the experimental light irradiation are shown. Color codes: Fe orange, N blue, C grey, O red, F green, and H white

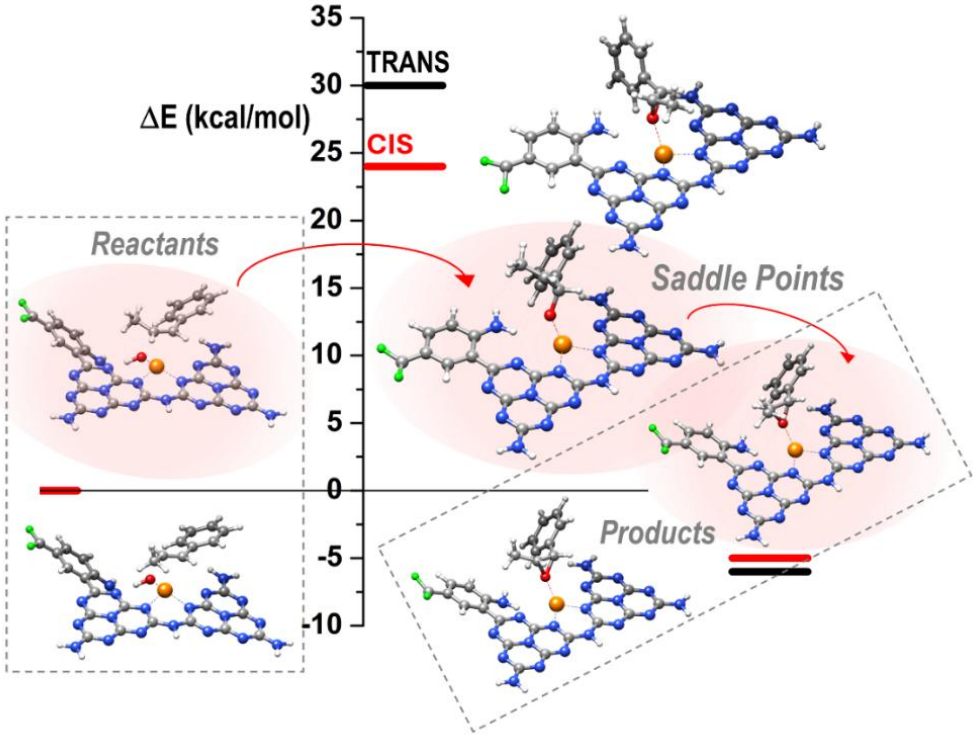

Fig. S44. Process showing the conversion of methyl-styrene to the corresponding epoxide promoted by the catalyst, where the Fe atom carries, initially, an adsorbed OH group. Color codes: Fe orange, N blue, C grey, O red, F green, and H white

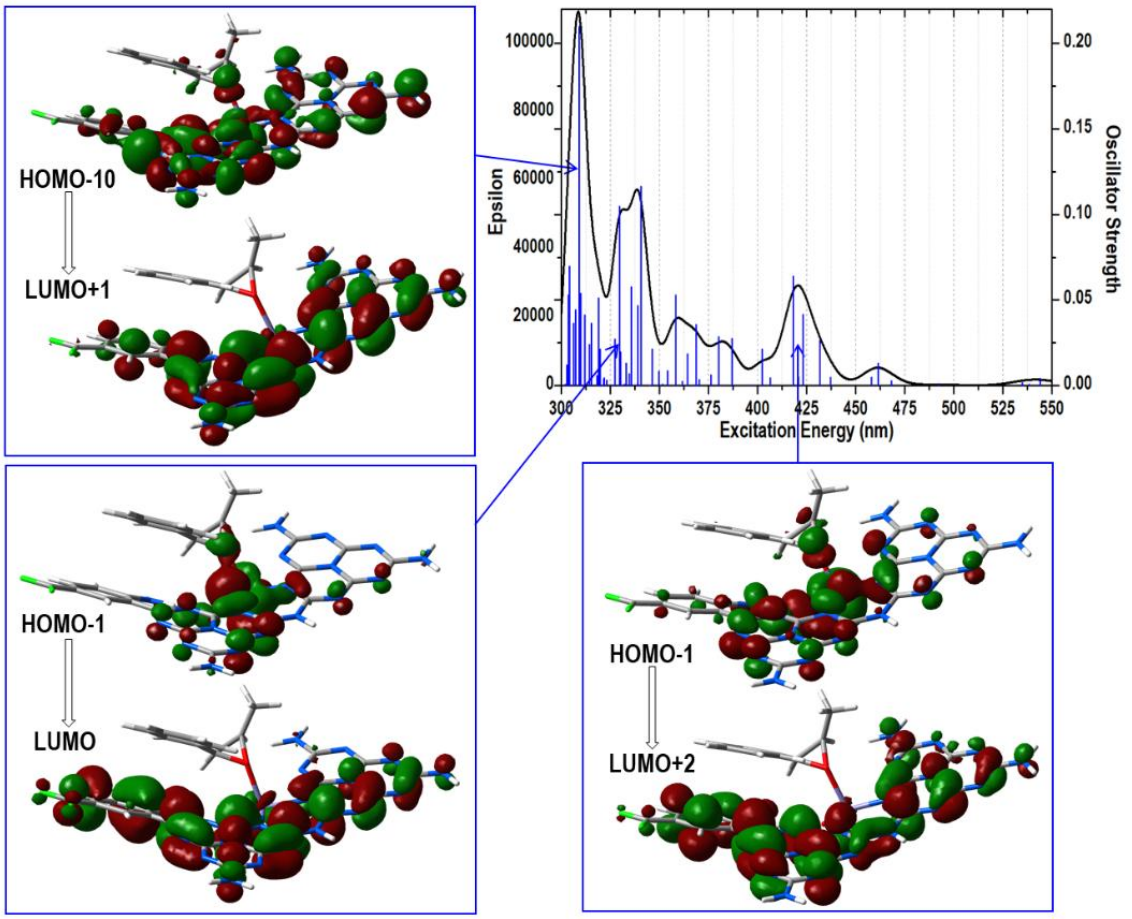

Fig. S45. Simulated adsorption profile of cis-epoxide reporting three main single-particle transitions to highlight the electron transfer process from the adsorbate to the catalyst. Color codes: Fe orange, N blue, C grey, O red, F green, and H white

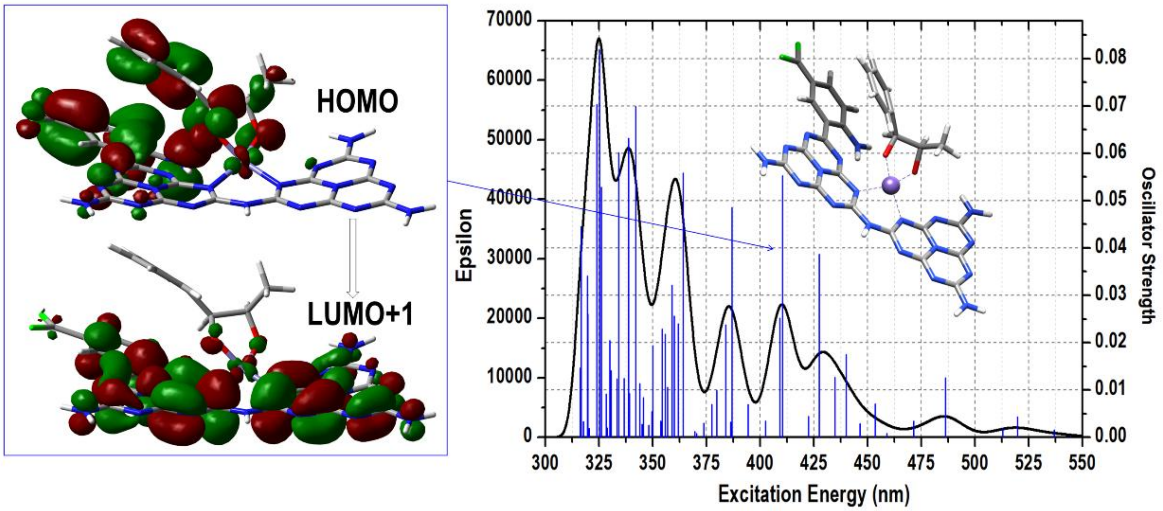

Fig. S46. Simulated adsorption profile of cyclic complex adsorbed on the Fe center consequent to the ring-opening activated by the photo-catalyst. On the left, a single-particle transition shows the electron transfer process from the adsorbate to the catalyst. Color codes: Fe purple, N blue, C grey, O red, F green, and H white

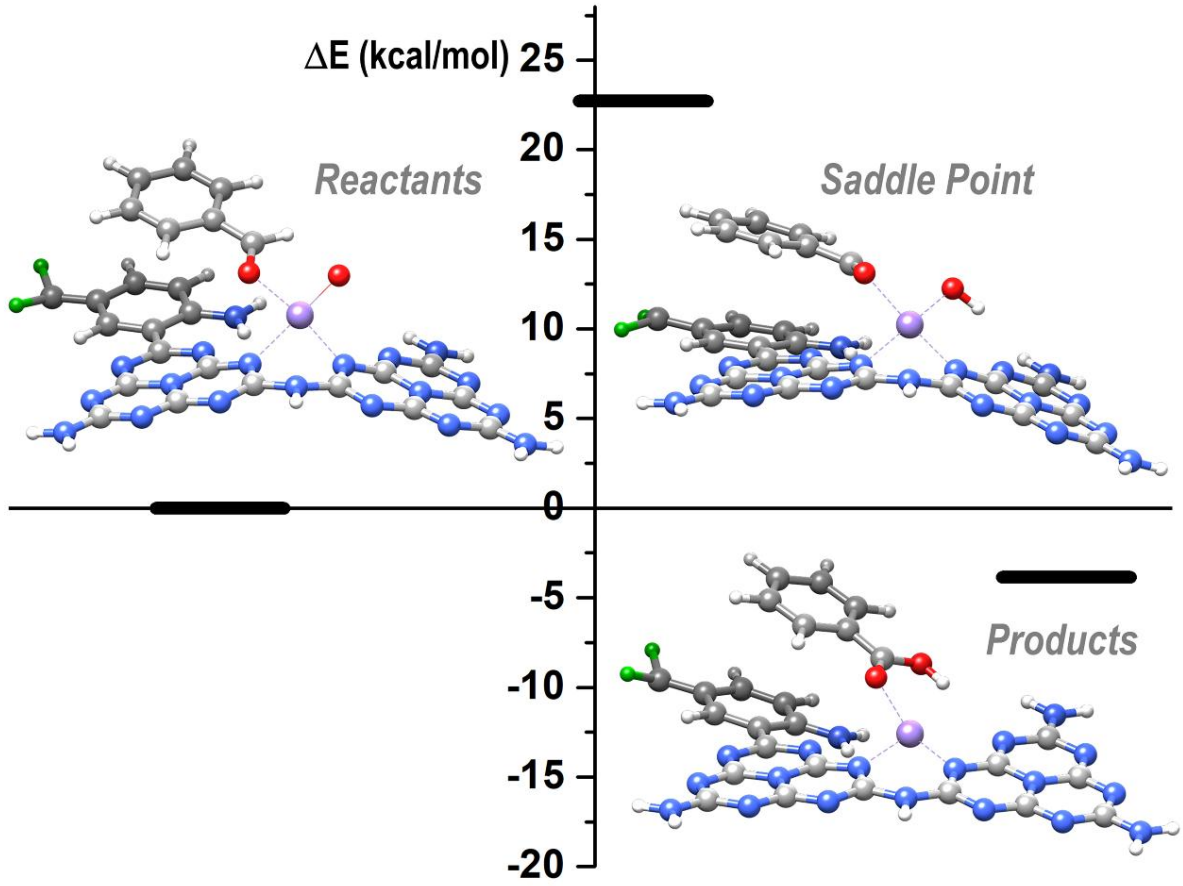

Fig. S47. conversion of benzaldehyde to benzoic acid promoted by the photocatalyst. Color codes: Fe purple, N blue, C grey, O red, F green, and H white

10. Characterization of starting materials and products

(1-cyclobutylvinyl)benzene (1q)

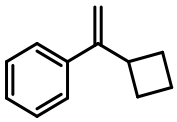

Colorless oil. **^{1}H NMR** (500 MHz, $CDCl_3$) δ 7.40 (d, *J* = 7.1 Hz, 2H), 7.34 (t, *J* = 7.7 Hz, 2H), 7.29 (d, *J* = 7.5 Hz, 1H), 5.22 (d, *J* = 154.4 Hz, 2H), 3.50 (p, *J* = 8.7 Hz, 1H), 2.24 (dq, *J* = 7.4, 4.3, 3.8 Hz, 2H), 2.07 – 1.91 (m, 3H), 1.84 – 1.76 (m, 1H). **^{13}C NMR** (126 MHz, $CDCl_3$) δ 151.97, 140.68, 128.13, 127.19, 126.05, 109.71, 39.53, 28.39, 17.76. Data in accordance with literature (*81*).

2-(hex-1-en-2-yl)thiophene (1x)

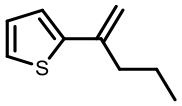

Yellow oil. **^{1}H NMR** (500 MHz, $CDCl_3$) δ 7.17 (dd, J = 5.1, 1.1 Hz, 1H), 7.05 (dd, J = 3.6, 1.1 Hz, 1H), 6.99 (dd, J = 5.1, 3.6 Hz, 1H), 5.41 (d, J = 0.9 Hz, 1H), 4.96 (d, J = 1.2 Hz, 1H), 2.46 (td, J = 7.5, 1.2 Hz, 2H), 1.68 – 1.57 (m, 2H), 0.98 (t, J = 7.3 Hz, 3H). **^{13}C NMR** (126 MHz, $CDCl_3$) δ 145.49, 141.58, 127.24, 123.93, 123.18, 110.74, 37.58, 21.56, 13.84. Data in accordance with literature (*82*).

2-(pent-1-en-2-yl)furan (1y)

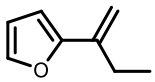

Yellow oil. **^{1}H NMR** (500 MHz, $CDCl_3$) δ 7.37 (d, *J* = 1.7 Hz, 1H), 6.39 (dd, *J* = 3.4, 1.8 Hz, 1H), 6.31 (d, *J* = 3.3 Hz, 1H), 5.54 (s, 1H), 4.99 (t, *J* = 1.5 Hz, 1H), 2.40 (q, *J* = 7.5, 6.9 Hz, 2H), 1.19 (t, *J* = 7.5 Hz, 3H). **^{13}C NMR** (126 MHz, $CDCl_3$) δ 154.80, 141.65, 139.07, 111.00, 107.97, 105.69, 25.82, 12.96. Data in accordance with literature (*83*).

2-(4-(1-phenylvinyl)phenoxy)ethan-1-ol (1ab)

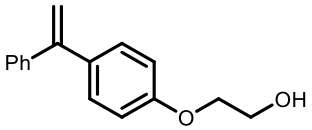

White solid. **^{1}H NMR** (500 MHz, $CDCl_3$) δ 7.83 (d, *J* = 8.3 Hz, 2H), 7.76 (d, *J* = 7.8 Hz, 2H), 7.57 (t, *J* = 7.4 Hz, 1H), 7.48 (t, *J* = 7.6 Hz, 2H), 6.99 (d, *J* = 8.6 Hz, 2H), 4.25 – 4.13 (m, 2H), 4.09 – 3.97 (m, 2H), 2.02 (q, *J* = 6.3 Hz, 1H), 1.57 (d, *J* = 4.4 Hz, 1H). **^{13}C NMR** (126 MHz, $CDCl_3$) δ 158.31, 149.37, 141.69, 134.44, 129.45, 128.27, 128.12, 127.66, 114.11, 113.13, 69.15, 61.49. Data in accordance with literature (*84*).

4-(4-(1-phenylvinyl)phenoxy)butanal (1ac)

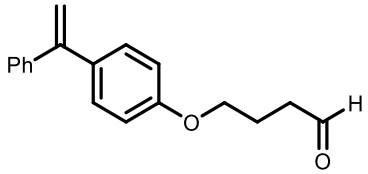

White solid. **^{1}H NMR** (500 MHz, $CDCl_3$) δ 9.85 (t, *J* = 1.3 Hz, 1H), 7.43 – 7.34 (m, 5H), 7.32 (d, *J* = 8.8 Hz, 2H), 6.89 (d, *J* = 8.8 Hz, 2H), 5.45 (d, *J* = 1.2 Hz, 1H), 5.41 (d, *J* = 1.3 Hz, 1H), 4.03 (t, *J* = 6.0 Hz, 2H), 2.68 (td, *J* = 7.1, 1.4 Hz, 2H), 2.19 – 2.11 (m, 2H). **^{13}C NMR** (126 MHz, $CDCl_3$) δ 201.52, 158.26, 149.25, 141.54, 133.89, 129.23, 128.11, 127.96, 127.50, 113.86, 112.82, 66.47, 40.40, 21.81. **HRMS–ESI** (m/z): $[M+H]^+$ calcd. for $C_{18}H_{19}O_2$, 267.1380; found, 267.1376.

1-(pent-2-yn-1-yloxy)-4-(1-phenylvinyl)benzene (1ad)

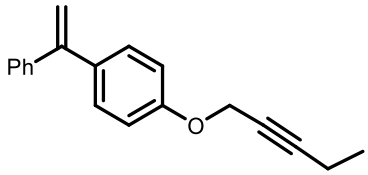

White solid. **^{1}H NMR** (500 MHz, $CDCl_3$) δ 7.39 – 7.32 (m, 5H), 7.14 (dd, J = 173.7, 8.0 Hz, 4H), 5.41 (d, J = 23.3 Hz, 2H), 4.70 (t, J = 2.2 Hz, 2H), 2.27 (qt, J = 7.5, 2.2 Hz, 2H), 1.18 (t, J = 7.4 Hz, 3H). **^{13}C NMR** (126 MHz, $CDCl_3$) δ 154.57, 146.38, 138.69, 131.39, 126.25, 125.26, 125.07, 124.60, 111.40, 110.05, 86.55, 71.12, 53.46, 10.57, 9.48. **HRMS–ESI** (m/z): $[M+H]^+$ calcd. for $C_{19}H_{19}O$, 263.1430; found, 263.1428.

3-methylbut-3-en-1-yl benzoate (1ae)

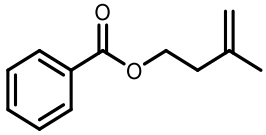

Colorless oil. **^{1}H NMR** (500 MHz, $CDCl_3$) δ 8.03 (d, *J* = 8.1 Hz, 2H), 7.54 (t, *J* = 7.9 Hz, 1H), 7.42 (t, *J* = 7.7 Hz, 2H), 4.83 (d, *J* = 12.9 Hz, 2H), 4.43 (t, *J* = 6.8 Hz, 2H), 2.52 – 2.44 (m, 2H), 1.81 (s, 3H). **^{13}C NMR** (126 MHz, $CDCl_3$) δ 166.49, 141.65, 132.80, 130.30, 129.49,

128.27, 112.37, 63.09, 36.75, 22.49. Data in accordance with literature (*85*).

2-(3-methylbut-3-en-1-yl)isoindoline-1,3-dione (1af)

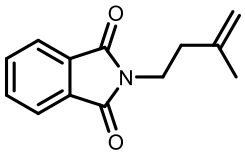

Colorless oil. **^{1}H NMR** (500 MHz, $CDCl_3$) δ 7.81 (dd, *J* = 5.4, 3.1 Hz, 2H), 7.69 (dd, *J* = 5.5, 3.0 Hz, 2H), 4.69 (d, *J* = 32.0 Hz, 2H), 3.81 (t, *J* = 7.2 Hz, 2H), 2.38 (t, *J* = 6.9 Hz, 2H), 1.79 (s, 3H). **^{13}C NMR** (126 MHz, $CDCl_3$) δ 168.22, 142.07, 133.79, 132.02, 123.10, 112.71, 36.38, 36.31, 21.98. Data in accordance with literature (*86*).

triisopropyl((3-methylbut-3-en-2-yl)oxy)silane (1ag)

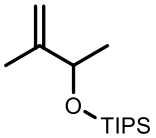

Colourless oil. **^{1}H NMR** (500 MHz, $CDCl_3$) δ 4.91 (d, *J* = 1.2 Hz, 1H), 4.71 (t, *J* = 1.8 Hz, 1H), 4.32 (q, *J* = 6.3 Hz, 1H), 1.72 (s, 3H), 1.25 (d, *J* = 6.4 Hz, 3H), 1.08 – 1.01 (m, 21H). **^{13}C NMR** (126 MHz, $CDCl_3$) δ 149.51, 108.90, 72.42, 23.69, 18.06, 18.05, 17.28, 12.30. **HRMS–ESI** (m/z): $[M+H]^+$ calcd. for $C_{14}H_{31}OSi$, 243.2138; found, 243.2143.

6-methyleneundecane (1ah)

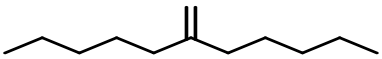

Colourless oil. **^{1}H NMR** (500 MHz, $CDCl_3$) δ 4.71 (d, *J* = 1.3 Hz, 2H), 2.01 (t, *J* = 7.8 Hz, 4H), 1.48 – 1.39 (m, 4H), 1.39 – 1.24 (m, 8H), 0.91 (t, *J* = 7.1 Hz, 6H). **^{13}C NMR** (126 MHz, $CDCl_3$) δ 150.26, 108.38, 36.09, 31.75, 27.57, 22.67, 14.07.

Methylenecyclododecane (1an)

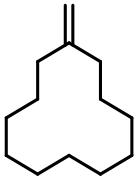

Colourless oil. **^{1}H NMR** (500 MHz, $CDCl_3$) δ 4.85 – 4.74 (m, 2H), 2.06 (t, *J* = 6.3 Hz, 4H), 1.57 – 1.46 (m, 4H), 1.38 – 1.23 (m, 14H). **^{13}C NMR** (126 MHz, $CDCl_3$) δ 147.45, 110.30, 33.04, 24.43, 24.12, 23.69, 23.24, 22.59. Data in accordance with literature (*87*).

***tert*-butyl 6-methylene-2-azaspiro[3.3]heptane-2-carboxylate (1ao)**

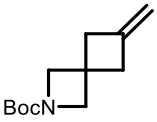

White solid. **^{1}H NMR** (500 MHz, $CDCl_3$) δ 4.80 (p, *J* = 2.4 Hz, 2H), 3.92 (s, 4H), 2.84 (t, *J* = 2.4 Hz, 4H), 1.43 (s, 9H). **^{13}C NMR** (126 MHz, $CDCl_3$) δ 156.24, 142.84, 107.18, 79.30, 42.85, 33.06, 28.37. **HRMS–ESI** (m/z): $[M+H]^+$ calcd. for $C_{12}H_{20}NO_2$, 210.1489; found, 210.1489.

***tert*-butyl 2-methylene-7-azaspiro[3.5]nonane-7-carboxylate (1ap)**

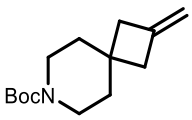

White solid. **^{1}H NMR** (500 MHz, $CDCl_3$) δ 4.82 (s, 2H), 3.31 (s, 4H), 2.41 (s, 4H), 1.54 (s, 4H), 1.44 (s, 9H). **^{13}C NMR** (126 MHz, $CDCl_3$) δ 154.91, 144.46, 144.44, 107.65, 79.23, 41.71, 36.54, 33.59, 28.42. **HRMS–ESI** (m/z): $[M+Na]^+$ calcd. for $C_{14}H_{23}NO_2Na$, 260.1621; found, 260.1650.

3-methylbut-3-en-1-yl (tert-butoxycarbonyl)tryptophanate (1aq)

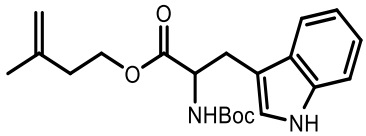

White solid. **^{1}H NMR** (500 MHz, $CDCl_3$) δ 8.18 (br, 1H), 7.56 (d, *J* = 7.8 Hz, 1H), 7.35 (d, *J* = 8.1 Hz, 1H), 7.19 (t, *J* = 7.6 Hz, 1H), 7.12 (d, *J* = 7.0 Hz, 1H), 7.00 (s, 1H), 5.08 (d, *J* = 7.8 Hz, 1H), 4.78 (s, 1H), 4.68 (s, 1H), 4.64 (dt, *J* = 8.2, 5.6 Hz, 1H), 4.17 (dt, *J* = 6.9, 3.5 Hz, 2H), 3.28 (qd, *J* = 14.8, 5.7 Hz, 2H), 2.25 (t, *J* = 7.0 Hz, 2H), 1.71 (s, 3H), 1.43 (s, 9H). **^{13}C NMR** (126 MHz, $CDCl_3$) δ 172.28, 155.21, 141.29, 136.05, 127.68, 122.67, 122.12, 119.52, 118.75, 112.43, 111.10, 110.25, 79.75, 63.52, 54.20, 36.40, 28.30, 27.99, 22.45. **HRMS–ESI** (m/z): $[M+Na]^+$ calcd. for $C_{21}H_{28}N_2O_4Na$, 395.1941; found, 395.1936.

3-methylbut-3-en-1-yl 2-(1,3-dioxo-2,3-dihydro-1H-inden-2-yl)-3-phenylpropanoate (1ar)

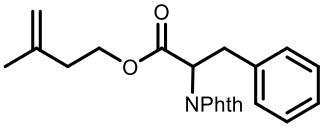

White solid. **^{1}H NMR** (500 MHz, $CDCl_3$) δ 7.73 (dd, *J* = 5.5, 3.1 Hz, 2H), 7.63 (dd, *J* = 5.5, 3.1 Hz, 2H), 7.16 (d, *J* = 4.5 Hz, 4H), 7.13 – 7.07 (m, 1H), 5.16 (dd, *J* = 11.2, 5.4 Hz, 1H), 4.61 (d, *J* = 13.1 Hz, 2H), 4.28 (td, *J* = 6.7, 3.6 Hz, 2H), 3.66 – 3.47 (m, 2H), 2.33 – 2.27 (m, 2H), 1.66 (s, 3H). **^{13}C NMR** (126 MHz, $CDCl_3$) δ 168.56, 167.22, 140.82, 136.59, 133.84, 131.35, 128.60, 128.31, 126.59, 123.14, 112.36, 63.63, 53.12, 36.28, 34.35, 21.95. **HRMS–ESI** (m/z): $[M+H]^+$ calcd. for $C_{22}H_{22}NO_4$, 364.1544; found, 364.1540.

(*E*)-hex-3-en-1-yl benzoate (1as)

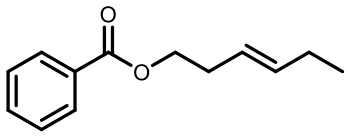

Colourless oil. **^{1}H NMR** (500 MHz, $CDCl_3$) δ 8.04 (dd, *J* = 8.3, 1.4 Hz, 2H), 7.59 – 7.51 (m, 1H), 7.44 (dd, *J* = 8.3, 7.1 Hz, 2H), 5.72 – 5.55 (m, 1H), 5.52 – 5.36 (m, 1H), 4.32 (t, *J* = 6.8 Hz, 2H), 2.46 (dddd, *J* = 8.1, 6.9, 5.7, 1.2 Hz, 2H), 2.03 (qdd, *J* = 7.5, 6.3, 1.3 Hz, 2H), 0.97 (t, *J* = 7.5 Hz, 3H). **^{13}C NMR** (126 MHz, $CDCl_3$) δ 166.53, 135.18, 132.76, 130.40, 129.49, 128.25, 124.01, 64.56, 32.01, 25.62, 13.71. Data in accordance with literature (*88*).

(*E*)-1,3-dichloro-2-(hex-3-en-1-yloxy)benzene (1at)

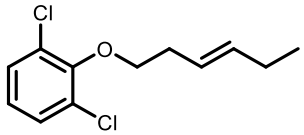

Colourless oil. **^{1}H NMR** (500 MHz, $CDCl_3$) δ 7.28 (d, *J* = 8.1 Hz, 2H), 6.97 (t, *J* = 8.1 Hz, 1H), 5.70 – 5.60 (m, 1H), 5.58 – 5.48 (m, 1H), 4.03 (t, *J* = 7.0 Hz, 2H), 2.56 (q, *J* = 6.9 Hz, 2H), 2.04 (p, *J* = 7.4 Hz, 2H), 0.99 (t, *J* = 7.5 Hz, 3H). **^{13}C NMR** (126 MHz, $CDCl_3$) δ 151.66, 134.80, 129.57, 128.83, 124.84, 124.21, 73.35, 33.26, 25.62, 13.67. **HRMS–ESI** (m/z): $[M+H]^+$ calcd. for $C_{12}H_{15}OCl_2$, 245.0494; found, 245.0498.

isopropyl 2-(4-(1-(4-chlorophenyl)vinyl)phenoxy)-2-methylpropanoate (1au)

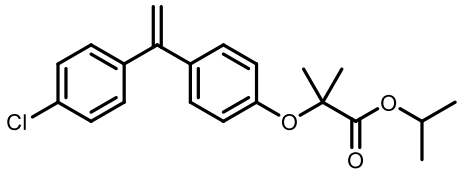

White solid. ^{1}H NMR (500 MHz, $CDCl_3$) δ 7.35 – 7.26 (m, 4H), 7.21 (d, *J* = 8.7 Hz, 2H), 6.83 (d, *J* = 8.7 Hz, 2H), 5.42 (d, *J* = 1.2 Hz, 1H), 5.36 (d, *J* = 1.2 Hz, 1H), 5.12 (p, *J* = 6.3 Hz, 1H), 1.64 (s, 6H), 1.26 (s, 3H), 1.25 (s, 3H). **^{13}C NMR** (126 MHz, $CDCl_3$) δ 173.54, 155.40, 148.24, 140.08, 134.33, 133.41, 129.53, 128.81, 128.22, 118.25, 113.52, 79.00, 68.91, 25.32, 21.49. Data in accordance with literature (*23*).

1-benzyl-4-((5,6-dimethoxy-1-methylene-2,3-dihydro-1H-inden-2-yl)methyl)piperidine (1av)

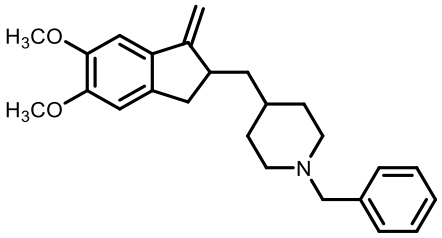

White solid. **^{1}H NMR** (500 MHz, $CDCl_3$) δ 7.34 – 7.29 (m, 4H), 7.26 – 7.22 (m, 1H), 6.94 (s, 1H), 6.73 (s, 1H), 5.27 (d, *J* = 2.3 Hz, 1H), 4.83 (d, *J* = 1.8 Hz, 1H), 3.89 (s, 3H), 3.87 (s, 3H), 3.51 (s, 2H), 3.13 – 2.99 (m, 2H), 2.90 (td, *J* = 9.8, 9.3, 3.7 Hz, 2H), 2.56 (dd, *J* = 15.0, 3.4 Hz, 1H), 1.96 (tdd, *J* = 11.6, 6.3, 2.7 Hz, 2H), 1.76 (dt, *J* = 12.9, 3.0 Hz, 1H), 1.70 – 1.63 (m, 2H), 1.58 (ddd, *J* = 13.0, 8.2, 4.6 Hz, 1H), 1.50 – 1.16 (m, 5H). **^{13}C NMR** (126 MHz, $CDCl_3$) δ 155.20, 150.11, 148.49, 138.52, 137.51, 133.02, 129.23, 128.10, 126.86, 107.48, 103.04, 99.87, 63.54, 55.94, 53.93, 53.89, 43.04, 40.81, 37.13, 33.74, 33.33, 31.80. Data in accordance with literature (*89*).

cyclohexyl 2-(4-((2-methylenecyclopentyl)methyl)phenyl)propanoate (1ax)

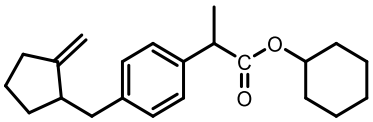

Colourless oil. **^{1}H NMR** (500 MHz, $CDCl_3$) δ 7.21 (d, *J* = 8.1 Hz, 2H), 7.13 (d, *J* = 8.0 Hz, 2H), 4.91 (s, 1H), 4.81 (s, 1H), 4.79 – 4.72 (m, 1H), 3.66 (q, *J* = 7.2 Hz, 1H), 2.93 (dd, *J* = 13.5, 5.1 Hz, 1H), 2.61 (dtdd, *J* = 9.4, 7.2, 4.8, 2.2 Hz, 1H), 2.44 (dd, *J* = 13.6, 9.8 Hz, 1H), 2.40 – 2.31 (m, 2H), 1.86 – 1.75 (m, 1H), 1.76 – 1.62 (m, 5H), 1.62 – 1.53 (m, 1H), 1.48 (d, *J* = 7.2 Hz, 3H), 1.46 – 1.41 (m, 1H), 1.38 – 1.20 (m, 6H). **^{13}C NMR** (500 MHz, $CDCl_3$) δ 174.13, 156.20, 140.05, 138.21, 129.04, 127.20, 104.62, 72.49, 45.57, 45.38, 40.35, 33.25, 32.54, 31.40, 31.16, 25.36, 23.93, 23.48, 23.36, 18.40, 18.38. **HRMS–ESI** (m/z): $[M+H]^+$ calcd. for $C_{22}H_{31}O_2$, 327.2319; found, 327.2314.

1-(4-chlorophenyl)-4-(4-(4-fluorophenyl)pent-4-en-1-yl)cyclohexan-1-ol (1ay)

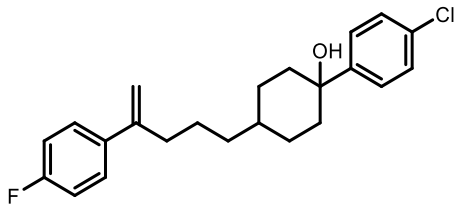

White solid. **^{1}H NMR** (500 MHz, $CDCl_3$) δ 7.43 (d, *J* = 8.6 Hz, 2H), 7.37 (dd, *J* = 8.8, 5.4 Hz, 2H), 7.31 (d, *J* = 8.7 Hz, 2H), 7.01 (t, *J* = 8.7 Hz, 2H), 5.23 (d, *J* = 1.5 Hz, 1H), 5.07 (d, *J* = 1.4 Hz, 1H), 2.77 (d, *J* = 11.0 Hz, 2H), 2.51 (t, *J* = 7.3 Hz, 2H), 2.48 – 2.38 (m, 2H), 2.38 (d, *J* = 2.5 Hz, 2H), 2.09 (td, *J* = 13.2, 4.5 Hz, 2H), 1.76 – 1.61 (m, 5H). **^{13}C NMR** (126 MHz, $CDCl_3$) δ 162.21 (d, *J* = 246.0 Hz), 147.14, 146.87, 137.15 (d, *J* = 3.4 Hz), 132.73, 128.38, 127.67 (d, *J* = 7.8 Hz), 126.07, 115.06 (d, *J* = 21.0 Hz), 112.33, 71.13, 58.27, 49.45, 38.50, 33.37, 25.55. **HRMS–ESI** (m/z): $[M+H]^+$ calcd. for $C_{23}H_{27}ClFNO$, 373.1729; found, 373.1730.

(8*S*,9*S*,13*S*,14*S*)-3-methoxy-13-methyl-17-methylene-7,8,9,11,12,13,14,15,16,17-decahydro-6H-cyclopenta[a]phenanthrene (1az)

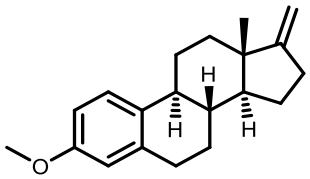

White solid. **^{1}H NMR** (500 MHz, $CDCl_3$) δ 7.23 (d, *J* = 7.6 Hz, 1H), 6.72 (dd, *J* = 8.6, 2.8 Hz, 1H), 6.64 (d, *J* = 2.7 Hz, 1H), 4.68 (t, *J* = 1.9 Hz, 2H), 3.78 (s, 3H), 2.94 – 2.80 (m, 2H), 2.61 – 2.48 (m, 1H), 2.36 (ddt, *J* = 10.9, 3.9, 1.9 Hz, 1H), 2.31 (d, *J* = 8.6 Hz, 1H), 2.22 (dt, *J* = 10.8, 5.6 Hz, 1H), 1.95 (dddd, *J* = 14.9, 8.5, 4.1, 2.5 Hz, 2H), 1.82 (dddd, *J* = 11.8, 8.6, 6.3, 1.8 Hz, 1H), 1.55 (tdd, *J* = 13.0, 11.8, 3.6 Hz, 1H), 1.49 – 1.33 (m, 4H), 1.31 – 1.18 (m, 1H), 0.83 (s, 3H). **^{13}C NMR** (126 MHz, $CDCl_3$) δ 161.79, 157.37, 138.02, 132.79, 126.31, 113.75, 111.41, 100.80, 55.19, 53.41, 44.35, 44.00, 38.75, 35.70, 29.89, 29.43, 27.59, 26.60, 23.89, 18.53. Data in accordance with literature (*90*).

1-(4-fluorophenyl)-3-(3-(4-fluorophenyl)but-3-en-1-yl)-4-(4-methoxyphenyl)azetidin-2-one-methane (1ba)

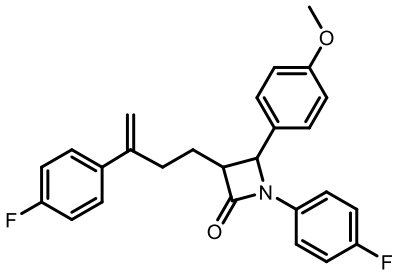

White solid. **^{1}H NMR** (500 MHz, $CDCl_3$) δ 7.39 – 7.32 (m, 2H), 7.31 – 7.24 (m, 4H), 7.04 – 6.96 (m, 2H), 6.95 – 6.88 (m, 4H), 5.23 (d, *J* = 1.2 Hz, 1H), 5.02 (d, *J* = 1.3 Hz, 1H), 4.61 (d, *J* = 2.4 Hz, 1H), 3.80 (s, 3H), 3.16 (ddd, *J* = 8.9, 6.8, 2.4 Hz, 1H), 2.83 – 2.59 (m, 2H), 2.10 (ddt, *J* = 13.4, 9.3, 6.6 Hz, 1H), 2.04 – 1.94 (m, 1H). **^{13}C NMR** (126 MHz, $CDCl_3$) δ 167.29, 162.13 (d, *J* = 246.6 Hz), 159.64, 158.70 (d, *J* = 243.1 Hz), 145.85, 136.39 (d, *J* = 3.2 Hz), 133.84 (d, *J* = 2.7 Hz), 129.27, 127.51 (d, *J* = 8.0 Hz), 127.06, 118.17 (d, *J* = 7.9 Hz), 115.59 (d, *J* = 22.7 Hz), 115.07 (d, *J* = 21.4 Hz), 114.43, 113.07, 60.90, 59.90, 55.08, 32.64, 27.49. **HRMS–ESI** (m/z): $[M+H]^+$ calcd. for $C_{28}H_{32}F_2NO_2$, 452.2396; found, 452.2391.

(3*S*,5*S*,8*R*,9*S*,10*S*,13*S*,14*S*)-10,13-dimethyl-17-methylenehexadecahydro-1H-cyclopenta [a] phenanthren-3-yl benzoate (1bb)

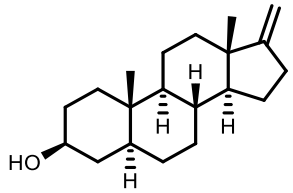

White solid. **^{1}H NMR** (500 MHz, $CDCl_3$) δ 4.59 (ddt, *J* = 9.0, 2.5, 1.6 Hz, 2H), 3.56 (tt, *J* =

11.1, 4.8 Hz, 1H), 2.45 (ddq, *J* = 17.1, 10.1, 2.3 Hz, 1H), 2.19 (dtt, *J* = 17.4, 8.7, 2.0 Hz, 1H), 1.94 (br, 1H), 1.78 (ddd, *J* = 12.4, 4.0, 2.6 Hz, 2H), 1.73 – 1.64 (m, 3H), 1.61 – 1.57 (m, 1H), 1.56 -1.52 (m, 1H), 1.43 – 1.35 (m, 2H), 1.34 – 1.29 (m, 1H), 1.30 – 1.22 (m, 4H), 1.22 – 1.16 (m, 1H), 1.15 – 1.05 (m, 1H), 0.97 (ddd, *J* = 12.7, 10.5, 6.4 Hz, 2H), 0.93 – 0.85 (m, 1H), 0.80 (s, 3H), 0.75 (s, 3H), 0.63 (ddd, *J* = 12.3, 10.5, 4.2 Hz, 1H). **^{13}C NMR** (126 MHz, $CDCl_3$) δ 161.85, 100.57, 71.12, 54.48, 54.34, 44.82, 44.04, 38.07, 36.95, 35.64, 35.52, 35.37, 31.84, 31.38, 29.31, 28.59, 24.07, 21.07, 18.46, 12.28. Data in accordance with literature (*91*).

(*E/Z*)-(prop-1-en-1-yl-1-d)benzene (1bc)

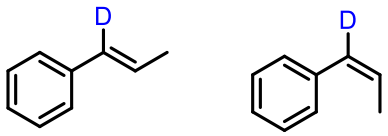

The synthesis procedure of substrate **1bc** followed the reported literature (*92*). Colorless oil. D/H = 89%. *trans* : *cis* = 2 : 3. **^{1}H NMR** (500 MHz, $CDCl_3$) δ 7.42 – 7.32 (m, 10.5H), 7.31 – 7.27 (m, 1H), 7.26 – 7.21 (m, 1H), 6.38 – 6.21 (m, 1H), 5.85 (tdd, *J* = 7.2, 6.4, 5.6, 2.1 Hz, 1.5H), 1.96 (dd, *J* = 7.2, 1.1 Hz, 4.5H), 1.94 (d, *J* = 6.6 Hz, 3H). **^{13}C NMR** (126 MHz, $CDCl_3$) δ 137.82, 137.50, 130.64 (t, *J* = 22.7 Hz), 129.47 (t, *J* = 23.9 Hz), 128.79, 128.44, 128.08, 126.69, 126.37, 125.54, 18.44, 14.58. Data in accordance with literature.

methyl 5-methyl-2,2-diphenylhex-4-enoate (1bd)

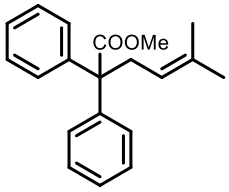

The synthesis procedure of substrate **1bd** followed the reported literature (*93*). Colourless oil. **^{1}H NMR** (500 MHz, $CDCl_3$) δ 7.42 – 6.93 (m, 10H), 5.01 (t, *J* = 7.1 Hz, 1H), 3.69 (s, 3H), 3.08 (d, *J* = 7.1 Hz, 2H), 1.56 (s, 3H), 1.26 (s, 3H). **^{13}C NMR** (126 MHz, $CDCl_3$) δ 174.84, 142.64, 134.86, 128.98, 127.67, 126.63, 119.41, 60.59, 52.30, 36.85, 25.86, 17.50. Data in accordance with literature.

Benzoic acid (2a)

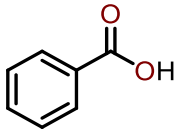

White solid. **^{1}H NMR** (500 MHz, $CDCl_3$) δ 8.14 (d, *J* = 7.9 Hz, 2H), 7.63 (t, *J* = 7.4 Hz, 1H), 7.49 (t, *J* = 7.8 Hz, 2H). **^{13}C NMR** (126 MHz, $CDCl_3$) δ 172.46, 133.83, 130.20, 129.28, 129.27, 128.48.

4-methoxybenzoic acid (2b)

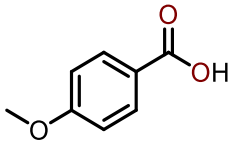

White solid. **^{1}H NMR** (500 MHz, DMSO-d_6) δ 12.63 (br, 1H), 7.89 (d, *J* = 8.9 Hz, 2H), 7.01 (d, *J* = 8.9 Hz, 2H), 3.82 (s, 3H). **^{13}C NMR** (126 MHz, DMSO-d_6) δ 167.03, 162.84, 131.36, 122.97, 113.83, 55.46.

4-methylbenzoic acid (2d)

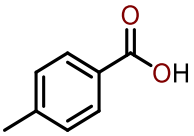

White solid.**^{1}H NMR** (500 MHz, DMSO-d_6) δ 7.81 (d, J = 8.2 Hz, 2H), 7.28 (d, J = 7.9 Hz, 2H), 3.77 (s, 1H), 2.34 (s, 3H). **^{13}C NMR** (126 MHz, DMSO-d_6) δ 167.78, 143.53, 129.68, 129.51, 128.21, 21.45.

4-(trifluoromethyl)benzoic acid (2f)

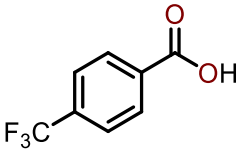

White solid. **^{1}H NMR** (500 MHz, DMSO-d_6) δ 13.50 (br, 1H), 8.13 (d, J = 8.1 Hz, 2H), 7.88 (d, J = 6.5 Hz, 2H). **^{13}C NMR** (126 MHz, DMSO-d_6) δ 166.23, 134.62, 132.49 (q, J = 31.9 Hz), 130.14, 125.65 (q, J = 3.8 Hz), 123.84 (q, J = 272.7 Hz).

terephthalic acid (2g)

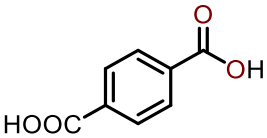

White solid. **^{1}H NMR** (500 MHz, DMSO-d_6) δ 13.31 (br, 1H), 8.04 (s, 4H). **^{13}C NMR** (126 MHz, DMSO-d_6) δ 166.71, 134.47, 129.50.

4-chlorobenzoic acid (2h)

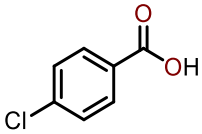

White solid. **^{1}H NMR** (500 MHz, DMSO-d_6) δ 7.94 (d, J = 8.5 Hz, 2H), 7.57 (d, J = 8.5 Hz, 2H). **^{13}C NMR** (126 MHz, DMSO-d_6) δ 166.48, 137.81, 131.17, 129.64, 128.78.

Acetophenone (2i)

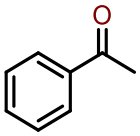

Colorless oil. ^{1}H NMR (500 MHz, $CDCl_3$) δ 7.95 (d, J = 8.3 Hz, 2H), 7.55 (t, J = 7.6 Hz, 1H), 7.44 (t, J = 7.7 Hz, 2H), 2.59 (s, 3H). **^{13}C NMR** (126 MHz, $CDCl_3$) δ 198.05, 136.97, 133.01, 128.46, 128.19, 26.53.

1-(4-(*tert*-butyl)phenyl)ethan-1-one (2j)

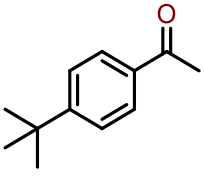

Colorless oil. **^{1}H NMR** (500 MHz, $CDCl_3$) δ 7.90 (d, J = 8.5 Hz, 2H), 7.48 (d, J = 8.5 Hz, 2H), 2.59 (s, 3H), 1.34 (s, 9H). **^{13}C NMR** (126 MHz, $CDCl_3$) δ 197.86, 156.79, 134.56, 128.26,

125.48, 35.08, 31.06, 26.56.

1-(4-methoxyphenyl)ethan-1-one (2k)

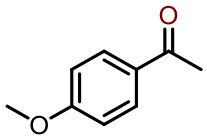

White solid. **^{1}H NMR** (500 MHz, $CDCl_3$) δ 7.94 (d, *J* = 8.9 Hz, 2H), 6.93 (d, *J* = 8.8 Hz, 2H), 3.87 (s, 3H), 2.56 (s, 3H). **^{13}C NMR** (126 MHz, $CDCl_3$) δ 196.79, 163.43, 130.57, 130.29, 113.64, 55.45, 26.35.

1-(4-hydroxyphenyl)ethan-1-one (2l)

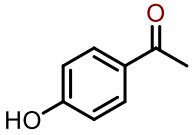

White solid. **^{1}H NMR** (500 MHz, $CDCl_3$) δ 7.92 (d, *J* = 8.8 Hz, 2H), 6.92 (d, *J* = 8.8 Hz, 2H), 6.49 (br, 1H), 2.58 (s, 3H). **^{13}C NMR** (126 MHz, $CDCl_3$) δ 197.71, 160.53, 131.07, 130.07, 115.38, 26.35.

1-(4-fluorophenyl)ethan-1-one (2m)

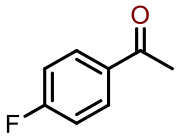

White solid. **^{1}H NMR** (500 MHz, $CDCl_3$) δ 7.97 (dd, *J* = 8.9, 5.4 Hz, 2H), 7.12 (t, *J* = 8.6 Hz, 2H), 2.58 (s, 3H). ^{13}C NMR (126 MHz, $CDCl_3$) δ 196.45, 165.70 (d, *J* = 254.7 Hz), 133.51 (d, *J* = 3.1 Hz), 130.89 (d, *J* = 9.2 Hz), 115.60 (d, *J* = 21.8 Hz), 26.51.

1-(4-chlorophenyl)ethan-1-one (2n)

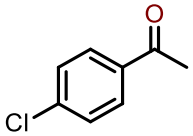

White solid. **^{1}H NMR** (500 MHz, $CDCl_3$) δ 7.89 (d, *J* = 8.5 Hz, 2H), 7.43 (d, *J* = 8.6 Hz, 2H), 2.58 (s, 3H). **^{13}C NMR** (126 MHz, $CDCl_3$) δ 196.77, 139.49, 135.33, 129.66, 128.82, 26.52.

1-(4-bromophenyl)ethan-1-one (2o)

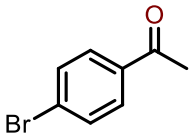

White solid. **^{1}H NMR** (500 MHz, $CDCl_3$) δ 7.82 (d, *J* = 8.5 Hz, 2H), 7.61 (d, *J* = 8.5 Hz, 2H), 2.59 (s, 3H). **^{13}C NMR** (126 MHz, $CDCl_3$) δ 197.02, 135.78, 131.88, 129.83, 128.30, 26.56.

1-(4-nitrophenyl)ethan-1-one (2p)

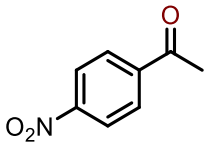

Yellow solid. **^{1}H NMR** (500 MHz, $CDCl_3$) δ 8.32 (d, *J* = 8.9 Hz, 2H), 8.11 (d, *J* = 8.8 Hz, 2H),

2.68 (s, 3H). **^{13}C NMR** (126 MHz, $CDCl_3$) δ 196.29, 150.35, 141.33, 129.30, 123.86, 27.01.

cyclobutyl(phenyl)methanone (2q)

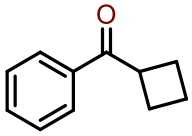

White solid. **^{1}H NMR** (500 MHz, $CDCl_3$) δ 7.90 (d, *J* = 6.9 Hz, 2H), 7.54 (t, *J* = 7.4 Hz, 1H), 7.44 (t, *J* = 7.6 Hz, 2H), 4.00 (p, *J* = 8.6 Hz, 1H), 2.49 – 2.36 (m, 2H), 2.35 – 2.26 (m, 2H), 2.09 (dt, *J* = 11.0, 8.8 Hz, 1H), 1.99 – 1.82 (m, 1H). **^{13}C NMR** (126 MHz, $CDCl_3$) δ 200.95, 135.57, 132.80, 128.51, 128.29, 42.17, 25.06, 18.14.

3-methyl-1,3-diphenylbutan-1-one (2r)

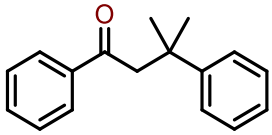

Colorless oil. **^{1}H NMR** (500 MHz, $CDCl_3$) δ 7.82 (dd, J = 8.4, 1.3 Hz, 2H), 7.54 – 7.44 (m, 1H), 7.42 – 7.34 (m, 4H), 7.28 (dd, J = 8.5, 7.1 Hz, 2H), 7.20 – 7.10 (m, 1H), 3.31 (s, 2H), 1.51 (s, 6H). **^{13}C NMR** (126 MHz, $CDCl_3$) δ 198.99, 148.84, 138.09, 132.64, 128.35, 128.13, 128.03, 125.75, 125.41, 50.84, 37.49, 29.09. Data in accordance with literature (*94*).

Benzophenone (2s)

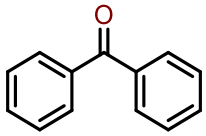

White solid. **^{1}H NMR** (500 MHz, $CDCl_3$) δ 7.81 (d, *J* = 6.9 Hz, 4H), 7.60 (t, *J* = 7.4 Hz, 2H), 7.50 (d, *J* = 7.9 Hz, 4H). **^{13}C NMR** (126 MHz, $CDCl_3$) δ 196.77, 137.56, 132.41, 130.05, 128.26.

(4-methoxyphenyl)(phenyl)methanone (2t)

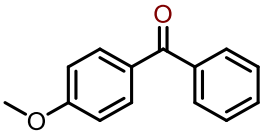

White solid. **^{1}H NMR** (500 MHz, $CDCl_3$) δ 7.83 (d, *J* = 8.8 Hz, 2H), 7.76 (d, *J* = 6.9 Hz, 2H), 7.57 (t, *J* = 7.4 Hz, 1H), 7.47 (t, *J* = 7.5 Hz, 2H), 6.97 (d, *J* = 8.8 Hz, 2H), 3.89 (s, 3H). **^{13}C NMR** (126 MHz, $CDCl_3$) δ 195.56, 163.18, 138.24, 132.55, 131.87, 130.11, 129.71, 128.16, 113.52, 55.48.

4-benzoylbenzonitrile (2u)

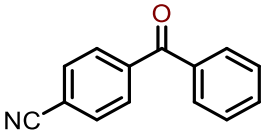

Brown solid. **^{1}H NMR** (500 MHz, $CDCl_3$) δ 7.88 (d, *J* = 8.5 Hz, 2H), 7.83 – 7.76 (m, 4H), 7.69 – 7.61 (m, 1H), 7.56 – 7.48 (m, 2H). **^{13}C NMR** (126 MHz, $CDCl_3$) δ 195.05, 141.20, 136.29, 133.33, 132.16, 130.23, 130.06, 128.63, 118.01, 115.65.

anthracene-9,10-dione (2v)

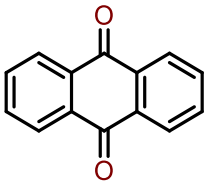

White solid. **^{1}H NMR** (500 MHz, $CDCl_3$) δ 8.32 (dd, *J* = 5.8, 3.3 Hz, 4H), 7.81 (dd, *J* = 5.8, 3.3 Hz, 4H). **^{13}C NMR** (126 MHz, $CDCl_3$) δ 183.15, 134.12, 133.48, 127.22.

1-(pyridin-2-yl)ethan-1-one (2w)

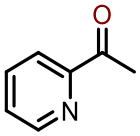

Yellow oil. **^{1}H NMR** (500 MHz, $CDCl_3$) δ 8.67 (d, *J* = 4.4 Hz, 1H), 8.03 (d, *J* = 7.9 Hz, 1H), 7.83 (d, *J* = 7.7 Hz, 1H), 7.46 (dd, *J* = 7.5, 4.8 Hz, 1H), 2.71 (s, 3H). **^{13}C NMR** (126 MHz, $CDCl_3$) δ 200.10, 153.51, 148.94, 136.80, 127.06, 121.61, 25.78.

1-(Thiophen-2-yl)butan-1-one (2x)

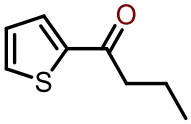

Colorless oil. **^{1}H NMR** (500 MHz, $CDCl_3$) δ 7.73 (dd, *J* = 3.8, 1.2 Hz, 1H), 7.63 (dd, *J* = 5.0, 1.2 Hz, 1H), 7.14 (dd, *J* = 4.9, 3.7 Hz, 1H), 2.90 (t, *J* = 7.4 Hz, 2H), 1.80 (q, *J* = 7.4 Hz, 2H), 1.02 (t, *J* = 7.4 Hz, 3H). **^{13}C NMR** (126 MHz, $CDCl_3$) δ 193.37, 144.50, 133.28, 131.63, 127.98, 41.23, 18.17, 13.84.

1-(furan-2-yl)butan-1-one (2y)

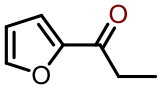

Colorless oil. **^{1}H NMR** (500 MHz, $CDCl_3$) δ 7.57 (dd, *J* = 1.8, 0.8 Hz, 1H), 7.17 (dd, *J* = 3.5, 0.8 Hz, 1H), 6.52 (dd, *J* = 3.5, 1.7 Hz, 1H), 2.86 (q, *J* = 7.4 Hz, 2H), 1.21 (t, *J* = 7.4 Hz, 3H). **^{13}C NMR** (126 MHz, $CDCl_3$) δ 190.20, 152.62, 146.07, 116.62, 112.05, 31.66, 8.06.

1-(4-hydroxyphenyl)propan-1-one (2z)

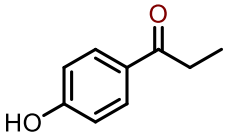

White solid. **^{1}H NMR** (500 MHz, $CDCl_3$) δ 7.92 (d, *J* = 8.7 Hz, 2H), 6.88 (d, *J* = 8.7 Hz, 2H), 5.42 (br, 1H), 2.95 (q, *J* = 7.3 Hz, 2H), 1.21 (t, *J* = 7.3 Hz, 3H). **^{13}C NMR** (126 MHz, $CDCl_3$) δ 199.76, 159.77, 130.57, 130.14, 115.26, 31.44, 8.44.

isobenzofuran-1,3-dione (2aa)

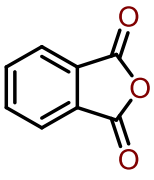

White solid. **^{1}H NMR** (500 MHz, $CDCl_3$) δ 8.03 (dd, *J* = 5.6, 3.0 Hz, 2H), 7.92 (dd, *J* = 5.6,

3.1 Hz, 2H). **^{13}C NMR** (126 MHz, $CDCl_3$) δ 162.75, 136.04, 131.25, 125.69.

(4-(2-hydroxyethoxy)phenyl)(phenyl)methanone (2ab)

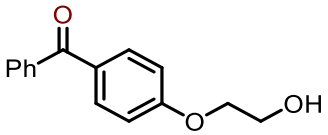

White solid. **^{1}H NMR** (500 MHz, $CDCl_3$) δ 7.83 (d, *J* = 8.9 Hz, 2H), 7.76 (d, *J* = 6.9 Hz, 2H), 7.61 – 7.54 (m, 1H), 7.48 (t, *J* = 7.6 Hz, 2H), 6.99 (d, *J* = 8.8 Hz, 2H), 4.20 – 4.15 (m, 2H), 4.02 (t, *J* = 4.5 Hz, 2H). **^{13}C NMR** (126 MHz, $CDCl_3$) δ 195.53, 162.20, 138.14, 132.58, 131.96, 130.52, 129.74, 128.20, 114.04, 69.37, 61.30. Data in accordance with literature (*85*).

4-(4-benzoylphenoxy)butanal (2ac)

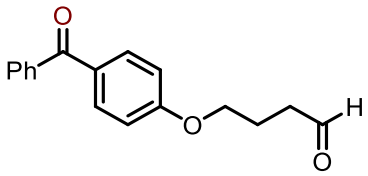

Colorless oil. **^{1}H NMR** (500 MHz, $CDCl_3$) δ 9.80 (t, *J* = 1.3 Hz, 1H), 7.77 (d, *J* = 8.8 Hz, 2H), 7.75 – 7.68 (m, 2H), 7.52 (d, *J* = 7.5 Hz, 1H), 7.44 (d, *J* = 7.9 Hz, 2H), 6.90 (d, *J* = 8.9 Hz, 2H), 4.04 (t, *J* = 6.1 Hz, 2H), 2.65 (td, *J* = 7.0, 1.3 Hz, 2H), 2.16 – 2.07 (m, 2H). **^{13}C NMR** (126 MHz, $CDCl_3$) δ 201.38, 195.32, 162.16, 137.99, 132.37, 131.76, 129.97, 129.51, 128.02, 113.80, 66.76, 40.25, 21.61. **HRMS–ESI** (m/z): $[M+H]^+$ calcd. for $C_{17}H_{17}O_3$, 269.1172; found, 269.1170.

(4-(pent-2-yn-1-yloxy)phenyl)(phenyl)methanone (2ad)

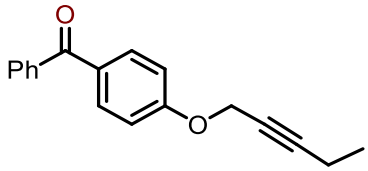

White solid. **^{1}H NMR** (500 MHz, $CDCl_3$) δ 7.83 (d, *J* = 8.8 Hz, 2H), 7.76 (d, *J* = 7.3 Hz, 2H), 7.56 (t, *J* = 7.4 Hz, 1H), 7.47 (t, *J* = 7.6 Hz, 2H), 7.03 (d, *J* = 8.8 Hz, 2H), 4.74 (t, *J* = 2.1 Hz, 2H), 2.24 (qt, *J* = 7.5, 2.2 Hz, 2H), 1.14 (t, *J* = 7.5 Hz, 3H). **^{13}C NMR** (126 MHz, $CDCl_3$) δ 195.50, 161.35, 138.12, 132.37, 131.88, 130.48, 129.69, 128.14, 114.38, 90.20, 73.43, 56.56, 13.50, 12.43. **HRMS–ESI** (m/z): $[M+H]^+$ calcd. for $C_{18}H_{17}O_2$, 265.1223; found, 265.1220.

3-oxobutyl benzoate (2ae)

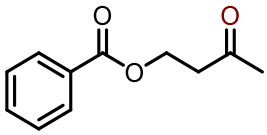

White solid. **^{1}H NMR** (500 MHz, $CDCl_3$) δ 7.98 (d, *J* = 7.2 Hz, 2H), 7.53 (t, *J* = 7.3 Hz, 1H), 7.41 (t, *J* = 7.7 Hz, 2H), 4.56 (t, *J* = 6.2 Hz, 2H), 2.89 (t, *J* = 6.2 Hz, 2H), 2.21 (s, 3H). **^{13}C NMR** (126 MHz, $CDCl_3$) δ 205.59, 166.31, 132.97, 129.83, 129.48, 128.28, 59.75, 42.28, 30.23. **HRMS–ESI** (m/z): $[M+H]^+$ calcd. for $C_{11}H_{13}O_3$, 193.0859; found, 193.0859.

2-(3-oxobutyl)isoindoline-1,3-dione (2af)

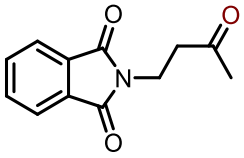

White solid. **^{1}H NMR** (500 MHz, $CDCl_3$) δ 7.84 (dd, *J* = 4.3, 2.4 Hz, 2H), 7.71 (dd, *J* = 4.3, 2.4 Hz, 2H), 3.96 (t, *J* = 5.9 Hz, 2H), 2.88 (t, *J* = 5.9 Hz, 2H), 2.19 (s, 3H). **^{13}C NMR** (500 MHz, $CDCl_3$) δ 205.86, 167.86, 134.34, 132.58, 123.62, 41.86, 33.06, 30.16. **HRMS–ESI** (m/z): $[M+H]^+$ calcd. for $C_{12}H_{12}NO_3$, 218.0812; found, 218.0810.

3-((trimethylsilyl)oxy)butan-2-one (2ag)

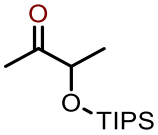

Colorless oil. **^{1}H NMR** (500 MHz, $CDCl_3$) δ 4.22 (q, *J* = 6.7 Hz, 1H), 2.21 (s, 3H), 1.30 (d, *J* = 6.8 Hz, 3H), 1.13 – 1.02 (m, 21H). **^{13}C NMR** (126 MHz, $CDCl_3$) δ 212.96, 75.41, 24.23, 21.16, 17.93, 12.13. **HRMS–ESI** (m/z): $[M+Na]^+$ calcd. for $C_{13}H_{28}O_2SiNa$, 267.1751; found, 267.1718.

undecan-6-one (2ah)

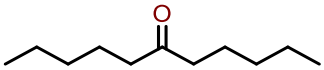

Colorless oil. **^{1}H NMR** (500 MHz, $CDCl_3$) δ 2.38 (t, *J* = 7.5 Hz, 4H), 1.56 (p, *J* = 7.3 Hz, 4H), 1.41 – 1.16 (m, 8H), 0.88 (t, *J* = 7.2 Hz, 6H). **^{13}C NMR** (126 MHz, $CDCl_3$) δ 211.77, 42.76, 31.43, 23.55, 22.45, 13.92.

4-phenylcyclohexan-1-one (2ai)

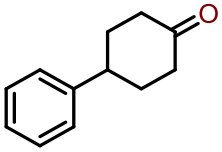

White solid. **^{1}H NMR** (500 MHz, $CDCl_3$) δ 7.33 (td, *J* = 7.3, 1.5 Hz, 2H), 7.26 – 7.22 (m, 3H), 3.03 (tt, *J* = 12.1, 3.5 Hz, 1H), 2.72 – 2.43 (m, 4H), 2.23 (dtd, *J* = 11.8, 3.5, 2.0 Hz, 2H), 2.09 – 1.82 (m, 2H). **^{13}C NMR** (126 MHz, $CDCl_3$) δ 211.20, 144.75, 128.58, 126.66, 126.56, 42.75, 41.37, 33.95.

(2*R*,5*S*)-2-isopropyl-5-methylcyclohexan-1-one (2aj)

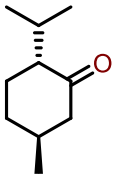

Colourless oil. **^{1}H NMR** (500 MHz, $CDCl_3$) δ 2.33 (ddq, *J* = 13.0, 3.5, 1.8 Hz, 1H), 2.12 (dddd, *J* = 8.2, 5.2, 4.1, 1.5 Hz, 1H), 2.02 (dddd, *J* = 18.4, 9.2, 4.1, 2.2 Hz, 2H), 1.95 (dd, *J* = 12.7, 1.5 Hz, 1H), 1.90 – 1.75 (m, 2H), 1.40 – 1.24 (m, 2H), 0.99 (dt, *J* = 6.4, 1.4 Hz, 3H), 0.89 (dt, *J* = 6.9, 1.4 Hz, 3H), 0.84 – 0.82 (m, 3H). **^{13}C NMR** (126 MHz, $CDCl_3$) δ 212.43, 55.84, 50.84, 35.44, 33.89, 27.81, 25.84, 22.26, 21.19, 18.66.

Adamantan-2-one (2ak)

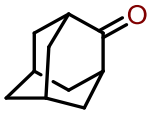

White solid. **^{1}H NMR** (500 MHz, $CDCl_3$) δ 2.59 – 2.49 (m, 2H), 2.11 – 2.05 (m, 4H), 2.05 – 1.97 (m, 6H), 1.93 (dd, *J* = 2.6, 1.4 Hz, 2H). **^{13}C NMR** (126 MHz, $CDCl_3$) δ 218.56, 46.96, 39.24, 36.27, 27.42.

1,4-dioxaspiro[4.5]decan-8-one (2al)

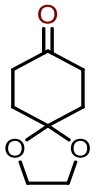

White solid. **^{1}H NMR** (500 MHz, $CDCl_3$) δ 4.02 (dd, *J* = 2.6, 1.5 Hz, 4H), 2.55 – 2.46 (m, 4H), 2.07 – 1.95 (m, 4H). **^{13}C NMR** (126 MHz, $CDCl_3$) δ 210.38, 107.10, 64.64, 38.16, 33.85.

Cyclooctenone (2am)

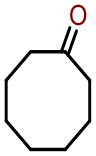

White solid. **^{1}H NMR** (500 MHz, $CDCl_3$) δ 2.46 – 2.33 (m, 4H), 1.94 – 1.82 (m, 4H), 1.64 – 1.49 (m, 4H), 1.38 (td, *J* = 7.4, 6.7, 4.7 Hz, 2H). **^{13}C NMR** (126 MHz, $CDCl_3$) δ 218.38, 41.94, 27.15, 25.65, 24.68.

Cyclododecanone (2an)

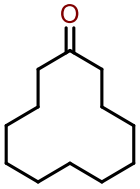

White solid. **^{1}H NMR** (500 MHz, $CDCl_3$) δ 2.79 – 2.33 (m, 4H), 1.99 – 1.63 (m, 4H), 1.53 – 1.07 (m, 14H). **^{13}C NMR** (126 MHz, $CDCl_3$) δ 212.99, 40.37, 24.72, 24.56, 24.19, 22.55, 22.29.

***tert*-butyl 6-oxo-2-azaspiro[3.3]heptane-2-carboxylate (2ao)**

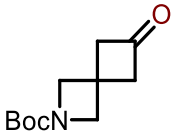

White solid. **^{1}H NMR** (500 MHz, $CDCl_3$) δ 4.13 (s, 4H), 3.29 (s, 4H), 1.45 (s, 9H). **^{13}C NMR** (126 MHz, $CDCl_3$) δ 204.80, 156.03, 79.85, 57.82, 28.34, 27.76.

***tert*-butyl 2-oxo-7-azaspiro[3.5]nonane-7-carboxylate (2ap)**

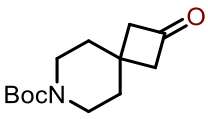

White solid. **^{1}H NMR** (500 MHz, $CDCl_3$) δ 3.46 – 3.32 (m, 4H), 2.81 (s, 4H), 1.70 (t, *J* = 5.6 Hz, 4H), 1.46 (s, 9H). **^{13}C NMR** (126 MHz, $CDCl_3$) δ 206.68, 154.78, 79.68, 56.39, 36.46, 29.12, 28.42.

3-oxobutyl (tert-butoxycarbonyl)tryptophanate (2aq)

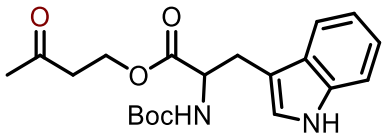

White solid. **^{1}H NMR** (500 MHz, $CDCl_3$) δ 8.63 (br, 1H), 7.55 (d, *J* = 7.9 Hz, 1H), 7.33 (d, *J* = 8.1 Hz, 1H), 7.21 – 7.14 (m, 1H), 7.14 – 7.06 (m, 1H), 7.00 (s, 1H), 5.16 (d, *J* = 8.1 Hz, 1H), 4.58 – 4.62 (m, 1H), 4.43 – 4.13 (m, 2H), 3.24 (dd, *J* = 5.9, 3.3 Hz, 2H), 2.64 – 2.44 (m, 2H), 2.04 (s, 3H), 1.43 (s, 9H). **^{13}C NMR** (126 MHz, $CDCl_3$) δ 205.62, 172.17, 155.21, 136.03, 127.49, 123.02, 121.87, 119.31, 118.48, 111.20, 109.53, 79.82, 59.88, 54.25, 41.58, 30.02, 28.19, 27.80. **HRMS–ESI** (m/z): $[M+Na]^+$ calcd. for $C_{20}H_{26}N_2O_5Na$, 397.1734; found, 397.1732.

3-oxobutyl 2-(1,3-dioxoisoindolin-2-yl)-3-phenylpropanoate (2ar)

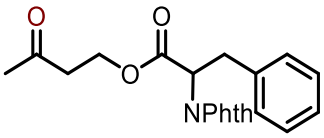

White solid. **^{1}H NMR** (500 MHz, $CDCl_3$) δ 7.71 (dd, *J* = 5.4, 3.1 Hz, 2H), 7.62 (dd, *J* = 5.5, 3.0 Hz, 2H), 7.16 – 7.05 (m, 5H), 5.10 (dd, *J* = 11.3, 5.1 Hz, 1H), 4.41 (ddt, *J* = 36.7, 11.1, 6.3 Hz, 2H), 3.58 – 3.40 (m, 2H), 2.73 (td, *J* = 6.2, 4.6 Hz, 2H), 2.08 (s, 3H). **^{13}C NMR** (126 MHz, $CDCl_3$) δ 204.89, 168.48, 167.10, 136.35, 133.95, 131.19, 128.59, 128.28, 126.61, 123.17, 60.43, 52.92, 41.60, 34.44, 29.94. **HRMS–ESI** (m/z): $[M+H]^+$ calcd. for $C_{21}H_{20}NO_5$, 366.1336; found, 366.1338.

3-(benzoyloxy)propanoic acid (2as)

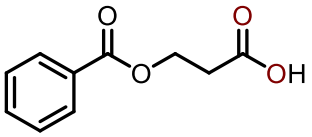

White solid. **^{1}H NMR** (500 MHz, $CDCl_3$) δ 8.03 (dd, *J* = 8.3, 1.4 Hz, 2H), 7.61 – 7.53 (m, 1H), 7.47 – 7.39 (m, 2H), 4.60 (t, *J* = 6.3 Hz, 2H), 2.86 (t, *J* = 6.3 Hz, 2H). **^{13}C NMR** (126 MHz, $CDCl_3$) δ 176.50, 166.29, 133.13, 129.72, 129.63, 128.38, 59.93, 33.67. **HRMS–ESI** (m/z): $[M-H]^-$ calcd. for $C_{10}H_9O_4$, 193.0506; found, 193.0516.

3-(2,6-dichlorophenoxy)propanoic acid (2at)

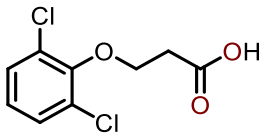

Yellow oil. **^{1}H NMR** (500 MHz, $CDCl_3$) δ 7.19 (d, *J* = 8.1 Hz, 2H), 6.90 (t, *J* = 8.1 Hz, 1H), 4.25 (t, *J* = 6.5 Hz, 2H), 2.85 (t, *J* = 6.5 Hz, 2H). **^{13}C NMR** (126 MHz, $CDCl_3$) δ 177.34, 151.03, 129.38, 128.86, 125.26, 68.38, 35.05. **HRMS–ESI** (m/z): $[M-H]^-$ calcd. for $C_9H_7O_3Cl_2$, 232.9777; found, 232.9702.

***isopropyl* 2-(4-(4-chlorobenzoyl)phenoxy)-2-methylpropanoate (2au)**

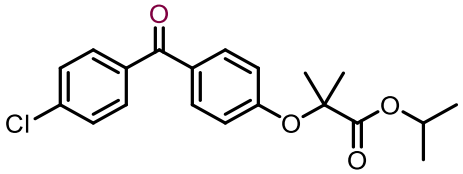

White solid. **^{1}H NMR** (500 MHz, Chloroform-*d*) δ 7.73 (d, *J* = 8.8 Hz, 2H), 7.70 (d, *J* = 8.5 Hz, 2H), 7.45 (d, *J* = 8.5 Hz, 2), 6.86 (d, *J* = 8.8 Hz, 2H), 5.09 (p, *J* = 6.3 Hz, 1H), 1.66 (s, 6H), 1.20 (d, *J* = 6.3 Hz, 6H). **^{13}C NMR** (126 MHz, $CDCl_3$) δ 194.26, 173.09, 159.70, 138.33, 136.39, 131.94, 131.15, 130.17, 128.52, 117.18, 79.38, 69.34, 25.34, 21.51. Data in accordance with literature (94).

2-((1-benzylpiperidin-4-yl)methyl)-5,6-dimethoxy-2,3-dihydro-1H-inden-1-one (2av)

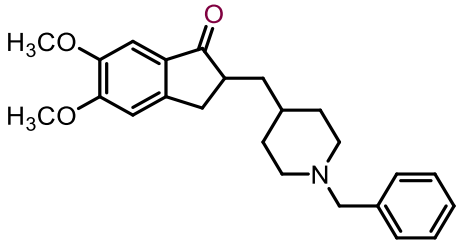

White solid. **^{1}H NMR** (500 MHz, $CDCl_3$) δ 7.35 – 7.28 (m, 4H), 7.26 (s, 1H), 7.17 (s, 1H), 6.85 (s, 1H), 3.96 (s, 3H), 3.90 (s, 3H), 3.51 (s, 2H), 3.23 (dd, *J* = 17.6, 8.1 Hz, 1H), 2.99 – 2.85 (m, 2H), 2.76 – 2.65 (m, 2H), 2.05 – 1.86 (m, 3H), 1.70 (dd, *J* = 35.5, 12.9 Hz, 2H), 1.49 (s, 1H), 1.43 – 1.26 (m, 3H). **^{13}C NMR** (126 MHz, $CDCl_3$) δ 207.84, 155.39, 149.37, 148.75, 138.46, 129.29, 129.23, 128.12, 126.90, 107.30, 104.33, 63.43, 56.20, 56.08, 53.79, 53.76, 45.44, 38.70, 34.45, 33.33, 33.01, 31.76. **HRMS–ESI** (m/z): $[M+H]^+$ calcd. for $C_{24}H_{30}NO_3$, 380.2221; found, 380.2220.

pyridin-2-yl(*p*-tolyl)methanone (2aw-1)

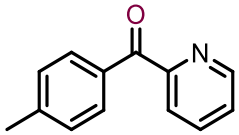

Colourless oil. **^{1}H NMR** (500 MHz, $CDCl_3$) δ 8.72 (d, *J* = 4.3 Hz, 1H), 8.02 (dt, *J* = 7.8, 1.1 Hz, 1H), 7.97 (d, *J* = 8.2 Hz, 2H), 7.89 (d, *J* = 1.7 Hz, 1H), 7.48 (ddd, *J* = 7.6, 4.8, 1.3 Hz, 1H), 7.29 (d, *J* = 7.9 Hz, 2H), 2.43 (s, 3H). **^{13}C NMR** (126 MHz, $CDCl_3$) δ 193.62, 155.38, 148.49, 143.80, 136.98, 133.59, 131.11, 128.89, 125.98, 124.54, 21.74. **HRMS–ESI** (m/z): $[M+H]^+$ calcd. for $C_{13}H_{12}NO$, 198.0913; found, 198.0913.

2-(pyrrolidin-1-yl)acetic acid (2aw-2)

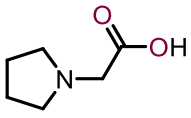

Yellow solid. **^{1}H NMR** (500 MHz, $CDCl_3$) δ 3.70 (s, 2H), 3.43 (br, 4H), 2.05 (h, *J* = 3.4 Hz, 4H). **^{13}C NMR** (126 MHz, $CDCl_3$) δ 169.07, 57.96, 54.05, 23.41.

cyclohexyl 2-(4-((2-oxocyclopentyl)methyl)phenyl)propanoate (2ax)

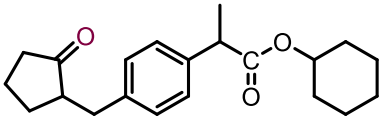

White solid. **^{1}H NMR** (500 MHz, $CDCl_3$) δ 7.20 (d, *J* = 8.0 Hz, 2H), 7.09 (d, *J* = 8.1 Hz, 2H),

4.78 – 4.64 (m, 1H), 3.64 (q, *J* = 7.2 Hz, 1H), 3.10 (dd, *J* = 13.9, 4.1 Hz, 1H), 2.50 (dd, *J* = 13.9, 9.5 Hz, 1H), 2.38 – 2.25 (m, 2H), 2.14 – 2.02 (m, 2H), 1.93 (tdd, *J* = 8.9, 6.5, 3.3 Hz, 1H), 1.82 – 1.62 (m, 4H), 1.59 – 1.48 (m, 3H), 1.45 (d, *J* = 7.2 Hz, 3H), 1.43 – 1.37 (m, 1H), 1.37 – 1.25 (m, 3H), 1.23 (dd, *J* = 9.7, 2.8 Hz, 1H). **^{13}C NMR** (126 MHz, $CDCl_3$) δ 220.22, 173.97, 138.64, 138.54, 128.93, 127.43, 72.52, 50.93, 45.32, 38.17, 35.11, 31.36, 31.14, 29.09, 25.31, 23.45, 23.34, 20.49, 18.38, 18.36. **HRMS–ESI** (m/z): $[M+Na]^+$ calcd. for $C_{21}H_{28}O_3Na$, 351.1931; found, 351.1927.

4-(4-(4-chlorophenyl)-4-hydroxycyclohexyl)-1-(4-fluorophenyl) butan-1-one (2ay)

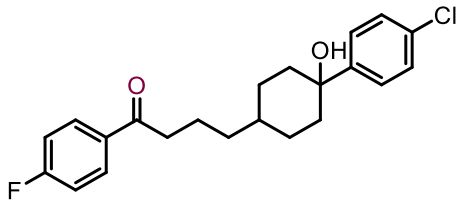

White solid. **^{1}H NMR** (500 MHz, $CDCl_3$) δ 8.02 (dd, *J* = 8.9, 5.4 Hz, 2H), 7.38 (d, *J* = 8.7 Hz, 2H), 7.30 (d, *J* = 8.6 Hz, 2H), 7.14 (t, *J* = 8.6 Hz, 2H), 2.99 (t, *J* = 7.0 Hz, 2H), 2.79 (d, *J* = 11.3 Hz, 2H), 2.48 (t, *J* = 7.1 Hz, 2H), 2.41 (t, *J* = 11.9 Hz, 2H), 1.99 (p, *J* = 7.5, 7.0 Hz, 4H), 1.67 (dq, *J* = 14.4, 3.0 Hz, 2H), 1.60 – 1.50 (m, 1H). **^{13}C NMR** (126 MHz, $CDCl_3$) δ 198.34, 165.59 (d, *J* = 254.3 Hz), 146.87, 133.65 (d, *J* = 3.1 Hz), 132.71, 130.66 (d, *J* = 9.4 Hz), 128.34, 126.05, 115.59 (d, *J* = 21.8 Hz), 71.10, 57.83, 49.31, 38.40, 36.24, 21.91. **HRMS–ESI** (m/z): $[M+H]^+$ calcd. for $C_{22}H_{25}CFO_2$, 375.1522; found, 375.1520.

(8*R*,9*S*,13*S*,14*S*)-3-methoxy-13-methyl-6,7,8,9,11,12,13,14,15,16-decahydro-17*H*-cyclop enta [a]phenanthren-17-one (2az)

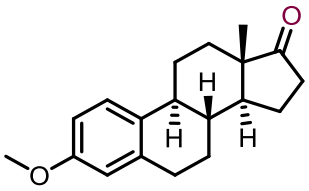

White solid. **^{1}H NMR** (500 MHz, $CDCl_3$) δ 7.21 (d, *J* = 9.1 Hz, 1H), 6.73 (dd, *J* = 8.6, 2.9 Hz, 1H), 6.65 (d, *J* = 2.7 Hz, 1H), 3.78 (s, 3H), 2.98 – 2.81 (m, 2H), 2.51 (ddd, *J* = 18.9, 8.7, 0.9 Hz, 1H), 2.43 – 2.34 (m, 1H), 2.26 (d, *J* = 4.4 Hz, 1H), 2.15 (dt, *J* = 19.0, 8.9 Hz, 1H), 2.09 – 1.98 (m, 2H), 1.98 – 1.92 (m, 1H), 1.71 – 1.37 (m, 6H), 0.91 (s, 3H). **^{13}C NMR** (126 MHz, $CDCl_3$) δ 221.00, 157.54, 137.73, 131.99, 126.33, 113.84, 111.54, 55.20, 50.37, 48.00, 43.95, 38.34, 35.87, 31.55, 29.66, 26.53, 25.91, 21.57, 13.84. **HRMS–ESI** (m/z): $[M+H]^+$ calcd. for $C_{19}H_{25}O_2$, 285.1849; found, 285.1845.

1-(4-fluorophenyl)-3-(3-(4-fluorophenyl)-3-oxopropyl)-4-(4-methoxyphenyl)azetidin-2-one (2ba)

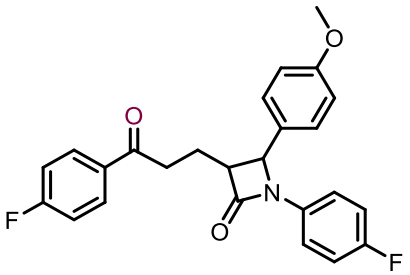

White solid. **^{1}H NMR** (500 MHz, $CDCl_3$) δ 8.06 – 7.96 (m, 2H), 7.33 – 7.23 (m, 4H), 7.14 (t, *J* = 8.6 Hz, 2H), 6.95 (dd, *J* = 9.1, 8.3 Hz, 2H), 6.90 (d, *J* = 8.7 Hz, 2H), 4.70 (d, *J* = 2.3 Hz, 1H), 3.81 (s, 3H), 3.31 (ddd, *J* = 17.7, 8.4, 5.6 Hz, 1H), 3.23 – 3.09 (m, 2H), 2.42 (ddt, *J* = 13.9,

8.4, 6.9 Hz, 1H), 2.35 – 2.20 (m, 1H). **^{13}C NMR** (126 MHz, $CDCl_3$) δ 197.32, 167.22, 165.77 (d, *J* = 255.1 Hz), 158.91 (d, *J* = 243.4 Hz), 159.77, 133.83 (d, *J* = 2.7 Hz), 133.01 (d, *J* = 2.9 Hz), 130.67 (d, *J* = 9.3 Hz), 129.13, 127.15, 118.36 (d, *J* = 7.8 Hz), 115.82 (d, *J* = 8.1 Hz), 115.65 (d, *J* = 7.3 Hz), 114.57, 61.09, 59.74, 55.27, 35.51, 23.14. **HRMS–ESI** (m/z): $[M+H]^+$ calcd. for $C_{25}H_{22}NO_3F_2$, 422.1562; found, 422.1559.

(3*S*,5*S*,8*R*,9*S*,10*S*,13*S*,14*S*)-10,13-dimethyl-17-oxohexadecahydro-1*H*-cyclopenta [a] ph enanthren-3-yl benzoate (2bb)

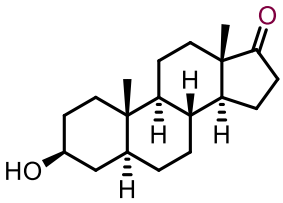

White solid. **^{1}H NMR** (500 MHz, $CDCl_3$) δ 3.64 – 3.52 (m, 1H), 2.43 (dd, *J* = 18.3, 9.0 Hz, 1H), 2.14 – 1.98 (m, 1H), 1.95 – 1.89 (m, 1H), 1.86 – 1.75 (m, 3H), 1.71 (dt, *J* = 13.3, 3.7 Hz, 1H), 1.68 – 1.62 (m, 1H), 1.60 – 1.54 (m, 2H), 1.54 – 1.46 (m, 2H), 1.45 – 1.38 (m, 1H), 1.37 – 1.18 (m, 6H), 1.13 (ddd, *J* = 15.9, 7.8, 3.4 Hz, 1H), 0.97 (dtd, *J* = 17.4, 12.9, 12.4, 4.9 Hz, 2H), 0.85 (s, 3H), 0.83 (s, 3H), 0.69 (ddd, *J* = 12.2, 10.5, 4.1 Hz, 1H). **^{13}C NMR** (126 MHz, $CDCl_3$) δ 221.42, 71.13, 54.40, 51.39, 47.78, 44.81, 38.04, 36.91, 35.83, 35.62, 35.02, 31.52, 31.42, 30.87, 28.37, 21.76, 20.48, 13.80, 12.29. **HRMS–ESI** (m/z): $[M+H]^+$ calcd. for $C_{19}H_{31}O_2$, 291.2319; found, 291.2320.

2-methyl-3-phenyloxirane (2a″)

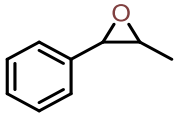

Colourless oil. **^{1}H NMR** (500 MHz, Chloroform-*d*) δ 7.39 – 7.35 (m, 2H), 7.34 – 7.31 (m, 1H), 7.31 – 7.27 (m, 2H), 3.61 (d, *J* = 2.0 Hz, 1H), 3.07 (qd, *J* = 5.1, 2.1 Hz, 1H), 1.49 (d, *J* = 5.1 Hz, 3H). **^{13}C NMR** (126 MHz, $CDCl_3$) δ 137.70, 128.39, 127.99, 125.51, 59.50, 59.03, 17.89. Data in accordance with literature (*92*).

Benzaldehyde-α-d$_1$ (4a)

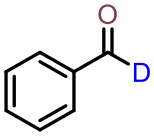

Colourless oil. D/H = 88%. **^{1}H NMR** (500 MHz, Chloroform-*d*) δ 7.91 – 7.85 (m, 1H), 7.67 – 7.60 (m, 1H), 7.53 (t, *J* = 7.6 Hz, 1H). **^{13}C NMR** (126 MHz, $CDCl_3$) δ 192.05 (t, *J* = 26.5 Hz), 136.26 (t, *J* = 3.8 Hz), 134.44, 129.70, 128.96.

5-(2-hydroxypropan-2-yl)-3,3-diphenyldihydrofuran-2(3H)-one (5a)

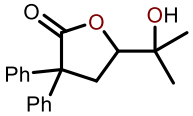

Colourless oil. **^{1}H NMR** (500 MHz, $CDCl_3$) δ 7.31 (d, *J* = 3.1 Hz, 4H), 7.28 – 7.20 (m, 2H), 7.20 – 7.15 (m, 2H), 7.06 (dd, *J* = 6.5, 1.3 Hz, 1H), 4.09 (dd, *J* = 8.7, 4.0 Hz, 1H), 2.95 (dd, *J* = 10.3, 8.7 Hz, 1H), 2.78 (dd, *J* = 10.3, 4.0 Hz, 1H), 1.30 (s, 3H), 1.14 (s, 3H). **^{13}C NMR** (500 MHz, $CDCl_3$) δ 177.06, 141.81, 139.65, 129.29, 128.98, 128.34, 127.94, 127.75, 127.31, 82.46, 70.16, 58.52, 29.80, 27.14, 23.79. **HRMS–ESI** (m/z): $[M+H]^+$ calcd. for $C_{19}H_{21}O_3$, 297.1486; found, 297.1489.

11. NMR spectra

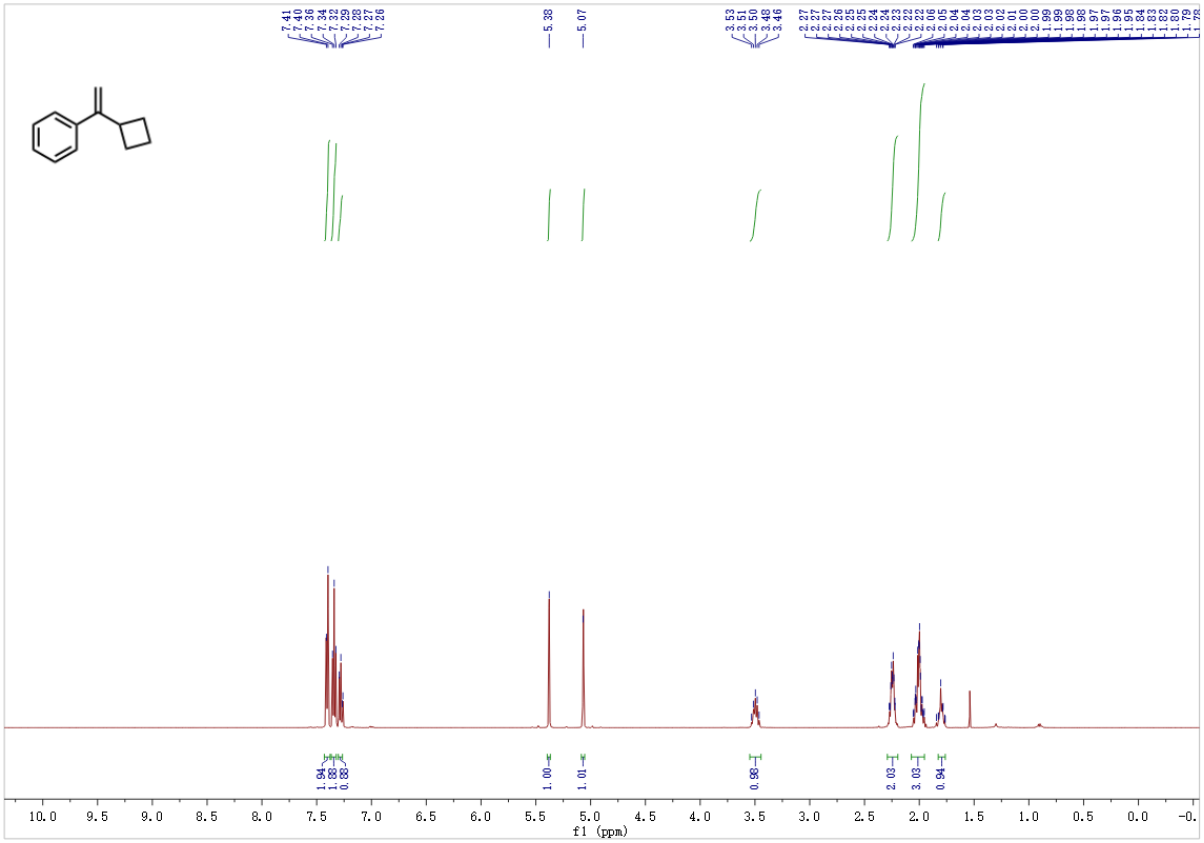

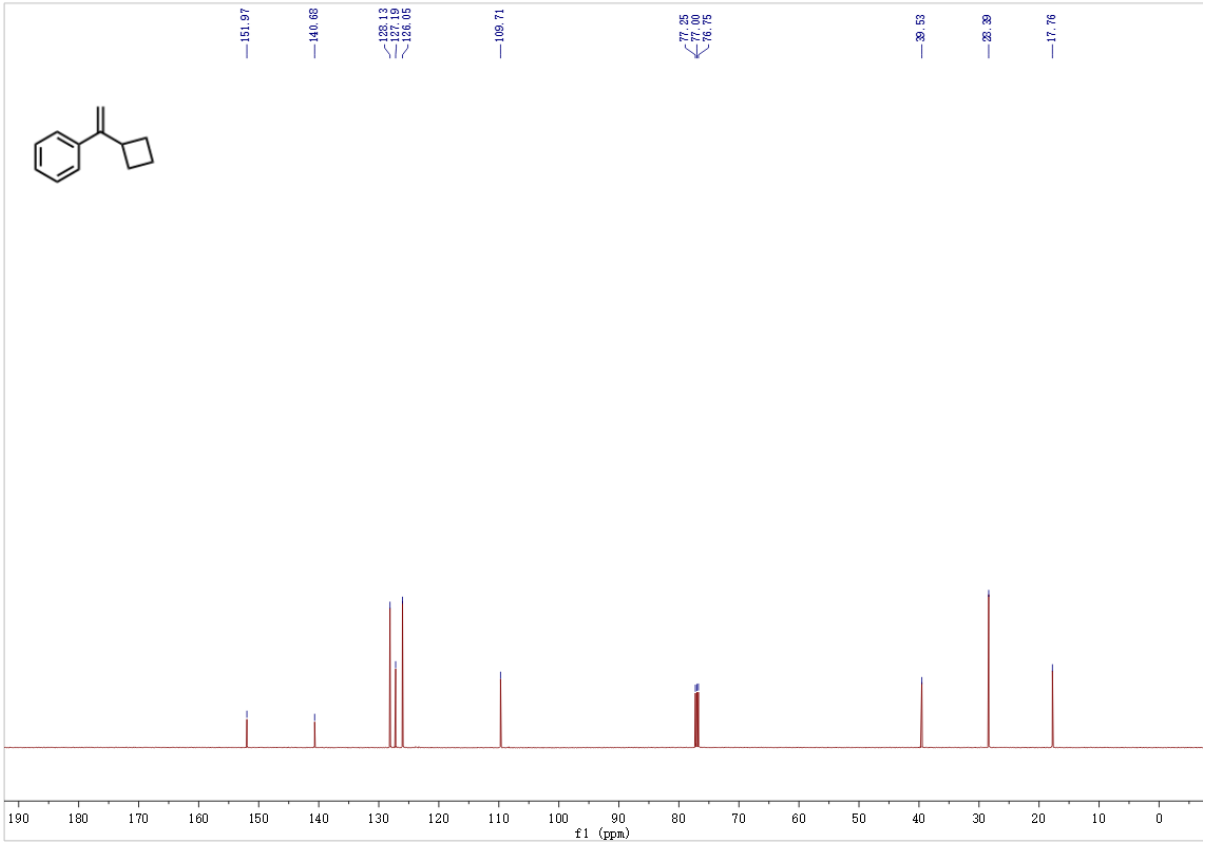

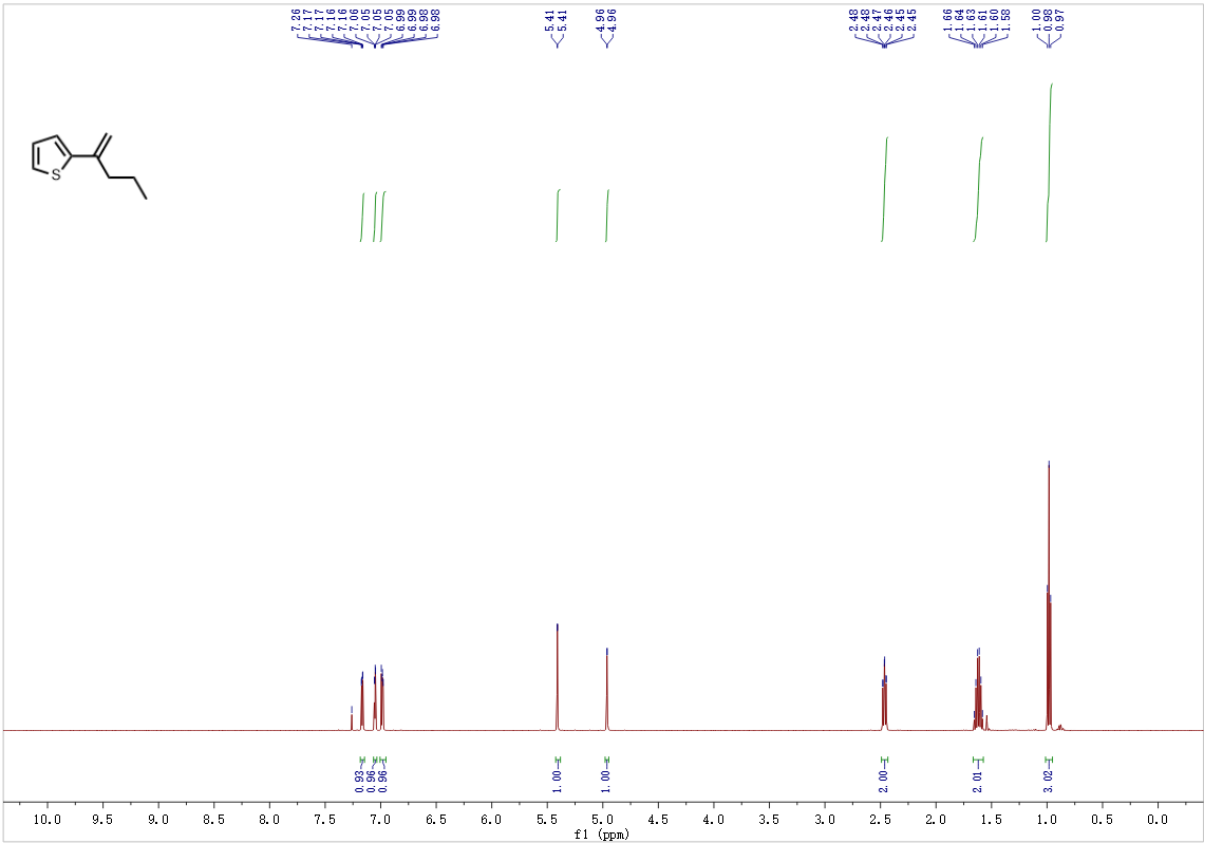
7.26
7.17
7.17
7.16
7.16
7.06
7.05
7.05
6.99
6.99
6.98
6.98
5.41
5.41
4.96
4.96
2.48
2.48
2.47
2.46
2.45
2.45
1.66
1.64
1.63
1.61
1.60
1.58
1.00
0.98
0.97
0.93
0.96
0.96
1.00
1.00
2.00
2.01
3.02
10.0 9.5 9.0 8.5 8.0 7.5 7.0 6.5 6.0 5.5 5.0 4.5 4.0 3.5 3.0 2.5 2.0 1.5 1.0 0.5 0.0
f1 (ppm)

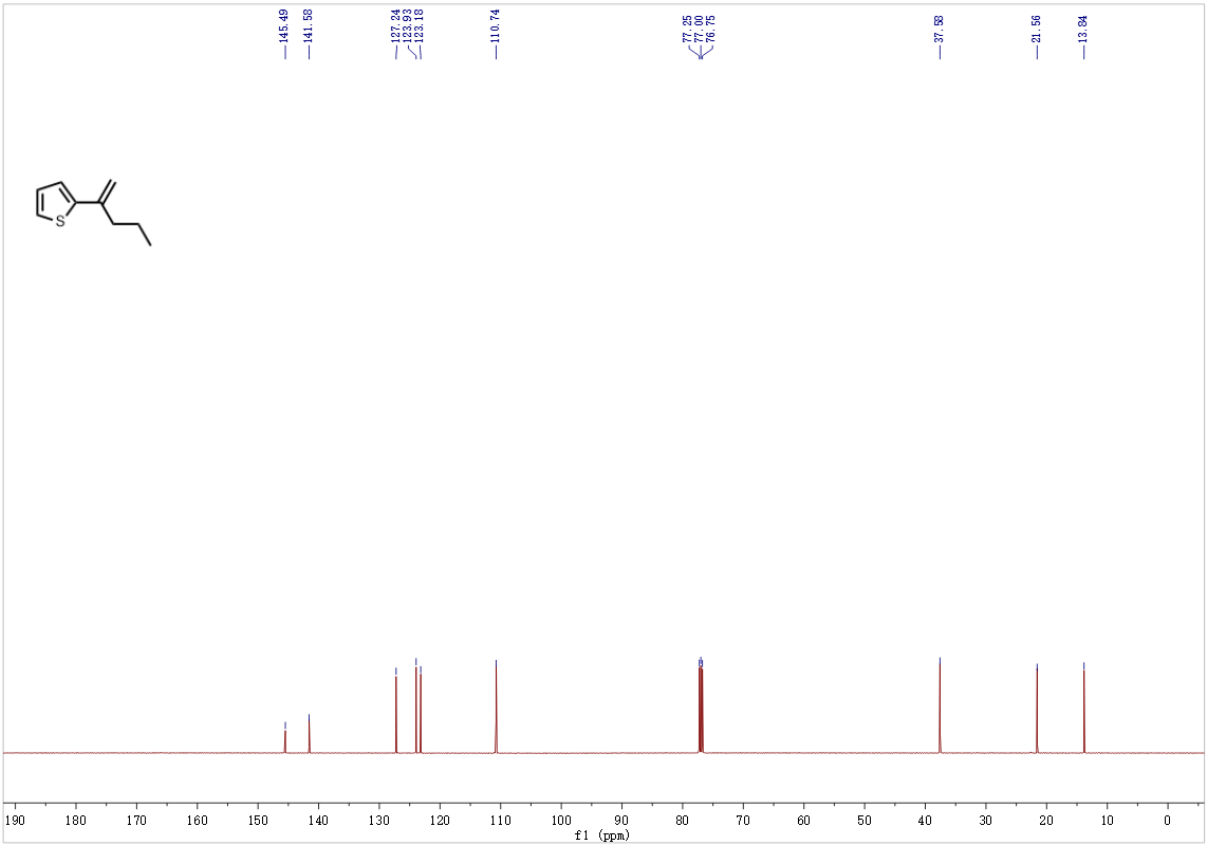
145.49
141.58
127.24
123.93
123.18
110.74
77.25
77.00
76.75
37.58
21.56
13.84
190 180 170 160 150 140 130 120 110 100 90 80 70 60 50 40 30 20 10 0
f1 (ppm)

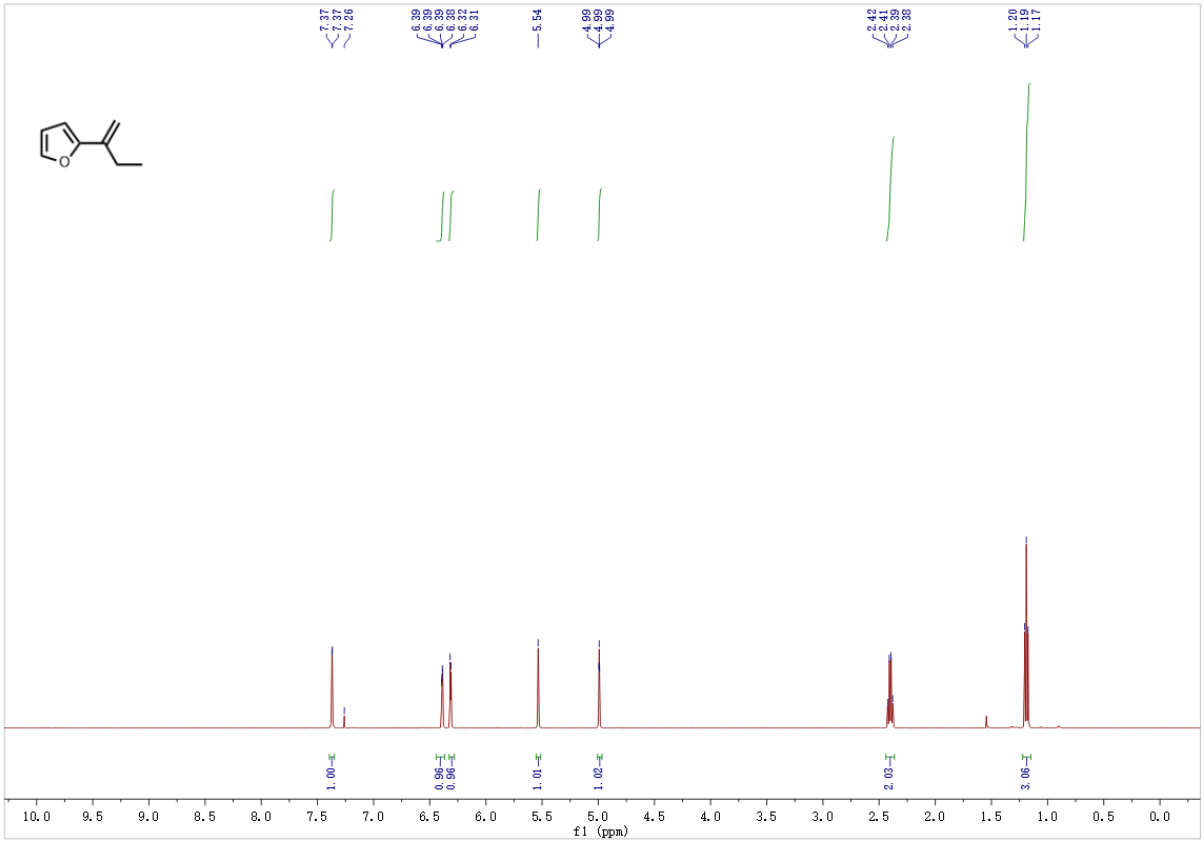
7.37
7.37
7.26
6.39
6.39
6.39
6.33
6.32
6.31
5.54
4.99
4.99
4.99
2.42
2.41
2.39
2.38
1.20
1.19
1.17
1.00
0.96
0.96
1.01
1.02
2.03
3.06
f1 (ppm)

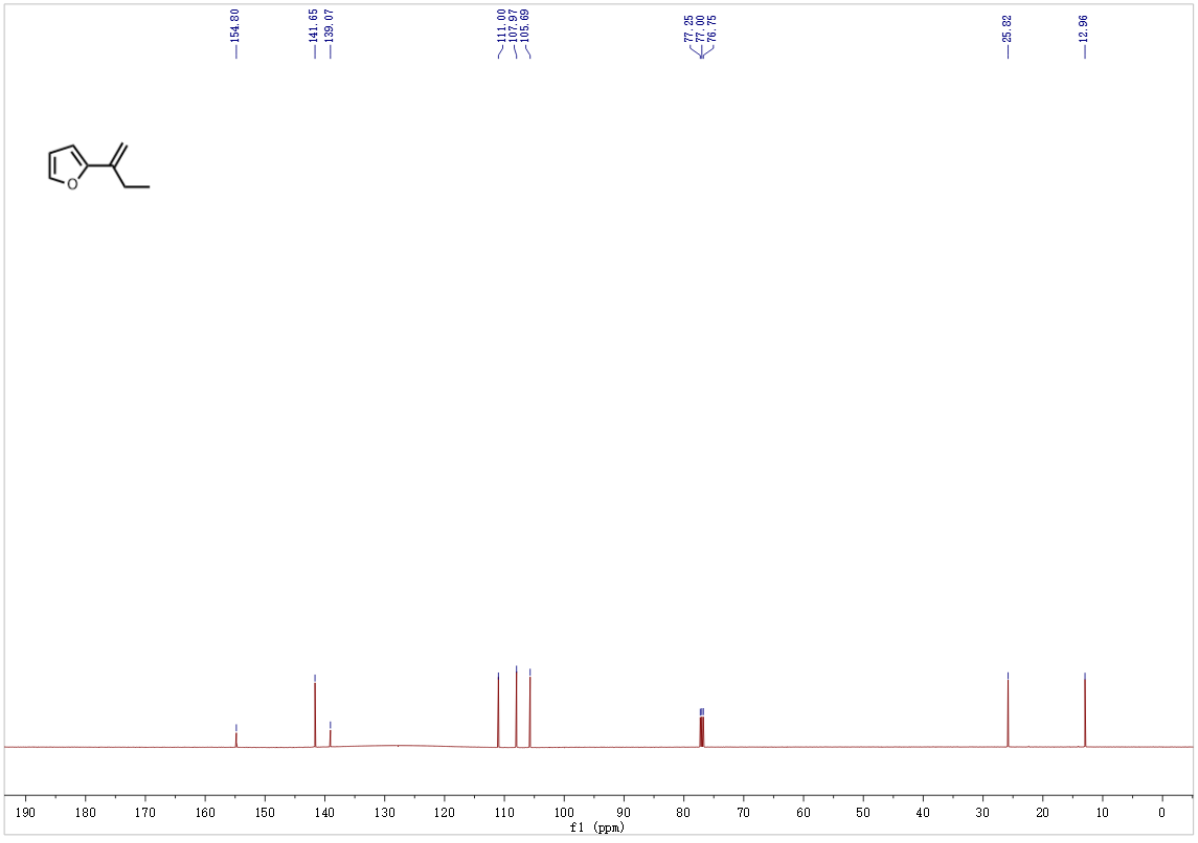
154.80
141.65
139.07
111.00
107.97
105.69
77.25
77.00
76.75
25.82
12.96
f1 (ppm)

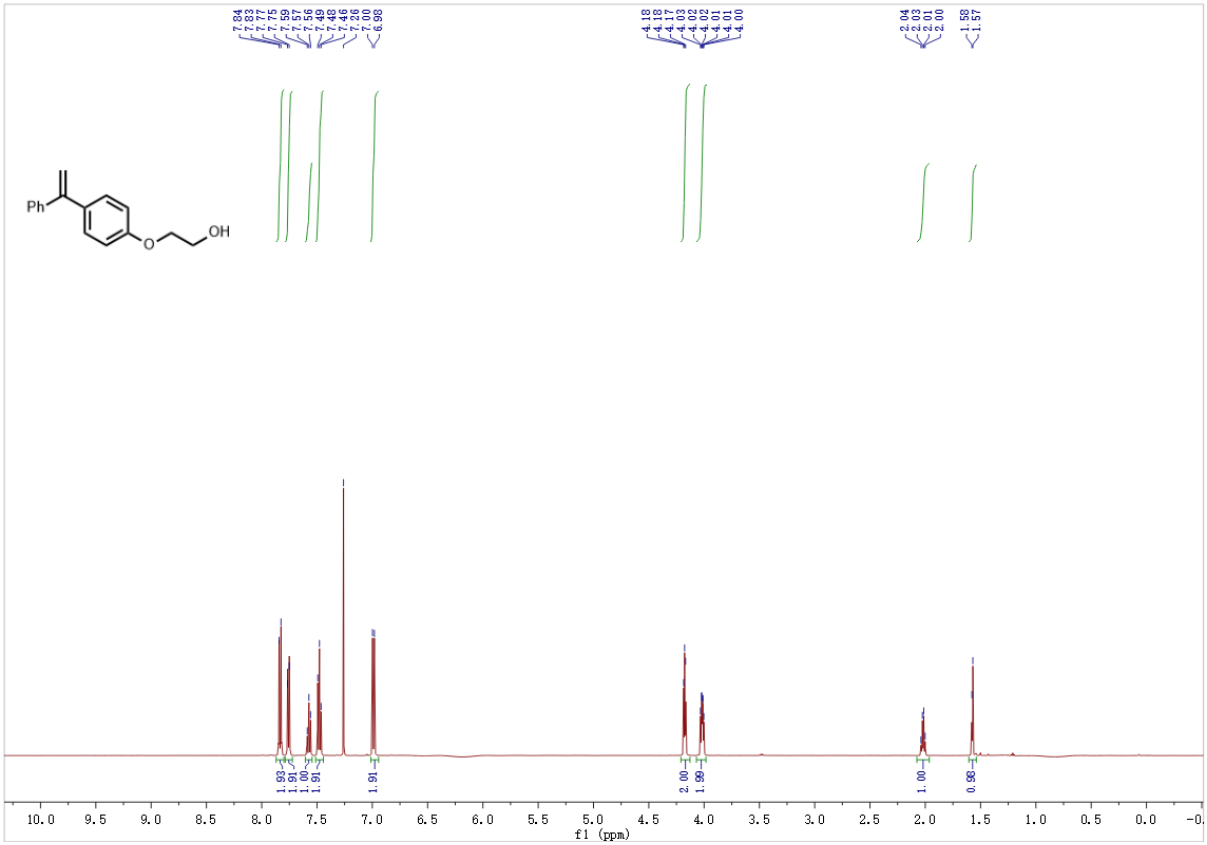
7.84
7.83
7.77
7.75
7.59
7.57
7.56
7.49
7.48
7.46
7.26
7.00
6.98
4.18
4.18
4.17
4.03
4.02
4.02
4.01
4.01
4.00
2.04
2.03
2.01
2.00
1.58
1.57
Ph
O
OH
1.93
1.91
1.00
1.91
1.91
2.00
1.99
1.00
0.98
10.0 9.5 9.0 8.5 8.0 7.5 7.0 6.5 6.0 5.5 5.0 4.5 4.0 3.5 3.0 2.5 2.0 1.5 1.0 0.5 0.0
f1 (ppm)

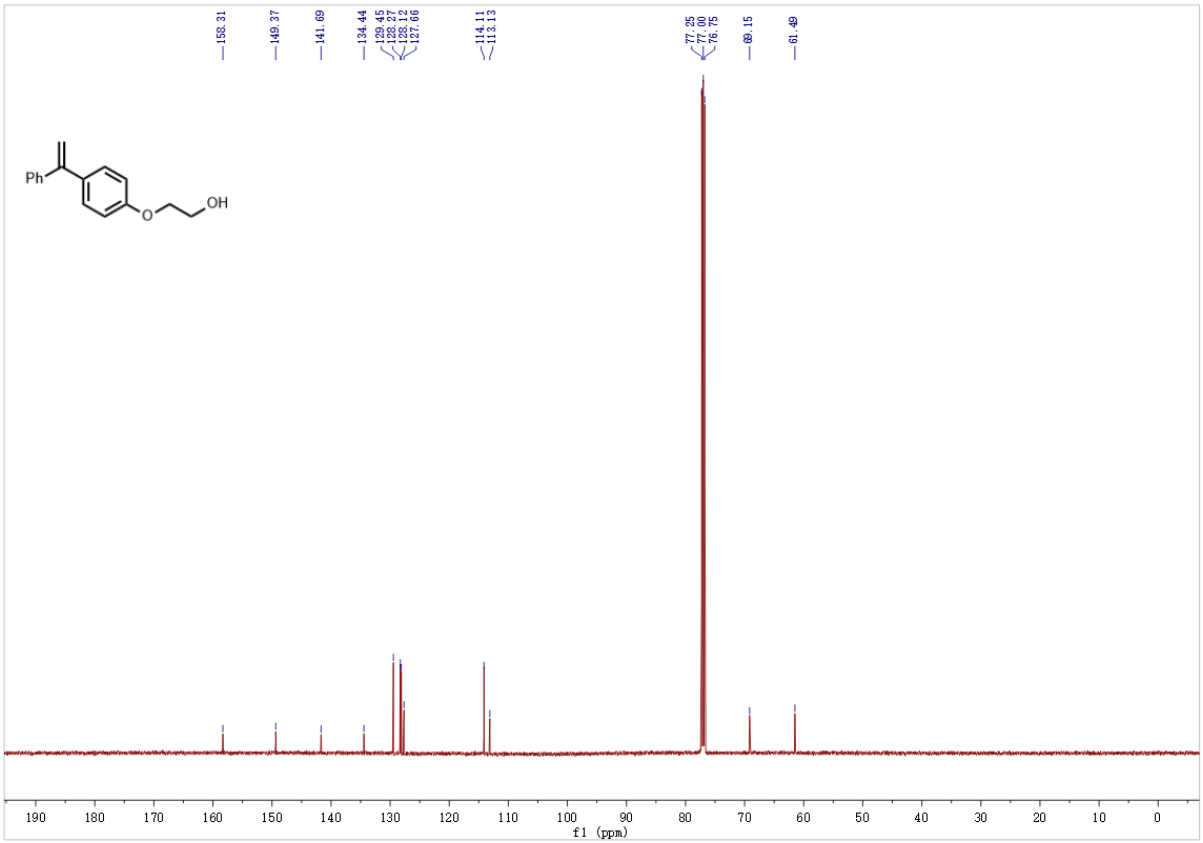
158.31
149.37
141.69
134.44
129.45
128.27
128.12
127.66
114.11
113.13
77.25
77.00
76.75
69.15
61.49
Ph
O
OH
190 180 170 160 150 140 130 120 110 100 90 80 70 60 50 40 30 20 10 0
f1 (ppm)

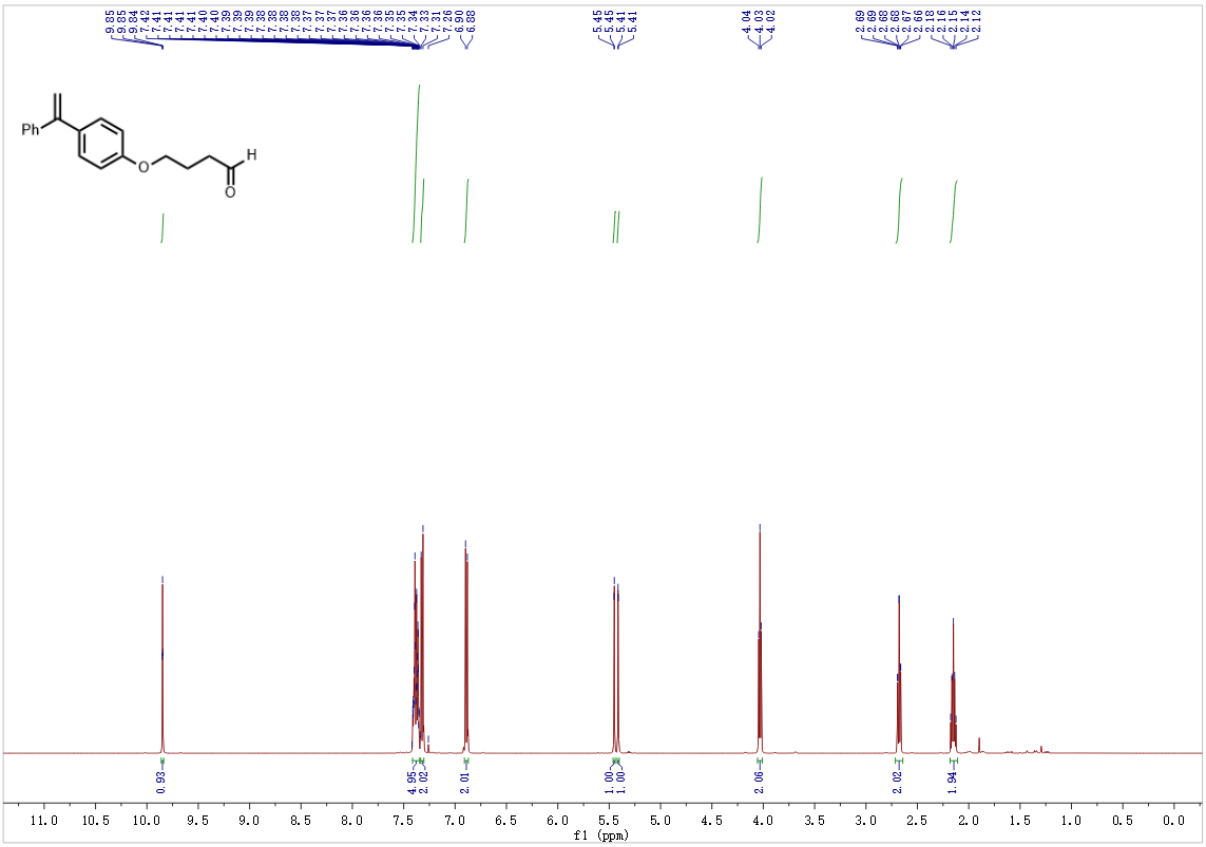
9.85
9.84
7.42
7.41
7.40
7.39
7.38
7.37
7.36
7.35
7.34
7.33
7.31
7.26
6.90
6.88
5.45
5.41
4.04
4.03
4.02
2.69
2.68
2.67
2.66
2.18
2.15
2.14
2.12
Ph
O
H
O
0.93
4.95
2.02
2.01
1.00
1.00
2.06
2.02
1.94
11.0 10.5 10.0 9.5 9.0 8.5 8.0 7.5 7.0 6.5 6.0 5.5 5.0 4.5 4.0 3.5 3.0 2.5 2.0 1.5 1.0 0.5 0.0
f1 (ppm)

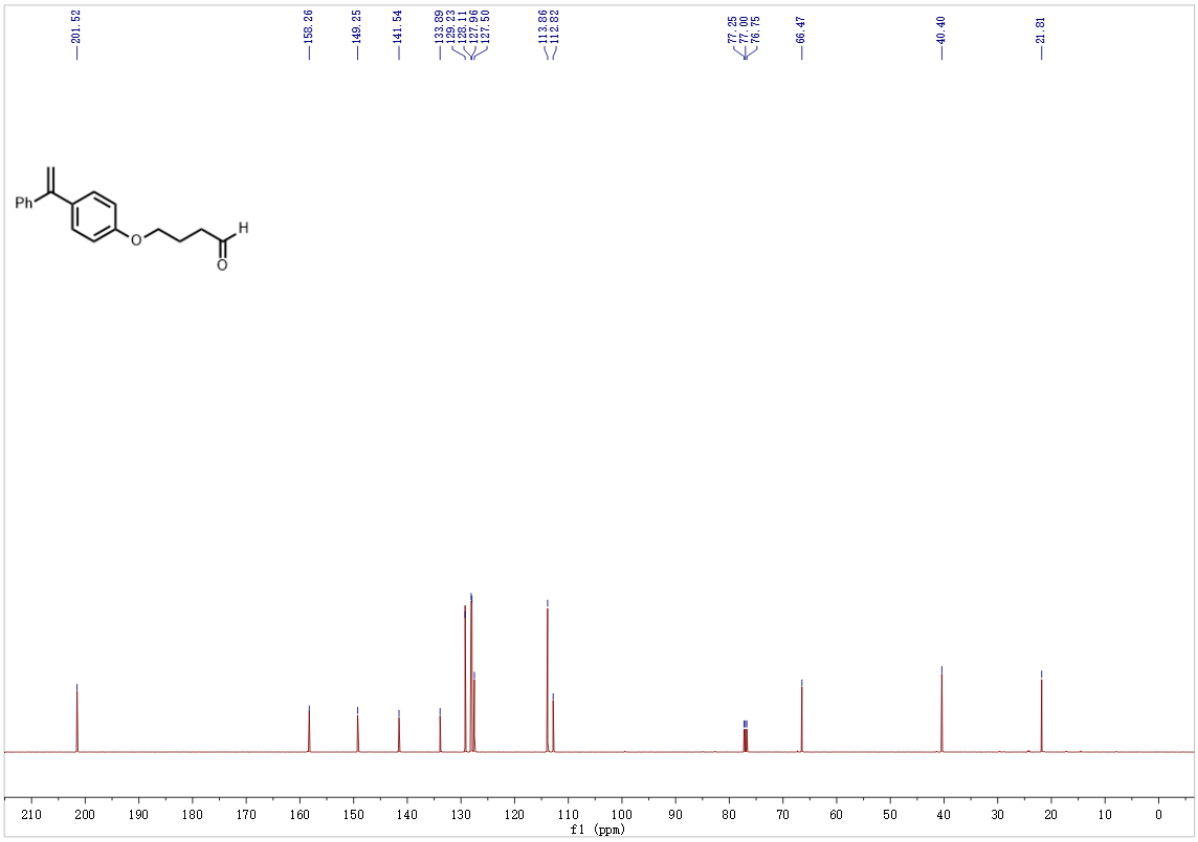
201.52
158.26
149.25
141.54
133.89
129.23
128.11
127.96
127.50
113.86
112.82
77.25
77.00
76.75
66.47
40.40
21.81
Ph
O
H
O
210 200 190 180 170 160 150 140 130 120 110 100 90 80 70 60 50 40 30 20 10 0
f1 (ppm)

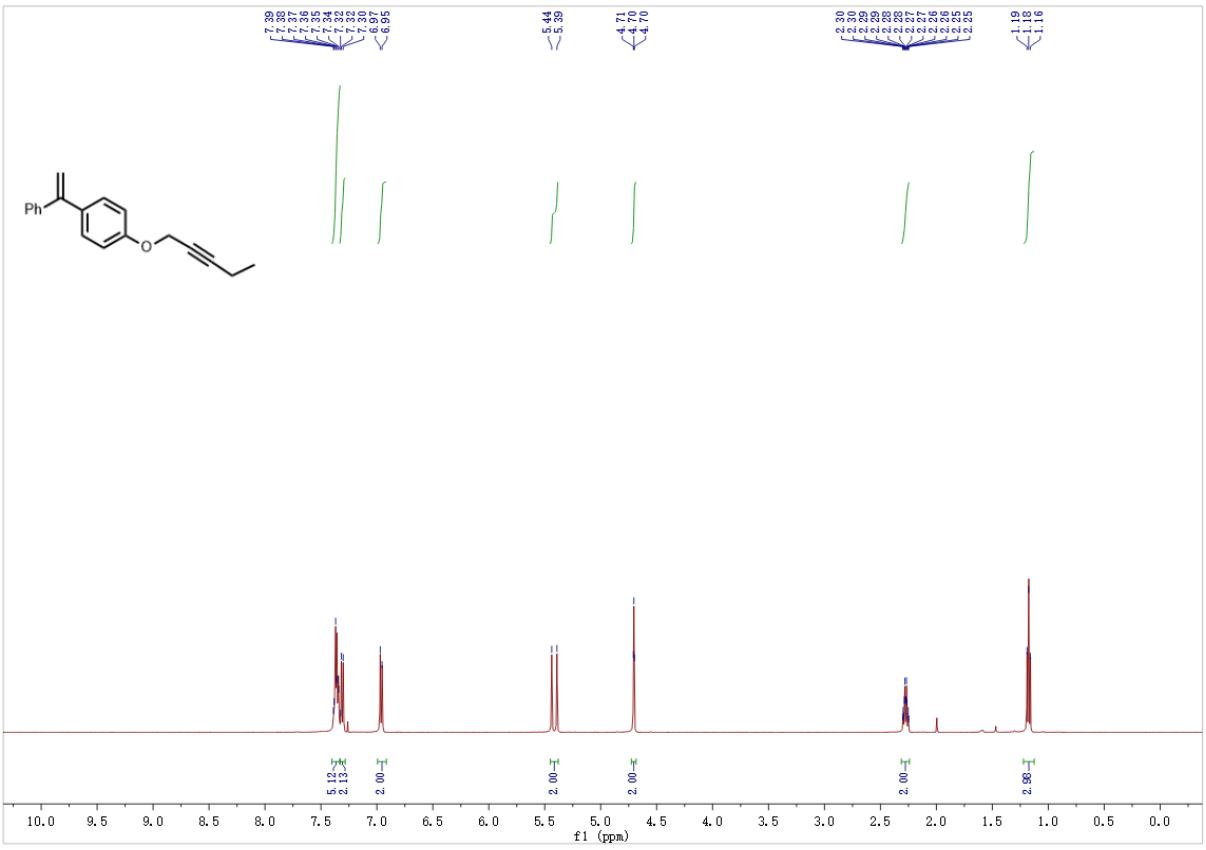
7.39
7.38
7.37
7.36
7.35
7.34
7.32
7.30
6.97
6.95
5.44
5.39
4.71
4.70
4.70
2.30
2.30
2.29
2.29
2.28
2.28
2.27
2.27
2.26
2.26
2.25
2.25
1.19
1.18
1.16
Ph
O
5.13
2.13
2.00
2.00
2.00
2.00
2.98
10.0 9.5 9.0 8.5 8.0 7.5 7.0 6.5 6.0 5.5 5.0 4.5 4.0 3.5 3.0 2.5 2.0 1.5 1.0 0.5 0.0
f1 (ppm)

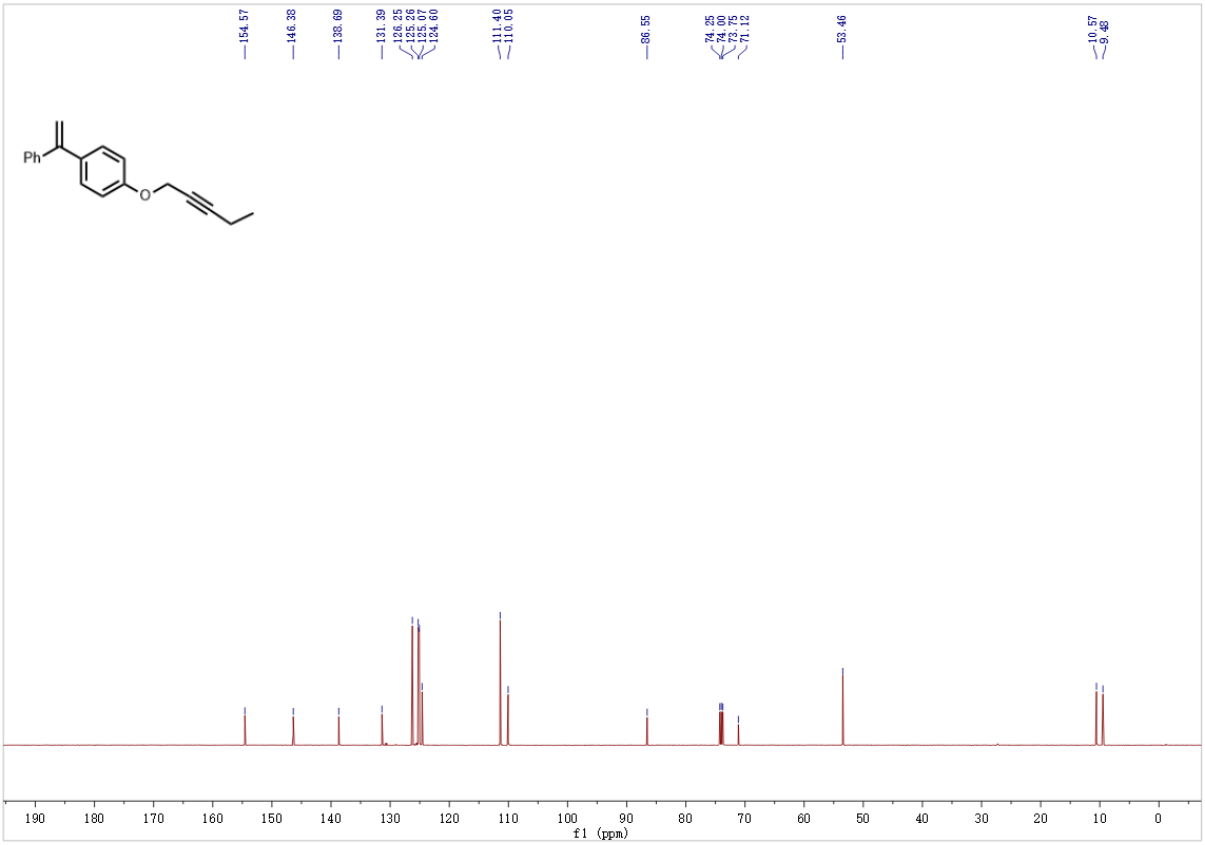
154.57
146.38
138.69
131.39
126.25
125.66
125.07
124.60
111.40
110.65
86.55
74.25
74.00
73.75
71.12
53.46
10.57
9.48
Ph
O
190 180 170 160 150 140 130 120 110 100 90 80 70 60 50 40 30 20 10 0
f1 (ppm)

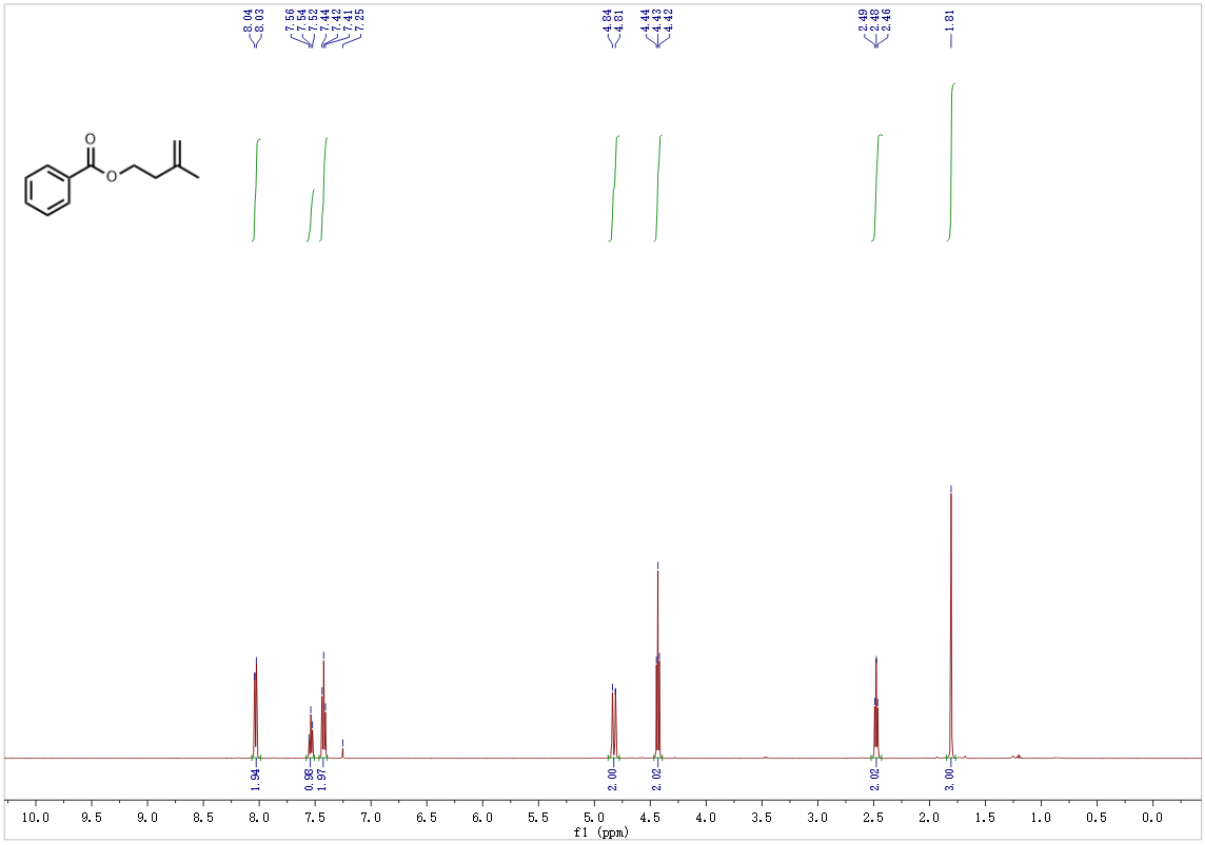
8.04
8.03
7.56
7.54
7.52
7.44
7.42
7.41
7.25
4.84
4.81
4.44
4.43
4.42
2.49
2.48
2.46
1.81
1.94
0.98
1.97
2.00
2.02
2.02
3.00
f1 (ppm)

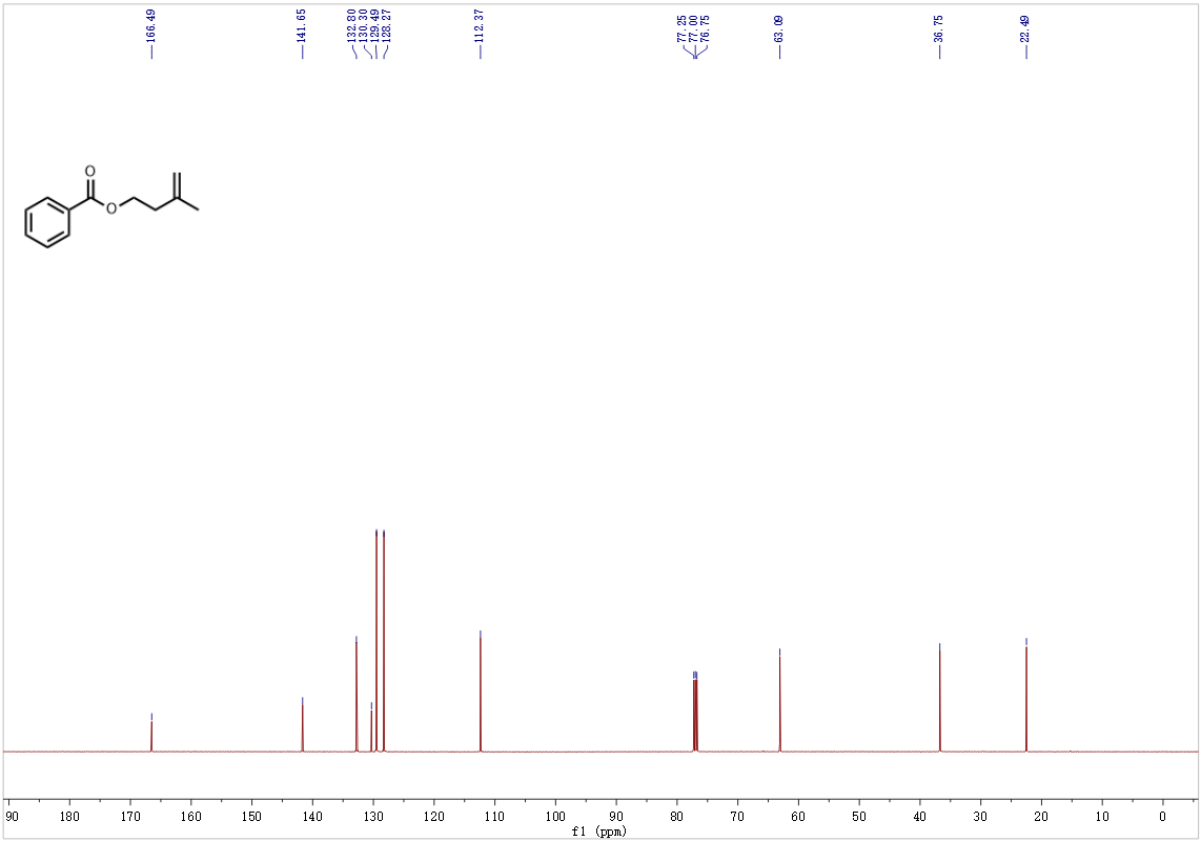
166.49
141.65
132.80
130.30
129.49
128.27
112.37
77.25
77.00
76.75
63.09
36.75
22.49
f1 (ppm)

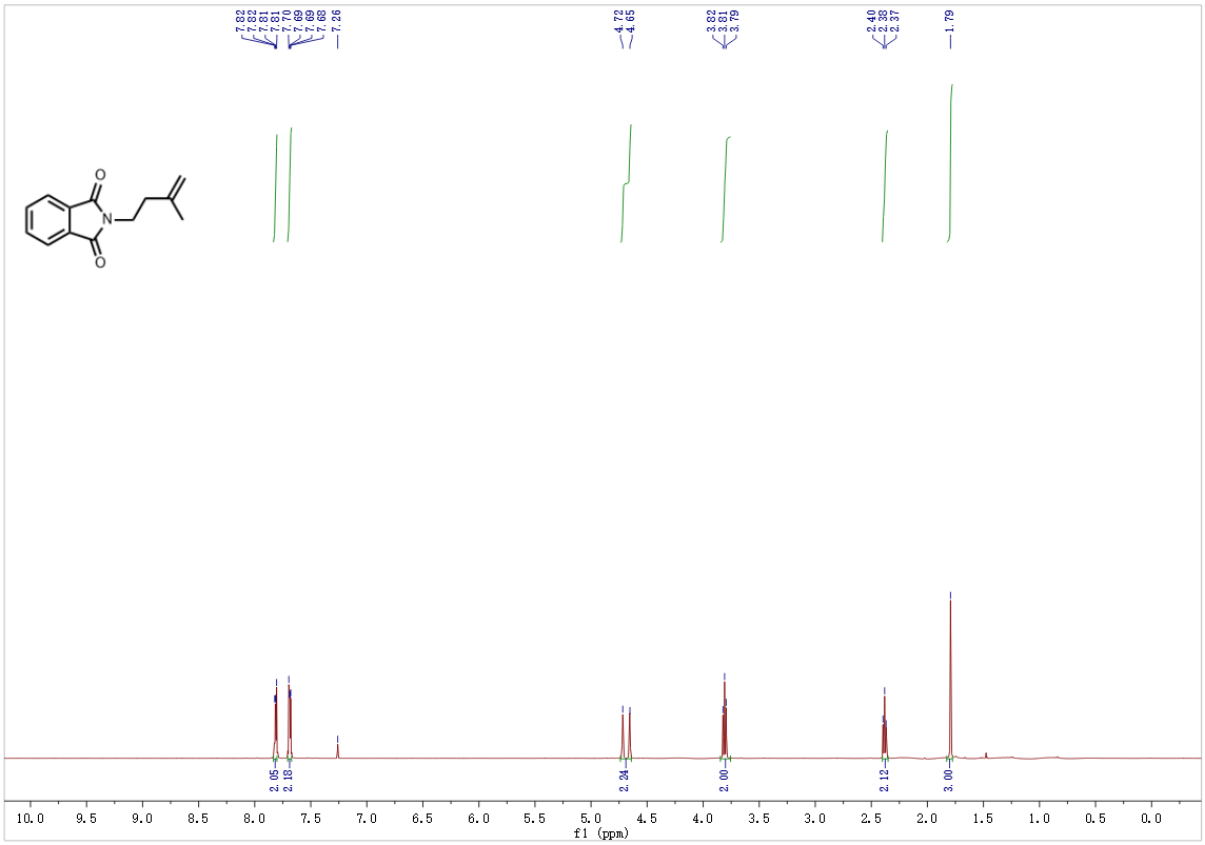
7.82
7.82
7.81
7.81
7.70
7.69
7.68
7.68
7.26
4.72
4.65
3.82
3.81
3.79
2.40
2.38
2.37
1.79
2.05
2.18
2.24
2.00
2.12
3.00
10.0 9.5 9.0 8.5 8.0 7.5 7.0 6.5 6.0 5.5 5.0 4.5 4.0 3.5 3.0 2.5 2.0 1.5 1.0 0.5 0.0
f1 (ppm)

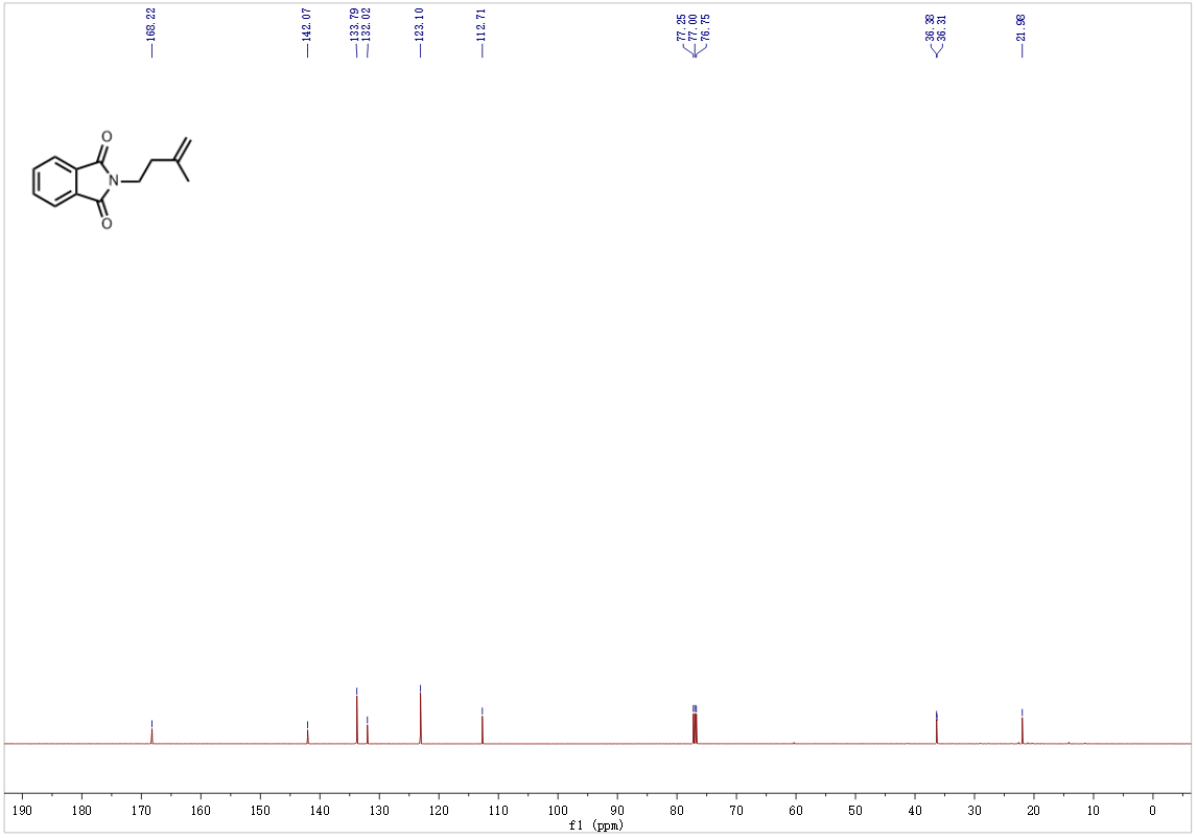
168.22
142.07
133.79
132.02
123.10
112.71
77.25
77.00
76.75
36.88
36.31
21.98
190 180 170 160 150 140 130 120 110 100 90 80 70 60 50 40 30 20 10 0
f1 (ppm)

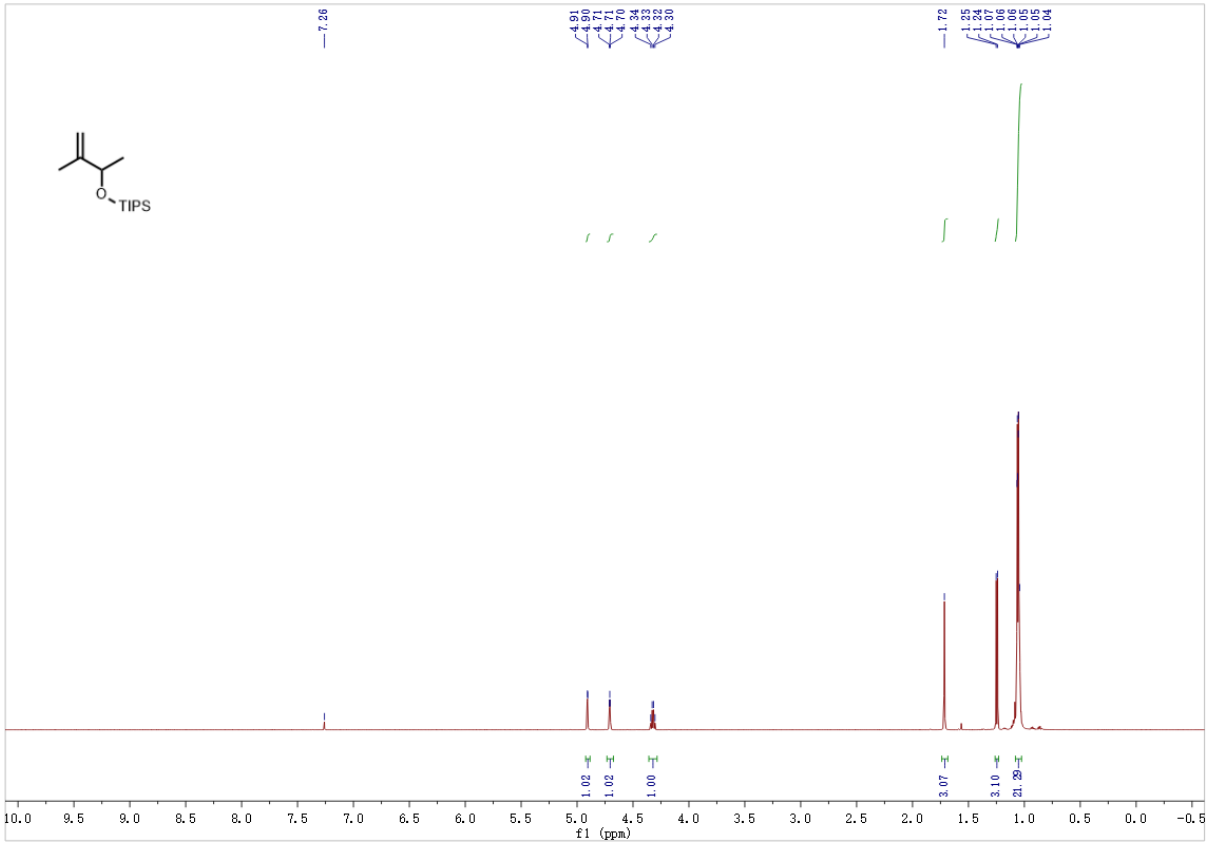
7.26
4.91
4.90
4.71
4.70
4.34
4.33
4.32
4.30
1.72
1.25
1.24
1.07
1.06
1.05
1.05
1.05
1.04
TIPS
1.02
1.02
1.00
3.07
3.10
21.29
f1 (ppm)

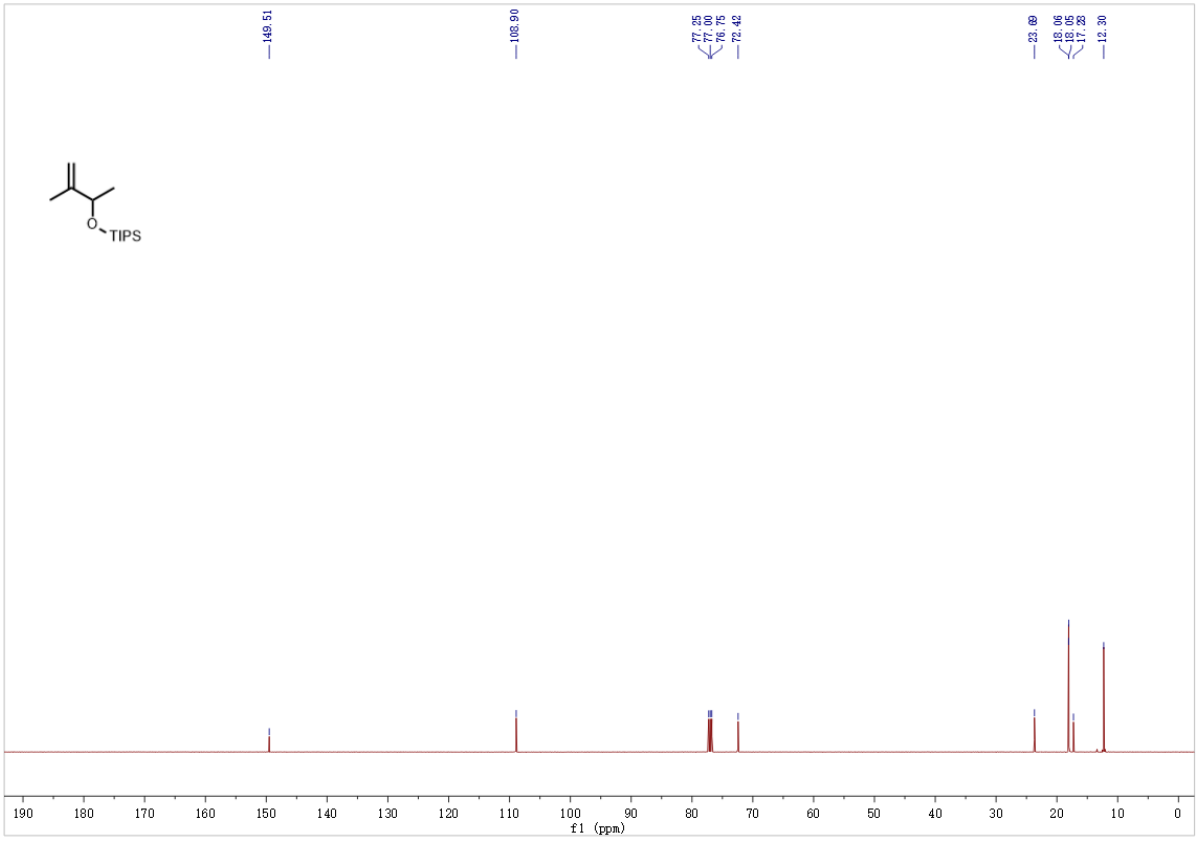
149.51
108.90
77.25
77.00
76.75
72.42
23.89
18.06
18.05
17.28
12.30
TIPS
f1 (ppm)

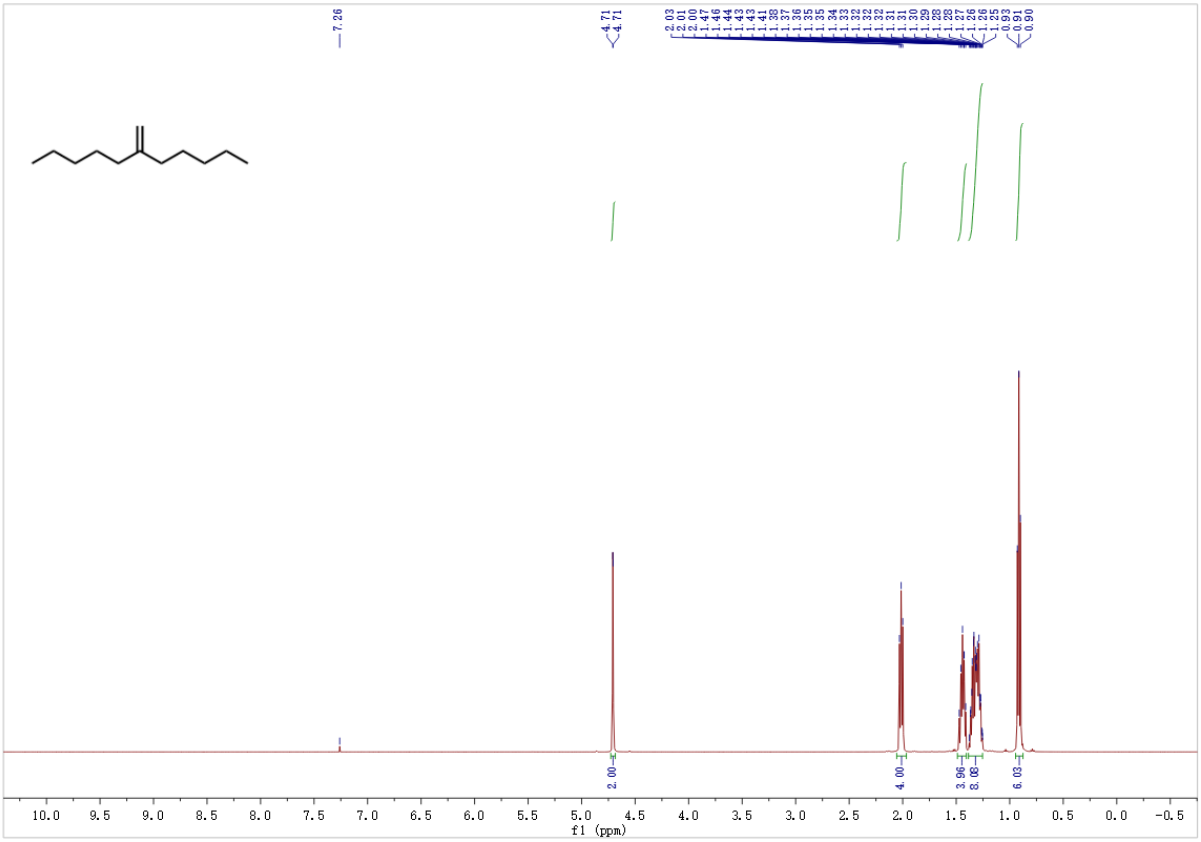
7.26
4.71
4.71
2.03
2.01
2.00
1.47
1.46
1.44
1.43
1.41
1.38
1.37
1.36
1.35
1.34
1.33
1.32
1.32
1.31
1.30
1.29
1.28
1.27
1.26
0.93
0.91
0.90
2.00
4.00
3.96
8.08
6.03
10.0 9.5 9.0 8.5 8.0 7.5 7.0 6.5 6.0 5.5 5.0 4.5 4.0 3.5 3.0 2.5 2.0 1.5 1.0 0.5 0.0 -0.5
f1 (ppm)

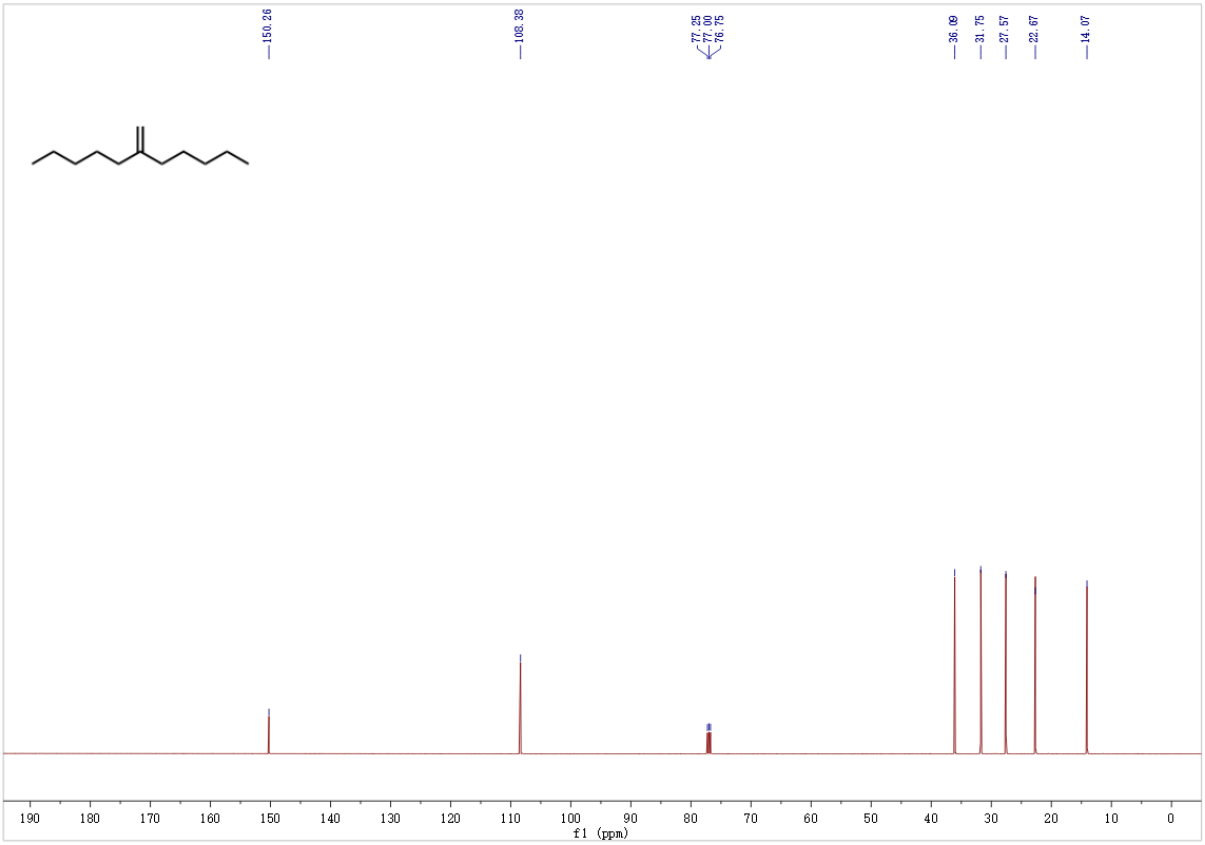
150.26
108.38
77.25
77.00
76.75
36.09
31.75
27.57
22.67
14.07
190 180 170 160 150 140 130 120 110 100 90 80 70 60 50 40 30 20 10 0
f1 (ppm)

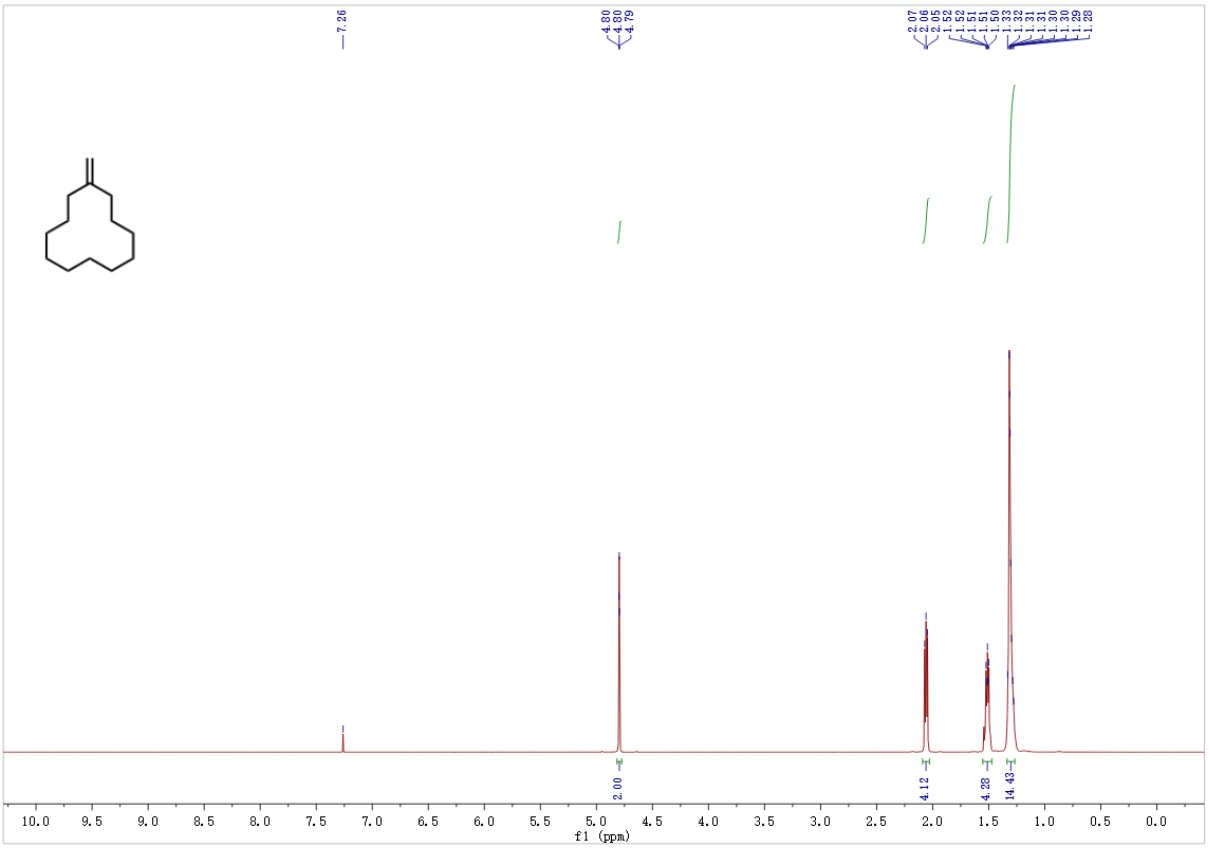
7.26
4.80
4.80
4.79
2.07
2.06
2.05
1.52
1.52
1.51
1.51
1.50
1.33
1.32
1.31
1.31
1.30
1.30
1.29
1.28
2.00
4.12
4.28
14.43
10.0 9.5 9.0 8.5 8.0 7.5 7.0 6.5 6.0 5.5 5.0 4.5 4.0 3.5 3.0 2.5 2.0 1.5 1.0 0.5 0.0
f1 (ppm)

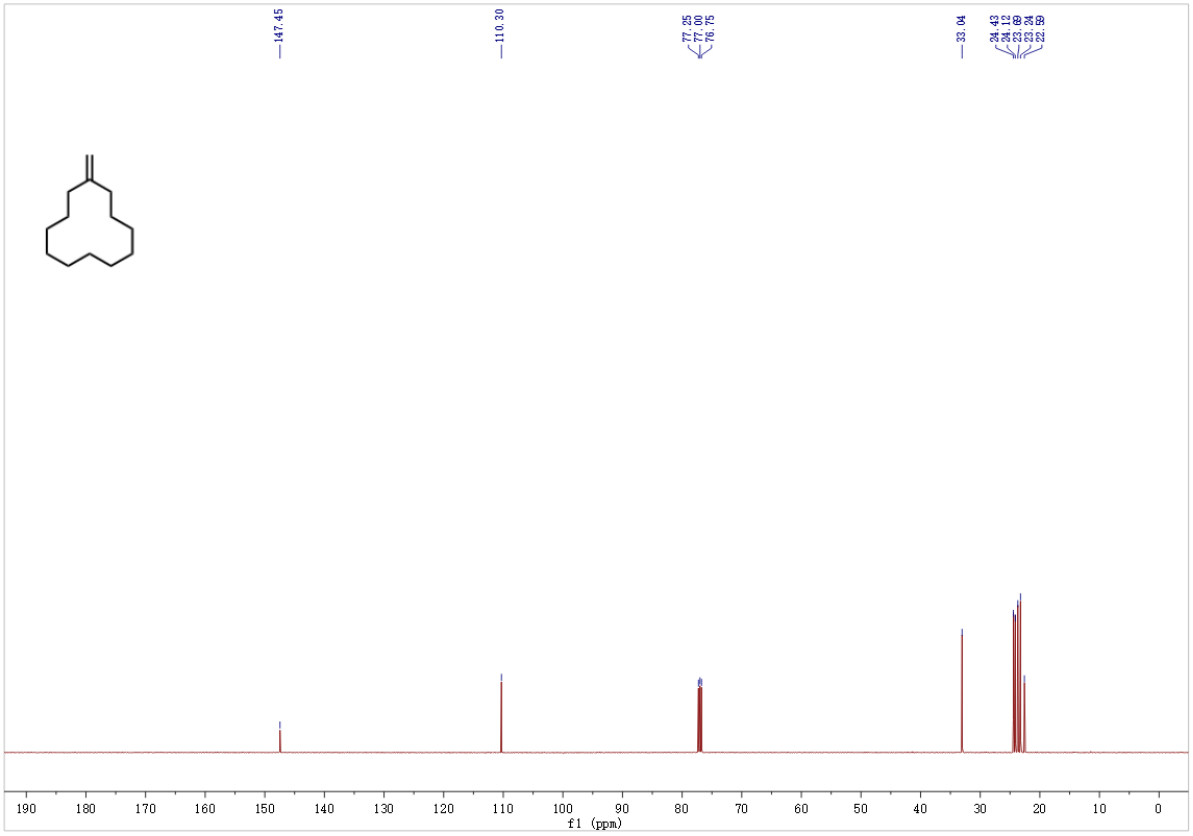
147.45
110.30
77.25
77.00
76.75
33.04
24.43
24.12
23.69
23.24
22.59
190 180 170 160 150 140 130 120 110 100 90 80 70 60 50 40 30 20 10 0
f1 (ppm)

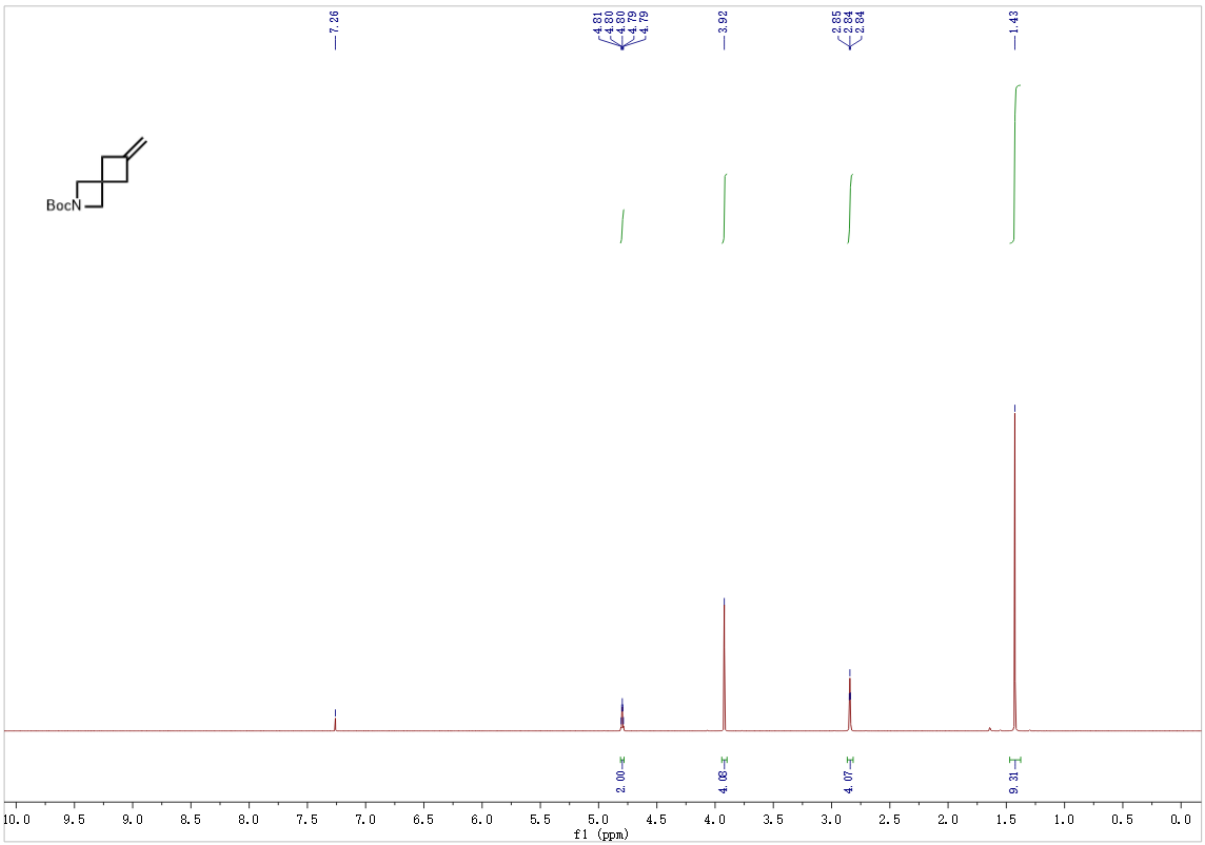
7.26
4.81
4.80
4.80
4.79
4.79
3.92
2.85
2.84
2.84
1.43
BocN
2.00
4.08
4.07
9.31
10.0 9.5 9.0 8.5 8.0 7.5 7.0 6.5 6.0 5.5 5.0 4.5 4.0 3.5 3.0 2.5 2.0 1.5 1.0 0.5 0.0
f1 (ppm)

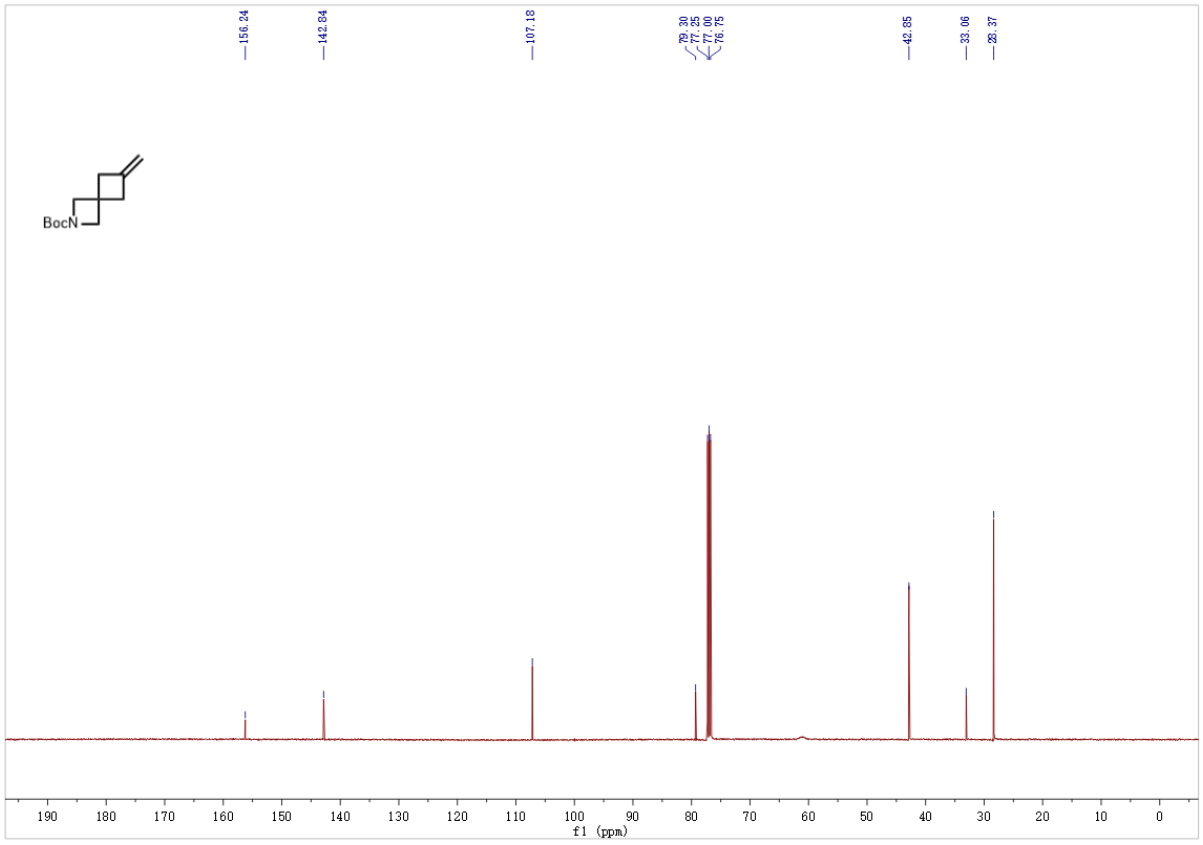
156.24
142.84
107.18
79.30
77.25
77.00
76.75
42.85
33.06
28.37
BocN
190 180 170 160 150 140 130 120 110 100 90 80 70 60 50 40 30 20 10 0
f1 (ppm)

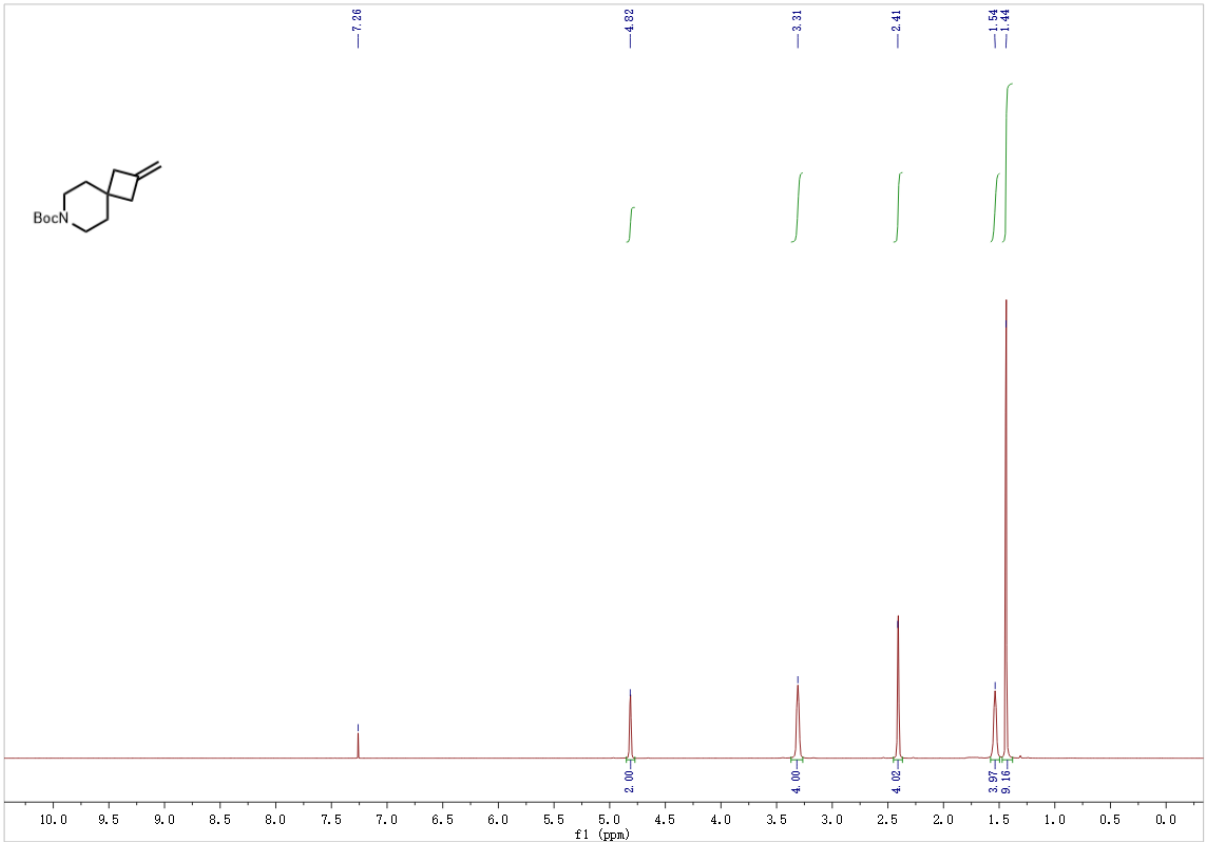
7.26
4.82
3.31
2.41
1.54
1.44
BocN
2.00
4.00
4.02
3.97
9.16
f1 (ppm)

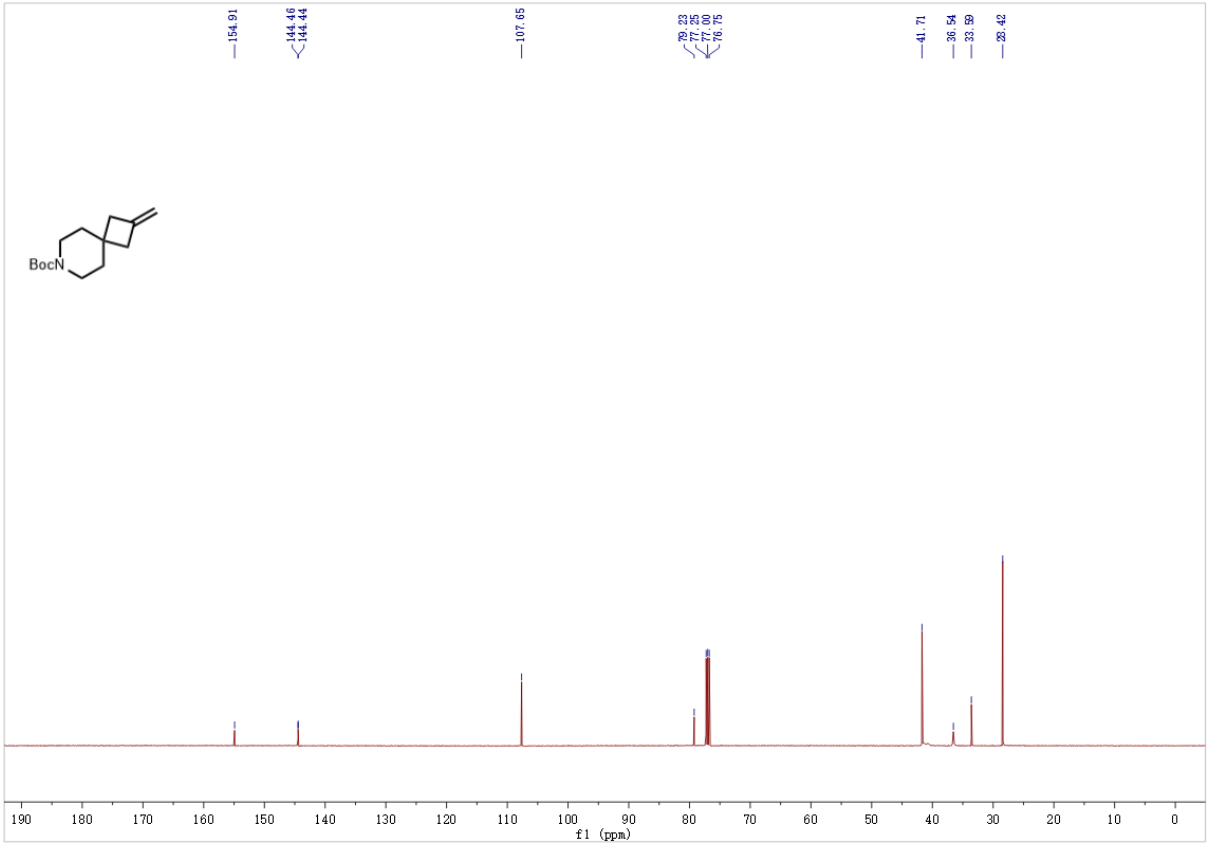
154.91
144.46
144.44
107.65
79.23
77.25
77.00
76.75
41.71
36.54
33.99
28.42
BocN
f1 (ppm)

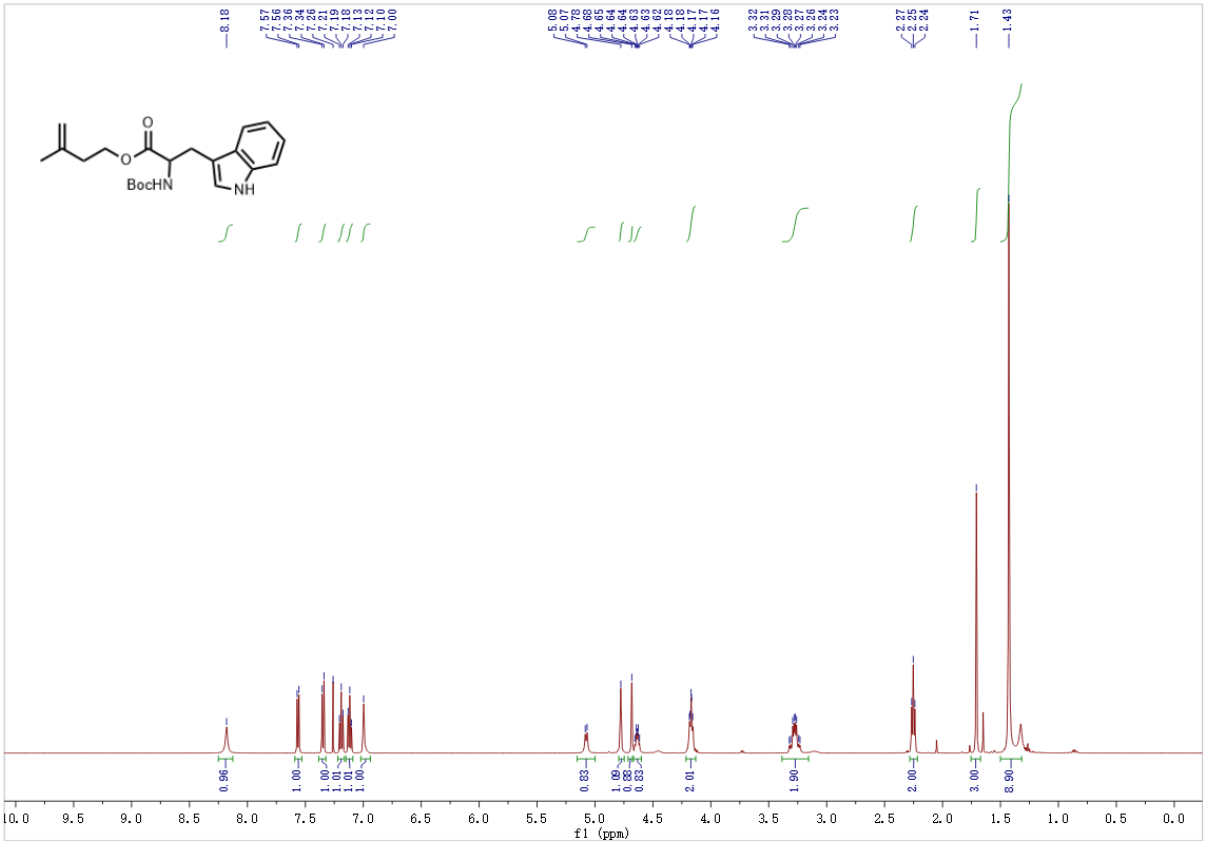
8.18
7.57
7.56
7.36
7.34
7.26
7.21
7.19
7.18
7.13
7.12
7.10
7.00
5.08
5.07
4.78
4.68
4.65
4.64
4.64
4.63
4.63
4.62
4.18
4.18
4.17
4.17
4.16
3.32
3.31
3.29
3.28
3.27
3.26
3.24
3.23
2.27
2.25
2.24
1.71
1.43
O
O
BocHN
NH
0.96
1.00
1.00
1.01
1.01
1.00
0.83
1.09
0.88
0.83
2.01
1.90
2.00
3.00
8.90
f1 (ppm)

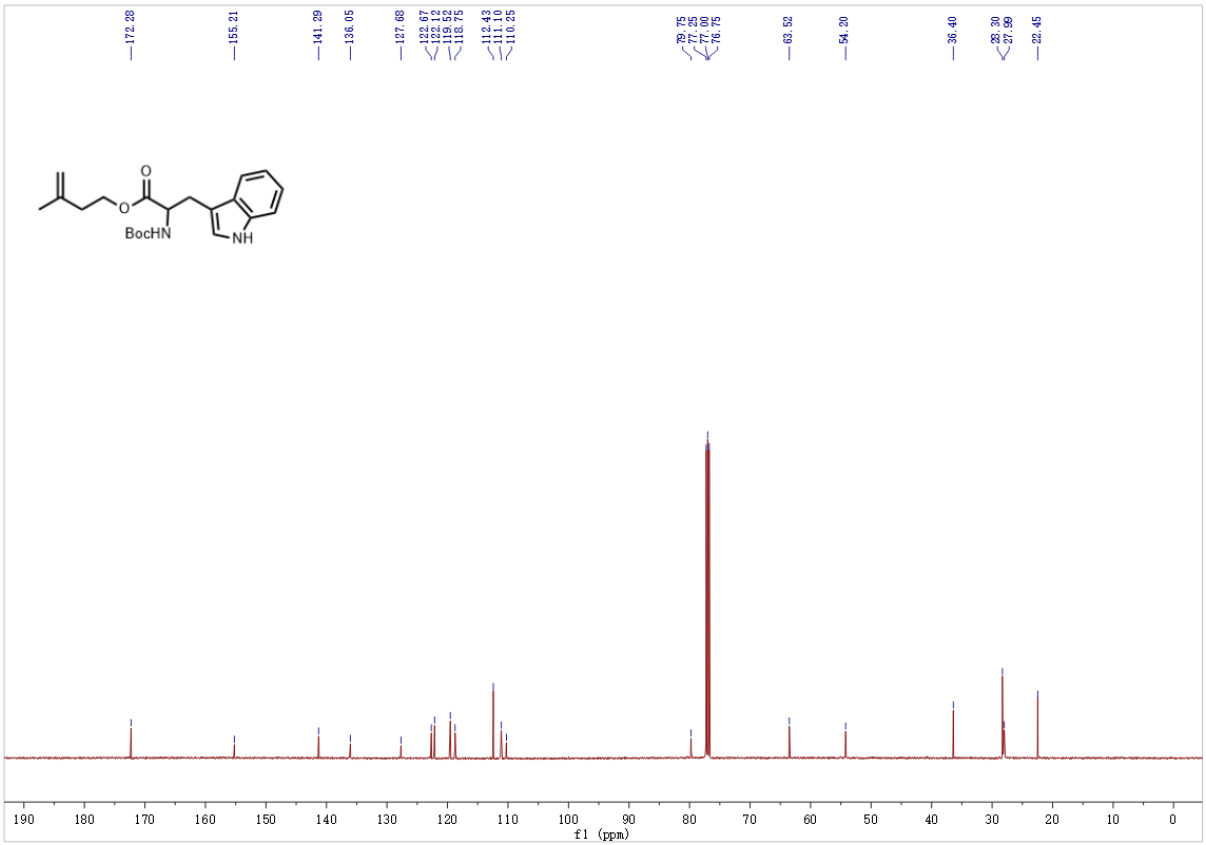
172.28
155.21
141.29
136.05
127.68
122.67
122.12
119.52
118.75
112.43
111.10
110.25
79.75
77.25
77.00
76.75
63.52
54.20
36.40
28.30
27.99
22.45
O
O
BocHN
NH
f1 (ppm)

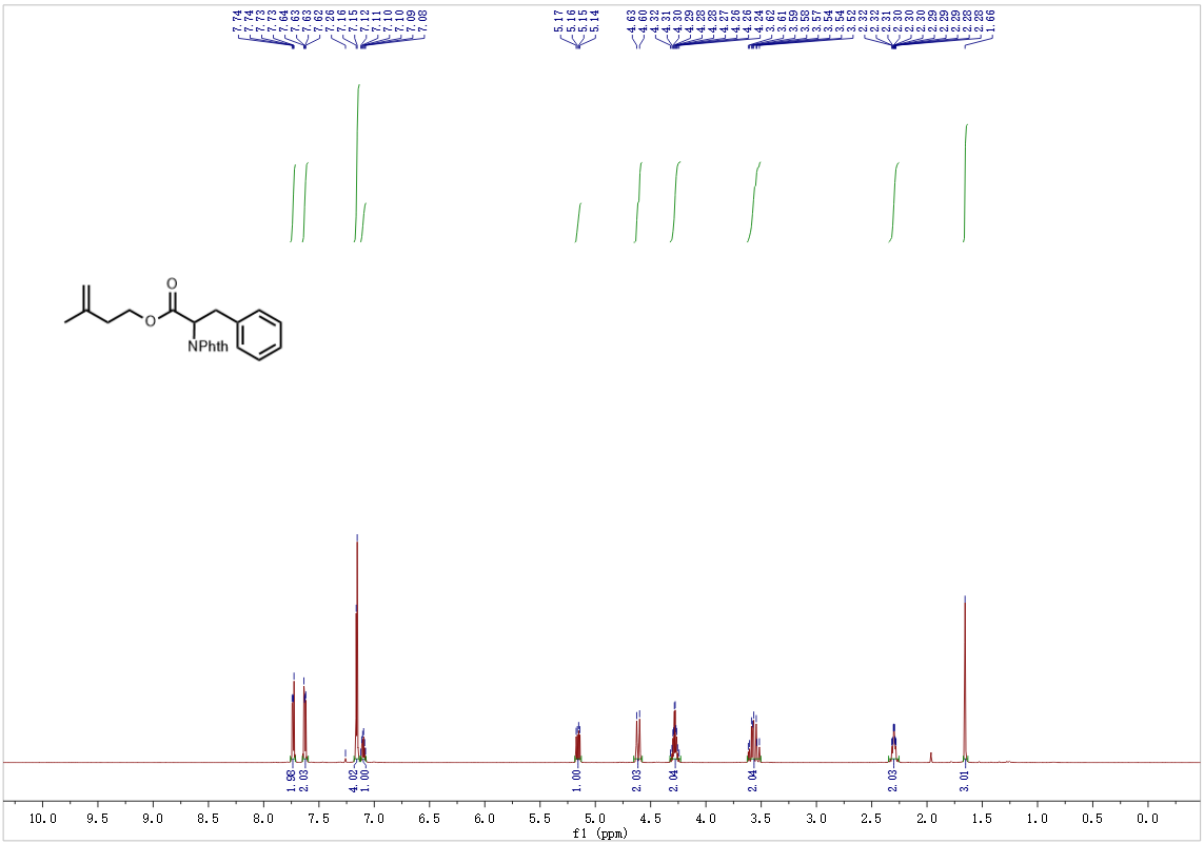
NPhth
f1 (ppm)

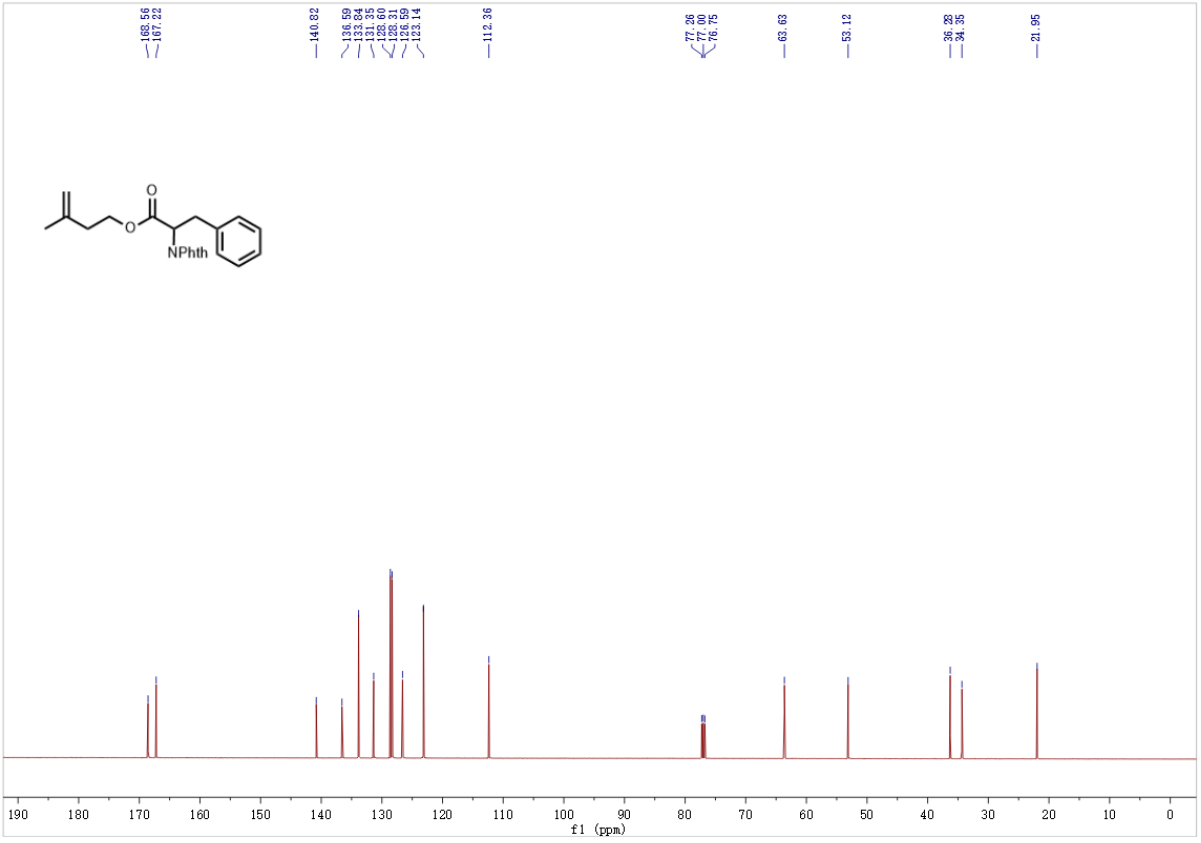
NPhth
f1 (ppm)

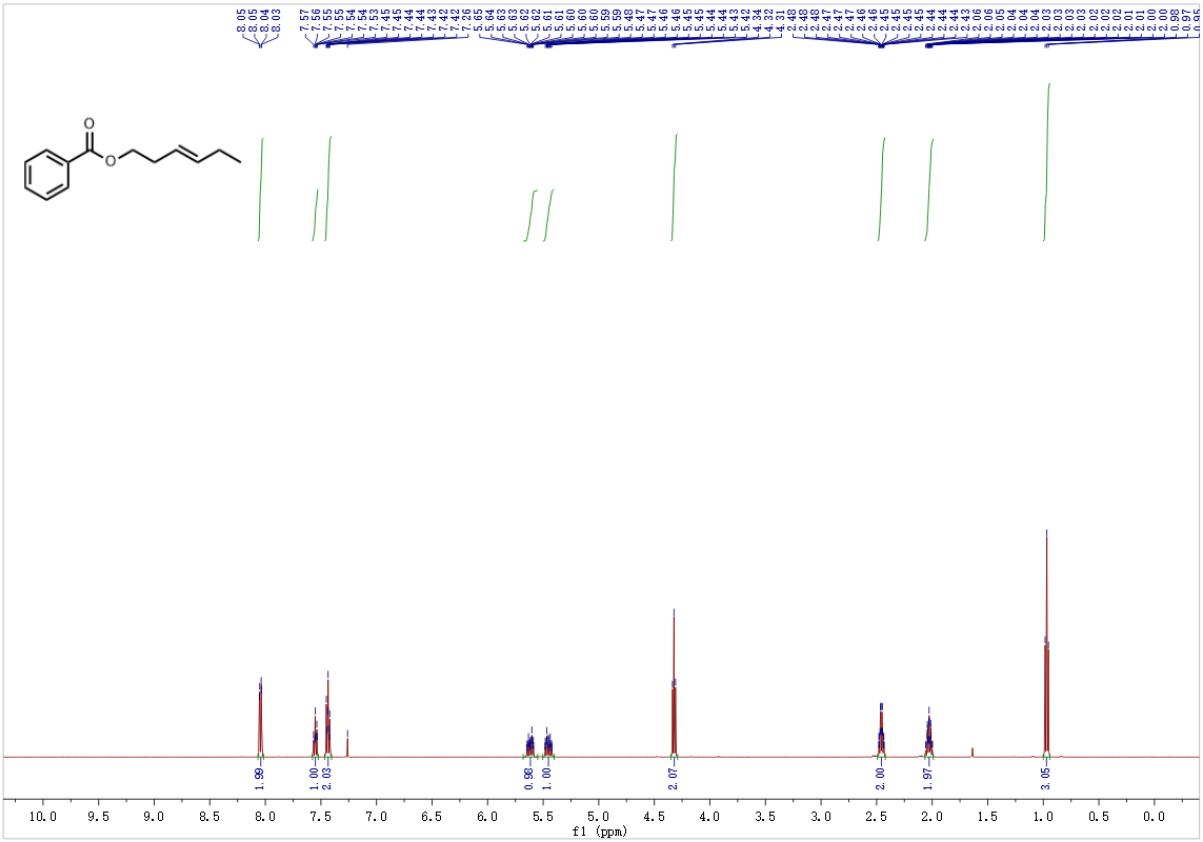
f1 (ppm)

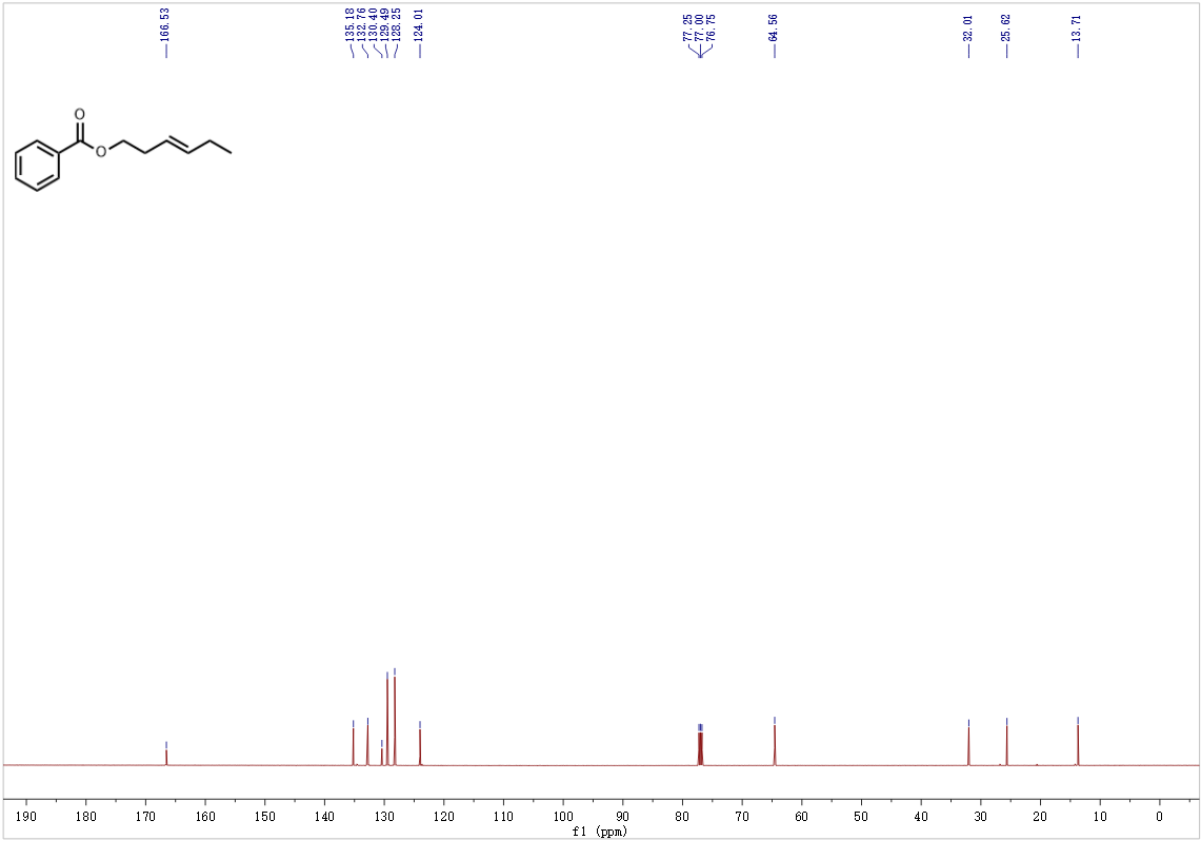
166.53
135.18
132.76
130.40
129.49
128.25
124.01
77.25
77.00
76.75
64.56
32.01
25.62
13.71
f1 (ppm)

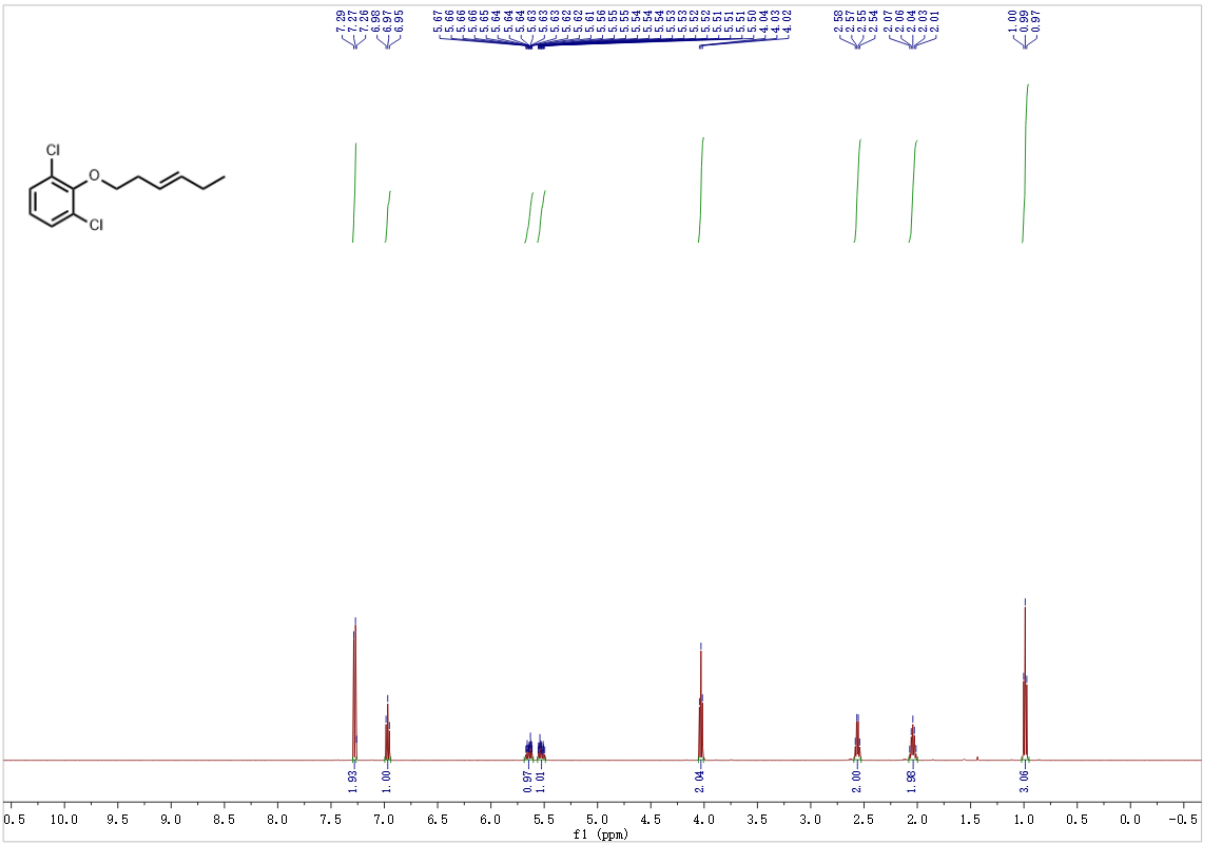
Cl
O
Cl
7.29
7.27
7.26
6.98
6.97
6.95
5.67
5.66
5.66
5.65
5.64
5.64
5.63
5.63
5.63
5.62
5.62
5.61
5.56
5.55
5.55
5.54
5.54
5.54
5.53
5.53
5.52
5.52
5.51
5.51
5.51
5.50
4.04
4.03
4.02
2.58
2.57
2.55
2.54
2.07
2.06
2.04
2.03
2.01
1.00
0.99
0.97
1.93
1.00
0.97
1.01
2.04
2.00
1.98
3.06
f1 (ppm)

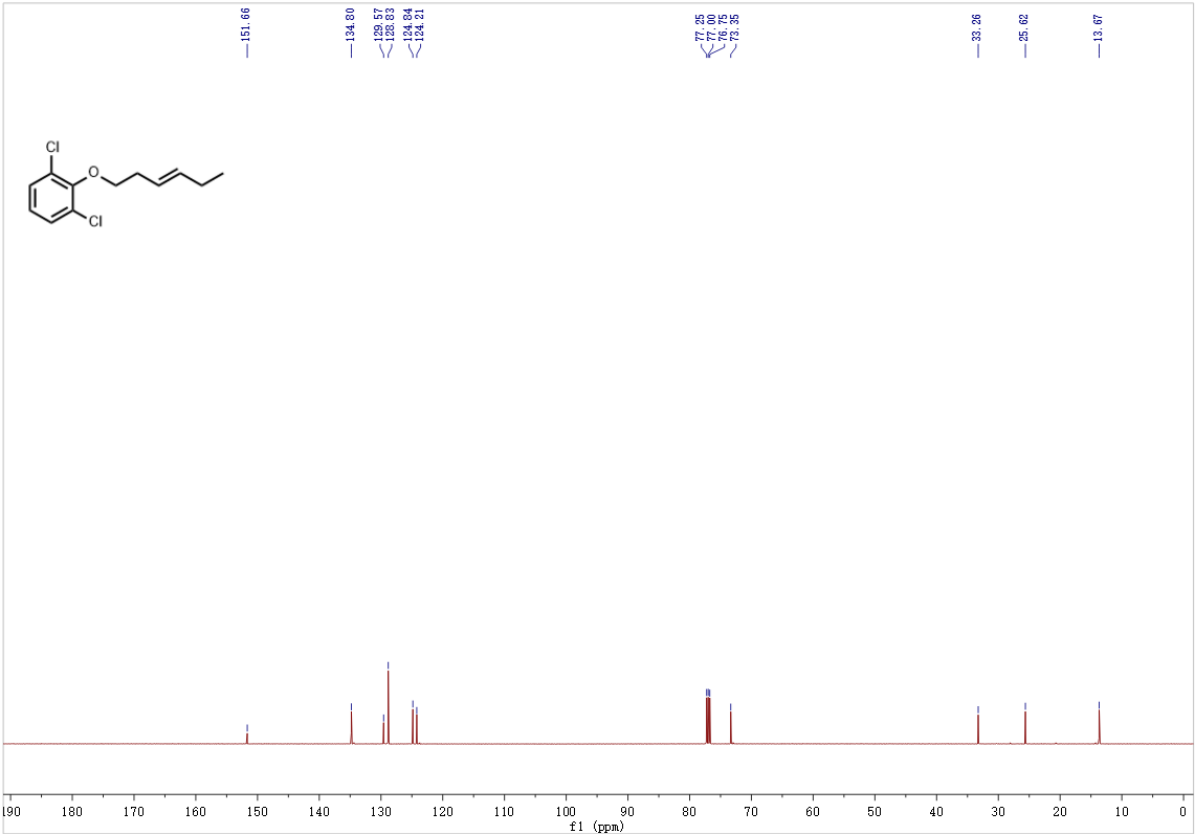
Cl
O
Cl
151.66
134.80
129.57
128.83
124.84
124.21
77.25
77.00
76.75
73.35
33.26
25.62
13.67
f1 (ppm)

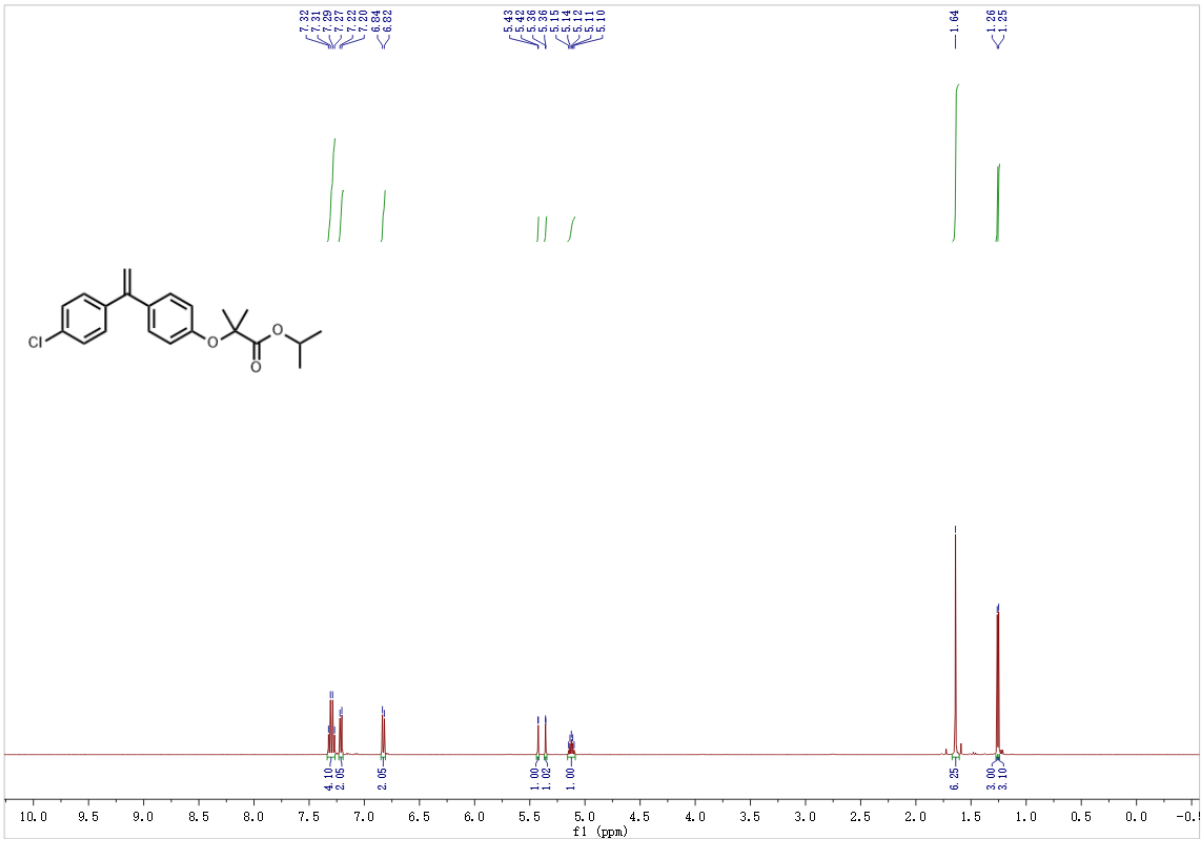
7.32
7.31
7.29
7.27
7.23
7.20
6.84
6.82
5.43
5.42
5.36
5.15
5.14
5.12
5.11
5.10
1.64
1.26
1.25
Cl
O
O
O
4.10
2.05
2.05
1.00
1.02
1.00
6.25
3.00
3.10
10.0 9.5 9.0 8.5 8.0 7.5 7.0 6.5 6.0 5.5 5.0 4.5 4.0 3.5 3.0 2.5 2.0 1.5 1.0 0.5 0.0
f1 (ppm)

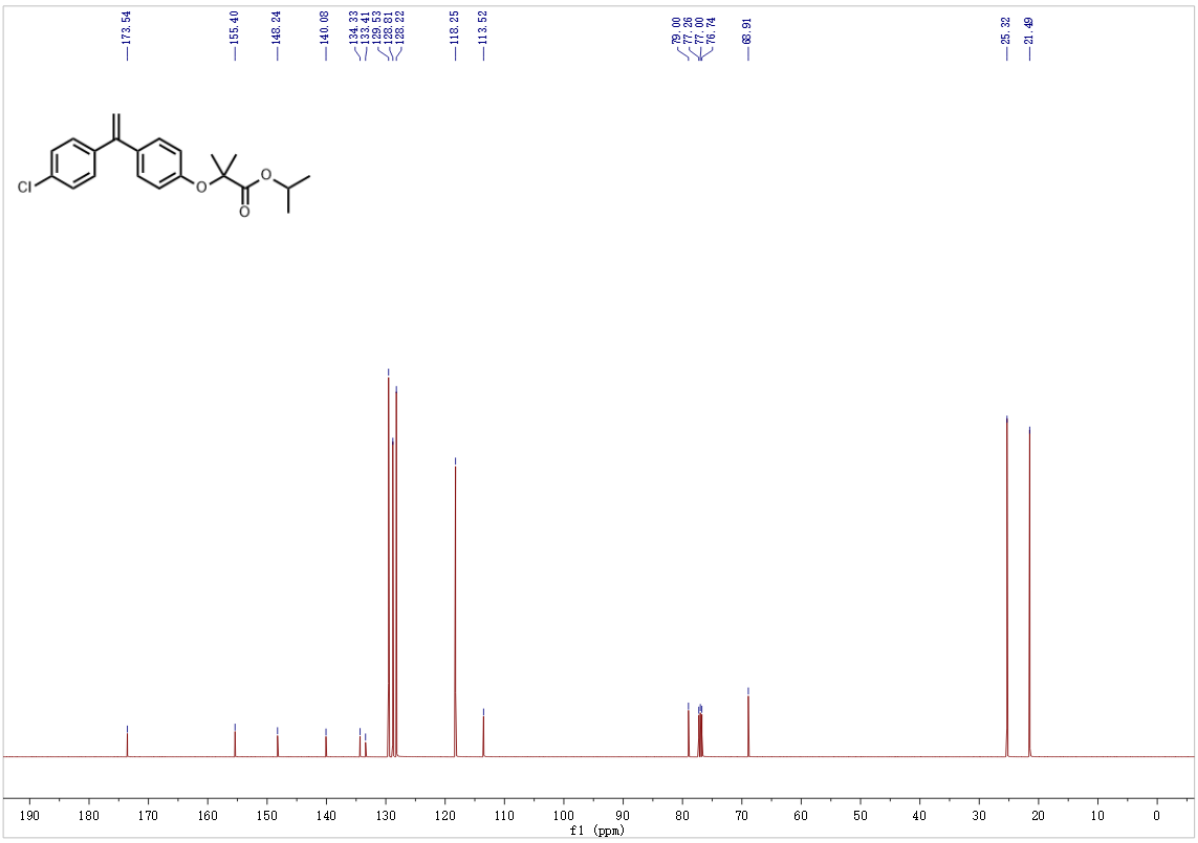
173.54
155.40
148.24
140.08
134.33
133.41
129.53
128.81
128.22
118.25
113.52
79.00
77.26
77.00
76.74
68.91
25.32
21.49
Cl
O
O
O
190 180 170 160 150 140 130 120 110 100 90 80 70 60 50 40 30 20 10 0
f1 (ppm)

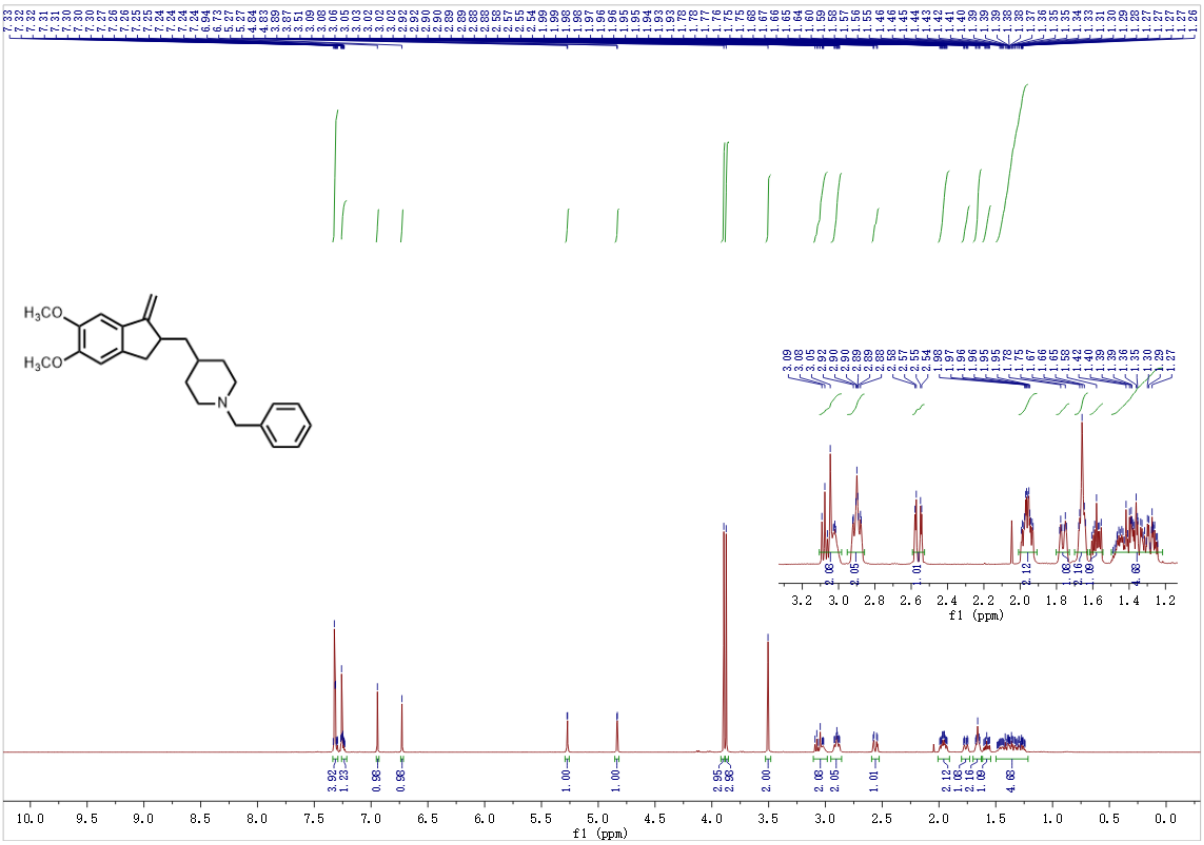
H3CO
H3CO
N
f1 (ppm)


H3CO
H3CO
N
f1 (ppm)

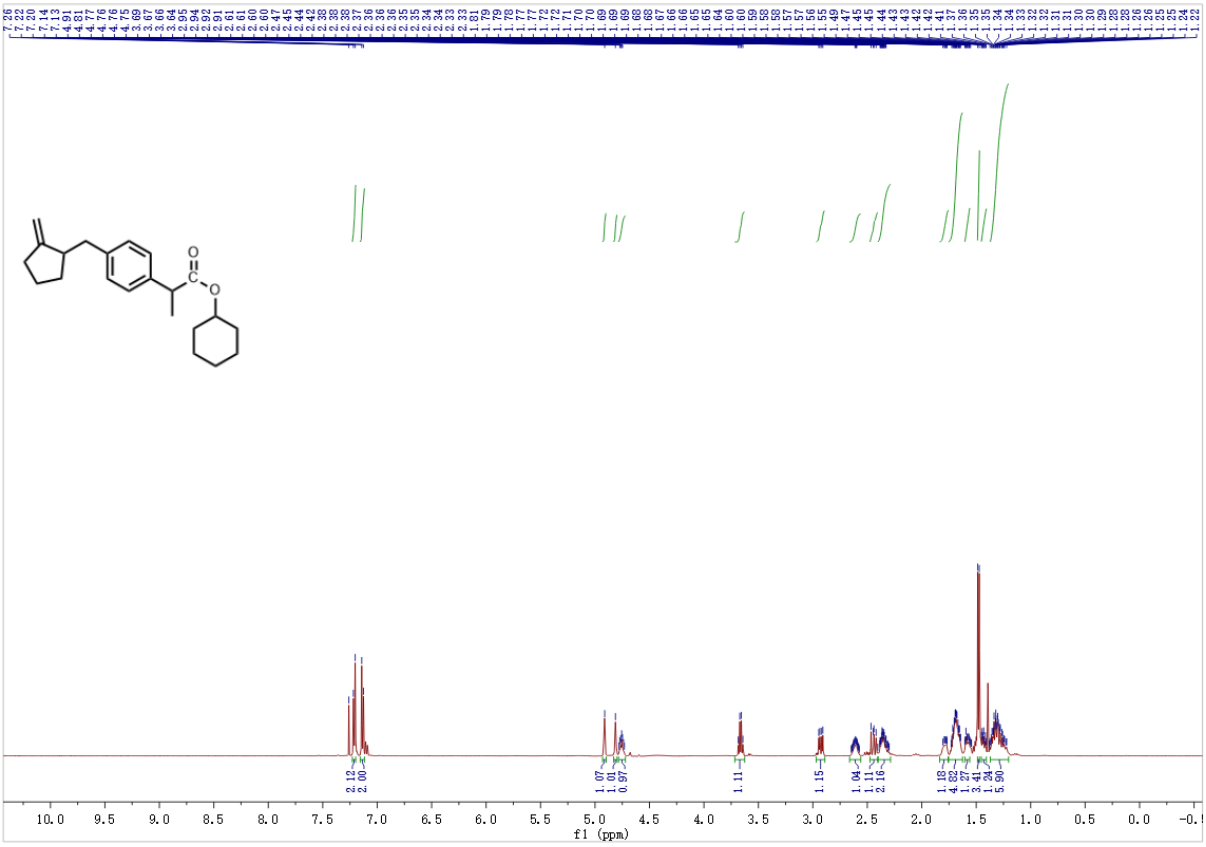
f1 (ppm)

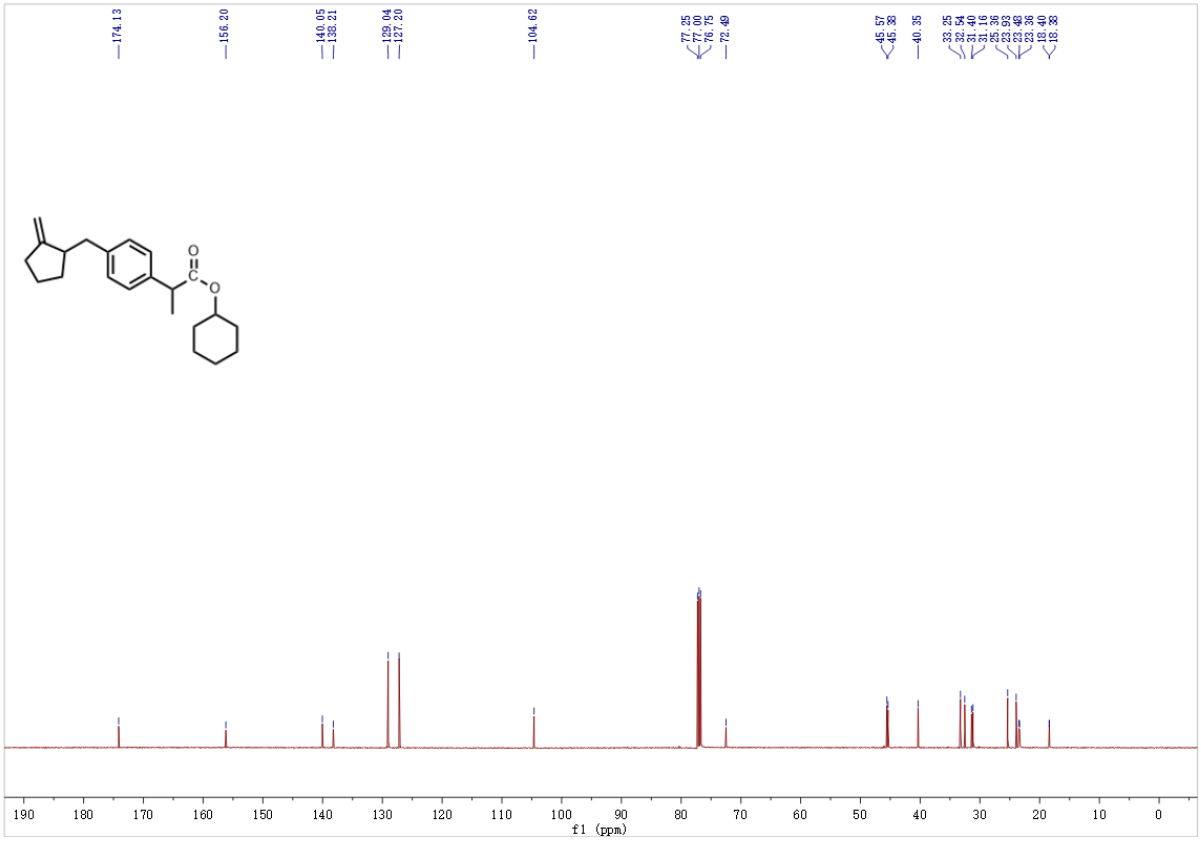
f1 (ppm)

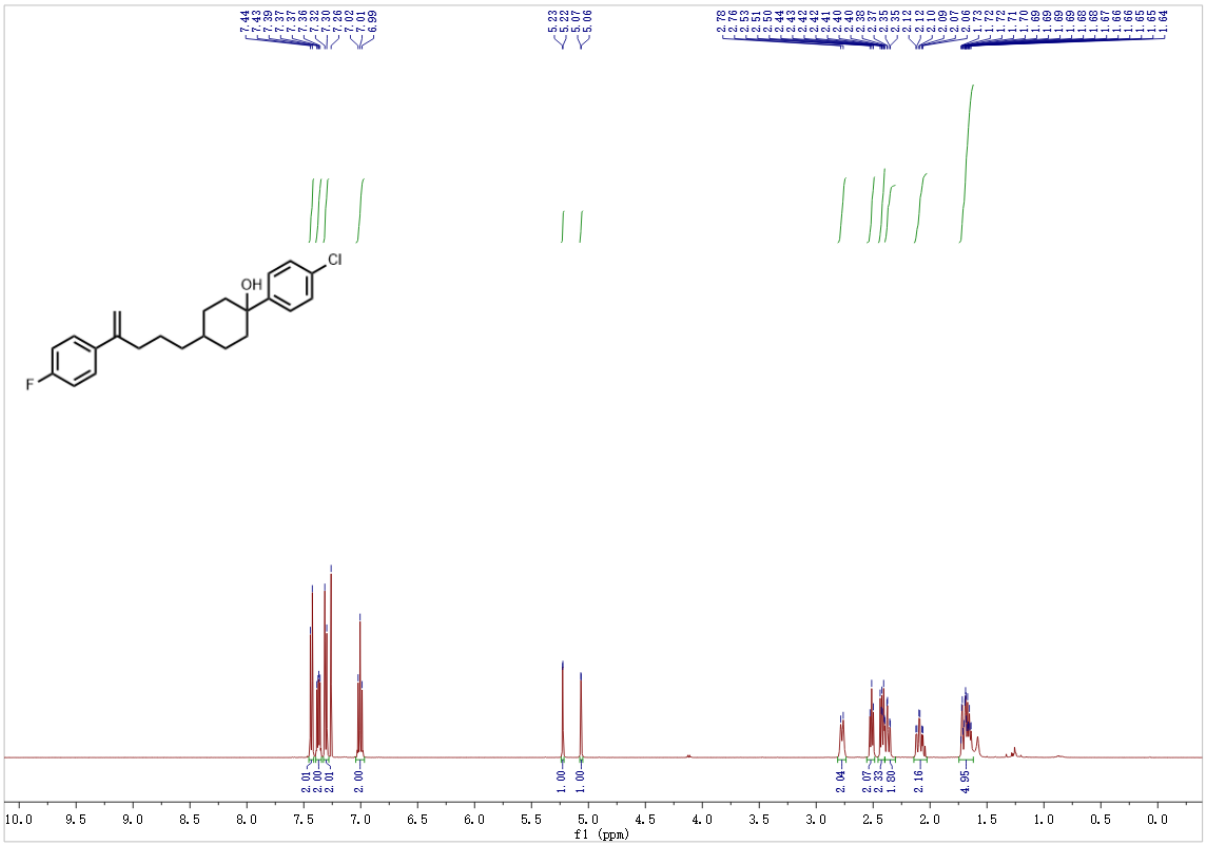
Cl
OH
F
f1 (ppm)

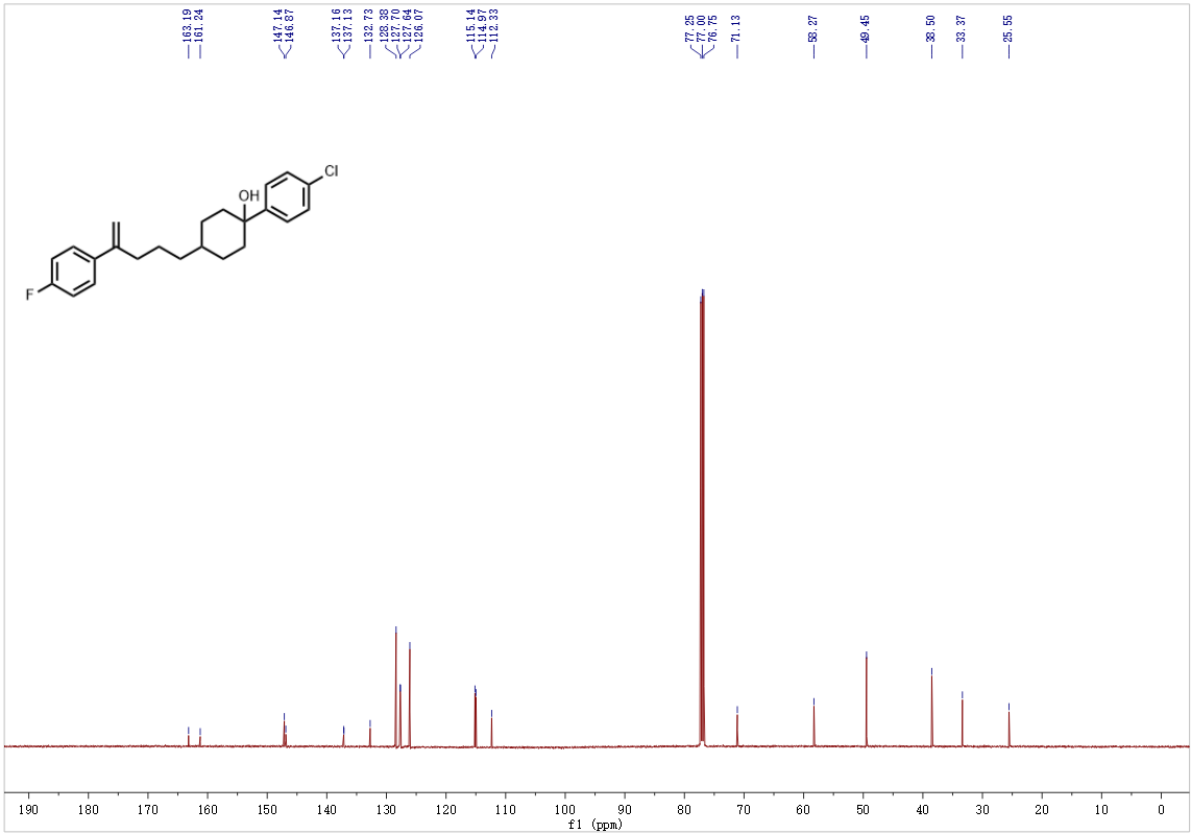
Cl
OH
F
f1 (ppm)

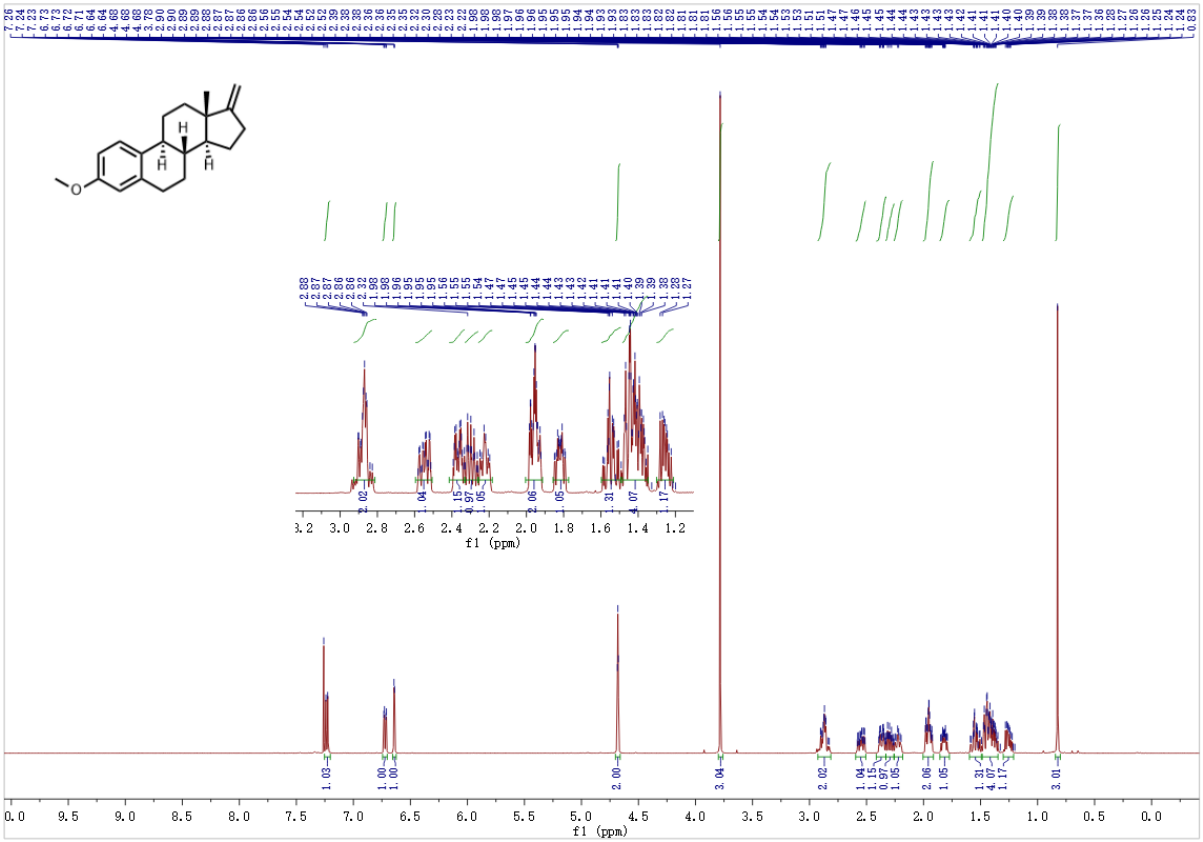
f1 (ppm)

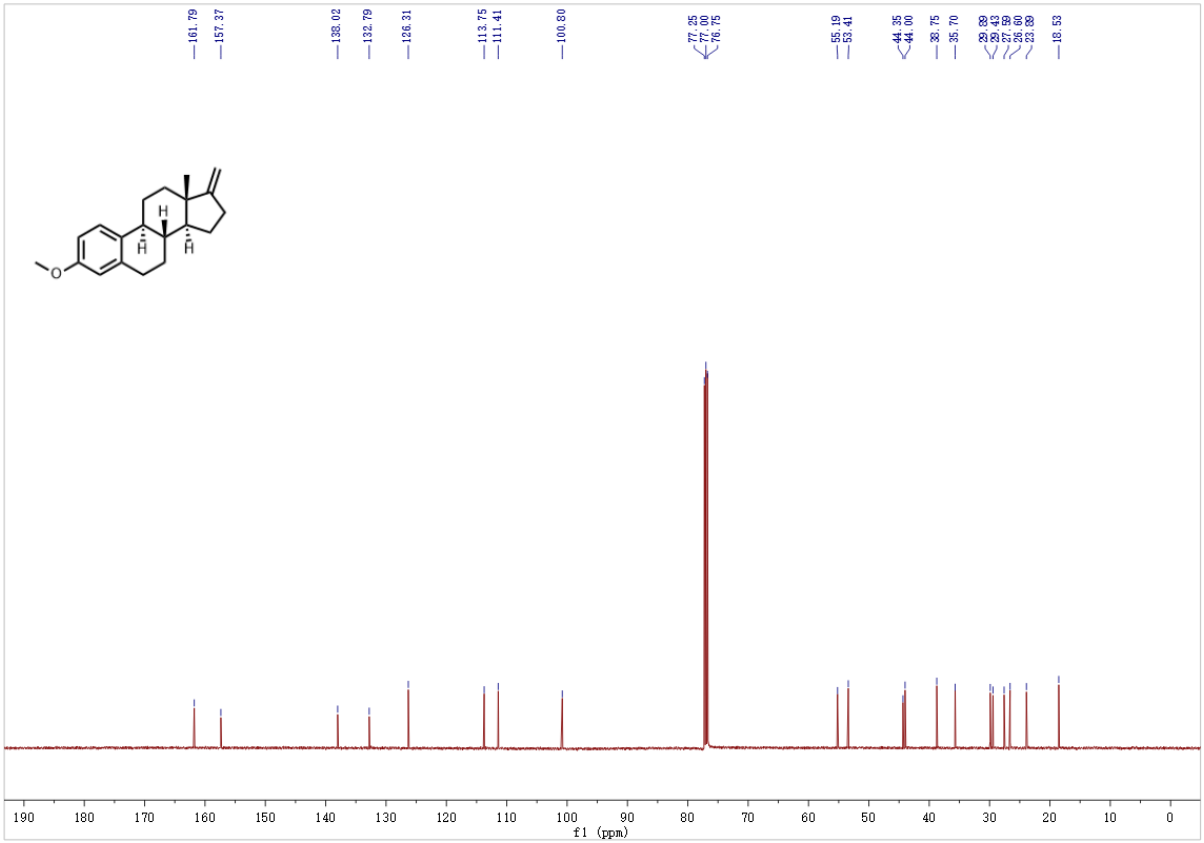
f1 (ppm)

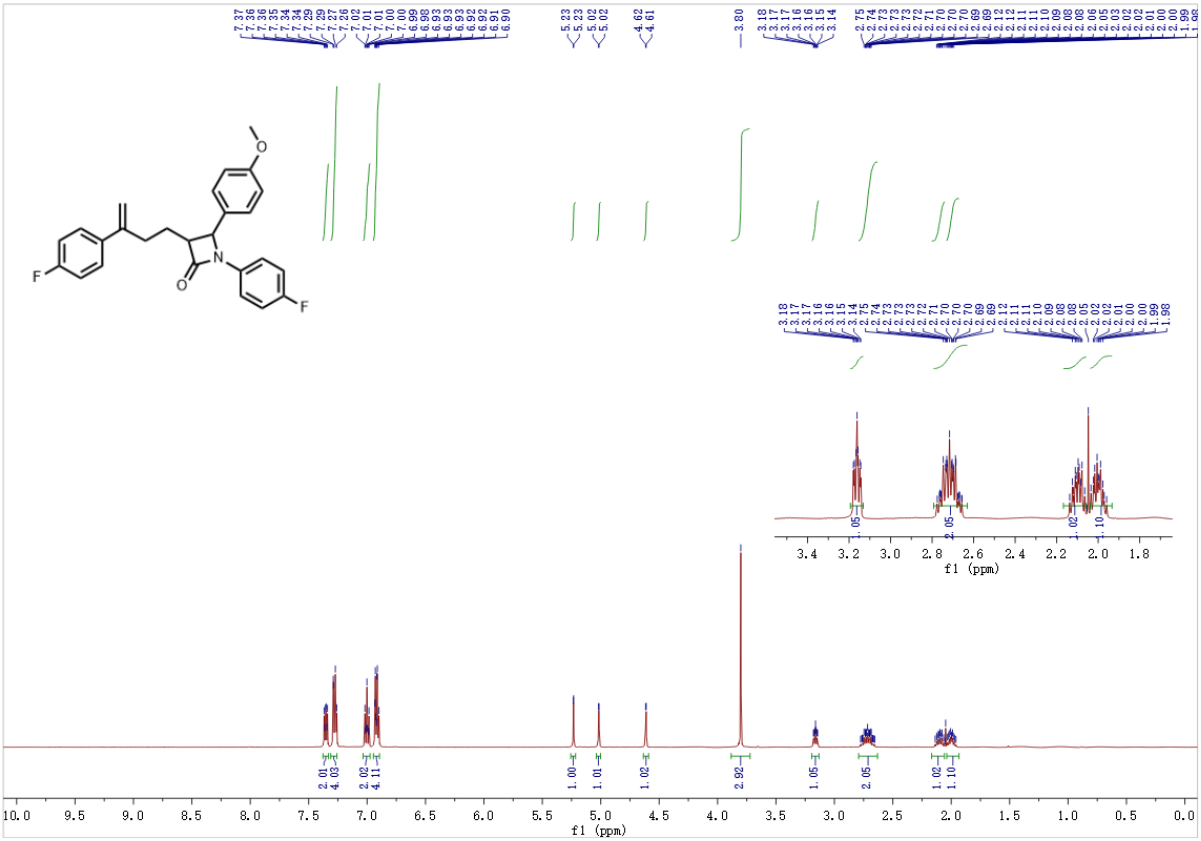

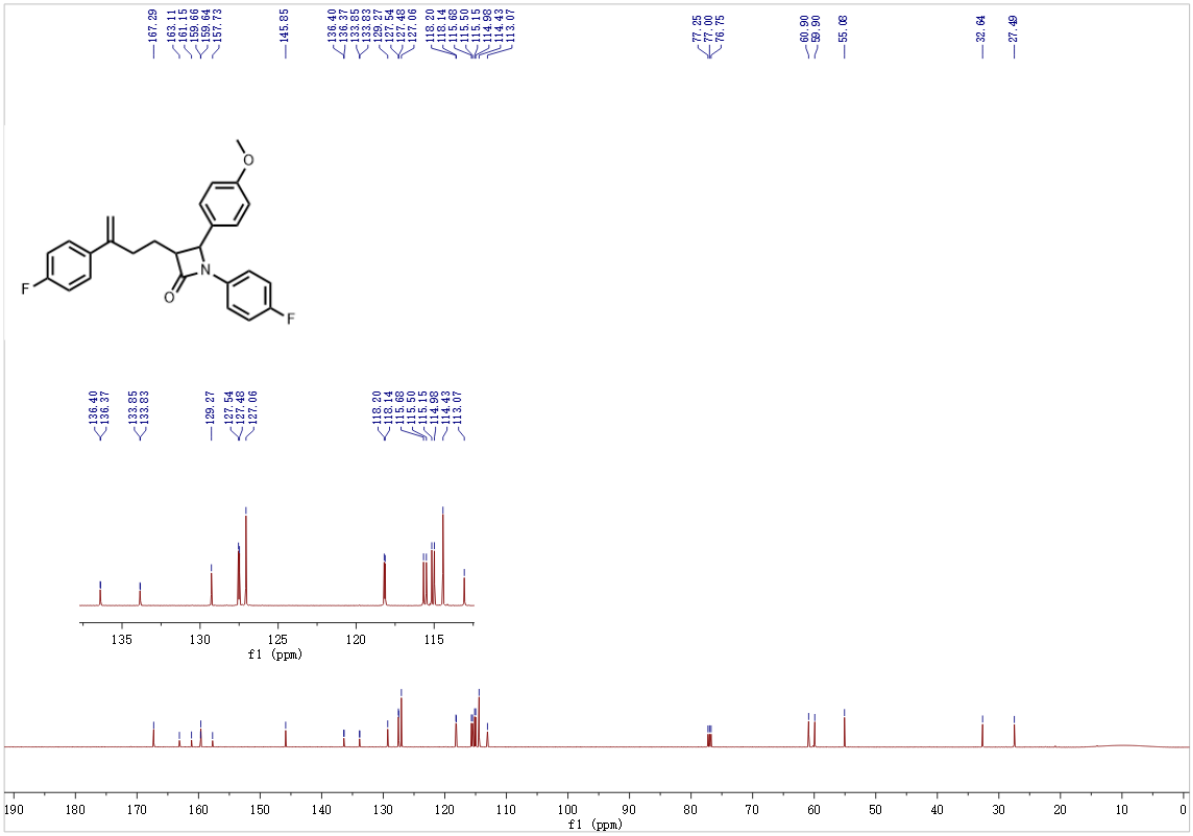

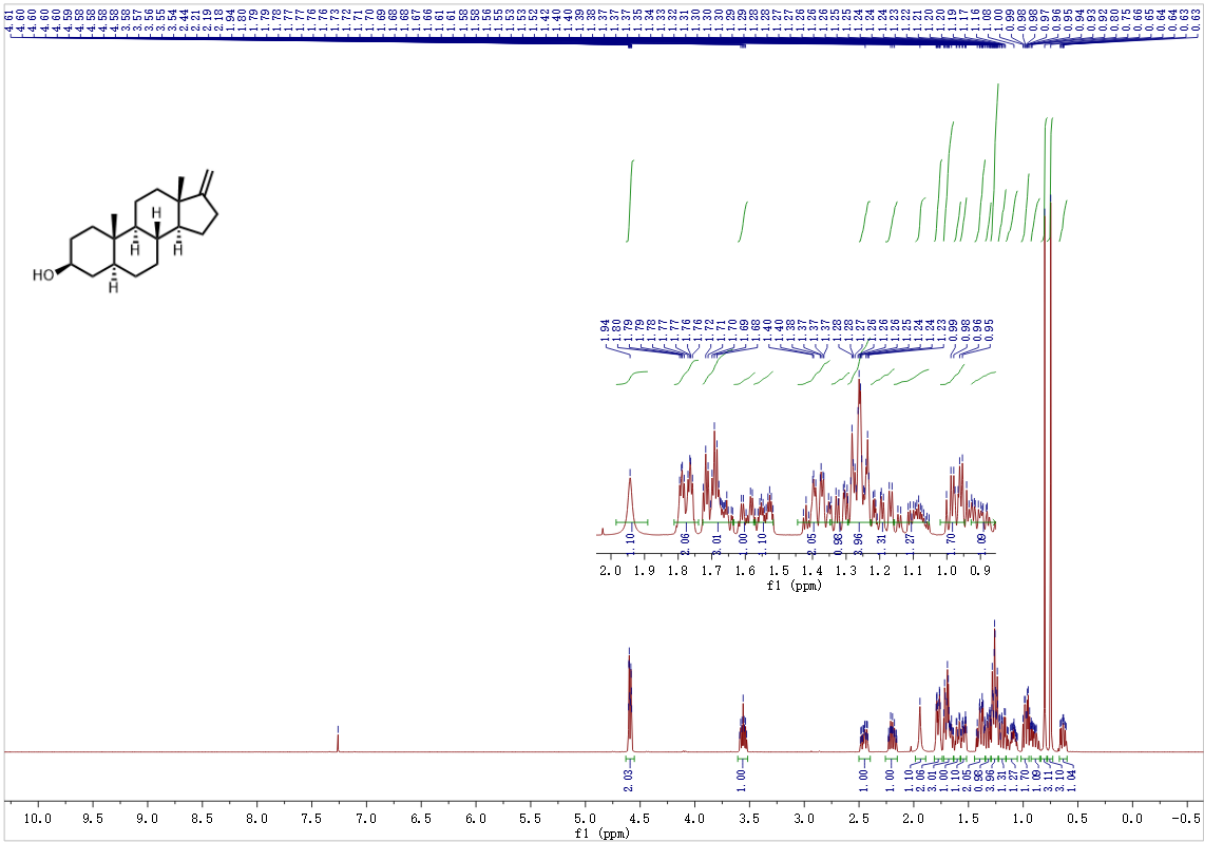
HO
f1 (ppm)

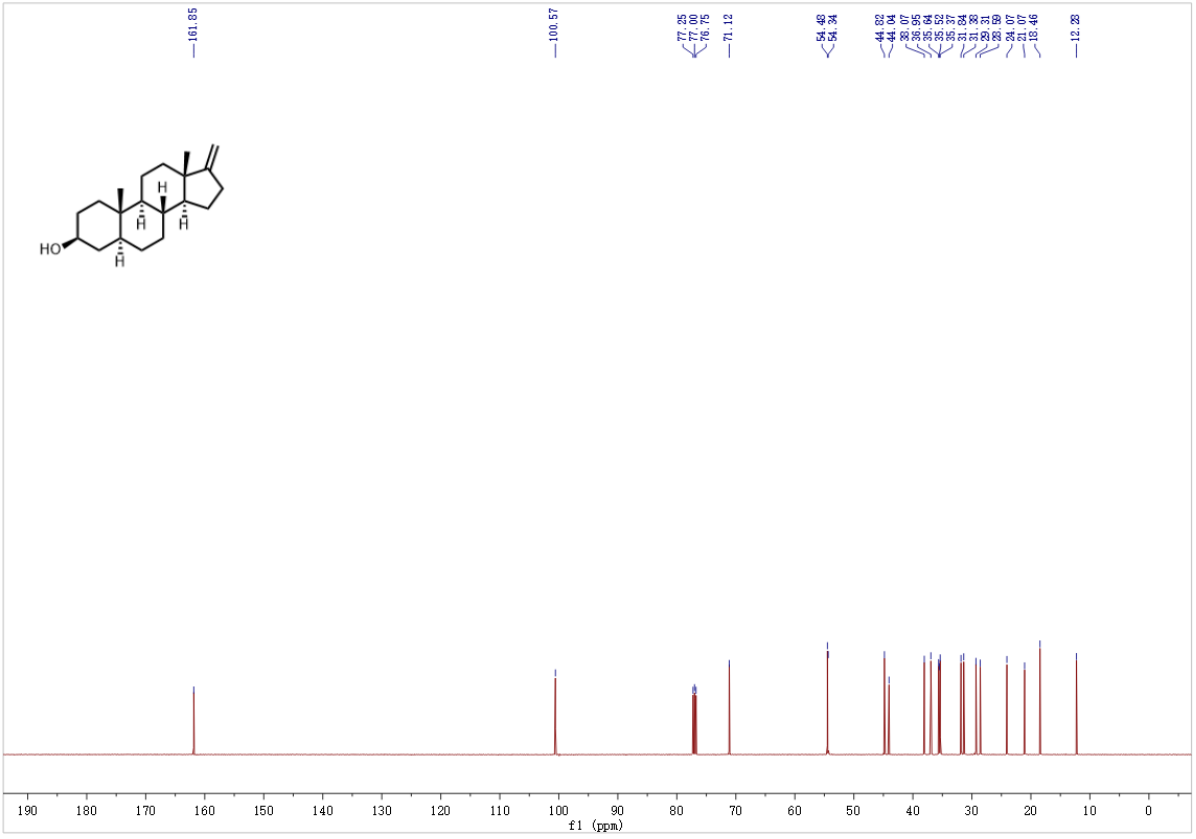
HO
f1 (ppm)

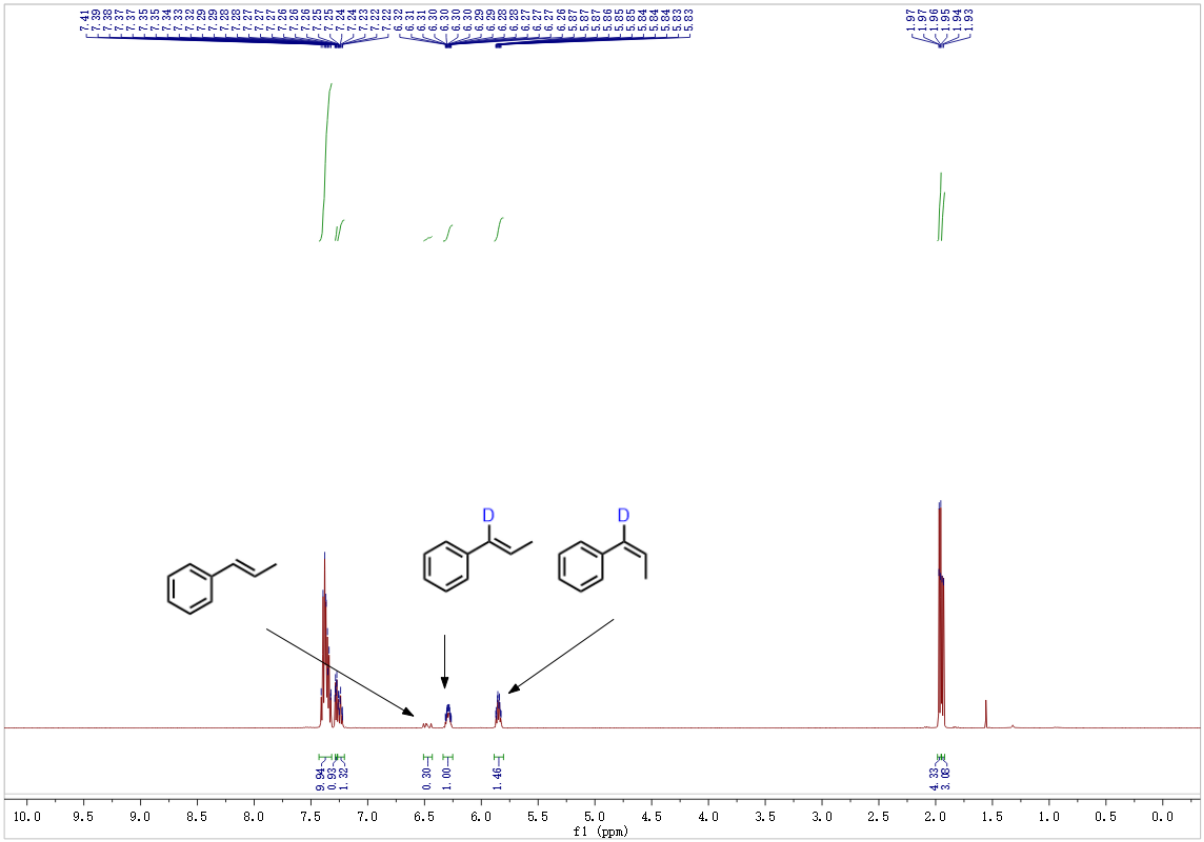
D
D
f1 (ppm)

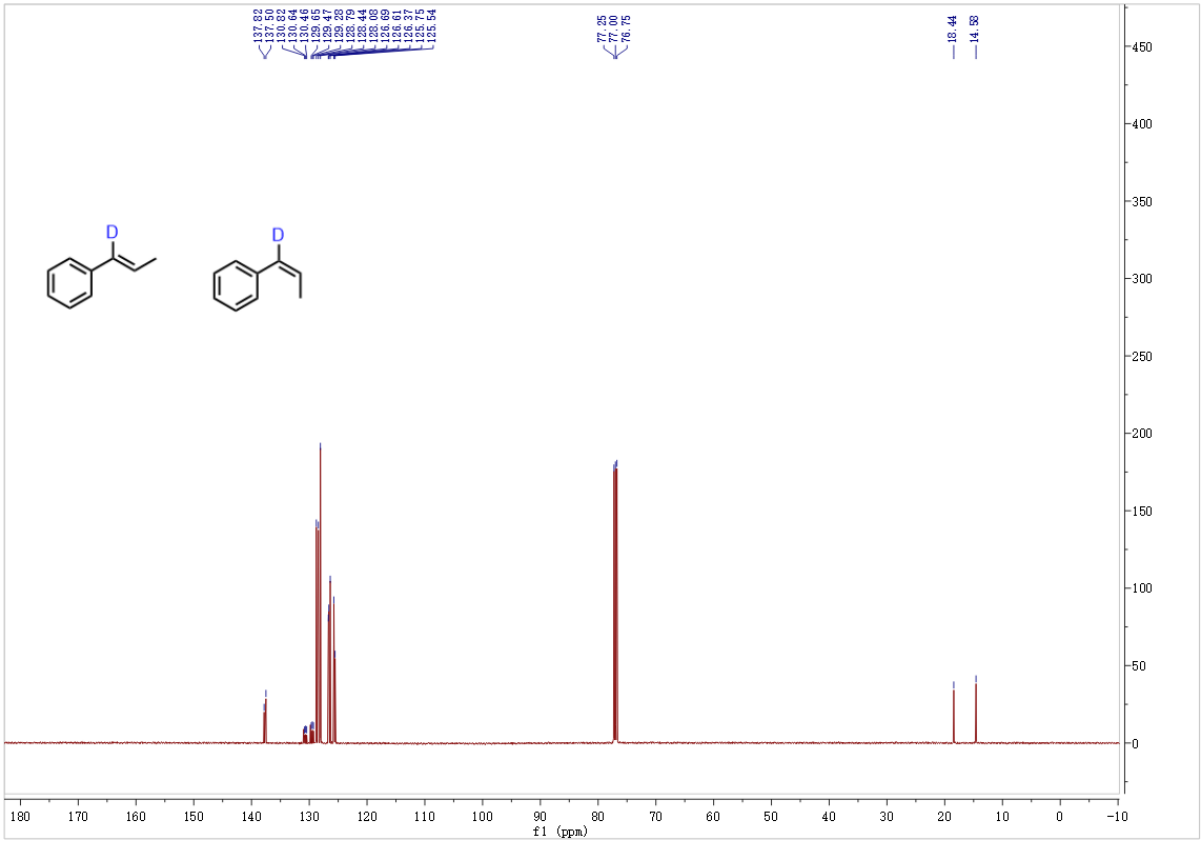
D
D
f1 (ppm)

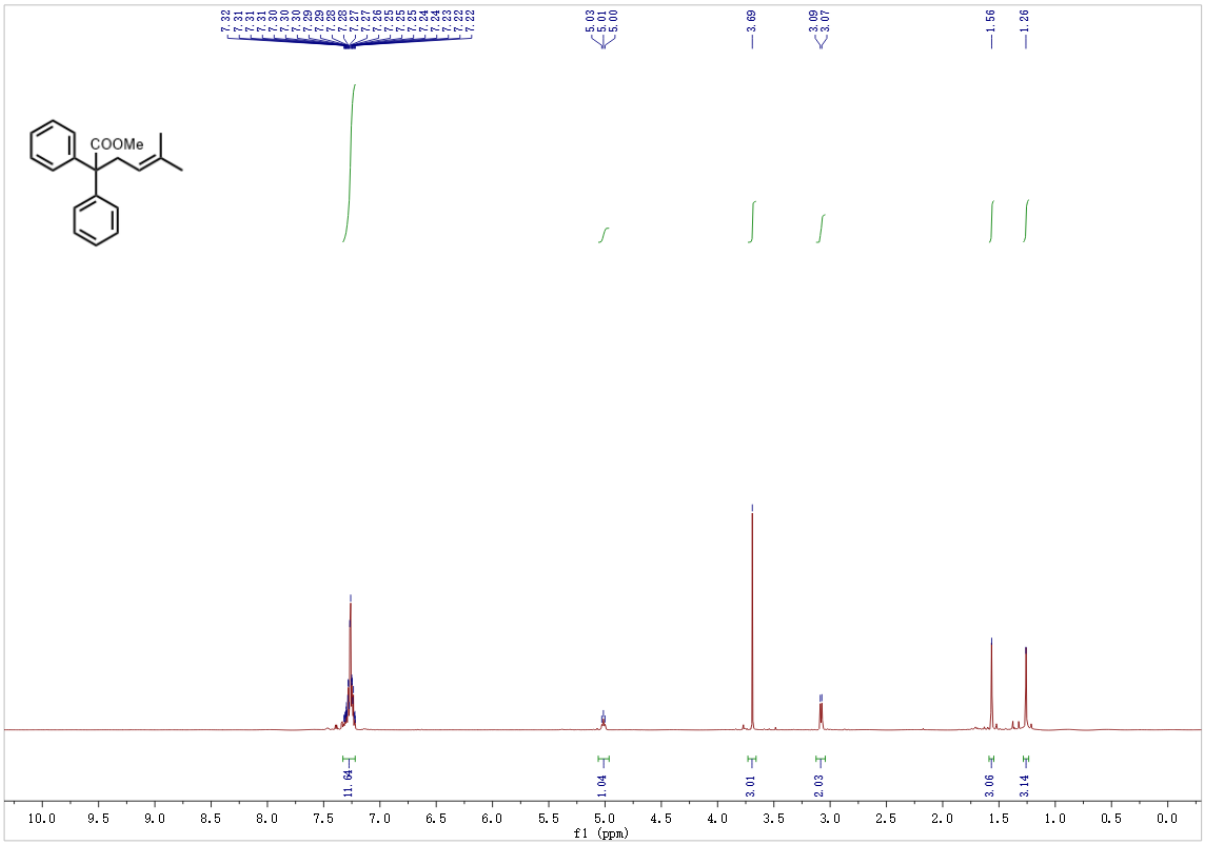
COOMe
7.32
7.31
7.31
7.31
7.30
7.30
7.30
7.29
7.28
7.28
7.27
7.27
7.26
7.25
7.25
7.24
7.24
7.23
7.22
7.22
5.03
5.01
5.00
3.69
3.09
3.07
1.56
1.26
11.64
1.04
3.01
2.03
3.06
3.14
10.0
9.5
9.0
8.5
8.0
7.5
7.0
6.5
6.0
5.5
5.0
4.5
4.0
3.5
3.0
2.5
2.0
1.5
1.0
0.5
0.0
f1 (ppm)

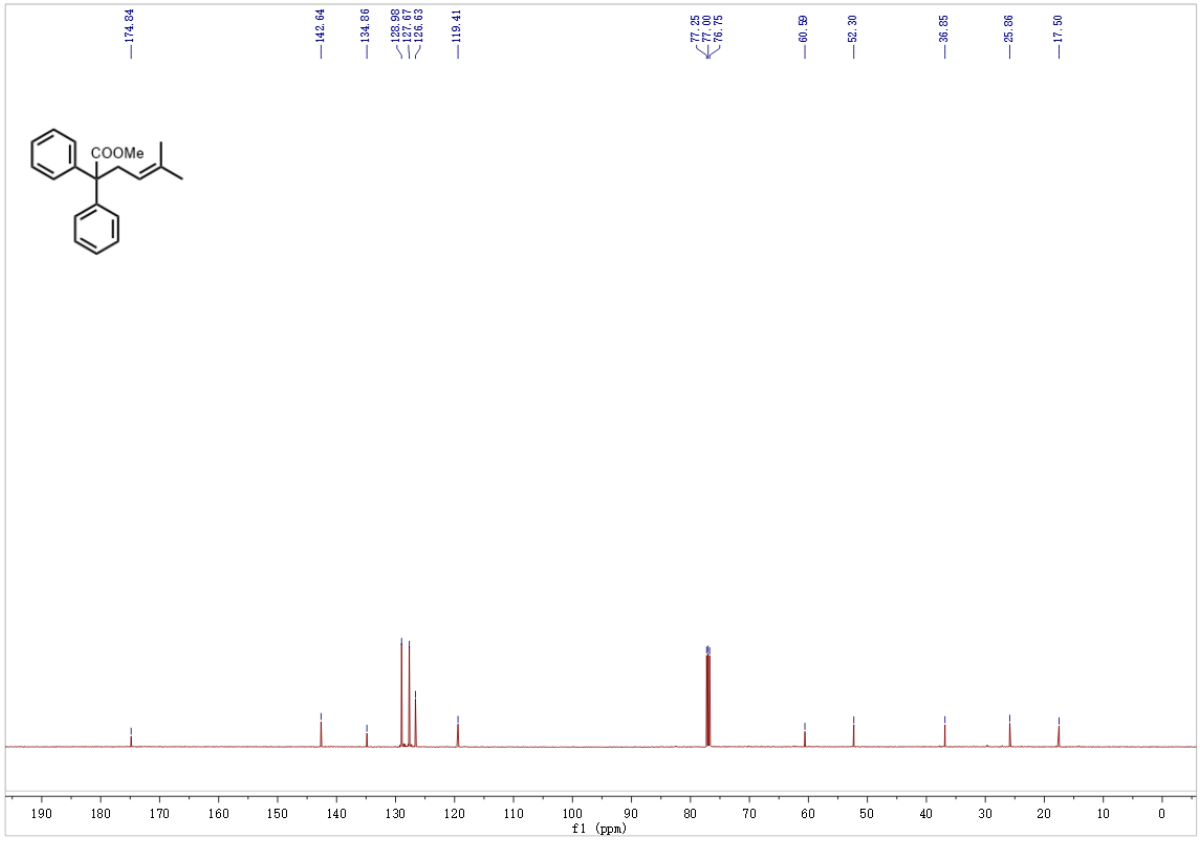
COOMe
174.84
142.64
134.86
128.98
127.67
126.63
119.41
77.25
77.00
76.75
60.89
52.30
36.85
25.86
17.50
190
180
170
160
150
140
130
120
110
100
90
80
70
60
50
40
30
20
10
0
f1 (ppm)

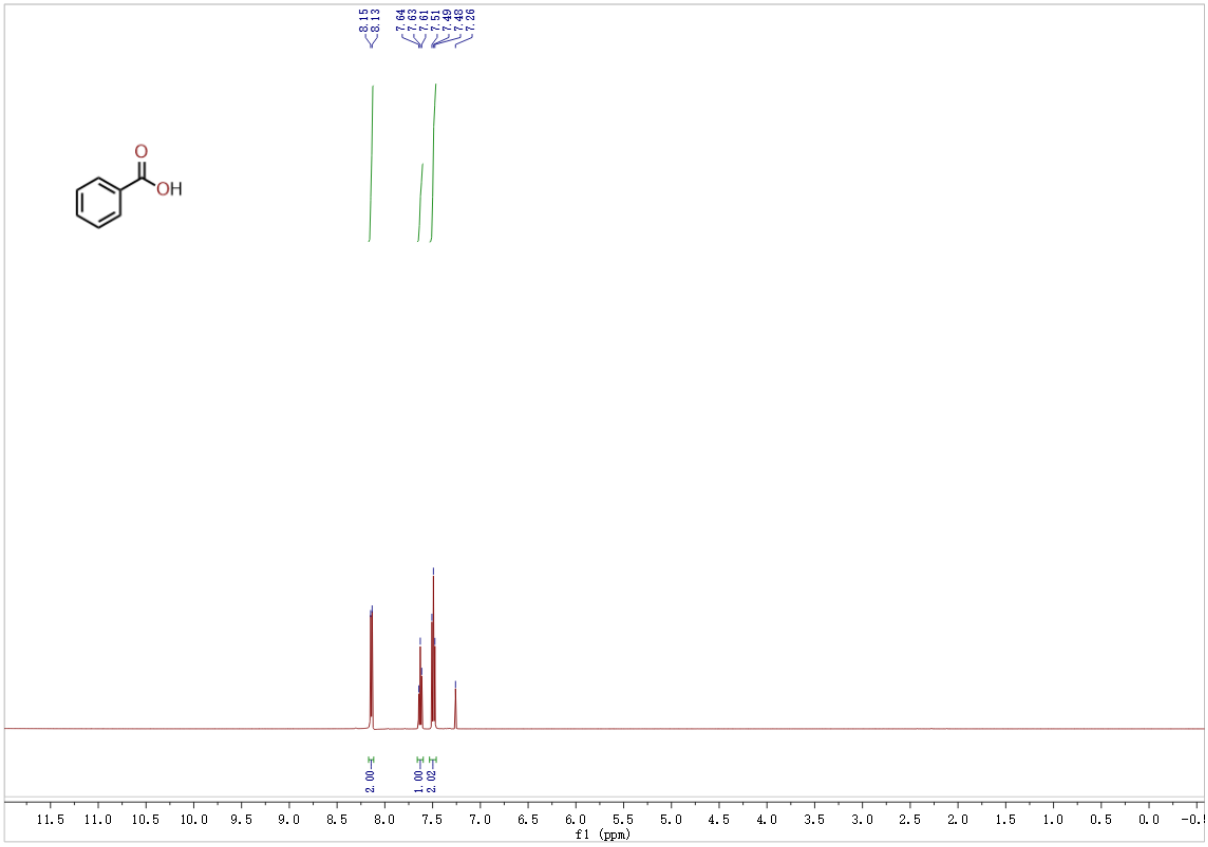
8.15
8.13
7.64
7.63
7.61
7.51
7.49
7.48
7.26
O
OH
2.00
1.00
2.02
f1 (ppm)

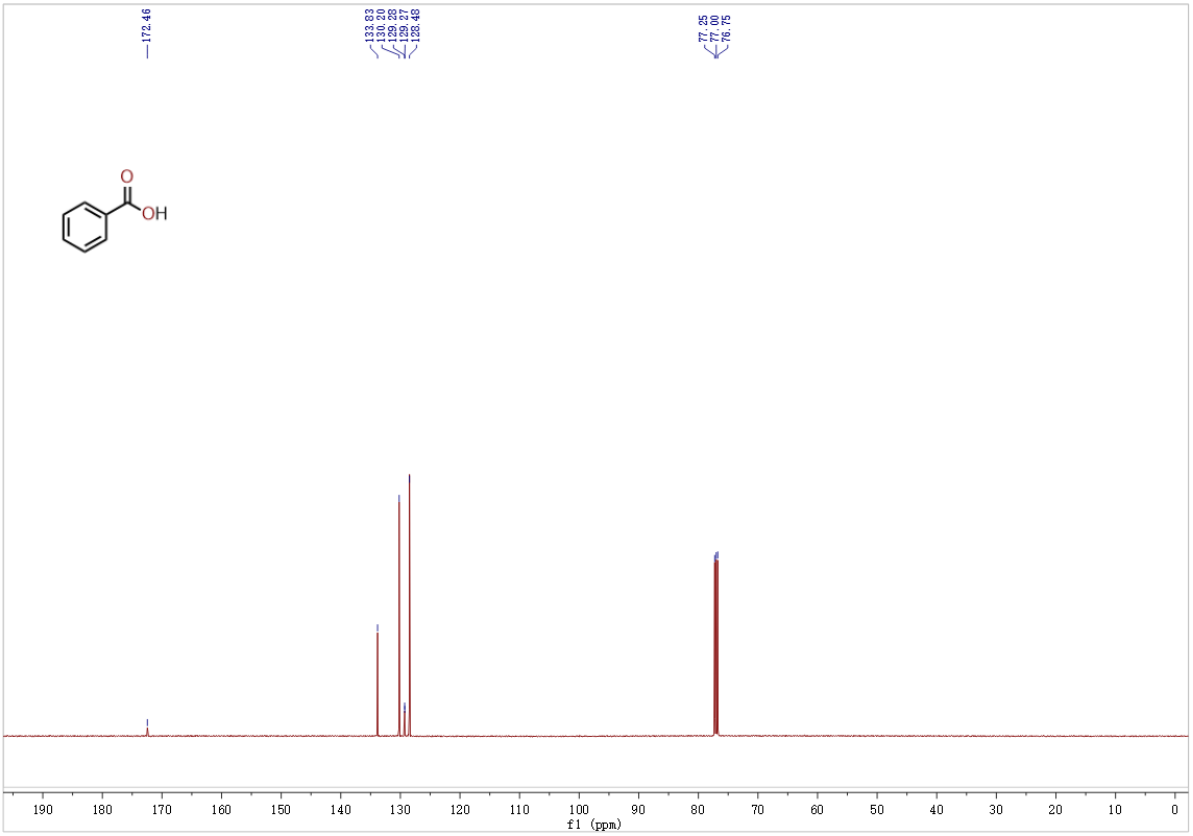
172.46
133.83
130.00
129.28
129.27
128.48
77.25
77.00
76.75
O
OH
f1 (ppm)

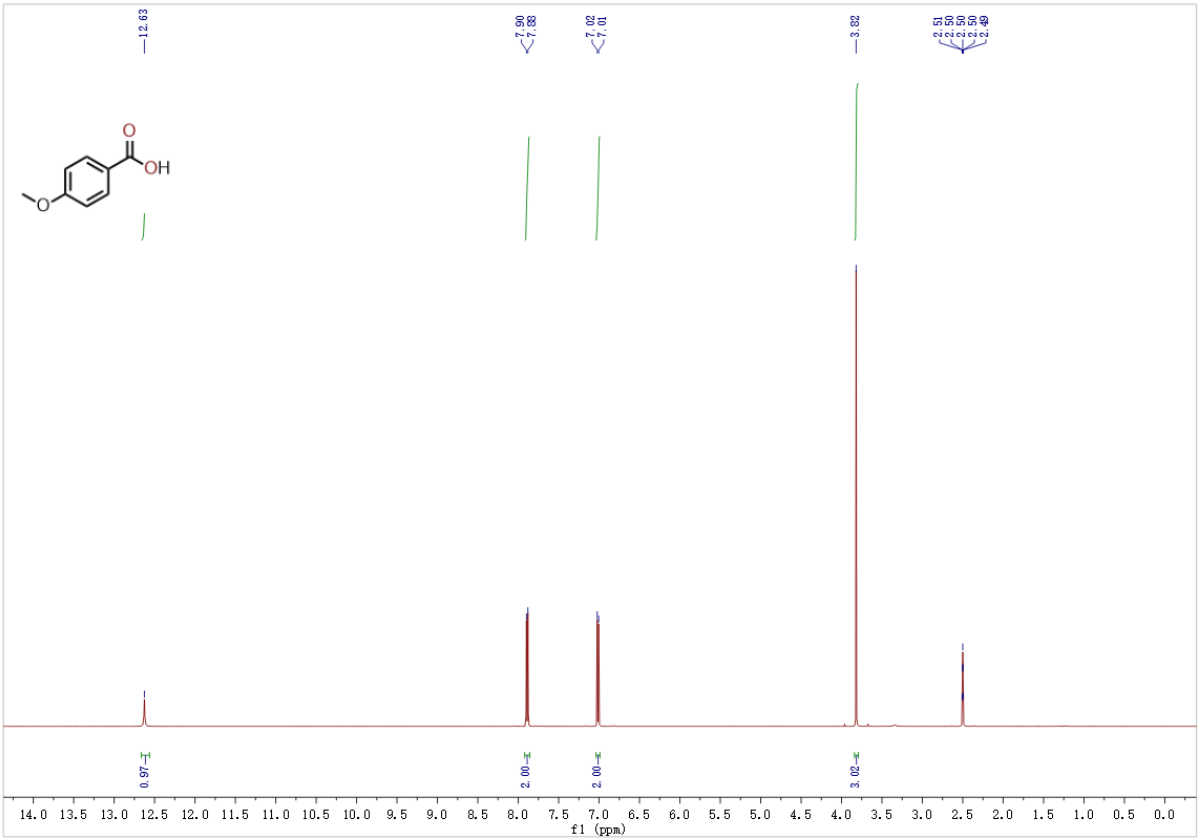
12.63
7.90
7.88
7.02
7.01
3.82
2.51
2.50
2.50
2.50
2.49
O
OH
O
0.97
2.00
2.00
3.02
14.0 13.5 13.0 12.5 12.0 11.5 11.0 10.5 10.0 9.5 9.0 8.5 8.0 7.5 7.0 6.5 6.0 5.5 5.0 4.5 4.0 3.5 3.0 2.5 2.0 1.5 1.0 0.5 0.0
f1 (ppm)

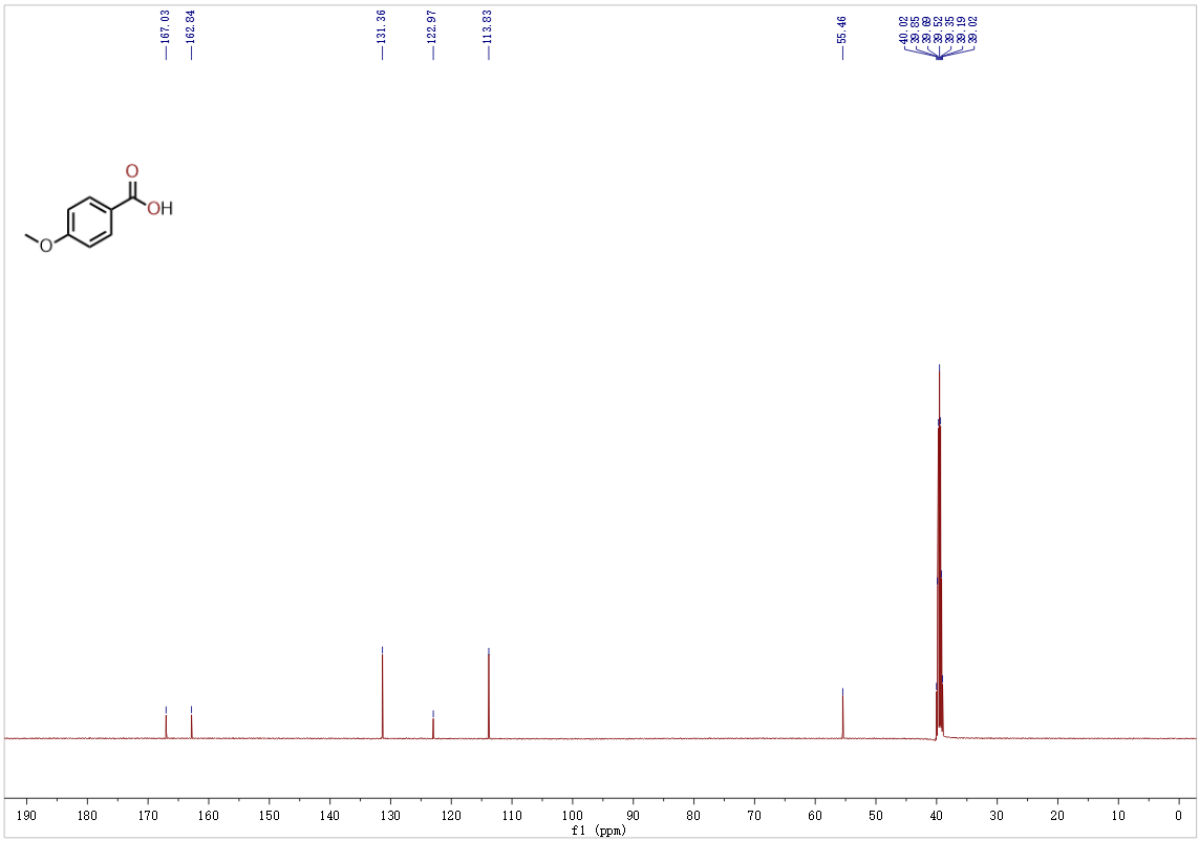
167.03
162.84
131.36
122.97
113.83
55.46
40.02
39.85
39.69
39.52
39.35
39.19
39.02
O
OH
O
190 180 170 160 150 140 130 120 110 100 90 80 70 60 50 40 30 20 10 0
f1 (ppm)

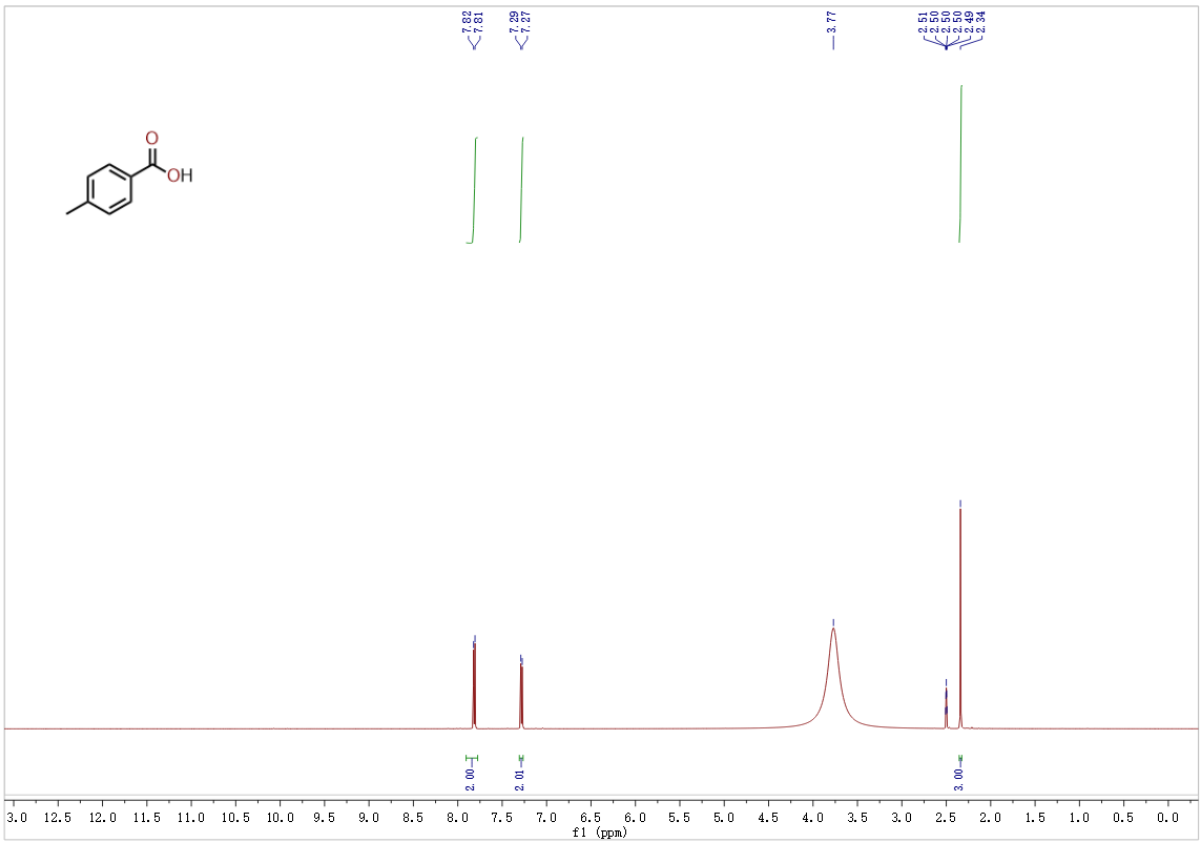
7.82
7.81
7.29
7.27
3.77
2.51
2.50
2.50
2.50
2.49
2.34
O
OH
2.00
2.01
3.00
f1 (ppm)

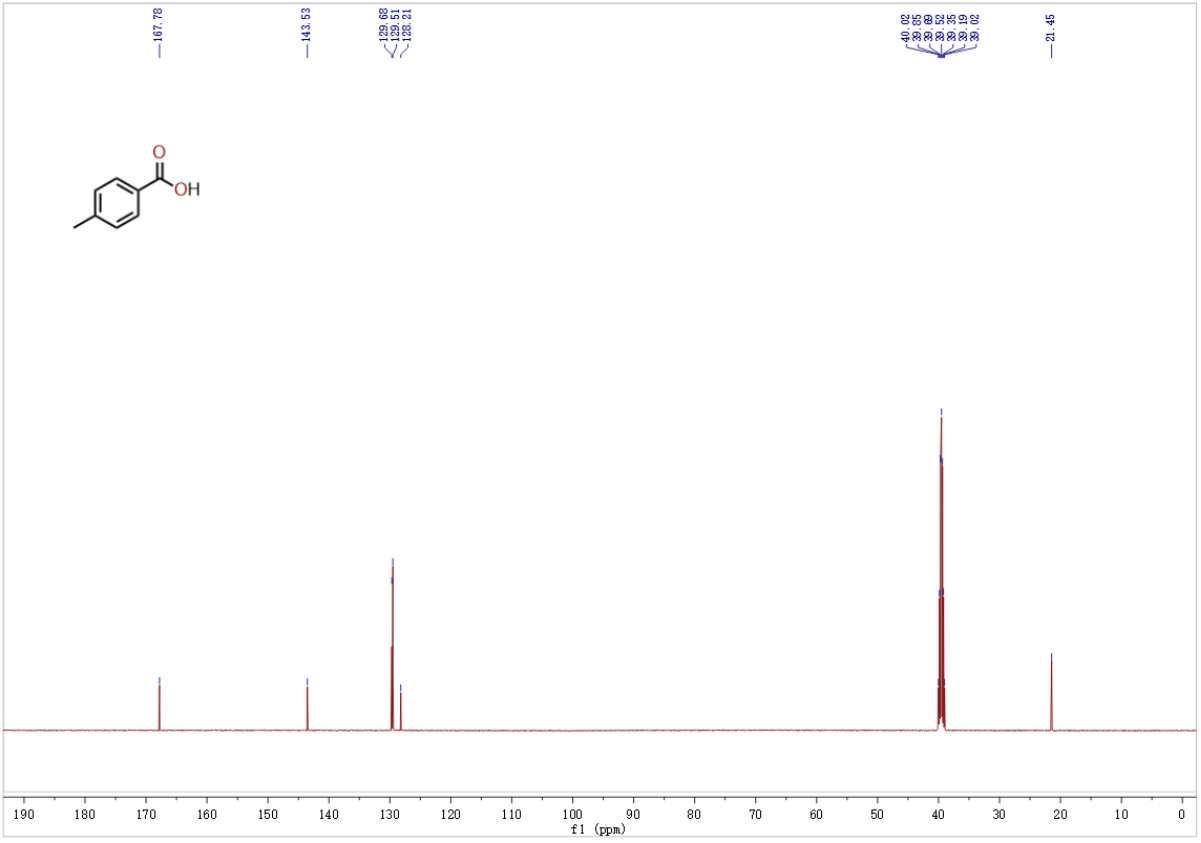
167.78
143.53
129.68
129.51
128.21
40.02
39.85
39.69
39.52
39.35
39.19
39.02
21.45
O
OH
f1 (ppm)

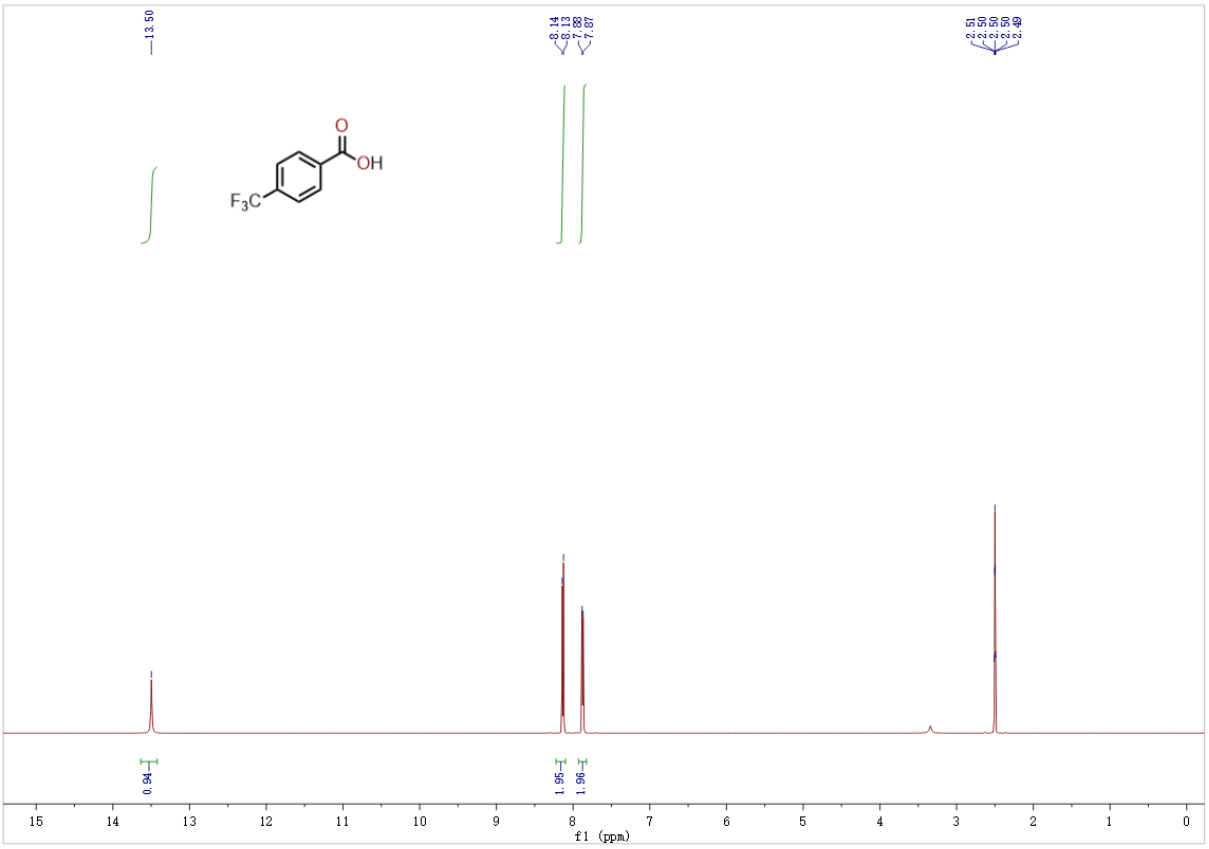
13.50
8.14
8.13
7.88
7.87
2.51
2.50
2.50
2.50
2.49
O
OH
F3C
0.94
1.95
1.96
f1 (ppm)

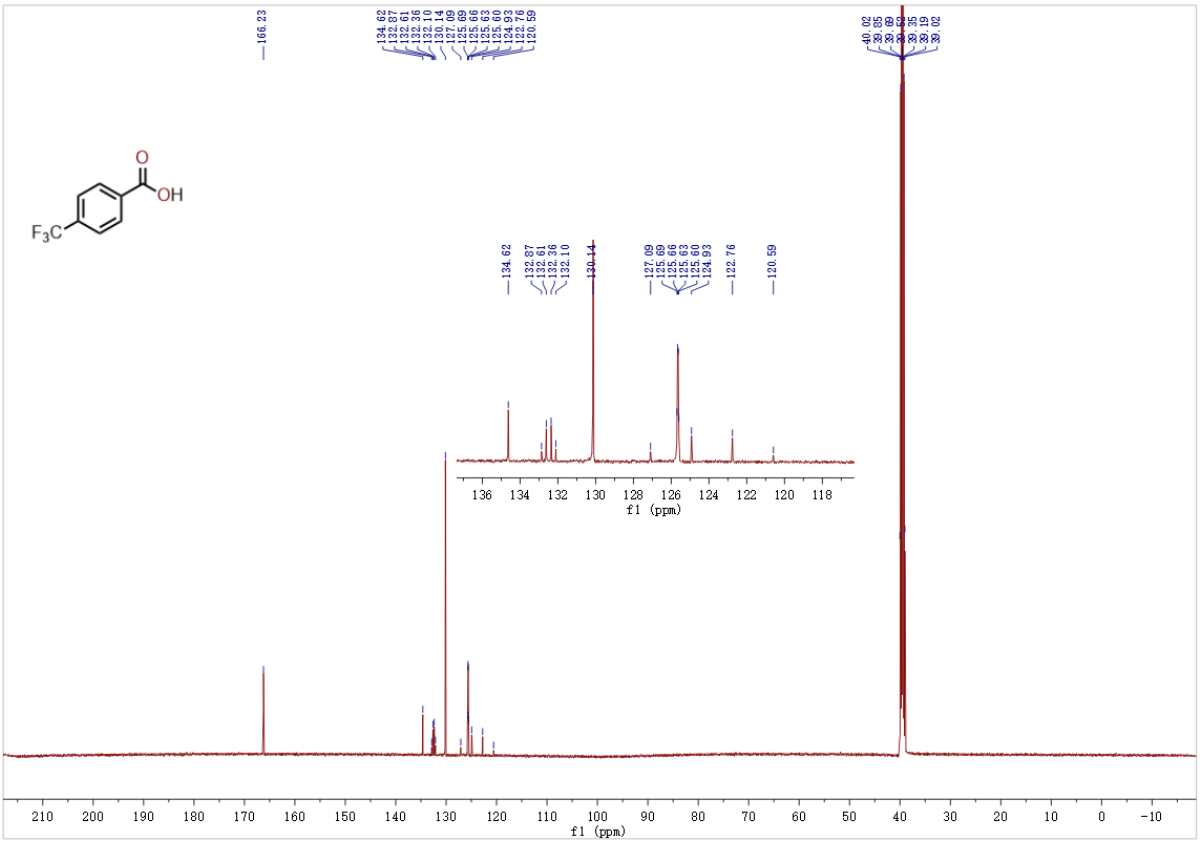
166.23
134.62
132.87
132.61
132.36
132.10
130.14
127.09
125.69
125.66
125.63
125.60
124.93
122.76
120.59
40.02
39.85
39.69
39.52
39.35
39.19
39.02
O
OH
F3C
f1 (ppm)
f1 (ppm)

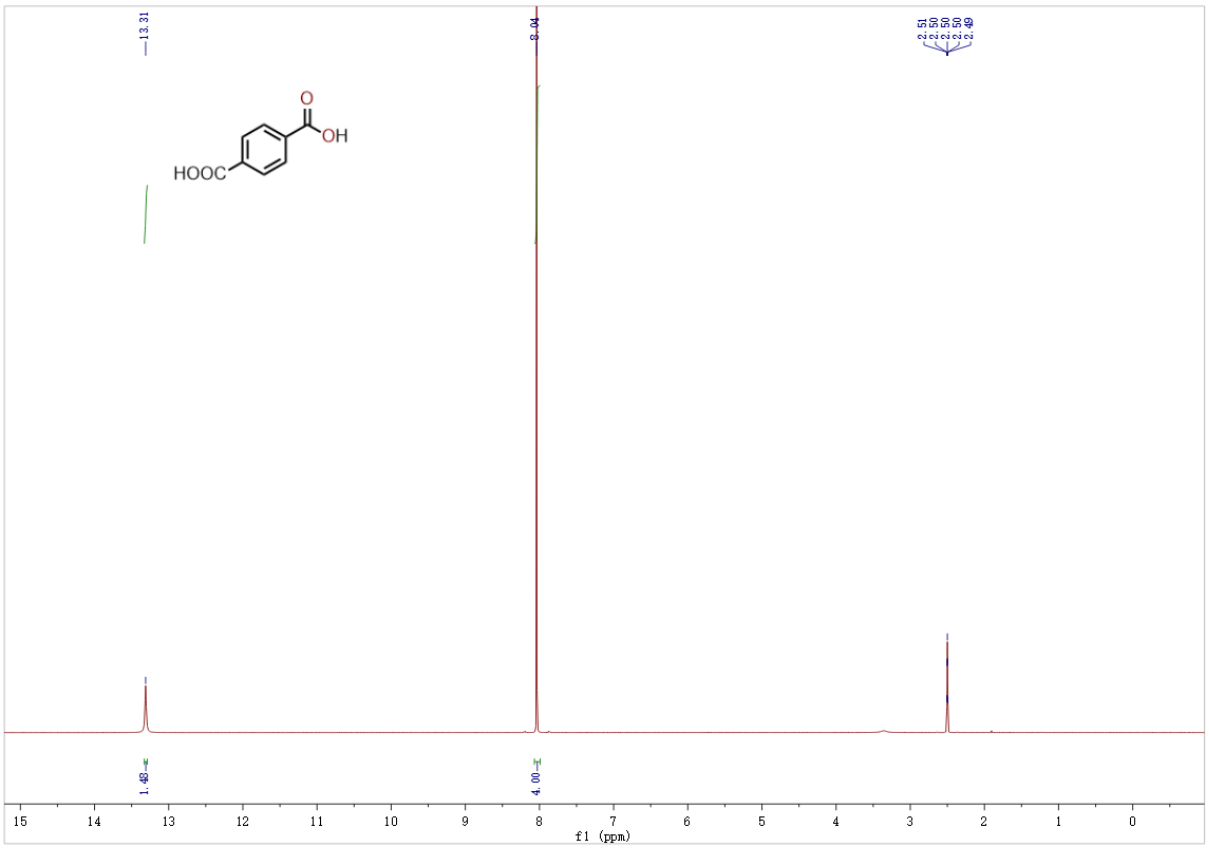
13.31
8.04
2.51
2.50
2.50
2.50
2.49
O
OH
HOOC
1.48
4.00
15
14
13
12
11
10
9
8
7
6
5
4
3
2
1
0
f1 (ppm)

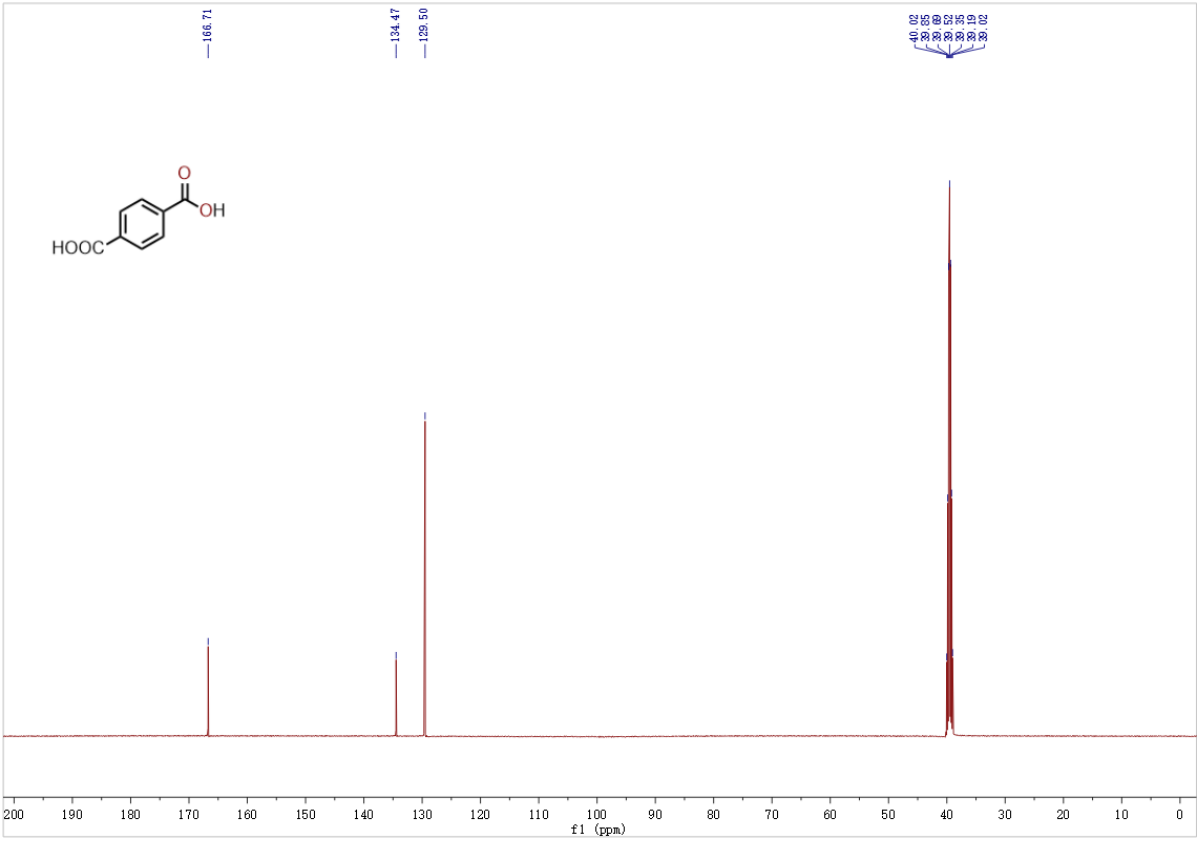
166.71
134.47
129.50
40.02
39.85
39.69
39.52
39.35
39.19
39.02
O
OH
HOOC
200
190
180
170
160
150
140
130
120
110
100
90
80
70
60
50
40
30
20
10
0
f1 (ppm)

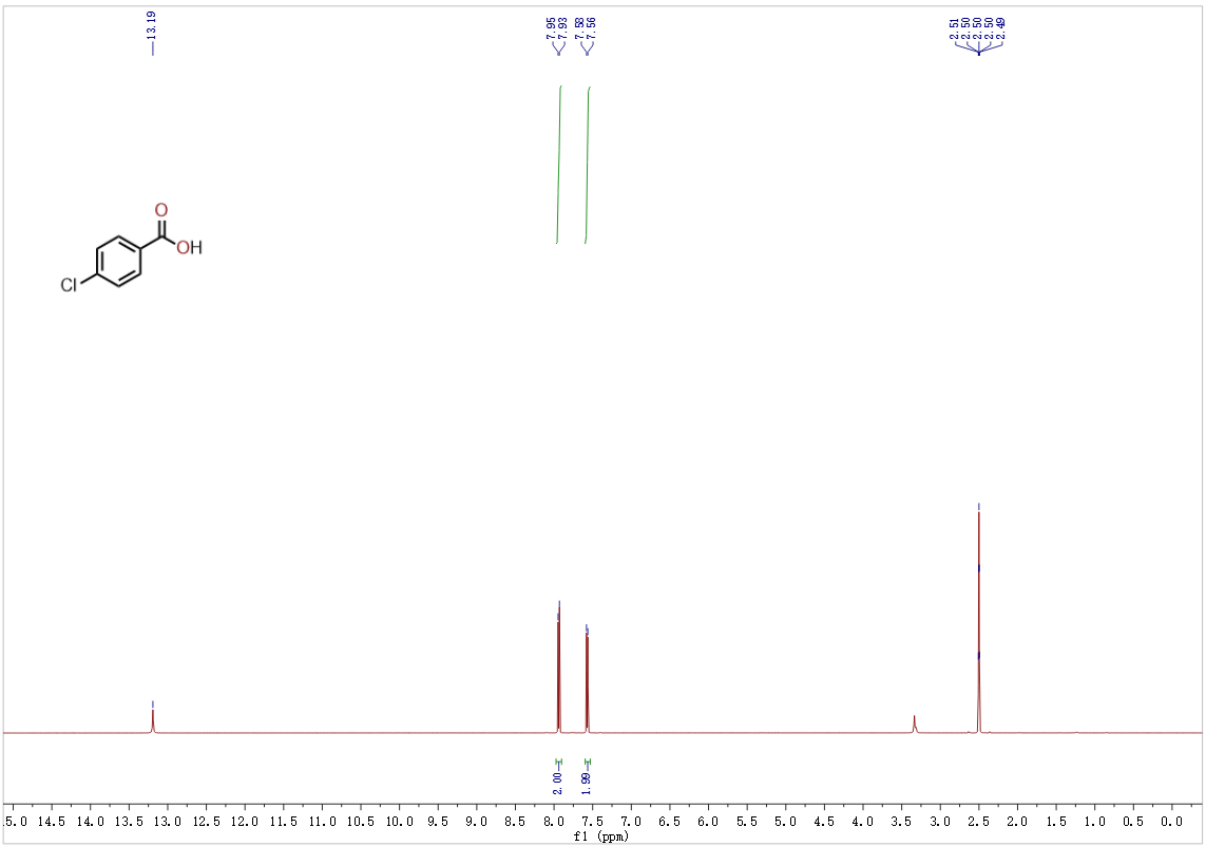
13.19
7.95
7.93
7.58
7.56
2.51
2.50
2.50
2.50
2.49
O
OH
Cl
2.00
1.99
f1 (ppm)

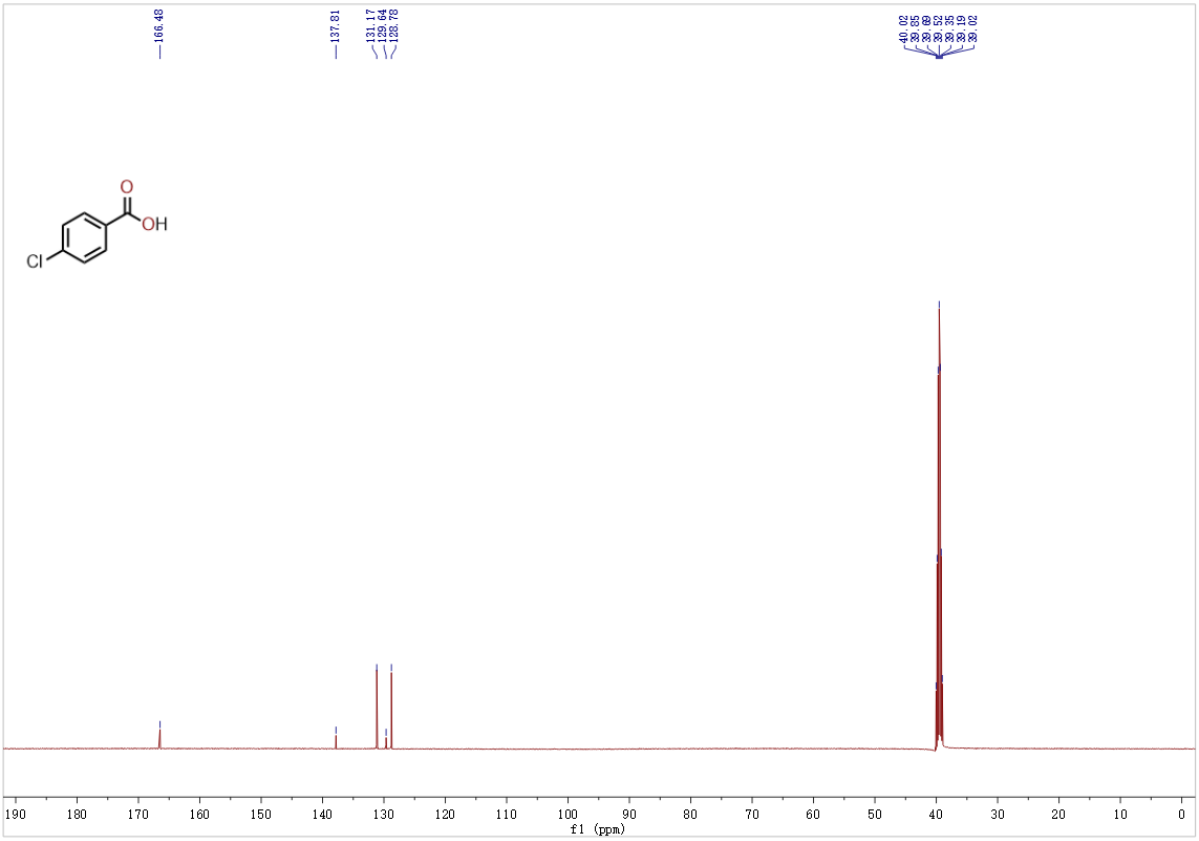
166.48
137.81
131.17
129.64
128.70
40.02
39.85
39.69
39.52
39.35
39.19
39.02
O
OH
Cl
f1 (ppm)

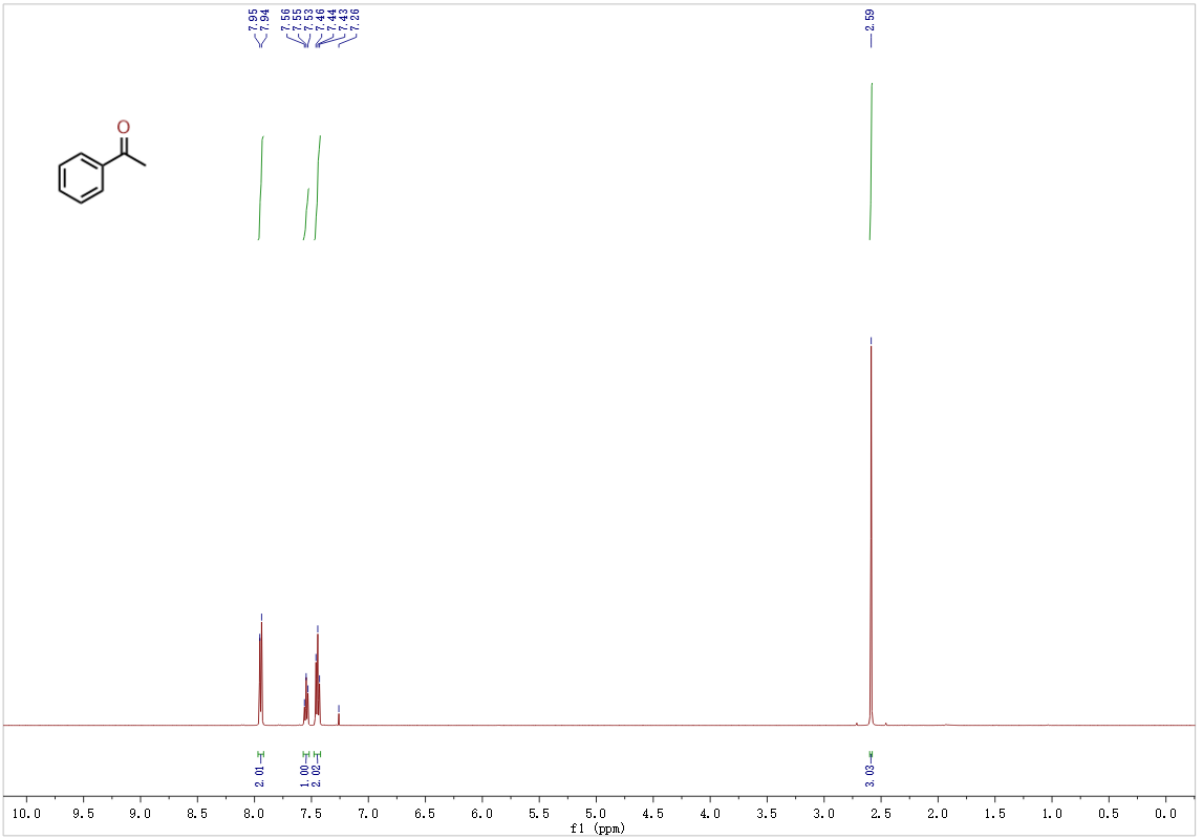
7.95
7.94
7.56
7.55
7.53
7.46
7.44
7.43
7.26
2.59
O
2.01
1.00
2.02
3.03
10.0 9.5 9.0 8.5 8.0 7.5 7.0 6.5 6.0 5.5 5.0 4.5 4.0 3.5 3.0 2.5 2.0 1.5 1.0 0.5 0.0
f1 (ppm)

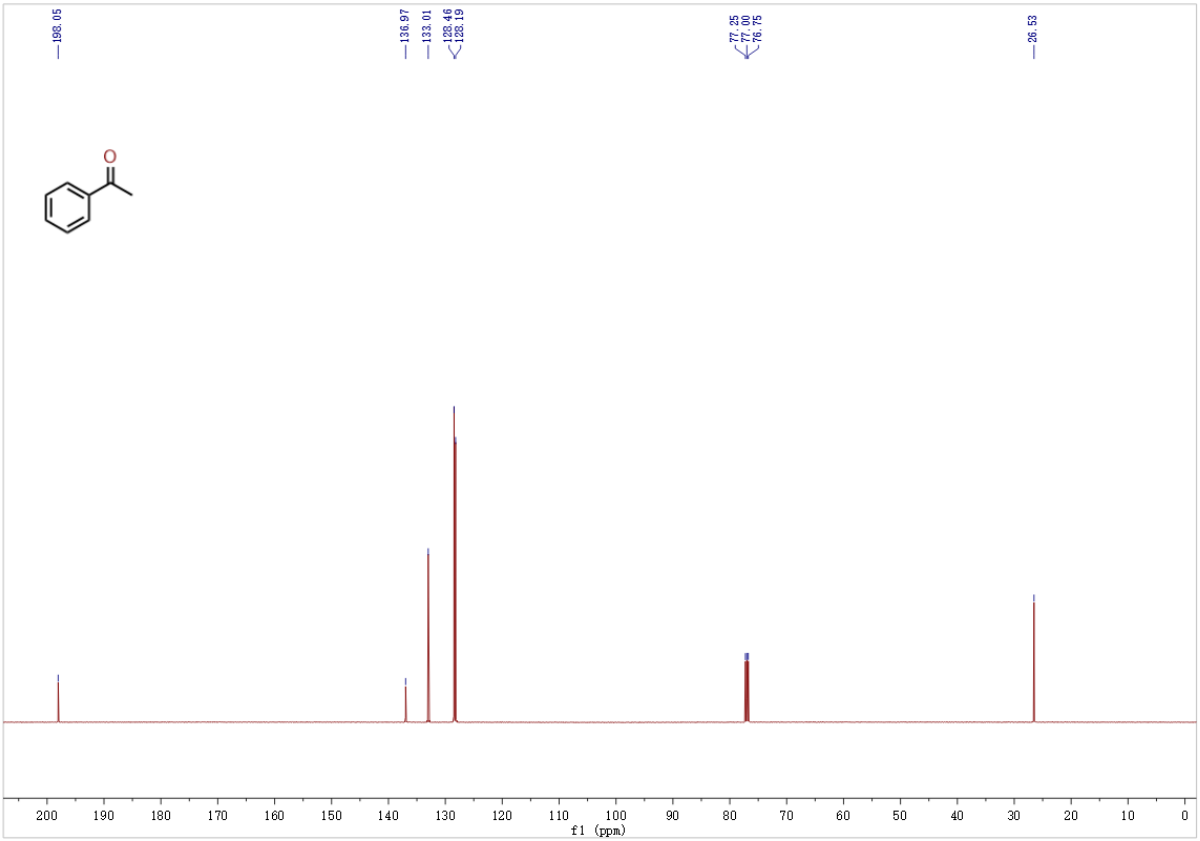
198.05
136.97
133.01
128.46
128.19
77.25
77.00
76.75
26.53
O
200 190 180 170 160 150 140 130 120 110 100 90 80 70 60 50 40 30 20 10 0
f1 (ppm)

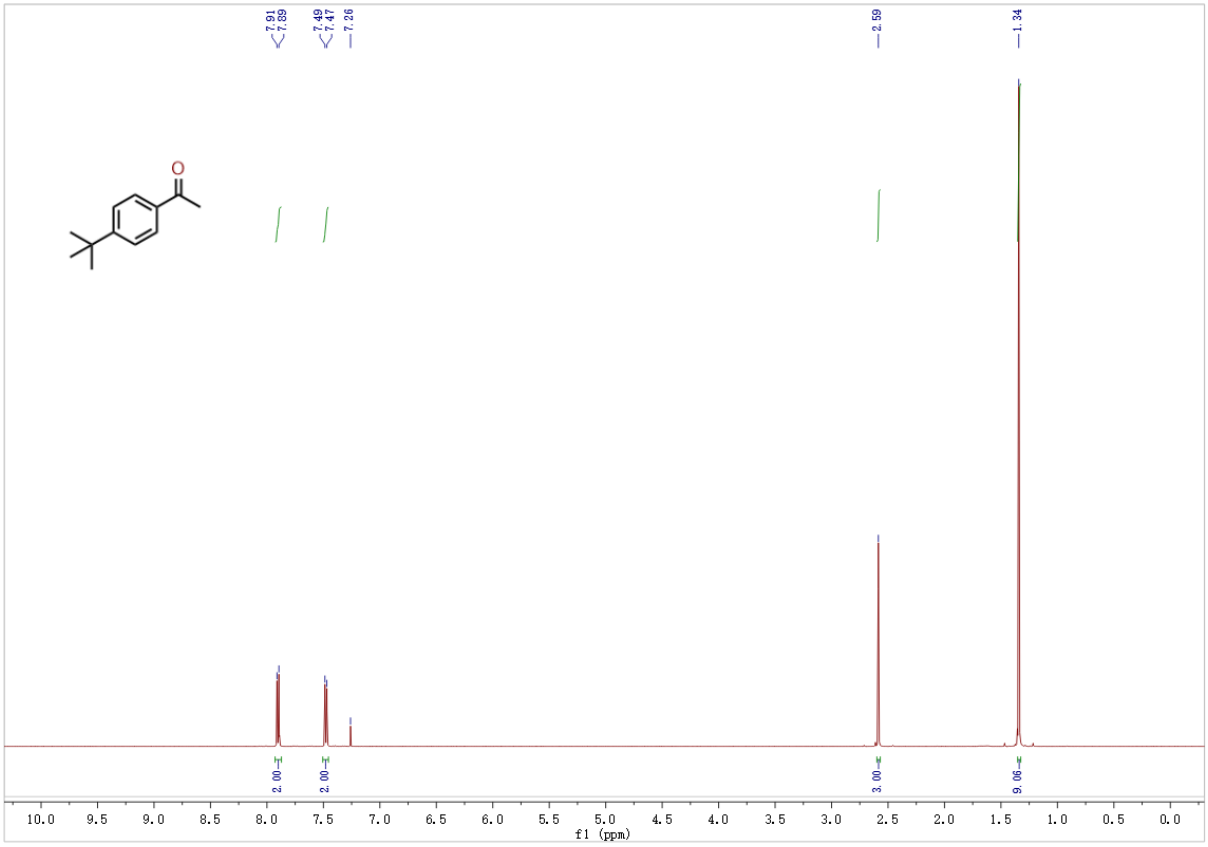
7.91
7.89
7.49
7.47
7.26
2.59
1.34
2.00
2.00
3.00
9.06
f1 (ppm)

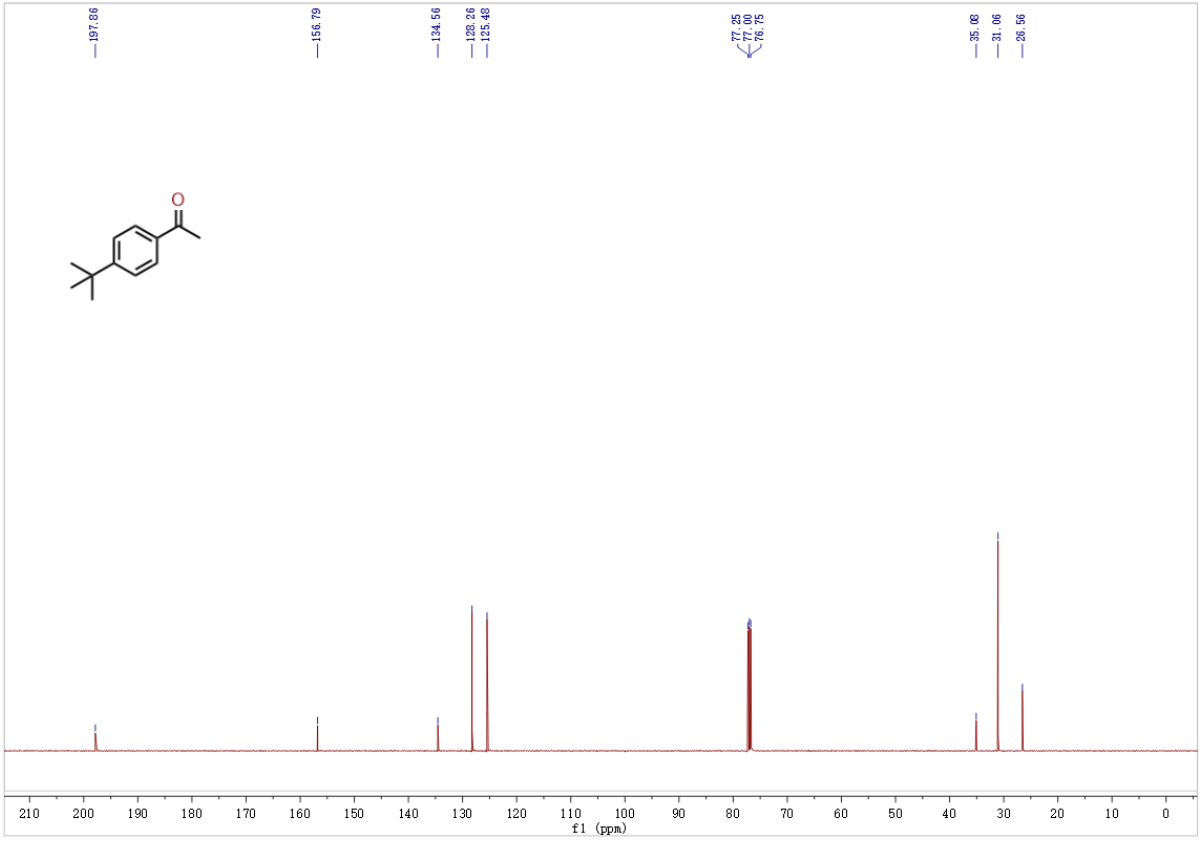
197.86
156.79
134.56
128.26
125.48
77.25
77.00
76.75
35.08
31.06
28.56
f1 (ppm)

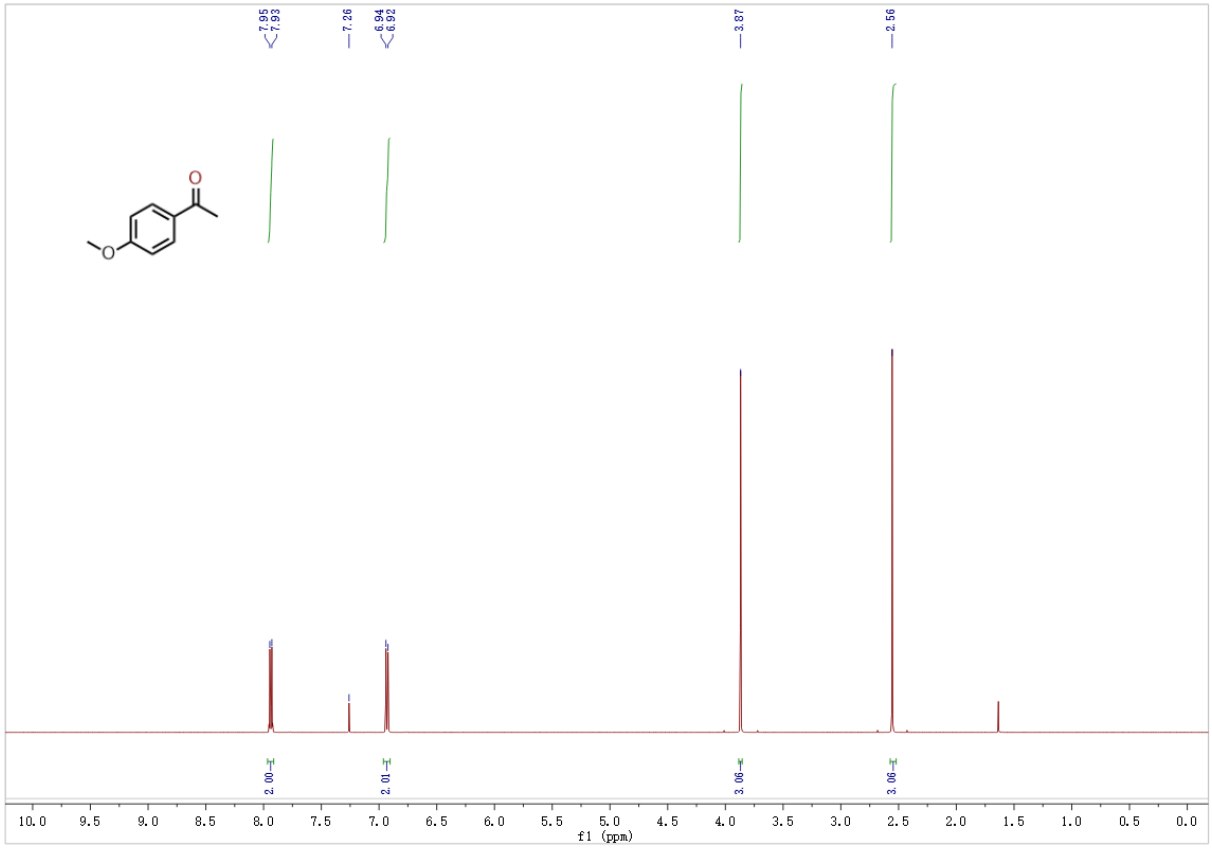
7.95
7.93
7.26
6.94
6.92
3.87
2.56
O
O
2.00
2.01
3.06
3.06
10.0 9.5 9.0 8.5 8.0 7.5 7.0 6.5 6.0 5.5 5.0 4.5 4.0 3.5 3.0 2.5 2.0 1.5 1.0 0.5 0.0
f1 (ppm)

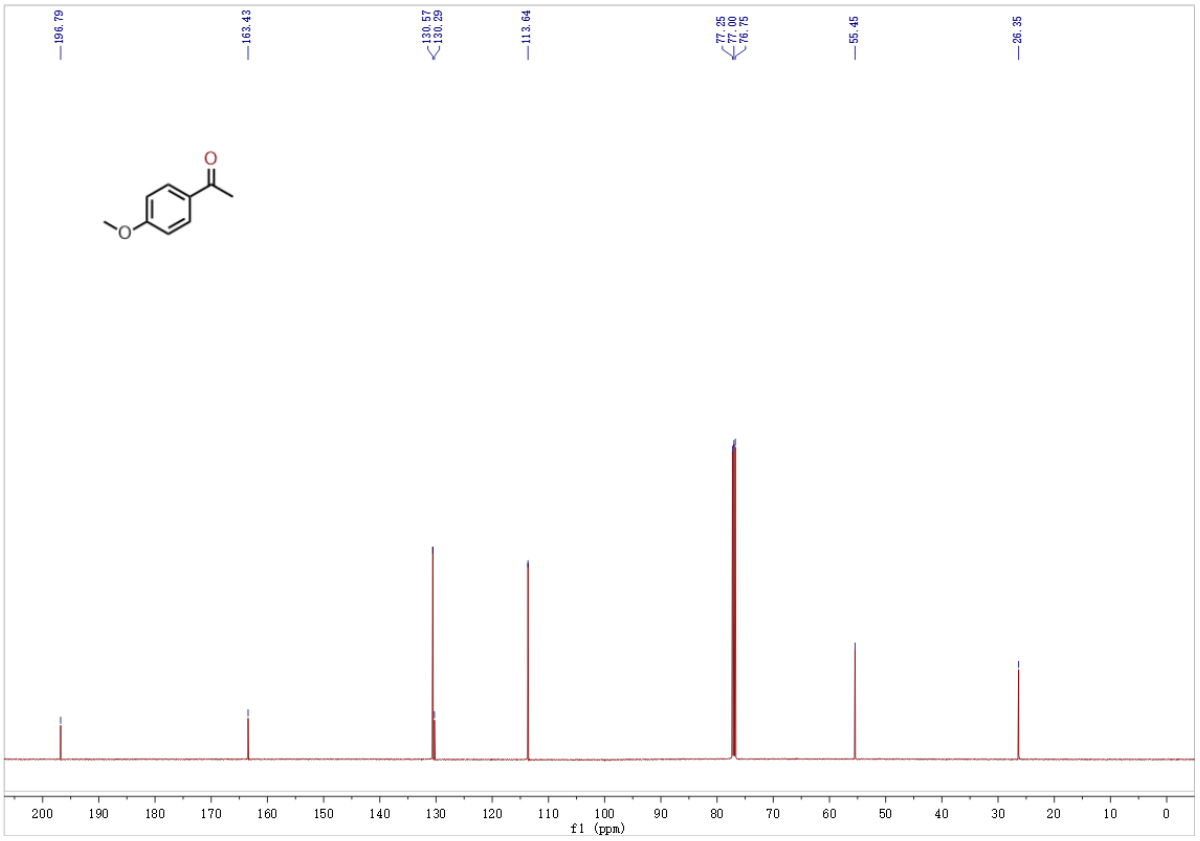
196.79
163.43
130.57
130.29
113.64
77.25
77.00
76.75
55.45
26.35
O
O
200 190 180 170 160 150 140 130 120 110 100 90 80 70 60 50 40 30 20 10 0
f1 (ppm)

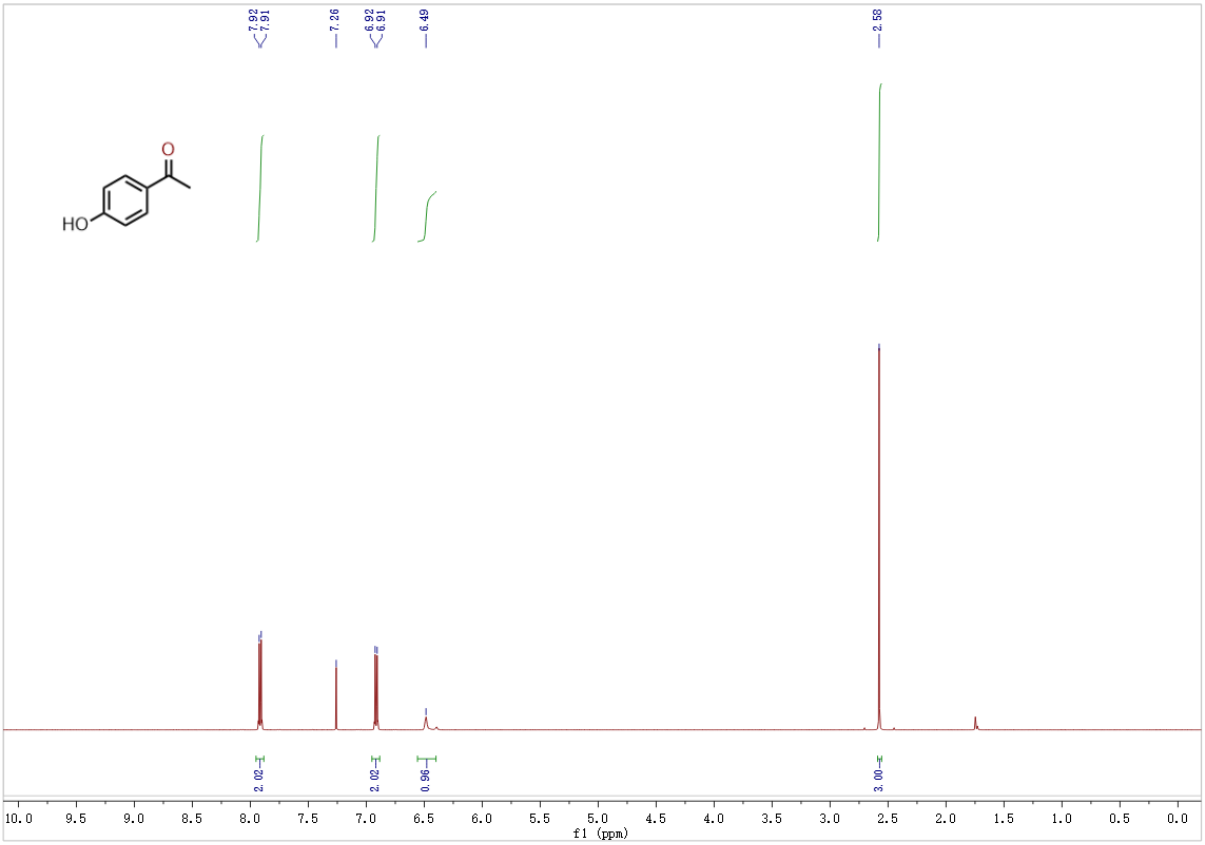
7.92
7.91
7.26
6.92
6.91
6.49
2.58
O
HO
2.02
2.02
0.96
3.00
10.0 9.5 9.0 8.5 8.0 7.5 7.0 6.5 6.0 5.5 5.0 4.5 4.0 3.5 3.0 2.5 2.0 1.5 1.0 0.5 0.0
f1 (ppm)

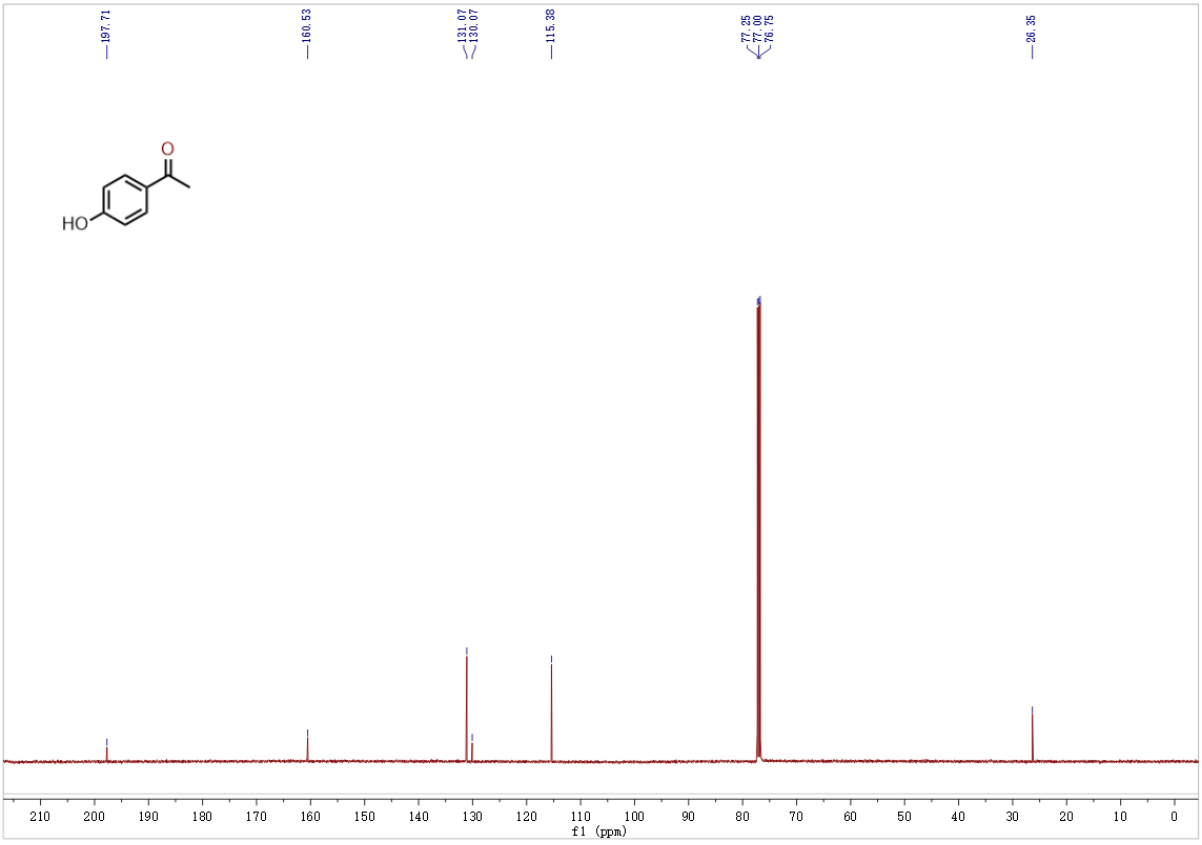
197.71
160.53
131.07
130.07
115.38
77.25
77.00
76.75
26.35
O
HO
210 200 190 180 170 160 150 140 130 120 110 100 90 80 70 60 50 40 30 20 10 0
f1 (ppm)

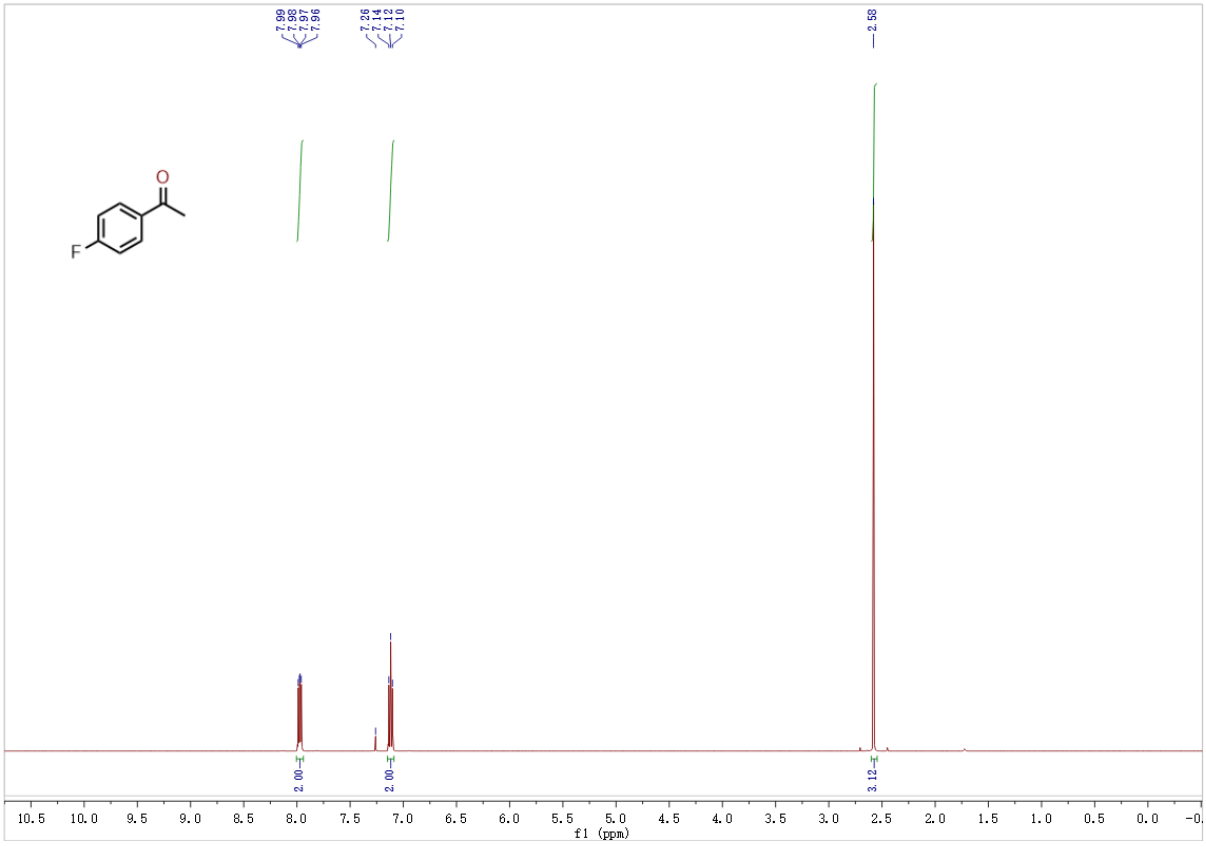
7.99
7.98
7.97
7.96
7.26
7.14
7.12
7.10
2.58
O
F
2.00
2.00
3.12
10.5 10.0 9.5 9.0 8.5 8.0 7.5 7.0 6.5 6.0 5.5 5.0 4.5 4.0 3.5 3.0 2.5 2.0 1.5 1.0 0.5 0.0
f1 (ppm)

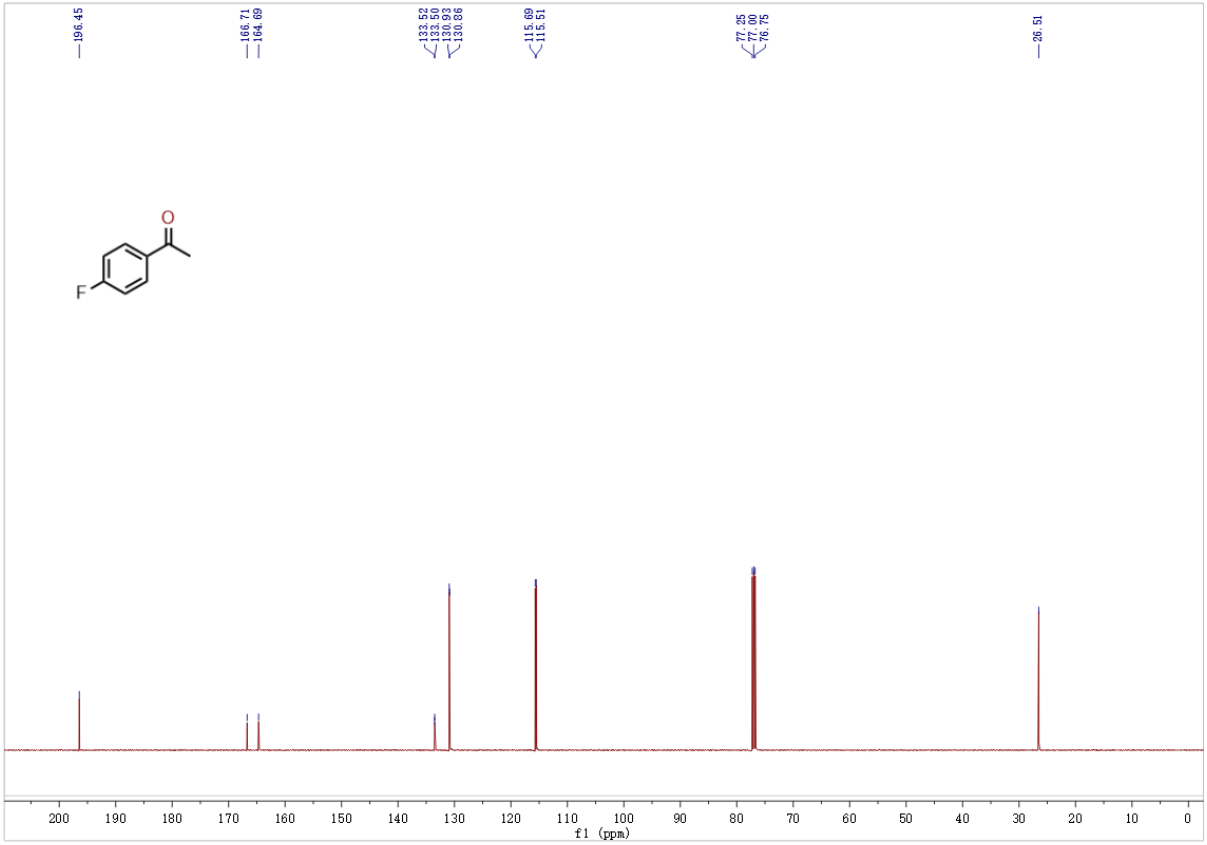
196.45
166.71
164.69
133.52
133.50
130.93
130.86
115.69
115.51
77.25
77.00
76.75
26.51
O
F
200 190 180 170 160 150 140 130 120 110 100 90 80 70 60 50 40 30 20 10 0
f1 (ppm)

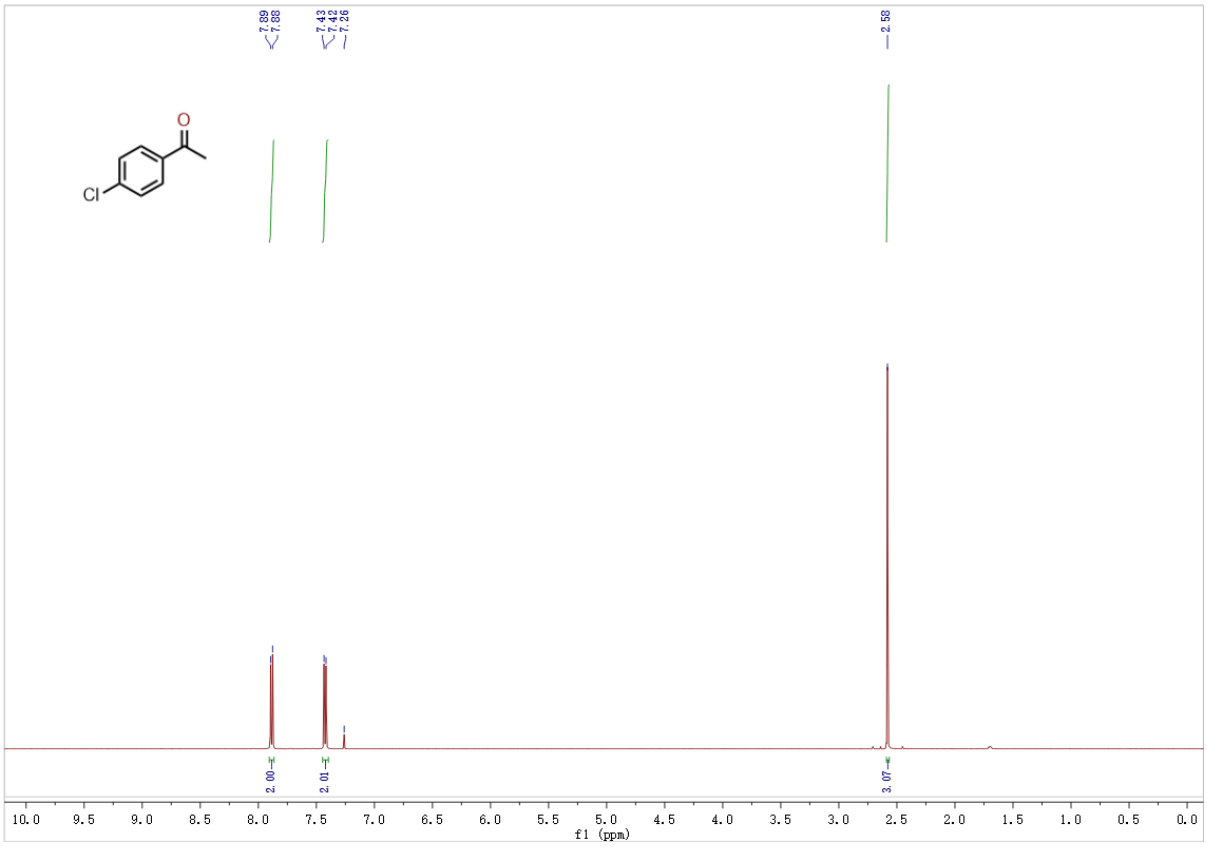
7.89
7.88
7.43
7.42
7.26
2.58
O
Cl
2.00
2.01
3.07
10.0 9.5 9.0 8.5 8.0 7.5 7.0 6.5 6.0 5.5 5.0 4.5 4.0 3.5 3.0 2.5 2.0 1.5 1.0 0.5 0.0
f1 (ppm)

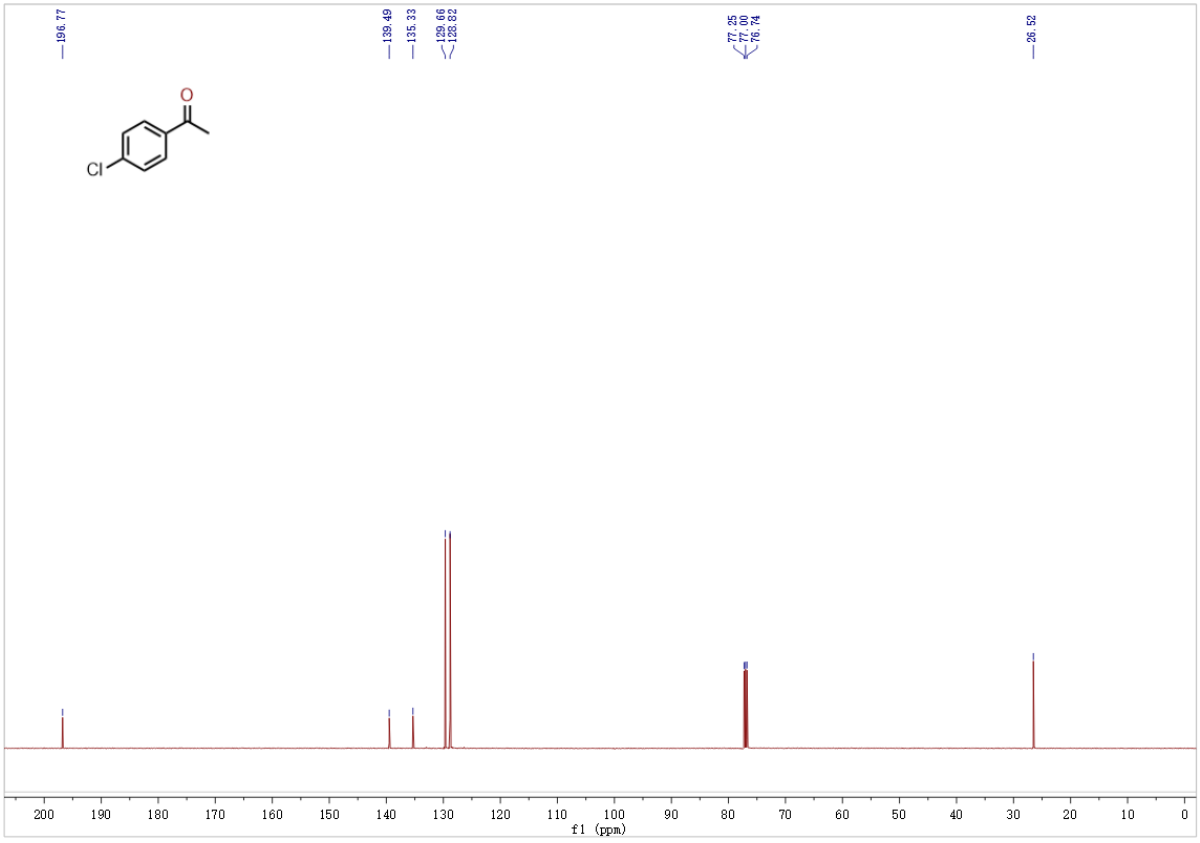
196.77
139.49
135.33
129.66
128.82
77.25
77.00
76.74
26.52
O
Cl
200 190 180 170 160 150 140 130 120 110 100 90 80 70 60 50 40 30 20 10 0
f1 (ppm)

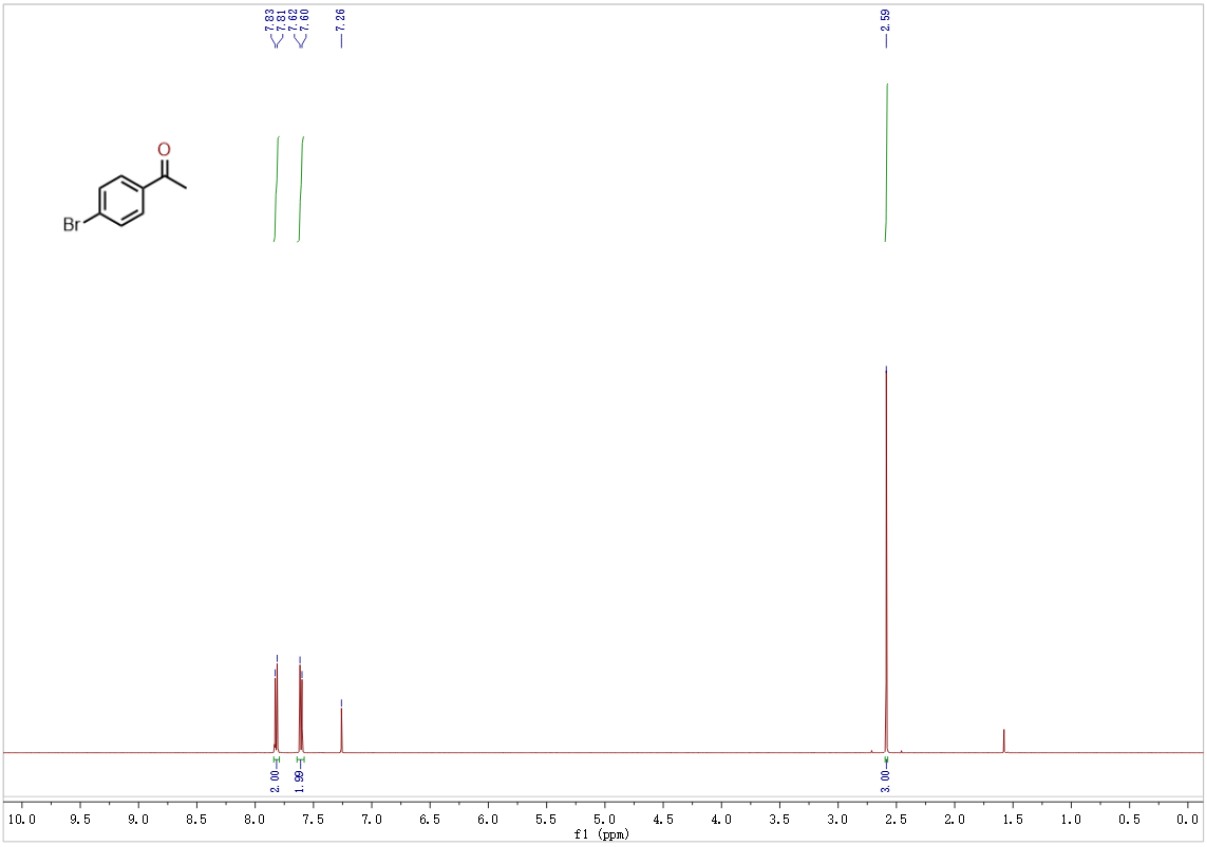
7.83
7.81
7.62
7.60
7.26
2.59
O
Br
2.00
1.99
3.00
10.0 9.5 9.0 8.5 8.0 7.5 7.0 6.5 6.0 5.5 5.0 4.5 4.0 3.5 3.0 2.5 2.0 1.5 1.0 0.5 0.0
f1 (ppm)

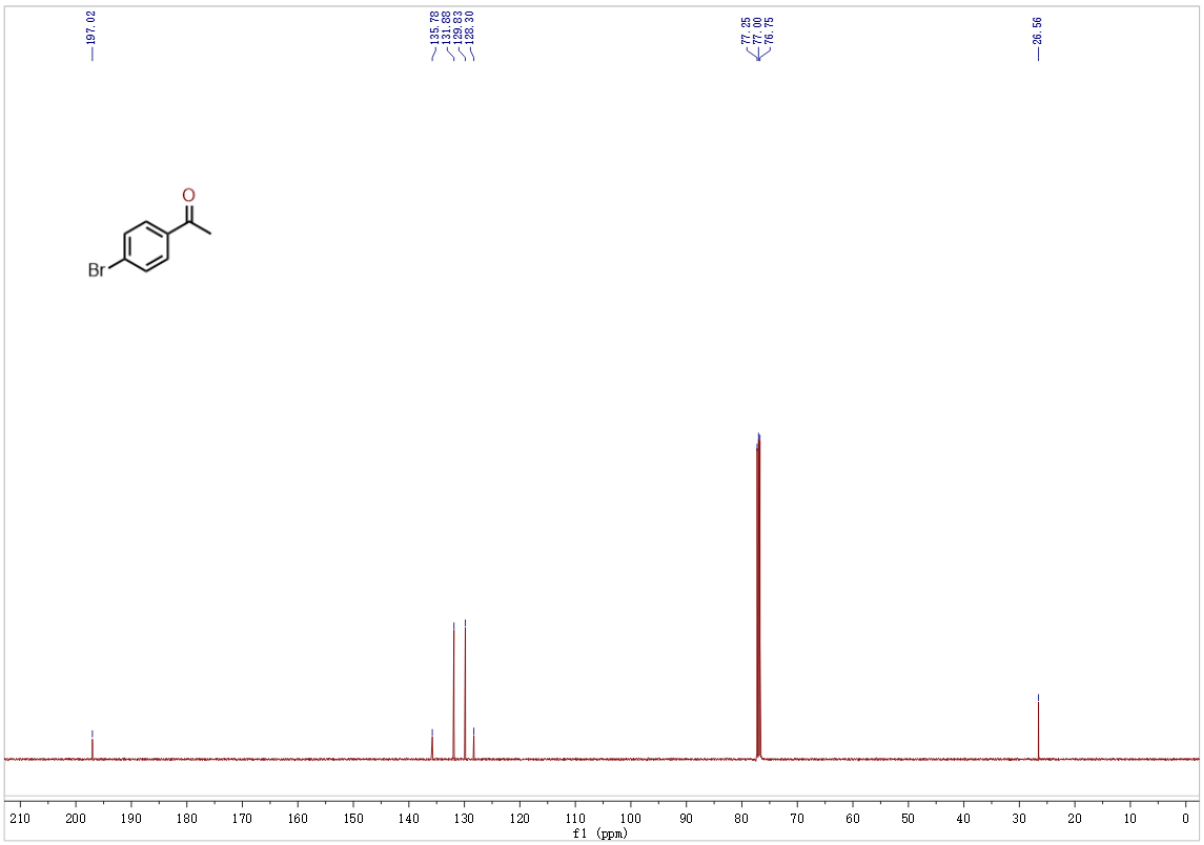
197.02
135.78
131.88
129.83
128.30
77.25
77.00
76.75
26.56
O
Br
210 200 190 180 170 160 150 140 130 120 110 100 90 80 70 60 50 40 30 20 10 0
f1 (ppm)

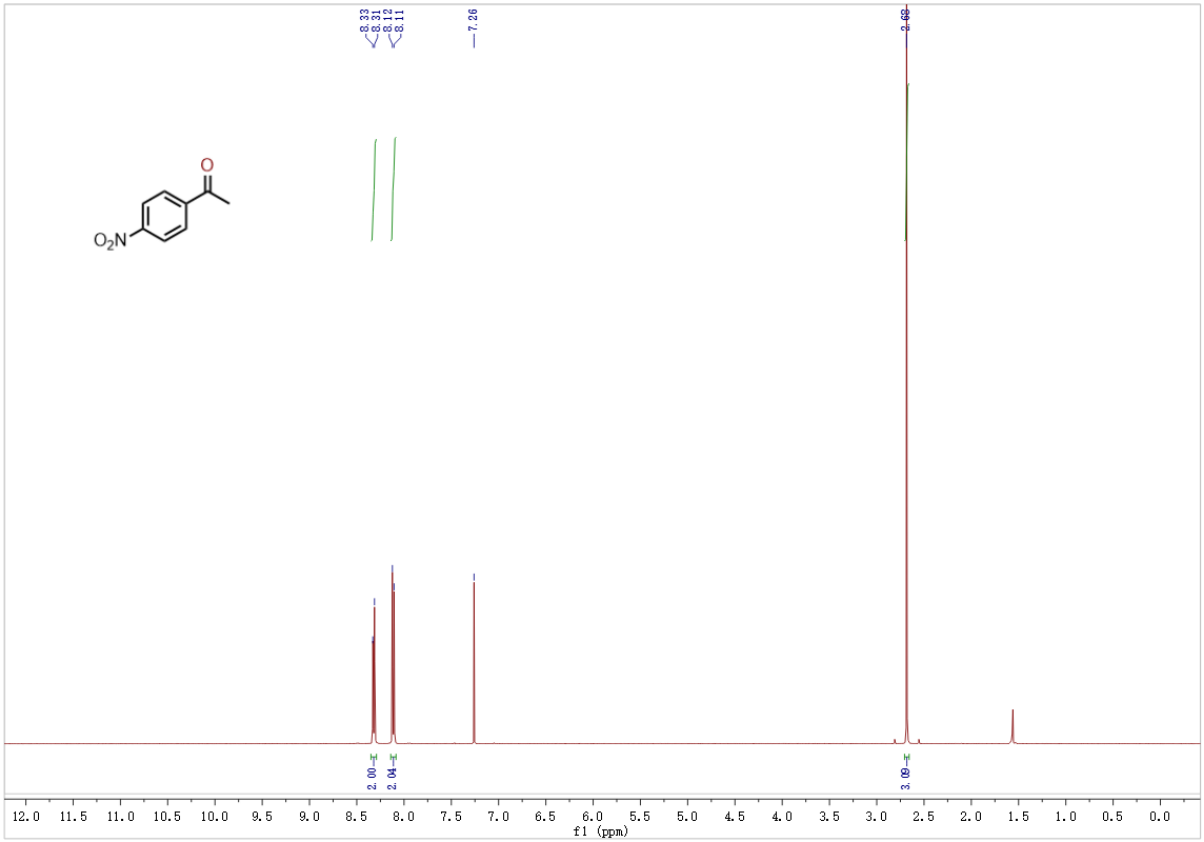
8.33
8.31
8.12
8.11
7.26
2.68
O
O2N
2.00
2.04
3.09
12.0 11.5 11.0 10.5 10.0 9.5 9.0 8.5 8.0 7.5 7.0 6.5 6.0 5.5 5.0 4.5 4.0 3.5 3.0 2.5 2.0 1.5 1.0 0.5 0.0
f1 (ppm)

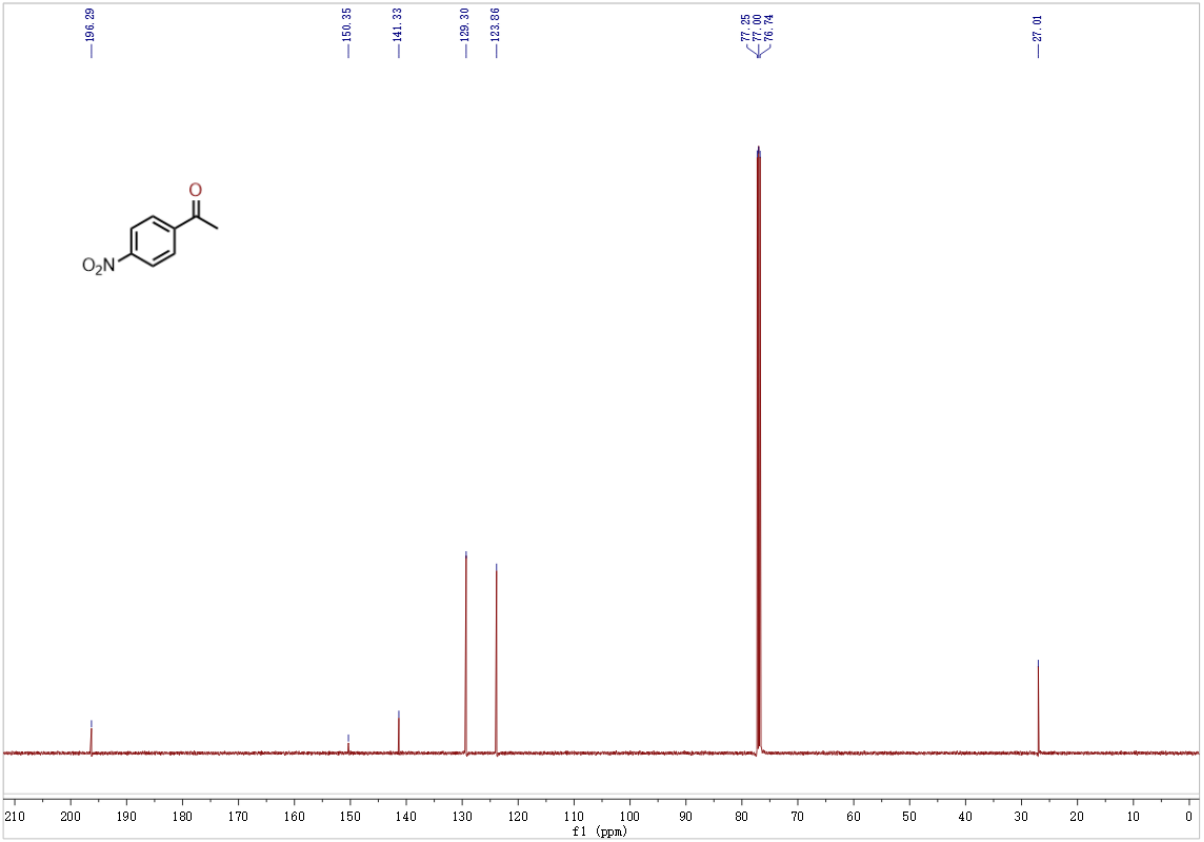
196.29
150.35
141.33
129.30
123.86
77.25
77.00
76.74
27.01
O
O2N
210 200 190 180 170 160 150 140 130 120 110 100 90 80 70 60 50 40 30 20 10 0
f1 (ppm)

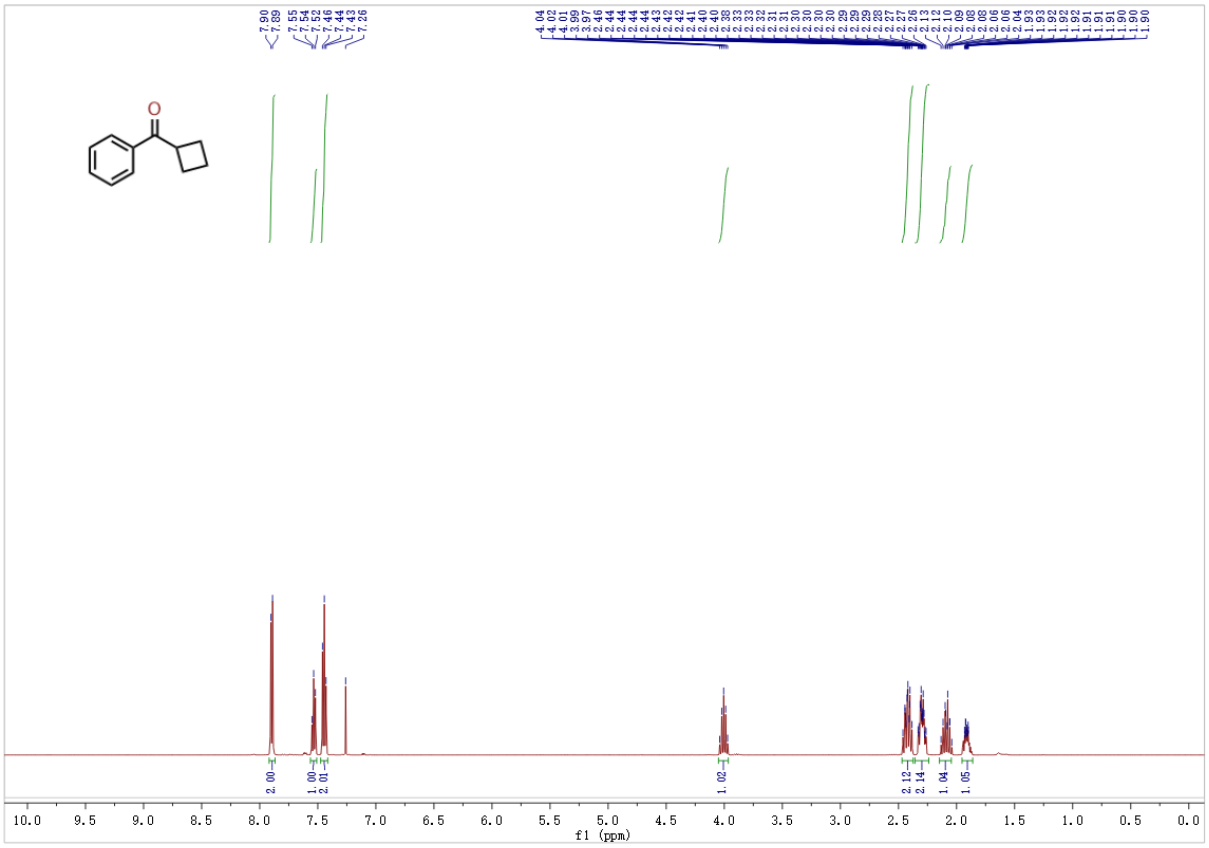
7.90
7.89
7.55
7.54
7.52
7.46
7.44
7.43
7.26
2.00
1.00
2.01
1.02
2.12
2.14
1.04
1.05
10.0 9.5 9.0 8.5 8.0 7.5 7.0 6.5 6.0 5.5 5.0 4.5 4.0 3.5 3.0 2.5 2.0 1.5 1.0 0.5 0.0
f1 (ppm)

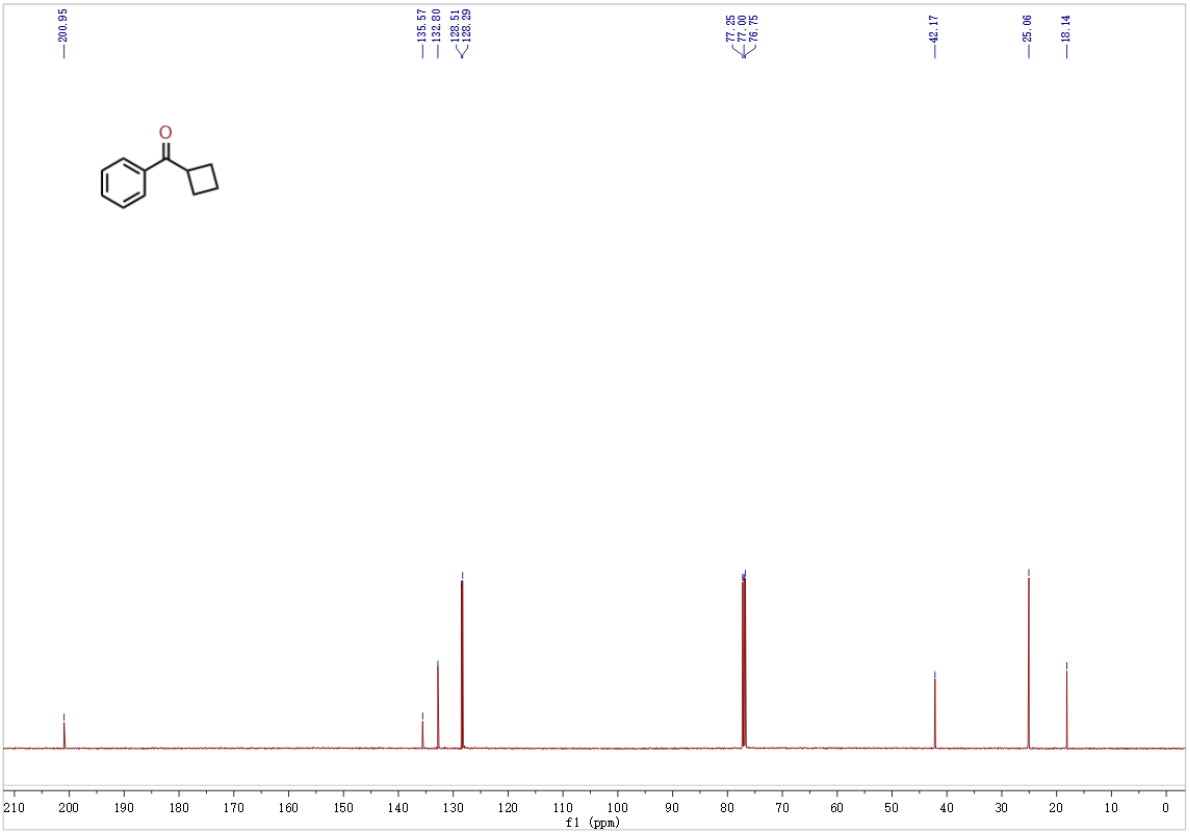
200.95
135.57
132.80
128.51
128.29
77.25
77.00
76.75
42.17
25.06
18.14
210 200 190 180 170 160 150 140 130 120 110 100 90 80 70 60 50 40 30 20 10 0
f1 (ppm)

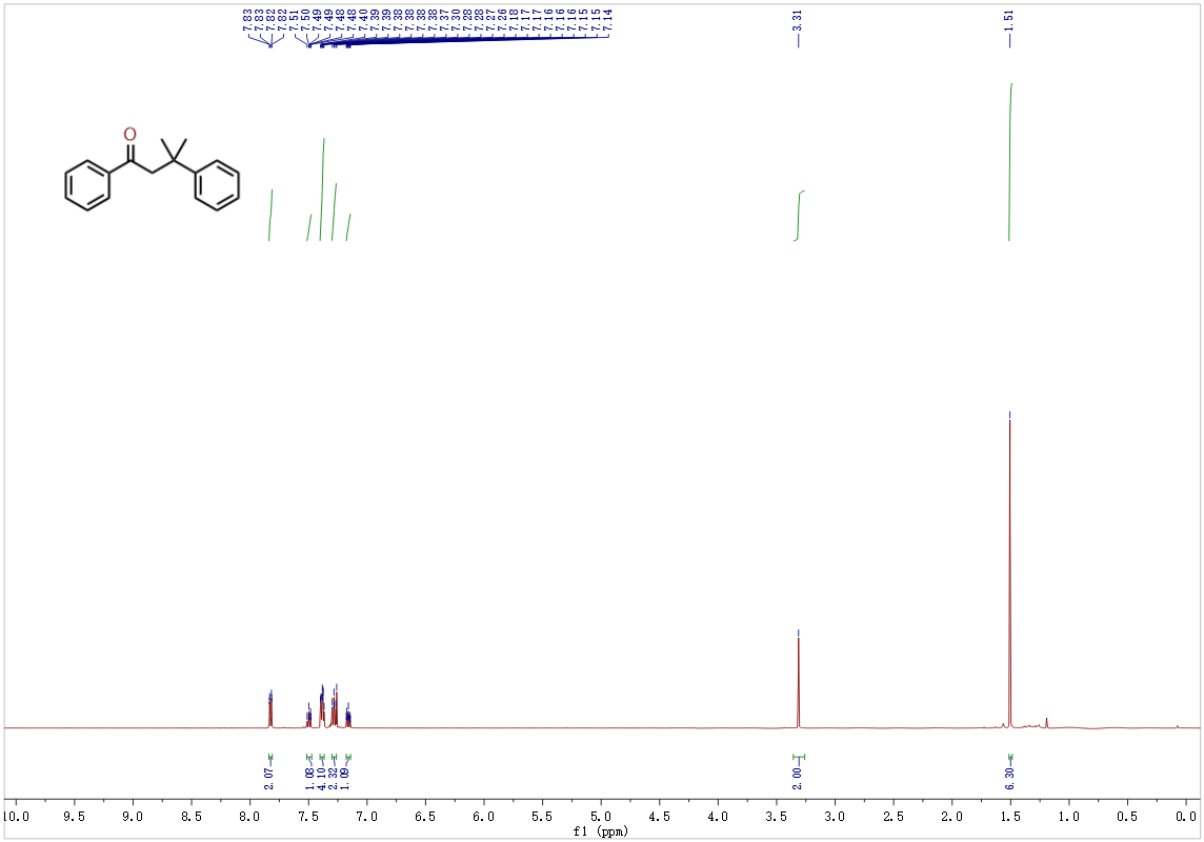
7.83
7.83
7.82
7.82
7.51
7.50
7.49
7.49
7.48
7.46
7.40
7.39
7.39
7.38
7.38
7.38
7.37
7.30
7.28
7.28
7.27
7.26
7.18
7.17
7.17
7.17
7.16
7.16
7.15
7.15
7.14
3.31
1.51
O
2.07
1.08
4.10
2.32
1.09
2.00
6.30
10.0 9.5 9.0 8.5 8.0 7.5 7.0 6.5 6.0 5.5 5.0 4.5 4.0 3.5 3.0 2.5 2.0 1.5 1.0 0.5 0.0
f1 (ppm)

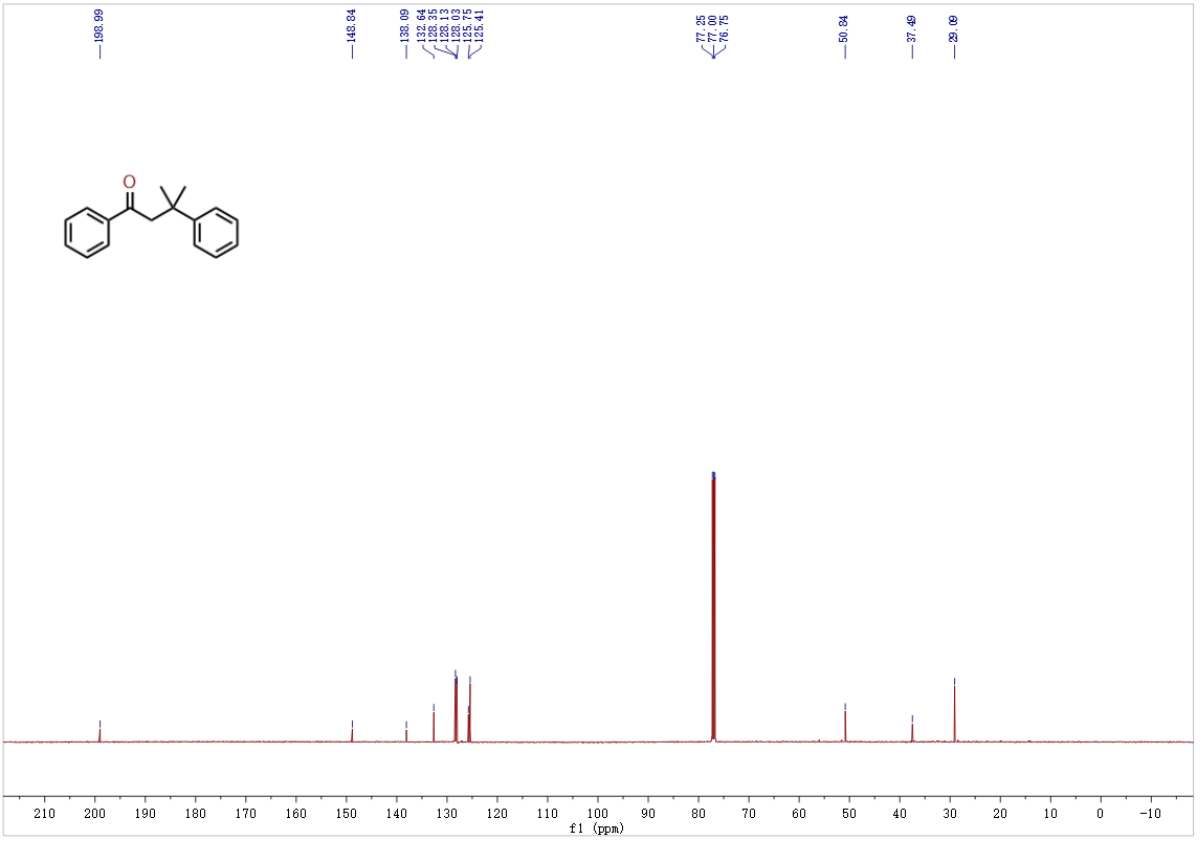
198.99
148.64
138.09
132.64
128.35
128.13
128.03
125.75
125.41
77.25
77.00
76.75
50.84
37.49
29.09
O
210 200 190 180 170 160 150 140 130 120 110 100 90 80 70 60 50 40 30 20 10 0 -10
f1 (ppm)

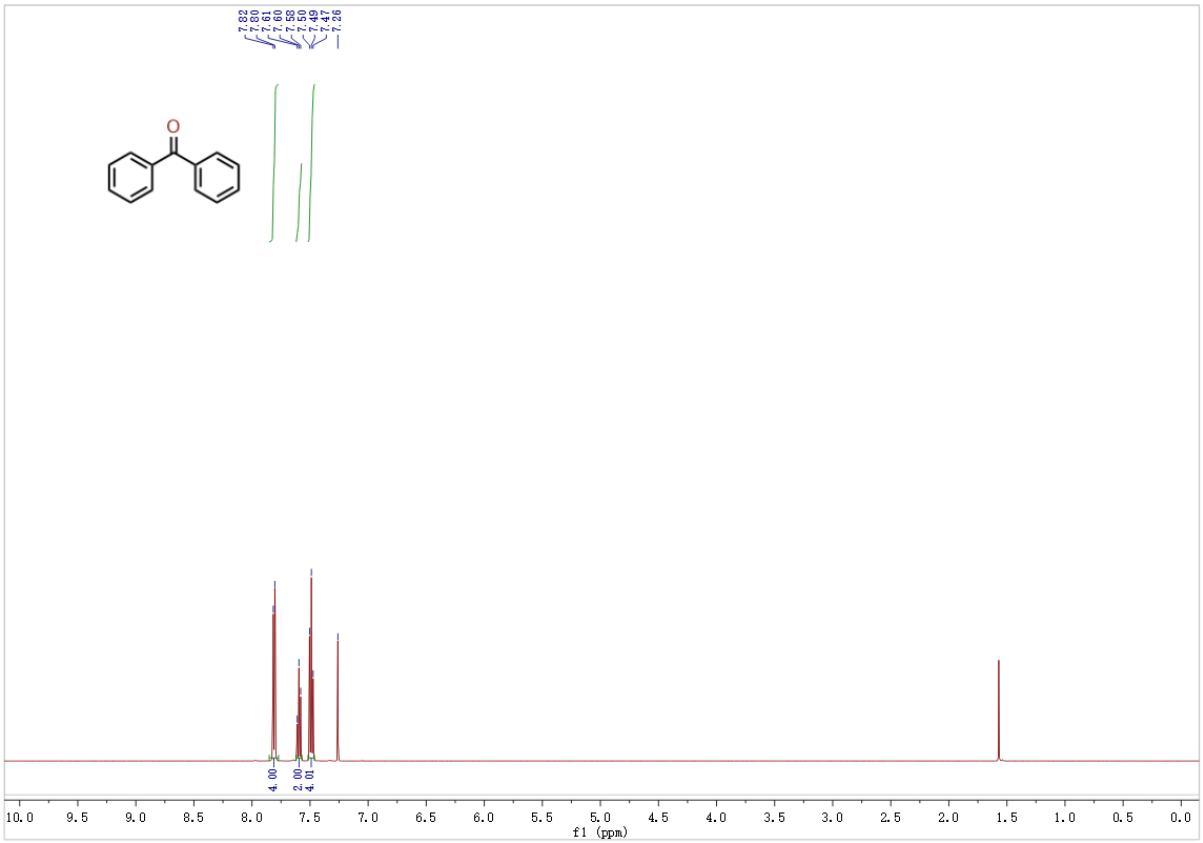
7.82
7.80
7.61
7.60
7.58
7.50
7.49
7.47
7.26
O
4.00
2.00
4.01
10.0 9.5 9.0 8.5 8.0 7.5 7.0 6.5 6.0 5.5 5.0 4.5 4.0 3.5 3.0 2.5 2.0 1.5 1.0 0.5 0.0
f1 (ppm)

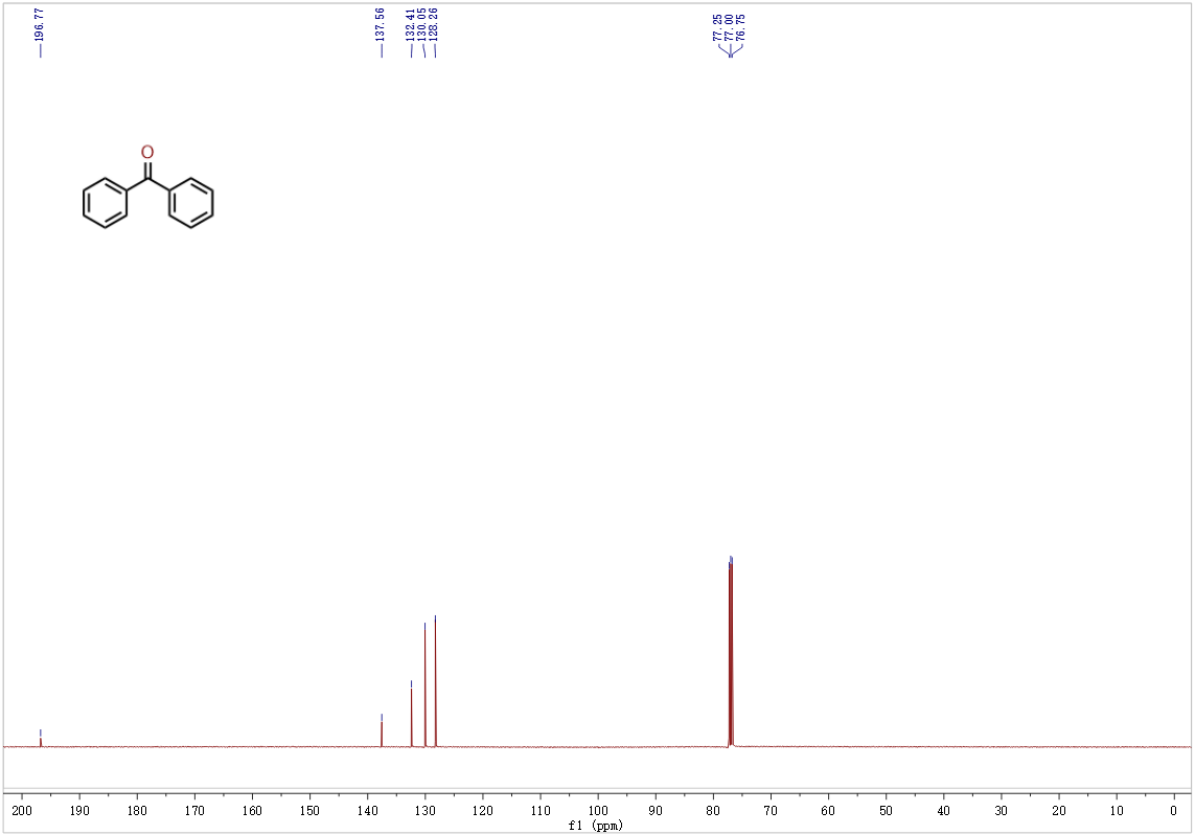
196.77
137.56
132.41
130.05
128.26
77.25
77.00
76.75
O
200 190 180 170 160 150 140 130 120 110 100 90 80 70 60 50 40 30 20 10 0
f1 (ppm)

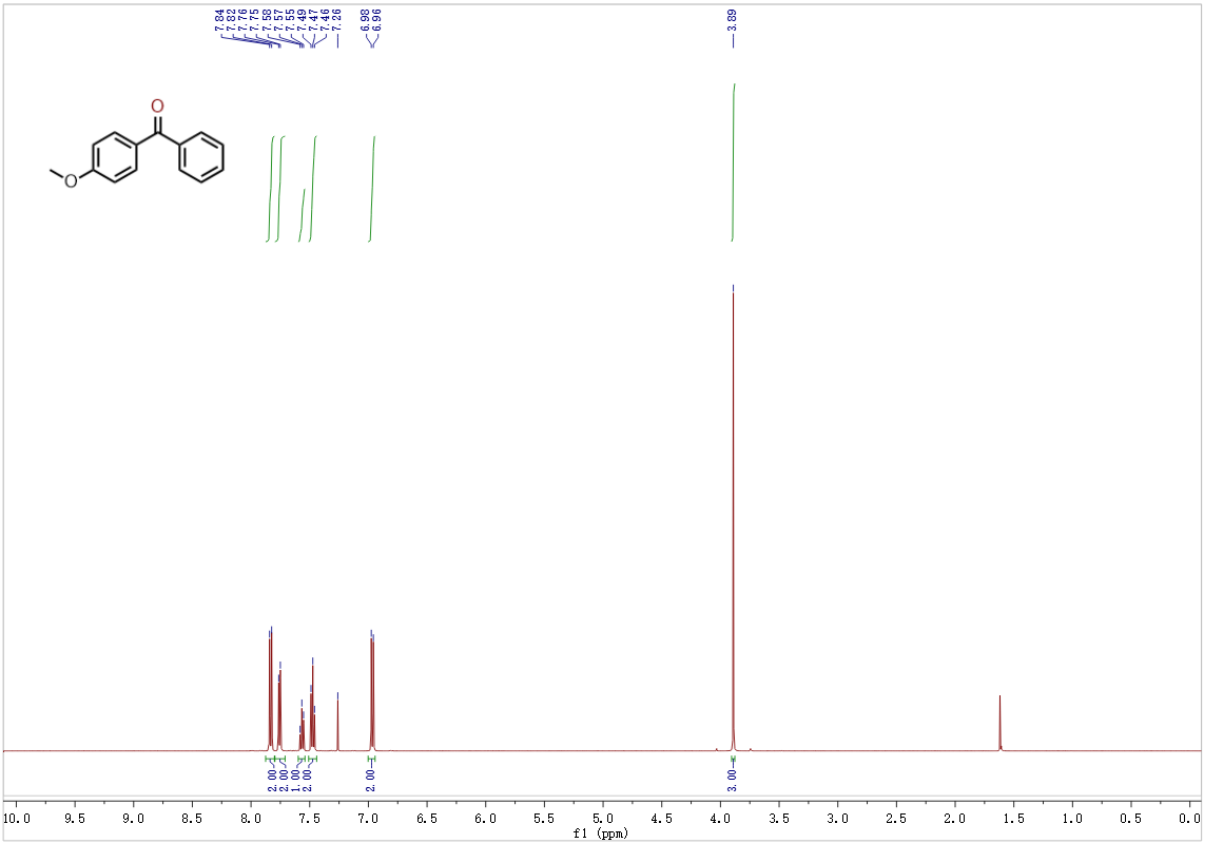
7.84
7.82
7.76
7.75
7.58
7.57
7.55
7.49
7.47
7.45
7.26
6.98
6.96
3.89
2.00
2.00
1.00
2.00
2.00
3.00
10.0 9.5 9.0 8.5 8.0 7.5 7.0 6.5 6.0 5.5 5.0 4.5 4.0 3.5 3.0 2.5 2.0 1.5 1.0 0.5 0.0
f1 (ppm)

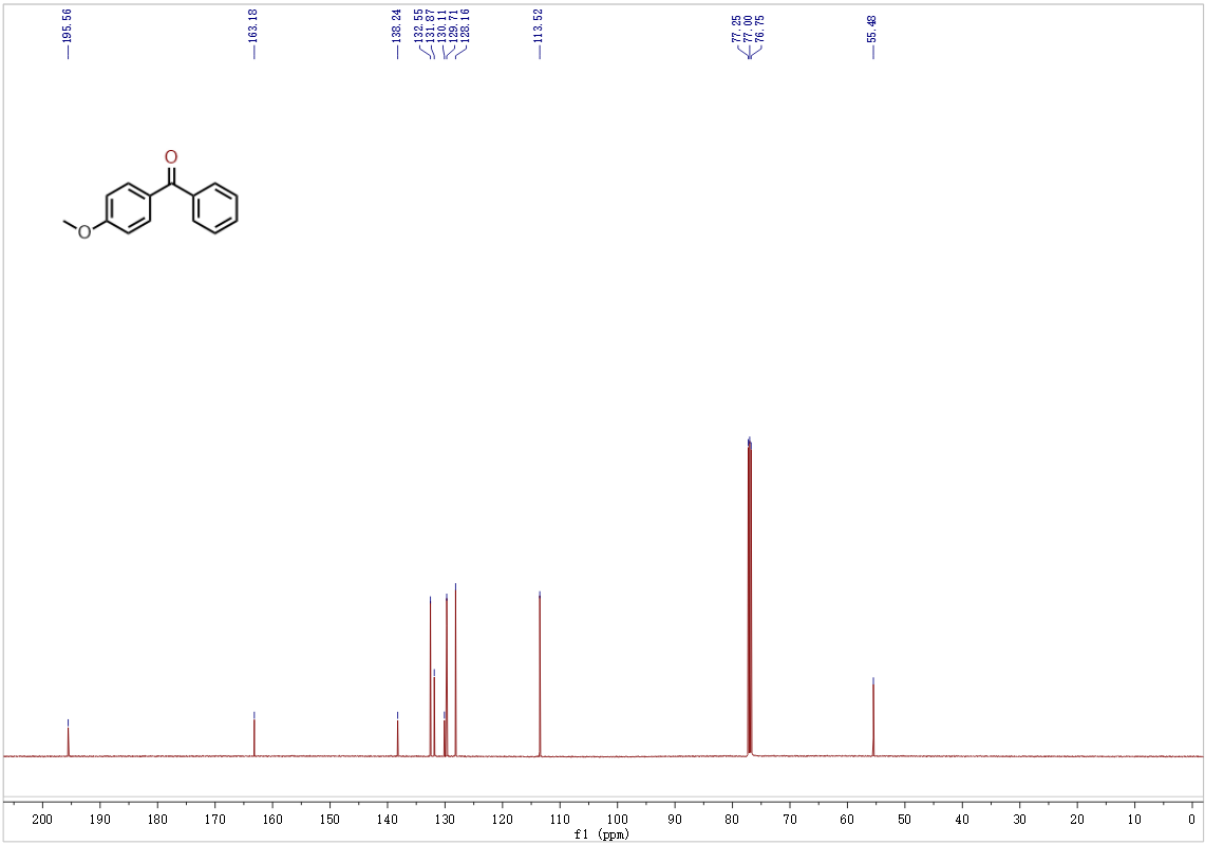
195.56
163.18
138.24
132.55
131.87
130.11
129.71
128.16
113.52
77.25
77.00
76.75
55.48
200 190 180 170 160 150 140 130 120 110 100 90 80 70 60 50 40 30 20 10 0
f1 (ppm)

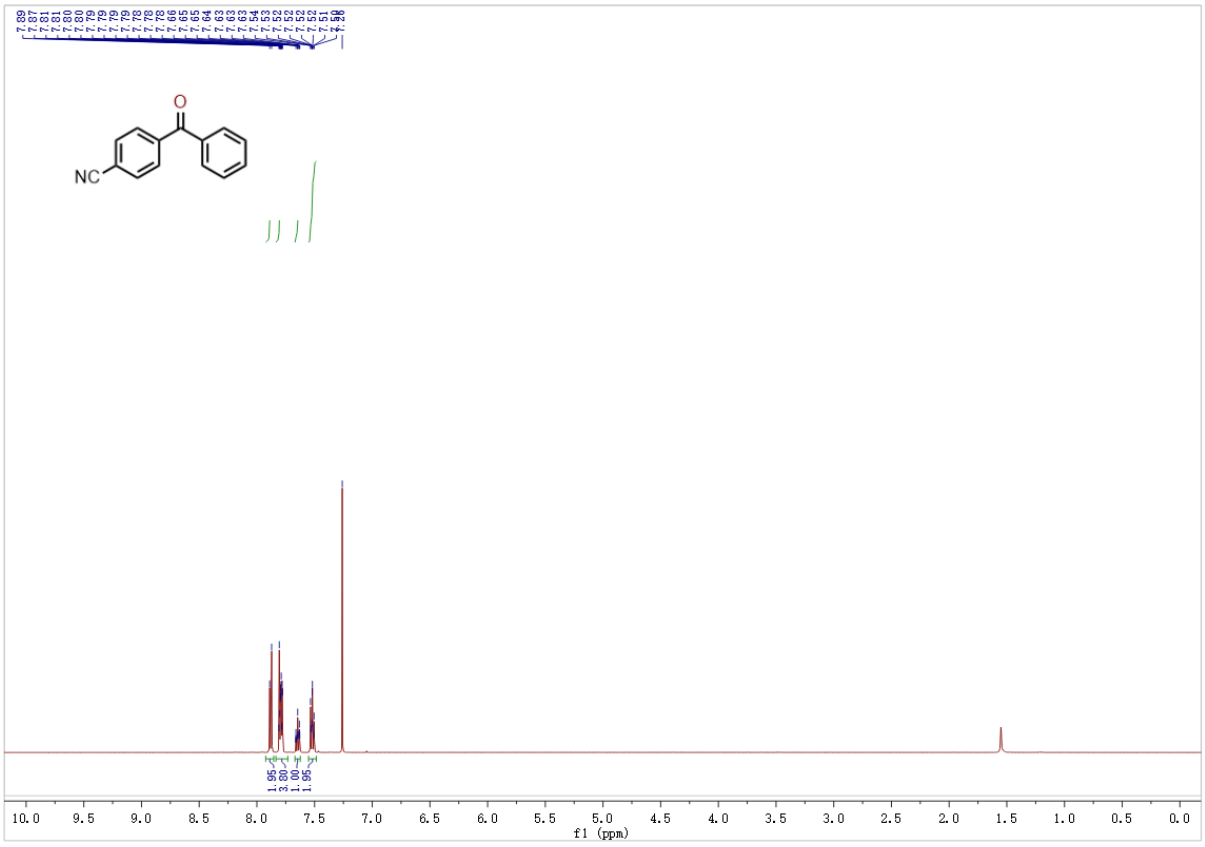
NC
O
f1 (ppm)

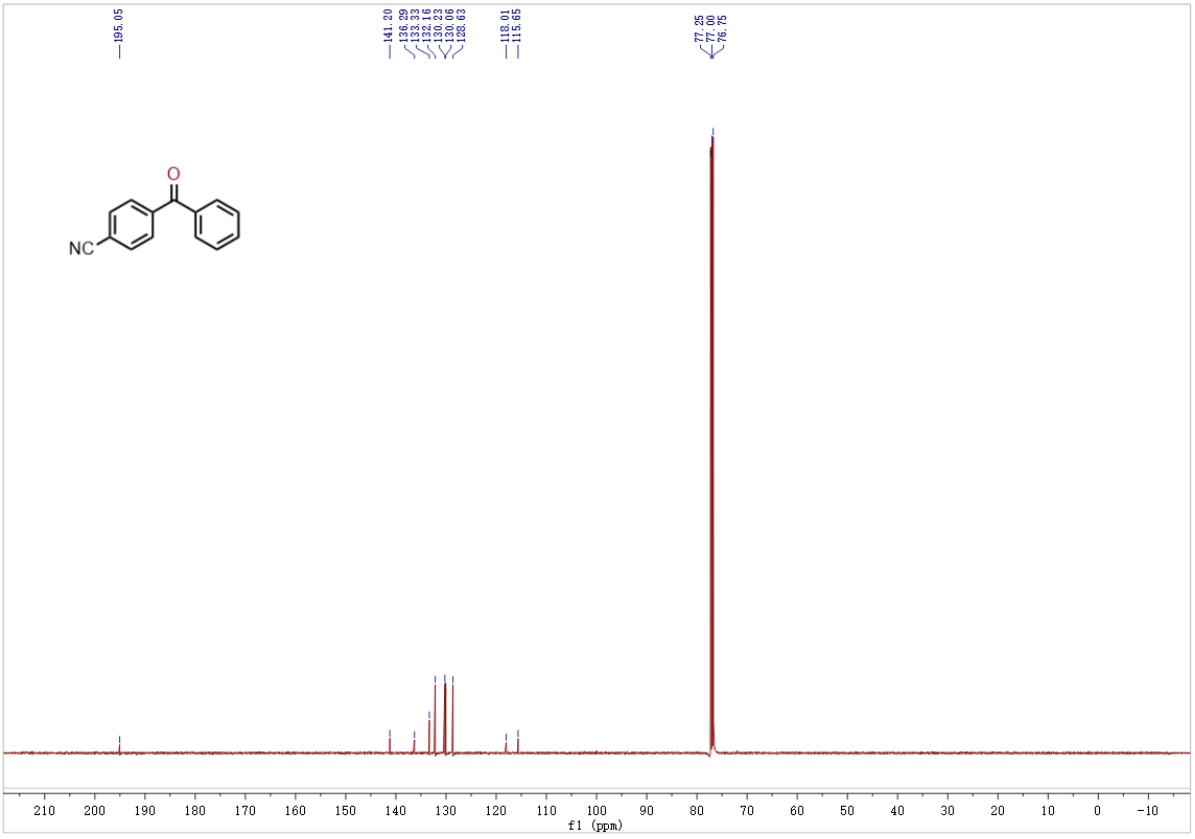
NC
O
f1 (ppm)

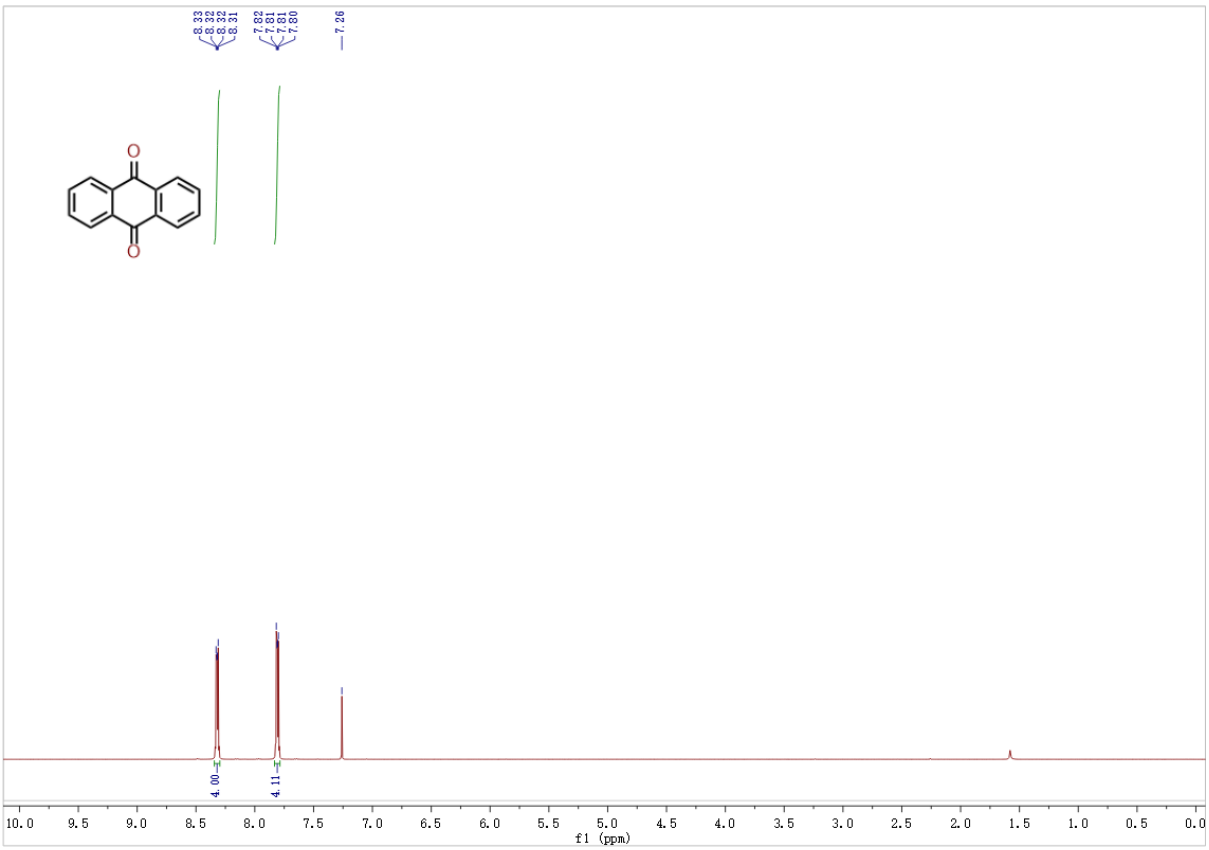
8.33
8.32
8.32
8.31
7.82
7.81
7.81
7.80
7.26
4.00
4.11
10.0 9.5 9.0 8.5 8.0 7.5 7.0 6.5 6.0 5.5 5.0 4.5 4.0 3.5 3.0 2.5 2.0 1.5 1.0 0.5 0.0
f1 (ppm)

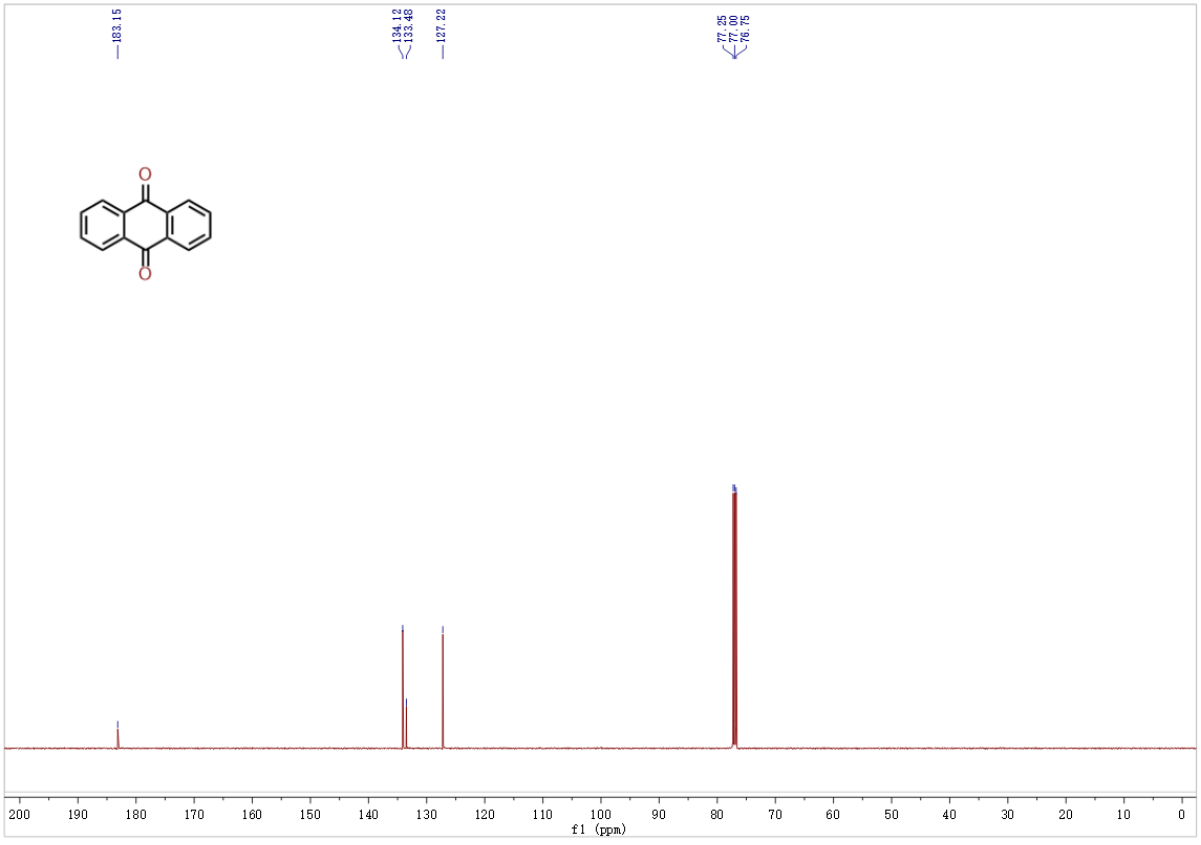
183.15
134.12
133.48
127.22
77.25
77.00
76.75
200 190 180 170 160 150 140 130 120 110 100 90 80 70 60 50 40 30 20 10 0
f1 (ppm)

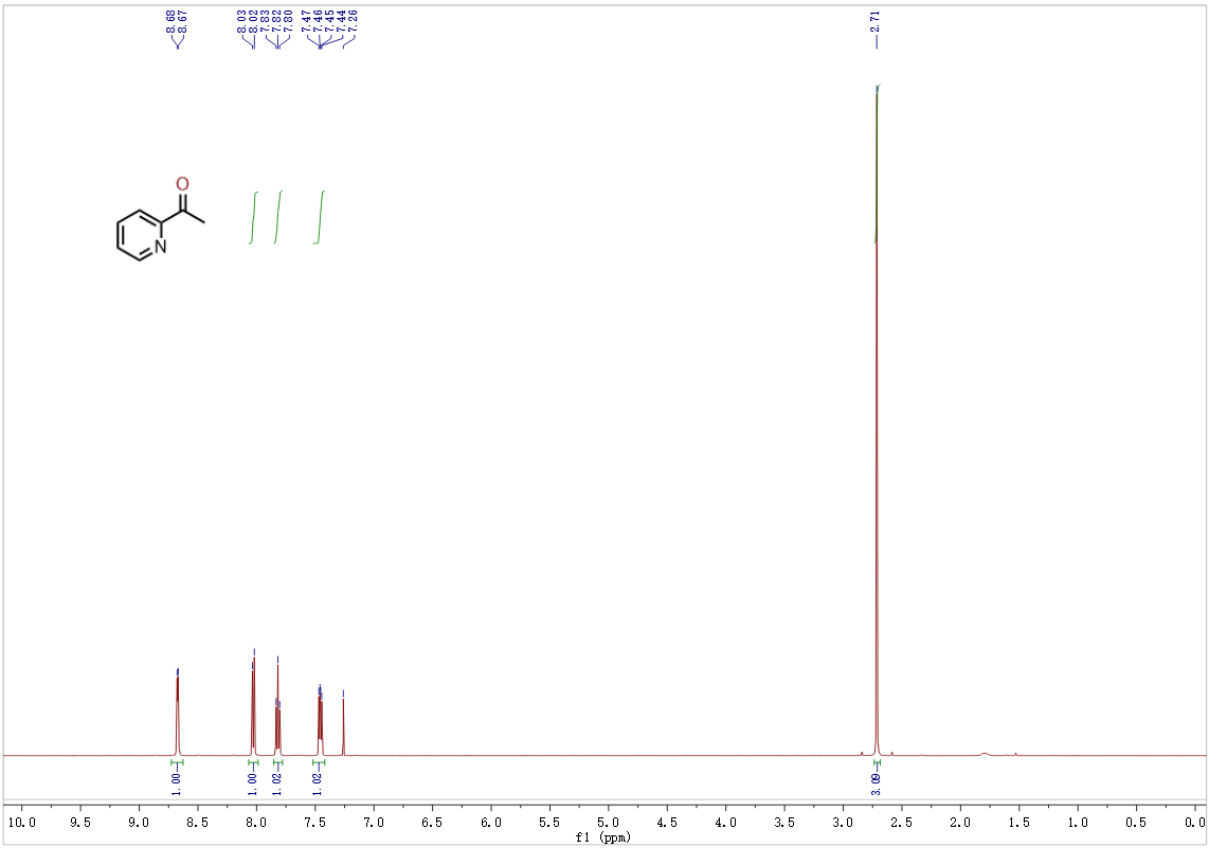
8.68
8.67
8.03
8.02
7.83
7.82
7.80
7.47
7.46
7.45
7.44
7.43
7.26
2.71
O
N
1.00
1.00
1.02
1.02
3.09
10.0
9.5
9.0
8.5
8.0
7.5
7.0
6.5
6.0
5.5
5.0
4.5
4.0
3.5
3.0
2.5
2.0
1.5
1.0
0.5
0.0
f1 (ppm)

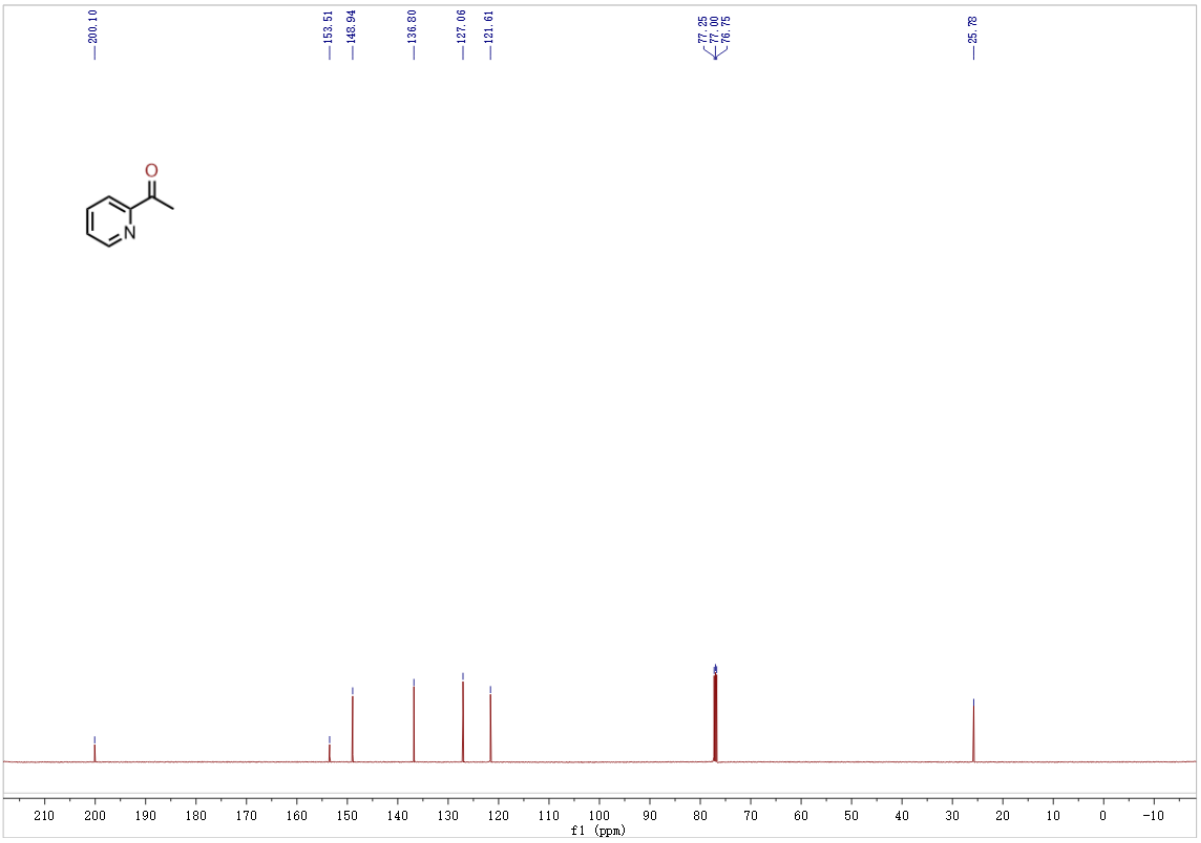
200.10
153.51
148.94
136.80
127.06
121.61
77.25
77.00
76.75
25.78
O
N
210
200
190
180
170
160
150
140
130
120
110
100
90
80
70
60
50
40
30
20
10
0
-10
f1 (ppm)

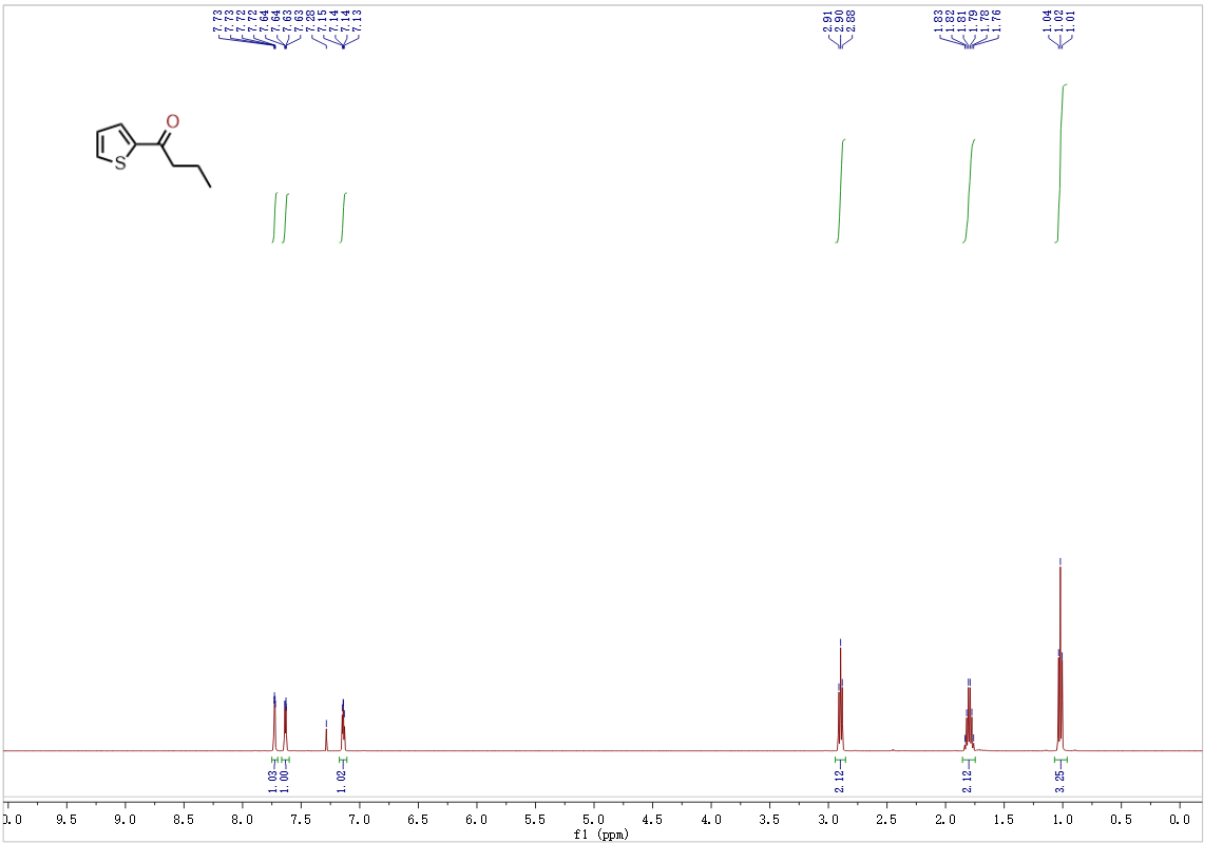
7.73
7.73
7.72
7.72
7.64
7.64
7.63
7.63
7.15
7.14
7.14
7.13
2.91
2.90
2.88
1.83
1.82
1.81
1.79
1.78
1.76
1.04
1.02
1.01
O
S
1.03
1.00
1.02
2.12
2.12
3.25
f1 (ppm)

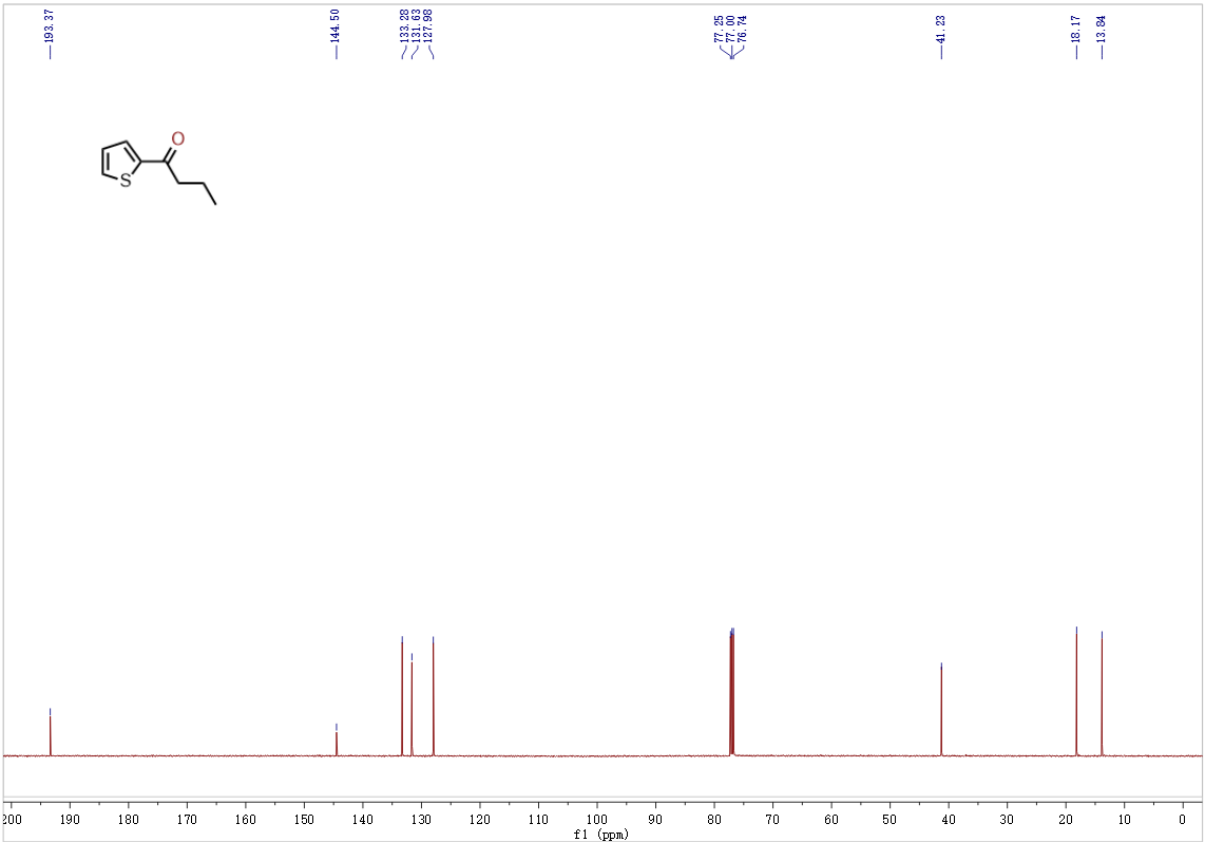
193.37
144.50
133.28
131.63
127.98
77.25
77.00
76.74
41.23
18.17
13.84
O
S
f1 (ppm)

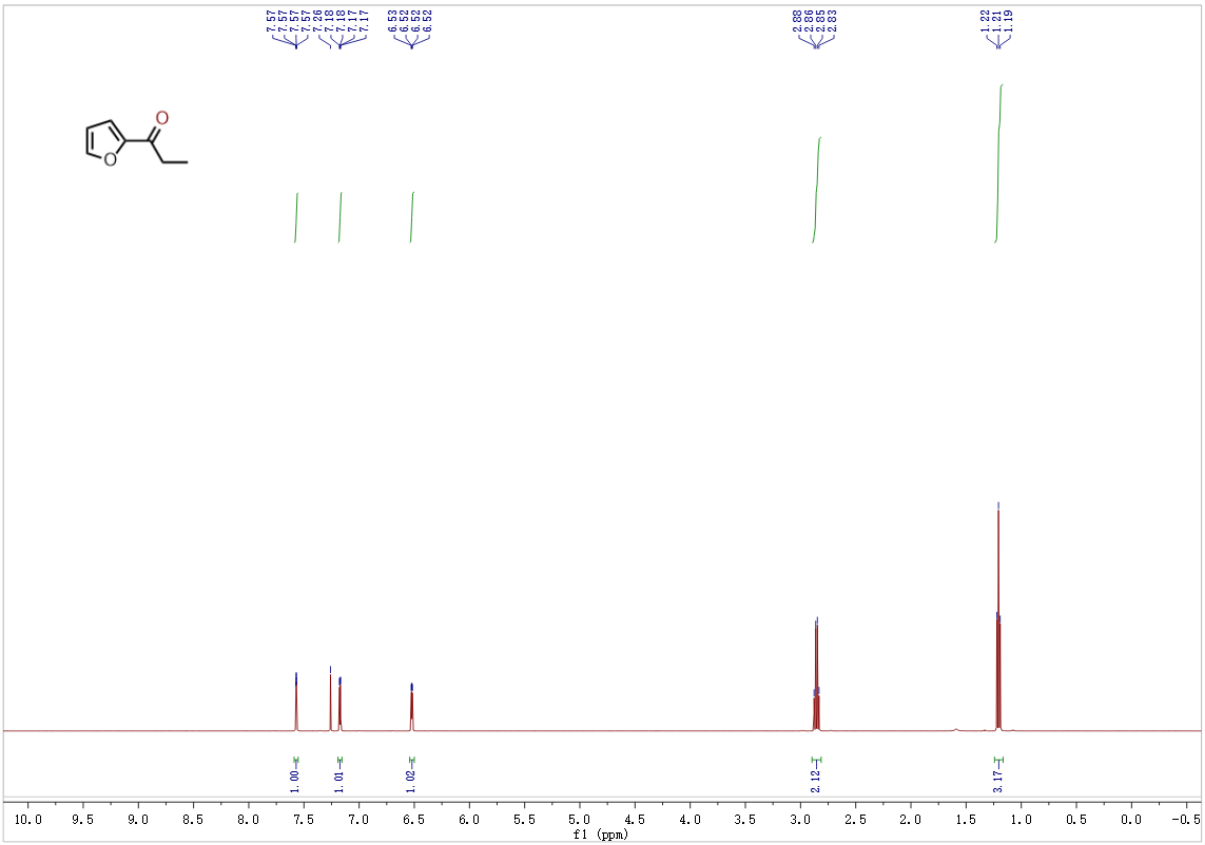
7.57
7.57
7.57
7.57
7.26
7.18
7.18
7.17
7.17
6.53
6.52
6.52
6.52
6.52
2.88
2.86
2.85
2.83
1.22
1.21
1.19
1.00
1.01
1.02
2.12
3.17
10.0 9.5 9.0 8.5 8.0 7.5 7.0 6.5 6.0 5.5 5.0 4.5 4.0 3.5 3.0 2.5 2.0 1.5 1.0 0.5 0.0 -0.5
f1 (ppm)

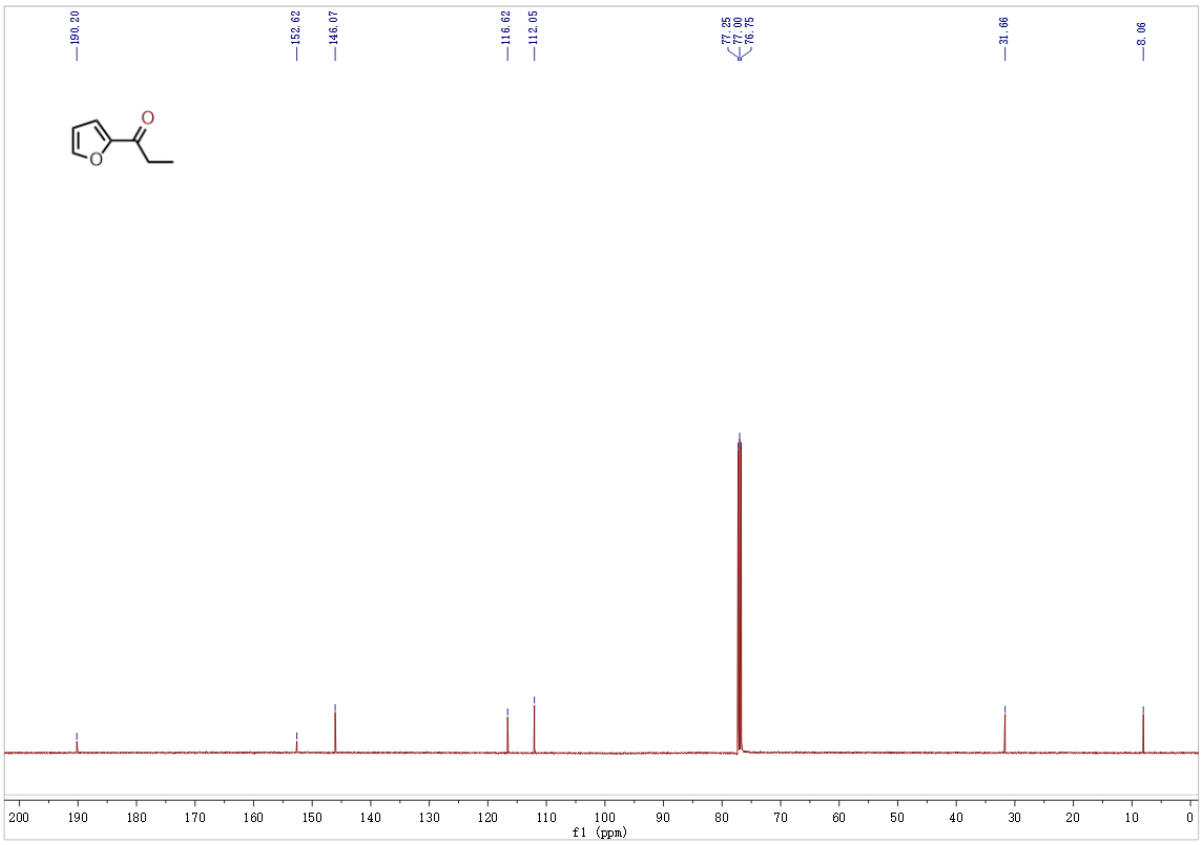
190.20
152.62
146.07
116.62
112.05
77.25
77.00
76.75
31.66
8.06
200 190 180 170 160 150 140 130 120 110 100 90 80 70 60 50 40 30 20 10 0
f1 (ppm)

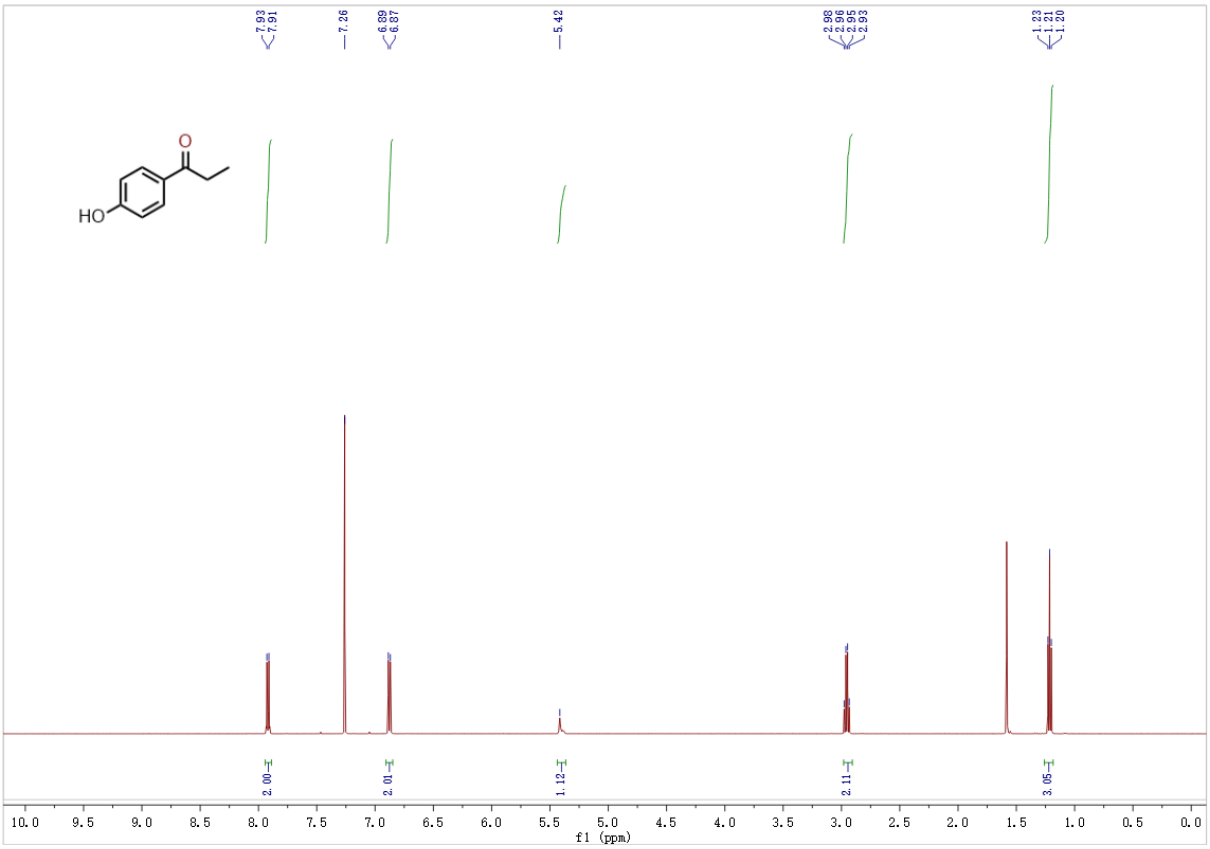
7.93
7.91
7.26
6.89
6.87
5.42
2.98
2.96
2.95
2.93
1.23
1.21
1.20
O
HO
2.00
2.01
1.12
2.11
3.05
10.0 9.5 9.0 8.5 8.0 7.5 7.0 6.5 6.0 5.5 5.0 4.5 4.0 3.5 3.0 2.5 2.0 1.5 1.0 0.5 0.0
f1 (ppm)

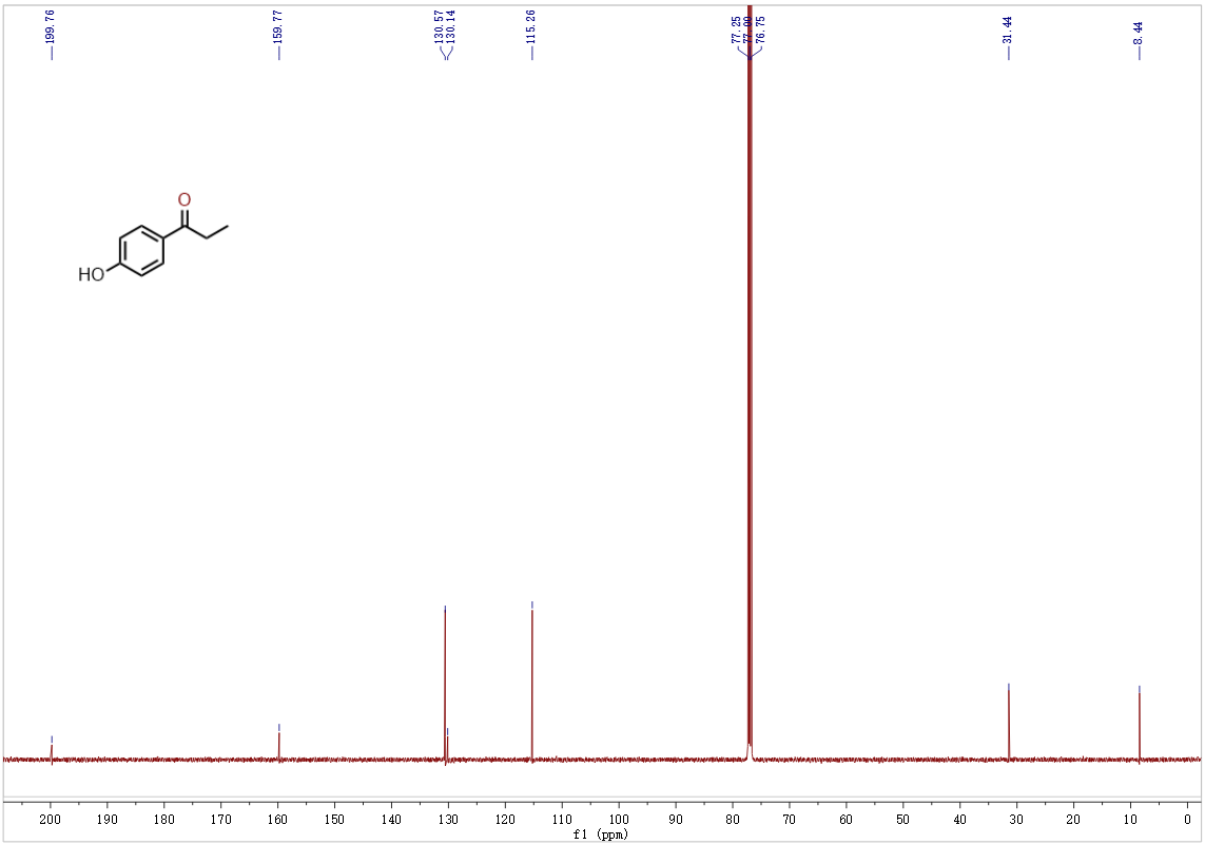
199.76
159.77
130.57
130.14
115.26
77.25
77.00
76.75
31.44
8.44
O
HO
200 190 180 170 160 150 140 130 120 110 100 90 80 70 60 50 40 30 20 10 0
f1 (ppm)

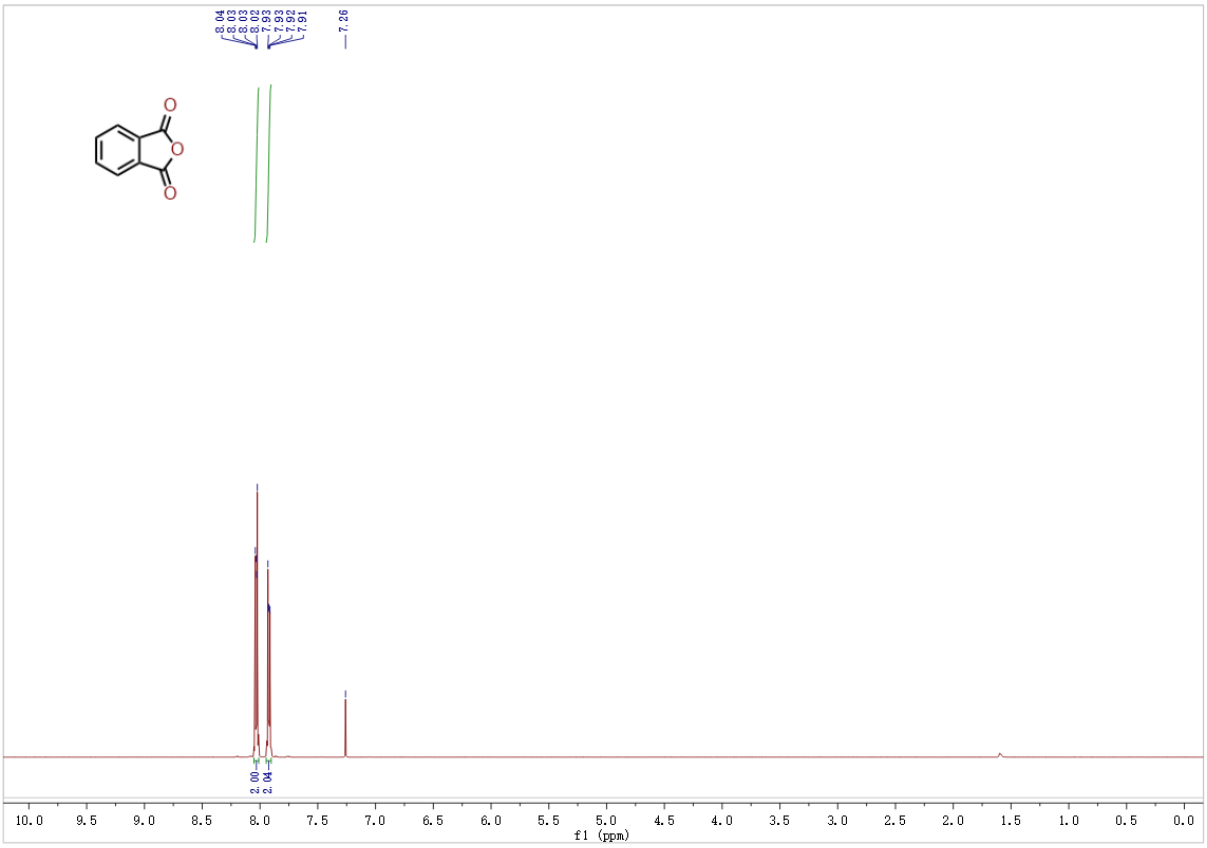
8.04
8.03
8.03
8.02
7.93
7.93
7.92
7.91
7.26
O
O
O
2.00
2.04
10.0
9.5
9.0
8.5
8.0
7.5
7.0
6.5
6.0
5.5
5.0
4.5
4.0
3.5
3.0
2.5
2.0
1.5
1.0
0.5
0.0
f1 (ppm)

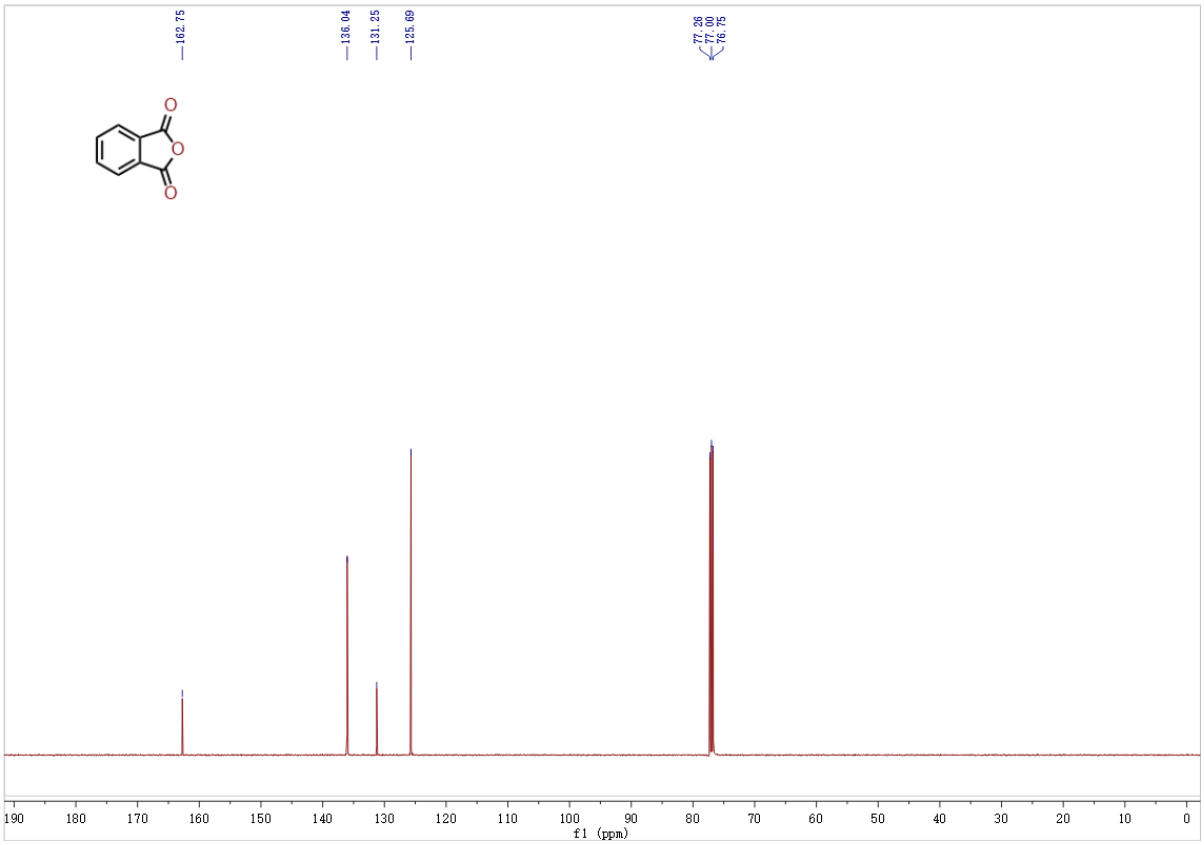
162.75
136.04
131.25
125.69
77.26
77.00
76.75
O
O
O
190
180
170
160
150
140
130
120
110
100
90
80
70
60
50
40
30
20
10
0
f1 (ppm)

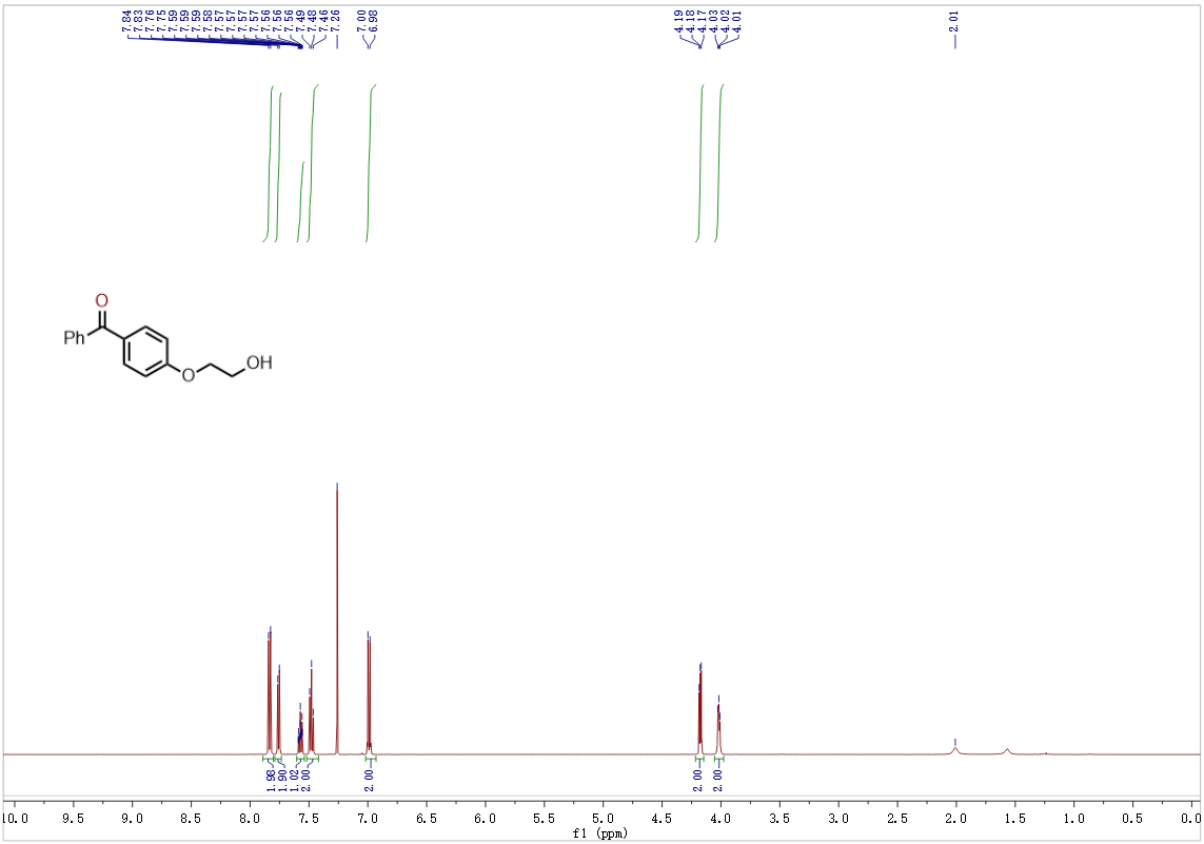
7.84
7.83
7.76
7.75
7.59
7.59
7.59
7.58
7.57
7.57
7.57
7.57
7.56
7.56
7.56
7.49
7.48
7.46
7.26
7.00
6.98
4.19
4.18
4.17
4.03
4.02
4.01
2.01
O
Ph
O
OH
1.90
1.96
1.02
2.00
2.00
2.00
2.00
f1 (ppm)

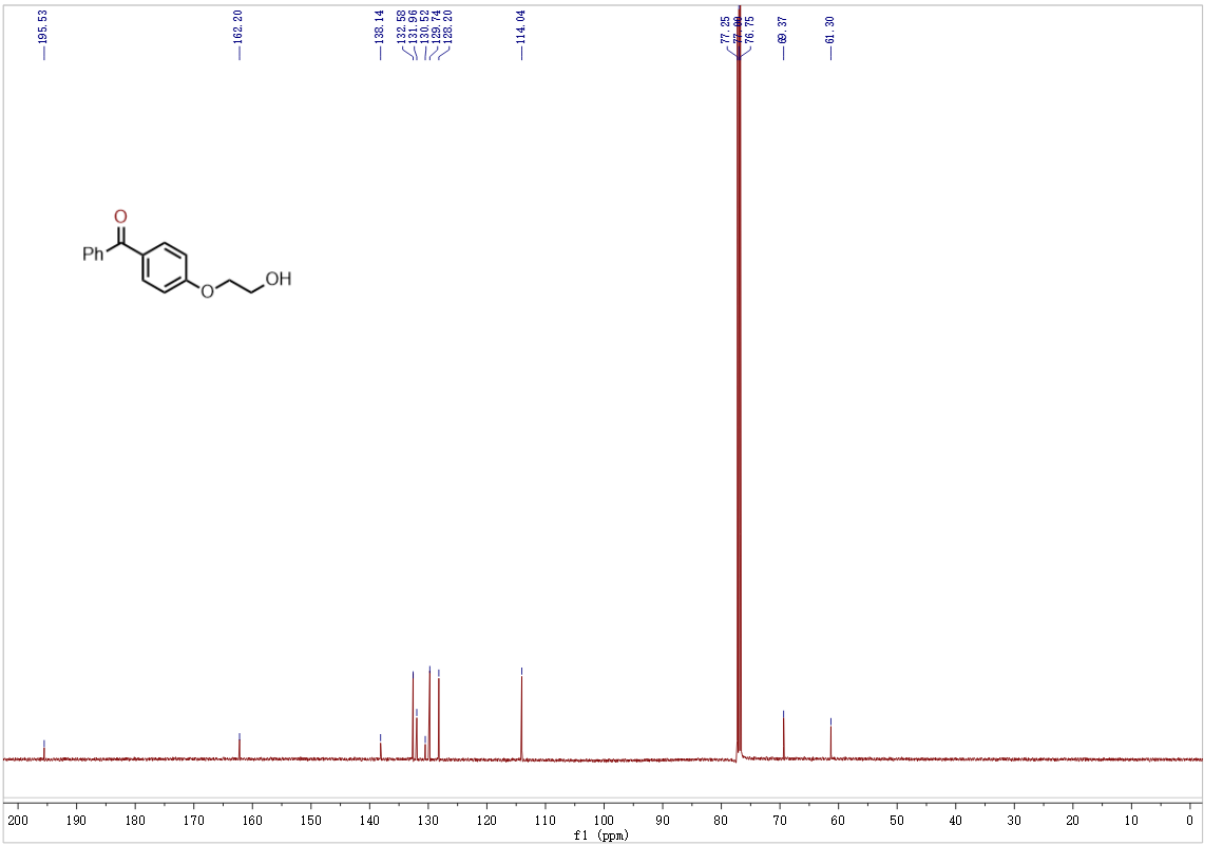
195.53
162.20
138.14
132.58
131.96
130.52
129.74
128.20
114.04
77.25
77.00
76.75
69.37
61.30
O
Ph
O
OH
f1 (ppm)

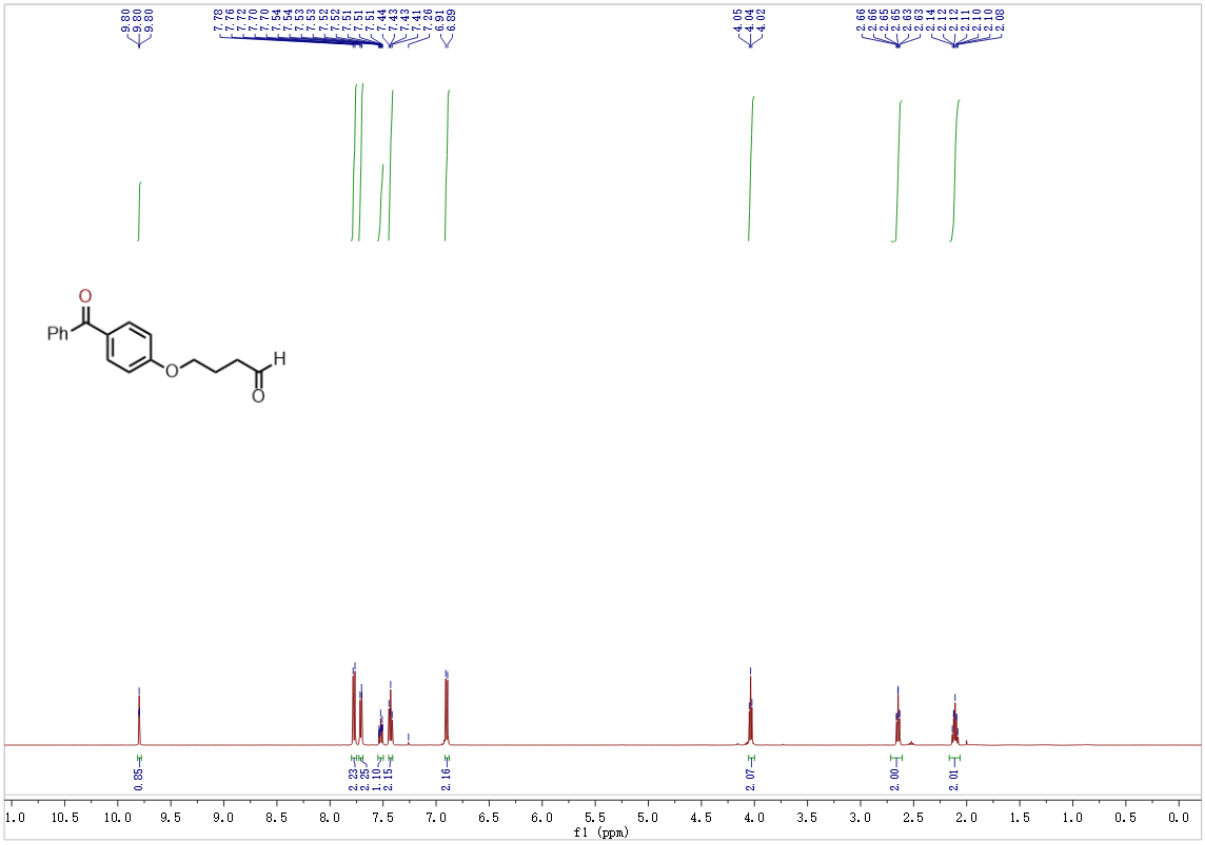
9.80
9.80
9.80
7.78
7.76
7.72
7.70
7.70
7.54
7.54
7.53
7.53
7.52
7.52
7.51
7.51
7.51
7.51
7.44
7.43
7.43
7.41
7.26
6.91
6.89
4.05
4.04
4.02
2.66
2.66
2.65
2.65
2.63
2.63
2.14
2.13
2.12
2.11
2.10
2.10
2.08
O
Ph
O
O
H
0.85
2.22
2.25
1.10
2.15
2.16
2.07
2.00
2.01
1.0 10.5 10.0 9.5 9.0 8.5 8.0 7.5 7.0 6.5 6.0 5.5 5.0 4.5 4.0 3.5 3.0 2.5 2.0 1.5 1.0 0.5 0.0
f1 (ppm)

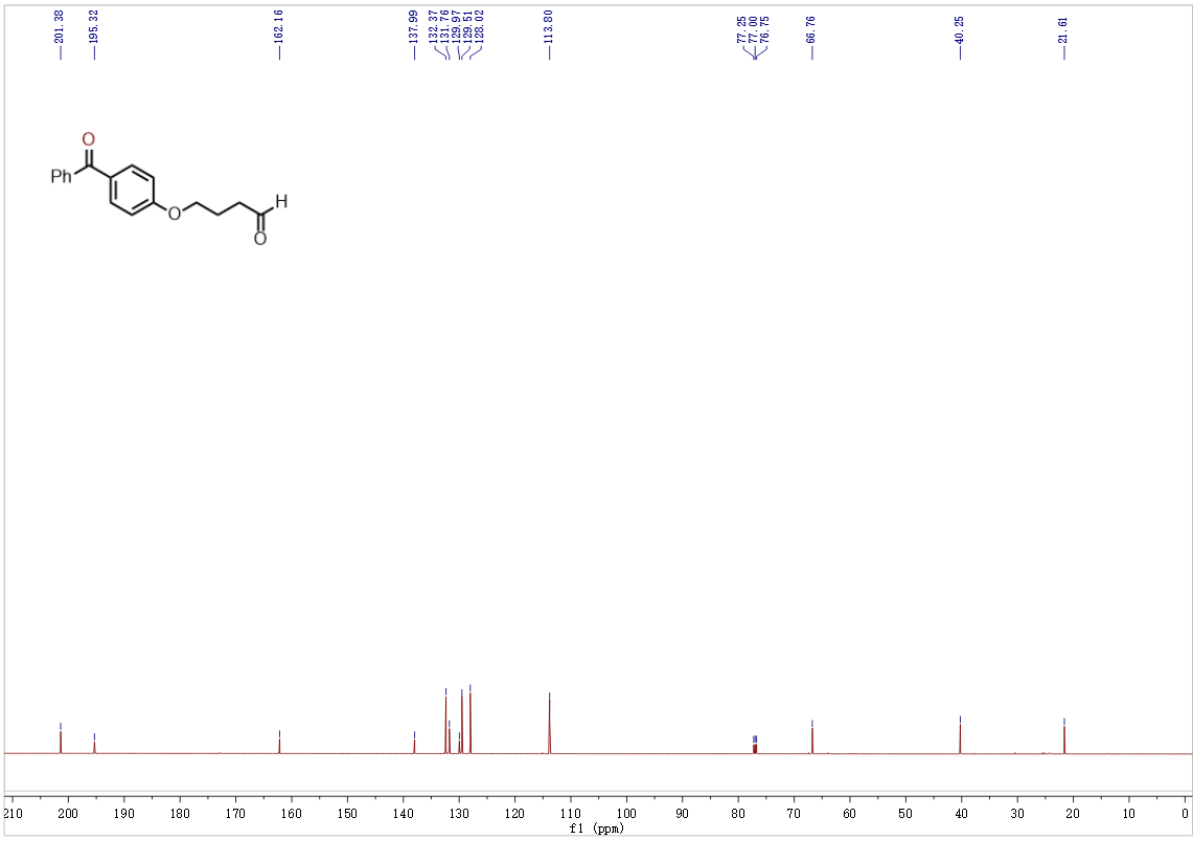
201.38
195.32
162.16
137.99
132.37
131.76
129.97
129.51
128.02
113.80
77.25
77.00
76.75
66.76
40.25
21.61
O
Ph
O
O
H
210 200 190 180 170 160 150 140 130 120 110 100 90 80 70 60 50 40 30 20 10 0
f1 (ppm)

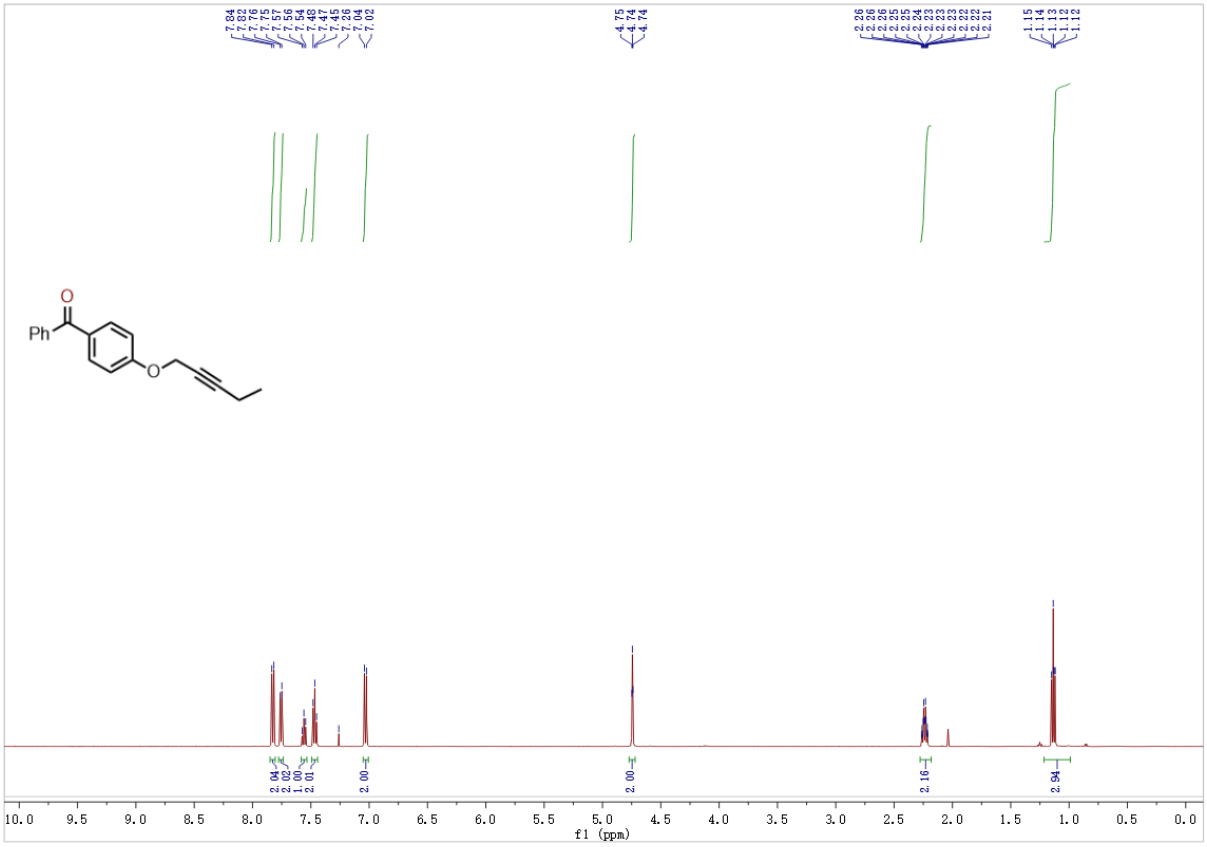
7.84
7.82
7.76
7.75
7.57
7.56
7.54
7.49
7.47
7.45
7.26
7.04
7.02
4.75
4.74
4.74
2.26
2.26
2.26
2.25
2.25
2.24
2.23
2.23
2.23
2.22
2.22
2.21
1.15
1.14
1.13
1.12
1.12
O
Ph
O
2.04
2.03
2.00
2.01
2.00
2.00
2.16
2.94
10.0
9.5
9.0
8.5
8.0
7.5
7.0
6.5
6.0
5.5
5.0
4.5
4.0
3.5
3.0
2.5
2.0
1.5
1.0
0.5
0.0
f1 (ppm)

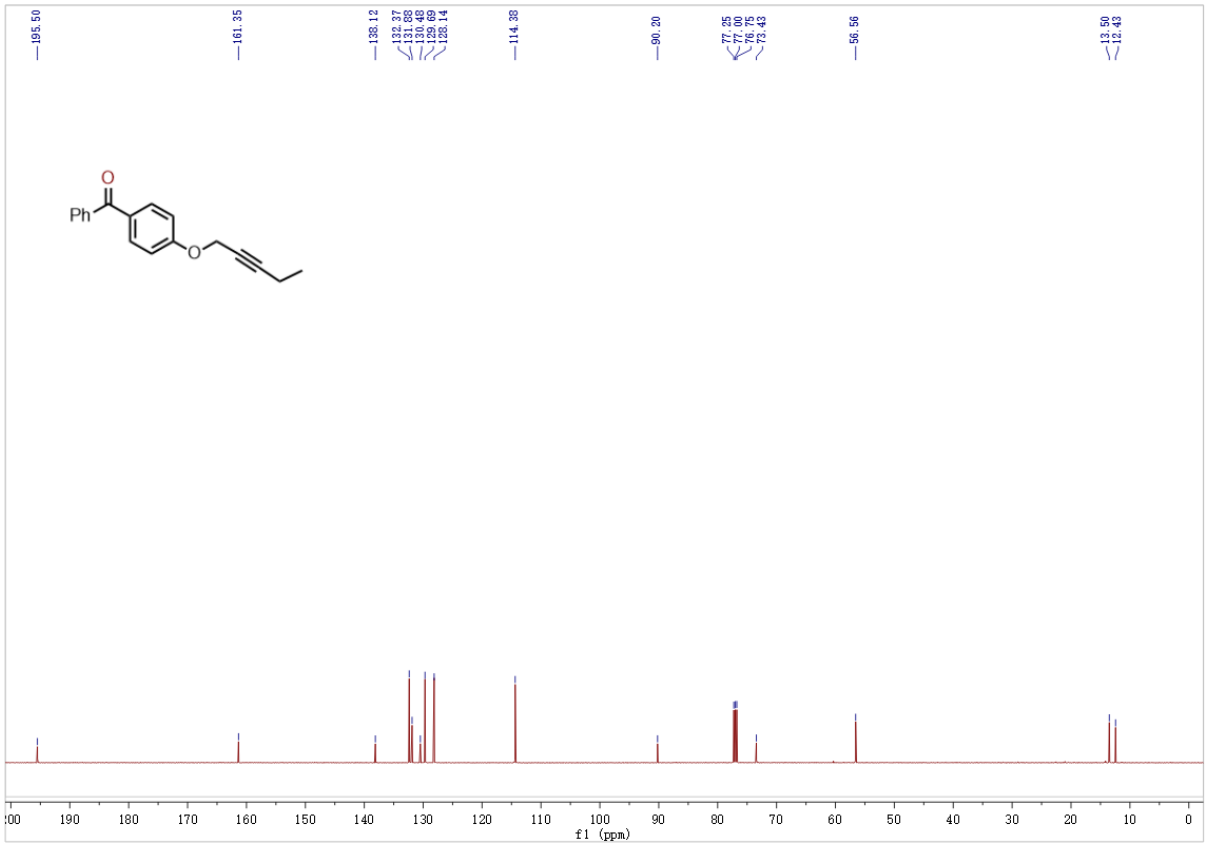
195.50
161.35
138.12
132.37
131.88
130.48
129.69
128.14
114.38
90.20
77.25
77.00
76.75
73.43
56.56
13.50
12.43
O
Ph
O
200
190
180
170
160
150
140
130
120
110
100
90
80
70
60
50
40
30
20
10
0
f1 (ppm)

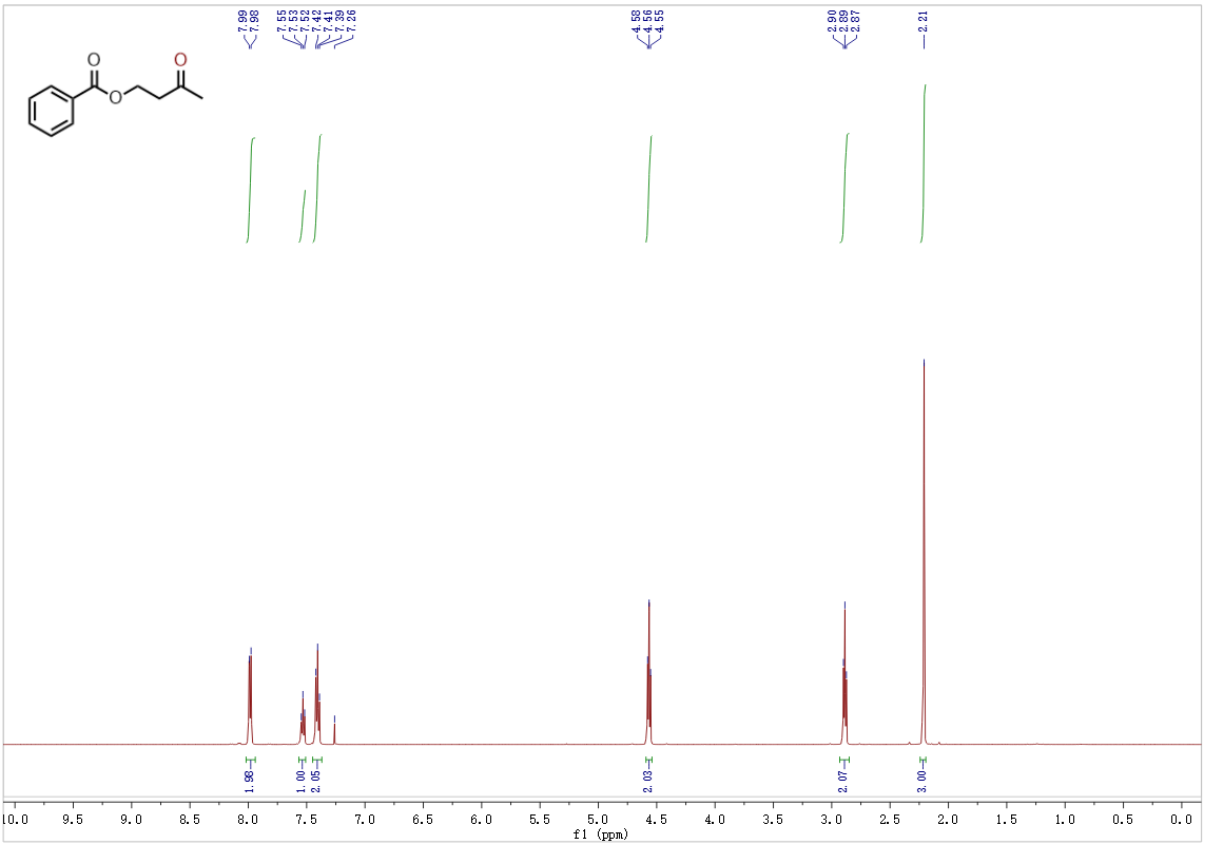
7.99
7.98
7.55
7.53
7.52
7.42
7.41
7.39
7.26
4.58
4.56
4.55
2.90
2.89
2.87
2.21
1.98
1.00
2.05
2.03
2.07
3.00
f1 (ppm)

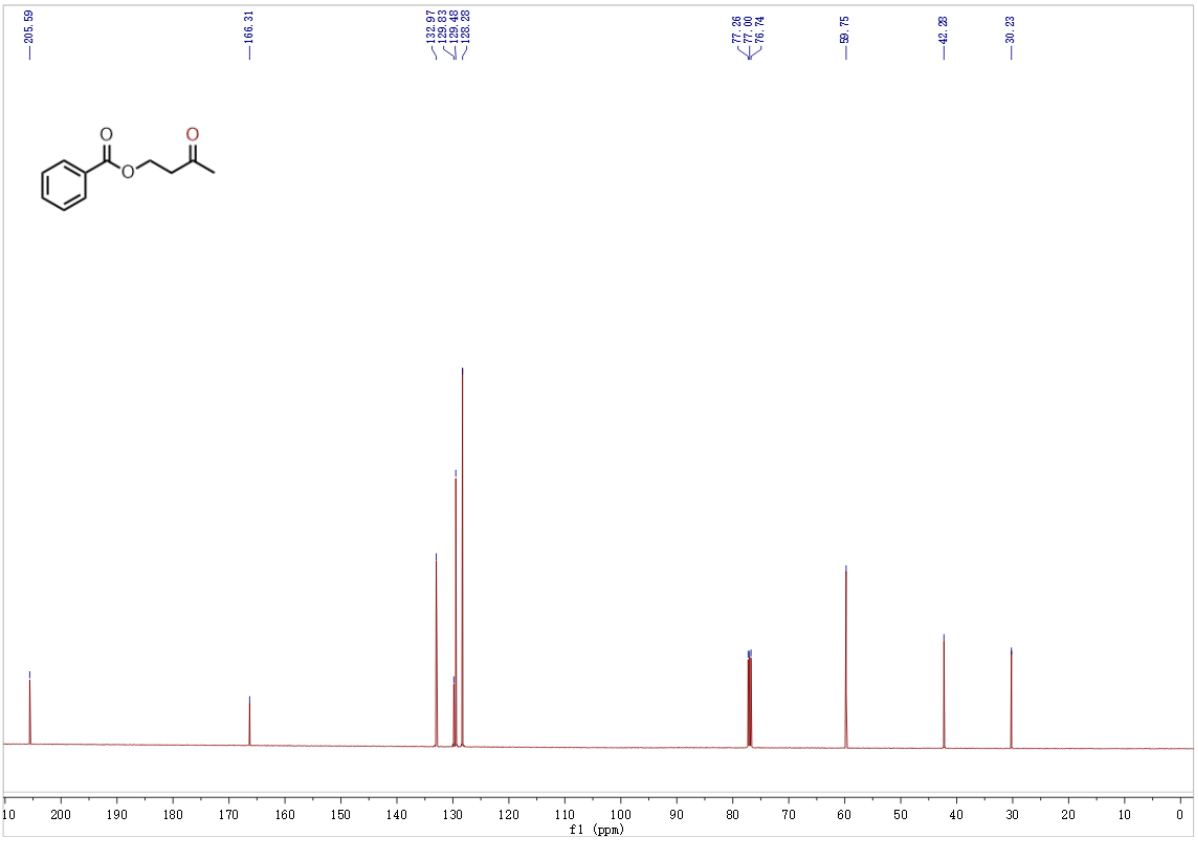
205.59
166.31
132.97
129.83
129.48
128.28
77.26
77.00
76.74
59.75
42.28
30.23
f1 (ppm)

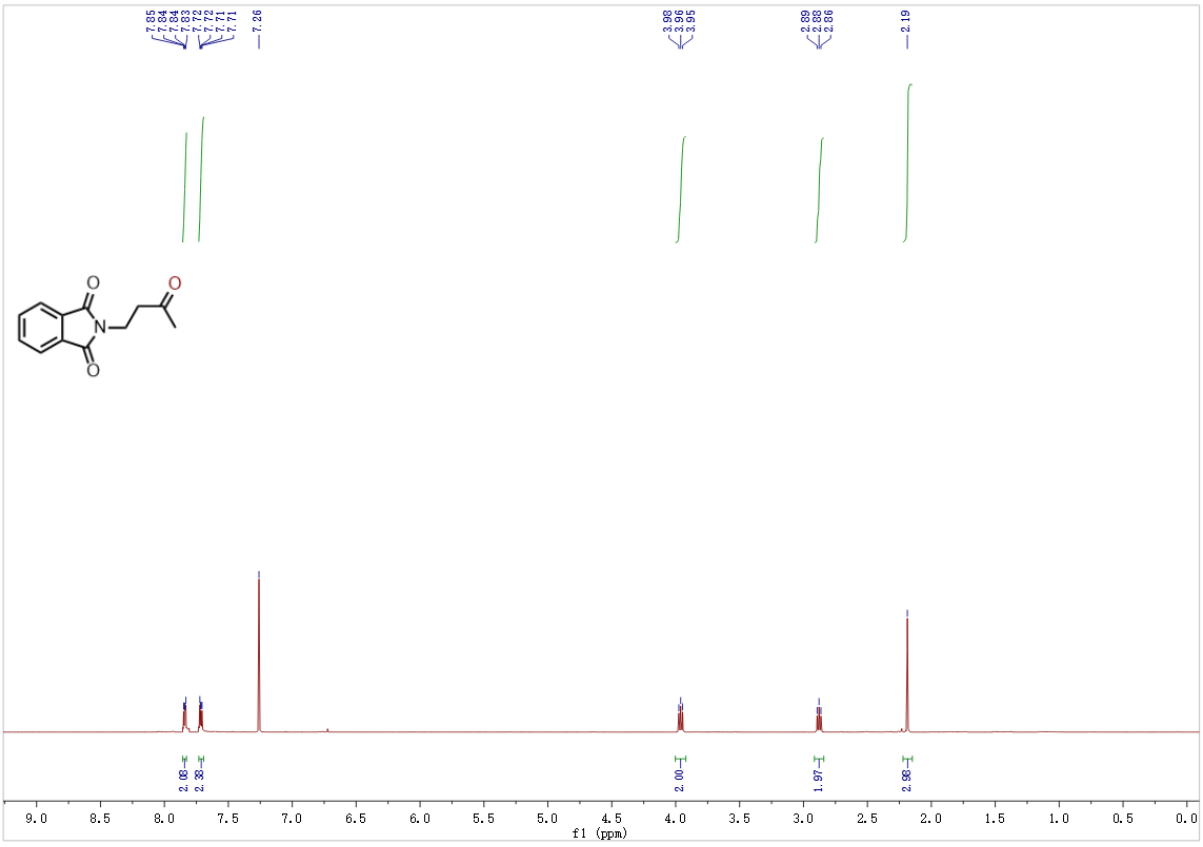
7.85
7.84
7.84
7.83
7.73
7.72
7.71
7.71
7.26
3.98
3.96
3.95
2.89
2.88
2.86
2.19
2.09
2.33
2.00
1.97
2.98
9.0
8.5
8.0
7.5
7.0
6.5
6.0
5.5
5.0
4.5
4.0
3.5
3.0
2.5
2.0
1.5
1.0
0.5
0.0
f1 (ppm)

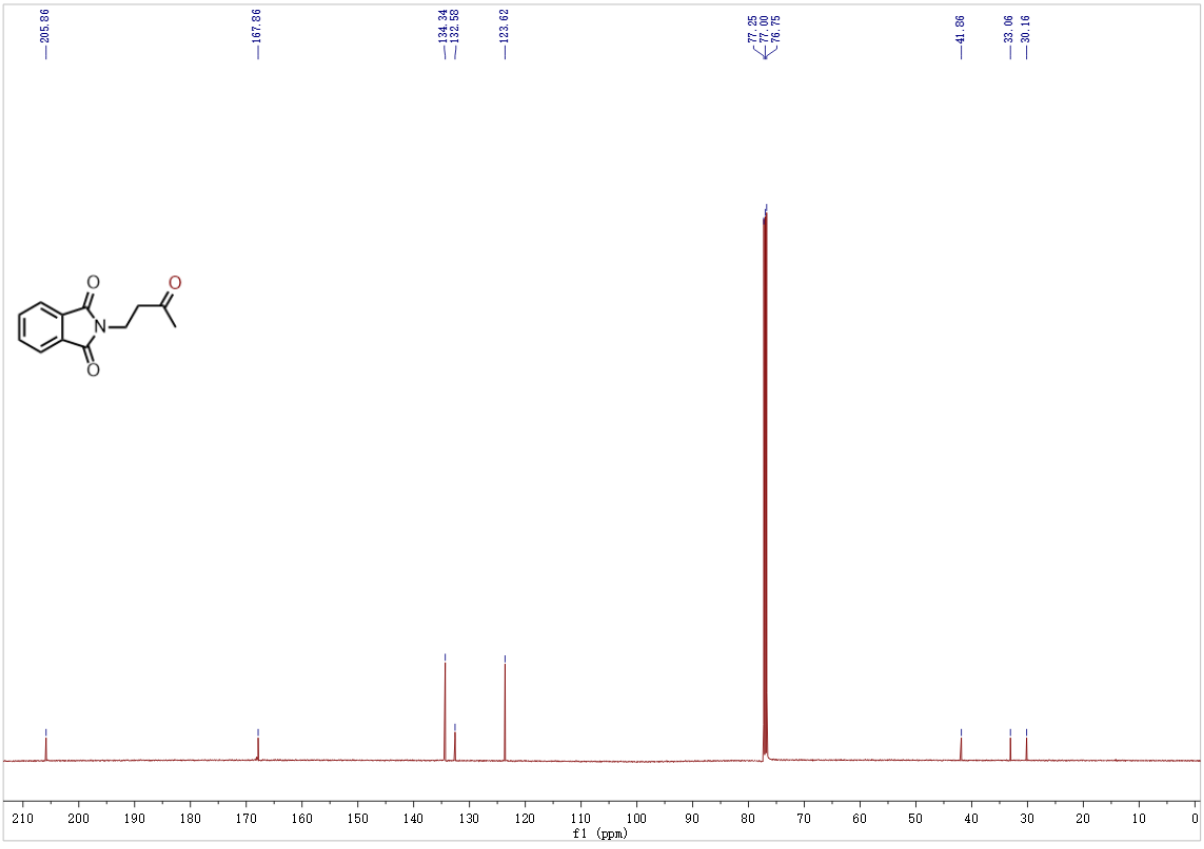
205.86
167.86
134.34
132.58
123.62
77.25
77.00
76.75
41.86
33.06
30.16
210
200
190
180
170
160
150
140
130
120
110
100
90
80
70
60
50
40
30
20
10
0
f1 (ppm)

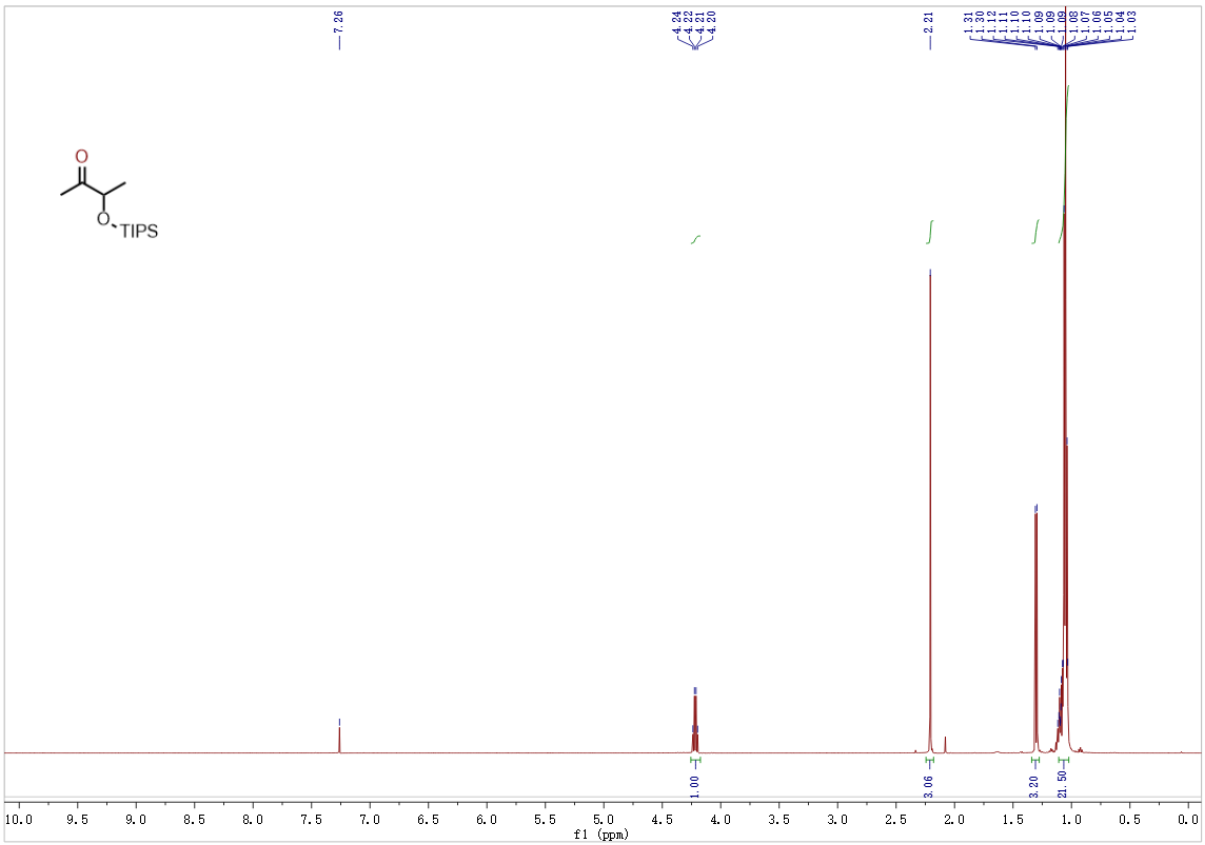
7.26
4.24
4.22
4.21
4.20
2.21
1.31
1.30
1.12
1.11
1.10
1.10
1.09
1.09
1.08
1.07
1.06
1.05
1.04
1.03
O
O
TIPS
1.00
3.06
3.20
21.50
f1 (ppm)

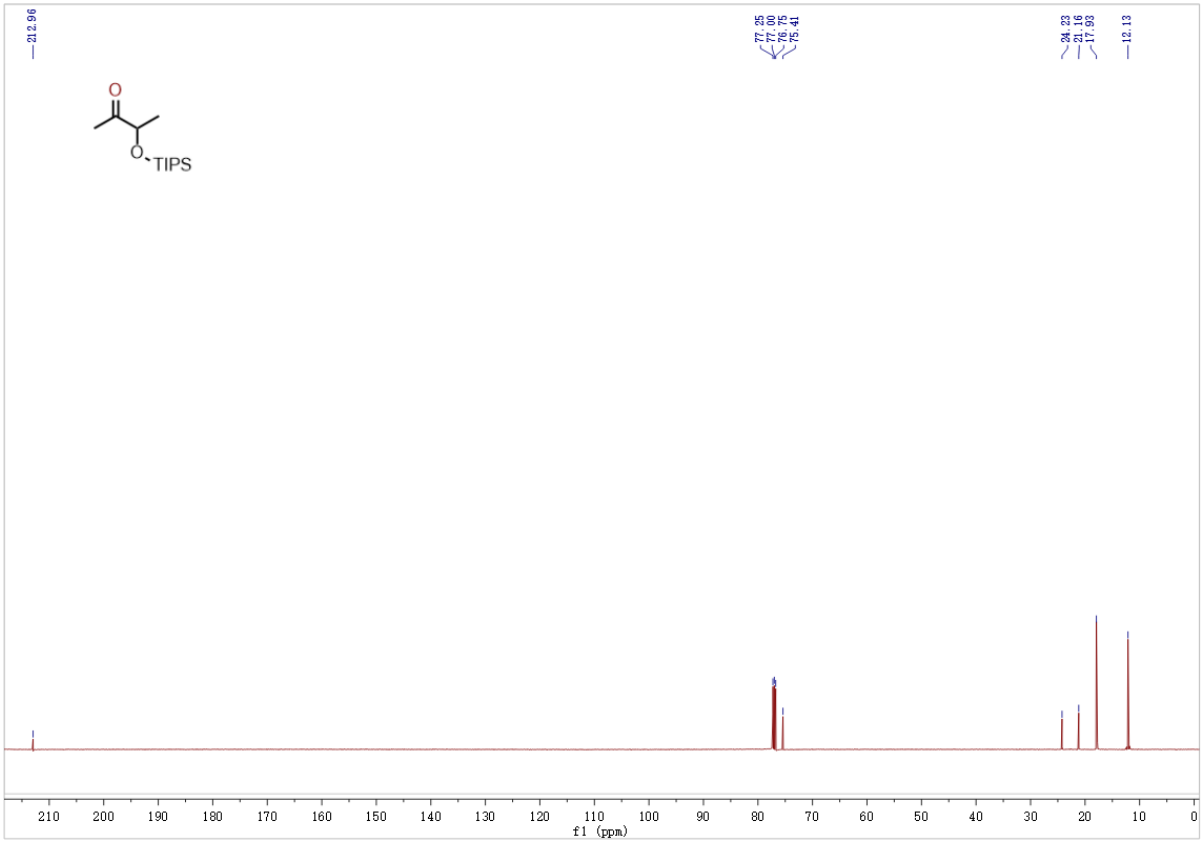
212.96
77.25
77.00
76.75
75.41
24.23
21.16
17.93
12.13
O
O
TIPS
f1 (ppm)

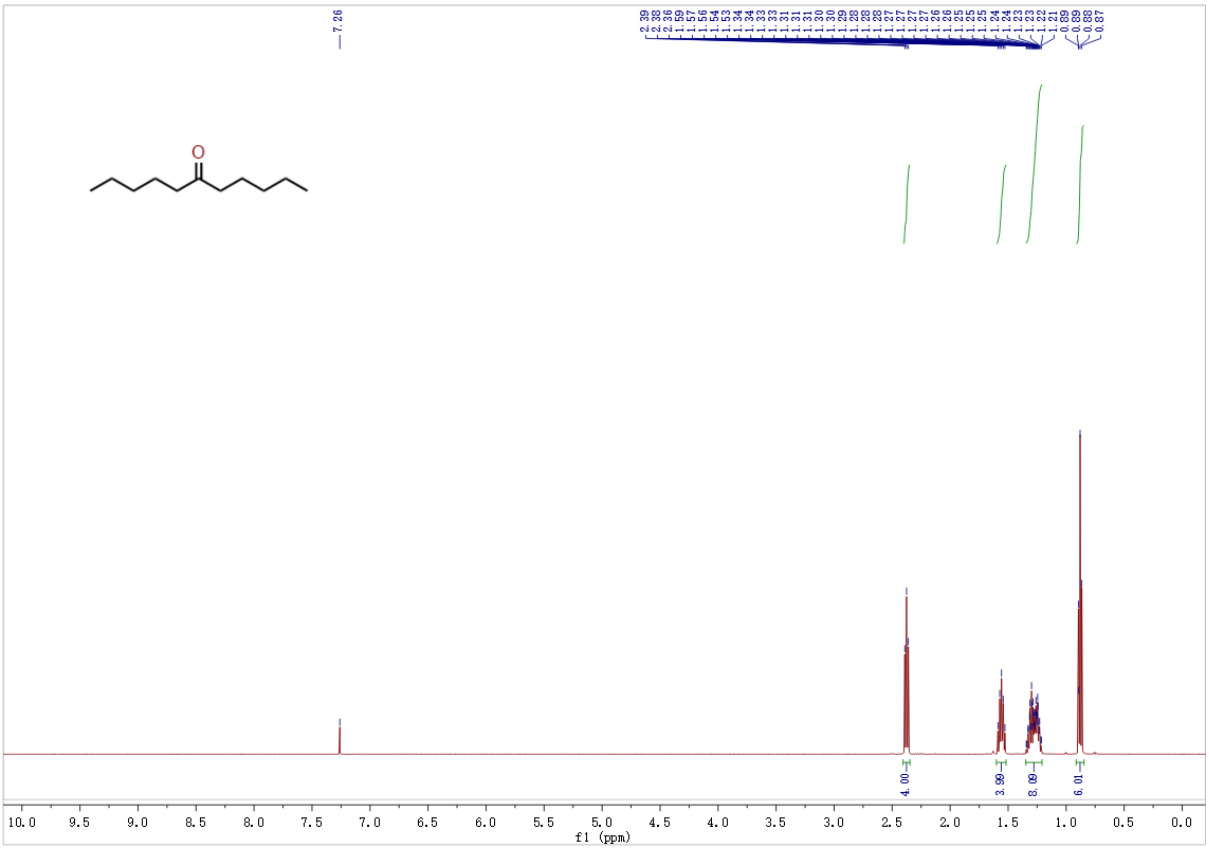
7.26
4.00
3.99
8.09
6.01
f1 (ppm)

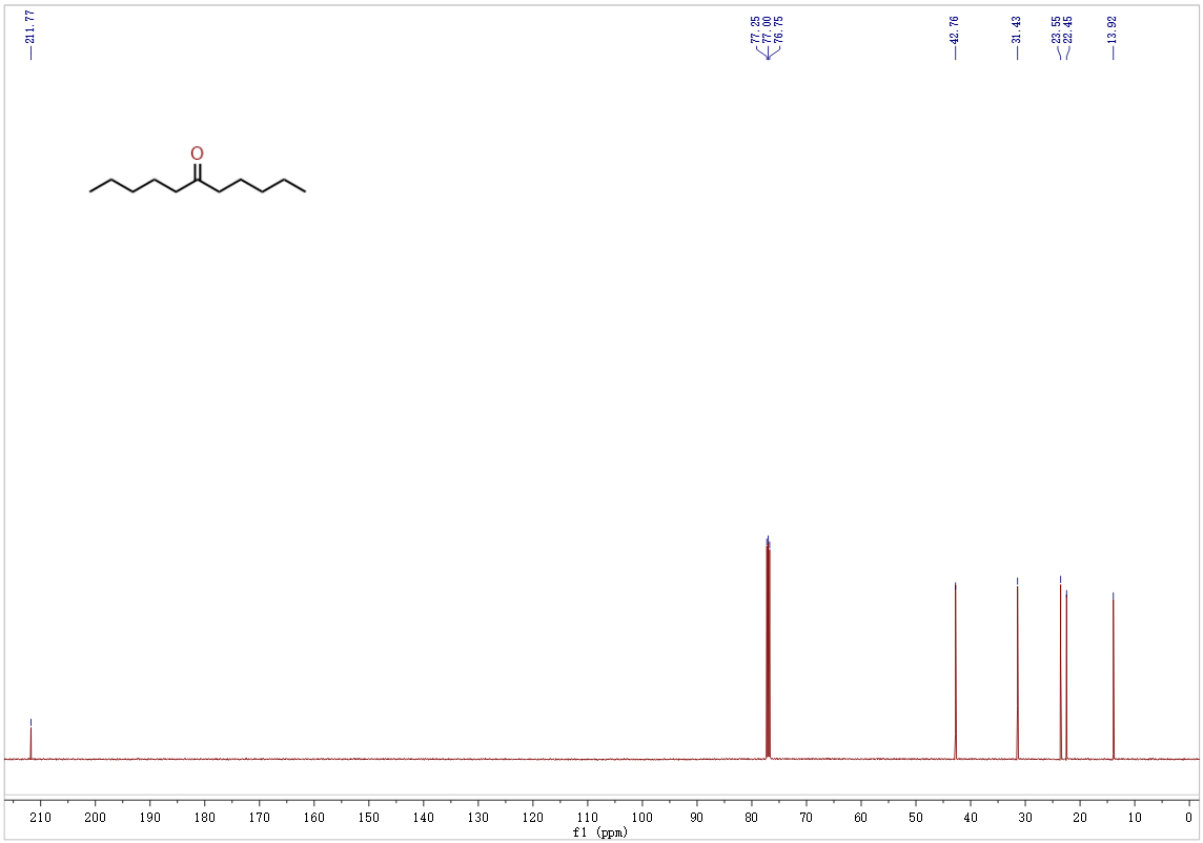
211.77
77.25
77.00
76.75
42.76
31.43
23.55
22.45
13.92
f1 (ppm)

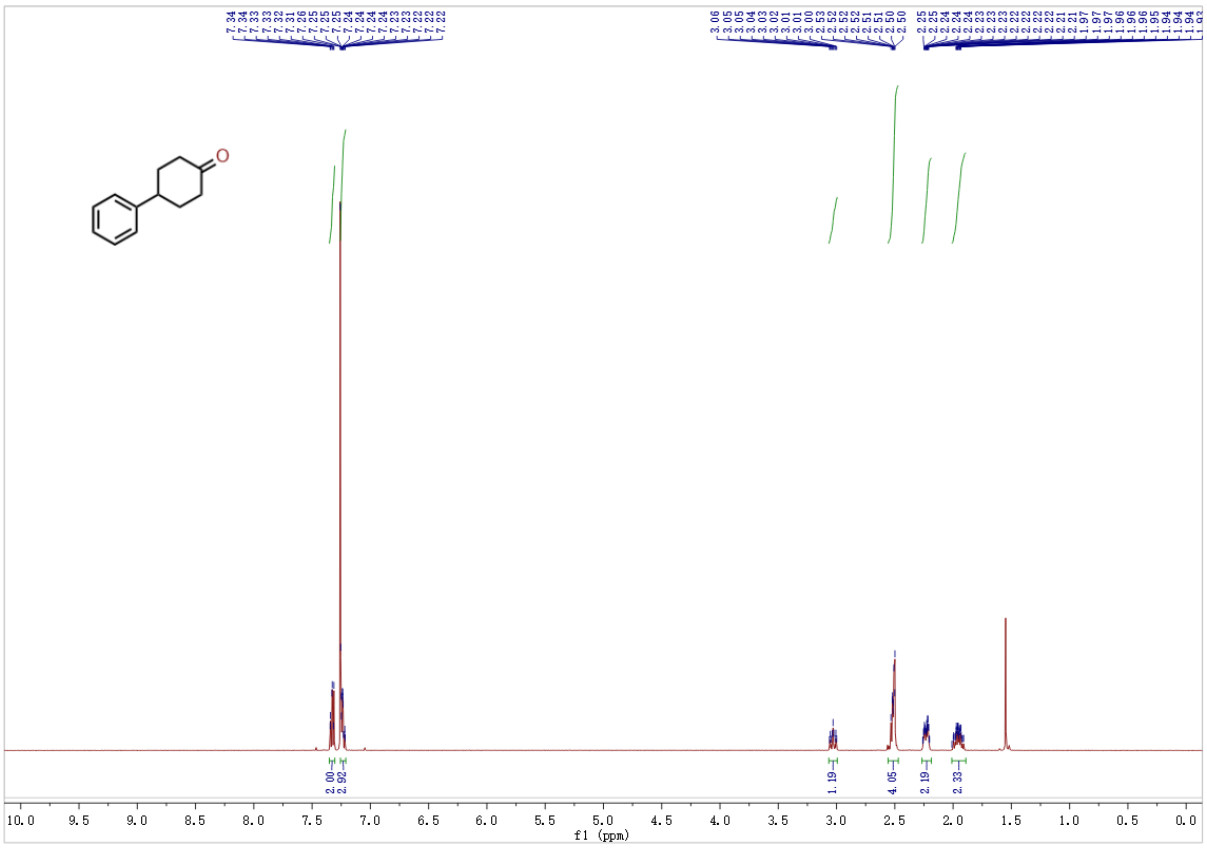
O
f1 (ppm)

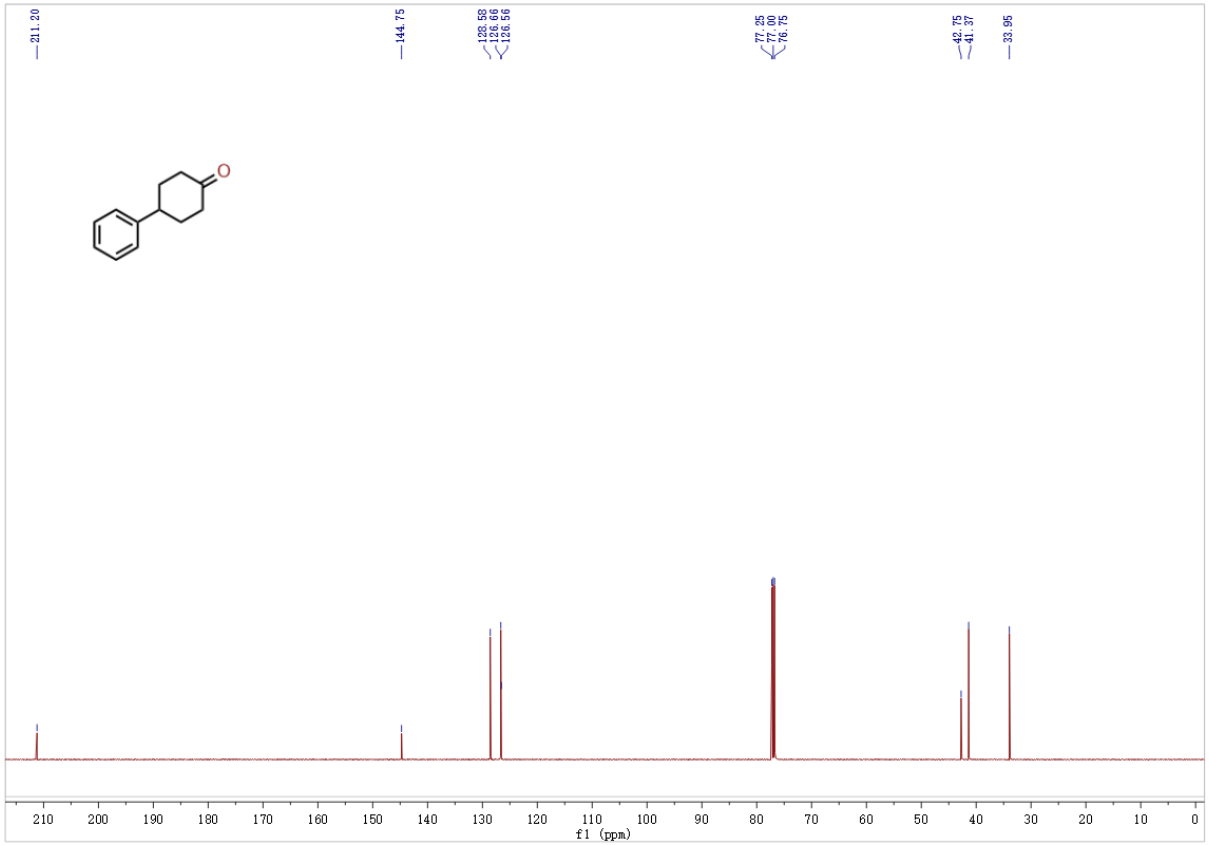
211.20
144.75
128.58
126.66
126.56
77.25
77.00
76.75
42.75
41.37
33.96
O
f1 (ppm)

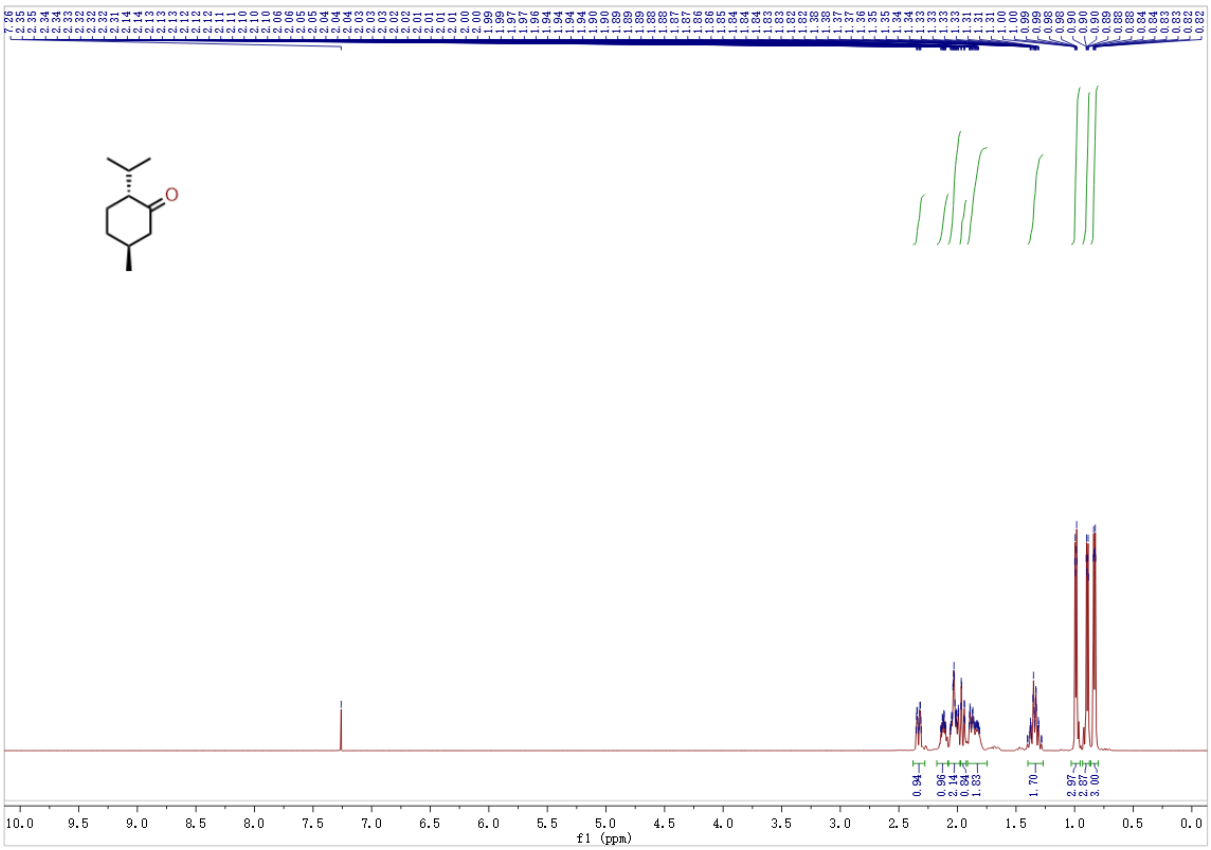
O
0.94
0.96
2.14
0.84
1.83
1.70
2.97
2.87
3.00
10.0 9.5 9.0 8.5 8.0 7.5 7.0 6.5 6.0 5.5 5.0 4.5 4.0 3.5 3.0 2.5 2.0 1.5 1.0 0.5 0.0
f1 (ppm)

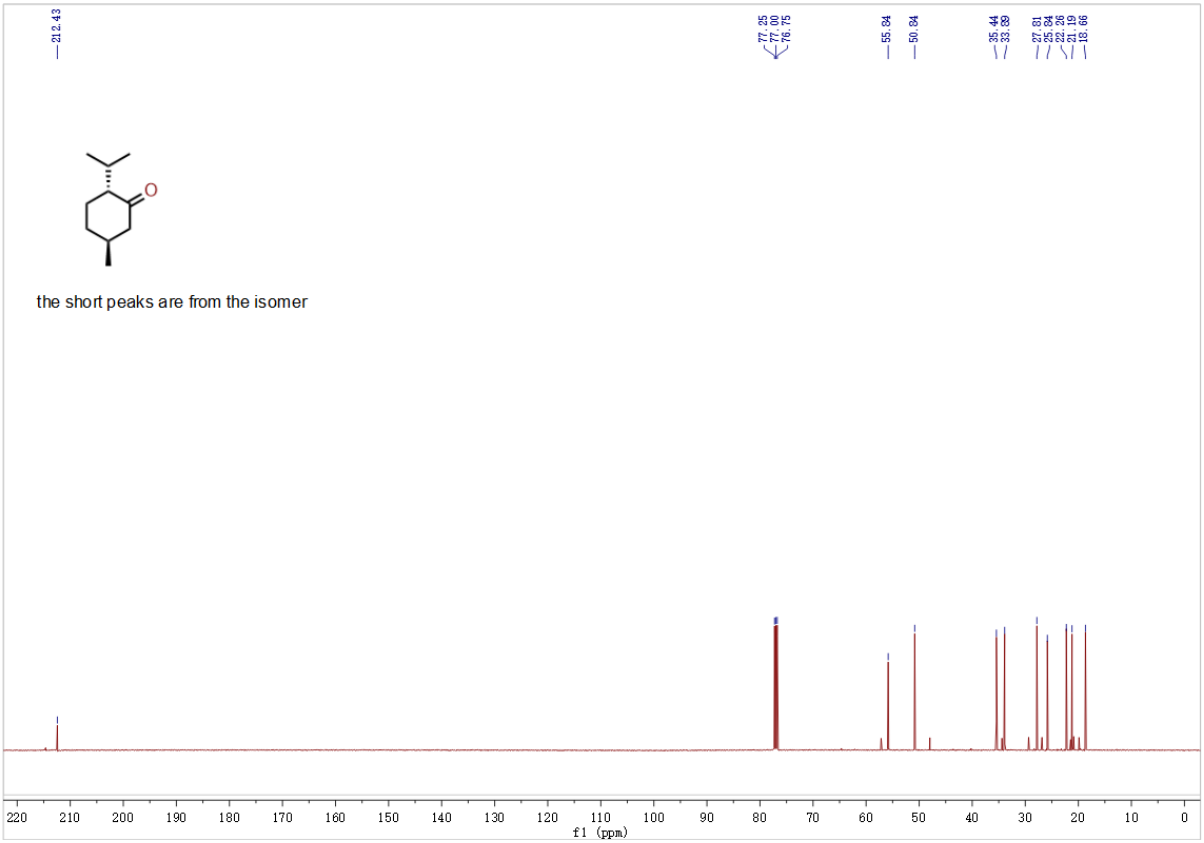
212.43
77.25
77.00
76.75
55.84
50.84
35.44
33.89
27.81
25.84
22.26
21.19
18.66
O
the short peaks are from the isomer
220 210 200 190 180 170 160 150 140 130 120 110 100 90 80 70 60 50 40 30 20 10 0
f1 (ppm)

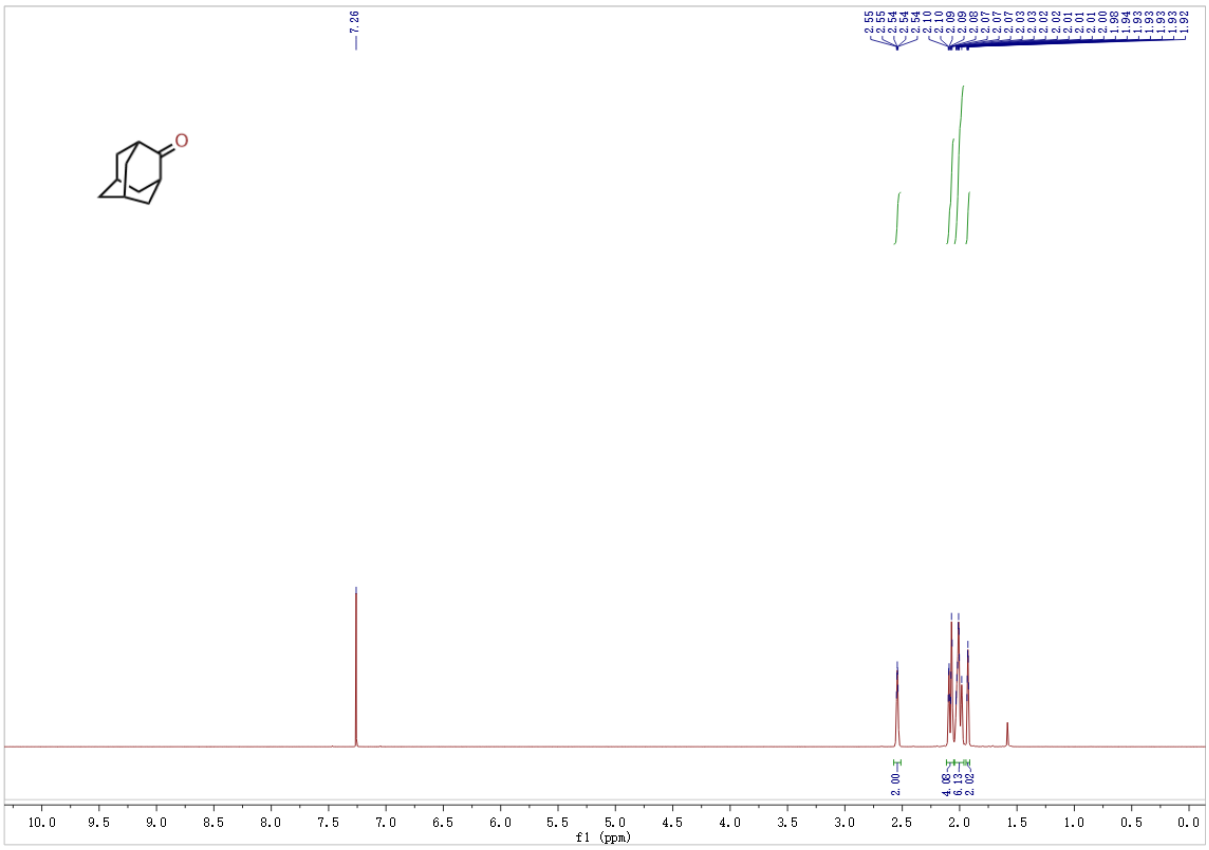
7.26
2.55
2.54
2.10
2.09
2.08
2.07
2.03
2.02
2.01
2.00
1.98
1.94
1.93
1.92
O
2.00
4.08
6.13
2.02
10.0
9.5
9.0
8.5
8.0
7.5
7.0
6.5
6.0
5.5
5.0
4.5
4.0
3.5
3.0
2.5
2.0
1.5
1.0
0.5
0.0
f1 (ppm)

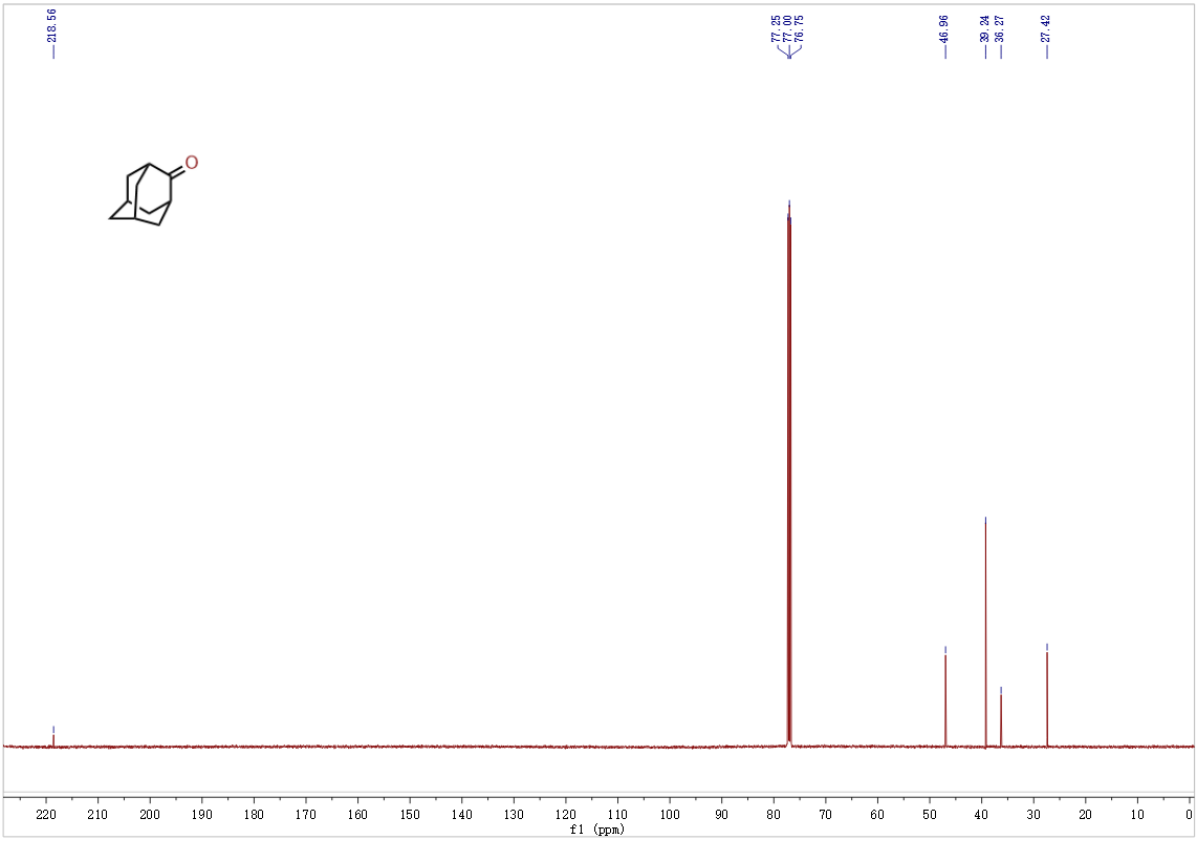
218.56
77.25
77.00
76.75
46.96
39.24
36.27
27.42
O
220
210
200
190
180
170
160
150
140
130
120
110
100
90
80
70
60
50
40
30
20
10
0
f1 (ppm)

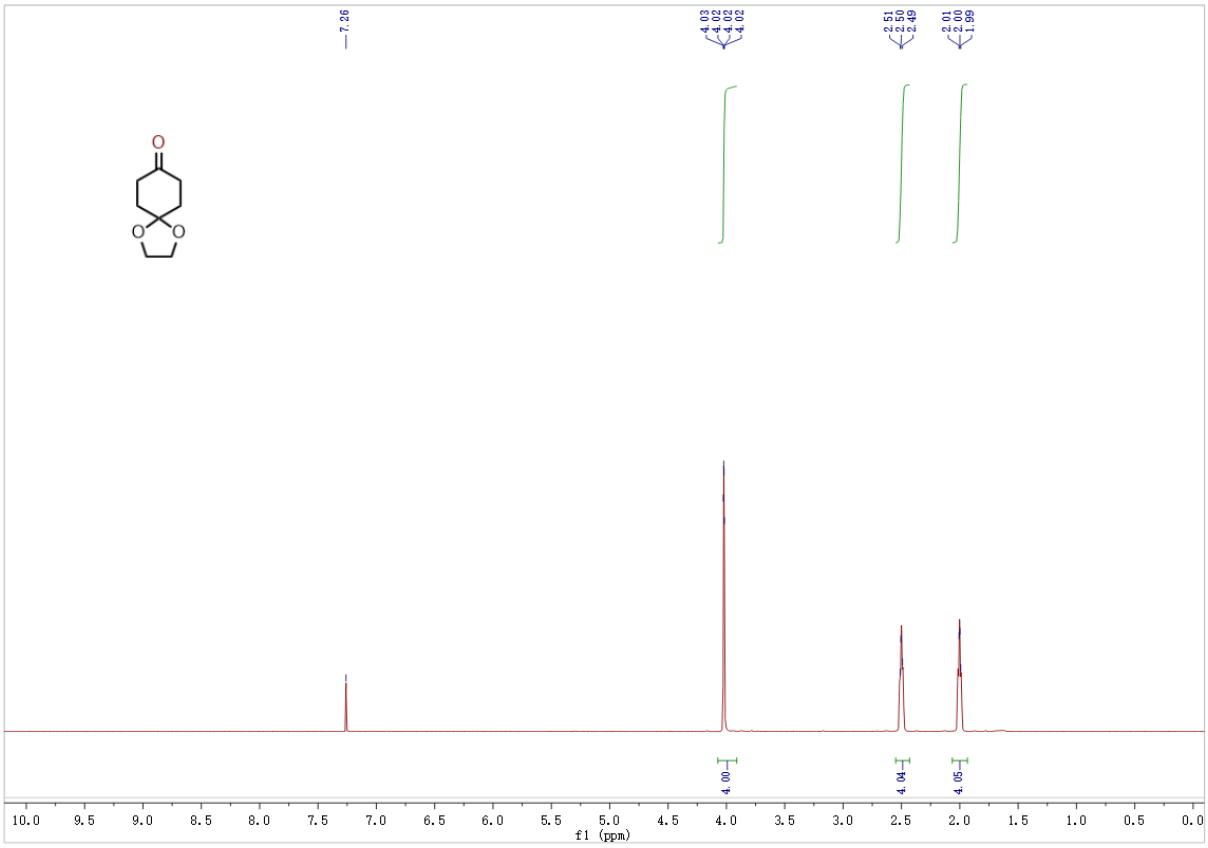
7.26
4.03
4.02
4.02
4.02
2.51
2.50
2.49
2.01
2.00
1.99
4.00
4.04
4.05
f1 (ppm)

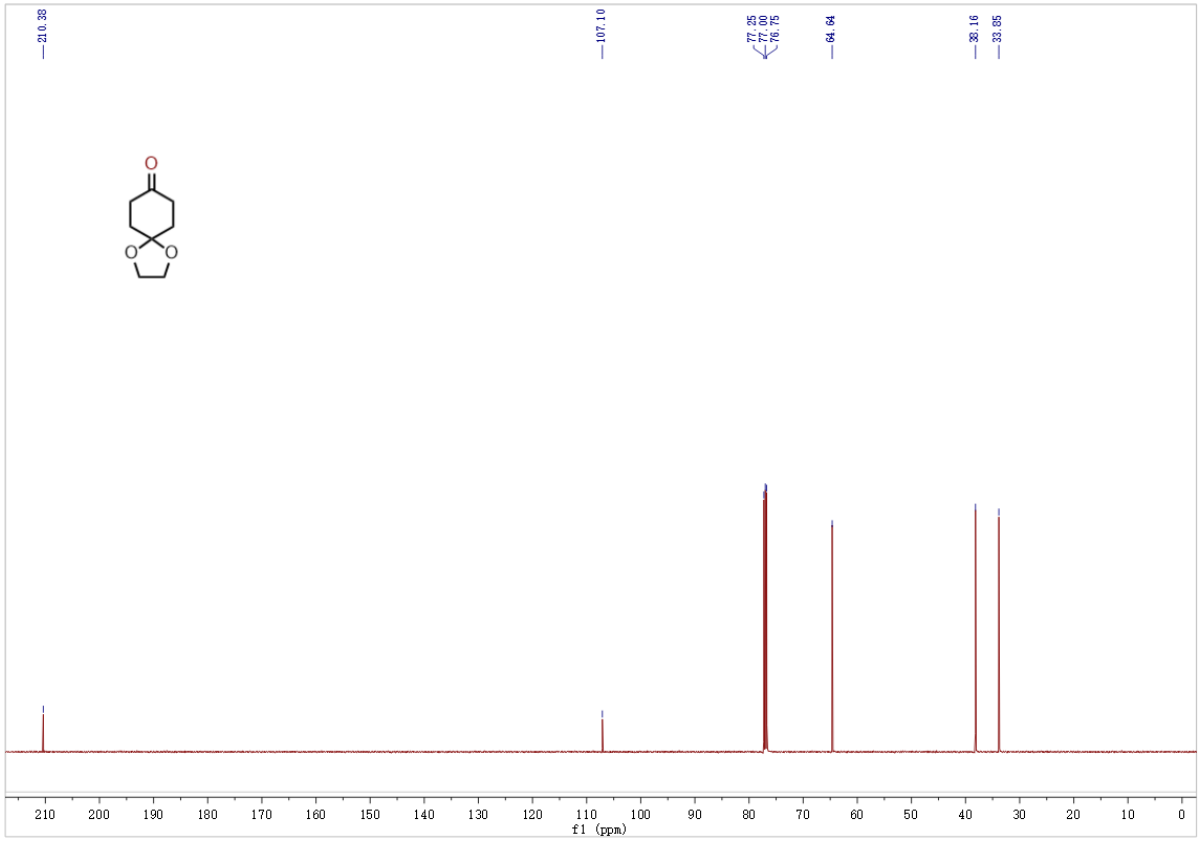
210.38
107.10
77.25
77.00
76.75
64.64
38.16
33.85
f1 (ppm)

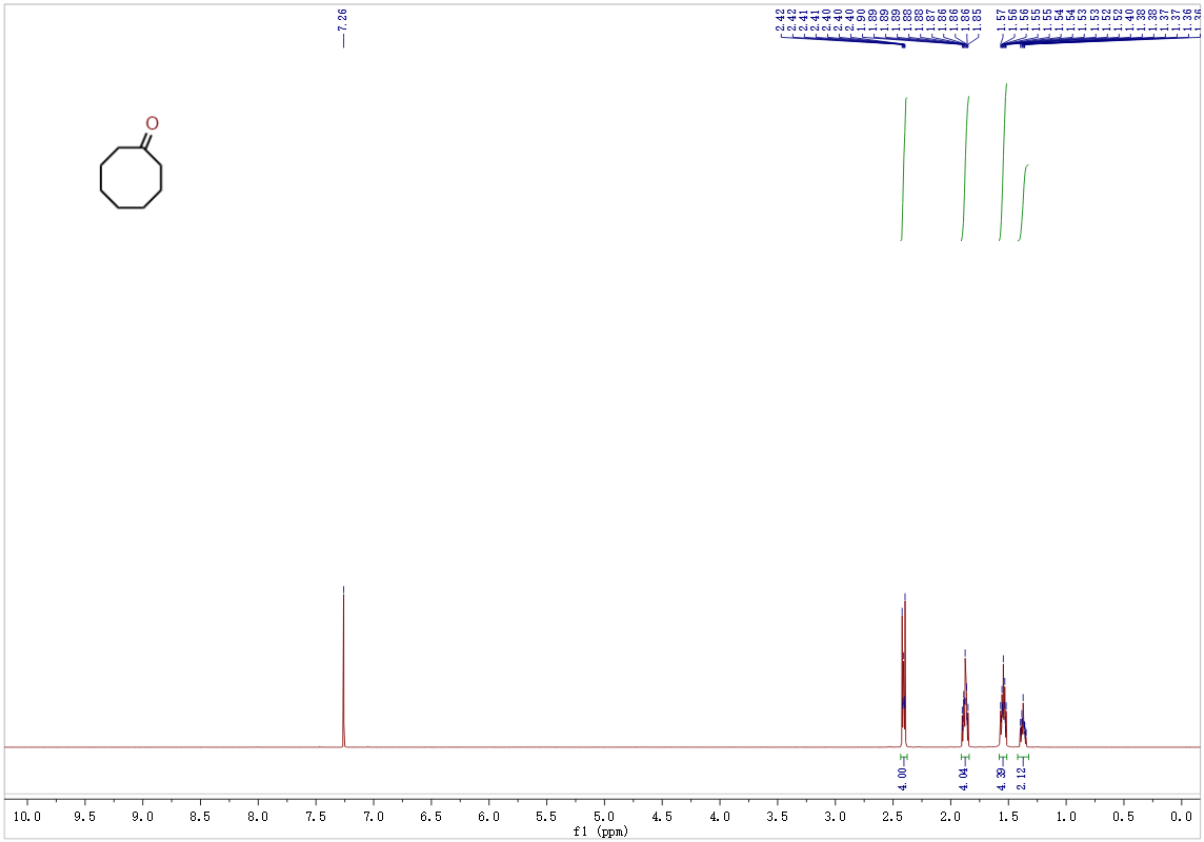
7.26
2.42
2.42
2.41
2.41
2.40
2.40
1.90
1.89
1.89
1.89
1.88
1.88
1.87
1.86
1.86
1.86
1.85
1.57
1.56
1.55
1.55
1.55
1.54
1.54
1.53
1.53
1.52
1.52
1.40
1.38
1.38
1.37
1.37
1.36
O
4.00
4.04
4.39
2.12
10.0 9.5 9.0 8.5 8.0 7.5 7.0 6.5 6.0 5.5 5.0 4.5 4.0 3.5 3.0 2.5 2.0 1.5 1.0 0.5 0.0
f1 (ppm)

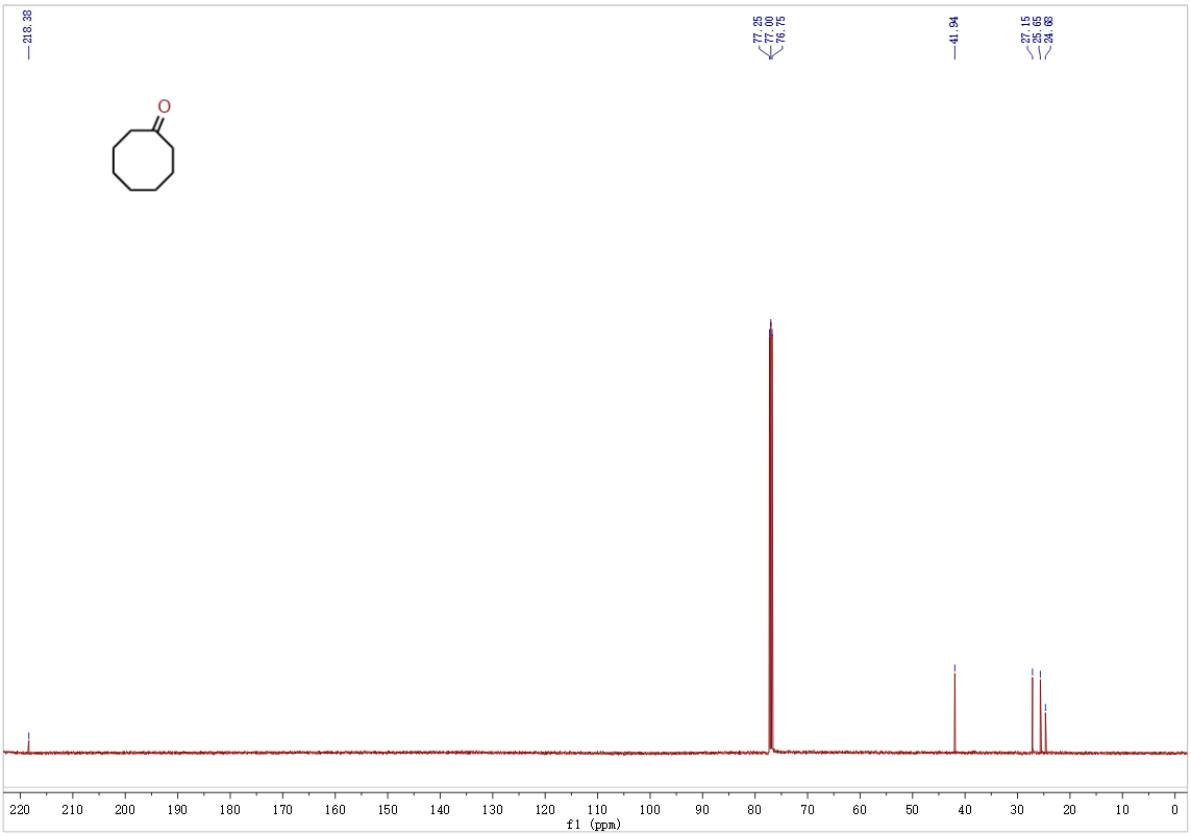
218.38
77.25
77.00
76.75
41.94
27.15
25.65
24.68
O
220 210 200 190 180 170 160 150 140 130 120 110 100 90 80 70 60 50 40 30 20 10 0
f1 (ppm)

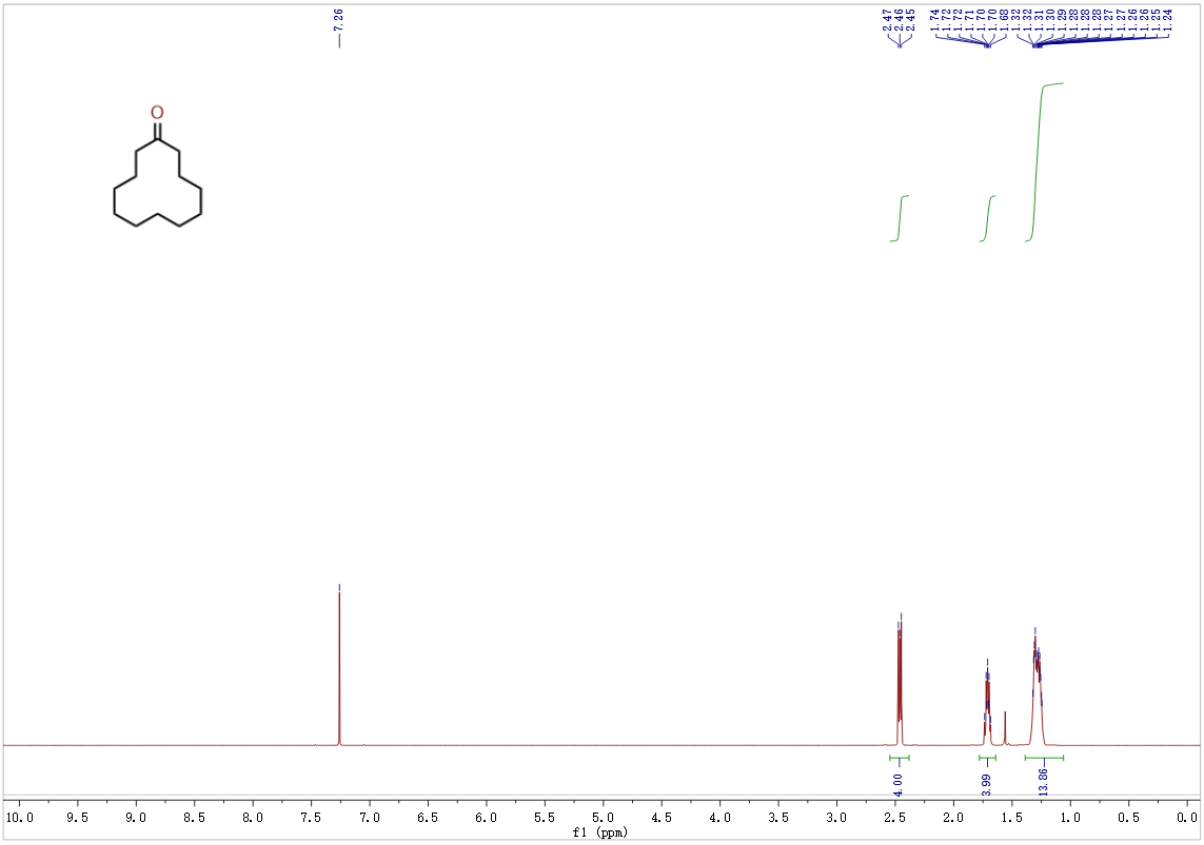
7.26
2.47
2.46
2.45
1.74
1.72
1.71
1.70
1.68
1.32
1.31
1.30
1.29
1.28
1.27
1.26
1.25
1.24
O
4.00
3.99
13.88
10.0 9.5 9.0 8.5 8.0 7.5 7.0 6.5 6.0 5.5 5.0 4.5 4.0 3.5 3.0 2.5 2.0 1.5 1.0 0.5 0.0
f1 (ppm)

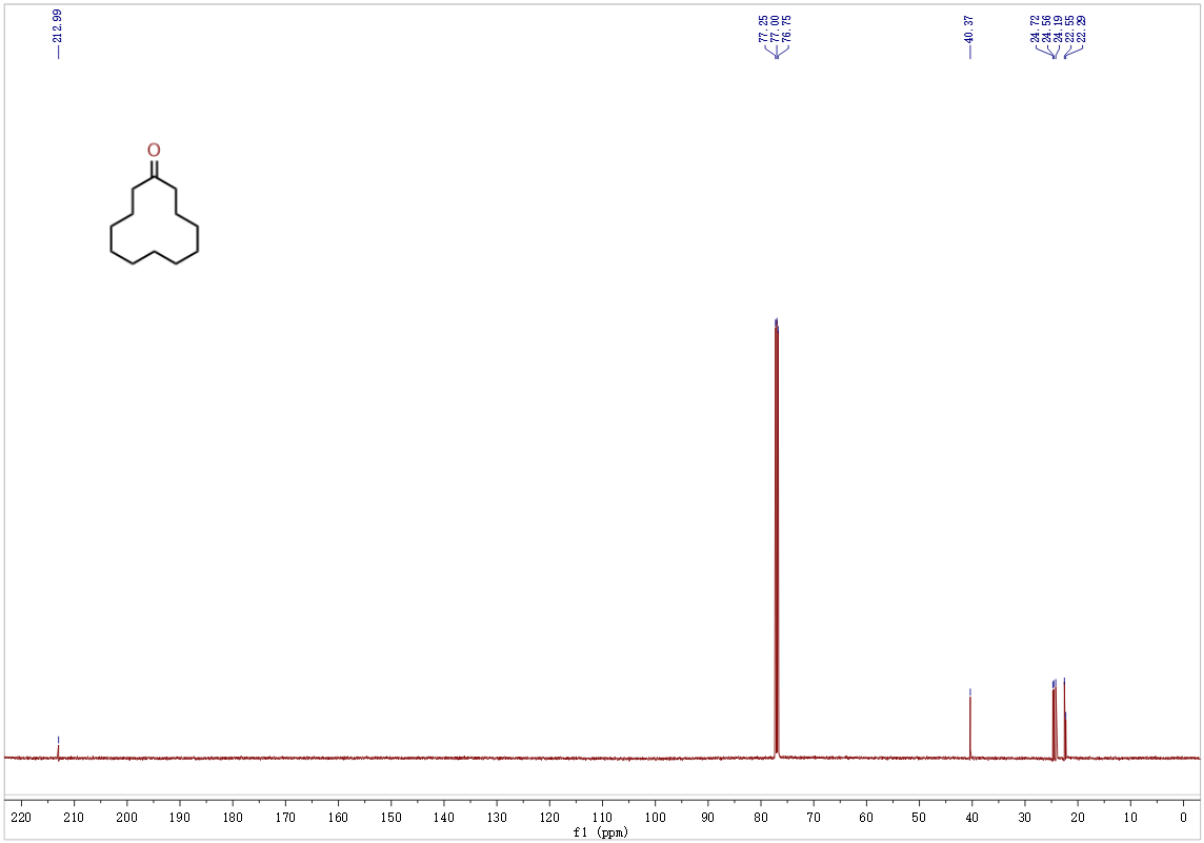
212.99
77.25
77.00
76.75
40.37
24.72
24.56
24.19
23.55
22.29
O
220 210 200 190 180 170 160 150 140 130 120 110 100 90 80 70 60 50 40 30 20 10 0
f1 (ppm)

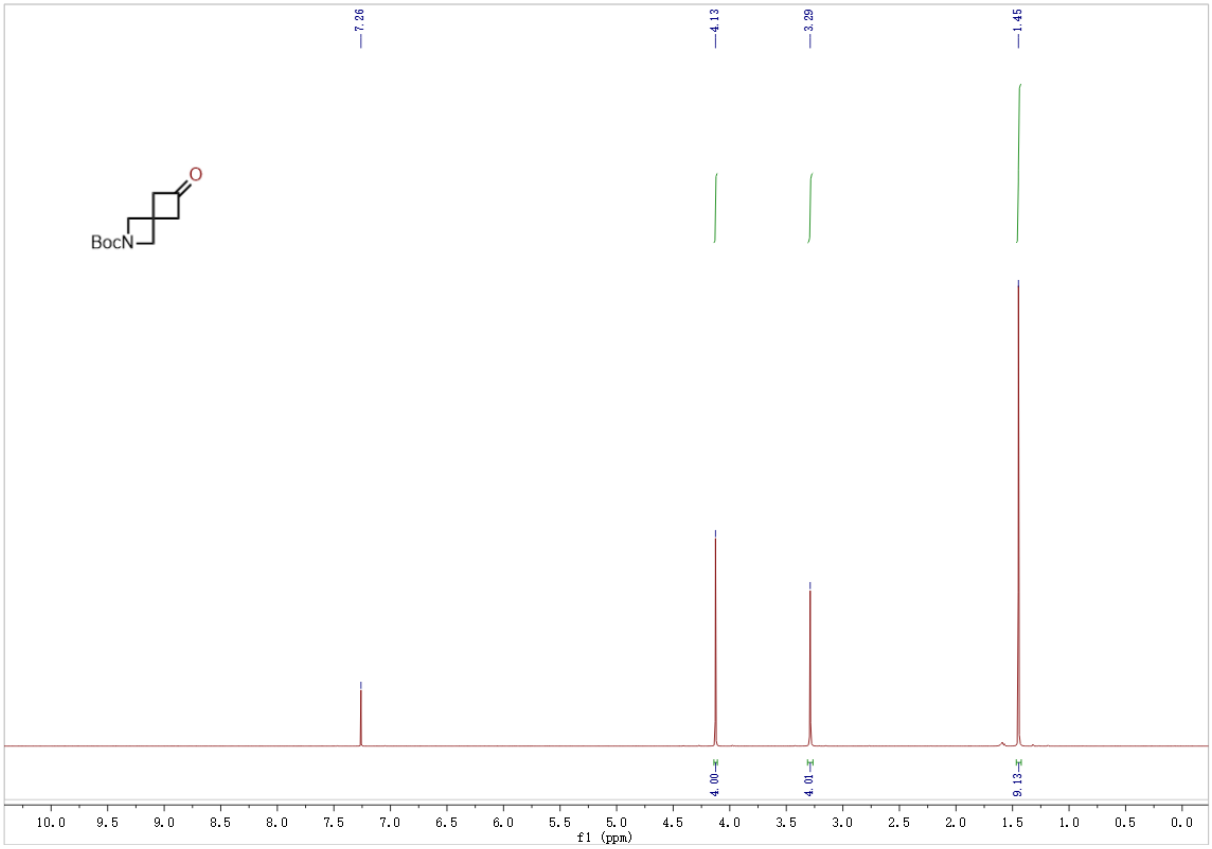
7.26
4.13
3.29
1.45
BocN
O
4.00
4.01
9.13
10.0 9.5 9.0 8.5 8.0 7.5 7.0 6.5 6.0 5.5 5.0 4.5 4.0 3.5 3.0 2.5 2.0 1.5 1.0 0.5 0.0
f1 (ppm)

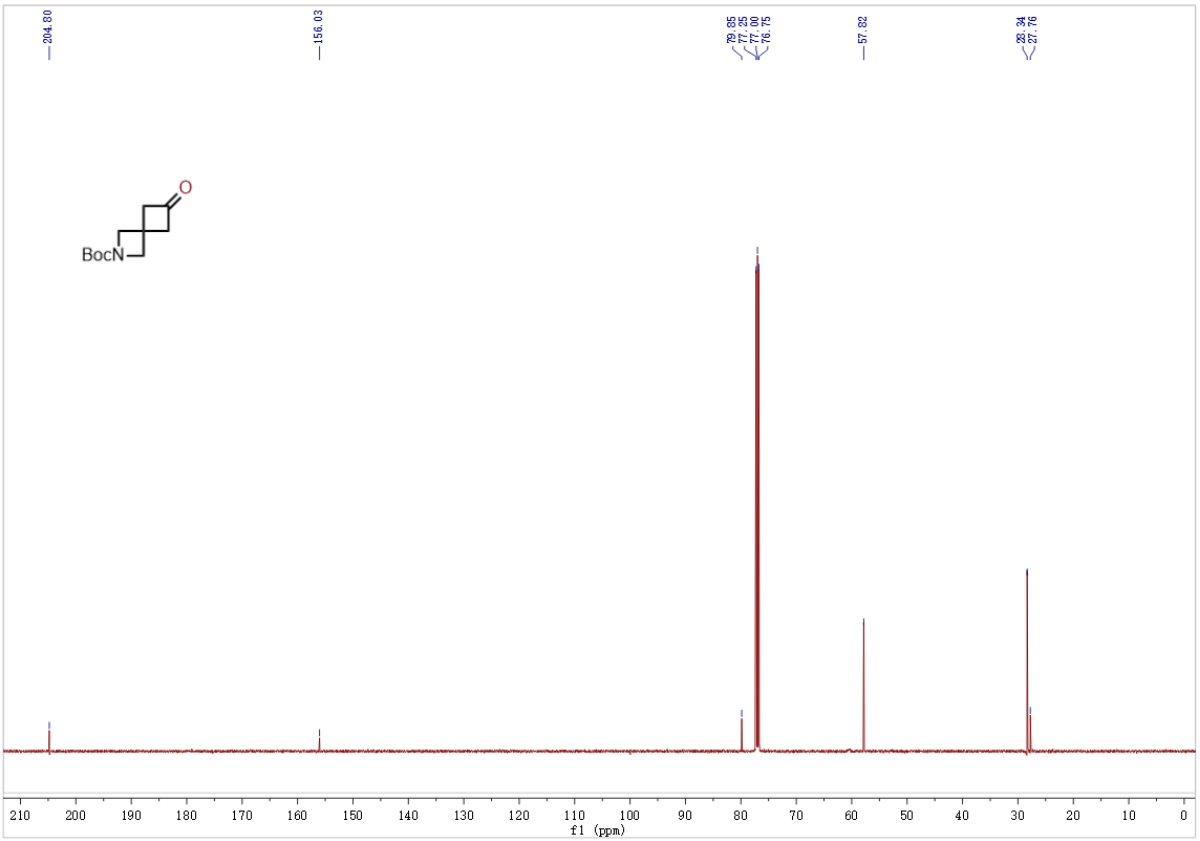
204.80
156.03
79.85
77.25
77.00
76.75
57.82
28.34
27.76
BocN
O
210 200 190 180 170 160 150 140 130 120 110 100 90 80 70 60 50 40 30 20 10 0
f1 (ppm)

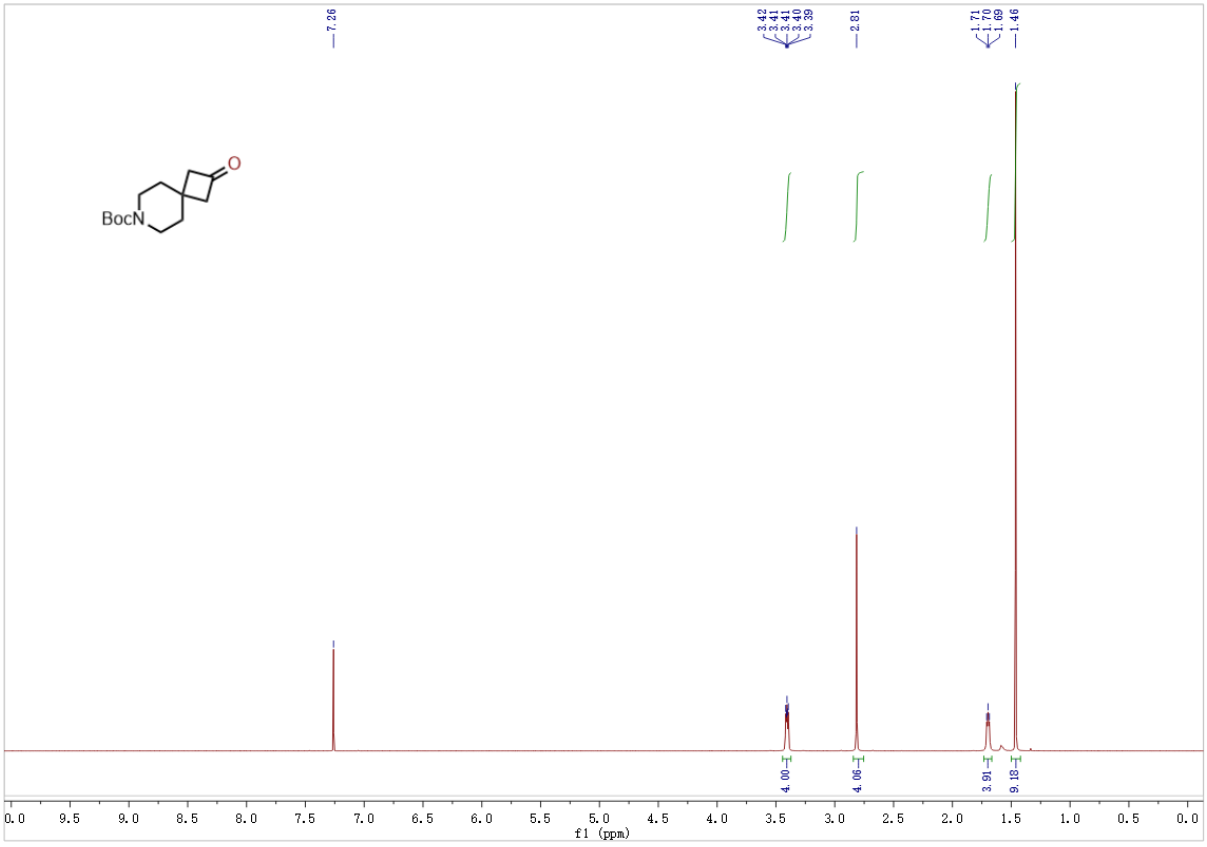
7.26
3.42
3.41
3.41
3.40
3.39
2.81
1.71
1.70
1.69
1.46
BocN
O
4.00
4.06
3.91
9.18
f1 (ppm)

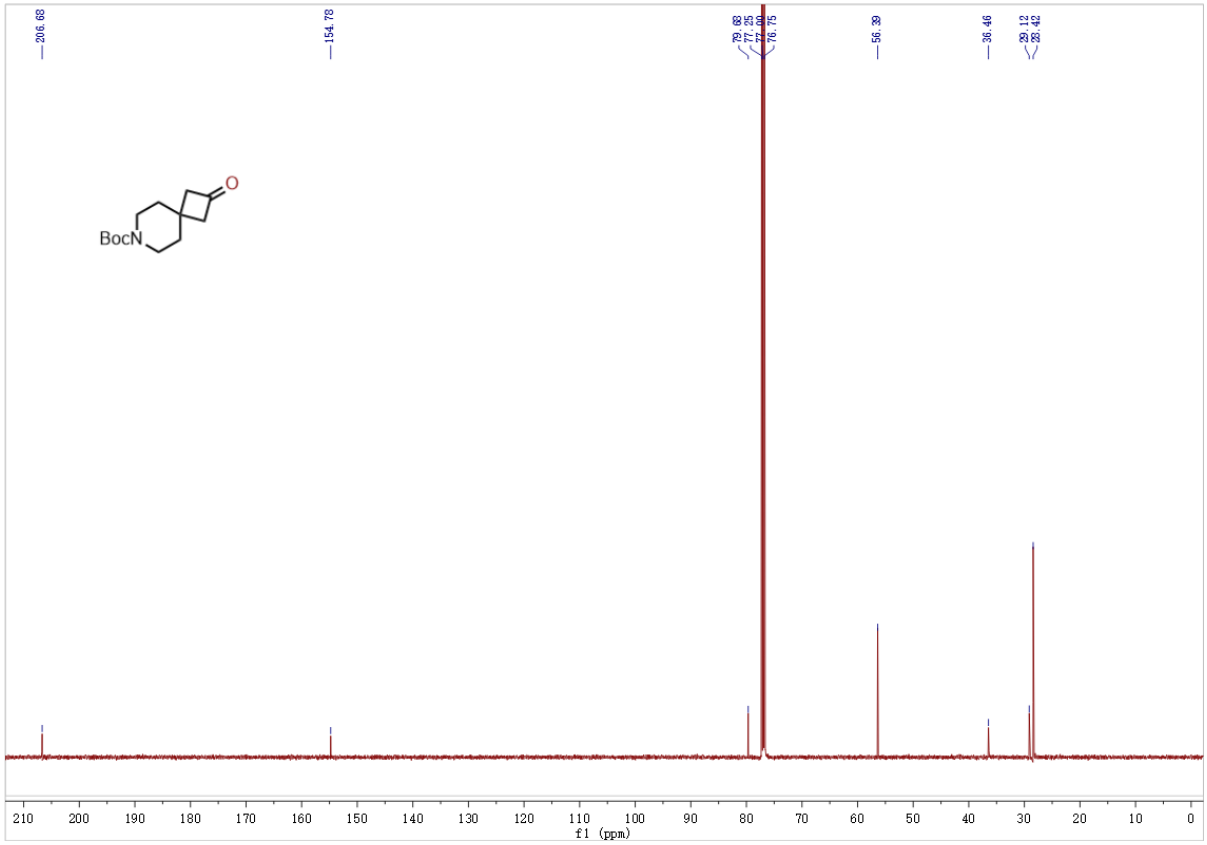
206.68
154.78
79.68
77.25
77.00
76.75
56.39
36.46
29.12
28.42
BocN
O
f1 (ppm)

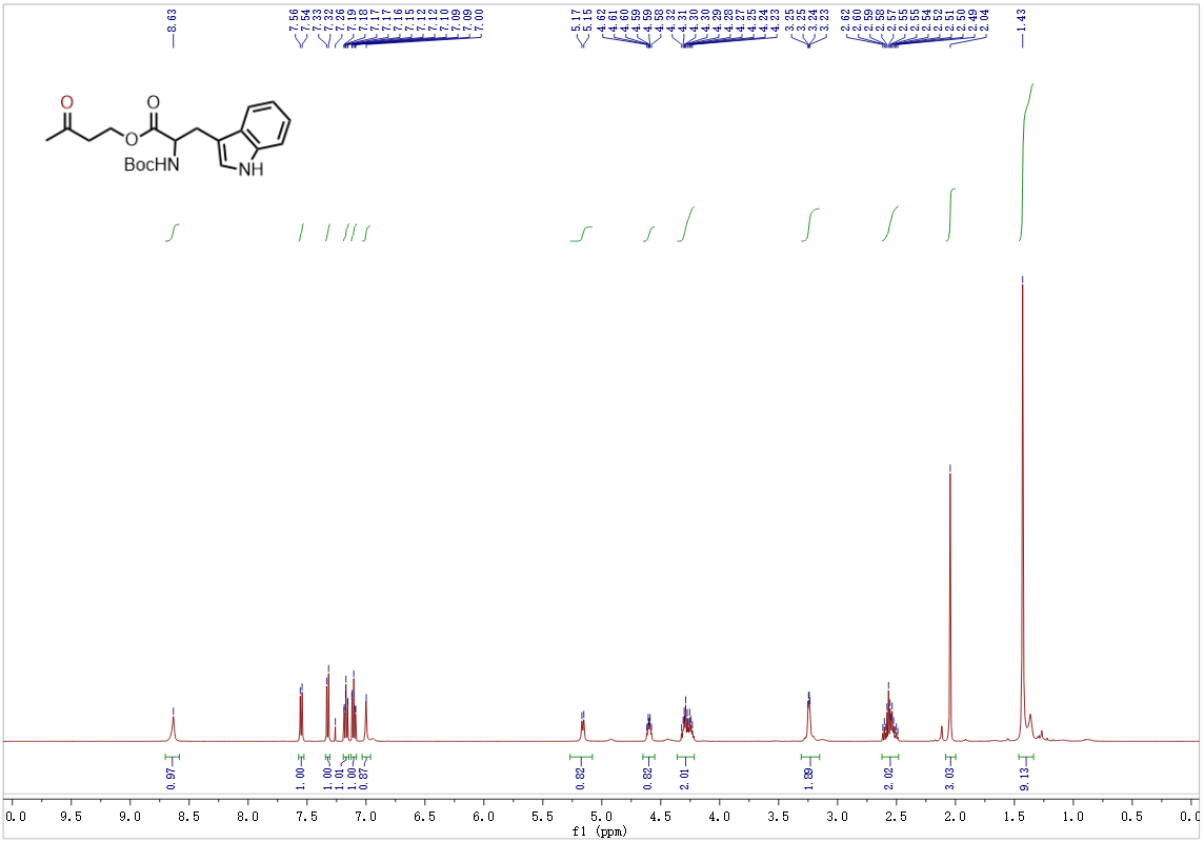
8.63
7.56
7.54
7.33
7.32
7.26
7.19
7.18
7.17
7.17
7.16
7.15
7.12
7.10
7.09
7.09
7.00
5.17
5.15
4.62
4.61
4.60
4.59
4.58
4.58
4.32
4.31
4.30
4.30
4.29
4.28
4.27
4.25
4.24
4.23
3.25
3.24
3.24
3.23
2.62
2.60
2.59
2.58
2.57
2.55
2.54
2.52
2.51
2.50
2.49
2.04
1.43
O
O
O
BocHN
NH
0.97
1.00
1.08
1.15
1.00
0.87
0.82
0.83
2.01
1.89
2.02
3.03
9.13
f1 (ppm)

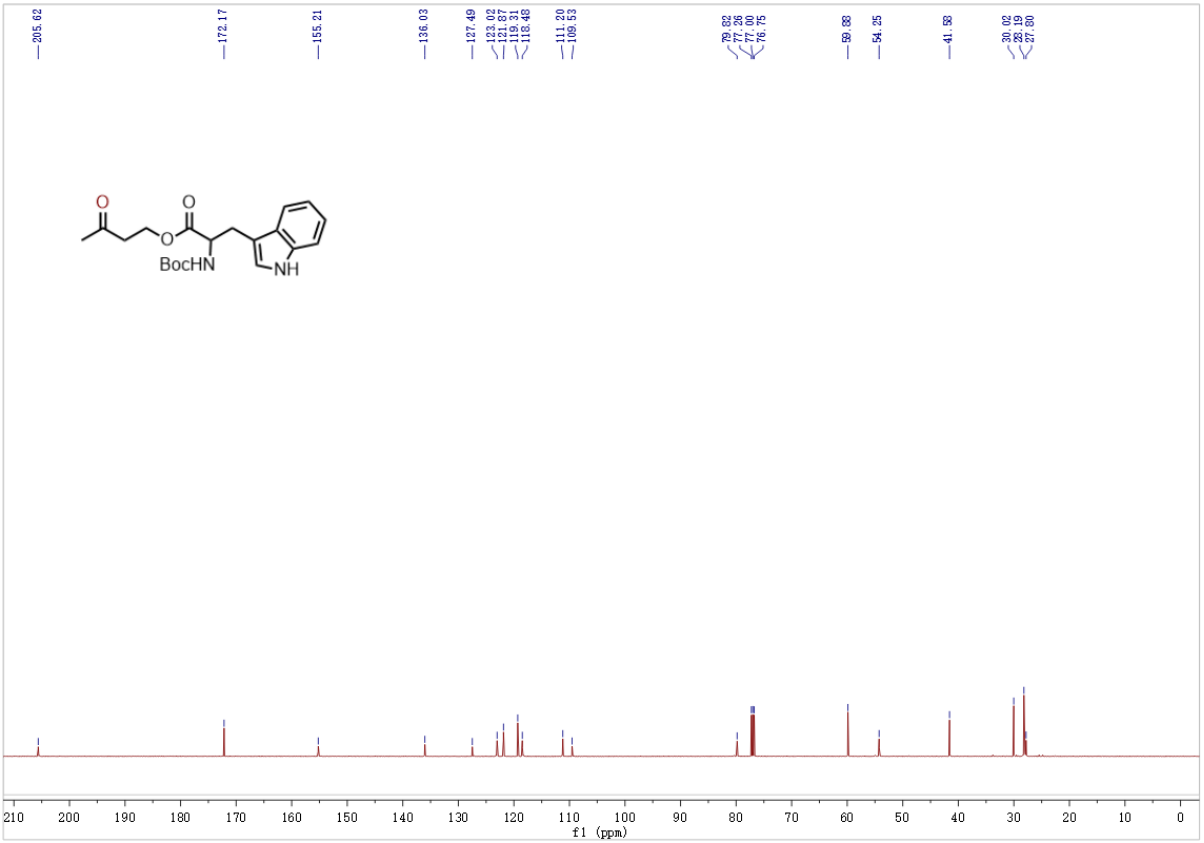
205.62
172.17
155.21
136.03
127.49
123.02
121.87
119.31
118.48
111.20
109.53
79.82
77.26
77.00
76.75
59.88
54.25
41.58
30.02
28.19
27.80
O
O
O
BocHN
NH
f1 (ppm)

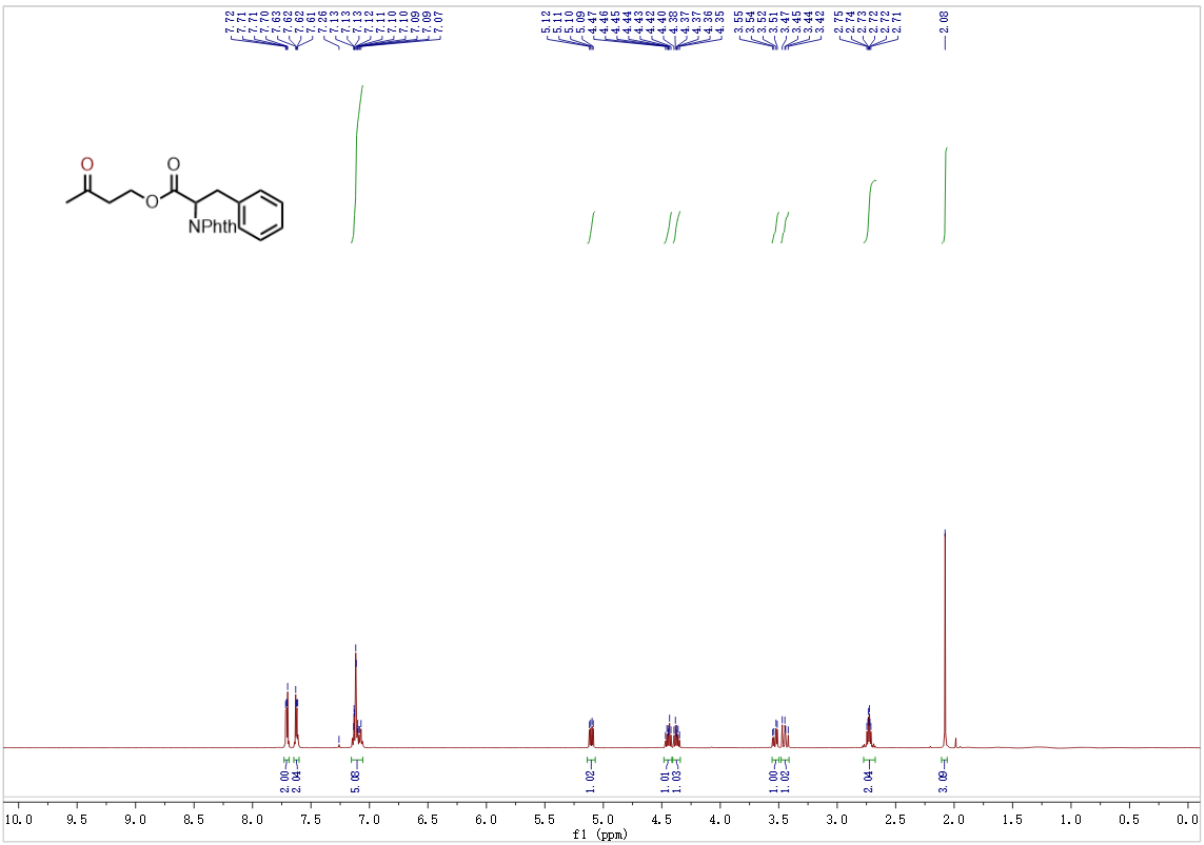
7.72
7.71
7.71
7.70
7.63
7.62
7.62
7.61
7.26
7.13
7.13
7.12
7.11
7.11
7.10
7.10
7.09
7.09
7.07
5.12
5.11
5.10
5.09
4.47
4.46
4.45
4.44
4.43
4.42
4.40
4.38
4.37
4.37
4.36
4.35
3.55
3.54
3.52
3.51
3.47
3.45
3.44
3.42
2.75
2.74
2.73
2.72
2.72
2.71
2.08
O
O
O
NPhth
2.00
2.04
5.08
1.02
1.01
1.03
1.00
1.02
2.04
3.09
10.0
9.5
9.0
8.5
8.0
7.5
7.0
6.5
6.0
5.5
5.0
4.5
4.0
3.5
3.0
2.5
2.0
1.5
1.0
0.5
0.0
f1 (ppm)

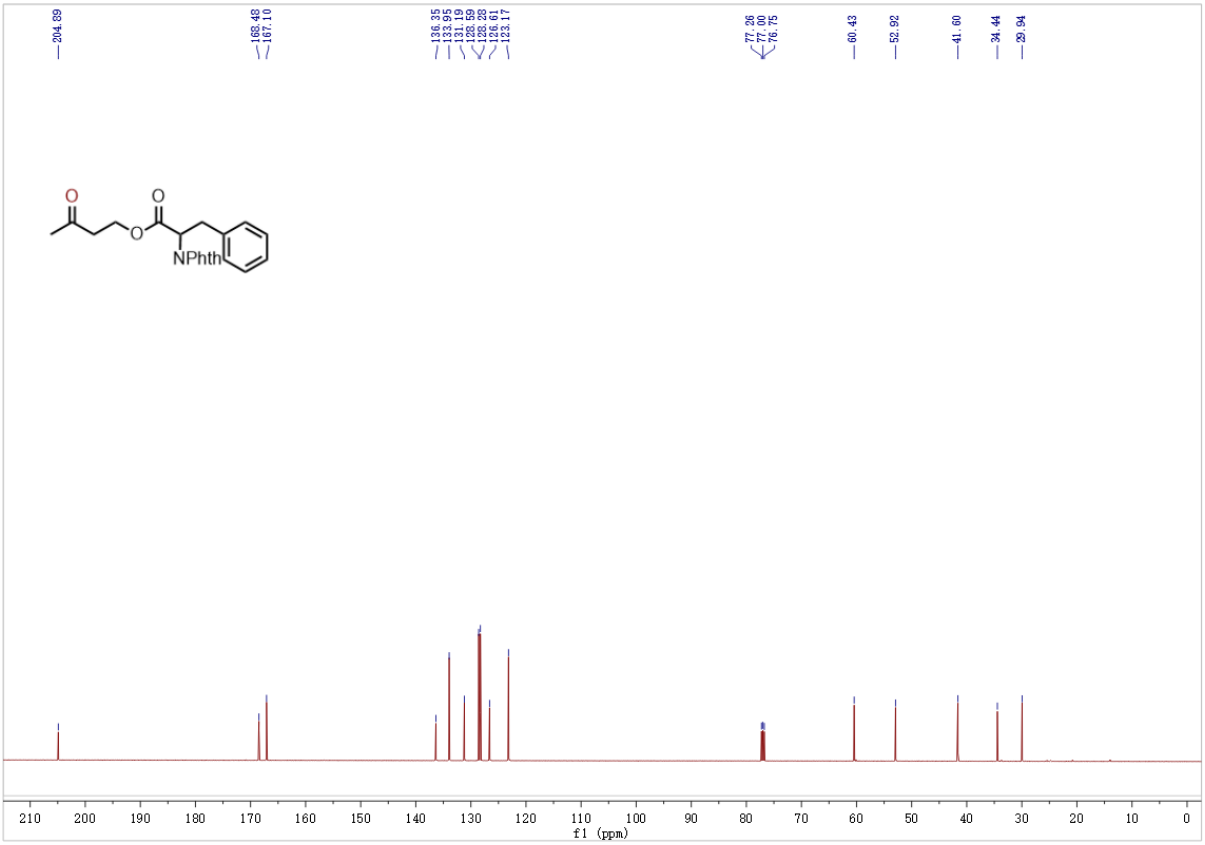
204.89
168.48
167.10
136.35
133.95
131.19
128.59
128.23
126.61
123.17
77.38
77.00
76.75
60.43
52.92
41.60
34.44
29.94
O
O
O
NPhth
210
200
190
180
170
160
150
140
130
120
110
100
90
80
70
60
50
40
30
20
10
0
f1 (ppm)

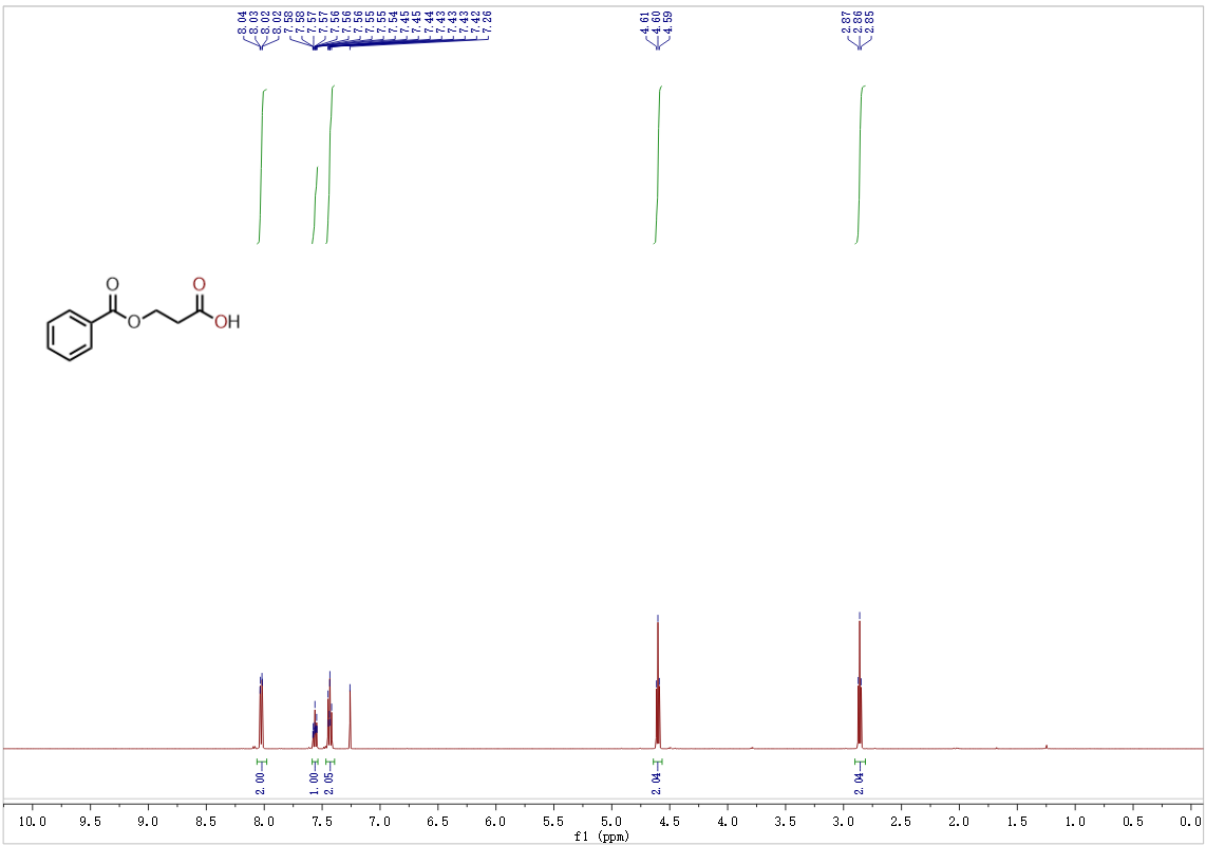
8.04
8.03
8.02
8.02
7.58
7.57
7.57
7.56
7.56
7.56
7.55
7.55
7.54
7.45
7.44
7.43
7.43
7.43
7.42
7.26
4.61
4.60
4.59
2.87
2.86
2.85
O
O
O
OH
2.00
1.00
2.05
2.04
2.04
10.0
9.5
9.0
8.5
8.0
7.5
7.0
6.5
6.0
5.5
5.0
4.5
4.0
3.5
3.0
2.5
2.0
1.5
1.0
0.5
0.0
f1 (ppm)

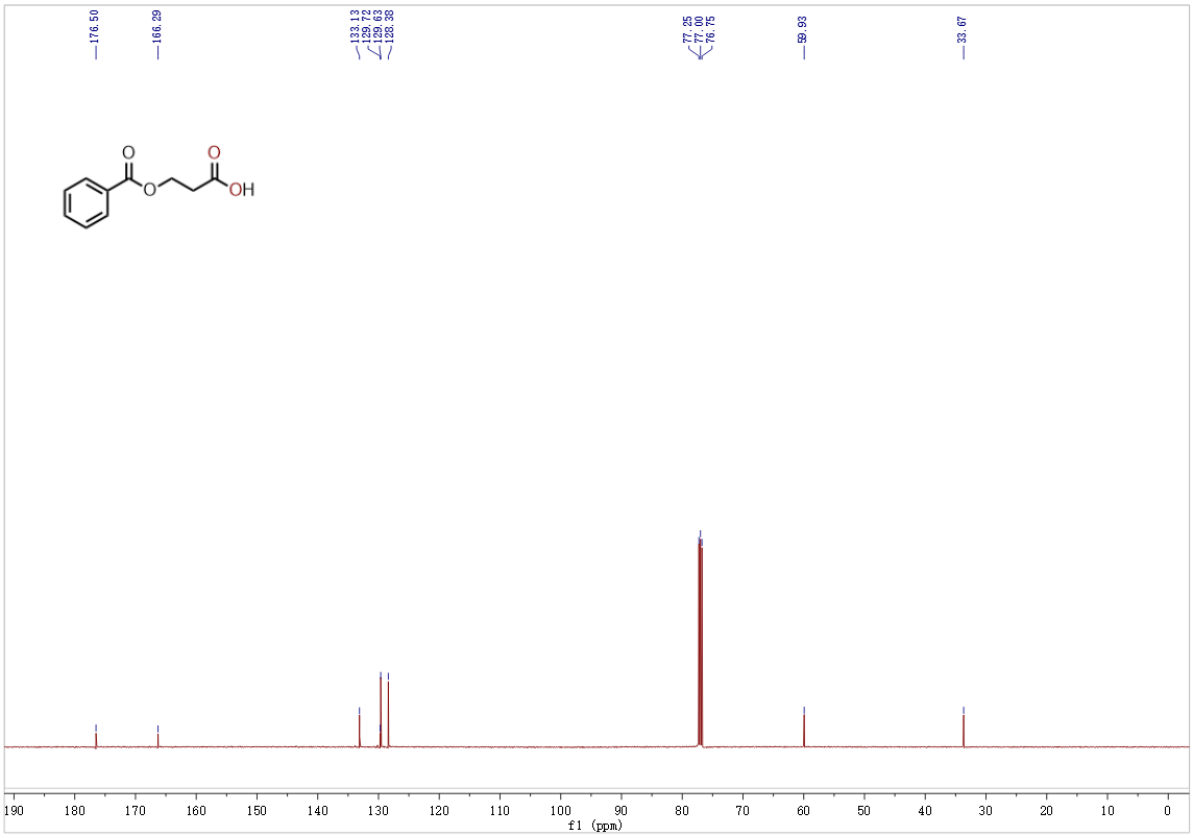
176.50
166.29
133.13
130.72
129.63
128.38
77.25
77.00
76.75
59.93
33.07
O
O
O
OH
190
180
170
160
150
140
130
120
110
100
90
80
70
60
50
40
30
20
10
0
f1 (ppm)

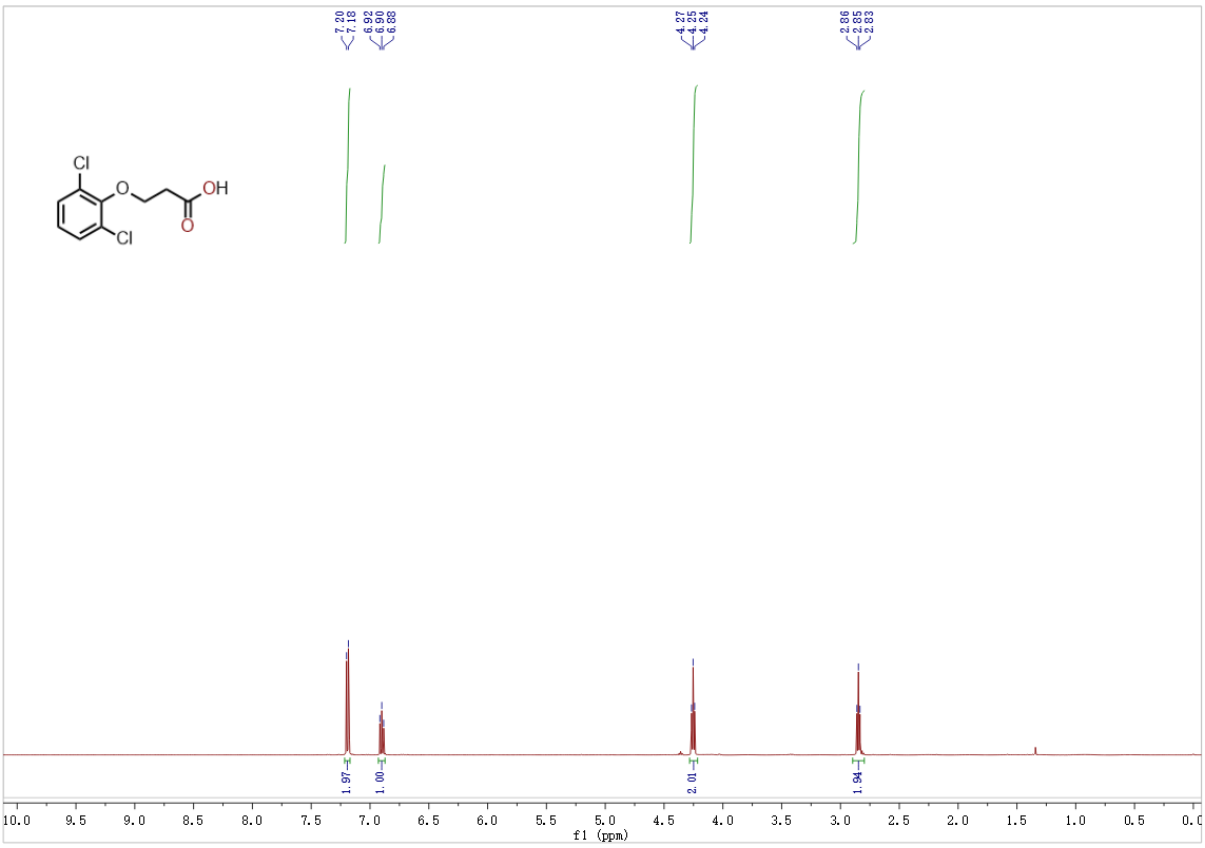
7.20
7.18
6.92
6.90
6.88
4.27
4.25
4.24
2.86
2.85
2.83
Cl
O
OH
O
Cl
1.97
1.00
2.01
1.94
10.0
9.5
9.0
8.5
8.0
7.5
7.0
6.5
6.0
5.5
5.0
4.5
4.0
3.5
3.0
2.5
2.0
1.5
1.0
0.5
f1 (ppm)

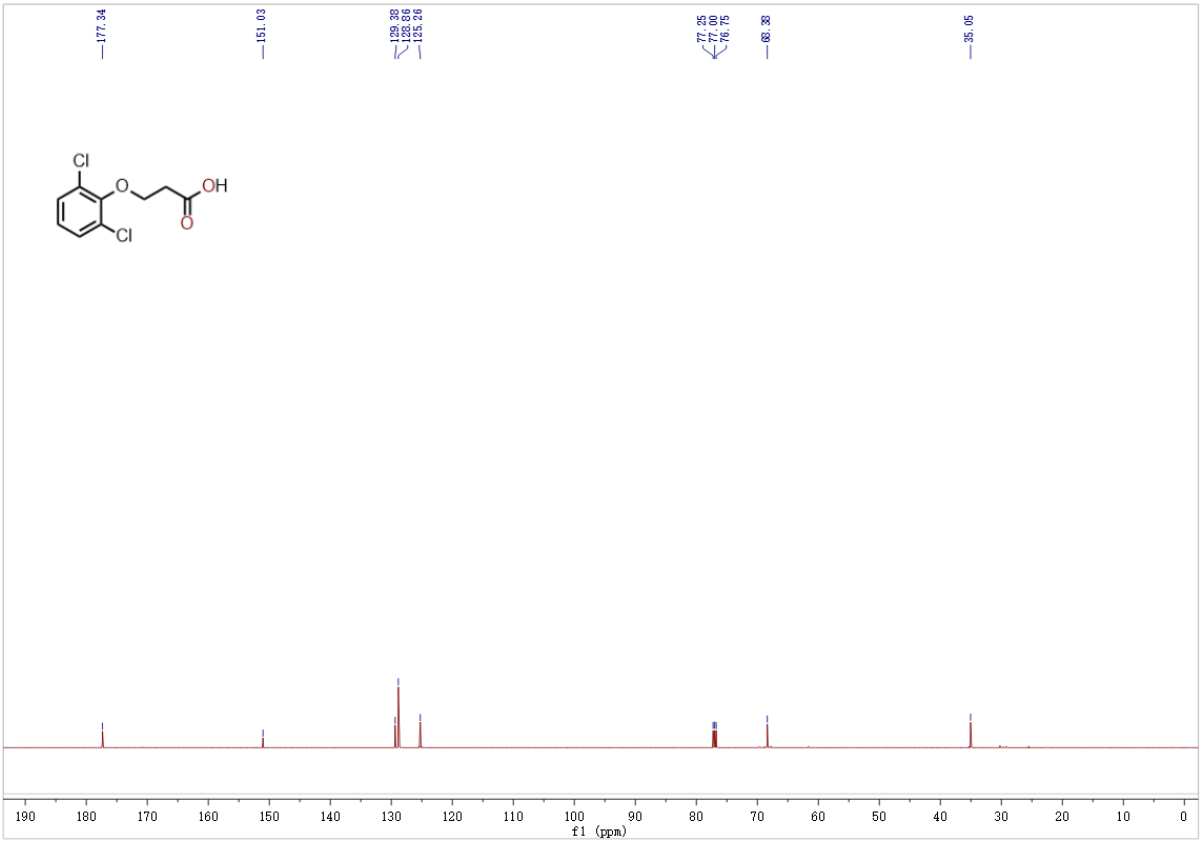
177.34
151.03
129.38
128.86
125.26
77.25
77.00
76.75
68.38
35.05
Cl
O
OH
O
Cl
190
180
170
160
150
140
130
120
110
100
90
80
70
60
50
40
30
20
10
0
f1 (ppm)

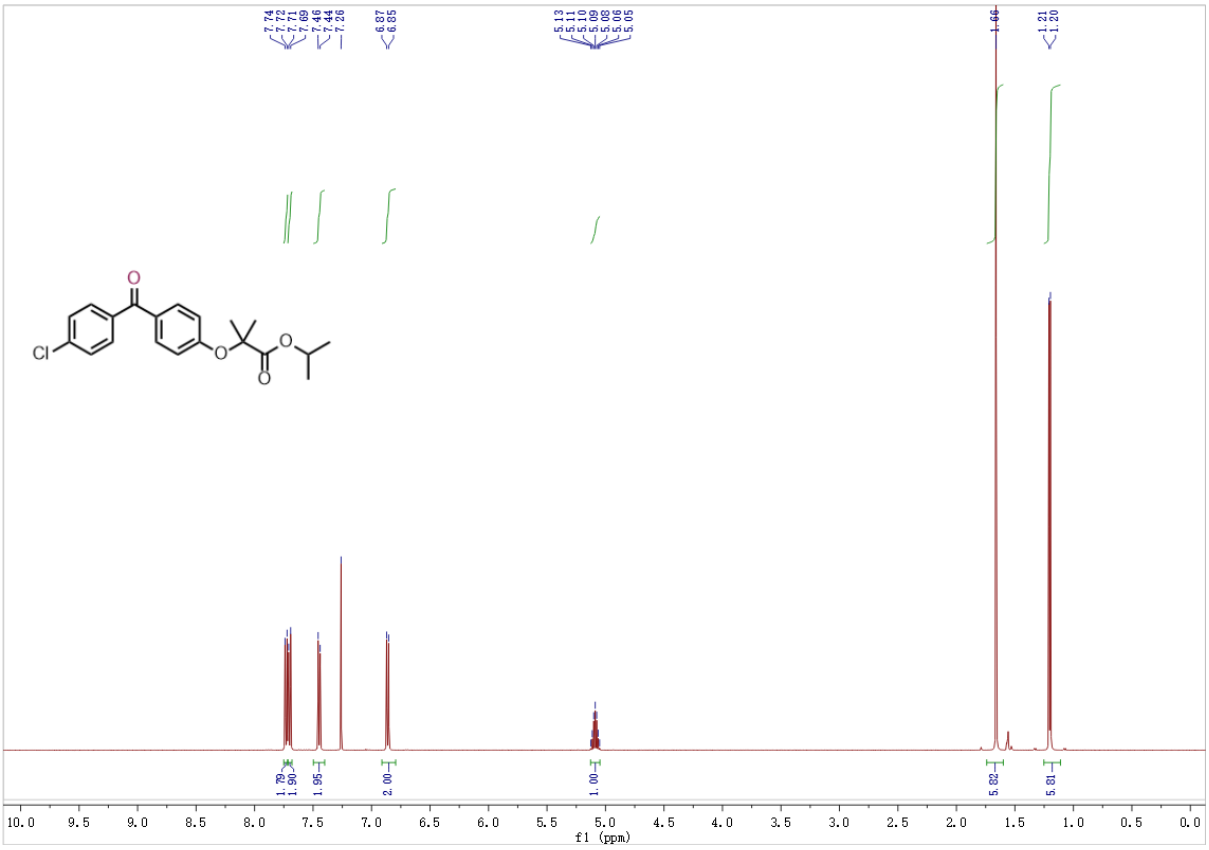
7.74
7.72
7.71
7.69
7.46
7.44
7.26
6.87
6.85
5.13
5.11
5.10
5.09
5.08
5.06
5.05
1.66
1.21
1.20
O
Cl
O
O
O
1.79
1.90
1.95
2.00
1.00
5.82
5.81
10.0 9.5 9.0 8.5 8.0 7.5 7.0 6.5 6.0 5.5 5.0 4.5 4.0 3.5 3.0 2.5 2.0 1.5 1.0 0.5 0.0
f1 (ppm)

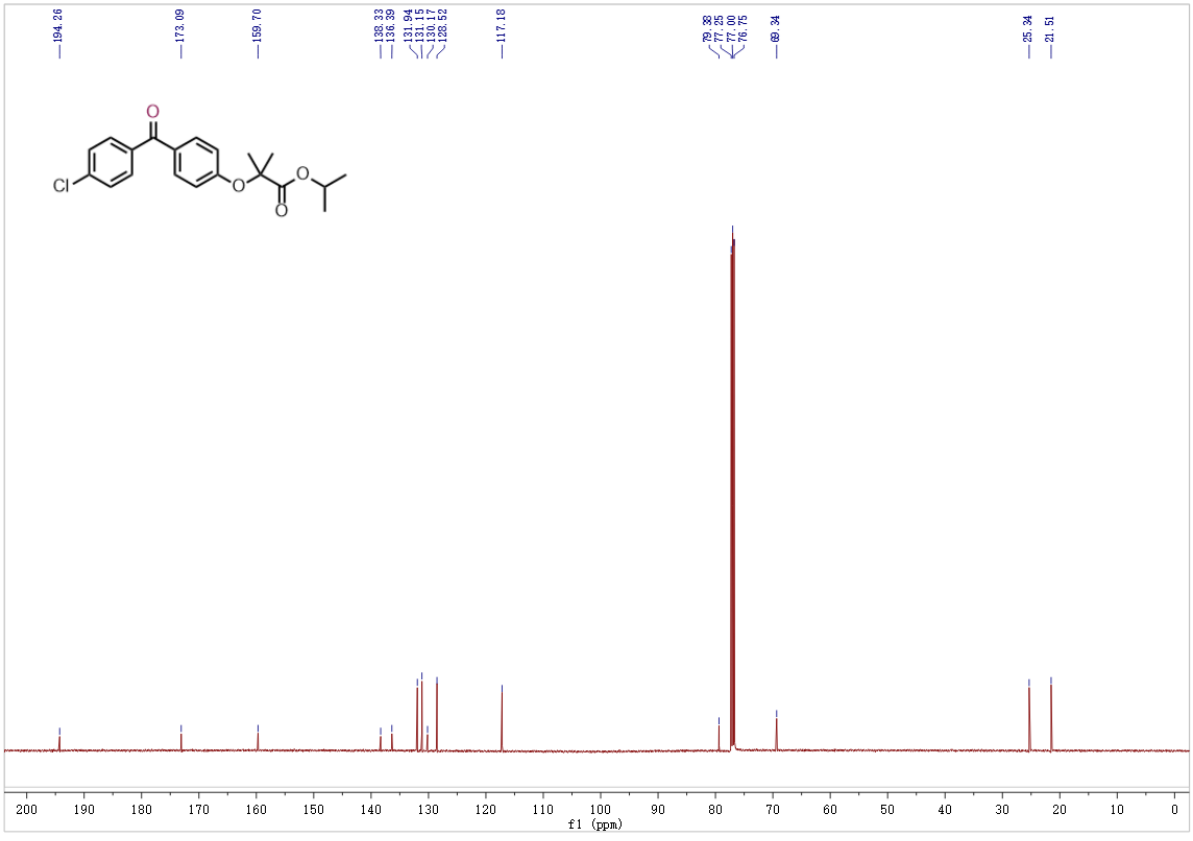
194.26
173.09
159.70
138.33
136.39
131.94
131.15
130.17
128.52
117.18
79.38
77.25
77.00
76.75
69.34
25.34
21.51
O
Cl
O
O
O
200 190 180 170 160 150 140 130 120 110 100 90 80 70 60 50 40 30 20 10 0
f1 (ppm)

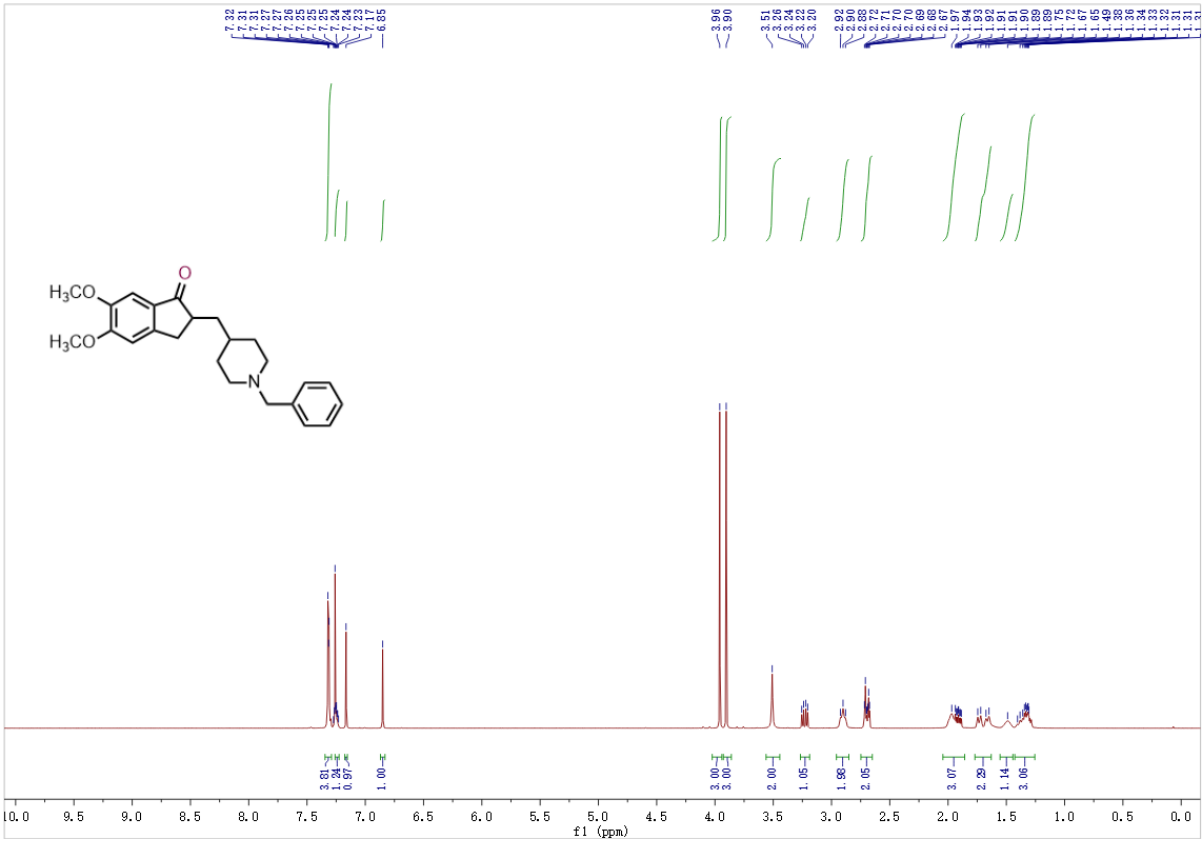
H3CO
H3CO
O
N
f1 (ppm)

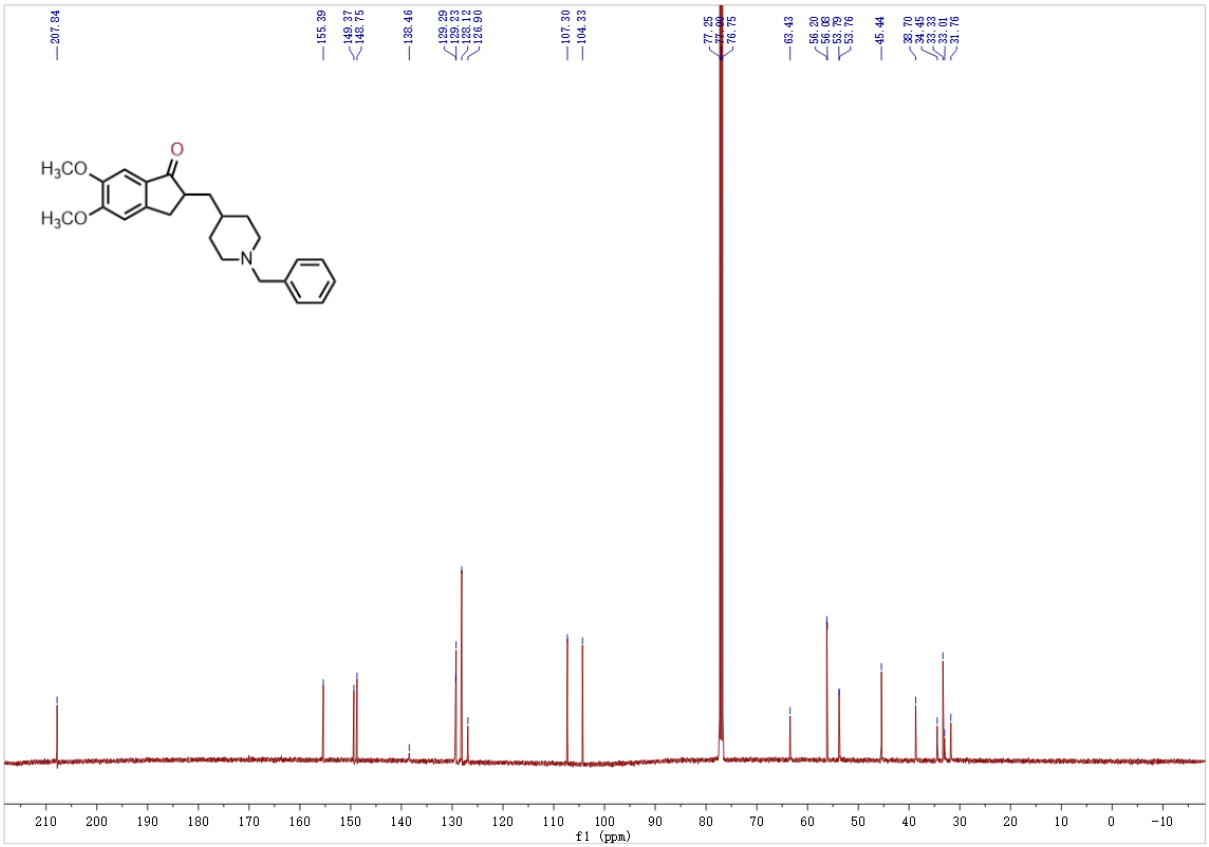
H3CO
H3CO
O
N
f1 (ppm)

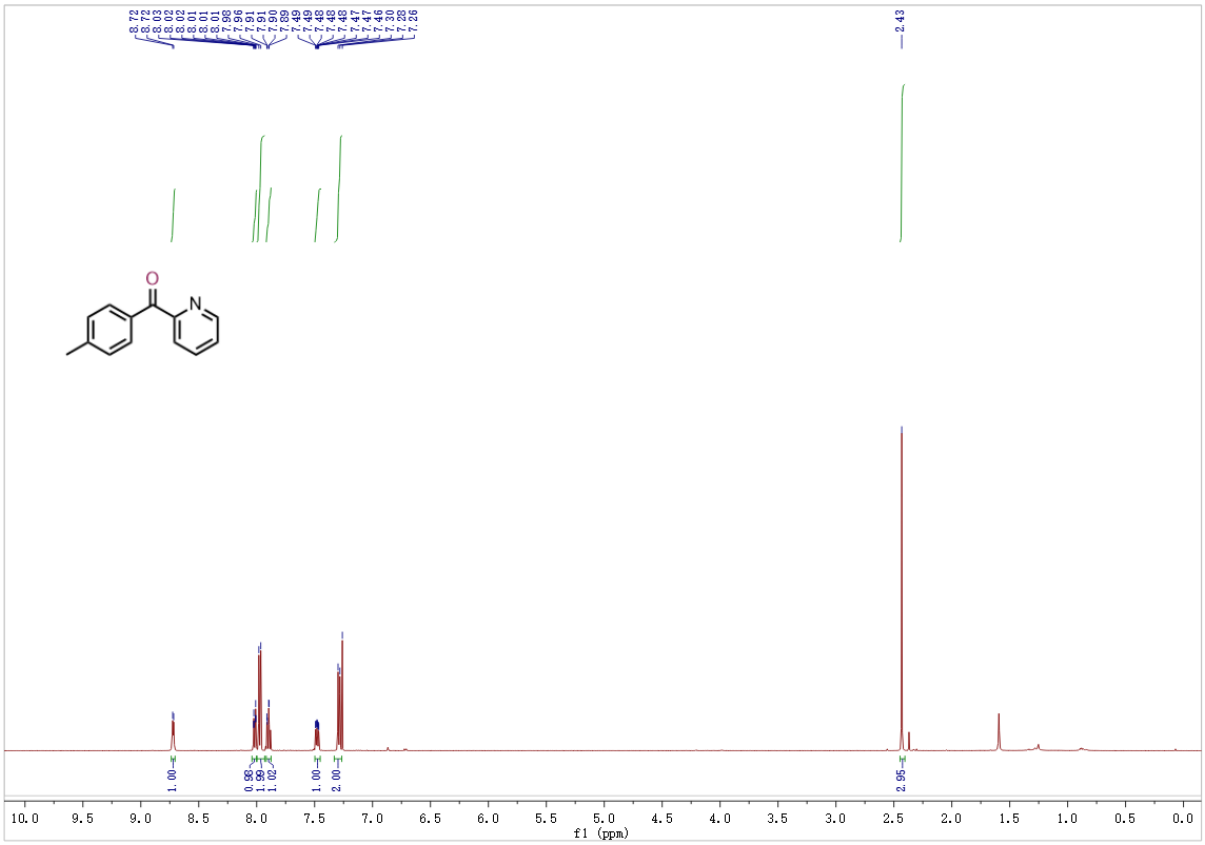
8.72
8.72
8.03
8.03
8.02
8.02
8.02
8.01
8.01
8.01
7.98
7.96
7.91
7.91
7.90
7.89
7.49
7.49
7.48
7.48
7.48
7.47
7.47
7.46
7.30
7.28
7.26
2.43
1.00
0.98
1.99
1.02
1.00
2.00
2.95
10.0 9.5 9.0 8.5 8.0 7.5 7.0 6.5 6.0 5.5 5.0 4.5 4.0 3.5 3.0 2.5 2.0 1.5 1.0 0.5 0.0
f1 (ppm)

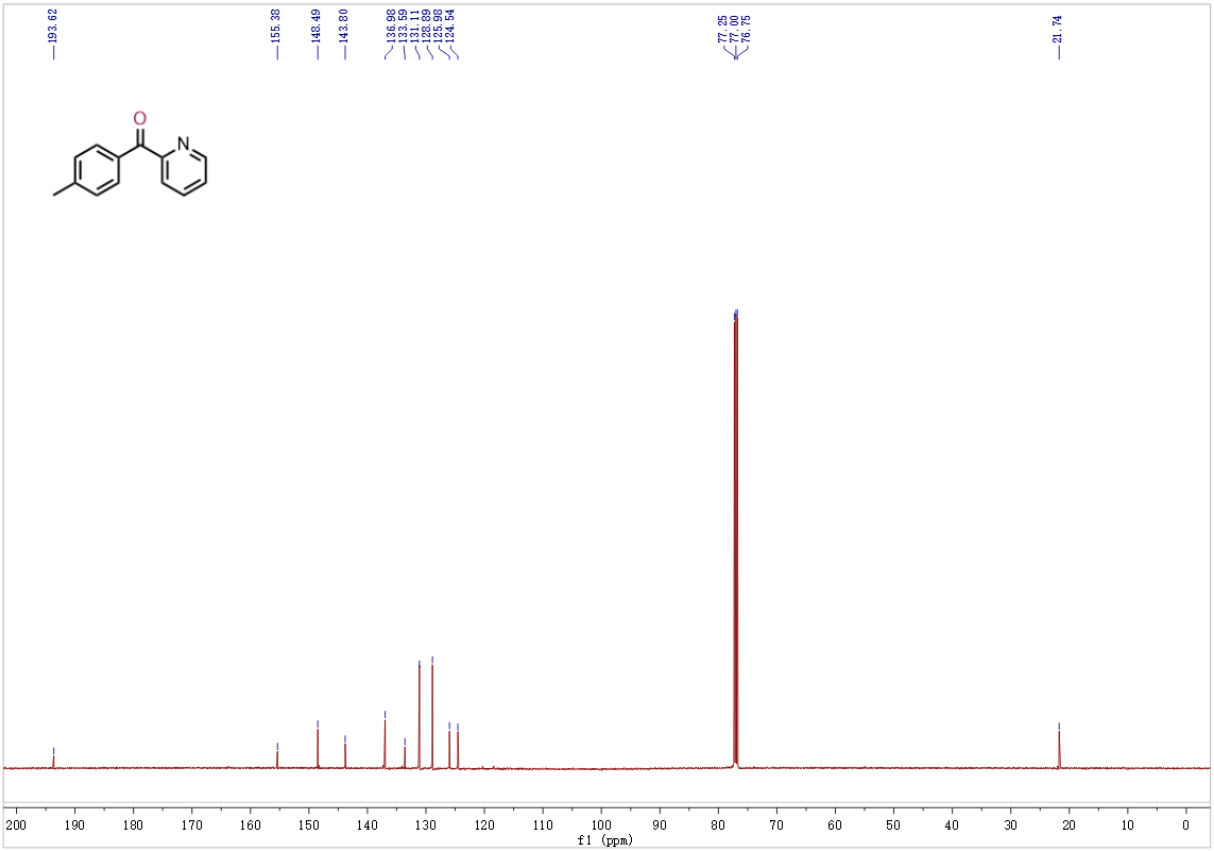
193.62
155.38
148.49
143.80
136.98
133.59
131.11
128.89
125.98
124.94
77.25
77.00
76.75
21.74
200 190 180 170 160 150 140 130 120 110 100 90 80 70 60 50 40 30 20 10 0
f1 (ppm)

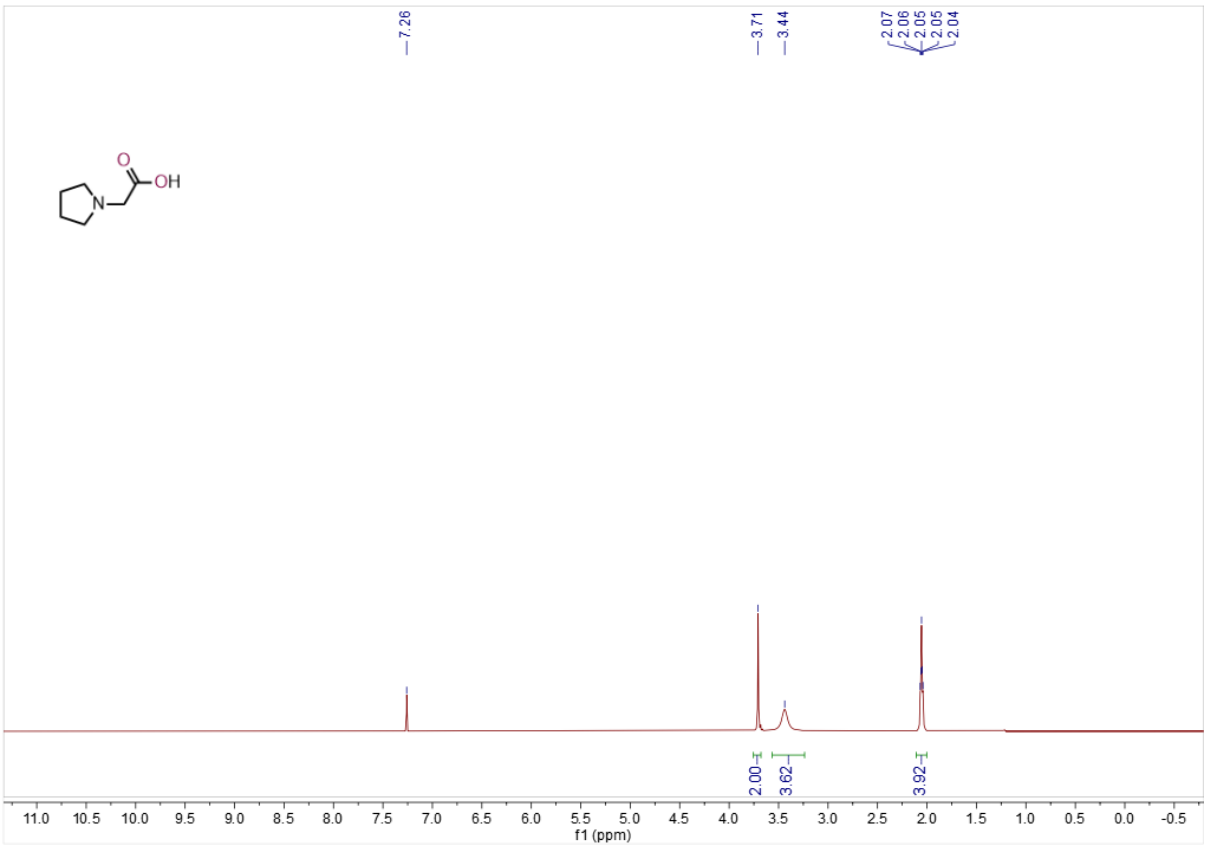
7.26
3.71
3.44
2.07
2.06
2.05
2.05
2.04
O
OH
N
2.00
3.62
3.92
11.0 10.5 10.0 9.5 9.0 8.5 8.0 7.5 7.0 6.5 6.0 5.5 5.0 4.5 4.0 3.5 3.0 2.5 2.0 1.5 1.0 0.5 0.0 -0.5
f1 (ppm)

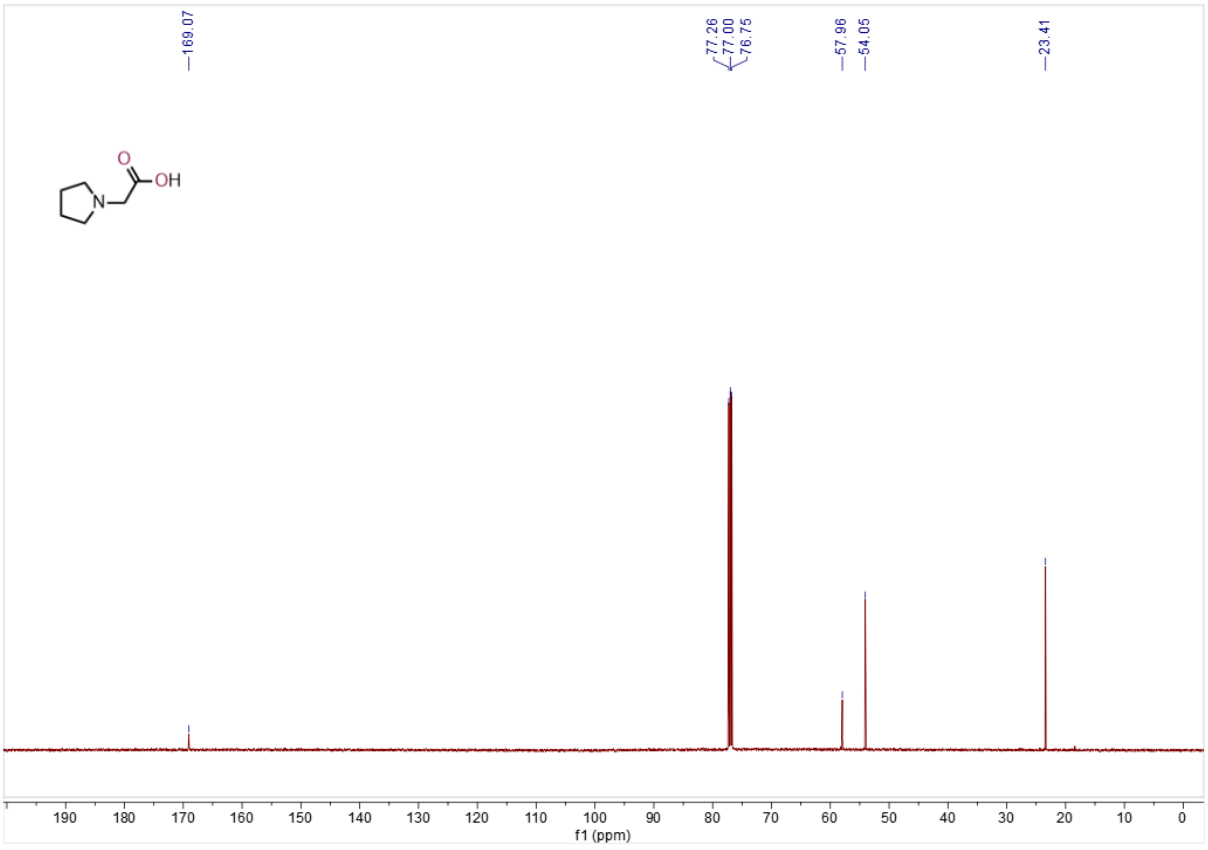
169.07
77.26
77.00
76.75
57.96
54.05
23.41
O
OH
N
190 180 170 160 150 140 130 120 110 100 90 80 70 60 50 40 30 20 10 0
f1 (ppm)

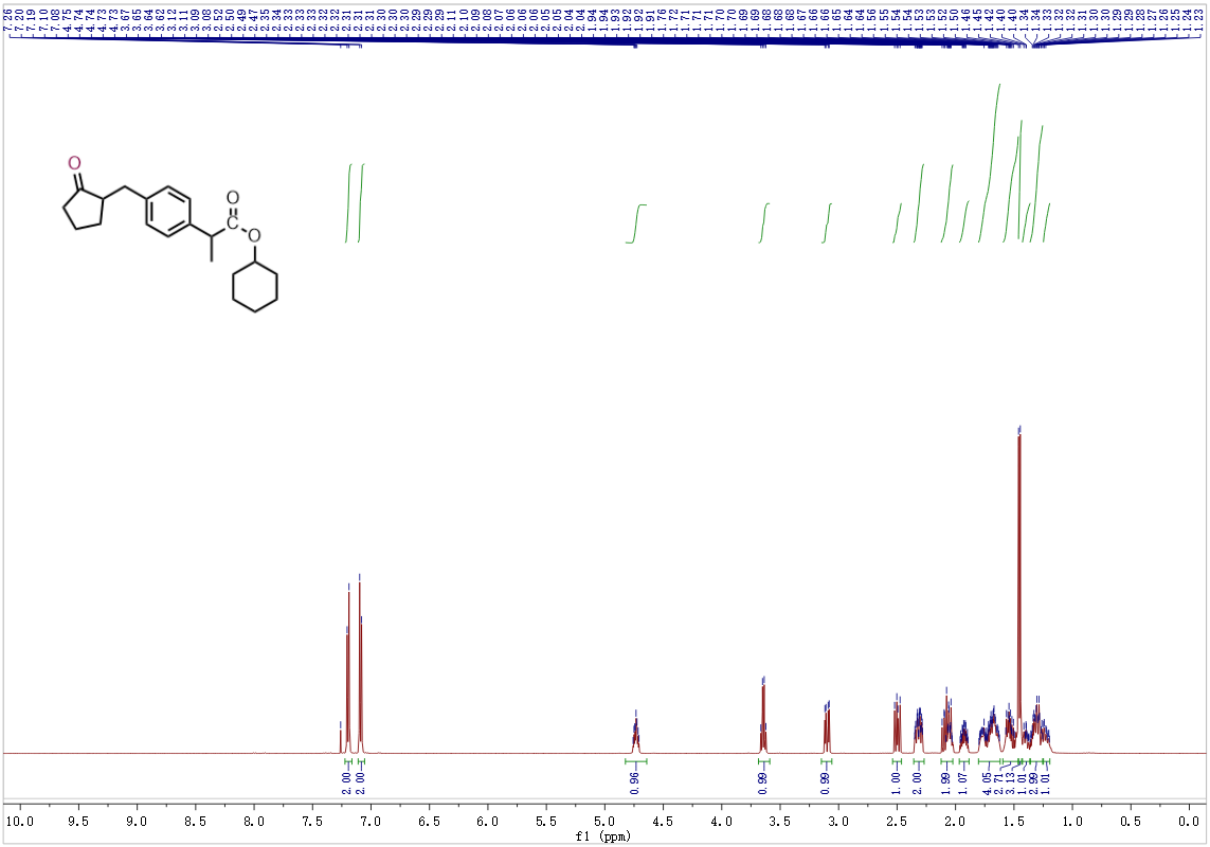
f1 (ppm)

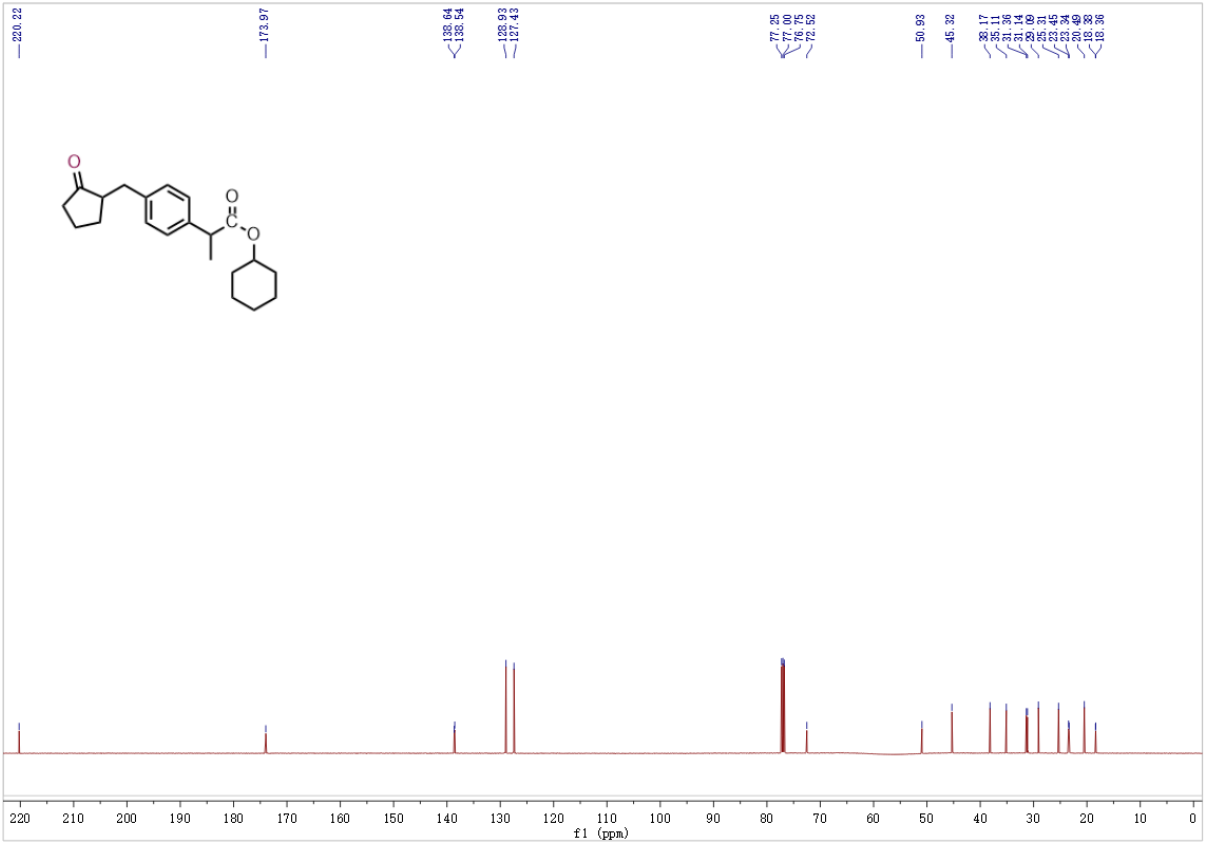
f1 (ppm)

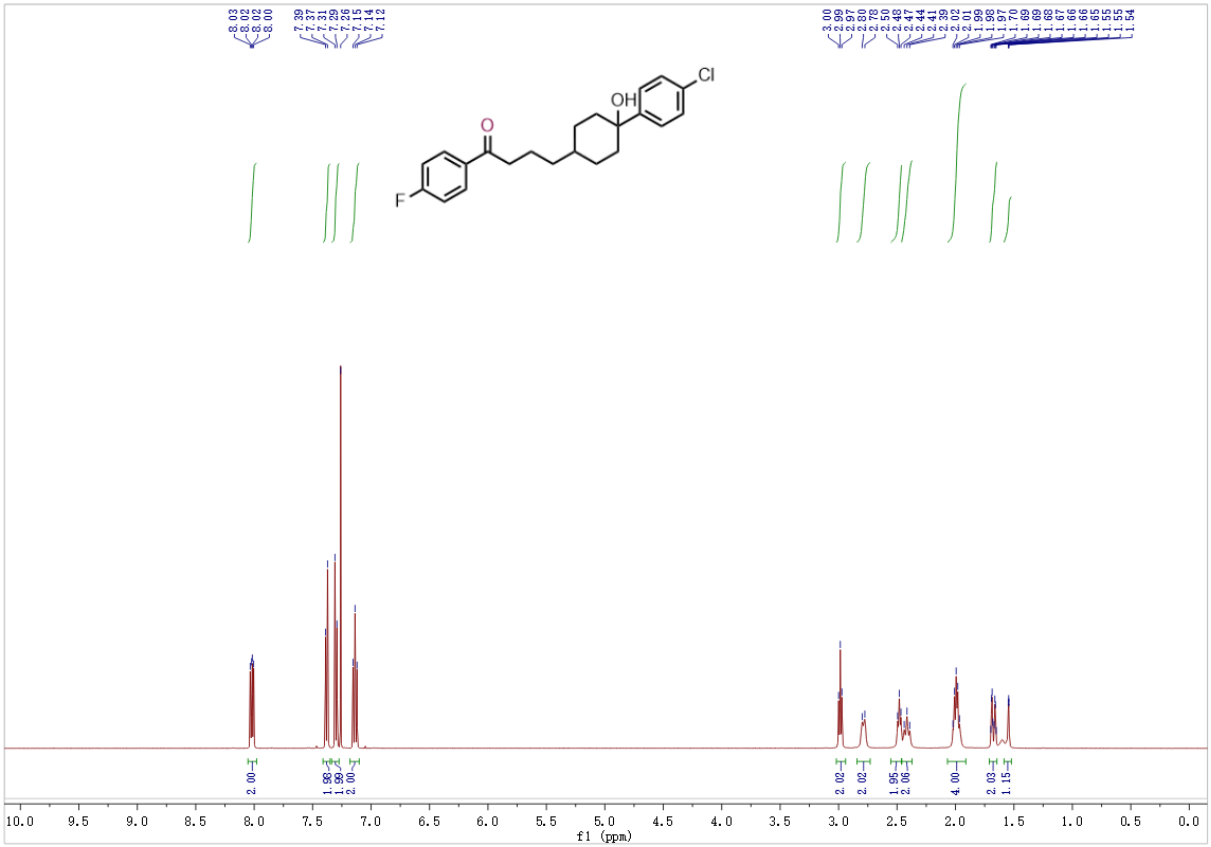
Cl
OH
O
F
f1 (ppm)

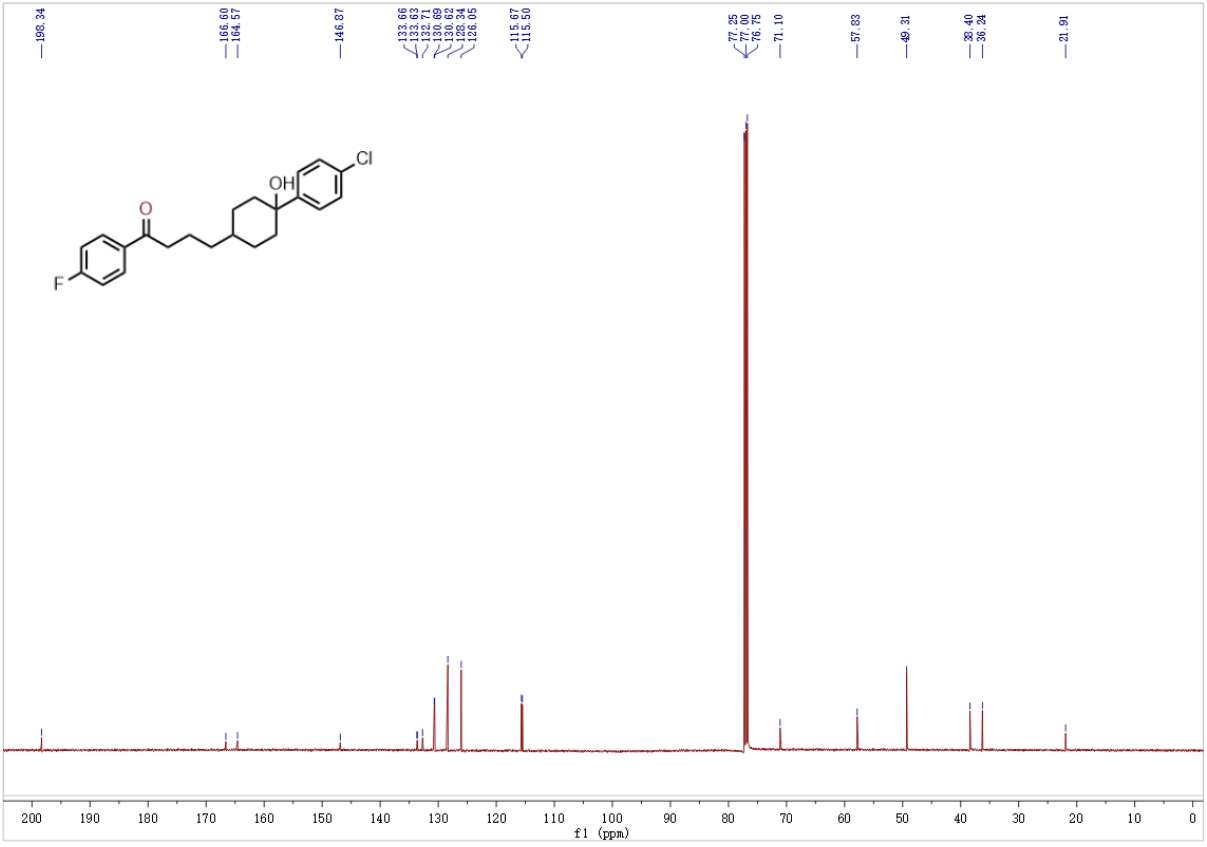
Cl
OH
O
F
f1 (ppm)

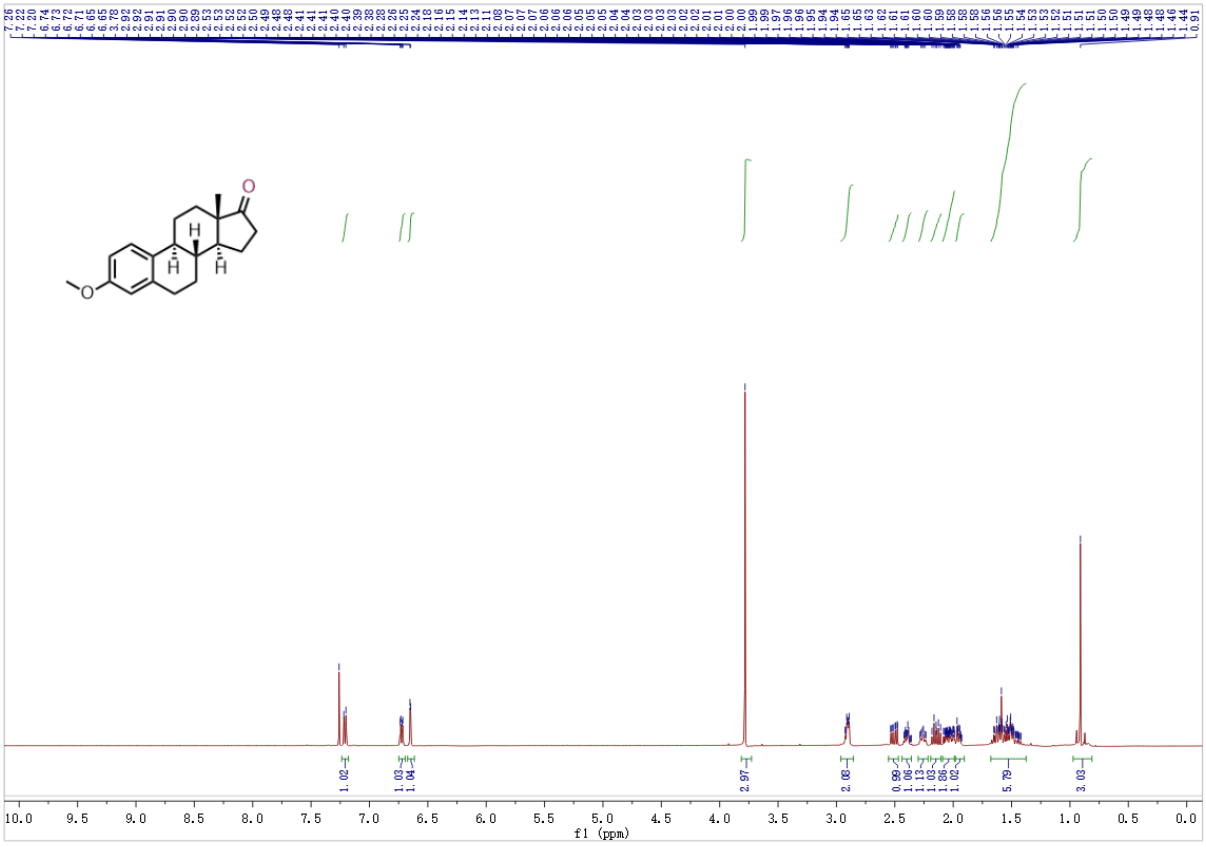
f1 (ppm)

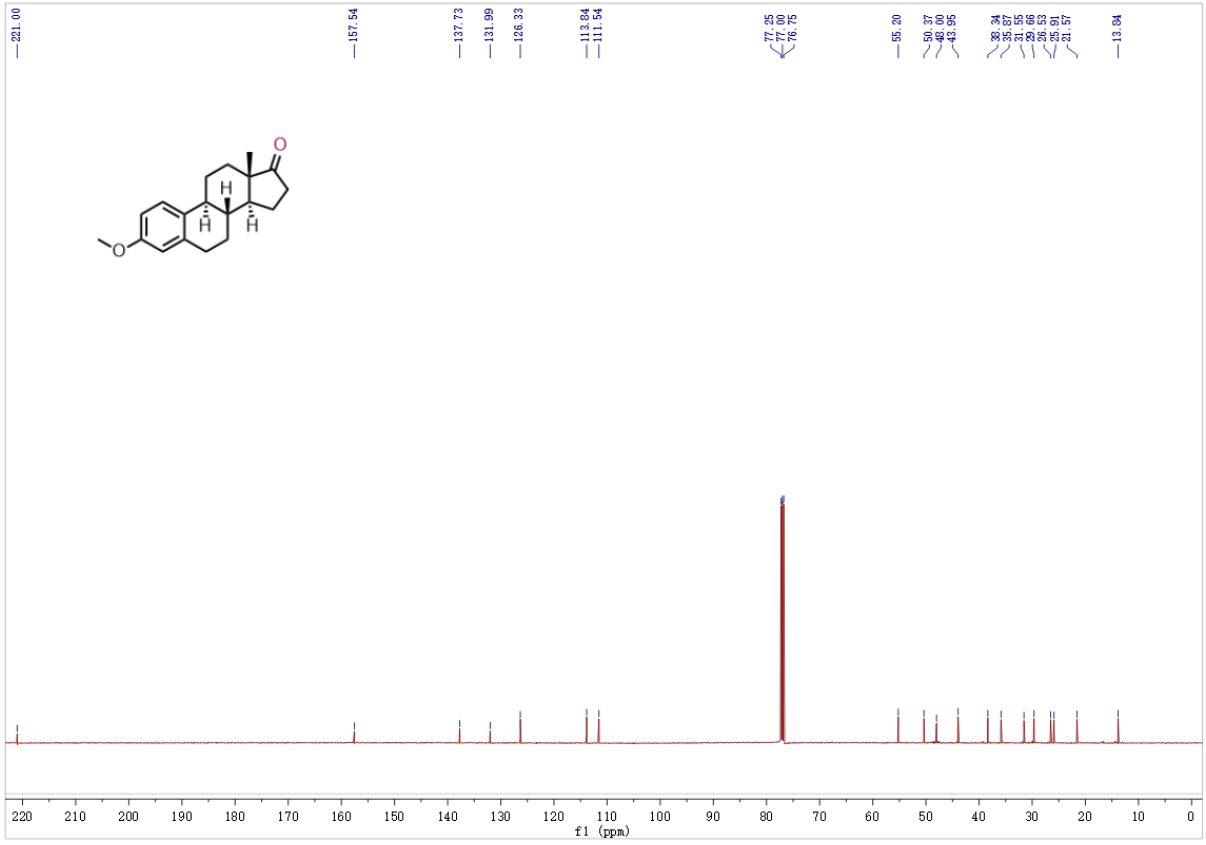
f1 (ppm)

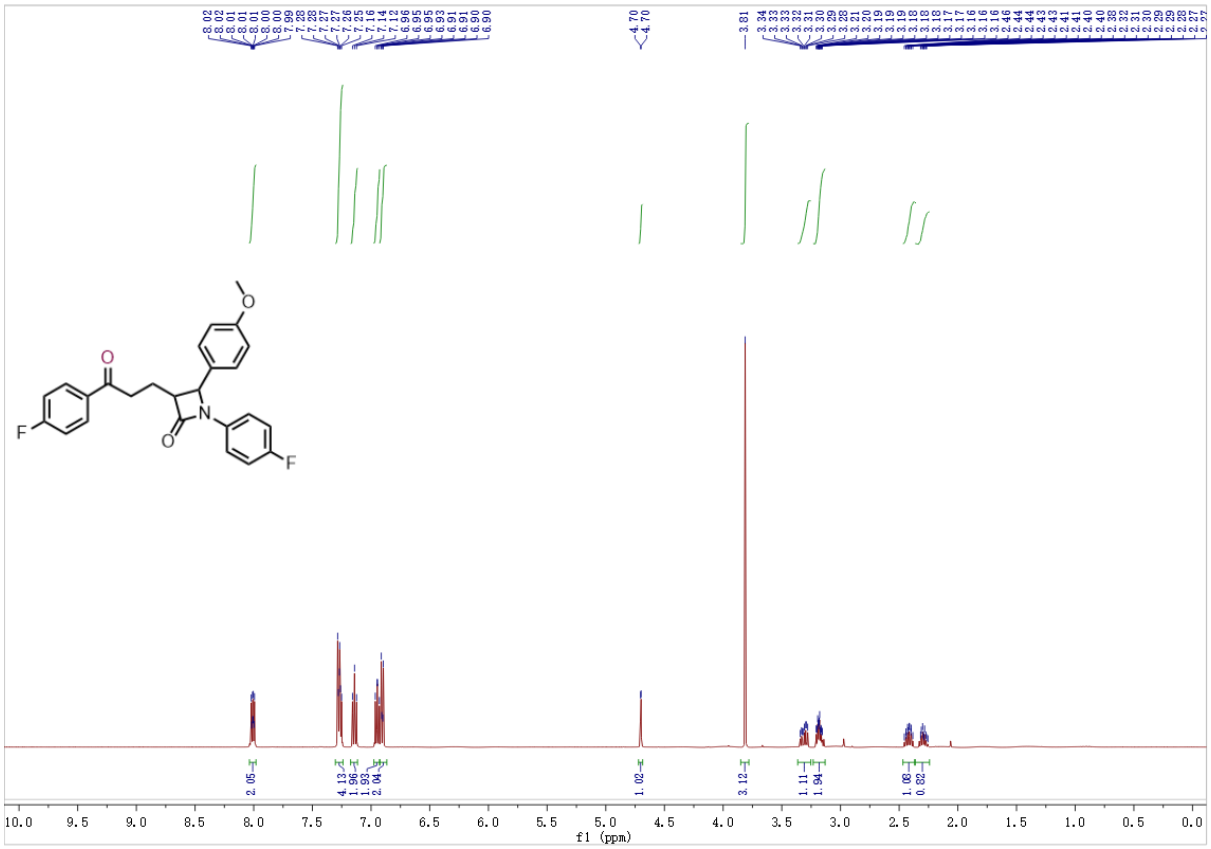
f1 (ppm)

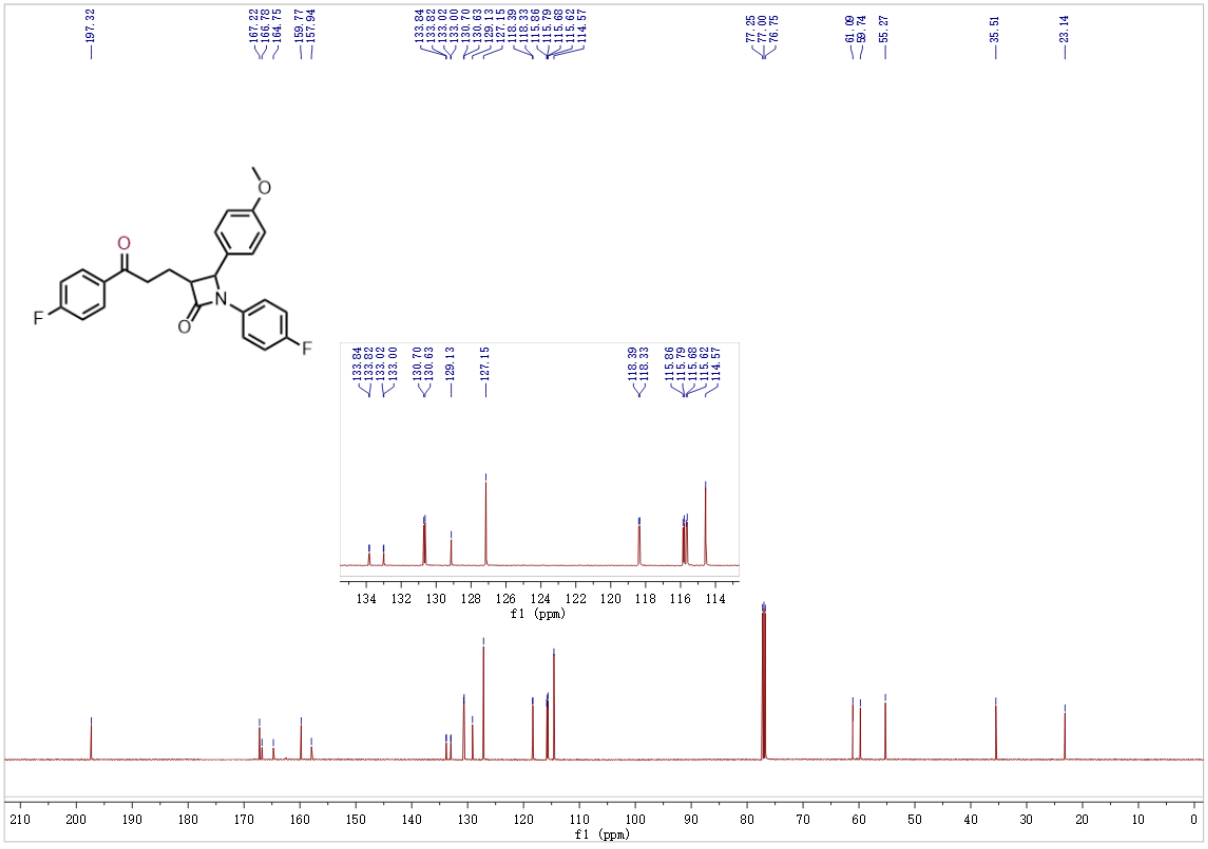
f1 (ppm)
f1 (ppm)

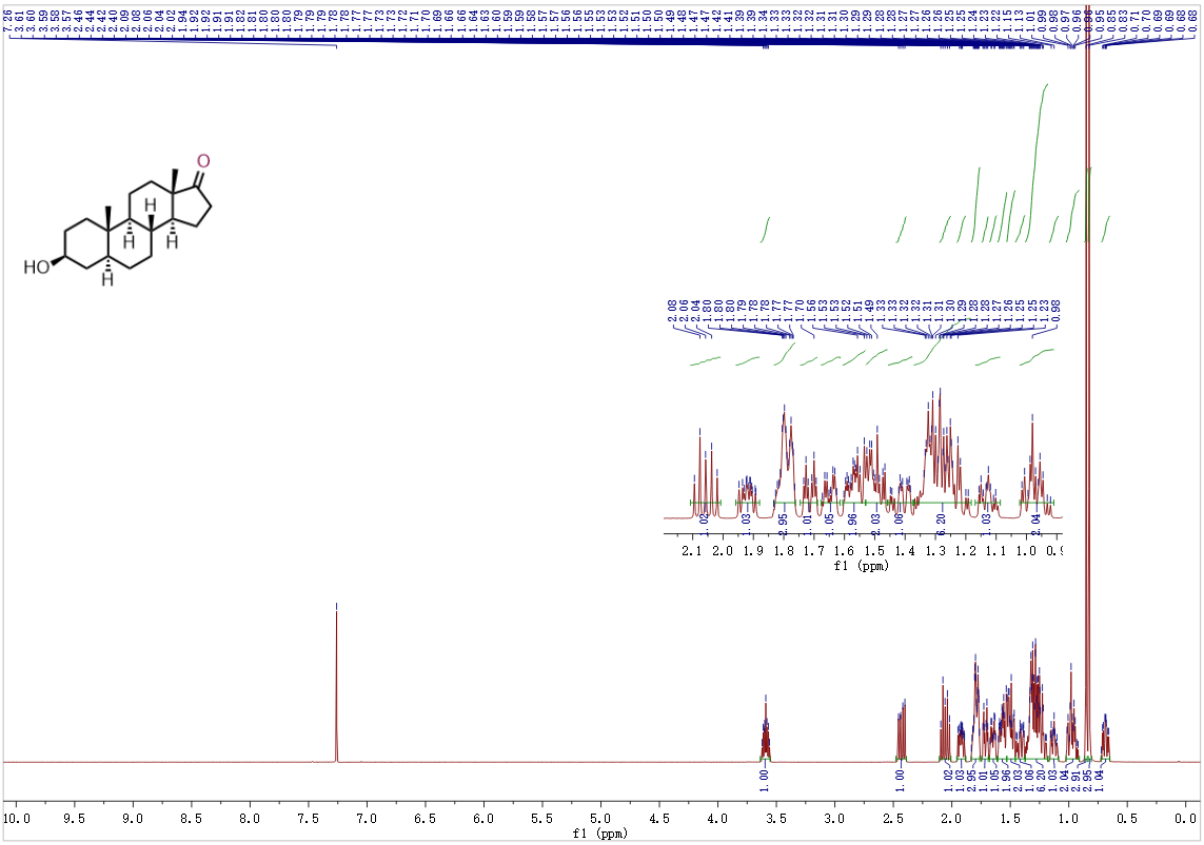
HO
O
f1 (ppm)

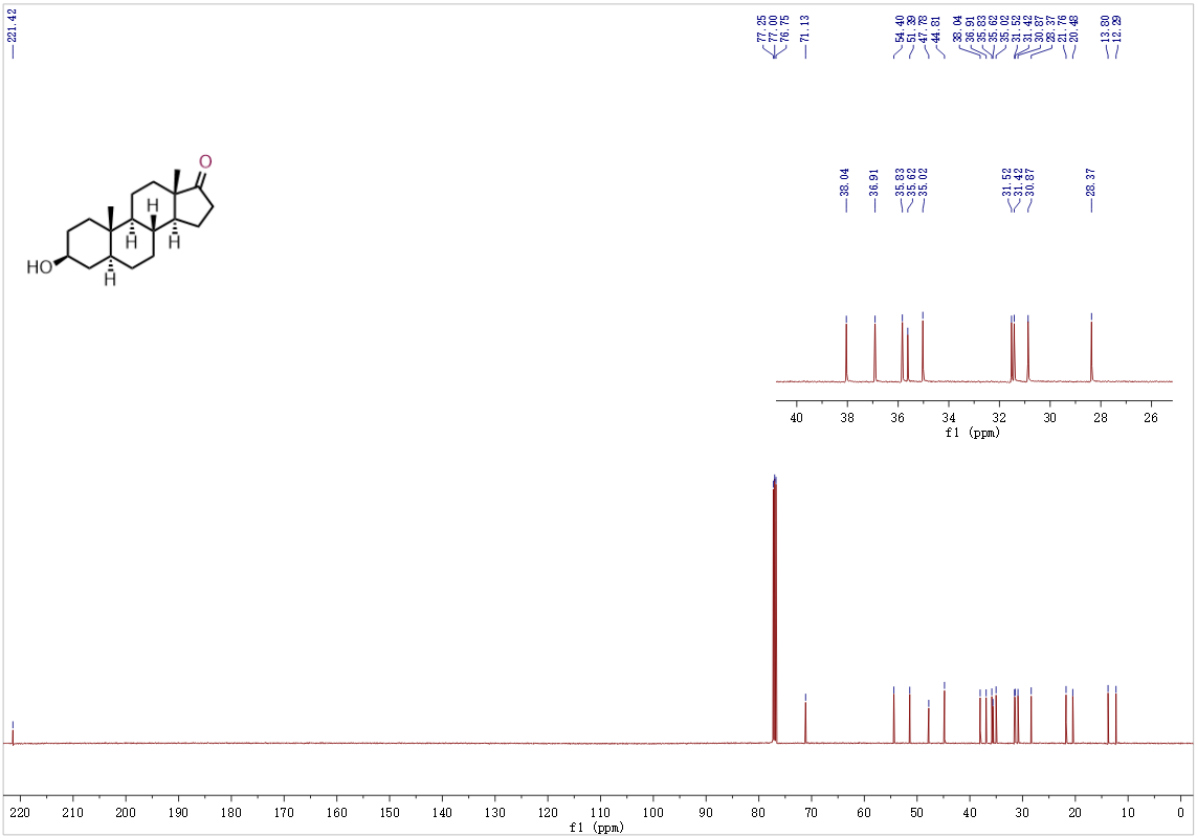
HO
O
f1 (ppm)

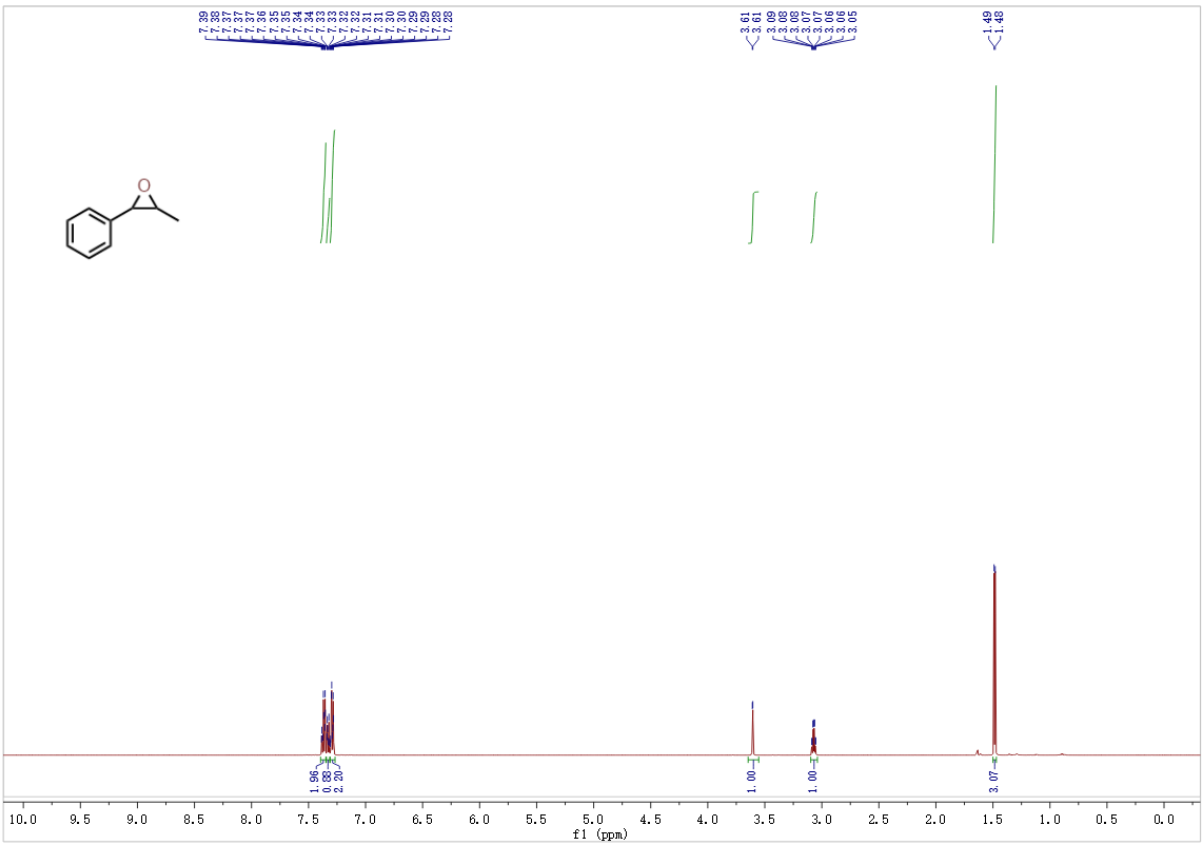
7.39
7.38
7.37
7.37
7.37
7.36
7.35
7.35
7.34
7.34
7.33
7.33
7.32
7.32
7.31
7.31
7.30
7.30
7.29
7.29
7.28
7.28
3.61
3.61
3.09
3.08
3.08
3.07
3.07
3.06
3.06
3.05
1.49
1.48
1.96
0.88
2.20
1.00
1.00
3.07
10.0
9.5
9.0
8.5
8.0
7.5
7.0
6.5
6.0
5.5
5.0
4.5
4.0
3.5
3.0
2.5
2.0
1.5
1.0
0.5
0.0
f1 (ppm)

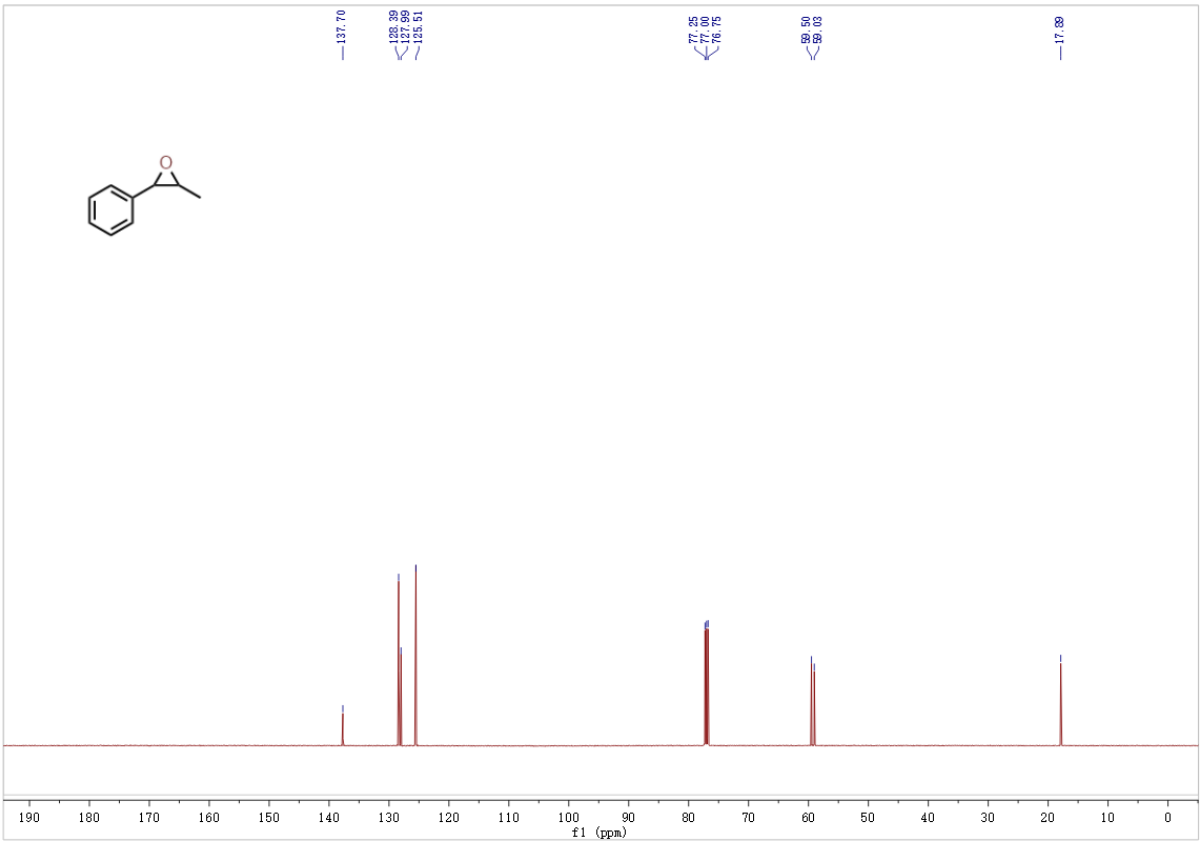
137.70
128.39
127.99
125.51
77.25
77.00
76.75
59.50
59.03
17.89
190
180
170
160
150
140
130
120
110
100
90
80
70
60
50
40
30
20
10
0
f1 (ppm)

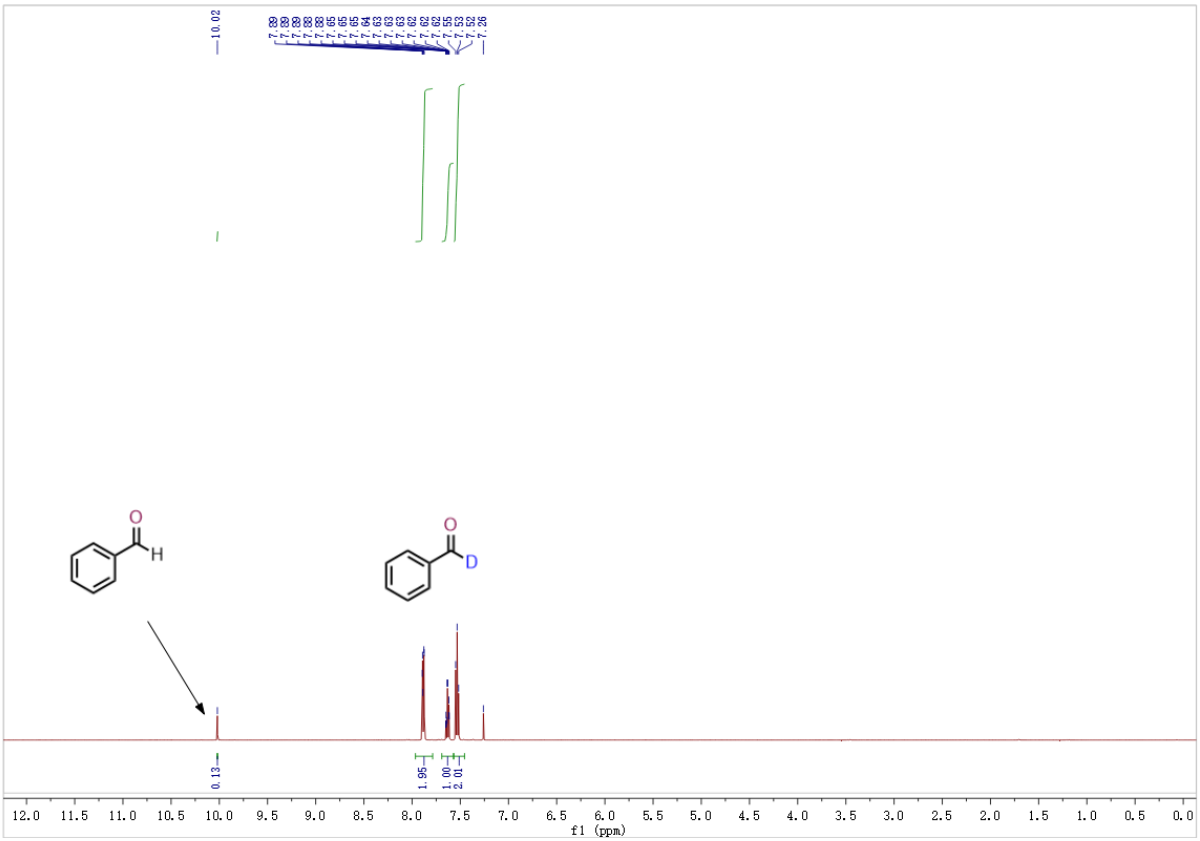
10.02
7.89
7.89
7.89
7.88
7.88
7.65
7.65
7.65
7.64
7.63
7.63
7.62
7.62
7.62
7.55
7.53
7.52
7.26
O
H
O
D
0.13
1.95
1.00
2.01
12.0 11.5 11.0 10.5 10.0 9.5 9.0 8.5 8.0 7.5 7.0 6.5 6.0 5.5 5.0 4.5 4.0 3.5 3.0 2.5 2.0 1.5 1.0 0.5 0.0
f1 (ppm)

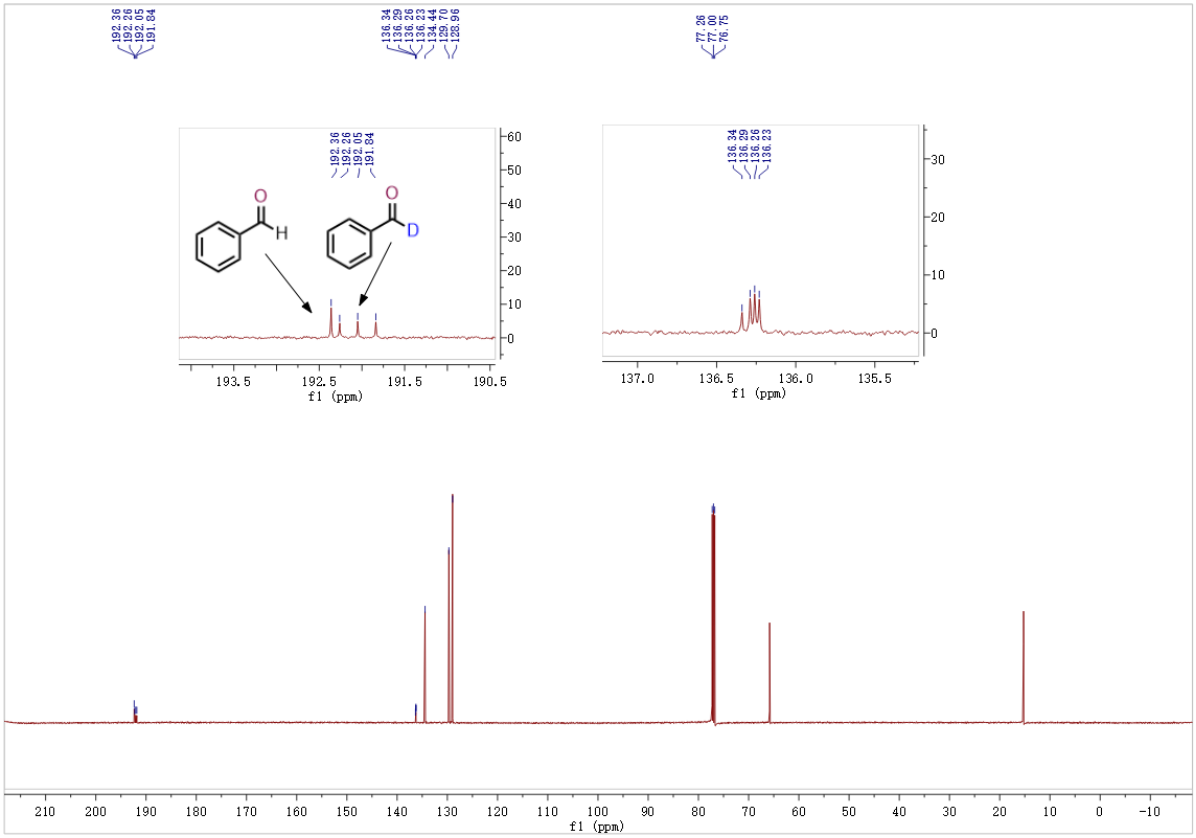
192.36
192.26
192.05
191.84
136.34
136.29
136.25
136.23
134.44
129.70
128.96
77.26
77.00
76.75
O
H
O
D
193.5 192.5 191.5 190.5
f1 (ppm)
137.0 136.5 136.0 135.5
f1 (ppm)
210 200 190 180 170 160 150 140 130 120 110 100 90 80 70 60 50 40 30 20 10 0 -10
f1 (ppm)

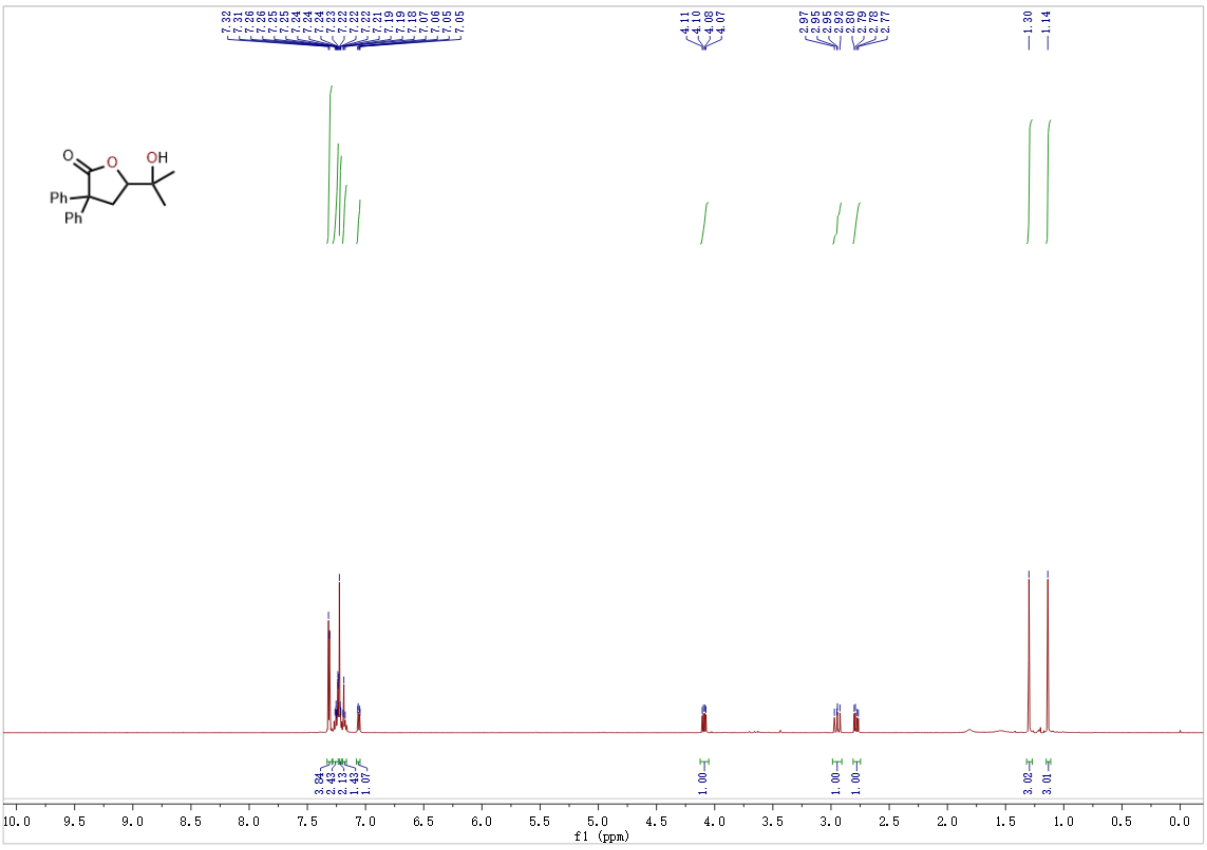
7.32
7.31
7.26
7.26
7.25
7.25
7.24
7.24
7.23
7.23
7.22
7.22
7.22
7.21
7.19
7.19
7.18
7.07
7.06
7.05
7.05
4.11
4.10
4.08
4.07
2.97
2.95
2.95
2.92
2.80
2.79
2.78
2.77
1.30
1.14
O
O
OH
Ph
Ph
3.84
2.43
2.13
1.43
1.07
1.00
1.00
1.00
3.02
3.01
10.0
9.5
9.0
8.5
8.0
7.5
7.0
6.5
6.0
5.5
5.0
4.5
4.0
3.5
3.0
2.5
2.0
1.5
1.0
0.5
0.0
f1 (ppm)

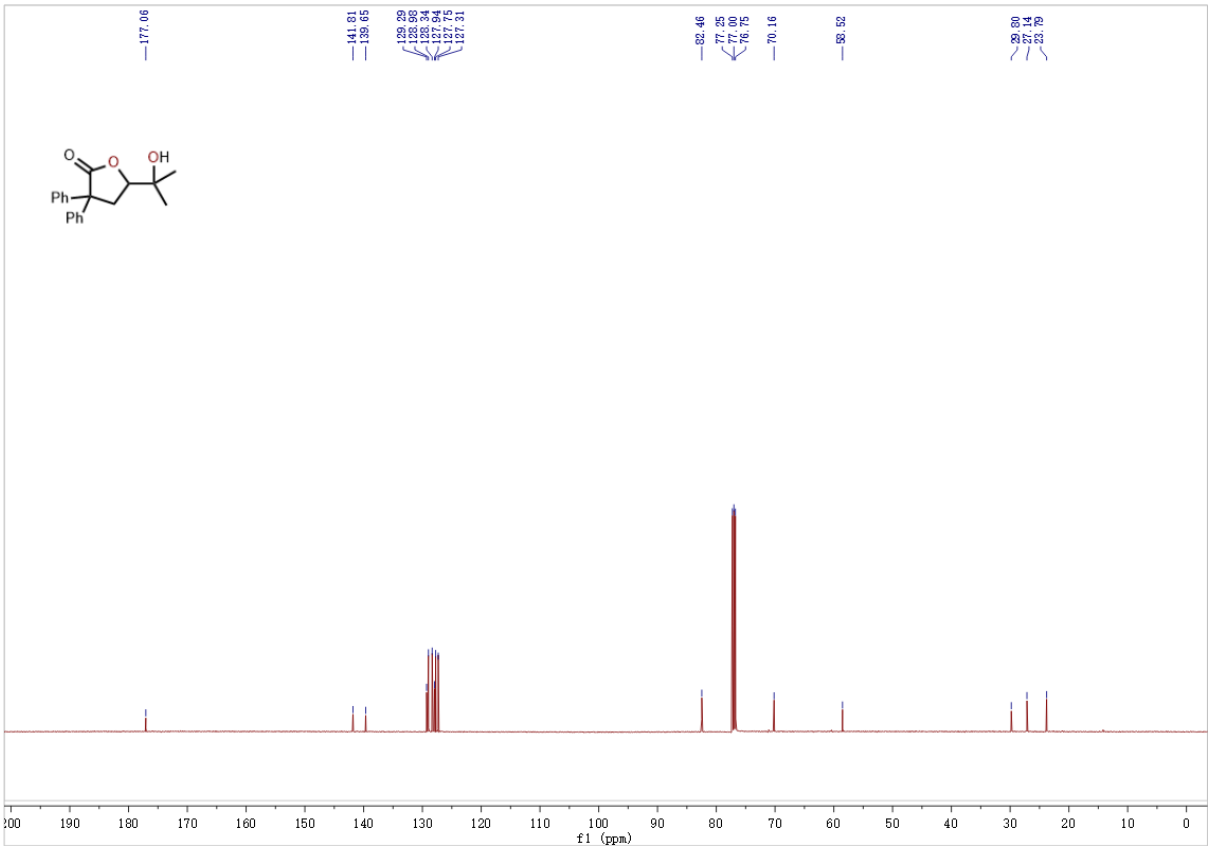
177.06
141.81
139.65
129.29
128.98
128.94
127.94
127.75
127.31
82.46
77.25
77.00
76.75
70.16
58.52
29.80
27.14
23.79
O
O
OH
Ph
Ph
200
190
180
170
160
150
140
130
120
110
100
90
80
70
60
50
40
30
20
10
0
f1 (ppm)

References and Notes

1. Z. Guo, B. Liu, Q. Zhang, W. Deng, Y. Wang, Y. Yang, Recent advances in heterogeneous selective oxidation catalysis for sustainable chemistry. *Chem. Soc. Rev.* **43**, 3480–3524 (2014). doi:10.1039/c3cs60282f Medline

2. H. Baumann, M. Bühler, H. Fochem, F. Hirsinger, H. Zoebelein, J. Falbe, Natural fats and oils—Renewable raw materials for the chemical industry. *Angew. Chem. Int. Ed.* **27**, 41–62 (2003). doi:10.1002/anie.198800411

3. S. Caron, R. W. Dugger, S. G. Ruggeri, J. A. Ragan, D. H. B. Ripin, Large-scale oxidations in the pharmaceutical industry. *Chem. Rev.* **106**, 2943–2989 (2006). doi:10.1021/cr040679f Medline

4. Z. Hassan, M. Stahlberger, N. Rosenbaum, S. Bräse, Criegee intermediates beyond ozonolysis: Synthetic and mechanistic insights. *Angew. Chem. Int. Ed.* **60**, 15138–15152 (2021). doi:10.1002/anie.202014974 Medline

5. M. Rossi, M. Freschi, L. de Camargo Nascente, A. Salerno, S. de Melo Viana Teixeira, F. Nachon, F. Chantegreil, O. Soukup, L. Prchal, M. Malaguti, C. Bergamini, M. Bartolini, C. Angeloni, S. Hrelia, L. A. Soares Romeiro, M. L. Bolognesi, Sustainable drug discovery of multi-target-directed ligands for alzheimer's disease. *J. Med. Chem.* **64**, 4972–4990 (2021). doi:10.1021/acs.jmedchem.1c00048 Medline

6. B. R. Travis, R. S. Narayan, B. Borhan, Osmium tetroxide-promoted catalytic oxidative cleavage of olefins: An organometallic ozonolysis. *J. Am. Chem. Soc.* **124**, 3824–3825 (2002). doi:10.1021/ja017295g Medline

7. K. Salzmann, C. Segarra, M. Albrecht, Donor-flexible bis(pyridylidene amide) ligands for highly efficient ruthenium-catalyzed olefin oxidation. *Angew. Chem. Int. Ed.* **59**, 8932–8936 (2020). doi:10.1002/anie.202002014 Medline

8. P. Spannring, P. C. A. Bruijnincx, B. M. Weckhuysen, R. J. M. Klein Gebbink, Transition metal-catalyzed oxidative double bond cleavage of simple and bio-derived alkenes and unsaturated fatty acids. *Catal. Sci. Technol.* **4**, 2182 (2014). doi:10.1039/c3cy01095c

9. C. Wang, J. Xiao, Activation of molecular oxygen and selective oxidation with metal complexes. *Acc. Chem. Res.* **58**, 714–731 (2025). doi:10.1021/acs.accounts.4c00731 Medline

10. Y. Deng, X.-J. Wei, H. Wang, Y. Sun, T. Noël, X. Wang, Disulfide-catalyzed visible-light-mediated oxidative cleavage of C=C bonds and evidence of an olefin-disulfide charge-transfer complex. *Angew. Chem. Int. Ed.* **56**, 832–836 (2017). doi:10.1002/anie.201607948 Medline

11. Z. Huang, R. Guan, M. Shanmugam, E. L. Bennett, C. M. Robertson, A. Brookfield, E. J. L. McInnes, J. Xiao, Oxidative cleavage of alkenes by O_2 with a non-heme manganese catalyst. *J. Am. Chem. Soc.* **143**, 10005–10013 (2021). doi:10.1021/jacs.1c05757 Medline

12. Z. Cheng, K. Huang, C. Wang, L. Chen, X. Li, Z. Hu, X. Shan, P.-F. Cao, H. Sun, W. Chen, C. Li, Z. Zhang, H. Tan, X. Jiang, G. Zhang, Z. Zhang, M. Lin, L. Wang, A. Zheng, C. Xia, T. Wang, S. Song, X. Shu, N. Jiao, Catalytic remodeling of complex alkenes to oxonitriles through C=C double bond deconstruction. *Science* **387**, 1083–1090 (2025). doi:10.1126/science.adq8918 Medline

13. European Industrial Gases Association, Fire hazards of oxygen and oxygen-enriched atmospheres (EIGA, doc 04/18, 2018); https://www.eiga.eu/uploads/documents/DOC004.pdf.

14. A. Ruffoni, C. Hampton, M. Simonetti, D. Leonori, Photoexcited nitroarenes for the oxidative cleavage of alkenes. *Nature* **610**, 81–86 (2022). doi:10.1038/s41586-022-05211-0 Medline

15. D. E. Wise, E. S. Gogarnoiu, A. D. Duke, J. M. Paolillo, T. L. Vacala, W. A. Hussain, M. Parasram, Photoinduced oxygen transfer using nitroarenes for the anaerobic cleavage of alkenes. *J. Am. Chem. Soc.* **144**, 15437–15442 (2022). doi:10.1021/jacs.2c05648 Medline

16. F. Le Vaillant, A. Mateos Calbet, S. González-Pelayo, E. J. Reijerse, S. Ni, J. Busch, J. Cornella, Catalytic synthesis of phenols with nitrous oxide. *Nature* **604**, 677–683 (2022). doi:10.1038/s41586-022-04516-4 Medline

17. H. Seo, M. H. Katcher, T. F. Jamison, Photoredox activation of carbon dioxide for amino acid synthesis in continuous flow. *Nat. Chem.* **9**, 453–456 (2017). doi:10.1038/nchem.2690 Medline

18. J. H. Ye, T. Ju, H. Huang, L. L. Liao, D. G. Yu, Radical carboxylative cyclizations and carboxylations with CO_2. *Acc. Chem. Res.* **54**, 2518–2531 (2021). doi:10.1021/acs.accounts.1c00135 Medline

19. W. Xiao, J. Zhang, J. Wu, Recent advances in reactions involving carbon dioxide radical anion. *ACS Catal.* **13**, 15991–16011 (2023). doi:10.1021/acscatal.3c04125

20. R. Cauwenbergh, V. Goyal, R. Maiti, K. Natte, S. Das, Challenges and recent advancements in the transformation of CO_2 into carboxylic acids: Straightforward assembly with homogeneous 3d metals. *Chem. Soc. Rev.* **51**, 9371–9423 (2022). doi:10.1039/D1CS00921D Medline

21. L. Piccirilli, B. Rabell, R. Padilla, A. Riisager, S. Das, M. Nielsen, Versatile CO_2 hydrogenation-dehydrogenation catalysis with a Ru-PNP/ionic liquid system. *J. Am. Chem. Soc.* **145**, 5655–5663 (2023). doi:10.1021/jacs.2c10399 Medline

22. Q. Liu, L. Wu, R. Jackstell, M. Beller, Using carbon dioxide as a building block in organic synthesis. *Nat. Commun.* **6**, 5933 (2015). doi:10.1038/ncomms6933 Medline

23. Y. Qin, R. Cauwenbergh, S. Pradhan, R. Maiti, P. Franck, S. Das, Straightforward synthesis of functionalized γ-Lactams using impure CO_2 stream as the carbon source. *Nat. Commun.* **14**, 7604 (2023). doi:10.1038/s41467-023-43289-w Medline

24. P. K. Sahoo, Y. Zhang, S. Das, CO_2-promoted reactions: An emerging concept for the synthesis of fine chemicals and pharmaceuticals. *ACS Catal.* **11**, 3414–3442 (2021). doi:10.1021/acscatal.0c05681

25. J. Wu, Y. Huang, W. Ye, Y. Li, CO_2 reduction: From the electrochemical to photochemical approach. *Adv. Sci.* **4**, 1700194 (2017). doi:10.1002/advs.201700194 Medline

26. T. Y. Takeshita, B. A. Lindquist, T. H. Dunning Jr., Insights into the electronic structure of ozone and sulfur dioxide from generalized valence bond theory: Bonding in O_3 and SO_2. *J. Phys. Chem. A* **119**, 7683–7694 (2015). doi:10.1021/acs.jpca.5b00998 Medline

27. Z. Lu, Y. C. Chang, Q. Z. Yin, C. Y. Ng, W. M. Jackson, Photochemistry. Evidence for direct molecular oxygen production in CO_2 photodissociation. *Science* **346**, 61–64 (2014). doi:10.1126/science.1257156 Medline

28. H. Xu, M. Shaban, S. Wang, A. Alkayal, D. Liu, M. G. Kong, F. Plasser, B. R. Buckley, F. Iza, Oxygen harvesting from carbon dioxide: Simultaneous epoxidation and CO formation. *Chem. Sci.* **12**, 13373–13378 (2021). doi:10.1039/D1SC04209B Medline

29. W. Li, X. Mu, S. Yang, D. Wang, Y. Wang, H. Zhou, P. He, Artificial carbon neutrality through aprotic CO_2 splitting. *Angew. Chem. Int. Ed.* **64**, e202422888 (2025). doi:10.1002/anie.202422888 Medline

30. F. Goettmann, A. Thomas, M. Antonietti, Metal-free activation of CO_2 by mesoporous graphitic carbon nitride. *Angew. Chem. Int. Ed.* **46**, 2717–2720 (2007). doi:10.1002/anie.200603478 Medline

31. H. Qi, S. Mao, J. Rabeah, R. Qu, N. Yang, Z. Chen, F. Bourriquen, J. Yang, J. Li, K. Junge, M. Beller, Water-promoted carbon-carbon bond cleavage employing a reusable Fe single-atom catalyst. *Angew. Chem. Int. Ed.* **62**, e202311913 (2023). doi:10.1002/anie.202311913 Medline

32. C. Copéret, A. Comas-Vives, M. P. Conley, D. P. Estes, A. Fedorov, V. Mougel, H. Nagae, F. Núñez-Zarur, P. A. Zhizhko, Surface organometallic and coordination chemistry toward single-site heterogeneous catalysts: Strategies, methods, structures, and activities. *Chem. Rev.* **116**, 323–421 (2016). doi:10.1021/acs.chemrev.5b00373 Medline

33. T. Hartman, R. G. Geitenbeek, G. T. Whiting, B. M. Weckhuysen, Operando monitoring of temperature and active species at the single catalyst particle level. *Nat. Catal.* **2**, 986–996 (2019). doi:10.1038/s41929-019-0352-1

34. A. E. Nieuwelink, J. C. Vollenbroek, R. M. Tiggelaar, J. G. Bomer, A. van den Berg, M. Odijk, B. M. Weckhuysen, High-throughput activity screening and sorting of single catalyst particles with a droplet microreactor using dielectrophoresis. *Nat. Catal.* **4**, 1070–1079 (2021). doi:10.1038/s41929-021-00718-7

35. A. Wang, J. Li, T. Zhang, Heterogeneous single-atom catalysis. *Nat. Rev. Chem.* **2**, 65–81 (2018). doi:10.1038/s41570-018-0010-1

36. X. Shi, Z. Wen, Q. Gu, L. Jiao, H.-L. Jiang, H. Lv, H. Wang, J. Ding, M. P. Lyons, A. Chang, Z. Feng, S. Chen, Y. Lin, X. Xu, P. Du, W. Xu, M. Sun, Y. Li, B. Yang, T. Zhang, X. Wu, J. Lu, Metal-support frontier orbital interactions in single-atom catalysis. *Nature* **640**, 668–675 (2025). doi:10.1038/s41586-025-08747-z Medline

37. I. Ghosh, J. Khamrai, A. Savateev, N. Shlapakov, M. Antonietti, B. König, Organic semiconductor photocatalyst can bifunctionalize arenes and heteroarenes. *Science* **365**, 360–366 (2019). doi:10.1126/science.aaw3254 Medline

38. S. Ji, Y. Chen, X. Wang, Z. Zhang, D. Wang, Y. Li, Chemical synthesis of single atomic site catalysts. *Chem. Rev.* **120**, 11900–11955 (2020). doi:10.1021/acs.chemrev.9b00818 Medline

39. W. J. Ong, L. L. Tan, Y. H. Ng, S. T. Yong, S. P. Chai, Graphitic carbon nitride ($g\text{-}C_3N_4$)-based photocatalysts for artificial photosynthesis and environmental remediation: Are we

a step closer to achieving sustainability? *Chem. Rev.* **116**, 7159–7329 (2016). doi:10.1021/acs.chemrev.6b00075 Medline

40. S. Bhunia, A. Ghatak, A. Dey, Second sphere effects on oxygen reduction and peroxide activation by mononuclear iron porphyrins and related systems. *Chem. Rev.* **122**, 12370–12426 (2022). doi:10.1021/acs.chemrev.1c01021 Medline

41. X. Chen, J. Zhang, X. Fu, M. Antonietti, X. Wang, Fe-g-C_3N_4-catalyzed oxidation of benzene to phenol using hydrogen peroxide and visible light. *J. Am. Chem. Soc.* **131**, 11658–11659 (2009). doi:10.1021/ja903923s Medline

42. W. Nam, High-valent iron(IV)-oxo complexes of heme and non-heme ligands in oxygenation reactions. *Acc. Chem. Res.* **40**, 522–531 (2007). doi:10.1021/ar700027f Medline

43. B. Meunier, Metalloporphyrins as versatile catalysts for oxidation reactions and oxidative DNA cleavage. *Chem. Rev.* **92**, 1411–1456 (1992). doi:10.1021/cr00014a008

44. Z. Chen, J. J. Concepcion, M. K. Brennaman, P. Kang, M. R. Norris, P. G. Hoertz, T. J. Meyer, Splitting CO_2 into CO and O_2 by a single catalyst. *Proc. Natl. Acad. Sci. U.S.A.* **109**, 15606–15611 (2012). doi:10.1073/pnas.1203122109 Medline

45. T. Kong, Y. Jiang, Y. Xiong, Photocatalytic CO_2 conversion: What can we learn from conventional CO_x hydrogenation? *Chem. Soc. Rev.* **49**, 6579–6591 (2020). doi:10.1039/C9CS00920E Medline

46. J. Schneider, H. Jia, J. T. Muckerman, E. Fujita, Thermodynamics and kinetics of CO_2, CO, and H^+ binding to the metal centre of CO_2 reduction catalysts. *Chem. Soc. Rev.* **41**, 2036–2051 (2012). doi:10.1039/C1CS15278E Medline

47. P. Ren, T. Zhang, N. Jain, H. Y. V. Ching, A. Jaworski, G. Barcaro, S. Monti, J. Silvestre-Albero, V. Celorrio, L. Chouhan, A. Rokicińska, E. Debroye, P. Kuśtrowski, S. Van Doorslaer, S. Van Aert, S. Bals, S. Das, An atomically dispersed Mn-photocatalyst for generating hydrogen peroxide from seawater via the water oxidation reaction (WOR). *J. Am. Chem. Soc.* **145**, 16584–16596 (2023). doi:10.1021/jacs.3c03785 Medline

48. P. K. Sahoo, R. Maiti, P. Ren, J. J. Delgado Jaén, X. Dai, G. Barcaro, S. Monti, A. Skorynina, A. Rokicińska, A. Jaworski, L. Simonelli, P. Kuśtrowski, J. Rabeah, S. Das, An atomically dispersed Mn photocatalyst for vicinal dichlorination of nonactivated alkenes. *J. Am. Chem. Soc.* **147**, 11829–11840 (2025). doi:10.1021/jacs.4c16413 Medline

49. T. Zhang, W. Schilling, S. U. Khan, H. Y. V. Ching, C. Lu, J. Chen, A. Jaworski, G. Barcaro, S. Monti, K. De Wael, A. Slabon, S. Das, Atomic-level understanding for the enhanced generation of hydrogen peroxide by the introduction of an aryl amino group in polymeric carbon nitrides. *ACS Catal.* **11**, 14087–14101 (2021). doi:10.1021/acscatal.1c03733

50. E. Murphy, B. Sun, M. Rüscher, Y. Liu, W. Zang, S. Guo, Y.-H. Chen, U. Hejral, Y. Huang, A. Ly, I. V. Zenyuk, X. Pan, J. Timoshenko, B. R. Cuenya, E. D. Spoerke, P. Atanassov, Synergizing Fe_2O_3 nanoparticles on single atom Fe-N-C for nitrate reduction to ammonia at industrial current densities. *Adv. Mater.* **36**, 2401133 (2024). doi:10.1002/adma.202401133 Medline

51. S. Ding, J. A. Barr, Z. Lyu, F. Zhang, M. Wang, P. Tieu, X. Li, M. H. Engelhard, Z. Feng, S. P. Beckman, X. Pan, J.-C. Li, D. Du, Y. Lin, Effect of phosphorus modulation in iron

single-atom catalysts for peroxidase mimicking. *Adv. Mater.* **36**, 2209633 (2024). doi:10.1002/adma.202209633 Medline

52. Y. Deng, B. Chi, J. Li, G. Wang, L. Zheng, X. Shi, Z. Cui, L. Du, S. Liao, K. Zang, J. Luo, Y. Hu, X. Sun, Atomic Fe-doped MOF-derived carbon polyhedrons with high active-center density and ultra-high performance toward PEM fuel cells. *Adv. Energy Mater.* **9**, 1802856 (2019). doi:10.1002/aenm.201802856

53. Y. Zhou, G. Chen, Q. Wang, D. Wang, X. Tao, T. Zhang, X. Feng, K. Müllen, Fe-N-C electrocatalysts with densely accessible Fe-N_4 sites for efficient oxygen reduction reaction. *Adv. Funct. Mater.* **31**, 2102420 (2021). doi:10.1002/adfm.202102420

54. S. Ni, D. Spinnato, J. Cornella, Reductive cyclopropanation through bismuth photocatalysis. *J. Am. Chem. Soc.* **146**, 22140–22144 (2024). doi:10.1021/jacs.4c07262 Medline

55. T. Ghosh, P. Ren, P. Franck, M. Tang, A. Jaworski, G. Barcaro, S. Monti, L. Chouhan, J. Rabeah, A. Skorynina, J. Silvestre-Albero, L. Simonelli, A. Rokicińska, E. Debroye, P. Kuśtrowski, S. Bals, S. Das, A robust Fe-based heterogeneous photocatalyst for the visible-light-mediated selective reduction of an impure CO_2 stream. *Chem. Sci.* **15**, 11488–11499 (2024). doi:10.1039/D4SC02773F Medline

56. Y. Gao, M. Pink, V. Carta, J. M. Smith, Ene reactivity of an Fe=NR bond enables the catalytic α-deuteration of nitriles and alkynes. *J. Am. Chem. Soc.* **144**, 17165–17172 (2022). doi:10.1021/jacs.2c07462 Medline

57. H. A. Obeid, J. Hannedouche, Iron-catalyzed positional and geometrical isomerization of alkenes. *Adv. Synth. Catal.* **365**, 1100–1111 (2023). doi:10.1002/adsc.202300052

58. M. Alves, B. Grignard, R. Mereau, C. Jerome, T. Tassaing, C. Detrembleur, Organocatalyzed coupling of carbon dioxide with epoxides for the synthesis of cyclic carbonates: Catalyst design and mechanistic studies. *Catal. Sci. Technol.* **7**, 2651–2684 (2017). doi:10.1039/C7CY00438A

59. C. H. Oh, H. H. Jung, K. S. Kim, N. Kim, The palladium-catalyzed addition of organoboronic acids to alkynes. *Angew. Chem. Int. Ed.* **42**, 805–808 (2003). Medline

60. G. Wittig, From diyls to ylides to my idyll. *Science* **210**, 600–604 (1980). doi:10.1126/science.210.4470.600 Medline

61. M. Sasikumar, M. D. Nikalje, M. Muthukrishnan, A convenient synthesis of enantiomerically pure (R)-mexiletine using hydrolytic kinetic resolution method. *Tetrahedron Asymmetry* **20**, 2814–2817 (2009). doi:10.1016/j.tetasy.2009.11.014

62. S. Yasui, S. Banjo, Y. Nagashima, Y. Okada, K. Yoshikawa, K. Nakata, N. Chida, T. Okamura, T. Sato, Total synthesis of lobatamides A and C. *Angew. Chem. Int. Ed.* **63**, e202402335 (2024). doi:10.1002/anie.202402335 Medline

63. A. Jordan, K. D. Whymark, J. Sydenham, H. F. Sneddon, A solvent-reagent selection guide for Steglich-type esterification of carboxylic acids. *Green Chem.* **23**, 6405–6413 (2021). doi:10.1039/D1GC02251B

64. F. H. Lutter, L. Grokenberger, M. S. Hofmayer, P. Knochel, Cobalt-catalyzed acylation-reactions of (hetero)arylzinc pivalates with thiopyridyl ester derivatives. *Chem. Sci.* **10**, 8241–8245 (2019). doi:10.1039/C9SC01817D Medline

65. A. A. Rafaniello, R. Kumar, R. C. Phillips, M. J. Gaunt, Modular synthesis of heterobenzylic amines via carbonyl azinylative amination. *Angew. Chem. Int. Ed.* **63**, e202408287 (2024). Medline

66. Q. Q. Li, Z. Shah, J. P. Qu, Y. B. Kang, Direct wittig olefination of alcohols. *J. Org. Chem.* **83**, 296–302 (2018). doi:10.1021/acs.joc.7b02720 Medline

67. M. Conte, K. Wilson, V. Chechik, Radical intermediates in chloroform reactions over triphenylphosphine-protected Au nanoparticles. *Org. Biomol. Chem.* **7**, 1361–1367 (2009). doi:10.1039/b819627c Medline

68. G. R. Buettner, Spin trapping: ESR parameters of spin adducts. *Free Radic. Biol. Med.* **3**, 259–303 (1987). doi:10.1016/S0891-5849(87)80033-3 Medline

69. L. Eberson, O. Persson, Generation of acyloxyl spin adducts from *N-tert-butyl-α*-phenylnitrone†(PBN) and 4,5-dihydro-5,5-dimethylpyrrole 1-oxide (DMPO) *via* nonconventional mechanisms. *J. Chem. Soc., Perkin Trans. 2* **2**, 1689–1696 (1997). doi:10.1039/a701479a

70. F. Neese, The ORCA program system. *Wiley Interdiscip. Rev. Comput. Mol. Sci.* **2**, 73–78 (2011). doi:10.1002/wcms.81

71. F. Neese, F. Wennmohs, U. Becker, C. Riplinger, The ORCA quantum chemistry program package. *J. Chem. Phys.* **152**, 224108 (2020). doi:10.1063/5.0004608 Medline

72. B. Ravel, M. Newville, ATHENA, ARTEMIS, HEPHAESTUS: Data analysis for X-ray absorption spectroscopy using IFEFFIT. *J. Synchrotron Radiat.* **12**, 537–541 (2005). doi:10.1107/S0909049505012719 Medline

73. M. J. Frisch *et al*., *Gaussian 16, Revision C.01* (Gaussian, Inc., 2016).

74. L. E. Roy, P. J. Hay, R. L. Martin, Revised basis sets for the LANL effective core potentials. *J. Chem. Theory Comput.* **4**, 1029–1031 (2008). doi:10.1021/ct8000409 Medline

75. A. V. Marenich, C. J. Cramer, D. G. Truhlar, Universal solvation model based on solute electron density and on a continuum model of the solvent defined by the bulk dielectric constant and atomic surface tensions. *J. Phys. Chem. B* **113**, 6378–6396 (2009). doi:10.1021/jp810292n Medline

76. C. Peng, H. B. Schlegel, Combining synchronous transit and quasi-newton methods for finding transition states. *Isr. J. Chem.* **33**, 449–454 (1993). doi:10.1002/ijch.199300051

77. P. Giannozzi, O. Andreussi, T. Brumme, O. Bunau, M. Buongiorno Nardelli, M. Calandra, R. Car, C. Cavazzoni, D. Ceresoli, M. Cococcioni, N. Colonna, I. Carnimeo, A. Dal Corso, S. de Gironcoli, P. Delugas, R. A. DiStasio Jr., A. Ferretti, A. Floris, G. Fratesi, G. Fugallo, R. Gebauer, U. Gerstmann, F. Giustino, T. Gorni, J. Jia, M. Kawamura, H.-Y. Ko, A. Kokalj, E. Küçükbenli, M. Lazzeri, M. Marsili, N. Marzari, F. Mauri, N. L. Nguyen, H.-V. Nguyen, A. Otero-de-la-Roza, L. Paulatto, S. Poncé, D. Rocca, R. Sabatini, B. Santra, M. Schlipf, A. P. Seitsonen, A. Smogunov, I. Timrov, T. Thonhauser, P. Umari, N. Vast, X. Wu, S. Baroni, Advanced capabilities for materials modelling with Quantum ESPRESSO. *J. Phys. Condens. Matter* **29**, 465901 (2017). doi:10.1088/1361-648X/aa8f79 Medline

78. G. Kresse, D. Joubert, From ultrasoft pseudopotentials to the projector augmented-wave method. *Phys. Rev. B* **59**, 1758–1775 (1999). doi:10.1103/PhysRevB.59.1758

79. J. P. Perdew, K. Burke, M. Ernzerhof, Generalized gradient approximation made simple. *Phys. Rev. Lett.* **77**, 3865–3868 (1996). doi:10.1103/PhysRevLett.77.3865 Medline

80. S. Grimme, J. Antony, S. Ehrlich, H. Krieg, A consistent and accurate ab initio parametrization of density functional dispersion correction (DFT-D) for the 94 elements H-Pu. *J. Chem. Phys.* **132**, 154104 (2010). doi:10.1063/1.3382344 Medline

81. V. Palani, A. E. Wendlandt, Strain inducing positional alkene isomerization. *J. Am. Chem. Soc.* **145**, 20053–20061 (2023). doi:10.1021/jacs.3c06935 Medline

82. J. Mazuela, J. J. Verendel, M. Coll, B. Schäffner, A. Börner, P. G. Andersson, O. Pàmies, M. Diéguez, Iridium phosphite-oxazoline catalysts for the highly enantioselective hydrogenation of terminal alkenes. *J. Am. Chem. Soc.* **131**, 12344–12353 (2009). doi:10.1021/ja904152r Medline

83. C. R. Larsen, D. B. Grotjahn, Stereoselective alkene isomerization over one position. *J. Am. Chem. Soc.* **134**, 10357–10360 (2012). doi:10.1021/ja3036477 Medline

84. T. Nagashima, H. M. L. Davies, Catalytic asymmetric solid-phase cyclopropanation. *J. Am. Chem. Soc.* **123**, 2695–2696 (2001). doi:10.1021/ja005776e Medline

85. B. Gaspar, E. M. Carreira, Mild cobalt-catalyzed hydrocyanation of olefins with tosyl cyanide. *Angew. Chem. Int. Ed.* **46**, 4519–4522 (2007). doi:10.1002/anie.200700575 Medline

86. J. Ren, F.-H. Du, M.-C. Jia, Z.-N. Hu, Z. Chen, C. Zhang, Ring expansion fluorination of unactivated cyclopropanes mediated by a new monofluoroiodane(III) reagent. *Angew. Chem. Int. Ed.* **60**, 24171–24178 (2021). doi:10.1002/anie.202108589 Medline

87. Q. Feng, Q. Wang, J. Zhu, Oxidative rearrangement of 1,1-disubstituted alkenes to ketones. *Science* **379**, 1363–1368 (2023). doi:10.1126/science.adg3182 Medline

88. M. Behera, P. D. Dharpure, A. K. Sahu, R. G. Bhat, Visible light-induced organophotoredox-catalyzed *β*-hydroxytrifluoromethylation of unactivated alkenes. *J. Org. Chem.* **89**, 14695–14709 (2024). doi:10.1021/acs.joc.4c00967 Medline

89. L. Gao, X. Liu, G. Li, S. Chen, J. Cao, G. Wang, S. Li, 1,2-Silylpyridylation reaction of aryl alkenes with silylboronate. *Org. Lett.* **24**, 5698–5703 (2022). doi:10.1021/acs.orglett.2c02074 Medline

90. S. A. Green, T. R. Huffman, R. O. McCourt, V. van der Puyl, R. A. Shenvi, Hydroalkylation of olefins to form quaternary carbons. *J. Am. Chem. Soc.* **141**, 7709–7714 (2019). doi:10.1021/jacs.9b02844 Medline

91. H. Zeng, R. Yin, Y. Zhao, J. A. Ma, J. Wu, Modular alkene synthesis from carboxylic acids, alcohols and alkanes *via* integrated photocatalysis. *Nat. Chem.* **16**, 1822–1830 (2024). doi:10.1038/s41557-024-01642-6 Medline

92. J. Wang, F. He, X. Yang, Asymmetric construction of acyclic quaternary stereocenters *via* direct enantioselective additions of *α*-alkynyl ketones to allenamides. *Nat. Commun.* **12**, 6700 (2021). doi:10.1038/s41467-021-27028-7 Medline

93. H. Qian, X. Han, R. A. Widenhoefer, Platinum-catalyzed intramolecular hydroalkoxylation of *γ*- and *δ*-hydroxy olefins to form cyclic ethers. *J. Am. Chem. Soc.* **126**, 9536–9537 (2004). doi:10.1021/ja0477773 Medline

94. Y. Zhang, N. Hatami, N. S. Lange, E. Ronge, W. Schilling, C. Jooss, S. Das, A metal-free heterogeneous photocatalyst for the selective oxidative cleavage of C=C bonds in aryl olefins *via* harvesting direct solar energy. *Green Chem.* **22**, 4516–4522 (2020). doi:10.1039/D0GC01187H